VOL.29 NO.2
FEBRUARY
2026

AJSTR

ASEAN JOURNAL

of Scientific and Technological Report

ISSN 2773-8752 (online)

ASEAN
Journal of Scientific and Technological Reports
Online ISSN:2773-8752

ASEAN Journal of Scientific and Technological Reports (AJSTR)

Contact Us Institute of Research and Innovation, Thaksin University
222 M. 2 Ban-Prao sub-district, Pa-Pra-Yom district, Phatthalung province, Thailand
Tel. 0 7460 9600 # 7242 , E-mail: aseanjstr@tsu.ac.th

List of Contents

List of Contents

ASEAN
Journal of Scientific and Technological Reports
Online ISSN:2773-8752

ASEAN
Journal of Scientific and Technological Reports
Online ISSN:2773-8752

Research article

Enhancing Growth and Nutritional Components of Hydroponic Mulato II Grass Using Moringa Leaf Extract as a Priming Agent

Roger Y. Ibañez Jr.[1]*, and Manuel D. Gacutan, Jr.[2]

[1] Faculty of Cawayan Campus, Dr. Emilio B. Espinosa Sr. Memorial State College of Agriculture and Technology, 5405, Philippines
[2] Faculty of Department of Animal Science, Visayas State University, 6521, Philippines
* Correspondence: ryibanez@debesmscat.edu.ph

Citation:
Ibañez Jr., R.; Gacutan Jr., M. Enhancing growth and nutritional component of yydroponic mulato II grass using moringa leaf extract as a priming agent. *ASEAN J. Sci. Tech. Report.* **2026**, *29*(2), e259077. https://doi.org/10.55164/ajstr.v29i2.259077.

Article history:
Received: April 30, 2025
Revised: September 29, 2025
Accepted: October 1, 2025
Available online: January 18, 2026

Publisher's Note:
This article is published and distributed under the terms of Thaksin University.

Abstract: Forage grasses are vital for livestock nutrition and sustainability but face challenges due to climate change and land degradation. This study aimed to enhance the germination, growth, and nutritional quality of Mulato II grass by utilizing *Moringa oleifera* leaf extract (MLE) as a priming agent. A Completely Randomized Design (CRD) was employed, testing five treatments (unprimed seeds, hydropriming, and MLE priming for 6, 12, and 18 hours), and each treatment was replicated three times. Growth parameters, biomass, and nutritional composition were analyzed statistically at a 5% significance level, with post-hoc comparisons performed using Tukey's Honestly Significant Difference (HSD) test. MLE priming for 18 hours significantly ($p<0.05$) enhanced performance, yielding the highest vigor index (5326.67), fresh herbage yield (196.32 t/ha), and DM yield (57.70 t/ha). Nutritional analysis revealed a significant difference ($p < 0.0001$) in ether extract (EE) content (4.54%) with MLE priming for 12 hours, while crude protein content (16.76%) and total nitrogen content (3.05%) were significantly higher with MLE priming for 18 hours. Hydropriming and MLE priming for 18 hours also significantly ($p = 0.0137$) achieved the highest final emergence percentage (FEP = 53.33%). The findings show that MLE priming, especially when primed for 18 hours, significantly enhances the growth and nutritional value of Mulato II grass. It is recommended as a sustainable strategy for improving forage production, with future studies focusing on long-term effects and cost-effective scaling.

Keywords: Hydroponic; MLE; Mulato II; nutritional component; priming agent

1. Introduction

Forage grasses are essential for livestock production because they provide essential nutrients that enhance animal health, productivity, and the livelihoods of millions of farmers worldwide. The world population currently stands at 8.16 billion and is expected to continue growing in the coming years [1]. As a result, the demand for livestock products will also increase. However, there will be a reduction in land available for agricultural production due to land conversion to residential and commercial spaces, which will affect the forage supply chain in the future. In 2022, the global market for forage was valued at USD 773.12 million, and it is projected to continue increasing to US$131.0 billion by 2032 [2, 3]. Globally, 80% of the land, or 38 million km^2, is occupied or devoted to grazing and crops used for animal feed [4]. However, the global forage supply is facing a significant decrease due to the effects of traditional farming practices, such as pesticide pollution, land degradation,

population growth, loss of biodiversity, and climate change [3]. In the Philippines, this issue of declining forage supply is severe, with inconsistent forage availability threatening the sustainability of livestock farming—a vital sector for food security and rural economies [5]. Forages are essential not only for livestock nutrition but also for the overall health of the agricultural economy. They promote sustainable farming practices and enhance food security [6].

Climate change was affecting all countries, exacerbating the crisis of forage supply in the market, and impacting the livestock industry. These environmental stressors reduce forage quality and availability, increase feed costs, and lower livestock productivity [7]. In light of these challenges, innovative strategies are needed to enhance forage production, particularly in resource-limited environments. Michalk et al [8] pointed out that land conversion is one of the reasons for the declining supply of forages. One of the strategies adopted by some livestock farmers is the use of improved forage grass, which contains a high amount of essential nutrients the animals need to grow, utilizing only a small portion of the land. However, farmers often face the drawback of these improved forage grasses due to poor germination rates, which hampers the feed needed for their animals. Mulato II is one of the forage grasses yet to be widely cultivated in the Philippines. This three-way hybrid *(Urochloa ruziziensis x Urochloa decumbens x Urochloa brizantha)* is a yielding and nutritious perennial forage grass suitable for both large and small ruminants, promoting increased beef and milk production. According to the study by Bacorro et al [9], Mulato II contains 18.54-21.04% dry matter, 8.08-12.86% crude protein, 53.36-63.73% neutral detergent fiber (NDF), 30.25-38.93% acid detergent fiber (ADF), 0.23-0.30% phosphorus, and 0.21-0.37% calcium.

Seed priming has emerged as a promising technique to improve germination, growth, and stress resilience in various crops. *Moringa oleifera*, known for its rich content of growth-promoting compounds like zeatin (a cytokinin), ascorbic acid, phenolic compounds, and other antioxidants, has gained attention as a natural priming agent [10]. A study by Shrey et al. [11] has shown that moringa leaf extract can enhance seedling vigor, root development, and biomass in crops such as maize, and improve the growth performance of tomato and bell pepper. A similar result was obtained by Muneeba et al. [12], who found that moringa leaf extract enhances wheat seedling growth and mitigates salinity stress, indicating its potential to improve crop vigor and biomass in wheat. Studies have also demonstrated that moringa leaf extract can increase photosynthetic activity [13], delay senescence [14], and improve nutrient uptake [15] in treated crops and plants. Additionally, based on analysis conducted by Yasmeen et al. (2013), Moringa leaf extract contains 191.86 units of superoxide dismutase, 7.09 units of catalase, 21.99 units of peroxidase (IU/mg protein), 8.19 mg g–1 total phenolics, 0.36 mmol g–1 ascorbic acid, and 1.40 mg g–1 total soluble protein.

Despite these promising results, the application of moringa leaf extract (MLE) in forage grass production, particularly under hydroponic systems, remains underexplored. Previous studies have primarily focused on staple crops, such as maize, rice, and wheat, as well as vegetables, with limited evidence on how MLE affects the germination, growth, and nutritional composition of forage grasses. Furthermore, most existing work has concentrated on soil-based cultivation, leaving a knowledge gap regarding its potential in controlled, soilless systems, such as hydroponics, which are increasingly relevant in land- and resource-constrained environments. This study aims to address this gap by investigating the effects of MLE as a priming agent on the growth and nutritional value of hydroponically grown Mulato II grass—a promising but underutilized forage species in the Philippines. By sustainably enhancing forage production, this study aligns with several of the United Nations' Sustainable Development Goals (SDGs), including Zero Hunger (SDG 2), Climate Action (SDG 13), and Life on Land (SDG 15). Enhancing forage availability fosters more resilient livestock systems, mitigates the environmental footprint of feed production, and promotes sustainable land use practices, ultimately contributing to global food security and environmental sustainability.

2. Methodology

2.1 Site and Seed Selection

The study was conducted at the lower campus of Visayas State University in Baybay City, Leyte, Philippines, which has a microclimate characterized by localized atmospheric conditions differing from the surrounding climate. During the study, the average environmental conditions at the university were 28 °C temperature, 85.5% relative humidity, and a photoperiod of 11.8 hours per day. Mulato II grass was used as the forage material in this study. The seeds for this forage grass were procured from an online store through the Shopee shopping application. This forage grass was selected because it represented a new, improved variety that had never been tested under the conditions at Visayas State University, Baybay City, Leyte, Philippines.

2.2. Treatment Preparation

Moringa leaves were collected from the Department of Animal Science laboratory field. The leaves were separated from the stalks and primary veins and then thoroughly washed under running water using a strainer to remove insects and dirt. The cleaned leaves were extracted using a locally made hydraulic coconut presser. The extract was filtered through cheesecloth to remove any remaining particulates. After filtration, the Moringa leaf extract was stored overnight at 4°C in the Visayas State University, Baybay City, Leyte, Philippines, Department of Agronomy Laboratory refrigerator, which maintained freezing temperatures.

Figure 1 Moringa leaf extraction.

2.3 Seed Priming

Seeds of Mulato II were subjected to priming at room temperature using a 1:10 diluted Moringa leaf extract, following the method outlined in the study by Yasmeen et al. [16]. For uniformity, seeds were soaked in 44 mL of diluted extract. The soaking durations were varied: 6, 12, and 18 hours, as described by Ranmeechai et al [17]. In addition, hydropriming was performed for a 12-hour soaking duration for comparative analysis. Some Mulato II seeds were included as control samples without priming. After the priming treatments, the seeds were dried on a paper sheet at room temperature for 48 hours to restore them to their original weight.

2.4 Planting and Management

Both primed and unprimed Mulato II seeds were placed in a seedling tray for germination. The soil media in the seedling tray consisted of a mixture of garden soil and vermicast. After 15 days, healthy seedlings were selected and directly transplanted into plastic cups, each filled with coco peat, with one seedling per cup. Seedlings were chosen based on uniformity in height, absence of visible damage, and normal leaf color after 15 days of germination. The cups were placed in a Styrofoam box containing 14 liters of nutrient solution with a dilution rate of 2 mL per liter of water. The nutrient solution was enriched with essential macronutrients, including carbon, phosphorus, iron, hydrogen, nitrogen, oxygen, sulfur, potassium, magnesium, and calcium, which supported plant growth and development. Each Styrofoam box contained three plastic cups. These cups were harvested after 30 days to evaluate shoot and root development, plant vigor, and the analysis of nutritional components. The 30-day harvesting time was anchored on the standard forage evaluation intervals

to capture early biomass accumulation and nutritional quality [18]. Regular monitoring ensured that the coco peat remained moist until the roots made contact with the nutrient-rich water solution.

2.5 Seed Emergence

Seedling emergence was counted daily until the final emergence was reached. The formula from the studies by Yasmeen et al. [16] and Vujošević et al. [19] was adopted to compute the emergence index (EI), mean emergence time (MET), and final emergence percentage (FEP).

$$\text{Emergence Index} = \frac{\text{No.of emerged seeds}}{\text{Days of the first count}} + \ldots\ldots + \frac{\text{No.of emerged seeds}}{\text{Days of the final count}} \quad (1)$$

$$\text{Mean Emergence Time} = \frac{\sum(\text{Dn})}{\sum \text{n}} \quad (2)$$

where D represents the number of days from the emergence, and n is the number of seeds that emerged on each respective day.

$$\text{Final Emergence Percentage } \frac{\text{No.of emerged seeds}}{\text{Number of seeds sown}} \text{ x } 100 \quad (3)$$

2.6 Vigor Index and Growth Parameters Determination

After 30 days of emergence, plants per treatment were harvested to assess plant vigor and forage grass quality parameters. Plant height, shoot length, and root length were measured from the tip to the base using a ruler. Fresh and dry weights were determined using an analytical digital scale. Seed vigor was calculated using the formula developed by Abdul-Baki and Alderson [20].

$$\text{Vigor Index} = (\text{Shoot length} + \text{Root length}) \text{ x Germination Percentage} \quad (4)$$

The number of leaves and tillers was recorded by counting them 30 days after transplanting. Fresh herbage yield was determined by weighing the harvested parts at 30 days, while dry matter (DM) yield was calculated by multiplying the fresh weight by the DM percentage.

$$\text{DM yield} = \text{Fresh Weight x Dry Matter Percentage} \quad (5)$$

To facilitate comparison with standard agronomic studies, the yields recorded in grams per plant were extrapolated to tons per hectare, allowing for a direct comparison with standard agronomic studies. The extrapolation was based on the planting density equivalent to the hydroponic box area and then scaled up to one hectare. This approach assumes uniform growth under field conditions. However, field validation is required to confirm the applicability of the extrapolated hectare-level yields.

2.7 Chemical Analyses

Chemical assays involved collecting plant tissue samples from each treatment per replicate at 30 days. The samples were sent to the Visayas State University Central Analytical Laboratory for analysis of their nutrient content, including total nitrogen and available phosphorus. Other relevant parameters, including crude protein (CP), ether extract (EE), neutral detergent fiber (NDF), and acid detergent fiber (ADF), were analyzed at the Animal Nutrition Laboratory of the Department of Animal Science. Crude protein was determined using the Kjeldahl method, ether extract by Soxhlet extraction, and NDF and ADF following the procedure of Goering and Van Soest [21].

2.8 Research Design

The study was a one-factor experiment using a Completely Randomized Design (CRD). It involved five treatments: unprimed seeds, hydropriming for 12 hours, Moringa leaf extract priming for 6 hours, Moringa leaf extract priming for 12 hours, and Moringa leaf extract priming for 18 hours, with three replicates for each treatment. For the germination phase, ten seeds of Mulato II were placed in a petri dish for each replicate. After 15 days of germination, three healthy seedlings from each replicate were selected and transferred to a prepared hydroponics set-up. The hydroponic system consisted of 15 Styrofoam boxes, each

filled with a nutrient solution at a concentration of 2 mL/L of water. Each box held 3 cups filled with a cocopeat, which served as the rooting medium for the Mulato II seedlings.

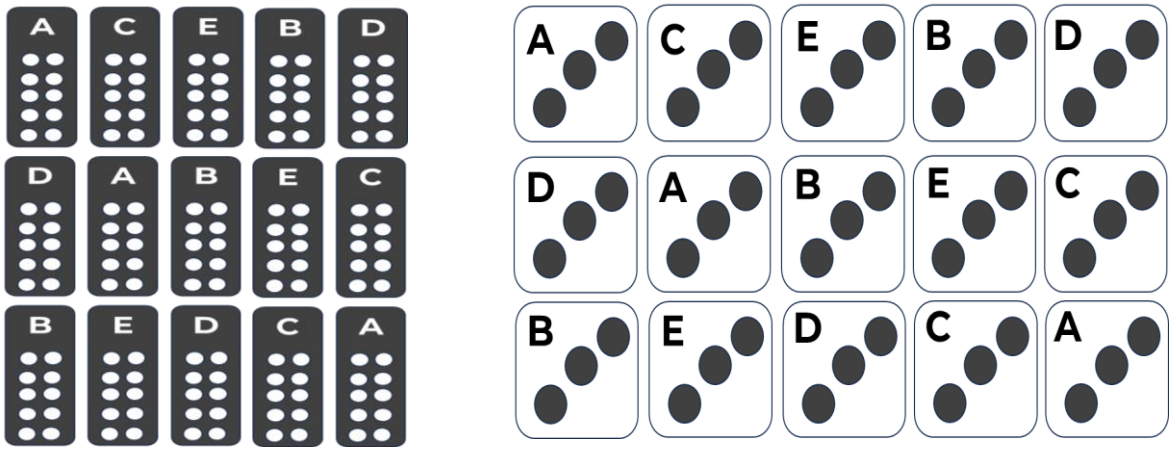

(a) Set-up for germination (b) Set-up for growth performance

Figure 2 Experimental layouts of the study

2.9 Data Analysis

The data obtained from the study were analyzed using the analysis of variance (ANOVA) in a one-factor Completely Randomized Design. The statistical analysis was performed using the PROC MIXED procedure of SAS Enterprise Guide statistical software. Significant differences among treatment means were declared at a 5% confidence level. A post hoc Test using Tukey's Honestly Significant Difference (HSD) test for pairwise comparison was conducted to determine which treatment groups differed significantly.

3. Results and Discussion

3.1 Seed emergence of Mulato II grass primed with moringa leaf extract

The seed emergence of Mulato II grass varied among treatments, including unprimed seeds, hydropriming, and priming with moringa leaf extract (MLE) for different durations. The emergence index (EI) did not show significant differences across treatments ($p = 0.1835$), with values ranging from 131.22 for seeds primed with MLE for 12 hours to 154.17 for hydropriming. The highest EI observed in hydropriming suggests that this method slightly enhanced seed vigor compared to others. Similarly, the mean emergence time (MET) showed no significant variation among treatments ($p = 0.0751$), remaining consistent between 12.15 and 12.75 days. These findings indicate that the speed of seed emergence was not notably affected by the treatments, aligning with research indicating that priming often has a limited effect on MET when seed moisture is uniformly maintained during germination [22].

Table 1. Seed emergence of Mulato II grass primed with moringa leaf extract

Treatments	Emergence Index	Mean Emergence Time	Final Emergence Percentage
Unprimed Seeds	152.20	12.27	50.00 [ab]
Hydropriming for 12 hours	154.17	12.15	53.33 [a]
Primed with Moringa leaf extract for 6 hours	144.20	12.58	50.00 [ab]
Primed with Moringa leaf extract for 12 hours	131.22	12.75	30.00 [b]
Primed with Moringa leaf extract for 18 hours	150.98	12.28	53.33 [a]
Mean	146.55	12.40	47.33
CV (%)	7.98	2.03	15.43
p-value	0.1835	0.0751	0.0137

Means with the same letter are not significantly different at (P>0.05.

However, significant differences were observed in the final emergence percentage (FEP), with a p-value of 0.0137, demonstrating that treatments substantially impacted germination success. Hydropriming for 12 hours and MLE priming for 18 hours achieved the highest FEP (53.33%), which was statistically comparable but significantly higher than the FEP of seeds primed with MLE for 12 hours (30.00%). Unprimed seeds and seeds primed with MLE for 6 hours produced intermediate FEP values of 50.00%, which were statistically comparable to those of both the highest- and lowest-performing treatments. The coefficient of variation (CV) for FEP was 15.43%, indicating moderate variability in response to the treatments. The superior FEP observed in hydropriming and MLE priming for 18 hours suggests that these treatments optimize seed hydration and metabolic activation, enhancing germination rates. MLE priming for 18 hours, in particular, benefits from bioactive compounds in Moringa, such as cytokinins, antioxidants, and vitamins, which improve seed vigor and support robust germination [23]. On the other hand, the reduced FEP seen with MLE priming for 12 hours (30.00%) may indicate insufficient uptake of these bioactive compounds or possible osmotic stress at this duration. The intermediate performance of unprimed seeds and seeds primed with MLE for 6 hours highlights the importance of optimizing priming duration to maximize the benefits of Moringa's bioactive properties. These results highlight the effectiveness of seed priming, particularly with MLE for 18 hours, as a sustainable and practical technique to enhance seed emergence in Mulato II grass. Hydropriming, while effective, lacks the added advantage of Moringa's bioactive compounds, which contribute to improved seed vigor and germination success. These findings are consistent with prior studies demonstrating that seed priming, especially with natural growth enhancers like MLE, can significantly improve germination outcomes, particularly under stress-prone environments [16].

3.2 *Vigor Index of Mulato II grass primed with moringa leaf extract.*

The vigor index of Mulato II grass was significantly influenced by seed priming treatments ($p = 0.0114$). At the same time, shoot and root lengths showed no significant differences among treatments ($p = 0.6134$ and $p = 0.0810$, respectively). For shoot length, values ranged from 56.60 cm for seeds primed with moringa leaf extract (MLE) for 12 hours to 62.37 cm for MLE priming for 18 hours, with a mean of 59.39 cm across all treatments. Root length varied more noticeably, with MLE priming for 18 hours producing the longest roots (37.17 cm) and MLE priming for 12 hours producing the shortest (25.33 cm). Although these differences were not statistically significant, the trends suggest that longer priming durations with MLE may enhance both shoot and root growth, potentially contributing to higher overall vigor. The vigor index, a composite measure of seedling quality, revealed significant differences among treatments. MLE priming for 18 hours resulted in the highest vigor index (5326.67), significantly greater than the lowest value (2458.33) observed in seeds primed with MLE for 12 hours. Unprimed seeds (4643.33), hydro-primed seeds (4822.67), and seeds primed with MLE for 6 hours (4626.67) produced intermediate vigor index values that were statistically comparable to both the highest and lowest-performing treatments.

Table 2. Vigor Index of Mulato II grass primed with moringa leaf extract

Treatments	Shoot Length (cm)	Root Length (cm)	Vigor Index
Unprimed Seeds	57.50	35.37	4643.33 ^{ab}
Hydropriming for 12 hours	60.83	29.60	4822.67 ^{ab}
Primed with Moringa leaf extract for 6 hours	59.67	32.87	4626.67 ^{ab}
Primed with Moringa leaf extract for 12 hours	56.60	25.33	2458.33 ^{b}
Primed with Moringa leaf extract for 18 hours	62.37	37.17	5326.67 ^{a}
Mean	59.39	32.07	4375.53
CV (%)	8.28	15.06	18.28
p-value	0.6134	0.0810	0.0114

Means with the same letter are not significantly different at (P>0.05.

The superior vigor index associated with MLE priming for 18 hours reflects the positive effects of Moringa's bioactive compounds, including cytokinins, vitamins, and antioxidants, which promote seedling

growth and enhance metabolic activity during germination. These properties stimulate cell division and elongation, contributing to the development of longer shoots and roots and, ultimately, higher vigor [24]. The relatively low vigor index observed in MLE priming for 12 hours may indicate suboptimal exposure to these compounds, limiting their physiological benefits or potentially creating mild osmotic stress that inhibits growth [25]. The intermediate vigor index values for unprimed, hydroprimed, and seeds primed with MLE for 6 hours highlight the importance of optimizing priming duration and the priming agent. While hydropriming can enhance seed hydration and activation of metabolic pathways, it lacks the additional growth-promoting benefits of Moringa's phytonutrients [26]. Similarly, the performance of MLE priming for 6 hours suggests that even short exposure to Moringa can improve seed vigor, although not to the same extent as longer durations. These findings emphasize the effectiveness of MLE priming for 18 hours in improving seedling vigor, offering a practical and sustainable strategy for enhancing the establishment and productivity of Mulato II grass. By leveraging the natural bioactive properties of Moringa, this technique provides a cost-effective and environmentally friendly alternative to chemical seed treatments, making it particularly valuable for resource-limited farming systems.

3.3 Average height of Mulato II grass primed with moringa leaf extract

The seed priming treatments affected the average height of Mulato II grass, with variations observed across different measurement weeks. At the initial measurement, plant heights ranged from 10.37 cm (MLE priming for 12 hours) to 14.43 cm (MLE priming for 6 hours), but the differences were not statistically significant ($p = 0.7790$). Similar trends of no significant differences continued through the first ($p = 0.4415$), second ($p = 0.2829$), third ($p = 0.0893$), and fourth weeks ($p = 0.1446$), indicating that while numerical differences were observed, they were not statistically distinct. Despite the lack of statistical significance, notable trends emerged. In the fourth week, seeds primed with MLE for 6 hours and 18 hours, respectively, exhibited the tallest plants, averaging 52.77 cm and 52.43 cm. These heights were greater than those of plants from hydroprimed seeds (48.47 cm) and unprimed seeds (41.30 cm). The lowest plant height at this stage was recorded for seeds primed with MLE for 12 hours (40.70 cm). Similar trends were observed across earlier weeks, with MLE priming for 6 hours consistently producing taller plants compared to other treatments.

Table 3. Average height (cm) of Mulato II grass primed with moringa leaf extract

Treatment	Plant height (cm)				
	Weeks				
	Initial	**1st**	**2nd**	**3rd**	**4th**
Unprimed Seeds	11.17	14.43	17.70	30.17	41.30
Hydropriming for 12 hours	11.70	15.93	20.17	32.43	48.47
Primed with Moringa leaf extract for 6 hours	14.43	20.50	26.53	43.33	52.77
Primed with Moringa leaf extract for 12 hours	10.37	13.80	17.13	28.23	40.70
Primed with Moringa leaf extract for 18 hours	11.70	16.87	22.00	38.57	52.43
Mean	11.87	16.31	20.71	34.55	47.13
CV (%)	33.78	27.71	26.22	18.96	14.56
p-value	0.7790	0.4415	0.2829	0.0893	0.1446

Means with the same letter are not significantly different at (P>0.05.

3.4 Average Number of Mulato II grass leaves primed with moringa leaf extract

The average number of leaves per plant in Mulato II grass was not significantly affected by seed priming treatments across the observation period, as indicated by the high p-values (0.9327 to 0.6819). At the initial stage, all treatments, except for seeds primed with moringa leaf extract (MLE) for 12 hours, exhibited

the same number of leaves (2.0). The exception was MLE priming for 12 hours, which yielded an average of 3.0 leaves; however, this difference was not statistically significant. By the first week, the number of leaves across treatments remained consistent, with a mean value of 3.0 leaves, regardless of the priming method. Similarly, during the second and third weeks, all treatments reached an average of 4.0 leaves, indicating uniform leaf production. By the fourth week, all treatments, except for MLE priming for 18 hours, maintained this average, with MLE priming for 18 hours resulting in a slight but non-significant reduction to 3.0 leaves. The uniformity in leaf number across treatments, including unprimed seeds, may be due to Mulato II grass's inherent genetic growth potential, which might not be significantly altered by seed priming in the short term.

Table 4. Average number of Mulato II grass leaves primed with moringa leaf extract.

Treatment	Number of Leaves				
	Weeks				
	Initial	**1st**	**2nd**	**3rd**	**4th**
Unprimed Seeds	2.0	3.0	4.0	4.0	4.0
Hydropriming for 12 hours	2.0	3.0	4.0	4.0	4.0
Primed with Moringa leaf extract for 6 hours	2.0	4.0	4.0	4.0	4.0
Primed with Moringa leaf extract for 12 hours	3.0	3.0	4.0	4.0	4.0
Primed with Moringa leaf extract for 18 hours	2.0	3.00	4.0	3.0	4.0
Mean	2.0	3.0	4.0	4.0	4.0
CV (%)	24.06	15.49	14.34	13.59	16.08
p-value	0.9327	0.6554	0.0886	0.2428	0.6819

Means with the same letter are not significantly different at (P>0.05.

3.5 Average Number of Mulato II grass tillers primed with moringa leaf extract

The number of tillers in Mulato II grass varied across treatments, with significant differences emerging during the later weeks of observation. Initially and during the first and second weeks, there were no significant differences among treatments ($p = 0.5121$ and $p = 0.4516$, respectively), with all treatments producing an average of one tiller. This similarity suggests that the priming treatments had a minimal influence on the early establishment phase of the grass, consistent with findings that priming effects are more pronounced as plants transition to active growth stages [27]. By the third week, significant differences among treatments were observed ($p = 0.0470$). Seeds primed with moringa leaf extract (MLE) for 6 and 18 hours produced three tillers, which were statistically comparable and significantly higher than the one tiller produced by seeds primed with MLE for 12 hours. Unprimed and hydro-primed seeds exhibited intermediate tiller numbers (two tillers each), statistically comparable to those of the highest- and lowest-performing treatments. The differences became more pronounced in the fourth week ($p = 0.0023$), where seeds primed with MLE for 18 hours produced the highest number of tillers (five tillers), significantly outperforming all other treatments. Seeds primed with MLE for 6 hours produced four tillers, statistically comparable to the 18-hour treatment but significantly greater than those observed in both unprimed seeds and seeds primed with MLE for 12 hours. Hydroprimed seeds produced three intermediate tillers and were statistically comparable to the other treatments. The coefficient of variation (CV) for tiller counts decreased from the third to the fourth week (35.34% to 18.98%), reflecting reduced variability as treatments exerted more pronounced effects on plant growth. The superior performance of MLE priming for 18 hours can be attributed to the bioactive compounds in Moringa, such as cytokinins, antioxidants, and nutrients, which enhance cell division, metabolic activity, and overall plant vigor [28]. These compounds likely promote more robust root and shoot development, facilitating better nutrient uptake and tillering. The intermediate performance of MLE priming for 6 hours suggests that even shorter priming durations provide benefits, though optimal results are achieved with 18-hour priming. Conversely, the reduced tiller counts observed with MLE priming for 12 hours may indicate

suboptimal exposure to Moringa's bioactive compounds, which could cause osmotic stress or inadequate physiological stimulation [29].

Table 5. Average number of Mulato II grass tillers primed with moringa leaf extract.

Treatment	Number of Tillers				
	Weeks				
	Initial	1st	2nd	3rd	4th
Unprimed Seeds	0.0	1.0	1.0	2.0 ab	2.0 c
Hydropriming for 12 hours	0.0	0.0	1.0	2.0 ab	3.0 abc
Primed with Moringa leaf extract for 6 hours	0.0	1.0	1.0	3.0 a	4.0 ab
Primed with Moringa leaf extract for 12 hours	0.0	0.0	1.0	1.0 b	2.0 c
Primed with Moringa leaf extract for 18 hours	0.0	1.0	1.0	3.0 a	5.0 a
Mean		1.0	1.0	2.0	4.0
CV (%)		36.07	24.21	35.34	18.98
p-value		0.5121	0.4516	0.0470	0.0023

Means with the same letter are not significantly different at (P>0.05.

These findings highlight the effectiveness of MLE priming, particularly for 18 hours, in improving the vegetative growth of Mulato II grass. The increase in tiller production reflects enhanced plant vigor and potential biomass, which are crucial for forage production. Hydropriming, while beneficial, lacked the additional growth-promoting effects of MLE, reaffirming the role of bioactive compounds in optimizing plant performance.

3.6 Herbage yield of Mulato II grass primed with moringa leaf extract

The herbage yield of Mulato II grass was significantly influenced by seed priming treatments, as indicated by both fresh and dry yield data. For fresh herbage yield, seeds primed with moringa leaf extract (MLE) for 18 hours produced the highest yield (196.32 t/ha), which was significantly greater than other treatments but statistically comparable to seeds primed with MLE for 6 hours (164.39 t/ha). In contrast, unprimed seeds had the lowest fresh herbage yield (78.95 t/ha). Hydropriming for 12 hours (115.44 t/ha) and MLE priming for 12 hours (116.93 t/ha) resulted in intermediate yields comparable to each other but significantly lower than those achieved with MLE priming for 6 and 18 hours. Similarly, for dry herbage yield, MLE priming for 18 hours produced the highest yield (57.70 t/ha), significantly surpassing all other treatments but comparable to MLE priming for 6 hours (45.35 t/ha). Unprimed seeds had the lowest dry yield (25.87 t/ha), while hydropriming (31.03 t/ha) and MLE priming for 12 hours (31.77 t/ha) produced comparable yields that were significantly lower than those of the MLE treatments for 6 and 18 hours. Statistical analysis revealed significant differences among treatments, as evidenced by low p-values for fresh ($p = 0.0013$) and dry yield ($p = 0.0014$). The superior performance of MLE priming for 18 hours can be attributed to the bioactive compounds in Moringa, such as zeatin (a natural cytokinin), vitamins, minerals, and antioxidants, which enhance seed metabolism, promote vigorous germination, and stimulate growth. The high yields observed in MLE-primed seeds align with findings that cytokinin-rich treatments improve biomass accumulation by promoting cell division and delaying senescence [30].

Interestingly, while MLE priming for 6 hours produced yields comparable to those of the 18-hour treatment, the slightly lower yields suggest that a longer priming duration may optimize the absorption of Moringa's bioactive compounds. Although beneficial in enhancing germination and hydration, hydropriming produced significantly lower yields than those of MLE priming treatments, emphasizing the added value of Moringa's phytonutrients [31]. Unprimed seeds consistently yielded the lowest biomass, underscoring the critical role of priming in improving herbage productivity.

Table 6. Herbage yield of Mulato II grass primed with moringa leaf extract.

Treatments	Herbage Yield (tons/ha)	
	Fresh	Dry
Unprimed Seeds	78.95 [c]	25.87 [c]
Hydropriming for 12 hours	115.44 [bc]	31.03 [bc]
Primed with Moringa leaf extract for 6 hours	164.39 [ab]	45.35 [ab]
Primed with Moringa leaf extract for 12 hours	116.93 [bc]	31.77 [bc]
Primed with Moringa leaf extract for 18 hours	196.32 [a]	57.70 [a]
Mean	134.40	38.35
CV (%)	16.27	16.23
p-value	0.0013	0.0014

Means with the same letter are not significantly different at (P>0.05.

These findings suggest that MLE priming, particularly for 18 hours, is a highly effective and sustainable strategy for enhancing both fresh and dry herbage yields of Mulato II grass. By leveraging the natural growth-promoting properties of Moringa, this approach offers a cost-effective alternative to synthetic inputs, particularly in tropical and subtropical regions where Moringa is abundant. The significant yield improvements achieved through MLE priming make it a practical solution for addressing the dual challenges of increasing forage production and promoting sustainable agriculture. The study emphasizes the potential of MLE priming to optimize forage yield and quality, benefiting resource-constrained farmers while contributing to sustainable livestock systems.

3.7 Nutritional component of Mulato II grass primed with moringa leaf extract.

The nutritional composition of Mulato II grass was influenced by seed priming treatments, with significant differences observed in ether extract (EE) content ($p < 0.0001$), crude protein (CP) content ($p < 0.0001$), and total nitrogen (TN) content ($p = 0.0001$) but no significant effects on moisture content (MC), dry matter (DM), organic matter (OM), ash, total phosphorus (TN), neutral detergent fiber (NDF), or acid detergent fiber (ADF). The moisture content ranged from 66.21% in unprimed seeds to 72.95% in seeds hydro-primed for 12 hours, with no statistically significant differences ($p = 0.6494$). Similarly, DM content varied from 27.05% (hydroprimed for 12 hours) to 33.79% (unprimed seeds), but remained statistically comparable among treatments. Likewise, OM content consistently exceeded 95% across all treatments ($p = 0.5801$). Ash content showed slight variations, ranging from 3.70% to 4.31%, but these differences were also not statistically significant ($p = 0.5801$). Ether extract (EE) content, an indicator of the fat content in the grass, exhibited significant differences among treatments. Seeds primed with moringa leaf extract (MLE) for 12 hours produced grass with the highest EE content (4.54%), significantly higher than that of all other treatments. Comparable EE values followed this in unprimed seeds (2.55%), hydroprimed seeds (2.73%), and seeds primed with MLE for 18 hours (2.34%). The lowest EE content was observed in seeds primed with MLE for 6 hours (0.63%), which was significantly lower than in all other treatments. The significant improvement in EE content following MLE priming for 12 hours can be attributed to the bioactive compounds in Moringa, such as zeatin, antioxidants, and vitamins, which may enhance lipid synthesis and accumulation in plant tissues. Similar findings have been reported by Nouman et al [25], highlighting the role of phytohormones in improving nutritional quality. However, the reduced EE content observed with MLE priming for 6 hours suggests that shorter priming durations may not allow sufficient uptake of these bioactive compounds, limiting their impact on lipid metabolism. Hydropriming and unprimed seeds resulted in intermediate EE content, indicating that while hydration enhances seed germination and subsequent growth, it lacks the additional nutritional benefits Moringa's phytonutrients provide. Crude protein (CP) content exhibited statistically significant differences across treatments ($p < 0.0001$), highlighting the impact of seed priming on protein synthesis. The highest CP content (16.76%) was recorded in grass from seeds primed with moringa leaf extract (MLE) for 18 hours, followed by 15.02% from the 6-hour priming treatment. Unprimed and hydroprimed seeds yielded intermediate CP levels (14.67% and 14.50%, respectively), while MLE priming for 12 hours resulted in the lowest CP value (14.09%). These variations are also reflected in the total nitrogen (TN)

content, which ranged from 2.56% to 3.05%. Notably, the TN content was highest in the 18-hour MLE priming treatment, aligning with its elevated CP value. This suggests that extended exposure to MLE may enhance nitrogen assimilation, likely through the synergistic action of Moringa's bioactive compounds such as cytokinins and micronutrients [21].

Table 7. Nutritional component of Mulato II grass primed with moringa leaf extract

Treatments	Nutritional Components									
	MC (%)	DM (%)	OM (%)	EE (%)	Ash (%)	CP (%)	TN (%)	TP (%)	NDF (%)	ADF (%)
Unprimed Seeds	66.21	33.79	95.69	2.55 [b]	4.31	14.67 [b]	2.67 [b]	0.25	47.77	24.47
Hydropriming for 12 hours	72.95	27.05	96.30	2.73 [b]	3.70	14.50 [b]	2.64 [b]	0.24	46.55	33.52
Primed with Moringa leaf extract for 6 hours	71.56	28.44	96.27	0.63 [c]	3.73	15.02 [b]	2.73 [b]	0.24	47.23	27.96
Primed with Moringa leaf extract for 12 hours	72.21	27.79	96.08	4.54 [a]	3.92	14.09 [b]	2.56 [b]	0.22	45.91	23.26
Primed with Moringa leaf extract for 18 hours	70.70	29.30	95.71	2.34 [b]	4.29	16.76 [a]	3.05 [a]	0.23	47.86	23.49
Mean	70.73	29.27	96.00	2.47	3.99	15.01	2.73	0.24	47.06	26.54
CV (%)	8.17	19.75	0.61	18.61	14.77	2.81	2.81	5.02	10.96	18.17
p-value	0.6494	0.6494	0.5801	<0.0001	0.5801	<0.0001	<0.0001	0.1077	0.9875	0.1171

Means with the same letter are not significantly different at (P>0.05)

Total phosphorus (TP), which is vital for energy transfer and root development, showed slight fluctuations among treatments, ranging from 0.22% to 0.25%. Though these differences were not statistically significant ($p = 0.1077$), the trend indicates a potential influence of MLE on phosphorus uptake or retention, particularly in the 6-hour priming group. The neutral detergent fiber (NDF) and acid detergent fiber (ADF) values showed no significant differences across treatments ($p = 0.9875$ and $p = 0.1171$, respectively). NDF values ranged from 45.91% in seeds primed with Moringa leaf extract for 12 hours to 47.86% in seeds primed for 18 hours. Similarly, ADF was lowest (23.26%) in seeds primed with Moringa leaf extract for 12 hours, suggesting improved digestibility due to reduced lignin and cellulose content. These findings underscore the potential of Moringa leaf extract to enhance forage quality for ruminants, particularly at optimal priming durations. The results demonstrate that seed priming, particularly with MLE priming for 12 hours, notably enhanced EE, while 18-hour priming maximized CP and TN levels. While other nutritional components, such as MC, DM, OM, Ash, TP, NDF, and ADF, remained unaffected, the marked improvement in EE, CP, and TN contents highlights the potential of MLE priming to enhance forage quality. The variation in optimal results across different priming durations may be attributed to differences in the uptake and physiological utilization of Moringa's bioactive compounds, suggesting that shorter durations may favor certain metabolic pathways, such as lipid synthesis. In contrast, longer durations are more effective in enhancing protein accumulation and nitrogen assimilation. These findings emphasize the value of MLE priming as a sustainable and cost-effective strategy for enhancing forage yield and quality, particularly in resource-constrained agricultural systems.

4. Conclusions

This study demonstrated the efficacy of MLE priming, particularly for 18 hours, in enhancing the growth performance and nutritional quality of Mulato II grass. MLE priming significantly improved key parameters, including vigor index, fresh and dry herbage yields, and final emergence percentage, compared

to unprimed seeds and hydropriming. The bioactive compounds in MLE, such as cytokinins, antioxidants, and vitamins, likely contributed to improved seed vigor, metabolic activity, and nutrient accumulation. While hydropriming was effective, it lacked the added benefits of MLE's phytonutrients. The study highlights the potential of MLE priming as a sustainable and eco-friendly strategy for enhancing forage production in controlled environments, such as hydroponics. Based on the results, MLE priming for 18 hours is recommended for maximizing seed vigor, nutrient contents, and forage yield. Further research could investigate other durations and concentrations to refine this practice. Field-based studies should be conducted to validate the effectiveness of MLE priming under real-world conditions, including different environmental stresses. To ensure widespread adoption, a detailed economic assessment of MLE extraction and application should be performed, particularly in resource-limited farming systems. Future research should also investigate the impact of MLE priming on plant growth and forage quality across multiple crop cycles to assess its sustainability and productivity. The application of MLE priming could be extended to other forage crops to evaluate its broader potential in improving livestock nutrition and sustainable agriculture. Additionally, combining MLE priming with advanced hydroponic techniques and nutrient management strategies could further enhance forage productivity and quality.

5. Acknowledgements

The authors express their sincere gratitude to the Central Analytical Soil Laboratory at Visayas State University for generously providing a discount for the tissue analysis.

Author Contributions: R.Y.I.J: Data collection, recording, discussion, interpretation of results validation, and editing; M.D.G.J: Conceptualization, methodology, Literature review, proofreading, and critiquing. All authors have read and agreed to the published version of the manuscript.

Funding: This research received no external funding.

Conflicts of Interest: The authors declare no conflict of interest.

References

[1] Ritchie, H.; Rodés-Guirao, L. Peak Global Population and Other Key Findings from the 2024 UN World Population Prospects. OurWorldInData.org. https://ourworldindata.org/un-population-2024-revision (accessed 2026-01-11).

[2] Polaris Market Research. *Forage Market Share, Size, Trends, Industry Analysis Report, By Crop Type; By Product Type; By Animal Type; By Region; Segment Forecast, 2023–2032*; Polaris Market Research: 2023. https://www.polarismarketresearch.com/industry-analysis/forage-market (accessed 2026-01-11).

[3] IMARC Group. *Forage Market Report by Crop Type, Product Type, Animal Type, and Region 2024–2032*; IMARC Group: 2024. https://www.imarcgroup.com/forage-market (accessed 2026-01-11).

[4] Ritchie, H.; Roser, M. Half of the World's Habitable Land is Used for Agriculture. OurWorldInData.org. https://ourworldindata.org/global-land-for-agriculture (accessed 2026-01-11).

[5] , J. D.; Delaquis, E.; Van Dung, P.; Douxchamps, S. Linking Up: The Role of Institutions and Farmers in Forage Seed Exchange Networks of Southeast Asia. *Hum. Ecol.* **2022**, *50*(1), 61–78. https://doi.org/10.1007/s10745-021-00274-5

[6] Deepika, M. Forage Crops and its Importance in Agriculture. Kisanvedika | BigHaat. https://kisanvedika.bighaat.com/crop/forage-crops-and-its-importance-in-agriculture/ (accessed 2026-01-11).

[7] Rojas-Downing, M. M.; Nejadhashemi, A. P.; Harrigan, T.; Woznicki, S. A. Climate Change and Livestock: Impacts, Adaptation, and Mitigation. *Clim. Risk Manage.* **2017**, *16*, 145–163. https://doi.org/10.1016/j.crm.2017.02.001

[8] Michalk, D. L.; Kemp, D. R.; Badgery, W. B.; Wu, J.; Zhang, Y.; Thomassin, P. J. Sustainability and Future Food Security—A Global Perspective for Livestock Production. *Land Degrad. Dev.* **2019**, *30*(5), 561–573. https://doi.org/10.1002/ldr.3217

[9] Bacorro, T.; Reyes, P. M.; Loresco, M. Herbage Dry Matter Yield, Nutrient Composition and In Vitro Gas Production of Mulato II and Mombasa Grasses at 30- and 45- Day Cutting Intervals. *Philipp. J. Vet. Anim. Sci.* **2018**, *44*(1), 86–89.

[10] Jassim, A. A.; Ali, R. S. Study of Phenolic Compounds of *Moringa oleifera* Leaf Extracts and Their Potential as Antioxidants. *Pak. J. Life Soc. Sci.* **2024**, *22*(1). https://doi.org/10.57239/pjlss-2024-22.1.00255

[11] Shrey, D. D.; Nasim, A.; Ansari, F.; Rana, G. K. A Miracle Multipurpose Tree (*Moringa oleifera*) with Recent Applications in Agriculture. *Curr. J. Appl. Sci. Technol.* **2023**, *42*(48), 197–208. https://doi.org/10.9734/cjast/2023/v42i484360

[12] Muneeba, M.; Khaliq, A.; Muhammad, F.; Khan, M. D.; Alharbi, S. A.; Ansari, M. J.; Umer, M.; Aslam, M. T.; Shahzad, H. Mitigating the Toxic Effects of Salinity in Wheat though Exogenous Application of Moringa Leaf Extract. *Inż. Ekol.* **2024**, *25*(5), 268–278. https://doi.org/10.12911/22998993/186503

[13] Khan, S.; Ibrar, D.; Hasnain, Z.; Nawaz, M.; Rais, A.; Ullah, S.; Gul, S.; Siddiqui, M. H.; Irshad, S. *Moringa* Leaf Extract Mitigates the Adverse Impacts of Drought and Improves the Yield and Grain Quality of Rice through Enhanced Physiological, Biochemical, and Antioxidant Activities. *Plants* **2023**, *12*(13), 2511. https://doi.org/10.3390/plants12132511

[14] Andriyani, S.; Rujitoningtyas, K.; Wigati, H. U.; Amalina, N. D. The Potential of *Moringa* Leaf Extract to Prevent Aging Targeted Cellular Senescence. *Int. J. Cell Biomed. Sci.* **2023**, *1*(3), 76–85. https://doi.org/10.59278/cbs.v1i3.21

[15] Buthelezi, N. M. D.; Ntuli, N. R.; Mugivhisa, L. L.; Gololo, S. S. *Moringa oleifera* Lam. Seed Extracts Improve the Growth, Essential Minerals, and Phytochemical Constituents of *Lessertia frutescens* L. *Horticulturae* **2023**, *9*(8), 886. https://doi.org/10.3390/horticulturae9080886

[16] Yasmeen, A. Exploring the Potential of Moringa (*Moringa oleifera*) Leaf Extract as Natural Plant Growth Enhancer. Ph.D. Dissertation, University of Agriculture, Faisalabad, Pakistan, **2011**.

[17] Ranmeechai, N.; Lacap, A.; Tac-an, M. I.; Bayogan, E. R. Seed Germination and Vigor of Four Philippine Rice Varieties as Influenced by Hydropriming and Storage at Various Durations. *Philipp. J. Sci.* **2022**, *151*(2), 755–765. https://doi.org/10.56899/151.02.18

[18] Rushing, J. B.; Lemus, R. W.; Lyles, J. C. Harvest Frequency and Native Warm-Season Grass Species Influence Nutritive Value. *Crop Forage Turfgrass Manage.* **2019**, *5*(1), 1–9. https://doi.org/10.2134/cftm2019.04.0030

[19] Vujošević, B.; Čanak, P.; Babić, M.; Mirosavljević, M.; Mitrović, B.; Stanisavljević, D.; Tatić, M. Field Performance of Abnormal Maize Seedlings. *Rat. Povrt.* **2018**, *55*(1), 34–38. https://doi.org/10.5937/ratpov55-15198

[20] Abdul-Baki, A. A.; Anderson, J. D. Vigor Determination in Soybean Seed by Multiple Criteria. *Crop Sci.* **1973**, *13* (6), 630–633. https://doi.org/10.2135/cropsci1973.0011183x001300060013x

[21] Goering, H. K.; Van Soest, P. J. *Forage Fiber Analyses*; Agricultural Research Service, U.S. Department of Agriculture: 1970. https://sl1nk.com/q7S0u (accessed 2026-01-11).

[22] Salomão, A. N.; José, S. C. B. R.; Santos, I. R. I. Effect of Pre-Germination Treatments on *Passiflora setacea* DC Seed Germination (Passifloraceae). *Delos* **2023**, *16*(43), 580–597. https://doi.org/10.55905/rdelosv16.n43-007

[23] Srivastava, S.; Pandey, V. K.; Dash, K. K.; Dayal, D.; Wal, P.; Debnath, B.; Singh, R.; Dar, A. H. Dynamic Bioactive Properties of Nutritional Superfood *Moringa oleifera*: A Comprehensive Review. *J. Agric. Food Res.* **2023**, *14*, 100860. https://doi.org/10.1016/j.jafr.2023.100860

[24] Soares, T. F. S. N.; Muniz, E. N.; Sousa, J. P. S.; Oliveira Júnior, L. F. G.; Barbosa, A. M.; Silva, A. V. C. Seed Priming as a Strategy to Increase the Performance of Drumstick Tree. *S. Afr. J. Bot.* **2023**, *157*, 279–286. https://doi.org/10.1016/j.sajb.2023.03.037

[25] Merewitz, E. Chemical Priming-Induced Drought Stress Tolerance in Plants. In *Drought Stress Tolerance in Plants*; Springer International Publishing: **2016**; 1, pp 77–103. https://doi.org/10.1007/978-3-319-28899-4_4

[26] Ahmed, A. A.; El-Mahdy, A. A. Improving Seed Germination and Seedling Growth of Maize (*Zea mays*, L.) Seed by Soaking in Water and *Moringa oleifera* Leaf Extract. *Curr. Chem. Lett.* **2022**, *11*(2), 147–156. https://doi.org/10.5267/j.ccl.2022.2.005

[27] Martinez-Medina, A.; Flors, V.; Heil, M.; Mauch-Mani, B.; Pieterse, C. M. J.; Pozo, M. J.; Ton, J.; van Dam, N. M.; Conrath, U. Recognizing Plant Defense Priming. *Trends Plant Sci.* **2016**, *21*(10), 818–822. https://doi.org/10.1016/j.tplants.2016.07.009

[28] Yasmeen, A.; Basra, S. M. A.; Wahid, A.; Nouman, W.; Rehman, H. U. R. Exploring the Potential of *Moringa oleifera* Leaf Extract (MLE) as a Seed Priming Agent in Improving Wheat Performance. *Turk. J. Bot.* **2013**, *37*(3), 512–520. https://doi.org/10.3906/bot-1205-19

[29] Nouman, W.; Siddiqui, M. T.; Basra, S. M. A. *Moringa oleifera* Leaf Extract: An Innovative Priming Tool for Rangeland Grasses. *Turk. J. Agric. For.* **2012**, *36*(1), 65–71. https://doi.org/10.3906/tar-1009-1261

[30] Rehman, H. U.; Basra, S. M. A.; Rady, M. M.; Ghoneim, A. M.; Wang, Q. *Moringa* Leaf Extract Improves Wheat Growth and Productivity by Delaying Senescence and Source-Sink Relationship. *Int. J. Agric. Biol.* **2017**, *19*(3), 479–484. https://doi.org/10.17957/IJAB/15.0316

[31] Basra, S. M. A.; Iftikhar, M. N.; Afzal, I. Potential of Moringa (*Moringa oleifera*) Leaf Extract as Priming Agent for Hybrid Maize Seeds. *Int. J. Agric. Biol.* **2011**, *13*(6), 1006–1010.

ASEAN
Journal of Scientific and Technological Reports
Online ISSN:2773-8752

Research article

Development and Performance Analysis of an Improved Biomass Stove for Krajood Dyeing: A Sustainable Appropriate Technology Approach

Palachai Khaonuan[1], Noppadon Podkumnerd[1*], Tidaporn Ruangroengkulrit[1], Jirapat Phookwantong[1], Kosin Teeparuksapun[1], and Worawit Sriwittayakul[1]

[1] Faculty of Liberal Arts, Rajamangala University of Technology Srivijaya, Songkhla, 90000, Thailand
* Correspondence: Noppadon.p@rmutsv.ac.th

Citation:
Khaonuan, P.; Podkumnerd, N.; Ruangroengkulrit, T.; Phookwantong, J.; Teeparuksapun, K.; Sriwittayakul, W. Development and performance analysis of an improved biomass atove for krajood dyeing: A sustainable appropriate technology approach. *ASEAN J. Sci. Tech. Report.* **2026**, *29*(2), e259614. https://doi.org/10.55164/ajstr.v29i2.259614.

Article history:
Received: June 2, 2025
Revised: October 13, 2025
Accepted: October 18, 2025
Available online: January 18, 2026

Abstract: This research developed an improved biomass stove for dyeing Krajood (*Lepironia articulata*) as a sustainable, appropriate technology for small-scale industry applications. The new design features an integrated water reserve tank, improved combustion chamber, heat shield, and robust support structure while maintaining operational simplicity. Performance evaluation revealed the improved stove reduced PM2.5 emissions at the operator position by 72.25% (from 191±16 to 53±7 μg/m³, p=0.0002), decreased water boiling time by 32.73% (from 55±6 to 37±3 minutes, p=0.0097), shortened dyeing time by 52.43% (from 103±7 to 49±3 minutes, p=0.0006), and lowered ambient temperature at the operator position by 46.45% (from 62.0±4.8°C to 33.2±1.7°C, p=0.0003). These improvements collectively enabled a five-fold increase in daily production capacity from 20 bundles (44 kg) to 100 bundles (220 kg) in an 8-hour workday. Colorimetric analysis confirmed no significant differences in L*ab** values between traditionally and newly dyed Krajood at all measurement positions (p>0.05), ensuring quality preservation despite the process modifications. Economic assessment indicates the 71.4% higher initial investment (12,000 vs. 7,000 THB) is rapidly offset by productivity gains. The design exemplifies appropriate technology principles through its simplicity, local material utilization, and alignment with existing production knowledge. This improved stove addresses critical health and efficiency constraints in traditional Krajood processing while preserving product quality, demonstrating how targeted technological interventions can enhance traditional craft productivity and worker wellbeing in rural communities.

Keywords: Biomass stove; krajood dyeing; appropriate technology; sustainable development; particulate matter reduction

1. Introduction

Krajood (*Lepironia articulata*) is a sedge plant that grows in wetland areas, characterized by its cylindrical green stems reaching heights of 1-2 meters. This plant possesses natural qualities of durability, flexibility, and resilience that make it particularly suitable for creating woven products [1]. In Thailand, especially in the central southern provinces of Nakhon Si Thammarat and Phatthalung, communities have developed a cultural heritage of transforming Krajood into various handicraft items, including bags, mats, baskets, fans, hats, and coasters. The economic significance of Krajood extends

beyond preserving traditional knowledge; it represents a primary source of income for communities in areas such as Thale Noi, Phanang Tung, and Chai Buri districts in Phatthalung Province. These crafts embody local wisdom passed down through multiple generations and contribute significantly to sustainable rural livelihoods [1]. The integration of Krajood crafting into creative economic development initiatives has further enhanced its importance in community-based production systems.

The transformation of Krajood into marketable products involves several processing steps, including harvesting, selection by length and size, mud soaking to enhance durability, sun drying, pressing, dyeing for aesthetic appeal, weaving, and final decoration. Among these processes, the dyeing step presents challenges in traditional production systems. The conventional dyeing method employs local wisdom techniques that utilize a rectangular container placed on brick supports referred to as a "Sao stove." This setup uses firewood as a heat source, with limited control over combustion efficiency. The traditional method can typically process only 20 bundles (approximately 44 kilograms) of Krajood within one working day (8 hours), creating a production bottleneck. Additionally, this open-flame design exposes operators to significant heat stress and particulate matter emissions, potentially compromising both health and working comfort. The traditional Krajood dyeing system suffers from numerous inefficiencies, including limited production capacity, prolonged boiling and dyeing times, high PM2.5 emissions that pose health risks, excessive heat exposure for operators, substantial thermal energy loss to the environment, and inability to maintain water temperature between dyeing batches, all of which reduce productivity and worker comfort.

Appropriate technology represents an approach to technological development that prioritizes solutions aligned with the specific needs, resources, and context of users. According to Dezord *et al*. [2], appropriate technology is characterized by design adaptations that suit user requirements while maintaining low costs, easy maintenance, and accessibility through locally available resources. This concept extends beyond mere technical functionality to encompass contextual suitability, sustainability, environmental friendliness, and the ability to address real community problems [3]. The fundamental principles of appropriate technology emphasize simplicity and sustainability. As noted by Lyman and Chung [4], effective appropriate technology incorporates participatory design elements that enhance social impact through direct engagement with community needs and capabilities. This approach ensures that technological interventions remain relevant, adoptable, and maintainable within local contexts. In the context of Krajood dyeing, appropriate technology must address the specific challenges faced by artisans while respecting cultural practices and economic constraints. The development of improved biomass stoves represents an opportunity to enhance productivity and working conditions without disrupting established production knowledge or requiring prohibitive investments.

This research aims to develop an enhanced biomass stove system for dyeing Krajood that increases work efficiency while adhering to appropriate technology principles. The specific design goals include creation of a dyeing system with minimal complexity to facilitate ease of use and maintenance, development of a configuration that reduces operator exposure to heat and harmful emissions, integration of a water reserve system to minimize waiting time between dyeing batches, design of a combustion chamber that improves fuel efficiency and heat transfer, implementation of features that maintain consistent dyeing quality compared to traditional methods, utilization of locally available materials to enable local production and repair, and ensuring affordability and economic viability within the context of small-scale Krajood production.

2. Materials and Methods

2.1 Design and construction of the new biomass stove

The traditional biomass stove for Krajood dyeing consists of a simple open fire stove (Figure 1a). This traditional biomass stove was made of a concrete brick with a height of 27 cm that elevates the container and creates a combustion space, and an open combustion area beneath the container for burning biomass fuel (typically wood). The dyeing container is a rectangular metal steel with a size of 25 cm × 70 cm × 25 cm. This traditional design represents local wisdom but suffers from several limitations, including heat loss, smoke exposure, and limited production capacity, as noted by Zube [5] in studies of similar open-design biomass cooking systems. The improved biomass stove design (Figure 1b) incorporates several significant

modifications while maintaining operational simplicity in accordance with appropriate technology principles [2]. Key design features include Integrated dyeing and water reserve containers: A corrosion-resistant metal sheet container (65 cm width × 100 cm length × 35 cm height) divided into two sections—a 40 cm wide dyeing chamber and a 25 cm wide hot water reserve chamber. This design allows for continuous operation by maintaining a supply of pre-heated water. Elevated support frame: A metal frame support structure (65 cm width × 100 cm length × 50 cm height) constructed from welded metal bars, featuring four corner posts extending 25 cm above the frame to secure the dyeing container and a 1.5 mm thick metal sheet (65 cm width × 45 cm height) installed at the rear to shield operators from heat. The biomass stove is made of 1.2 mm steel, providing better thermal conductivity, reflection, and radiation properties than the simple open fire stove [6-7] and is formed into a cylindrical container with a diameter of 58 cm and a height of 45 cm. The upper side wall opens a 40 cm wide and 15 cm high rectangular compartment to serve as a biomass fuel feeder, and a plate is installed at the bottom of the compartment to help support the biomass fuel. Inside the biomass stove, there is a steel frame reinforced with angle steel and round bars, and an expanded metal grate to support the biomass fuel. It is 20 cm high from the bottom of the biomass stove. Improved combustion chamber: A redesigned biomass stove positioned beneath the support frame, featuring controlled air intake to enhance combustion efficiency similar to designs evaluated by Bentson *et al*. [8]. Biomass support system: An extended rack to support longer pieces of biomass fuel, preventing spillage and enabling more effective fuel feeding. The new design prioritizes simplicity for ease of maintenance and repair while addressing the core inefficiencies of the traditional system. All materials were selected based on local availability to ensure sustainability and economic feasibility.

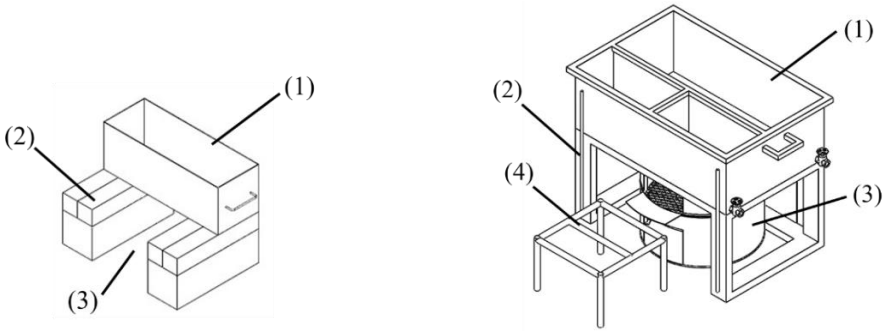

Figure 1. The design of a set of biomass stoves for krajood dyeing. (a) traditional biomass stove (b) improve biomass stove

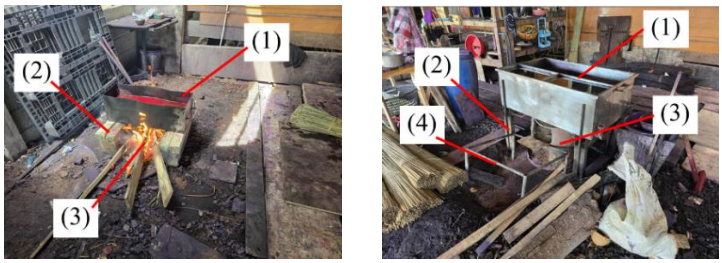

Figure 2. Dyeing of krajood using a biomass stove. (a) traditional stove (b) improve biomass stove

2.2 Experimental setup and testing procedures

The experimental evaluation followed a comparative methodology to assess performance differences between the traditional and improved biomass stove designs. The testing procedures were conducted under controlled conditions with the following protocol. Preparation of test materials: Three bundles of Krajood, each weighing 2.2 kilograms (6.6 kilograms total), measured using a digital scale (CTS model DRC-15), 25 liters of water at ambient temperature for each dyeing test, and Standard dyeing agents

prepared according to traditional formulations. Testing sequence: Both stove types were prepared and ignited with equivalent biomass fuel. Water was heated to the boiling point with measurements recorded continuously, Krajood bundles were processed through complete dyeing cycles, and Dyed Krajood samples were dried under standardized conditions for color evaluation. Replication: Tests were repeated three times for each stove design to ensure statistical reliability, and environmental conditions (ambient temperature, humidity) were recorded and maintained within a controlled range across all tests.

2.3 Measurement parameters and analytical methods

Particulate matter (PM2.5) concentrations were measured at the operator's position using a portable particle counter (CEM model DT9881) in accordance with methodologies used by Bentson *et al.* [8] for biomass combustion systems. Measurements were recorded at 15-minute intervals throughout the dyeing process to capture variations during different operational phases. Thermal performance was evaluated through multiple parameters:

1. Water boiling time: The time required to bring 20 liters of water from an ambient temperature to boiling point (100°C) was measured using a digital timer.

2. Operator position temperature: Ambient temperature at the standard operator position (0.5 meters from the stove at a height of 1.5 meters) was measured using a Fluke 54-2B thermometer with a Fluke 80pk-22 probe as utilized in similar studies by Hafner *et al.* [9].

3. Dyeing time: The total processing time for completing the dyeing cycle for all three Krajood bundles (6.6 kg) was recorded.

The color quality of dyed Krajood was analyzed using a colorimeter (Hunter Lab, Konica; Japan) to measure L* *a** b* color values [10]. Measurements were taken at three positions on each Krajood sample base section (closest to the root), middle section, and end section (tip of the Krajood). This comprehensive color analysis approach was used to determine whether the improved stove design maintained consistent dyeing quality compared to the traditional method. Statistical analysis was performed using independent t-tests at a significant level of 0.05. Production capacity was calculated based on the dyeing cycle time and the maximum loading capacity of each stove design. This was extrapolated to determine the number of Krajood bundles that could be processed in a standard 8-hour workday, providing practical data for economic assessment of the technology. Cost-benefit analysis was conducted by comparing initial investment costs for both stove designs, operational costs including fuel consumption and labor requirements, productivity differences in terms of throughput capacity, and expected service life based on construction materials and design. This economic assessment followed approaches recommended by Lyman and Chung [4] for appropriate technology evaluation in community-based production systems.

3. Results and Discussion

3.1 Reduction in PM2.5 emissions

The comparative analysis of PM2.5 emissions between the traditional and improved biomass stoves revealed significant differences in particulate matter concentrations at the operator position. As illustrated in Figure 3, the improved biomass stove design produced substantially lower PM2.5 emissions (53±7 μg/m³) compared to the traditional design (191±16 μg/m³). Statistical analysis confirmed that this 72.25% reduction was significant at the $p = 0.0002$ level. The substantial decrease in PM2.5 emissions can be attributed to several design improvements in the new stove. First, the improved combustion chamber incorporated dedicated air intake channels that enhanced combustion efficiency. This finding aligns with research by Bentson *et al*. [6], who demonstrated that forced jets of primary air in biomass cookstoves significantly improved combustion completeness, thereby reducing particulate emissions. The presence of controlled airflow into the combustion chamber of the improved design facilitated more complete burning of volatile compounds that would otherwise contribute to PM2.5 formation. Second, the installation of a heat shield at the operator's position in the improved design effectively redirected smoke and particulate flow away from the user. This simple structural modification substantially reduced operator exposure to combustion byproducts. As noted by Hafner *et al*. [9], even modest modifications to stove structure can significantly alter

heat and emission pathways, resulting in improved operator safety without necessarily requiring complex technological interventions. It is worth noting that while the improved design achieved a substantial reduction in PM2.5 emissions, the measured concentration (53±7 μg/m³) still exceeds the World Health Organization's recommended 24-hour exposure limit of 15 μg/m³ [11]. This suggests that while significant improvements have been achieved, additional modifications, such as a chimney system or further combustion optimization, might be warranted in future iterations to further reduce operator exposure to particulate matter.

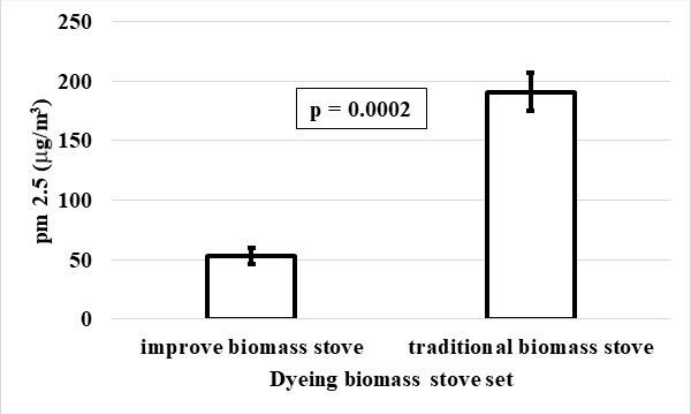

Figure 3. Comparison of PM 2.5 levels from the krajood dyeing process (n = 3).

3.2 Decreased water boiling time

The time required to bring 20 liters of water to a boil showed marked improvement with the new stove design. As shown in Figure 4, the improved biomass stove achieved boiling in 37±3 minutes compared to 55±6 minutes for the traditional design. This 32.73% reduction in boiling time was statistically significant ($p = 0.0097$). This decrease in water boiling time can be attributed to two primary design factors. First, the combustion chamber walls in the improved design effectively contained and directed heat upward toward the container, minimizing lateral heat loss to the surrounding environment. This improvement is due to the superior thermal conduction, reflection, and radiation characteristics of the metal-steel combustion chamber in the improved biomass stove compared to traditional biomass open-fire stoves [6-7]. Zube [5] identified similar principles in improved cooking stove designs, noting that heat transfer efficiency is substantially improved when combustion is contained within a defined chamber rather than in an open configuration. Second, the elevated grate design in the improved stove facilitated better air circulation beneath the fuel, promoting more complete combustion and higher flame temperatures. This design element creates what Bentson *et al*. [8] describe as a "high-power combustion zone" where primary air mixes with fuel gases to achieve more efficient burning. The result is more effective heat transfer to the dyeing container and, consequently, faster water heating. The practical implication of this reduced boiling time is significant for production workflow, as it reduces the initial setup time before dyeing can begin and increases the number of dyeing cycles that can be completed in a workday.

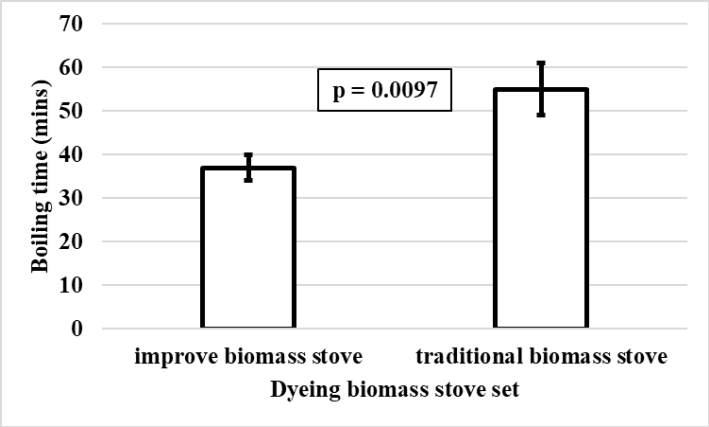

Figure 4. Comparison of the boiling time of water (n = 3).

3.3 Shortened dyeing time

The total time required to complete the dyeing process for three bundles of Krajood (6.6 kg) showed the most dramatic improvement among all measured parameters. As presented in Figure 5, the improved stove completed the dyeing process in 49±3 minutes, while the traditional stove required 103±7 minutes. This represents a 52.43% reduction in processing time ($p = 0.0006$). The substantial time savings can be primarily attributed to the integration of the hot water reserve tank in the improved design. This innovative feature maintains a continuous supply of pre-heated water that can be immediately transferred to the dyeing chamber when needed. In contrast, the traditional method requires operators to add ambient temperature water when levels decrease, necessitating additional heating time before dyeing can resume. This finding highlights how relatively simple design modifications can dramatically improve process efficiency when applied with careful consideration of workflow bottlenecks. The principle aligns with appropriate technology concepts described by Dezord *et al*. [2], where modest technological adaptations targeted at specific workflow constraints can yield disproportionate productivity benefits. The practical implication of this time reduction is substantial. Under an 8-hour workday scenario, the improved stove enables processing of approximately 100 bundles (220 kg) of Krajood compared to just 20 bundles (44 kg) with the traditional system—a five-fold increase in productivity.

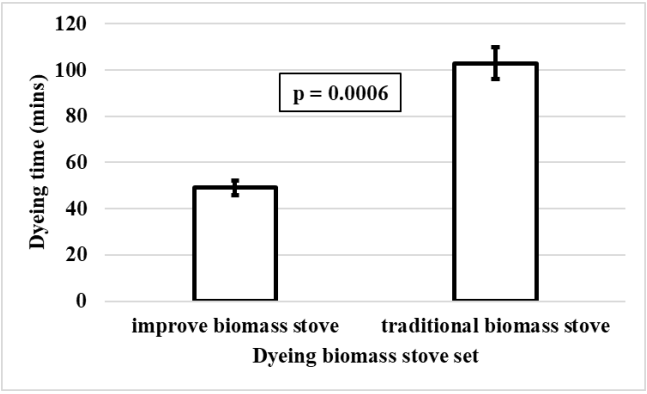

Figure 5. Comparison of dyeing time of krajood (n = 3).

3.4 Lower operating temperature

Ambient temperature measurements at the operator position revealed significant differences between the two stove designs. As shown in Figure 6, the improved stove design maintained a substantially lower temperature at the operator position (33.2±1.7°C) compared to the traditional stove (62.0±4.8°C). This 46.45% reduction in ambient temperature was statistically significant ($p = 0.0003$). The marked reduction in operator-position temperature can be attributed primarily to the 1.5 mm thick metal heat shield installed at

the rear of the improved stove design. This barrier effectively blocks direct thermal radiation from the combustion chamber and redirects it away from the operator. This result is in good agreement with the previous reports [9, 12, 6, 13]. Hafner *et al*. [9] observed similar benefits from heat shielding in improved cooking stove designs, noting that strategic placement of simple barriers can significantly improve operator comfort without compromising thermal efficiency. Liu *et al*. [12] discovered that installing a radiation shield between the combustion chamber walls would effectively control the temperature outside the stove. MacCarty and Bryden [6] reported that the shield can reduce the heat energy loss from the flame of a biomass stove. Yunusa *et al*. [13] have reported that the use of a shield to reflect heat radiation prevents heat radiation from being released to the outside. In contrast, the traditional brick support system creates an open combustion area that allows heat to radiate freely in all directions, resulting in substantially higher temperatures at the operator position. This unrestricted heat transfer not only creates uncomfortable working conditions but also represents wasted thermal energy that could otherwise contribute to the dyeing process. The lower operating temperature has important implications for both worker comfort and safety. Extended exposure to high temperatures can contribute to heat stress and fatigue, particularly in tropical environments where ambient temperatures are already elevated. The improved design creates more tolerable working conditions that may contribute to sustained productivity over full workdays.

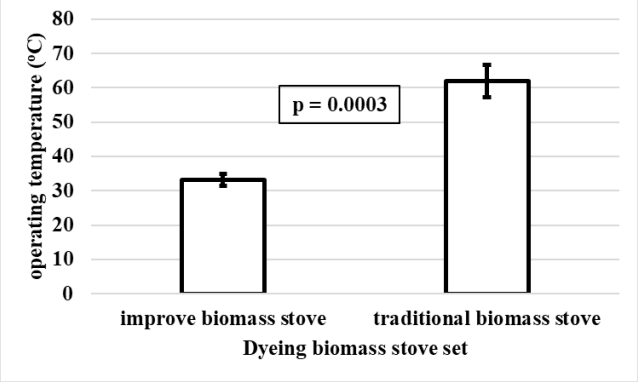

Figure 6. Comparison of the krajood dyeing operating temperature (n = 3).

3.5 Color quality comparison

A critical requirement for any improved Krajood dyeing technology is the maintenance of product quality. The color quality analysis aimed to determine whether the improved stove design affected the dyeing outcomes compared to the traditional method. As presented in Table 1, comprehensive colorimetric measurements (L*a*b* values) were taken at three positions on the Krajood (base, middle, and end). Statistical analysis using independent t-tests revealed no significant differences in color values between Krajood dyed using the traditional and improved stoves at any measurement position (all p-values > 0.05). This finding confirms that the improved stove maintains dyeing quality while delivering substantial efficiency improvements. The consistency in color outcomes despite the significant changes in processing time and temperature profiles suggests that the critical dyeing parameters (temperature and dye concentration) were effectively maintained in the improved system. Figure 7 provides a visual comparison of dyed Krajood samples, further illustrating the comparable color outcomes between the two methods. This quality preservation is particularly important for market acceptance of products made from Krajood dyed using the improved technology. As Kaewpradit *et al*. [1] noted, consistent quality is essential for maintaining the commercial value of traditional craft products when production processes are modified.

Table 1. Comparison of L* a* b* values measured at different parts of Krajood (base, middle, and end) using dyeing using a traditional biomass stove and dyeing using an improved biomass stove set (L* a* b* values (mean of three positions on each Krajood sample base, middle, and end section)).

	Biomass stove	Mean	S.D.	t	p value
L*_base	Improve the biomass stove	35.14	0.77	1.046	0.326
	Traditional biomass stove	34.65	0.69		
a*_base	Improve the biomass stove	32.30	2.88	-0.042	0.968
	Traditional biomass stove	32.36	1.26		
b*_base	Improve the biomass stove	11.28	1.94	-0.493	0.642
	Traditional biomass stove	11.74	0.80		
L*_middle	Improve the biomass stove	33.37	0.91	1.016	0.339
	Traditional biomass stove	32.91	0.42		
a*_middle	Improve the biomass stove	29.46	1.65	1.03	0.333
	Traditional biomass stove	28.50	1.30		
b*_middle	Improve the biomass stove	9.75	1.36	1.302	0.229
	Traditional biomass stove	8.91	0.50		
L*_end	Improve the biomass stove	33.60	0.18	0.876	0.429
	Traditional biomass stove	33.02	1.47		
a*_end	Improve the biomass stove	29.09	1.17	-0.087	0.933
	Traditional biomass stove	29.20	2.33		
b*_end	Improve the biomass stove	9.16	1.15	0.176	0.865
	Traditional biomass stove	9.04	1.07		

(a) (b) (c)

Figure 7. Comparison of colors obtained from the traditional biomass stove and the improved biomass stove of dyeing krajood at base (a), middle (b) end (c) on the krajood threads.

Figure 8. Krajood products are made from the improved biomass stove.

3.6 Economic viability

The economic analysis considered both the initial investment costs and operational benefits of the improved stove design. The traditional biomass stove costs approximately 7,000 THB, while the improved design costs 12,000 THB, representing a 71.4% increase in initial investment. However, this higher initial cost must be considered against the five-fold increase in production capacity (from 20 to 100 bundles per day). Assuming consistent market demand, this productivity improvement translates to significantly reduced labor costs per unit of production. Although this assumption streamlines the model, it might not accurately represent the dynamics of the actual market. The real economic results may be impacted by seasonal variations, competition, and variations in customer demand. As a result, given these possible market uncertainties, the anticipated profitability should be interpreted cautiously. Additionally, the more efficient combustion in the improved design is likely to reduce fuel consumption per unit of output, though this was not specifically quantified in the current study. A simple return-on-investment calculation indicates that the 5,000 THB additional investment could be recovered within a short operational period due to the substantial productivity gains. This economic viability is essential for the adoption of appropriate technology in small-scale industrial settings, as emphasized by Lyman and Chung [4]. Furthermore, the non-monetary benefits of reduced PM2.5 exposure and improved working conditions represent additional value that may contribute to long-term health benefits for operators, though these effects would require longitudinal studies to quantify fully.

Table 2. Cost-benefit analysis of biomass stove technologies.

Parameter	Traditional Stove	Improved Stove	Difference
Initial investment (THB)	7,000	12,000	+5,000
Daily production capacity (bundles)	20	100	+80
Daily production capacity (kg)	44	220	+176
Production increase factor	-	5x	-
Estimated daily revenue (THB)*	2,000	10,000	+8,000
Estimated payback period	-	<1 day	-

*Assuming 100 THB profit per bundle

4. Conclusions

This research has successfully developed and evaluated an improved biomass stove for Krajood dyeing that embodies the principles of sustainable appropriate technology. The new design maintains operational simplicity while achieving substantial performance improvements across multiple parameters. The most significant enhancements include a 72.25% reduction in PM2.5 emissions at the operator position, a 32.73% decrease in water boiling time, a 52.43% reduction in dyeing time, and a 46.45% lower operating temperature. These improvements collectively enabled a five-fold increase in production capacity from 20 to 100 bundles (44 kg to 220 kg) per eight-hour workday. The improved stove design demonstrates how

targeted modifications based on appropriate technology principles can simultaneously address health, efficiency, and productivity concerns without compromising traditional product quality. The integration of a water reserve tank, improved combustion chamber, and heat shield required only modest additional investment while delivering significant operational benefits. Importantly, the colorimetric analysis confirmed that the improved system maintained consistent dyeing quality, with no statistically significant differences in Lab* values between the traditional and improved methods. For small-scale Krajood processing enterprises, this technology offers particularly compelling advantages. The five-fold increase in production capacity enables microenterprises to scale operations without proportional increases in labor or workspace. This productivity enhancement strengthens their competitiveness in market environments where traditional crafts face pressure from mass-produced alternatives. Additionally, the significant reductions in ambient temperature and PM2.5 emissions create considerably healthier working conditions for artisans, potentially reducing occupational health risks associated with long-term exposure to heat and particulate matter. From a sustainability perspective, the improved stove represents a balanced approach to technological advancement that respects local capabilities and resources. The design uses locally available materials and maintains a level of simplicity that enables community-based production and maintenance. While not quantified in this study, the improved combustion efficiency likely reduces biomass fuel consumption per unit of output, contributing to resource conservation. Furthermore, by enhancing the economic viability of traditional Krajood processing, the technology supports the preservation of cultural heritage and sustainable livelihoods in rural communities. Future research directions should include long-term durability assessment, precise quantification of fuel efficiency improvements, and exploration of further PM2.5 reduction strategies such as chimney systems. The design principles demonstrated in this study may also be transferable to other natural fiber dyeing processes with similar technological challenges.

5. Acknowledgements

The authors would like to express our deepest gratitude to Rajamangala University of Technology Srivijaya and Program Management Unit on Area-Based Development (PMU A) for supporting the research project "Application and expansion of appropriate technology to increase efficiency in the chain of poverty-solving operating model of Phatthalung Province towards comprehensive and accurate poverty alleviation" for the fiscal year 2023 under contract number A11F660104-05. Special thanks to the anonymous reviewers for their constructive comments and suggestions, which helped improve the quality of this manuscript.

Author Contributions: Conceptualization, N.P., P.K., and K.T.; methodology, N.P., P.K., J.P., P.J., W.S., and T.R.; software, P.K.; validation, N.P., P.K., and K.T.; formal analysis, P.K.; investigation, N.P., R.K., and K.T.; resources, N.P. and R.K.; data curation, P.K., T.R., and J.P.; writing—original draft preparation, N.P., P.K., and K.T.; writing—review and editing, N.P. and P.K.; visualization, P.K.; supervision, N.P., and P.K.; project administration, N.P. and P.K.; funding acquisition, N.P. and P.K.

Funding: This research was funded by the Ministry of Higher Education, Thailand Science Research and Innovation (TSRI), Program Management Unit on Area-Based Development (PMU A). Fiscal year 2023.

Conflicts of Interest: The authors declare no conflict of interest. The funders had no role in the study's design, in the collection, analyses, or interpretation of data, in the writing of the manuscript, or in the decision to publish the results.

References

[1] Kaewpradit, K.; Keeratiburana, Y.; Janta-po, A. Krajood: Creative economics development in communities through indigenous handicraft of Southern Thailand. *International Journal of Academic Research in Business and Social Sciences*, **2013**, *3*(9), 707–716. https://doi.org/10.6007/IJARBSS/v3-i9/260

[2] Dezord, C.; Micolau, G.; Abbas, C.; Mesgouez, A.; Pozzo Di Borgo, E. Reliable, versatile and remotely controlled instrumentation of an hectometric loop antenna using appropriate technologies. *HardwareX*, **2023**, *15*, Article e00443. https://doi.org/10.1016/j.ohx.2023.e00443

[3] Auliani, R.; Suprawihadi, R.; Avinash, B. Application of appropriate technology for clean water (A case study in Lateri Village, Baguala District, Ambon City). *Pengabdian: Jurnal Abdimas,* **2023**, *1(1)*, 30–39. https://doi.org/10.55849/abdimas.v1i1.152

[4] Lyman, A.H.; Chung, K. A new model of participatory design to improve social impact: Incorporating action research into the design of appropriate technology in rural Zambia. *Design Studies,* **2025**, *97*, Article 101325. https://doi.org/10.1016/j.destud.2025.101296

[5] Zube, D. J. Heat transfer efficiency of biomass cookstoves [Master's thesis]. Colorado State University; **2010**.

[6] MacCarty, N.A.; Bryden, K.M. A generalized heat-transfer model for shielded-fire household cookstoves. *Energy for Sustainable Development*, **2016**, 96-107. https://doi.org/10.1016/j.esd.2016.03.003

[7] Pundle, A.; Sulliva, B.; Means, P.; Posner, J.D.; Kramlich, J.C. Predicting and analyzing the performance of biomass-burning natural draft rocket cookstoves using computational fluid dynamics. *Biomass and Bioenergy*, **2019**, 105402. https://doi.org/10.1016/j.biombioe.2019.105402

[8] Bentson, S.; Evitt, D.; Still, D.; Lieberman, D.; MacCarty, N. Retrofitting stoves with forced jets of primary air improves speed, emissions, and efficiency: Evidence from six types of biomass cookstoves. *Energy for Sustainable Development,* **2022**, *71*, 104–117. https://doi.org/10.1016/j.esd.2022.09.005

[9] Hafner, M.J.; Uckert, G.; Hoffmann, H. K.; Rosenstock, T. S.; Sieber, S.; Kimaro, A. A. Efficiency of three-stone fire and improved cooking stoves using on-farm and off-farm fuels in semi-arid Tanzania. *Energy for Sustainable Development,* **2020**, *59*, 199–207. https://doi.org/10.1016/j.esd.2020.10.012

[10] , K.; Prasongchan, N.; Wunsri, S.; Joyphod, P.; Podkumnerd, N. Dyeing of screw pine (*Pandanus tectorius*) leaves using natural dyes from local plants in Songkhla Province, Thailand. *Asia-Pacific Journal of Science and Technology,* **2024**, *29(4),* Article ID.:APST-29-04-17

[11] World Health Organization. *WHO Global Air Quality Guidelines: Particulate Matter (PM2.5 and PM10), Ozone, Nitrogen Dioxide, Sulfur Dioxide and Carbon Monoxide*; WHO: Geneva, 2021. https://www.who.int/publications/i/item/9789240034228 (accessed 2025-04-14).

[12] Liu, X.; Wang, K.; Shen, Z. A novel strategy of inserting radiation shields to enhance the performance of thermoelectric generator systems for industrial high-temperature heat recovery. *Energy*, **2024**, 301, 131704. https://doi.org/10.1016/j.energy.2024.131704

[13] Yunusa, S.U.; Mensah, E.; Preko, K.; Narra, S.; Saleh, A.; Sanfo, S.; Isiaka, M.; Dalha, I.B.; Abdulsalam, M. Biomass cookstoves: A review of technical aspects and recent advances. *Energy Nexus*, **2023**, 100225. https://doi.org/10.1016/j.nexus.2023.100225

ASEAN
Journal of Scientific and Technological Reports
Online ISSN:2773-8752

Academic article

Sterculia quadrifida R.Br: Utilization, Bioactive Compounds, and the Potential as a New Source of Seed Oil - A Comprehensive Review

Mery Rambu B. Djoru[1], Samatcha Krungkaew[1], Malinee Sriariyanun[2], Yu-Shen Cheng[3], Godlief F. Neonufa[4], and Patchanee Yasurin[1*]

[1] Theophane Venard School of Biotechnology, Assumption University, Bangkok, 10240, Thailand
[2] The Sirindhorn International Thai-German Graduate School of Engineering, King Mongkut's University of Technology North Bangkok, Bangkok, 10800, Thailand
[3] Department of Chemical and Materials Engineering, National Yunlin University of Science and Technology, Douliu, Yunlin, Taiwan
[4] Agricultural Technology Faculty, Artha Wacana Christian University, Kupang, Indonesia
[*] Correspondence: patchaneeYsr@au.edu

Citation:
Djoru, M.R.B.; Krungkaew, S.; Sriariyanun, M.; Yu-Shen, C.; Neonufa, G.F. *Sterculia quadrifida* R.Br: utilization, bioactive compounds, and the potential as a new source of seed oil - a comprehensive review. *ASEAN J. Sci. Tech. Report.* **2026**, *29*(2), e258593. https://doi.org/10.55164/ajstr.v29i2.258593.

Article history:
Received: April 2, 2025
Revised: October 11, 2025
Accepted: October 18, 205
Available online: January 18, 2026

Abstract: *Sterculia quadrifida* R.Br., a plant native to East Nusa Tenggara, Indonesia, and northern Australia, has gained increasing attention due to the diverse traditional uses of bark, roots, leaves, and seeds. Recent studies have shown that this plant is rich in bioactive compounds, including antioxidants, anticancer, antimicrobial, and antifungal agents present in all parts of the plant. This review aims to discuss the utilization of this plant by local communities and summarize various research findings on its bioactive compounds and their health benefits. Additionally, the review focuses on the potential of the seeds as a valuable new source of plant oil, as studies on *Sterculia quadrifida* R.Br. seeds have revealed high lipid content, diverse fatty acids including linoleic and palmitic acids, sterculic acid, triterpenoid, and β-sitosterol, which contribute to their antioxidant, anticancer, antimicrobial, and antifungal properties. This review provides opportunities for further research on the extraction of *Sterculia quadrifida* R.Br. seed oil and its applications in the food, pharmaceutical, and industrial sectors.

Keywords: Faloak tree; bioactivity; seed oil; extraction method; vegetable oil.

1. Introduction

Plants that traditional communities have long utilized may possess bioactive compounds that can be harnessed for modern applications [1]. Indonesia possesses abundant biodiversity in the world, with thousands of plant species widely distributed across tropical rainforests [2], with approximately 7,500 of its 30,000 species recognized for their medicinal potential [3]. Timor Island, Indonesia, has a dry soil structure, low rainfall intensity, and limited water supply, which has led to biodiversity that differs from other regions of Indonesia. One of the endemic plants on Timor Island is *Sterculia quadrifida* R.Br. This plant is categorized as a tropical tree and belongs to the family *Sterculiaceae* [4]. *Sterculia quadrifida* R.Br. exhibits various pharmacological properties and has long been utilized in traditional medicine. The bark is the most frequently used part by the local communities in East Nusa Tenggara for medicinal purposes, such as treating hepatitis or liver disorders, fatigue, gastroenteritis, and

rheumatoid arthritis [5]. Several products derived from the bark of *Sterculia quadrifida* R.Br have already been marketed in local markets and national marketplaces, such as tea and instant health beverages. It has also become one of the most sought-after plants for treating liver diseases.

Several studies have explored the roots, leaves, and seeds of *Sterculia quadrifida* R.Br, revealing a wealth of distinctive compounds [6-9]. Among the plant parts, the fruits of *Sterculia quadrifida* R.Br are particularly abundant each year, especially considering the dense distribution of trees on Timor Island [10]. However, these fruits are underutilized and are discarded seasonally. Research indicates that the seeds of *Sterculia quadrifida* R.Br are rich in fatty acids, including palmitic acid, heptadecenoic acid, stearic acid, and linoleic acid, which are vital components of many plant oils [11]. Additionally, bioactive compounds such as flavonoids, alkaloids, tannins, and phenolic acid found in the seeds demonstrate strong biological activities [7, 12]. The unique combination of fatty acids and bioactive compounds suggests that *Sterculia quadrifida* R.Br. seeds have a significant potential as a new and valuable source of plant-based oils.

This review aims to provide a comprehensive review of the potential of *Sterculia quadrifida* R.Br, particularly in terms of its utilization, bioactive compounds, and the prospects of its seed oil benefits. This review summarizes and analyzes various studies related to this plant, given the growing interest in natural and bioactive sources. A thorough review of *Sterculia quadrifida* R.Br can help identify new benefits and utilization opportunities across various sectors, such as health, food, and industry. Additionally, this article provides information about this plant in raising global awareness and understanding of this plant, encouraging further research that could unlock new economic and scientific opportunities.

2. Distribution and Morphology of *Sterculia quadrifida* R.Br

Sterculia quadrifida R.Br. is a tropical tree found in various regions across Australia and Asia [13]. Originally, this plant spread from northern New South Wales to Queensland and extended to Western Australia and parts of Indonesia (Figure 1). In Australia, this plant is known as the Peanut tree or Red Kurrajong [5], in China known as Wu wai zi [6], while in Timor Island, Indonesia, it is known by the local name Faloak [13, 14].

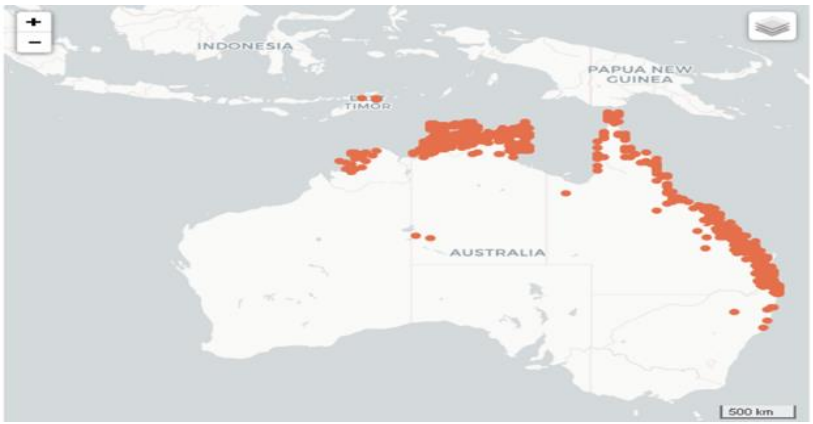

Figure 1. Map of the distribution of *Sterculia quadrifida* R.Br in Australia and Indonesia [15].

The ecology of *Sterculia quadrifida* R.Br. is characterized by its adaptability to a range of tropical and subtropical environments. This tree often grows in association with other native species and typically grows wildly in forest areas and can grow on rocky and drained soils [16]. Moreover, *Sterculia quadrifida* R.Br can grow up to a height of 20 meters, with a sturdy trunk featuring rough bark and thick fibers (Figure 2a). The fruiting season occurs annually between June to October. During this period, when the fruit is ripening, the seeds are protected by the green skin, and after the period ends at the age of 3 to 4 months, the skin of the fruit will turn orange, and the fruits split open, revealing black seeds that are elliptical in shape, typically containing 4-8 seeds per fruit. After 1-3 weeks, the skin of the fruits will turn brown, which indicates the seeds are old (Figure 2b). The seeds of *Sterculia quadrifida* R.Br are approximately 10 mm in size and are edible, with a taste resembling that of raw nuts [10].

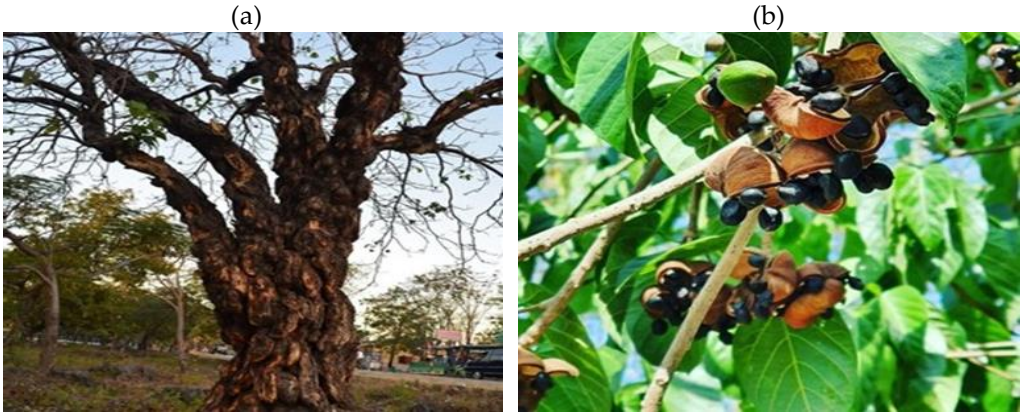

Figure 2. (a) Plant, and (b) Fruit and Seeds of *Sterculia quadrifida* R.Br.

Specific quantitative data regarding the annual fruit yield per tree is not available due to the limited research focusing on the seeds of this tree. However, research indicates that on Timor Island, Indonesia, the density of this plant is relatively high and widespread across various regions with differing densities [17]. Exploratory studies conducted in five districts on Timor Island revealed the distribution data of *Sterculia quadrifida* R.Br as follows: the highest density was found in the Timor Tengah Selatan District area (14.16 trees/ha), followed by the Kupang District area (7.94 trees/ha), the Belu District area (6.25 trees/ha), Kupang City (4.84 trees/ha), and the Timor Tengah Utara District area (1.4 trees/ha) (Figure 3). Given the high distribution density of this tree, it is expected and estimated to produce a substantial quantity of fruit and seeds from *the Sterculia quadrifida* R.Br plant each year.

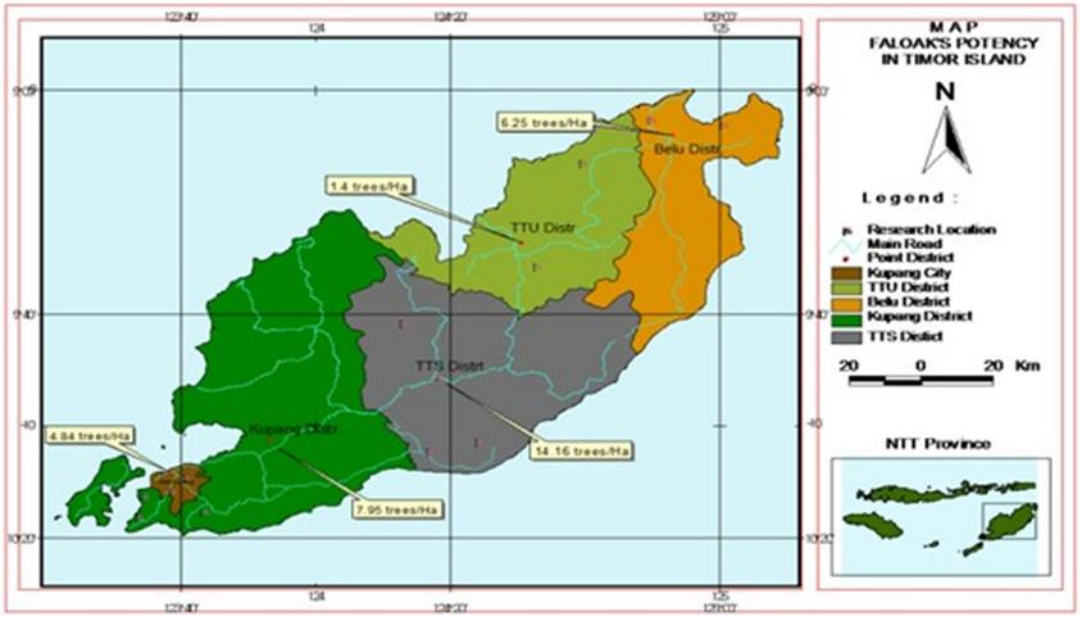

Figure 3. Map of Distribution of *Sterculia quadrifida* R.Br. Trees on Timor Island, Indonesia [17].

3. Utilization, Phytochemical Composition, and Bioactivity

3.1 Utilization of Sterculia quadrifida R.Br

Studying how indigenous and local communities use plants provides valuable insights into plant species, cultural significance, medicinal properties, and potential economic value [18]. *Sterculia quadrifida* R.Br has a history of traditional medicinal use in several regions where this species grows. In Australia, Aboriginal communities use the leaves of *Sterculia quadrifida* R.Br to treat wounds, skin disorders, eye diseases, and mouth

ulcers; the seeds are consumed, and the inner bark is used for weaving baskets and spinning ropes [14]. While in Timor Island, Indonesia utilize the bark of *Sterculia quadrifida* R.Br. is utilized as a medicinal and nutritional herbal drink to treat ailments such as liver disorders, digestive issues, fatigue, gastroenteritis, and rheumatoid [5,19]. In addition, besides the bark, the root extracts of *Sterculia quadrifida* R.Br. have also been traditionally used to treat diabetes and cancer [2]. The harvesting method practiced by the community involves slicing or peeling the tree bark into specific sizes or dimensions before using it or boiling it (Figure 4). Generally, they use clay pots to make a traditional herbal drink.

(a) (b)

Figure 4. (a) Bark, and (b) Sliced bark of *Sterculia quadrifida* R.Br Tree

Every local society has its own way of utilizing the bark of *Sterculia quadrifida* R.Br as a herbal drink. While most people use this bark without adding other ingredients, some have developed specific recipes to cure diseases by combining it with additional ingredients such as turmeric, garlic, lemongrass, onion, cinnamon, and sand ginger [19]. Traditionally, there are no specific guidelines for the dosage to boil *Sterculia quadrifida* R.Br bark. Residents who consume it only boil it with water, and the remaining decoction will be used again by adding water as needed, and this activity can be repeated up to 4 times, as long as the color of the boiled water remains red.

3.2 Phytochemical Composition of Sterculia quadrifida R.Br Seeds

Phytochemical investigations of *Sterculia quadrifida* R.Br. seeds have revealed the presence of diverse classes of bioactive compounds that contribute to their pharmacological potential. Ethanol extract analyses have identified major groups of secondary metabolites, including flavonoids, alkaloids, tannins, terpenoids, phenolic acids, and phytosterols such as β-sitosterol [11]. These compounds play important roles in various biological activities, including antioxidant, anticancer, antimicrobial, and antifungal effects. In particular, flavonoids and phenolic acids act as strong antioxidants that help protect cells from oxidative stress, while alkaloids and tannins exhibit antimicrobial properties through their ability to disrupt microbial cell membranes and inhibit enzymatic activity. Furthermore, triterpenoids and sterols such as β-sitosterol are reported to have immunomodulatory, anti-inflammatory, and anticancer activities [6,11,20]. The coexistence of these compounds highlights the pharmacological relevance of *Sterculia quadrifida* R.Br. seed extracts and provides a chemical basis for their traditional use in medicine. The presence of such diverse phytochemicals not only confirms the bioactivity of *Sterculia quadrifida* R.Br. seeds but also supports their potential as a novel source of natural compounds for pharmaceutical, nutraceutical, and food industries. These findings suggest that further exploration of seed phytochemistry, alongside biological assays, could open new opportunities for the utilization and development of *Sterculia quadrifida* R.Br. seed oil and its derivatives in modern applications.

3.3 Bioactivity Found in Sterculia quadrifida R.Br. Plant

Recent studies and research have increasingly focused on the potential health benefits and bioactive compounds derived from the plant part of *Sterculia quadrifida* R.Br., and the studies show that all parts of this

plant contain various bioactive compounds beneficial to health. Among them, the bark, root, leaf, and the seeds of *Sterculia quadrifida* R.Br have been identified to contain flavonoids, alkaloids, tannins, and unsaturated fatty acids [20]. These compounds exhibit various biological activities, including antioxidant [6,7], antifungal, and anticancer properties [16,21,22]. *Sterculia quadrifida* R.Br, which has been used for centuries as a traditional medicine in various regions, has attracted the attention of numerous researchers who have studied the chemical compounds and pharmacological properties of this species. Several phytochemical studies have led to the extraction and fractionation of various classes of compounds, including flavonoids, propanoids, alkaloids, and terpenoids, from this plant [3]. The potential health benefits of this plant underscore its importance, not only for the local population but also as a candidate for broader scientific exploration. Plants can produce diverse bioactive compounds. The bioactive compounds in plants produce pharmacological or toxicological effects on humans and animals [23]. Studies' results on *Sterculia quadrifida* R.Br seeds have identified varieties of bioactive compounds that will benefit human health, such as antioxidants, antimicrobial, antifungal, antitoxic, and anticancer (Table 1).

As a promising subject for broader scientific research, the potential health benefits of this plant emphasize its importance not only for the local community but also for further research. Although research on this plant is still limited to the local area, preliminary studies indicate that parts of this plant contain beneficial compounds that, if further explored, could contribute not only to the pharmaceutical field but also to the food and cosmetic fields. Reviewing the existing literature on the utilization and discovery of bioactivities of this plant positions *Sterculia quadrifida* R.Br as a promising candidate for a sustainable source of beneficial plants.

3.3.1 Antioxidant

Antioxidants are compounds that can protect body cells from damage caused by free radicals [35]. Free radicals are unstable molecules that can damage body cells, leading to various diseases and aging [36]. Antioxidants work by scavenging free radicals, thus preventing the damage they cause. The benefits of antioxidants for human health are diverse. Some key benefits include protecting cells from oxidative damage, reducing the risk of heart disease, combating the aging process, boosting the immune system, and even reducing the risk of some types of cancer [37]. Antioxidants can be found in various foods, especially in fruits, vegetables, grains, nuts, and spices [38]. Several bioactive compounds, including flavonoids, alkaloids, steroids, terpenoids, tannins, and fatty acids, are where these bioactive compounds can contribute to the ability of antioxidant activity [39]. Several research results have shown the presence of various secondary metabolites that act as antioxidant agents in *Sterculia quadrifida* R.Br bark, root, leaf, and seeds, such as flavonoids, phenols, and tannin content (Table 1). Flavonoids, phenols, and tannins also gain anti-inflammatory properties and can support cognitive function and brain health, including protection against cardiovascular diseases and some types of cancer [40]. Moreover, the extraction of *Sterculia quadrifida* R.Br has demonstrated strong antioxidant properties based on IC_{50} values. The bark showed very strong antioxidant activity with an IC_{50} value of 14.17±0.55 μg/mL, while the roots had an IC_{50} value of 20.55±0.42 μg/mL [7]. The leaves and seeds exhibited moderate antioxidant activity with IC_{50} values of 52.59±0.75 μg/mL and 76.62±0.32 μg/mL, respectively [7]. Some studies showed that the extract of new regrown stem bark and old regrown stem bark exhibited potent antioxidant activity with IC_{50} values of 2.51±0.03 and 3.43±0.12 μg/ml, respectively [41]. They are classified as strong antioxidants. In the context of IC_{50} values, the lower the IC_{50} value, the stronger the antioxidant ability of the substance. This indicates that the extract of *Sterculia quadrifida* R.Br. seeds can inhibit the activity of free radicals. It can also prevent oxidative damage to cells with high effectiveness.

Table 1. List of Bioactivity Found in Bark, Root, Leaf, and Seed of *Sterculia quadrifida* R.Br.

Bioactivity	Part of Plant	Research Result	Ref
Antioxidant	Bark	• The extract of *S. quadrifida* stem bark using ethanol solvent showed antioxidant activity classified as very strong (IC_{50} value was 14.17 ± 0.55 μg/ml).	[7,8]
		• Total content of flavonoid was found (62.76 ± 4.84 mg/g), phenols (45.37 ± 3.82 mg/g), and tannins (59.64 ± 9.64 mg/g).	[7]
		• The extract of the new regrown stem bark exhibited potent antioxidant activity with inhibitory concentration (IC_{50}) values of 2.51 ± 0.03 μg/ml, and the old regrown stem bark with 3.43 ± 0.12 μg/ml, is classified as a strong antioxidant.	[24]
	Root	• Based on IC_{50} values, the antioxidant activity of root extract was classified as very strong (20.55 ± 0.42 μg/ml), and the highest total tannins from all parts of the *S. quadrifida* plant are in the roots (71.26 ± 10.21 mg/g).	[7]
	Leaf	• The antioxidant activity based on IC_{50} values was 52.59 ± 0.75 μg/ml on a leaf of *S. quadrifida* (IC_{50} values of 51-100 μg/ml were classified as strong).	[7]
		• The total flavonoid content in the ethanol extract of *S. quadrifida* leaves was 5.31 ± 0.29% w/w, and the total polyphenol content was 1.79 ± 0.03% w/w.	[12]
	Seed	• The antioxidant activity was classified as strong based on IC_{50} values of 76.62 ± 0.32 μg/ml on the seeds of *S. quadrifida* R.Br.	[7]
		• Flavonoid content was found in the seeds of *S. quadrifida* extract (1.55 ± 1.44 mg/g). The flavonoid allegedly in the seeds of *S. quadrafida* causes a high ability to inhibit DPPH free radicals.	[3,7,25]
		• Phenol content was found in seeds (2.89 mg/g). Phenols are one of the bioactive compounds that can enhance antioxidant activity, alongside flavonoids and tannins.	[7,26,27]
		• β-sitosterol, also known as stigmast-5-en-3-ol, is a specific phytosterol. It is found in *S. quadrifida* seeds, which have been demonstrated to have antioxidant activities.	[6,28,29]

Table 1. List of Bioactivity Found in Bark, Root, Leaf, and Seed of *Sterculia quadrifida* R.Br. (Continue)

Bioactivity	Part of Plant	Research Result	Ref
Anticancer	Bark	• The *S. quadrifida* bark ethanol extract can inhibit the development of the breast cancer T47D cell line with an IC_{50} of 32.45 μg/ml.	[30]
		• The derivative compound Naptokuinon (*2,3-dihydro-6-hydroxy-2-methylenenaphtho [1,2-b] furan-4,5-dione*) has cytotoxic activity on breast cancer cell T47D with active category (IC_{50} = 9.88 μg/ml)	[31]
		• The *S. quadrifida* bark with ethyl acetate fraction can inhibit the development of T47D breast cancer by increasing the cytotoxic effect.	[9]
	Leaf	• The ethyl acetate fraction of the *S. quadrifida* leaf extract exhibited considerable cytotoxic activity in T47D and 4T1 breast cancer cells, with IC_{50} values of 19.86±3.48 and 16.70±3.33 μg/ml.	[32]
	Seed	• Methanol extract of *S. quadrifida* seeds is found to contain a cytotoxic compound, namely Tetramethoxyhydroxybiphenyl (*3,3',5,5'tetramethoxybiphenyl-2,2'-diol*), which can exhibit cytotoxic activity against various cancer cell lines, including human colon adenocarcinoma (HT-29), human breast adenocarcinoma (MCF-7), and human lung adenocarcinoma (A549) cells.	[6]
Antimicrobial	Bark	• The ethanol extract of *S. quadrifida* tree bark, at concentrations of 22.5% w/v, 45% w/v, 75% w/v, and 100% w/v, demonstrates antibacterial activity against the growth of *Staphylococcus aureus* bacteria.	[13]
		• Fractionation with 96% ethanol extract using the preparative thin-layer chromatography method on the bark of *S. quadrifida* exhibited strong antibacterial activity, with effective concentrations of 90.51 μg/ml against *Bacillus subtilis*, 80.12 μg/ml against *Escherichia coli*, and 77.87 μg/ml against *Staphylococcus aureus*.	[33]
Antifungal	Seeds	• Extraction with the diethyl ether fraction of *S. quadrifida* seeds has anti-fungal properties against the parasite *Candida albicans*, namely the compound 3-hydroxy octadecanoic acid ($C_{18}H_{36}O_3$), which showed an inhibition of 44.33 mm and a minimum inhibitory concentration (MIC) of 30.34 μg/ml.	[16,34]

3.3.2. Anticancer

Anticancer compounds can inhibit the growth of cancer cells, stimulate programmed cell death in cancer cells, or disrupt critical processes in the cancer cell cycle. Cancer treatments, such as chemotherapy and radiation, often lead to cytotoxic effects, which can harm healthy cells in addition to cancerous ones. Anticytotoxic agents may help mitigate these adverse effects by neutralizing or reducing the damage inflicted on normal tissues, thereby improving the overall efficacy and tolerability of cancer treatments. Moreover, some compounds with anticytotoxic properties might have direct anti-cancer effects, as they can also help in reducing oxidative stress and inflammation, which are commonly associated with cancer progression. Several studies have shown extracts and fractions of *Sterculia quadrifida* R.Br to have cytotoxic activity [6][9][31][32]. Ethanol extracts from the stem bark of *Sterculia quadrifida* R.Br demonstrated the ability to inhibit the growth of the T47D breast cancer cell line, with an IC_{50} value of 32.45 μg/ml [3,30]. Additionally, another study found that the ethyl acetate fraction from the bark of *Sterculia quadrifida* R.Br effectively inhibited the T47D breast cancer cell line, with an IC_{50} of 24.88 μg/ml and a selectivity index of 15.58. This ethyl acetate fraction was also capable of inducing cell cycle arrest in the S phase, with a percentage of 27.43%, and promoting apoptosis at a rate of 11.88% [9]. Some compounds that show various bioactivities found in *Sterculia quadrifida* R.Br. seeds are sterculic acid, triterpenoid, and β-sitosterol. These compounds are also known for antioxidant, anti-inflammatory, anticancer, antidiabetic, and cytotoxic activities [13]. This activity is often studied in the context of the development of anticancer drugs or other therapies. Furthermore, Dibenzalacetone (2E, 4E)-1, 5-diphenylpenta-2, 4-dien-1-one), a compound isolated from *Sterculia quadrifida* R.Br seeds, belongs to the group of phenylpropanoid compounds, which have anticancer activity through apoptosis induction [10]. In another study, isolation from the roots of *Piper sarmentosum* with cytotoxic activity against MDA-MB-231 breast cancer cells identified two phenylpropanoid compounds, asaricin and isoasarone [42]. Moreover, flavonoids found in the bark, root, leaf, and seeds of *Sterculia quadrifida* R.Br play a crucial role in inhibiting procarcinogen activation, inhibiting cancer cell proliferation, selective cancer cell death through apoptosis, inhibiting metastasis and angiogenesis, and activating immune responses to cancer cells [14]. Therefore, with the discovery of anticancer compounds from *Sterculia quadrifida* R.Br. seeds, they have the potential for use in cancer therapy. These compounds can serve as the basis for drug development or additional therapies. They can also be consumed as preventive measures and included in a healthy diet to help protect the body from cancer risks. Additionally, the utilization of antioxidant, anticancer, and antifungal activity from *Sterculia quadrifida* R.Br plant part in food products can enhance the nutritional value and health of these products. Anticancer-enriched food products can help strengthen the immune system and prevent diseases.

3.3.3 Antimicrobial

Sterculia quadrifida R.Br has been recognized for its antimicrobial properties, primarily attributed to compounds extracted from the bark of this plant. Previous research has shown that the ethanol extract of *Sterculia quadrifida* R.Br. bark has antimicrobial activity in gram-negative and gram-positive bacteria [43]. This antimicrobial activity is generally linked to the presence of bioactive compounds such as flavonoids, tannins, saponins, and alkaloids [44]. These phytochemicals are known to interfere with microbial cell membranes, inhibit enzyme activity essential for microbial growth, and disrupt cellular processes, thus exerting their antimicrobial effects. The analysis showed that the extract from *Sterculia quadrifida* R.Br bark demonstrated the effective inhibition of *Staphylococcus aureus* growth [13]. Another study reported that fractionation with 96% ethanol extract using the preparative thin-layer chromatography method on bark of *Sterculia quadrifida* R.Br exhibited strong antibacterial activity, with effective concentrations of 90.51 μg/ml against *Bacillus subtilis*, 80.12 μg/ml against *Escherichia coli*, and 77.87 μg/ml against *Staphylococcus aureus* [33]. The benefits of these antimicrobial properties are significant in both the food industry and pharmacology. In the food sector, *Sterculia quadrifida* R.Br extracts can be utilized as natural preservatives to extend shelf life and prevent microbial contamination, thus enhancing food safety. In pharmacology, the antimicrobial compounds from *Sterculia quadrifida* R.Br have potential applications in developing new antibiotics or antimicrobial agents,

which is crucial given the rising concerns of antibiotic resistance. The ability to harness these natural compounds can lead to more sustainable and effective treatments, reducing reliance on synthetic drugs and mitigating the impact of resistant pathogens.

3.3.4 Antifungal

Compounds with antifungal activity are compounds that can inhibit the growth or kill fungi. They can work through various mechanisms, including disrupting fungal cell membranes, inhibiting enzymes in fungal metabolic processes, and disrupting fungal reproduction processes [45]. *Sterculia quadrifida* R.Br. seeds have been found to contain various compounds with potential antifungal activity [16]. According to phytochemical studies, flavonoid derivatives, phenolic acids, and triterpenoids are a group of main compounds identified in plant parts such as leaves, seeds, and roots, which have biological activity and act as antifungal, antimicrobial, antiparasitic, anti-inflammatory, or antioxidant and cytotoxic[46-48]. The compound 3-hydroxyoctadecanoic acid ($C_{18}H_{36}O_3$) or *stearic* acid is the main antifungal compound found in *Sterculia quadrifida* R.Br. seeds. Analysis result of *Sterculia quadrifida* R.Br Seeds extraction with diethyl ether fractions against the parasitic fungus *Candida albicans* showed inhibition of 44.33 mm and minimum inhibitory concentration (MIC) of 30.34 µg m/l [12]. This indicates that the diethyl ether fraction from *Sterculia quadrifida* R.Br. seeds extract is capable of inhibiting the growth of *Candida albicans* fungus quite strongly, as evidenced by the significant inhibition zone size. The larger the diameter of the zone, the stronger the inhibitory activity of the tested compound against fungal growth. This suggests that at relatively low concentrations, the compound can effectively inhibit the growth of the parasitic fungus. This testing provides indications that *Sterculia quadrifida* R.Br. seeds contain compounds with significant antifungal activity, which may have applications in the development of drugs or antimicrobial products. The other research found that 3-hydroxyoctadecanoic acid ($C_{18}H_{36}O_3$) has been previously isolated from the extractive substance of *Hypericum lysimachioides* var. *lysimachioides* flower. This species is one of the flora that grows in Turkey, which is widely used as a medicine to heal wounds, antigastritis, antiseptic effect, and has anti-depressant, anti-cancer, and antimicrobial activities [34].

4. Potential Oil in *Sterculia quadrifida* R.Br seed

4.1 Fatty Acids in the Seeds

Research has been conducted to evaluate the chemical composition of *Sterculia quadrifida* R.Br. seeds using GC-MS analysis [11]. The results of the active compounds determination in *Sterculia quadrifida* R.Br. seeds using ethanol extract chromatograms showed that there are several fatty acids identified in these seeds (Figure 5).

Oils rich in saturated and unsaturated fatty acids, including monounsaturated and polyunsaturated fatty acids [49], have broad applications in the food, pharmaceutical, and cosmetic industries. Based on the analysis of the identified fatty acids, the seeds of *Sterculia quadrifida* R.Br. have the potential to offer various health benefits for humans. The fatty acid identified in *Sterculia quadrifida* R.Br. seeds using the GC-MS method with ethanol extract shows that the most dominant compound found in its seeds is hexadecanoic acid. Hexadecanoic acid is a saturated fatty acid commonly known as palmitic acid. Some other plants that contain relatively high levels of palmitic acid include coconut (*Cocos nucifera* L), palm (*Elaeis guineensis*) [37], candlenut (*Aleurites moluccana*) [50], peanut (*Arachis hypogaea*) [51], macadamia nut (*Macadamia Integrifolia*) [52], and almond seed (*Prunus dulcis*) [53]. Palmitic acid has several biological activities, such as hypocholesterolemic, nematicide, antioxidant, and pesticide [54]. Palmitic acid is also important and is often approached with caution due to its association with increased levels of bad cholesterol or Low-Density Lipoprotein (LDL) when consumed in excess. However, in balanced amounts, palmitic acid plays a vital role in the body, including as an energy source and as a structural component of various lipids within cell membranes. The high and dominant content of palmitic acid in *Sterculia quadrifida* R.Br. seeds indicates that these seeds contain a significant amount of plant oil that can be extracted. This oil has potential for use in various industrial and culinary applications. Additionally, the presence of palmitic acid provides stability and resistance to oxidation, which is important for the long-term storage of the oil. The significant amount of palmitic acid also suggests that this oil has good oxidative stability.

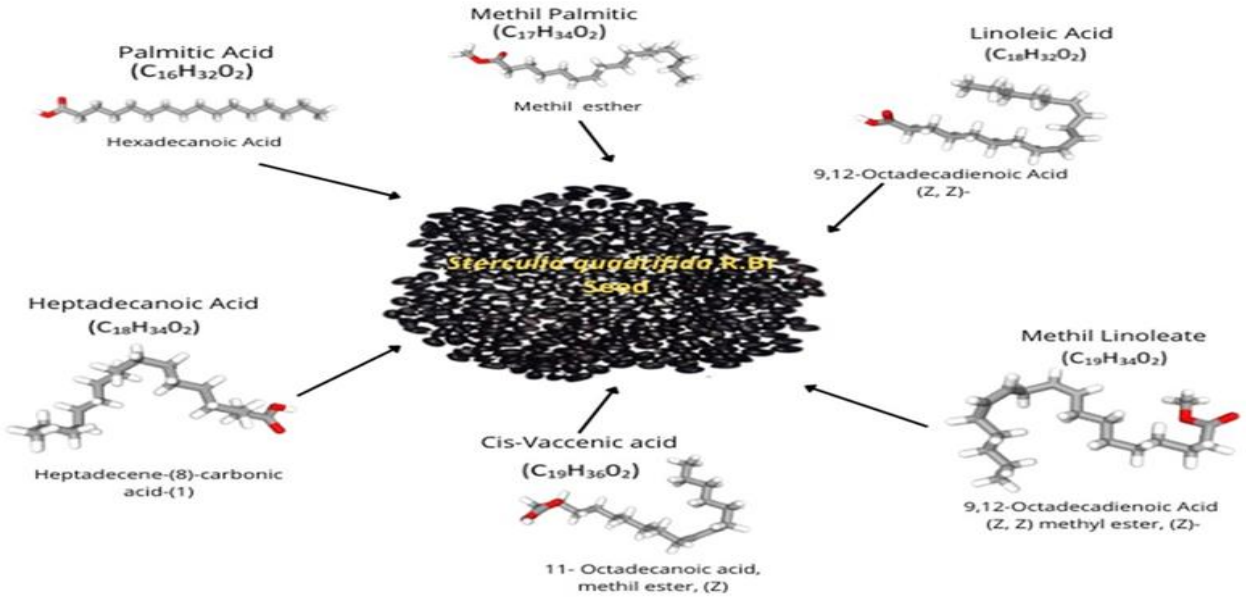

Figure 5. Fatty Acids Identified in *Sterculia quadrifida* R.Br Seed [11].

Heptadecene-8-carbonic acid-(1) or heptadecanoic acid is the following dominant compound found in *Sterculia quadrifida* R.Br. seeds. This compound, also known as margaric acid, is a saturated fatty acid with 17 carbon atoms that is commonly found in small amounts in some food sources, including grains, milk, and meat [55]. This compound is integrated with other compounds to provide antioxidant, antibacterial, and antiproliferative effects [56]. Research also shows that consuming odd-chain saturated fatty acids, such as heptadecanoic acid, may play a role in supporting heart health [57]. Another fatty acid discovery was 9,12-octadecadienoic acid, which is known as linoleic acid. Linoleic acid is an essential omega-6 fatty acid and the most beneficial for health. This fatty acid is essential for the growth and development of children, as it cannot be synthesized by the human body. It is also a major component of cell membranes and is important for nervous system function [58]. Linoleic acid offers several benefits to the human body, including maintaining lipid balance, regulating metabolism, and supporting optimal brain function, such as promoting brain development. Additionally, research indicates that linoleic acid plays a crucial role in protecting pancreatic β-cells [59]. Pancreatic β-cells are the type of cells responsible for producing insulin, a hormone that regulates blood sugar levels in the body. In other words, this acid helps maintain the health and function of pancreatic β-cells, which is important in preventing or reducing the risk of diseases such as diabetes. Moreover, linoleic acid reduces the risk of heart disease and contributes to metabolic health, making it highly valued in a healthy diet [49,60]. Additionally, cis-vaccenic acid and methyl linoleic acid are unsaturated fatty acids, both monounsaturated and polyunsaturated, that also offer health benefits. Cis-vaccenic acid is an omega-7 fatty acid that helps improve heart health by lowering bad cholesterol or LDL and increasing good cholesterol or High-Density Lipoprotein (HDL) [49,60]. Moreover, this omega-7 fatty acid contributes to skin and mucous membrane integrity and has potential anti-inflammatory properties [61]. As a polyunsaturated fatty acid (PUFA), methyl linoleic acid has antioxidant potential that can support immune function and prevent cellular damage [62]. Another beneficial fatty acid found is octadecanoic acid, also known as stearic acid, which is found in the extraction of Sterculia quadrifida R.Br seeds (Figure 5). Octadecanoic acid is a compound containing an 18-carbon chain. It is classified as an omega-9 fatty acid [63], and consuming omega-9 fatty acids can help lower LDL cholesterol levels in the blood, thus reducing the risk of heart disease [64]. Overall, the oil produced from these fatty acids has significant potential health benefits, particularly due to its content of polyunsaturated fatty acids like linoleic acid. The applications of this oil may include its use in functional foods, dietary supplements, and cosmetic products that support skin health and overall bodily functions. Thus, extracting oil from a source rich in such fatty acids can provide valuable contributions to enhancing human health.

4.2 Potential of the seed as a New Resource Supplying Oil

Plant oil is a key commodity in various food and non-food industries. Thus, identifying new plant oil sources can reduce dependence on a few types of oils. Extracting oil from the underutilized seeds of *Sterculia quadrifida* R.Br could provide a potential new source, offering health or nutritional benefits and economic advantages to society now and in the future. The discovery of various interesting bioactive and phytochemical compounds in *Sterculia quadrifida* R.Br. seeds by several researchers provides a deeper understanding of the potential of these seeds. A review and summary of the bioactive compounds found in *Sterculia quadrifida* R.Br. seeds is highly necessary, as this will provide valuable and useful information for obtaining high-quality oil in optimal quantities. Thus, this review makes an important contribution to further exploration of the benefits and potential of oil from these seeds, particularly in supporting broader industrial applications. Based on the findings from research on the bioactive compounds in *Sterculia quadrifida* R.Br. seeds, it has been demonstrated that these seeds contain various beneficial fatty acid compounds that are of significant interest [3,7]. A comprehensive analysis of the phytochemical composition indicates a substantial potential for extracting these compounds, thereby unveiling the prospective discovery of a new type of vegetable oil. The fatty acid components are particularly noteworthy, renowned for their promising properties across various industries, ranging from foods to pharmaceuticals. Sterculia quadrifida R.Br. seeds have the potential to be extracted into plant oil for several reasons (Figure 6).

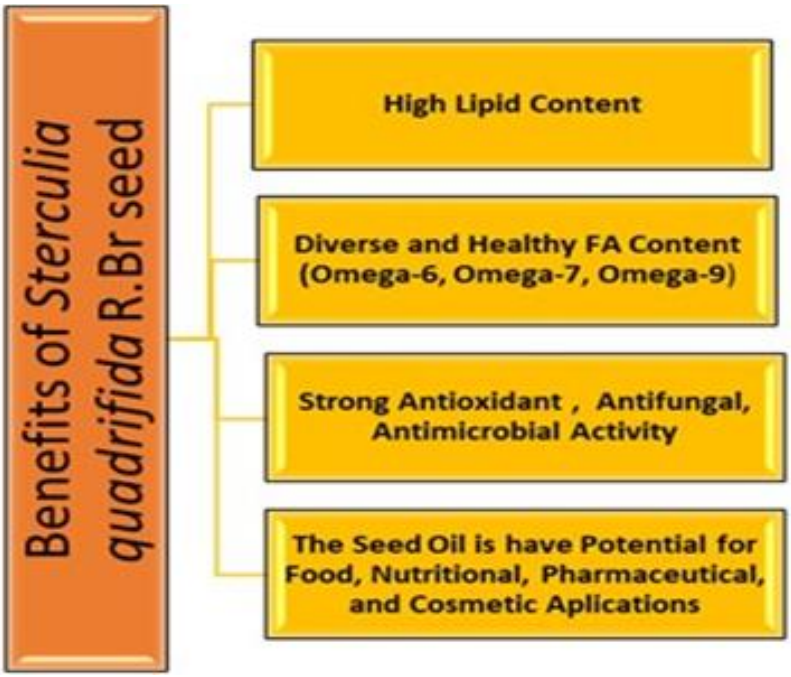

Figure 6. Benefits of *Sterculia quadrifida* R.Br. Seed

Continued research and development efforts are essential to unlock their full potential, paving the way for their integration into the food, pharmaceutical, and cosmetic industries. By leveraging the unique properties of *Sterculia quadrifida* R.Br oil, it is possible to enhance the diversity and sustainability of plant oil sources, contributing to improved health outcomes and economic resilience. Some of the potentials of *Sterculia quadrifida* R.Br. seeds are explained as follows;

- High lipid Content; *Sterculia quadrifida* R.Br. seeds are proven and have a relatively high lipid content [11]. Plant oil is obtained by extracting lipids from seeds, and seeds with high lipid content are a good choice for extraction into plant oil. Oil extracted from *Sterculia quadrifida* R.Br. seeds can become a potential source of new vegetable oil for the food, pharmaceutical, and cosmetic industries.
- Diverse, Healthy, and Beneficial Fatty Acid Content; *Sterculia quadrifida* R. Br seeds contain various types of fatty acids, including saturated, monounsaturated, and polyunsaturated fatty acids [4,11,15].

These fatty acids are the main components of plant oil and impart unique characteristics to the extracted oil. Some fatty acids found in *Sterculia quadrifida* R.Br. seeds, such as linoleic acid (omega-6), cis-vaccenic acid (omega-7), and octadecanoic acid (omega-9), are essential fatty acids required by the human body as the human body cannot synthesize them on its own [64]. The presence of these essential fatty acids makes vegetable oil extracted from *Sterculia quadrifida* R.Br. seeds nutritionally valuable.

- Potential Health Benefits: The fatty acids found in vegetable oil from *Sterculia quadrifida* R.Br seeds, such as monounsaturated and polyunsaturated fatty acids, have been associated with various health benefits, including maintaining heart health, skin health, pancreatic health, nervous system health, and brain health [64][65]. In addition to fatty acids, oil from *Sterculia quadrifida* R.Br seeds may also contain other bioactive compounds such as tocopherols (vitamin E) and phenolic compounds, which have antioxidant activity and other health benefits [11,20,40].
- Benefit in food, pharmaceutical, and cosmetic Applications: Oil extracted from *Sterculia quadrifida* R.Br seeds has great potential in various applications due to its unique physico-chemical properties. *Sterculia quadrifida* R.Br. oil contains a beneficial profile of fatty acids, vitamins, and antioxidants that are important for health, in addition to its unsaturated fatty acid content, which can support heart health and reduce the risk of cardiovascular disease. For culinary applications, this oil can be used as cooking oil or food additives, and in the cosmetic sector, antioxidant properties can help fight premature aging and protect the skin from damage caused by free radicals.

With the combination of these factors, the fruiting season that occurs every year, and the availability of fruit and seeds that have not been utilized, *Sterculia quadrifida* R.Br. seeds have the potential to be a valuable source of plant oil. Overall, the oil extracted from these seeds has great potential for application in various sectors, offering good health and economic benefits.

5. Conclusions

The bioactive components, including various fatty acids, exhibit antioxidant, anticancer, antimicrobial, and antifungal activities found in every part of *Sterculia quadrifida* R.Br., potentially contributing to more fundamental research on the utilization of this plant. The seeds of *Sterculia quadrifida* R.Br., rich in lipids, fatty acids, and significant bioactive compounds, have the potential to be extracted into plant seed oil that is beneficial for the food, health, and nutrition sectors. Further research is essential to fully characterize its bioactive compounds, optimize extraction methods, and explore new ways to utilize its diverse applications. Thus, *Sterculia quadrifida* R.Br. seed oil stands out as a promising natural resource for enhancing health and well-being, and this plant, from all parts, has the opportunity to be studied and used as a natural antioxidant agent.

6. Acknowledgements

The authors would like to express their sincere gratitude to the faculty and staff of Theophane Venard School of Biotechnology, Assumption University, Bangkok, Thailand, whose resources and guidance were invaluable in the preparation of this work. Special thanks go to Assistant Professor Patchanee Yasurin, Ph.D, and Samatcha Krungkaew, Ph.D, whose expertise in biotechnology and food science greatly contributed to the this article and who provided helpful discussions and insights, enriching the quality of this work. The authors also extend our appreciation to Artha Wacana Christian University in Kupang, Indonesia, and to the United Board for Christian Higher Education in Asia for their invaluable support, which made the completion of this review article possible

Author Contributions: Conceptualization: M.R, P.Y.,; Methodology: M.R, P.Y, S.K., M.S.,; Validation: P.Y., S.K.,Y.S.C., G.F.N.,; Investigation: M.R, S.K.,M.S., Y.S.C., G.F.N.,; Writing-oroginal draft preparation: M.R.,; Writing-review and editing: M.R, S.K.,; Supervision: P.Y, S.K., G.F.N.

Funding: This review article received no external funding.

Conflicts of Interest: The authors declare no conflict of interest.

References

[1] Dar, R. A.; Shahnawaz, M.; Ahanger, M. A.; Majid, I. ul. Exploring the Diverse Bioactive Compounds from Medicinal Plants: A Review. *J. Phytopharm.*, **2023**, *12*(3), 189–195. https://doi.org/10.31254/phyto.2023.12307

[2] Kristoferson Lulan, T. Y.; Fatmawati, S.; Santoso, M.; Ersam, T. Antioxidant Capacity of Some Selected Medicinal Plants in East Nusa Tenggara, Indonesia: The Potential of *Sterculia Quadrifida* R.Br. *Free Radicals Antioxidants*, **2018**, *8*(2), 96–101. https://doi.org/10.5530/fra.2018.2.15

[3] Rollando, R.; Warsito, W.; Masruri, M.; Widodo, W. Potential Therapeutic Use of *Sterculia Quadrifida* R.Br and Sterculia Foetida Linn.: Review. *Asian J. Plant Sci.*, **2020**, *19*(4), 325–334. https://doi.org/10.3923/ajps.2020.325.334

[4] Rollando, R.; Alfanaar, R. Cytotoxic Effect of 2,3-Dihydro-6-Hydroxy-2-Methylenenaphtho[1,2-b] Furan-4,5-Dione Compound from the Bark of Faloak (*Sterculia Quadrifida* R.Br) in Breast Cancer Cells T47D. *Pharmaciana*, **2017**, *7*(2), 289. https://doi.org/10.12928/pharmaciana.v7i2.6699

[5] Siswadi & Saragih, G. S. Kandungan Flavonoid Total Kulit Batang Beberapa Famili Sterculiaceae; Faloak (*Sterculia Quadrifida* R. Br.) Pterigota (Pterygota Alata (Roxb.) R. Br.) Dan Nitas (Sterculia Foetida L.). In *Prosiding Seminar Nasional POKJANAS TOI*; 2017; pp 112–118.

[6] Rollando, R.; Monica, E.; Afthoni, M. H.; Warsito, W.; Masruri, M.; Widodo, N. A Phenylpropanoid Compound from the Seeds of *Sterculia Quadrifida* and Its Cytotoxic Activity. *Trop. J. Nat. Prod. Res.*, **2023**, *7*(6), 3203–3208. https://doi.org/10.26538/tjnpr/v7i6.21

[7] Dillak, H. I.; Kristiani, E. B. E.; Kasmiyati, S. Secondary Metabolites and Antioxidant Activity of Ethanolic Extract of Faloak (*Sterculia Quadrifida*). *Biosaintifika*, **2019**, *11*(3), 296–303. https://doi.org/10.15294/biosaintifika.v11i3.20736

[8] Amin, A.; Wunas, J.; Anin, Y. M. UJI AKTIVITAS ANTIOKSIDAN EKSTRAK ETANOL KLIKA FALOAK (*Sterculia Quadrifida* R.Br) DENGAN METODE DPPH (2,2-Diphenyl-1-Picrylhydrazyl). *J. Fitofarmaka Indones.*, **2016**, *2*(2), 111–114. https://doi.org/10.33096/jffi.v2i2.180

[9] Rollando, R.; Prilianti, K. R. *Sterculia Quadrifida* R.Br Ethyl Acetate Fraction Increases Cisplatin Cytotoxicity on T47D Breast Cancer Cells. *Int. J. Pharm. Res.*, **2018**, *10*(3), 204–212. https://doi.org/10.31838/ijpr/2018.10.03.072

[10] Siswadi, S.; Saragih, G. S.; Rianawati, H. Potential Distributions and Utilization of Faloak (*Sterculia Quadrifida* R. Br 1844) on Timor Island , East Nusa Tenggara Potential Distributions and Utilization of Faloak. **2022**, No. March 2020.

[11] Siswadi, S.; Saragih, G. S. Phytochemical Analysis of Bioactive Compounds in Ethanolic Extract of *Sterculia Quadrifida* R.Br. *AIP Conf. Proc.*, **2021**, *2353*. https://doi.org/10.1063/5.0053057

[12] Faramayuda, F.; Julia Ratnawati; Akhirul Kahfi Syam. KARAKTERISASI FARMAKOGNOSI DAUN FALOAK (*Sterculia Quadrifida* R.Br). *Med. Sains J. Ilm. Kefarmasian*, **2022**, *7*(2), 173–180. https://doi.org/10.37874/ms.v7i2.322

[13] Soeharto, F.; Tenda, P. E. Soeharto, F., & Tenda, P. E. (2018). Antioxidant Activity of Instant Faloak (*Sterculia Quadrifida* R. Br.) from Kupang-East Nusa Tenggara by the Use DPPH (1, 1-Difenyl-2-Picrylhydrazyl) Free Radical Method. Proceeding 1st. International Conference Health P. In *Proceeding 1st. International Conference Health Polytechnic of Kupang*; 2018; pp 454–462.

[14] Darojati, U. A.; Murwanti, R.; Hertiani, T. *Sterqulia Quadrifida* R.Br: A Comprehensive Review of Ethnobotany, Phytochemistry, Pharmacology and Toxicology. *JPSCR J. Pharm. Sci. Clin. Res.*, **2022**, *7*(1), 1. https://doi.org/10.20961/jpscr.v7i1.52244

[15] Gardens, R. B. M. *Sterculia quadrifida* R.Br. https://bie.ala.org.au/species/https://id.biodiversity.org.au/node/apni/2914772#overview. (accessed Jul 27, 2024).

[16] Ranta, F.; Nawawi, D.; Pribadi, E.; Syafii, W. Aktivitas Anticendawan Zat Ekstraktif Faloak (*Sterculia Comosa Wallich*). *J. Ilmu dan Teknol. Kayu Trop.*, **2012**, *10*(1), 60.

[17] Siswadi; Saragih, G. S.; Rianawati, H. Potential Distributions and Utilization of Faloak (*Sterculia Quadrifida* R.Br 1844) on Timor Island, East Nusa Tenggara. *Int. Conf. For. Biodivers.*, **2013**, No. July 2013, 165–171.

[18] Cheikhyoussef, A.; Shapi, M.; Matengu, K.; Mu Ashekele, H. Ethnobotanical Study of Indigenous Knowledge on Medicinal Plant Use by Traditional Healers in Oshikoto Region, Namibia. *J. Ethnobiol. Ethnomed.*, **2011**, *7*(1), 10. https://doi.org/10.1186/1746-4269-7-10

[19] Siswadi, S.; Rianawati, H.; Saragih, G. *Utilization of Faloak Bark (Sterculia Quadrifida R. Br.) as Herbal Medicinal Raw Material on Timor Island. In Proceedings of the Savana Biodiversity of Nusa Tenggara*; 2016. https://doi.org/10.5281/zenodo.3353763

[20] Rollando, R.; Engracia, M.; Monica, E.; Siswadi, S. Immunomodulatory Activity Test of Syrup Dosage Form of Combination Phyllantus Niruri Linn. And *Sterculia Quadrifida* R.Br. Extract. *Int. J. Res. Pharm. Sci.*, **2020**, *11*(1), 191–199. https://doi.org/10.26452/ijrps.v11i1.1806

[21] Akter, K.; Barnes, E. C.; Brophy, J. J.; Harrington, D.; Community Elders, Y.; Vemulpad, S. R.; Jamie, J. F. Phytochemical Profile and Antibacterial and Antioxidant Activities of Medicinal Plants Used by Aboriginal People of New South Wales, Australia. *Evidence-based Complement. Altern. Med.*, **2016**, *2016*. https://doi.org/10.1155/2016/4683059

[22] Kale, A.; Gawande, S.; Kotwal, S. Cancer Phytotherapeutics: Role for Flavonoids at the Cellular Level. *Phyther. Res.*, **2008**, *22* (5), 567–577. https://doi.org/10.1002/ptr.2283

[23] Altemimi, A.; Lakhssassi, N.; Baharlouei, A.; Watson, D. G.; Lightfoot, D. A. Phytochemicals: Extraction, Isolation, and Identification of Bioactive Compounds from Plant Extracts. *Plants*, **2017**, *6*(4). https://doi.org/10.3390/plants6040042

[24] GRACE SEREPINA SARAGIH; SISWADI SISWADI. Antioxidant Activity of Plant Parts Extracts From *Sterculia Quadrifida* R. Br. *Asian J. Pharm. Clin. Res.*, **2019**, *12*(7), 143–148. https://doi.org/10.22159/ajpcr.2019.v12i7.33261

[25] Ben Ahmed, Z.; Yousfi, M.; Viaene, J.; Dejaegher, B.; Demeyer, K.; Mangelings, D.; Heyden, Y. Seasonal, Gender and Regional Variations in Total Phenolic, Flavonoid, and Condensed Tannins Contents and in Antioxidant Properties from *Pistacia Atlantica* Ssp. Leaves. *Pharm. Biol.*, **2017**, *55*. https://doi.org/10.1080/13880209.2017.1291690

[26] Santoso, B.; Anggraeni, R.; Aulia, P.; Suhendi, A.; Hanwar, D.; Haryoto, H.; Utami, W. *Aktivitas Antioksidan Ekstrak Etanol Dan Fraksi Kulit Batang Kepel (Stelechocarpus Burahol Blume Hook & Thomson) Menggunakan Metode DPPH Dan CUPRAC*; 2017.

[27] Nardini, M.; Garaguso, I. Characterization of Bioactive Compounds and Antioxidant Activity of Fruit Beers. *Food Chem.*, **2020**, *305*, 125437. https://doi.org/https://doi.org/10.1016/j.foodchem.2019.125437

[28] Bustanussalam; Hapsari, Y.; Rachman, F.; Septiana, E.; Simanjuntak, P.; Heliyawati, L.; Noviany, I. Antidiabetic Activity of Cinnamon Bark Extract (*Cinnamomum Burmannii* (Nees \\& T.Nees) Blume). *AIP Conf. Proc.*, **2023**, *2606*(1), 20009. https://doi.org/10.1063/5.0118405

[29] Nazarudin, M. F.; Alias, N. H.; Sharifuddin, N.; Zainal Abidin, A.; Ahmad, M. I.; Mazli, N. A. I. N.; Natrah, I.; Aliyu-Paiko, M.; Isha, A. Preliminary Evaluation of the Biochemical and Antioxidant Properties of Seaweed Species Predominantly Distributed in Peninsular Malaysia. *J. Fish. Environ.*, **2021**, *45*(2 SE-Articles), 119–133.

[30] Rollando, R.; Siswadi, S. Penelusuran Potensi Aktivitas Sitotoksik Fraksi Kulit Batang Tumbuhan Faloak (*Sterculia Quadrifida* R. Br). *J. Ilmu Farm. dan Farm. Klin.*, **2016**, *13*(1), 27–32.

[31] Rollando, R.; Alfanaar, R. Cytotoxic Effect of 2,3-Dihydro-6-Hydroxy 2-Methylenenaphtho[1,2-b] Furan-4,5-Dione Compound from the Bark of Faloak (*Sterculia Quadrifida* R.Br) in Breast Cancer Cells T47D. *Pharmaciana*, **2017**, *7*, 289–294. https://doi.org/10.12928/pharmaciana.v7i2.6699

[32] Rollando, R.; Afthoni, M.; Monica, E. In Vitro Cytotoxic Potential of *Sterculia Quadrifida* Leaf Extract Against Human Breast Cancer Cell Lines. *Trop. J. Nat. Prod. Res.*, **2022**, *6*, 1228–1232. https://doi.org/10.26538/tjnpr/v6i8.12

[33] Susanto, F. . Potential Fraction of Antibacterial and Anti-Radical Activity of Faloak Bark (*Sterculia Quadrifida* R.Br).; 2019.

[34] Özen, H.; Başhan, P. D. M.; Toker, Z.; Keskin, C. 3-Hydroxy Fatty Acids from the Flowers of Hypericum Lysimachioides Var. Lysimachioides. *Turkish J. Chem.*, **2004**, *28*, 223–226.

[35] Djoru, M. R.; Hetharia, G.; Adi, I.; Neonufa, G.; Tamonob, A.; Purwadi, R. *Characterization of Antioxidant Activity Forest Honey Enriched with Red Ginger Extract (Zingiber Officinale Var. Rubrum)*; 2024. https://doi.org/10.1063/5.0193707

[36] Martemucci, G.; Costagliola, C.; Mariano, M.; D'andrea, L.; Napolitano, P.; D'Alessandro, A. G. Free Radical Properties, Source and Targets, Antioxidant Consumption and Health. *Oxygen*, **2022**.

[37] Dauqan, E.; Halimah; Abdullah, A.; Mohd-Kasim, Z. Effect of Different Vegetable Oils (Red Palm Olein, Palm Olein, Corn Oil and Coconut Oil) on Lipid Profile in Rat. *Food Nutr. Sci.*, **2011**, *2*, 253–258. https://doi.org/10.4236/fns.2011.24036

[38] Lu, W.; Shi, Y.; Wang, R.; Su, D.; Tang, M.; Liu, Y.; Li, Z. Antioxidant Activity and Healthy Benefits of Natural Pigments in Fruits: A Review. *Int. J. Mol. Sci.*, **2021**, *22*, 4945. https://doi.org/10.3390/ijms22094945

[39] Do Nascimento, L. D.; de Moraes, A. A. B.; da Costa, K. S.; Galúcio, J. M. P.; Taube, P. S.; Costa, C. M. L.; Cruz, J. N.; Andrade, E. H. de A.; de Faria, L. J. G. Bioactive Natural Compounds and Antioxidant Activity of Essential Oils from Spice Plants: New Findings and Potential Applications. *Biomolecules*, **2020**, *10* (7), 1–37. https://doi.org/10.3390/biom10070988

[40] Hayat, J.; Akodad, M.; Moumen, A.; Baghour, M.; Skalli, A.; Ezrari, S.; Belmalha, S. Phytochemical Screening, Polyphenols, Flavonoids and Tannin Content, Antioxidant Activities and FTIR Characterization of *Marrubium Vulgare* L. from 2 Different Localities of Northeast of Morocco. *Heliyon*, **2020**, *6* (11), e05609. https://doi.org/https://doi.org/10.1016/j.heliyon.2020.e05609

[41] GRACE SEREPINA SARAGIH; SISWADI SISWADI. Antioxidant Activity of Plant Parts Extracts From *Sterculia Quadrifida* R. Br. *Asian J. Pharm. Clin. Res.*, **2019**, No. July 2019, 143–148. https://doi.org/10.22159/ajpcr.2019.v12i7.33261

[42] Hematpoor, A.; Paydar, M.; Liew, S. Y.; Sivasothy, Y.; Mohebali, N.; Looi, C. Y.; Wong, W. F.; Azirun, M. S.; Awang, K. Phenylpropanoids Isolated from *Piper Sarmentosum Roxb*. Induce Apoptosis in Breast Cancer Cells through Reactive Oxygen Species and Mitochondrial-Dependent Pathways. *Chem. Biol. Interact.*, **2018**, *279*, 210–218. https://doi.org/10.1016/j.cbi.2017.11.014

[43] Reid, K. A.; Jäger, A. K.; Light, M. E.; Mulholland, D. A.; Staden, J. Van. Phytochemical and Pharmacological Screening of Sterculiaceae Species and Isolation of Antibacterial Compounds. *J. Ethnopharmacol.*, **2005**, *97*(2), 285–291. https://doi.org/https://doi.org/10.1016/j.jep.2004.11.010

[44] Xia, P.; Shuang, S.; Feng, Z.; Zhang, P. Chemical Constituents from Leaves of *Sterculia Foetida*. *Zhongguo Zhong Yao Za Zhi*, **2009**, *34*, 2604–2606.

[45] Tian, F.; Woo, S. Y.; Lee, S. Y.; Park, S. B.; Zheng, Y.; Chun, H. S. Antifungal Activity of Essential Oil and Plant-Derived Natural Compounds against Aspergillus Flavus. *Antibiotics*, **2022**, *11*(12). https://doi.org/10.3390/antibiotics11121727.

[46] Mir, S. A.; Dar, A.; Hamid, L.; Nisar, N.; Malik, J. A.; Ali, T.; Bader, G. N. Flavonoids as Promising Molecules in the Cancer Therapy: An Insight. *Curr. Res. Pharmacol. Drug Discov.*, **2024**, *6* (November 2023), 100167. https://doi.org/10.1016/j.crphar.2023.100167

[47] Galli, C. L.; Cinelli, S.; Ciliutti, P.; Melzi, G.; Marinovich, M. Aloe-Emodin, a Hydroxyanthracene Derivative, Is Not Genotoxic in an in Vivo Comet Test. *Regul. Toxicol. Pharmacol.*, **2021**, *124*, 104967. https://doi.org/https://doi.org/10.1016/j.yrtph.2021.104967

[48] Loschi, F.; Faggian, M.; Sut, S.; Ferrarese, I.; Maccari, E.; Peron, G.; Dall'Acqua, S. Development of an LC–DAD–MS-Based Method for the Analysis of Hydroxyanthracene Derivatives in Food Supplements and Plant Materials. *Molecules*. 2022. https://doi.org/10.3390/molecules27061932

[49] Kapoor, B.; Kapoor, D.; Gautam, S.; Singh, R.; Bhardwaj, S. Dietary Polyunsaturated Fatty Acids (PUFAs): Uses and Potential Health Benefits. *Curr. Nutr. Rep.*, **2021**, *10*(3), 232–242. https://doi.org/10.1007/s13668-021-00363-3

[50] Shintawati; Widodo, Y. R.; Ermaya, D. Yield and Quality Improvement of Candlenut Oil by Microwave Assisted Extraction (MAE) Methods. *IOP Conf. Ser. Earth Environ. Sci.*, **2021**, *1012* (1). https://doi.org/10.1088/1755-1315/1012/1/012024

[51] Trustinah; Kasno, A. Karakterisasi Kandungan Asam Lemak Beberapa Genotipe Kacang Tanah. *Penelit. Pertan. Tanam. Pangan*, **2014**, *31*(3), 145–151.

[52] Aquino-Bolaños, E. N.; Mapel-Velazco, L.; Martín-del-Campo, S. T.; Chávez-Servia, J. L.; Martínez, A. J.; Verdalet-Guzmán, I. Fatty Acids Profile of Oil from Nine Varieties of Macadamia Nut. *Int. J. Food Prop.*, **2017**, *20*(6), 1262–1269. https://doi.org/10.1080/10942912.2016.1206125

[53] Özcan, M. M.; Matthäus, B.; Aljuhaimi, F.; Mohamed Ahmed, I. A.; Ghafoor, K.; Babiker, E. E.; Osman, M. A.; Gassem, M. A.; Alqah, H. A. S. Effect of Almond Genotypes on Fatty Acid Composition, Tocopherols and Mineral Contents and Bioactive Properties of Sweet Almond (*Prunus Amygdalus Batsch* Spp. Dulce) Kernel and Oils. *J. Food Sci. Technol.*, **2020**, *57*(11), 4182–4192. https://doi.org/10.1007/s13197-020-04456-9

[54] Sheela, D.; Uthayakumari, F. GC-MS Analysis of Bioactive Constituents from Coastal Sand Dune Taxon-Sesuvium Portulacastrum. *Biosci. Discov.*, **2013**, *4*, 47–53.

[55] Krishnaveni, M.; Dhanalakshmi, R.; Nandhini, N. GC-MS Analysis of Phytochemicals, Fatty Acid Profile, Antimicrobial Activity of Gossypium Seeds. *Int. J. Pharm. Sci. Rev. Res.*, **2014**, *27*(1), 273–276.

[56] Rahayu, A. A. D.; Prihantini, A. I.; Krisnawati; Nugraheni, Y. M. M. A. Chemical Components of Different Parts of Strychnos Ligustrina, a Medicinal Plant from Indonesia. *IOP Conf. Ser. Earth Environ. Sci.*, **2022**, *959*(1). https://doi.org/10.1088/1755-1315/959/1/012061

[57] Joshua, O.; Omowanle, J.; Ayo, R. J.; Habila, J.; Ilekhaize, J.; Adegbe, E. A. Physico-Chemical and Gc-Ms Analysis of Some Selected Plant Seed Oils; Castor, Neem and Rubber Seed Oils. *FUW Trends Sci. Technol. Journal, www.ftstjournal.com e-ISSN*, **2018**, *3*(2), 644–651.

[58] De Meester, F.; Watson, R. R. *Handbook of Lipids in Human Function: Fatty Acids*; 2015.

[59] Kumaravel, S.; Kalaiselvi, P. Determination of Bioactive Components of *Plectranthus Amboinicus Lour* by GC-MS Analysis. M. Uma; 2011.

[60] Msanne, J.; Kim, H.; Cahoon1, E. B. Biotechnology Tools and Applications for Development of Oilseed Crops with Healthy Vegetable Oils. **2020**.

[61] García, V. L. The Omega 7 as a Health Strategy for the Skin and Mucous Membranes. *EC Nutr.*, **2019**, *14*(6), 484–489.

[62] Zaloga, G. P. Narrative Review of N-3 Polyunsaturated Fatty Acid Supplementation upon Immune Functions, Resolution Molecules and Lipid Peroxidation. *Nutrients*. 2021. https://doi.org/10.3390/nu13020662

[63] Pretorius, C. J.; Zeiss, D. R.; Dubery, I. A. The Presence of Oxygenated Lipids in Plant Defense in Response to Biotic Stress: A Metabolomics Appraisal. *Plant Signal. Behav.*, **2021**, *16*(12). https://doi.org/10.1080/15592324.2021.1989215

[64] Delgado, G. E.; Krämer, B. K.; Lorkowski, S.; März, W.; von Schacky, C.; Kleber, M. E. Individual Omega-9 Monounsaturated Fatty Acids and Mortality-The Ludwigshafen Risk and Cardiovascular Health Study. *J. Clin. Lipidol.*, **2017**, *11*(1), 126-135.e5. https://doi.org/10.1016/j.jacl.2016.10.015.

[65] Chowdhury, R.; Steur, M.; Patel, P. S.; Franco, O. H. Chapter 10 - Individual Fatty Acids in Cardiometabolic Disease; Watson, R. R., De Meester, F. B. T.-H. of L. in H. F., Eds.; AOCS Press, 2016; pp 207–318. https://doi.org/https://doi.org/10.1016/B978-1-63067-036-8.00010-X

ASEAN
Journal of Scientific and Technological Reports
Online ISSN:2773-8752

Research article

Facile Assembly of Herbal-Organic and Inorganic Composite for Enhancing Antioxidant and Antibacterial Efficiency

Sonchai Intachai[1, 2], Thapat Jitthiang[3], Jiraporn Chomanee[3], Panita Sumanatrakul[4], and Tanchanok Poonsin[3*]

[1] Innovative Materials Chemistry for Environment Center, Thaksin University, Phatthalung, 93210, Thailand
[2] Faculty of Science and Digital Innovation, Thaksin University, Phatthalung, 93210, Thailand
[3] Faculty of Education, Thaksin University, Songkhla, 90000, Thailand
[4] Faculty of Engineering, Thaksin University, Phatthalung, 93210, Thailand
[*] Correspondence: tanchanok.p@tsu.ac.th

Citation:
Intachai, S.; Jitthiang, T.; Chomanee, J.; Sumanatrakul, P.; Poonsin, T. Facile assembly of herbal-organic and inorganic composite for enhancing antioxidant and antibacterial efficiency. *ASEAN J. Sci. Tech. Report.* **2026**, *29*(2), e260168. https://doi.org/10.55164/ajstr.v29i2.260168.

Article history:
Received: July 7, 2025
Revised: October 13, 2025
Accepted: October 18, 2025
Available online: January 18, 2026

Abstract: This study focused on the fabrication of multifunctional organic–inorganic composites composed of mixed herbal extracts from mangosteen peel (MP), pomelo peel (PP), and cucumber (CP) peel, biomass-derived activated carbon (AC), and zinc oxide@ZnAl-layered double hydroxide (ZnO@ZnAl-LDH) by a mechanochemical solid–solid process. The as-synthesized composites were characterized using XRD, FT-IR, and zeta potential analyses, and their biological activities were evaluated. The MP/PP/CP@AC/LDH composite exhibited superior antioxidant performance, with IC_{50} values of 136.6 μg/mL for DPPH radicals and 195.8 μg/mL for ABTS radicals, which were significantly lower than those of single-extract or single-host systems. The enhanced radical-scavenging behavior was attributed to the synergistic host–guest and guest–guest interactions among ZnO, ZnAl-LDH, AC, and bioactive compounds. Moreover, the composite demonstrated the pronounced antibacterial activity against *Staphylococcus aureus* and partial inhibition toward *Escherichia coli*, owing to reactive oxygen species (ROS) generation and membrane disruption. These findings suggested that MP/PP/CP@AC/LDH was a promising multifunctional herbal material for antioxidant and antimicrobial applications.

Keywords: Herbal extract; Zinc oxide; ZnAl-layered double hydroxide; antioxidant; antibacterial

1. Introduction

In Thailand, herbal remedies have for a long time played a significant role in drug, healthy innovation, and healthcare and body-cleaning goods [1, 2], especially, herbal extracts from mangosteen, pomelo, and cucumber, which are known for their remarkable antibacterial, antioxidant, moisturizing and anti-aging properties [3-6]. However, several active compounds are unstable organic substances that are easily degraded upon exposure to light, oxygen and chemical reactions, thereby reducing biological effectiveness [7]. Typically, the application of herbal extract-based ingredients is preferred in the solid state, because they are easy to use, cost-effective to store, and relatively stable [8]. To address, many attempts have been made to encapsulate crude extracts by surfactant [9] and inorganic host [10]. Furthermore, the antioxidant performance remains steadily high over a long period [7, 9]. In particular, the incorporation of herbal extract in activated carbon (AC) has received much interest as a host-

guest material, as the results of its stable 3D carbonaceous structure, low toxicity, large surface area and H-bonding active sites [11]. Moreover, AC also supports higher stability of organic compounds, and acts as an efficient adsorbent of toxic species [12, 13]. Because most crude extracts show lower antibacterial effectiveness than pure essential oil [14], their antibacterial function must be improved by mixing with another material such as metal oxide and metal hydroxide [7, 15].

Zinc oxide (ZnO), a well-known metal oxide, is recognized as an efficient UV-light absorber and antimicrobial agent [16]. Owing to its relatively low toxicity, ZnO particles have been a promising candidate for use in medical devices and pharmaceutical formulations for controlling *Staphylococcus aureus (S. aureus)* and *Escherichia coli* (*E. coli*) infections [15, 17]. However, bulk ZnO particles obtained by using a co-precipitation method exhibit lower biological activity due to the smaller surface area relative to ZnO nanoparticles [17]. The formation of ZnO nanoparticles in/on an inorganic host has been intensively studied because of the larger surface area, higher stability, and multifunctional merits. Layered double hydroxide (LDH), a general formula of $[M_{1-x}^{2+}M_x^{3+}(OH)_2]^{x+}(A^{n-})_{x/n}\cdot yH_2O$, where M^{2+} = divalent metal cation (Mg^{2+}, Co^{2+}, Zn^{2+}, Ni^{2+}), M^{3+} = trivalent metal cation (Al^{3+}, Fe^{3+}, Cr^{3+}), A^{n-} = interlayer anion (CO_3^{2-}, NO_3^-, Cl^-), has received much attention as a host material due to large surface area, anion exchange and swelling capacities, as well as optical, magnetic, antibacterial and catalytic properties [18]. However, LDH structures can be synthesized in various forms by adjusting the types of M^{2+}, M^{3+}, and A^{n-} species. Among them, ZnAl-LDH has been widely utilized for its antibacterial and pharmacological activities [19]. In addition, the incorporation of ZnO particles onto ZnAl-LDH can further tailor its antibacterial efficiency due to the co-functional effect [7].

The present research was focused on the utilization of AC and ZnAl-LDH solid materials for mixing herbal extracts by a mechanochemical solid-solid reaction [20], which was a simple method for generating a mixed herbal extract-powder based on an organic-inorganic host-guest composite. Many studies have reported that the incorporation of herbal organic compounds can provide synergistic effects on biological properties. However, the formation of such materials in the solid state still faces several challenges, including complicated synthesis procedures and the use of toxic substances [8-11]. In this work, the waste peels of mangosteen (*Garcinia mangostana L.*), pomelo (*Citrus maxima*), and cucumber (*Cucumis sativus L.*) were selected to attain organic extracts because they are abundant throughout Thailand, and contain abundant bioactive substances with strong antioxidant activity. The AC was developed from Krajood (*Lepironia articulata* Retz. Domin) residue, which is a waste-to-wealth route. This study aims to create a valuable material for herbal innovation with both efficient antioxidant and antibacterial activities.

2. Materials and Methods

2.1 Materials

Zinc nitrate hexahydrate ($Zn(NO_3)_2\cdot 6H_2O$) and aluminum nitrate nonahydrate ($Al(NO_3)_3\cdot 9H_2O$) were supported by Loba Chemie PVT. LTD. Gallic acid, 2,2-diphenyl-1-picrylhydrazyl (DPPH), and 2,2′-azino-bis(3-ethylbenzothiazoline-6-sulfonic acid-diammonium salt (ABTS)) were obtained from Sigma Aldrich. Folin-Ciocalteu reagent was obtained from Fisher Scientific. Ammonia (NH_3, 98%) and phosphoric acid (H_3PO_4, 98%) were purchased from Asia Pacific Specialty Chemicals LTD. All chemicals are AR-grade substances that were used directly without any characterization.

2.2 Preparation of AC

The long lines of waste Krajood were cut into small pieces, washed several times with water, collected and dried at 110 °C for 24 h, and finally carbonized at approximately 400 °C for 2 h. The black pieces were spun until achieving fine powder through a 60 mesh-sieve, soaked in distilled water containing excess H_3PO_4 under vigorous shaking for 24 h. The resulting powder was washed several times until achieving the supernatant pH ~ 7, separated with a thin white cloth, and dried at 110 °C for 24 h, finally calcined at 900 °C for 2 h. The activated carbon derived from Krajood residue was obtained, which was abbreviated as AC.

2.3 Preparation of ZnO@ZnAl-LDH

Firstly, the aqueous bimetallic mixture was conducted by mixing the appropriate $Zn(NO_3)_2$ and $Al(NO_3)_3$ amount of molar ratio of 3:1, and the concentrated ammonia was slowly dropped until the pH

reached 9.5 under strong magnetic stirring. The reactor was sealed with aluminium foil, and incubated at 80 °C for 24 h. After that, the precipitate was washed multiple times with DI water until obtaining the supernatant pH ~ 7, then separated with centrifugation, and dried at 80 °C for 24 h. The product powder was abbreviated as ZnO@ZnAl-LDH.

2.4 Preparation of herbal extracts

Each herbal peel (mangosteen, pomelo, or cucumber) was washed, cut into small pieces, and dried at 60 °C until its weight was constant. The extraction was soaked in 95% ethanol solvent at room temperature under vigorous shaking for 3 h, and ultrasonicated at 40 kHz for 30 min. To obtain the crude extract, the solution part was collected by a filter, and the mixed solvent was removed by evaporation and followed by freeze-dry. The crude extract of mangosteen, pomelo, and cucumber peels was abbreviated as MP, PP, and CP, respectively.

2.5 Preparation of organic-inorganic composites

The composites between organic (MP, PP, and/or CP) and inorganic (AC and/or ZnO@ZnAl-LDH) species were prepared by the solid-solid reaction, which comprised herbal extract, AC and ZnO@ZnAl-LDH with the weight ratio of 1:1:1. The reaction between 1 g extract and 1 g AC and/or 1 g ZnO@ZnAl-LDH in the presence of 1 mL acetone was carried out by grinding in the mortar for 30 min. For the mixed-extract batches, the total extract mass was 1.00 g, comprising 0.333 g mangosteen (MP), 0.333 g pomelo (PP), and 0.333 g cucumber (CP) (1:1:1 w/w/w), was then mechanically combined with 1.00 g AC and 1.00 g ZnO@ZnAl-LDH for 30 min, yielding composite powder.

2.6 Analysis of total phenolic content

Total phenolic contents of MP, PP, and CP extracts were analyzed by using the Folin-Ciocalteu colorimetric process. The appropriate amount of 10 mg/mL extract solution and 1.0 mL of 10% (v/v) Folin-Ciocalteu reagent were mixed under vortexing for 5 min, and then 1.6 mL of 7.5% (w/v) Na_2CO_3 solution was added under vortexing for further 30 s, and allowed the reaction in the dark for 30 min at room temperature. The absorbance of the resulting solution was measured at 725 nm to determine the total phenolic content (mg GAE/g extract) by the relationship to the calibration curve of gallic acid.

2.7 Antioxidant activities

For DPPH, 1.0 mg of sample was mixed with 5.0 mL of DPPH solution (10 ppm in ethanol), vortexed for 30 s, kept in the dark for 30 min, and read at 517 nm. For ABTS, the radicals were generated by mixing ABTS (7 mM) with potassium persulfate (2.45 mM) at a 1:1 (v/v) ratio in water and keeping the mixture in the dark for 16 h. Before use, the solution was diluted with ethanol to give an initial absorbance of 0.700 ± 0.020 at 734 nm. Then 1.0 mg of sample was added, and the volume was brought to 5.0 mL with the $ABTS^{\bullet+}$ solution, vortexed for 30 s, kept in the dark for 6 min, and read at 734 nm. Antioxidant activity (%) was calculated as the following equation,

$$\text{Antioxidant efficiency (\%)} = [(A_0 - A_s)/ A_0] \times 100$$

where A_0 is the control absorbance, and A_s is the sample absorbance. The half maximal inhibitory concentration (IC_{50}) of antioxidant (μg/mL) was also determined; all measurements were performed in triplicate and reported as mean ± SD.

2.8 Antibacterial activity

The antibacterial activities against *Staphylococcus aureus* (*S. aureus*) and *Escherichia coli* (*E. coli*) were evaluated using the Plate Count Agar (PCA) assay based on cell viability. Initially, the bacteria were precultured on the nutrient agar (NA) at 37 °C for 24 h, then suspended in 0.85% (w/v) NaCl solution, and adjusted to a turbidity of 10^8 CFU/mL. Subsequently, 5% (v/v) inoculum was introduced into 50 mL of nutrient broth (NB), followed by the addition of antibacterial samples. The inoculated cultures were incubated at 37 °C with shaking at 150 rpm for 24 h, where the bacterial viability was assessed using the spread plate technique on PCA at the serial dilutions ranging from 10^{-5} to 10^{-1} in comparison with the untreated control. The

experimental procedures for the preparation of precursors and their composites, as well as the biological evaluations, are summarized in Scheme 1.

2.9 Characterization

X-ray diffraction (XRD) pattern was recorded in the 2θ range of 5-70 ° by a PANalytical Empyrean powder diffractometer. The FT-IR spectra were analyzed by attenuated total reflection-Fourier transform infrared spectroscopy using a G8044AA-Agilent Technologies. Zeta potential of the product powder that was dispersed in DI water at 25 °C was measured using a Zetasizer (Nano ZS, Malvern, Worcestershire, UK). The absorption spectra of the herbal extract, and DPPH and ABTS radicals were investigated by a Shimadzu UV-1700 Pharmaspec UV-VIS spectrophotometer.

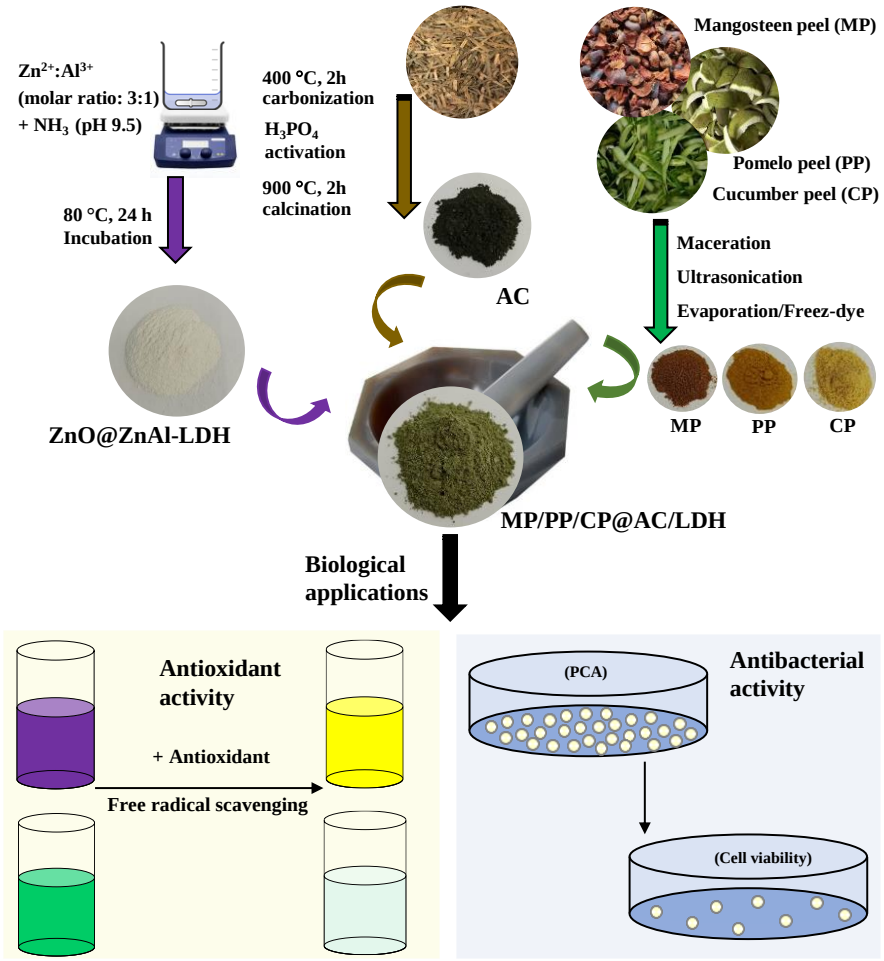

Scheme 1. Representation of preparation of herbal extracts, host materials, organic-inorganic composites, and their biological activities

3. Results and Discussion

3.1 Characterization

The crystalline features of the inorganic hosts and their composites were investigated by the XRD analysis, as depicted in Figure 1. The XRD pattern of AC (Figure 1a) displayed the broad diffraction peaks at 23.9 and 43.6° owing to the (*002*) and (*101*) reflections of a graphitic-like amorphous structure of activated carbon [20]. For ZnAl-LDH (Figure 1b), the diffraction peaks were observed at 11.6, 22.9, 33.8, 38.9, 45.5, 59.9 and 61.4° corresponding to the reflections of (*003*), (*006*), (*012*), (*015*), (*018*), (*110*) and (*113*) of a brucite-like LDH structure, respectively [8,10]. The basal spacing of the (*003*) plane was calculated to be 7.73 Å, and after subtracting the layer thickness (4.8 Å), the interlayer distance was 2.93 Å, which was consistent with the size

of intercalated carbonate ions (CO_3^{2-}) [18]. Additionally, the XRD peaks at 31.8, 34.5, 36.3, 47.5, 56.6, 62.9 and 68.0° were assigned to the (*100*), (*002*), (*101*), (*102*), (*110*), (*103*), and (*112*) planes of ZnO particles, respectively [16,17], indicating the presence of ZnO on the outer surface of ZnAl-LDH. For the MP/PP/CP@AC/LDH composite (Figure 1c), the XRD pattern displayed the reflections corresponding only to ZnAl-LDH and ZnO, with no distinct peaks attributable to AC or the organic extracts due to their low crystallinity [7, 20]. However, the presence of AC and herbal extracts in the composite was further described by later physicochemical characteristics.

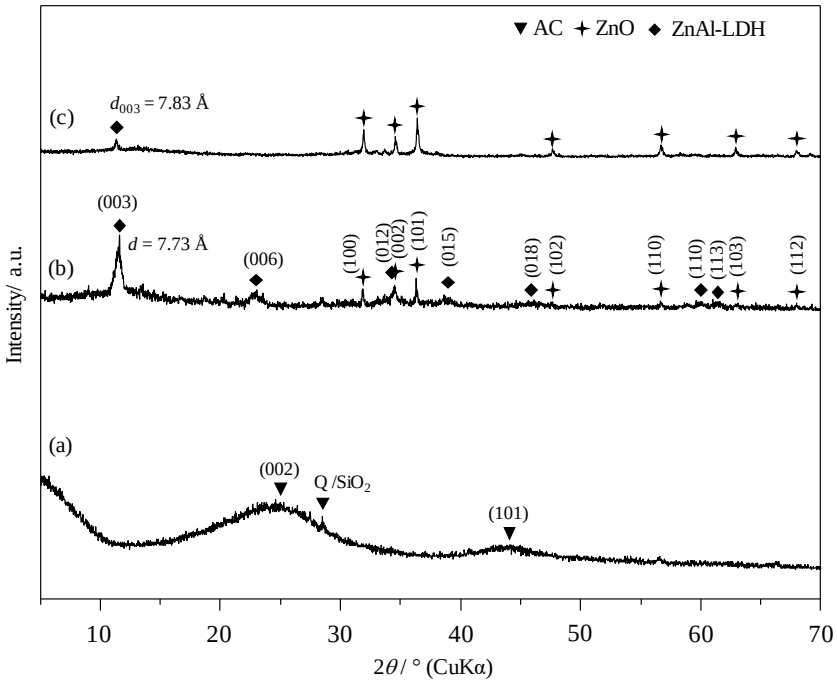

Figure 1. X-ray diffraction patterns of (a) AC, (b) ZnO@ZnAl-LDH, and (c) MP/PP/CP@AC/LDH

To consider the powder colors of the precursors and their corresponding products, ZnO@ZnAl-LDH, AC, and three plant extracts (MP, PP, and CP) showed distinct appearances, as seen in Figure 2. ZnO@ZnAl-LDH appeared white because both Zn^{2+} (d^{10}) and Al^{3+} ions are optically inactive in the visible light region [7]. The black color of AC was attributed to its strong light absorption capacity, resulting in almost no light reflection [20]. Meanwhile, the MP, PP, and CP extracts displayed dark brown, orange-brown, and yellow, respectively, which could be ascribed to the variations in their types and concentrations of bioactive compounds [18]. After the solid-state mixing of these precursors, the resulting composite powder of MP@AC/LDH, PP@AC/LDH, CP@AC/LDH, and MP/PP/CP@AC/LDH exhibited visibly different colors based on greenish-brown (Figure 2f), grayish-green (Figure 2g), yellowish-gray (Figure 2h), and brownish-green (Figure 2i), respectively. The color change might have resulted from blending the physical and chemical merits of white ZnO@ZnAl-LDH, black AC, and yellow-to-brown herbal extracts, suggesting the successful incorporation of AC, ZnO@ZnAl-LDH, and MP, PP, and/or CP in the composites [20].

Figure 2. Physical properties of powders (a) ZnO@ZnAl-LDH, (b) AC, (c) MP, (d) PP, (e) CP, (f) MP@AC/LDH, (g) PP@AC/LDH, (h) CP@AC/LDH, and (i) MP/PP/CP@AC/LDH

The FT-IR spectra were recorded to identify functional groups and confirm interactions among ZnO@ZnAl-LDH, AC, and the representative MP/PP/CP extract mixture. In Figure 3a, the characteristic bands attributed to M–O–M and/or M–O vibration modes appeared below 1000 cm^{-1}, while the broad absorption bands at 3286 and 1636 cm^{-1} were assigned to O–H stretching and H–O–H bending vibration modes of interlayer water, respectively [8, 19]. Additionally, the band at 1359 cm^{-1} corresponded to interlayer carbonate (CO_3^{2-}), confirming the successful formation of the LDH intercalated with CO_3^{2-} [7, 18]. In the FT-IR spectrum of AC (Figure 3b), the weak infrared bands at 1577 and 1027 cm^{-1} were observed, assigning to C=C and C–O vibration modes, in agreement with literature reports for activated carbon [13, 20]. For the MP/PP/CP@AC/LDH composite (Figure 3c), the combination of FT-IR features from ZnO@ZnAl-LDH (3286, 1539, and 1086 cm^{-1}), AC (1577 and 1027 cm^{-1}), and the plant extracts (2853–2962 cm^{-1} for C–H, 1605 and 1442 cm^{-1} for C=C aromatic/alkaloid rings, 1152–1280 cm^{-1} for C–O–C/C–O, and 600–1000 cm^{-1} for C–H out-of-plane) [1-2, 6]. The findings could further confirm that the bioactive organic compounds from the mixed extracts were successfully immobilized onto AC/LDH surface [8, 10].

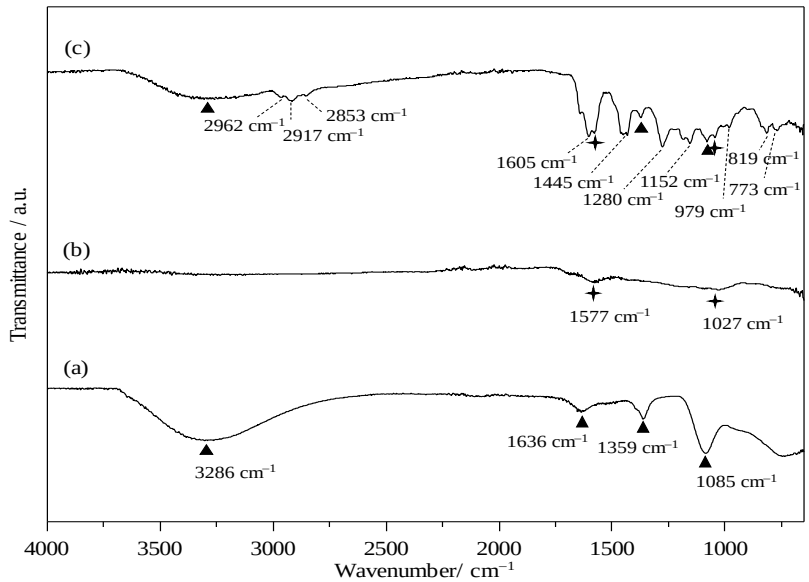

Figure 3. FT-IR spectra (a) ZnO@ZnAl-LDH, (b) AC, and (c) MP/PP/CP@AC/LDH

For further confirmation of the surface charge and interaction, the zeta potential of each sample was measured, as illustrated in Figure 4. It was found that ZnO@ZnAl-LDH, AC, MP, PP, CP, MP@AC/LDH, PP@AC/LDH, CP@AC/LDH and MP/PP/CP@AC/LDH exhibited the zeta potential values of +14.5, –28.2, –4.2, –3.6, –2.9, –11.2, –9.1, –7.7 and –6.8 mV, respectively. By referring, ZnO@ZnAl-LDH displayed positively charged surface because the LDH sheets were generated through the partial substitution of M^{2+} ions with M^{3+} ions [8,10]. In contrast, AC exhibited the negative surface-charge, which was attributed to the presence of functional groups such as hydroxyl (–OH) and carboxyl (–COOH) [20]. Regarding the composites, the zeta potential values were negative and intermediate between those of the pure extracts and AC (namely, more negative than the extracts but less negative than AC). The result might be due to the electrostatic interaction between the negatively charged AC and extracts, and the positively charged ZnO@ZnAl-LDH, confirming the integration of herbal extracts with both AC and ZnO@ZnAl-LDH in the composites [18, 20].

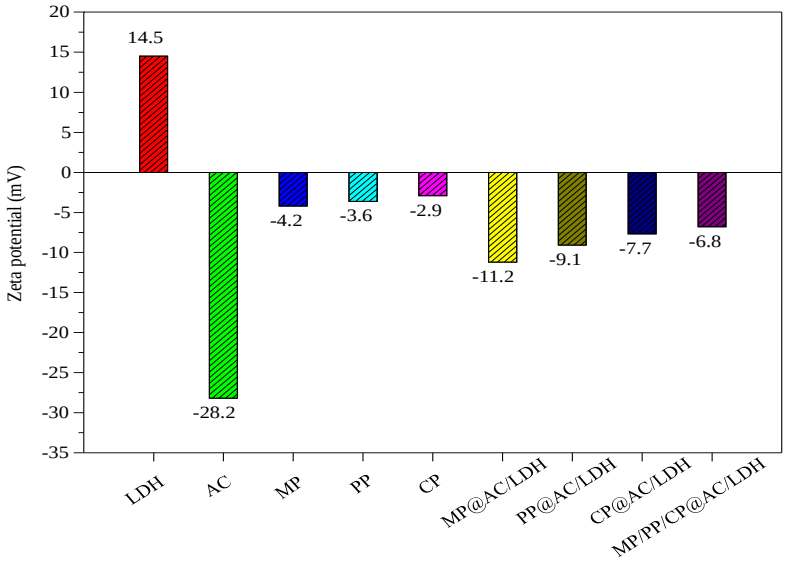

Figure 4. Zeta potential of precursors and composites

Table 1. Total phenolic content and capacity for radical scavenging activities

Material	Total phenolic content (mg GAE/g extract)	DPPH radical scavenging efficiency (%)	ABTS radical scavenging efficiency (%)	IC_{50} of radical scavenging (μg/mL)	
				DPPH	ABTS
ZnO@ZnAl-LDH	-	6.8 ± 0.35	5.6 ± 0.42	-	-
AC	-	1.7 ± 0.35	1.7 ± 0.40	-	-
MP	83.6	97.4 ± 1.79	87.3 ± 0.76	47.5 ± 0.65	61.0 ± 0.44
PP	55.2	86.0 ± 1.62	82.6 ± 0.45	77.3 ± 0.80	102.7 ± 0.72
CP	33.7	67.3 ± 0.71	64.8 ± 0.50	115.5 ± 0.86	143.3 ± 1.21
MP@AC	-	37.4 ± 0.53	33.4 ± 0.45	348.9 ± 1.40	387.7 ± 1.50
PP@AC	-	24.5 ± 0.50	21.1 ± 0.36	433.1 ± 1.21	500.2 ± 1.90
CP@AC	-	15.3 ± 0.50	13.8 ± 0.46	503.7 ± 2.26	563.3 ± 2.15
MP/PP/CP@AC	-	43.7 ± 0.30	40.3 ± 0.55	283.5 ± 1.35	342.5 ± 1.32
MP@LDH	-	48.0 ± 0.67	42.5 ± 0.56	253.1 ± 1.46	297.3 ± 1.23
PP@LDH	-	33.2 ± 0.50	29.1 ± 0.45	383.3 ± 1.53	416.2 ± 1.59
CP@LDH	-	27.6 ± 0.65	23.3 ± 0.56	408.7 ± 1.73	462.3 ± 1.76
MP/PP/CP@LDH	-	52.4 ± 0.62	46.1 ± 0.75	216.4 ± 2.20	247.2 ± 1.80
MP@AC/LDH	-	53.2 ± 0.45	47.8 ± 0.80	196.4 ± 2.10	235.6 ± 1.52
PP@AC/LDH	-	39.2 ± 0.56	33.3 ± 0.60	317.7 ±1.80	354.0 ± 1.31
CP@AC/LDH	-	34.9 ± 0.55	29.5 ± 0.72	366.3 ± 1.88	400.5 ± 1.75
MP/PP/CP@AC/LDH	-	62.4 ± 0.79	57.3 ± 0.35	136.6 ± 0.96	195.8 ± 1.36

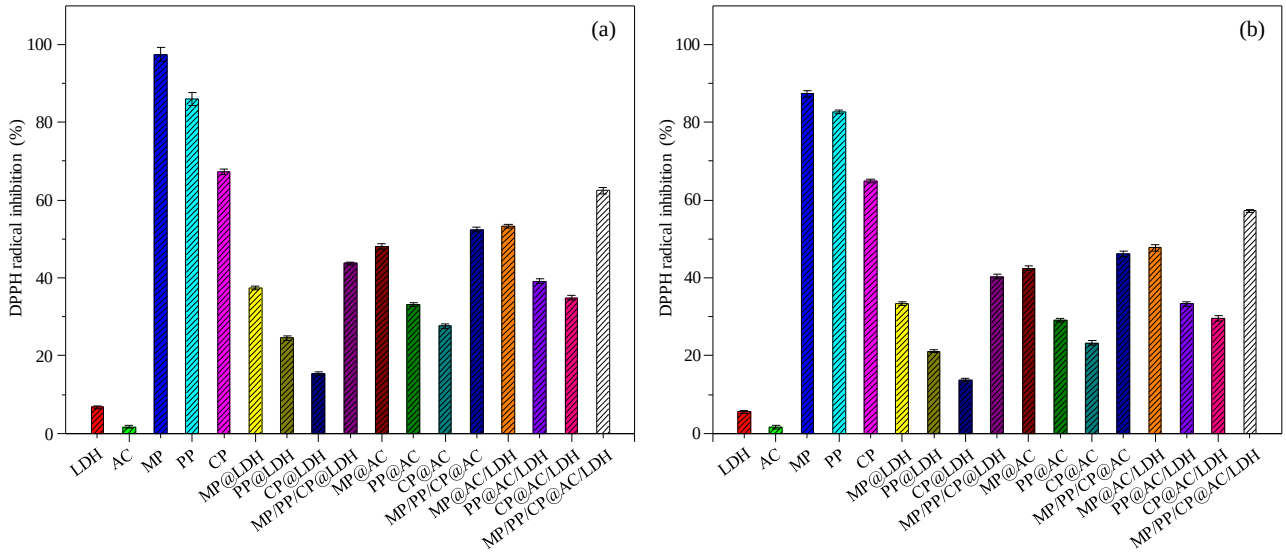

Figure 5. Inhibition efficiency of antioxidants for (a) DPPH radicals and (b) ABTS radicals in the dark.

3.2 Antioxidant activity

The antioxidant activities of various samples, including the herbal extracts (MP, PP, and CP), the host materials (AC, and ZnO@ZnAl-LDH), the composites of extracts with AC (MP@AC, PP@AC, CP@AC, and MP/PP/CP@AC), the composites of extracts with ZnO@ZnAl-LDH (MP@LDH, PP@LDH, CP@LDH, and MP/PP/CP@LDH), and the composites of extracts with both AC and ZnO@ZnAl-LDH (MP@AC/LDH, PP@AC/LDH, CP@AC/LDH, and MP/PP/CP@AC/LDH), were evaluated for scavenging DPPH and ABTS radicals. In Figure 5 and Table 1, the host materials (AC and ZnO@ZnAl-LDH) exhibited very low DPPH and ABTS radical scavenging efficiency (2-7%), suggesting poor antioxidant properties [4, 5]. Whereas all three extracts exhibited relatively high antioxidant activities, indicating strong radical-scavenging potential. In particular, MP showed the highest scavenging efficiencies with 97.4 ± 1.79% for DPPH radicals and 87.3 ± 0.76% for ABTS, compared with PP (86.0 ± 1.62% for DPPH radicals and 82.6 ± 0.45% for ABTS radicals) and CP (67.3 ± 0.71% for DPPH radicals and 64.8 ± 0.50% for ABTS radicals), which could be attributed to its higher total phenolic content (Table 1) [3-6]. For the composites formed between the extracts and ZnO@ZnAl-LDH, the DPPH radical scavenging profile ranged from 28 to 48% for DPPH radicals and 23 to 43% for ABTS radicals, which were higher than those observed in the composites formed with AC alone (15 to 37% for DPPH radicals and 14 to 33 for ABTS radicals). It could be explained by the advantageous properties of ZnO@ZnAl-LDH in the presence of hydroxyl groups and ZnO particles, acting as the effective reducing agents relative to AC [8,10]. Remarkably, by mixing the three extracts with a single host material, the antioxidant efficiencies significantly improved relative to the composites containing only a single extract. The findings might be due to the synergistic effects based on the host-guest and guest-guest interactions [21]. Furthermore, for the extracts combined with both host materials (AC and ZnO@ZnAl-LDH), the as-prepared composites displayed the higher antioxidant efficiency (44-52% for DPPH radicals and 40-46% for ABTS radicals) compared to those containing only a single host. It could be attributed to the cooperative interactions among host-guest and host-guest-host interactions, along with a more uniform distribution of the extracts on the surface of host materials [22, 23]. Importantly, the composite comprising the three extracts and both host materials (MP/PP/CP@AC/LDH) exhibited the highest scavenging inhibition of 62% for DPPH radicals and 57% for ABTS radicals, which might result from the stronger host-guest and host-guest-host interactions [21, 22].

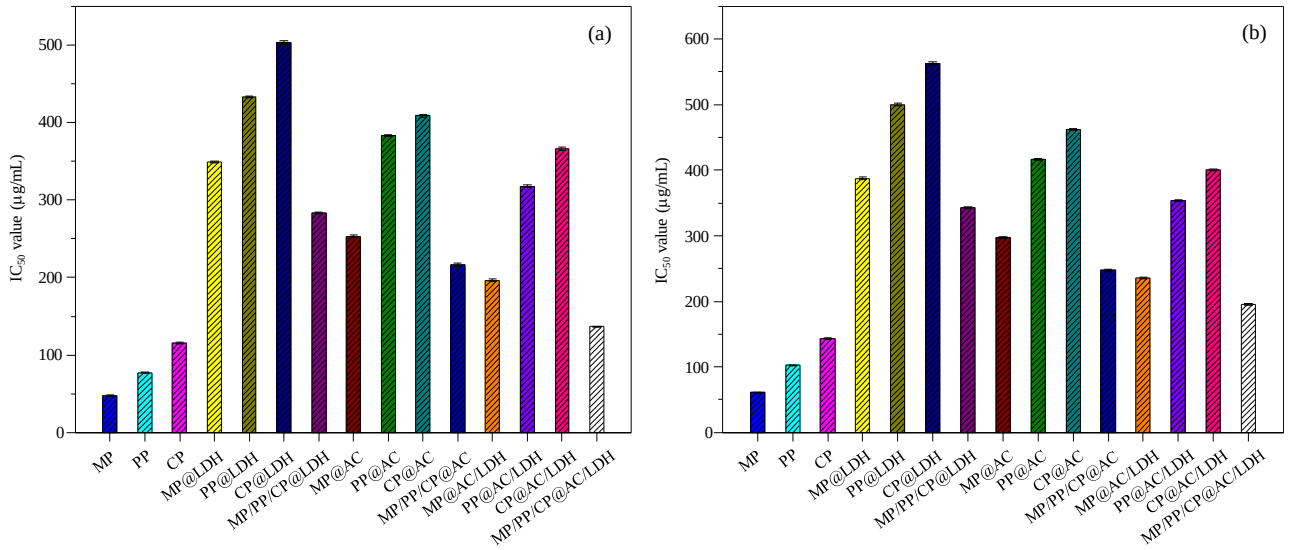

Figure 6. IC_{50} values (concentrations required to achieve 50% inhibition efficiency) of the antioxidant samples for (a) DPPH and (b) ABTS radicals.

The half inhibitory concentrations (IC_{50}) of DPPH and ABTS radicals for MP, PP, CP, MP@AC, PP@AC, CP@AC, MP/PP/CP@AC, MP@LDH, PP@LDH, CP@LDH, MP/PP/CP@LDH, MP@AC/LDH, PP@AC/LDH, CP@AC/LDH, and MP/PP/CP@AC/LDH are depicted in Figure 6 and listed in Table 1. The values ranged from 48–504 and 61–563 µg/mL for DPPH and ABTS radical scavenging activities, respectively, depending on the type of herbal extract, host material, and composite, as described above [1-2, 21-23]. Notably, DPPH showed higher inhibition than ABTS because DPPH was more sensitive to hydrogen-donating antioxidants, while ABTS involved both electron and hydrogen transfer, resulting in lower efficiency [24]. These findings could be indicative that MP/PP/CP@AC/LDH exhibited superior antioxidant performance compared to other herbal extracts such as *Zingiber officinale* extract (201.8 µg/mL) and its composite to LDH (349.2 µg/mL) [25], and essential oil of *Zingiber cassumunar* (1059.9 µg/mL) [26] for inhibiting DPPH radicals. Besides, the as-prepared composite exhibited the higher efficiency compared to Thai traditional herbal formulation, Ya-A (1600 µg/mL) [27], and the isolate of SWUF16-4.1 (283 µg/mL) [28].

Table 2. Antibacterial efficacy of precursors and composites

Antibacterial agents	Number of *S. aureus* viable cells (CFU/mL)			Number of *E. coli* viable cells (CFU/mL)		
	10^{-1}	10^{-3}	10^{-5}	10^{-1}	10^{-3}	10^{-5}
MP PP CP AC	> 300 colony			> 300 colony		
ZnO@ZnAl-LDH	< 30 colony	not detected	not detected			
MP/PP/CP@AC/LDH	not detected	not detected	not detected	> 300 colony	< 30 colony	< 30 colony

3.3 Antibacterial activity

The antibacterial activity against *Staphylococcus aureus* (*S. aureus*) and *Escherichia coli* (*E. coli*) of the herbal extracts (MP, PP and CP), host materials (AC and ZnO@ZnAl-LDH), and the composite (MP/PP/CP@AC/LDH) was evaluated using the plate count agar (PCA) method to determine the number of surviving bacterial colonies, as shown in Table 2. The results revealed that ZnO@ZnAl-LDH inhibited the growth of *S. aureus* more effectively than the single extract (MP, PP, and CP) or the AC host material. Among all tested samples, only ZnO@ZnAl-LDH precursor exhibited excellent antibacterial performance [15]. The antibacterial mechanism of ZnO and/or ZnAl-LDH could be attributed to their ability to generate reactive oxygen species (ROS), such as superoxide and hydroxyl radicals to damage bacterial cell membranes through lipid peroxidation.

Consequently, the loss of some essential substances (sugars, DNA, and proteins) caused the reduction of the bacteria's ability to survive, leading to their death [19]. Interestingly, MP/PP/CP@AC/LDH exhibited the highest antibacterial performance among all samples, which might be the result of the synergistic effect involving multiple integrating-parts of ZnO, ZnAl-LDH, extracts and AC. These phenomena were bases on the host–guest (between the host materials and extracts), guest-guest (among the different extracts), and host-guest-guest interactions, which collectively enhanced the antibacterial efficiency [22, 23]. Most samples exhibited no inhibitory effect against *E. coli*, showing dense bacterial growth (> 300 colonies). Only MP/PP/CP@AC/LDH showed partial inhibition, reducing viable cells to fewer than 30 colonies at higher concentrations. This limited efficacy was observed because *E. coli* possessed a more complex outer membrane structure relative to *S. aureus*, reducing the material's antibacterial penetration [3-5]. Therefore, the incorporation of ZnO@ZnAl-LDH with the mixed plant extracts in the composite significantly improved the antibacterial efficacy against *S. aureus*.

4. Conclusions

Organic–inorganic composite materials were successfully prepared by incorporating mangosteen peel (MP), pomelo peel (PP), and cucumber peel (CP) extracts with activated carbon (AC) and ZnO@ZnAl-LDH as host materials through a simple solid–solid method. The resulting MP/PP/CP@AC/LDH composite exhibited the most efficient antioxidant performance with IC_{50} values of 136.6 μg/mL for DPPH and 195.8 μg/mL for ABTS radicals, which were markedly lower than those of single-extract composites (253–563 μg/mL) or mixed-extract systems containing a single host (216–342 μg/mL). This improvement was mainly attributed to the synergistic effects among host–guest, guest–guest, and host–guest–guest interactions that enhanced the electron- and hydrogen-transfer capabilities of the composite. In terms of antibacterial behavior, ZnO@ZnAl-LDH and MP/PP/CP@AC/LDH effectively inhibited the growth of *Staphylococcus aureus*. In contrast, most samples showed no inhibition toward *Escherichia coli*, only MP/PP/CP@AC/LDH displayed partial *Escherichia coli* suppression, suggesting limited penetration through the Gram-negative bacterial membrane. The incorporation of ZnO@ZnAl-LDH and multiple herbal extracts significantly enhanced both antioxidant and antibacterial properties. These findings highlighted the potential of MP/PP/CP@AC/LDH composite as a multifunctional herbal powder, possessing strong DPPH and ABTS radical scavenging capacity together with antibacterial activity, particularly against *Staphylococcus aureus*, making it a promising candidate for further development in herbal-based cosmetic, pharmaceutical, and hygienic applications.

5. Acknowledgements

The scientific instrument support was gratefully provided by Faculty of Science and Digital Innovation and Faculty of Education, Thaksin University.

Author Contributions: Conceptualization; funding acquisition, T.P.; methodology; investigation, S.I., T.J., and T.P.; writing-original draft preparation, S.I., J.C., P.S and T.P.; writing-review and editing, S.I. and T.P.

Funding: This work was financially supported by the Thaksin University Research Fund, Thailand.

Conflicts of Interest: Declare conflicts of interest or state "The authors declare no conflict of interest."

References

[1] Siriyong, T.; Chanphool, H.; Jitjum, S.; Laohaprapanon, S.; Voravuthikunchai, S. P. Therapeutic Efficacy and Safety of Traditional Thai Herbal Medicines for Insomnia: A Double-Blind Randomized Controlled Trial. *Adv. Integr. Med.* **2025**, *12*, 100459. https://doi.org/10.1016/j.aimed.2025.01.006

[2] Limsuwan, S.; Thammathirata, T.; Yupanquic, C. T.; Wunnoo, S.; Eawsakul, K.; Noonong, K.; Punsawad, C.; Siripithaya, Y.; Bunluepuech, K. In Vitro Antimicrobial and NO Inhibitory Activities of a Thai Herbal Recipe against *Cutibacterium acnes*, *Staphylococcus aureus*, and *Staphylococcus epidermidis*. *Trends Sci.* **2025**, *22*, 9989. https://doi.org/10.48048/tis.2025.9989

[3] Semangoen, T.; Chotigawin, R.; Sangnim, T.; Chailerd, N.; Yodkeeree, S.; Pahasup-anan, T.; Huanbutta, K. Antimicrobial Efficacy of Mangosteen (*Garcinia mangostana*) Peel Extracts in Airborne Microbial

Control within Livestock Farming Environments. *Microb. Pathog.* **2025**, *204*, 107618. https://doi.org/10.1016/j.micpath.2025.107618

[4] Govindaiah, P. M.; Ruban, S. W.; Kiran, M.; Mohan, H. V.; Prabha, R. Exploring the In Vitro Antioxidant and Antimicrobial Properties of Pomelo Fruit Extract in Goat Meat: A Promising Alternative for Preservative and Health Benefits. *Sci. Hortic.* **2024**, *337*, 113534. https://doi.org/10.1016/j.scienta.2024.113534

[5] Anjani; Srivastava, N.; Mathur, J. Isolation, Purification, and Characterization of Quercetin from *Cucumis sativus* Peels: Antimicrobial, Antioxidant, and Cytotoxicity Evaluations. *3 Biotech* **2023**, *13*, 46. https://doi.org/10.1007/s13205-023-03464-8

[6] Xiao, L.; Ye, F.; Zhou, Y.; Zhao, G. Utilization of Pomelo Peels to Manufacture Value-Added Products: A Review. *Food Chem.* **2021**, *351*, 129247. https://doi.org/10.1016/j.foodchem.2021.129247

[7] Intachai, S.; Bosoy, S.; Thepthong, P.; Sumanatrakul, P.; Chanasit, W.; Khaorapapong, N. Effect of ZnAl-LDH-Based Host Material on Optical, Antioxidant, and Antibacterial Characteristics of *Zingiber montanum*. *Chem. Pap.* **2024**, *78*, 4119–4128. https://doi.org/10.1007/s11696-024-03305-9

[8] Kumari, S.; Sharma, V.; Soni, S.; Sharma, A.; Thakur, A.; Kumar, S.; Dhama, K.; Sharma, A. K.; Bhatia, S. K. Layered Double Hydroxides and Their Tailored Hybrids/Composites: Progressive Trends for Delivery of Natural/Synthetic Drug/Cosmetic Biomolecules. *Environ. Res.* **2023**, *238*, 117171. https://doi.org/10.1016/j.envres.2023.117171

[9] Thepthong, P.; Srirat, S.; Hiranrat, W.; Kongsune, P.; Chana, N. Development of Chitosan-Based Microencapsulation System for *Mitragyna speciosa* Alkaloids: A Novel Approach for Alzheimer's Disease Treatment. *J. Pharm. Innov.* **2025**, *20*, 58. https://doi.org/10.1007/s12247-025-09977-4

[10] Bahman, H.; Gharanjig, K.; Ghasemi, E.; Kazemian, H.; Hosseinnezhad, M.; Gharanjig, H. Synthesis and Characterization of an Eco-Friendly Nano-Hybrid Based on Luteolin-Loaded Zinc–Aluminum Layered Double Hydroxide for Biological Applications. *Int. J. Environ. Sci. Technol.* **2025**, *22*, 3545–3566. https://doi.org/10.1007/s13762-024-05960-7

[11] Suárez-Quiroz, M. L.; Campos, A. A.; Alfaro, G. V.; González-Ríos, O.; Villeneuve, P.; Figueroa-Espinoza, M. C. Isolation of Green Coffee Chlorogenic Acids Using Activated Carbon. *J. Food Compos. Anal.* **2014**, *33*, 55–58. https://doi.org/10.1016/j.jfca.2013.10.005

[12] Christodoulou, P.; Ladika, G.; Tsiantas, K.; Kritsi, E.; Tsiaka, T.; Cavouras, D.; Zoumpoulakis, P.; Sinanoglou, V. J. Quality Assessment of Greenhouse-Cultivated Cucumbers (*Cucumis sativus*) during Storage Using Instrumental and Image Analyses. *Appl. Sci.* **2024**, *14*, 8676. https://doi.org/10.3390/app14198676

[13] Zhang, Y.; Fu, X.; Wang, L.; Guo, X.; Dong, B. Sorption of Phenols and Flavonoids on Activated Charcoal Improves Protein Metabolism, Antioxidant Status, Immunity, and Intestinal Morphology in Broilers. *Front. Vet. Sci.* **2024**, *10*, 1327455. https://doi.org/10.3389/fvets.2023.1327455

[14] Zhao, Y.; Wei, J.; Li, C.; Ahmed, A. F.; Liu, Z.; Ma, C. A Comprehensive Review on Mechanism of Natural Products against *Staphylococcus aureus*. *J. Future Foods* **2022**, *2*, 25–33. https://doi.org/10.1016/j.jfutfo.2022.03.014

[15] Bizuayehu, T.; Kassaw, B.; Kendie, M. Green Synthesis, Characterization, and Antibacterial Activity Investigation of Zinc Oxide Nanoparticles Using *Rumex nervosus* Vahl Leaf Extract. *Results Chem.* **2025**, *13*, 102046. https://doi.org/10.1016/j.rechem.2025.102046

[16] Sobhy, M.; Ali, S. S.; Khalil, M. A.; Chen, X.; Cui, H.; Lin, L.; El-Sapagh, S. Exploring the Potential of Zinc Oxide Nanoparticles against Pathogenic Multidrug-Resistant *Staphylococcus aureus* from Ready-to-Eat Meat and Its Proposed Mechanism. *Food Control* **2024**, *156*, 110117. https://doi.org/10.1016/j.foodcont.2023.110117

[17] Almoneef, M. M.; Awad, M. A.; Aldosari, H. H.; Hendi, A. A.; Aldehish, H. A.; Merghani, N. M.; Alshammari, S. G. Exploring the Multi-Faceted Potential: Synthesized ZnO Nanostructure—Characterization, Photocatalysis, and Crucial Biomedical Applications. *Heliyon* **2024**, *10*, e32714. https://doi.org/10.1016/j.heliyon.2024.e32714

[18] Intachai, S.; Sumanatrakul, P.; Khaorapapong, N. Control of Particle Growth and Enhancement of Photoluminescence, Adsorption Efficiency, and Photocatalytic Activity for Zinc Sulfide and Cadmium

Sulfide Using CoAl-Layered Double Hydroxide System. *Environ. Sci. Pollut. Res.* **2023**, *30*, 63215–63229. https://doi.org/10.1007/s11356-023-26461-z

[19] Cardinale, A. M.; Alberti, S.; Reverberi, A. P.; Catauro, M.; Ghibaudo, N.; Fortunato, M. Antibacterial and Photocatalytic Activities of LDH-Based Sorbents of Different Compositions. *Microorganisms* **2023**, *11*, 1045. https://doi.org/10.3390/microorganisms11041045

[20] Intachai, S.; Sumanatrakul, P.; Pankam, P.; Suppaso, C.; Khaorapapong, N. Efficient Removal of Both Anionic and Cationic Dyes by Activated Carbon/NiFe-Layered Double Oxide. *J. Inorg. Organomet. Polym. Mater.* **2022**, *32*, 1999–2008. https://doi.org/10.1007/s10904-022-02254-8

[21] Ma, X.; Zhao, Y. Biomedical Applications of Supramolecular Systems Based on Host–Guest Interactions. *Chem. Rev.* **2015**, *115*, 7794–7839. https://doi.org/10.1021/cr500392w

[22] Acar, T.; Arayici, P. P.; Ucar, B.; Coksu, I.; Tasdurmazli, S.; Ozbek, T.; Acar, S. Host–Guest Interactions of Caffeic Acid Phenethyl Ester with β-Cyclodextrins: Preparation, Characterization, and In Vitro Antioxidant and Antibacterial Activity. *ACS Omega* **2024**, *9*, 3625–3634. https://doi.org/10.1021/acsomega.3c07643

[23] Swarnkar, N.; Kamalakaran, A. S.; Chintha, J.; Kambhampati, N. S. V.; Sripada, L.; Balakrishnan, S. B. Host–Guest Inclusion Complexes of Tafamidis with β-Cyclodextrin: Preparation, Characterization, and In Vitro Antibacterial and Antioxidant Approach. *J. Mol. Struct.* **2025**, *1332*, 141649. https://doi.org/10.1016/j.molstruc.2025.141649

[24] Lang, Y.; Gao, N.; Zang, Z.; Meng, X.; Lin, Y.; Yang, S.; Yang, Y.; Jin, Z.; Li, B. Classification and Antioxidant Assays of Polyphenols: A Review. *J. Future Foods* **2024**, *4*, 193–204. https://doi.org/10.1016/j.jfutfo.2023.07.002

[25] Jeung, D.-G.; Kim, H.-J.; Oh, J.-M. Incorporation of *Glycine max* Merrill Extract into Layered Double Hydroxide through Ion Exchange and Reconstruction. *Nanomaterials* **2019**, *9*, 1262. https://doi.org/10.3390/nano9091262

[26] Leelapornpisid, P.; Chansakaow, S.; Chaiyasut, C.; Wongwattananukul, N. Antioxidant Activity of Some Volatile Oils and Absolutes from Thai Aromatic Plants. *Acta Hortic.* **2008**, *786*, 61–65. https://doi.org/10.17660/ActaHortic.2008.786.5

[27] Mahadlek, J.; Tuntarawongsa, S.; Phaechamud, T. Antioxidant Activity and Total Phenolic Contents of Some Thai Traditional Formulations. *Isan J. Pharm. Sci.* **2017**, *13*, 97–105.

[28] Wangsawat, N.; Nahar, L.; Sarker, S. D.; Phosri, C.; Evans, A. R.; Whalley, A. J. S.; Choowongkomon, K.; Suwannasai, N. Antioxidant Activity and Cytotoxicity against Cancer Cell Lines of Extracts from Novel *Xylaria* Species Associated with Termite Nests and LC–MS Analysis. *Antioxidants* **2021**, *10*, 1557. https://doi.org/10.3390/antiox10101557

ASEAN
Journal of Scientific and Technological Reports
Online ISSN:2773-8752

Research article

Crickets As An Alternative Source of Protein: Development of Nutritious Local Foods and a Cost-Benefit Analysis

Natsima Tokhun[1], Kanokwan Punaaterkoon[1], Nahathai Chotklang[1], Chaloemphong Jansukar[2], Khanit Ruengkhajhon[3], Cheerawit Rattanapan[4], and Weerawat Ounsaneha[1*]

[1] Faculty of Science and Technology, Valaya Alongkorn Rajabhat University under the Royal Patronage, Pathum Thani Province, 13180, Thailand
[2] Faculty of Humanities and Social Science, Valaya Alongkorn Rajabhat University under the Royal Patronage, Pathum Thani Province, 13180, Thailand
[3] Faculty of Business Administration and Information Technology, Rajamangala University of Technology Suvarnabhumi, Phranakhon Si Ayutthaya Province, 13000, Thailand
[4] ASEAN Institute for Health Development, Mahidol University, Salaya, Phutthamonthon, Nakhon Pathom, 73170, Thailand
* Correspondence: weerawat@vru.ac.th

Citation:
Tokhun, N.; Punaaterkoon, F.; Lastname, F.; Chotklang, N.; Jansukar; C.; Ruengkhajhon; K.; Rattanapan, C.; Ounsaneha, W; Crickets as an alternative source of protein: development of nutritious local foods and a cost-benefit analysis. *ASEAN J. Sci. Tech. Report*. **2026**, *29*(2), e260796. https://doi.org/10.55164/ajstr.v29i2.260796.

Article history:
Received: August 11, 2025
Revised: October 13, 2025
Accepted: October 15, 2025
Available online: January 18, 2026

Abstract: This study aimed to develop processed food products incorporating cricket powder by creating formulas that optimize both nutritional benefits and consumer acceptability. The findings indicated that formulas incorporating cricket powder at 0.33%, 1.20%, and 0.33% by weight were optimal for pork sausages, grilled pork sausages, and pork meatballs, respectively. This aligned with the results regarding color and textural qualities, where the majority of scores were comparable to the control groups, while the water activity score was relatively high, potentially influencing microbial growth in the food. The three food products were rich in essential nutrients required by the body, including macronutrients and micronutrients such as carbohydrates, proteins, fats, vitamins B1 and B2, sodium, potassium, iron, and calcium. Furthermore, the protein content in pork meatball and pork sausage products complied with the Thai Community Product Standard (TCPS304/2555 and TCPS102/2555). The nutritional value per serving provided energy of 170, 150, and 80 kilocalories for grilled pork sausage, pressed sausage, and pork meatballs, respectively. Furthermore, the cost-benefit analysis indicated that project expenses comprised 93.33% fixed costs and 6.67% variable costs. The returns from this project will be beneficial over the following five years, as the NPV (38,790.29 USD) ≥ 0, the BCR (3.76) ≥ 0, and the IRR (31.80%) ≥ 5% interest rate of the cost of capital. The cricket protein serves as an alternative that can enhance the nutritional value of local food products and represents a prudent investment of project funds to bolster local community enterprises.

Keywords: Cricket powder; cricket processing; local food

1. Introduction

Despite crickets being economically viable insects with production potential and alternative protein sources that could address future food security issues [1], the majority of cricket farmers continue to experience elevated production costs and inconsistent yields [2]. A significant number of farmers are pursuing cricket farming as their primary vocation, leading to oversupply and diminished sales. However, food expenses constitute 48.9% to 60% of total production costs [3], resulting in financial losses and the eventual discontinuation of production.

Consequently, one potential solution to these issues is the enhancement of cricket's value as an alternative product, which can yield a market value tenfold greater [4], given that 100 g of cricket contains approximately 69% protein, whereas beef, pork, and chicken contain 43%, 29%, and 31% protein, respectively [5]. Cricket powders contained high levels of protein (42.0 to 45.8% of dry matter) and fat (23.6 to 29.1% of dry matter) [6]. Moreover, edible insects may offer enhanced health advantages owing to their elevated concentrations of vitamin B12, iron, zinc, fiber, essential amino acids, omega-3 and omega-6 fatty acids, and antioxidants [7]. The predominant cricket products in Thailand consist of frozen crickets, crispy baked crickets, and fried crickets [8]. Other processed cricket items are uncommon. Survey findings from farmers and small entrepreneurs reveal a demand for the development of cricket-based products that incorporate a straightforward production process and consist of a minimum of 60% cricket ingredients [9]. This strategy seeks to optimize the utilization of cricket raw materials in significant volumes while satisfying consumer preferences for product variety [10]. Additionally, it aims to enhance consumer acceptability of novel products—specifically edible insect products—by highlighting safety certifications and nutritional labeling, which have demonstrated an impact on purchasing decisions [11].

Finely comminuted products, including pork meatballs, pork sausages (Moo Yor), and grilled pork sausages (Naem Nuong), are created by blending deboned meat with seasonings and ingredients using a bowl cutter. This process results in emulsified meat, wherein the salt in the mixture facilitates fat extraction, enabling the emulsified meat to maintain cohesion. Additionally, modified starch may be incorporated to reduce costs, enhance texture, improve elasticity, and better retain moisture [12]. These pork-based products are popular among the Thai population and are commonly prepared in a variety of formulas or enjoyed with fresh vegetables by health-conscious consumers [13-15]. In response to growing interest in healthier and more sustainable food options, crickets have emerged as a valuable source of alternative protein. Currently, they are being utilized as a key ingredient in innovative food products [16]. This shift aligns with a broader trend in health-focused food development, which emphasizes the integration of high-protein ingredients—particularly cricket protein—into everyday items such as baked goods, muffins, flakes, and cookies [17-18].

Sa Kaeo Province, situated in eastern Thailand, is a multicultural society known for its Vietnamese-style Yuan cuisine, regional specialty dishes that both visitors and locals favor. The province holds significant geographical importance as the biggest hub for Thai-Cambodian border trade within ASEAN. According to the ASEAN Community Blueprint Plan (AEC blueprint), agriculture employs a substantial portion of the population and contributes significantly to the provincial GPP of 13,515 million Thai baht (THB) in 2022 [19-20]. Despite this economic contribution, the province experiences high levels of poverty, with Tapraya District among the nine districts reporting the lowest average income at 77,033.58 THB per person per year in 2022 [21-22]. Historically, the Tapraya District, Sa Kaeo Province, has engaged external organizations to foster diverse community economies, including organic agriculture and livestock, as well as the cultivation of economic insects such as crickets; yet, a significant risk remains concerning market volatility, input costs, and income instability [23-24]. The greater the risk associated with initiating a community business, the more essential it becomes to assess this risk through financial performance evaluations such as break-even analysis. A comprehensive cost-benefit analysis, alongside project cost-effectiveness indicators—including the Net Present Value (NPV), the Benefit-Cost Ratio (BCR), and the Internal Rate of Return (IRR)—can be employed to evaluate the efficiency of budget utilization and the socio-economic impact of the project. These tools are particularly valuable in measuring how such initiatives contribute to enhancing the overall quality of life within the community. Despite their importance, studies specifically examining cricket-based products developed by Community Enterprise Groups remain limited [23-24]. Therefore, the objective of this study was to examine the nutritional status and cost-benefit value of cricket protein supplementation. This aims to enhance cricket's viability as a protein supplement. By addressing low-yield production issues, cricket-based products can offer enhanced nutritional values, including potassium, protein, fat, sodium, carbohydrate, sugar, and vitamin A, B1, and B2, comprehensive nutritional information labels, and improved product acceptance. Furthermore, the findings can evaluate the project's cost-effectiveness, encourage community entrepreneurs, and facilitate more sustainable production and consumption models for local products.

The objective of this study was to develop suitable formulas for processed food products incorporating cricket powder as an ingredient. The study aimed to evaluate these products through consumer acceptance testing, nutritional analysis, and sensory profile assessment conducted by trained panelists. Additionally, the research sought to assess the economic viability of cricket-based food production through cost-benefit analysis.

2. Materials and Methods

2.1 Production of Food Products Supplemented with Cricket Protein

1. *Gryllus bimaculatus* field crickets obtained from the Ta Praya Community Enterprise in Sa Kaeo Province were utilized to generate cricket protein powder for incorporation into processed meat products supplemented with cricket protein. The area of the cricket farm is located in the agriculture community with the 1,800 m2 or 0.18 ha per one cultivation building with 35-45 days/crop. Water and commercial feed (21 % of protein, 5 % of fiber, and 4 % of fat) were provided after the incubation period. For animal ethical consideration, the research investigator (NT) was trained for an animal use license (U1-04867-2559) by the National Research Council of Thailand. The preparation method for cricket protein powder was adapted from Pansuntia et al. [18]. Seven kilograms of frozen crickets were thoroughly rinsed with clean water five to seven times or until pristine, and thereafter cooked at high temperature in a steam basket for thirty minutes. The roasted crickets were dehydrated in a hot-air oven (Series HT-D10P, Kitchen Mall Manufacturing, Thailand) at 85–105°C for approximately 10 hours or until completely desiccated. After chilling, the crickets were carefully pulverized, sieved through a 50-mesh filter (Test sieve, brand Endecotts, England), and then roasted with lemongrass at 60–70°C for 15 minutes. This process yielded one kilogram of cricket protein powder for the creation of food products supplemented with cricket protein.

2. The creation of food products supplemented with cricket protein was developed using formulas and processing techniques adapted from Wongnai Media Company Limited [25-27] and Wangkawan et al. [28], as illustrated in Table 1 and Figures 1–3, and implemented through the following procedures.

Table 1. Percentage by weight (% w/w) of processed food ingredients in each formula (F) and control (C).

Ingredients	Percent by weight of ingredients								
	Pork sausages			Grilled pork sausages			Pork meatballs		
	C 1.0	F 1.1	F 1.2	C 2.0	F 2.1	F 2.2	C 3.0	F 3.1	F 3.2
Pork loin	53.30	53.30	53.30	48.90	48.90	48.90	66.58	66.58	66.58
Pork lard	26.65	26.32	26.20	24.45	23.25	22.81	–	–	–
Cricket powder	–	0.33	0.45	–	1.20	1.64	–	0.33	0.45
Iodized refined salt	0.53	0.53	0.53	0.73	0.73	0.73	0.67	0.67	0.67
Seasoning powder	–	–	–	–	–	–	0.40	0.23	0.17
Tapioca flour	0.53	0.53	0.53	–	–	–	0.40	0.40	0.40
Pepper	2.66	2.66	2.66	1.22	1.22	1.22	0.40	0.40	0.40
Garlic	–	–	–	9.78	9.78	9.78	0.40	0.40	0.40
Pure refined sugar	–	–	–	0.49	0.49	0.49	1.20	1.04	0.98
Crushed ice	14.99	14.99	14.99	11.01	11.01	11.01	29.95	29.95	29.95
Baking powder	1.34	1.34	1.34	–	–	–	–	–	–
Seasoning sauce	–	–	–	3.42	3.42	3.42	–	–	–

Source: Adapted from Wongnai Media Company Limited [25-27] and Wangkawan et al. [28]

The preparation of cricket protein-supplemented pressed sausages involves the following steps: Initially, pork loin and lard undergo fine grinding before being subjected to freezing for 45 minutes. Concurrently, pre-measured dry ingredients—comprising seasoning salt, baking powder, tapioca flour, finely ground black pepper, and cricket protein powder—are homogeneously combined in a mixing vessel, followed by the incorporation of cold potable water. The mixture undergoes thorough agitation to ensure uniform ingredient distribution. The chilled pork loin and lard are subsequently incorporated into the prepared mixture and blended until achieving a homogeneous, cohesive consistency. The mixture is then subjected to a

secondary freezing period of approximately 15 minutes, after which it undergoes re-blending until attaining a sticky, aerated texture while maintaining an optimal processing temperature range of 10–15°C. Pre-cleaned banana leaves, lightly treated with vegetable oil, serve as the wrapping medium for the pork mixture, which is then tightly rolled and hermetically sealed at both termini. The encased sausages are secured with binding material and subjected to steam treatment in a steam basket positioned over vigorously boiling water for a duration of 30–45 minutes. Each packaged pressed sausage unit maintains a standardized net weight of 100 g.

The preparation of cricket protein-supplemented grilled pork sausages involves the following steps: Initially, pork loin and lard undergo fine grinding before being subjected to freezing at approximately -18°C for 45 minutes. Pre-measured dry ingredients (including seasoning salt, seasoning sauce, tapioca starch, granulated sugar, cricket protein powder, accord powder, granulated pepper, and garlic) are combined in a mixing vessel. The mixture undergoes thorough agitation, followed by the gradual incorporation of cold potable water until complete ingredient integration is achieved. Subsequently, the chilled pork loin and lard are incorporated into the prepared seasoning mixture using mechanical blending until a homogeneous, cohesive consistency is obtained. The mixture is then subjected to extended freezing for approximately 3 hours, after which it undergoes secondary blending until achieving a sticky, aerated texture. Throughout the blending process, the mixture temperature is maintained within the optimal range of 10–15°C through continuous cooling. The processed mixture is then formed into uniform rounds and secured onto skewers for grilling. The products undergo low-temperature grilling until achieving complete doneness, as determined by internal temperature monitoring. Following the cooking process, the grilled sausages are packaged in standardized units, with each package maintaining a net weight of 150 g.

The preparation of cricket protein-supplemented pork meatballs involves the following steps: Initially, pork is sectioned into small pieces and subjected to freezing for 45 minutes or until the meat achieves partial rigidity with visible ice crystal formation on the surface. The partially frozen pork then undergoes mechanical grinding until it achieves a fine, uniform texture. Pre-measured dry ingredients (including seasoned salt, tapioca flour, granulated sugar, ground pepper, garlic powder, and cricket protein powder) are combined in a mixing vessel. The mixture undergoes thorough agitation, followed by the gradual incorporation of cold potable water until complete homogenization is achieved. Subsequently, the ground pork is incorporated into the prepared seasoning mixture through mechanical blending. Ice is gradually added during the mixing process, and blending continues until a homogeneous, cohesive consistency is obtained. The mixture is then subjected to freezing for approximately 30 minutes, after which it undergoes secondary blending until it achieves optimal stickiness. Throughout all blending operations, the mixture temperature is maintained within the range of 10–15°C through continuous cooling. For the cooking process, water is brought to a rolling boil in a suitable vessel, then reduced to maintain a simmering temperature. The processed mixture is formed into uniform spherical shapes and carefully introduced into the heated water until the meatballs achieve buoyancy, indicating complete cooking. The cooked meatballs are subsequently removed and immersed in cold water for 10–15 minutes to halt the cooking process. Following drainage, the products are packaged in standardized units, with each package maintaining a net weight of 1,000 g. The research flow of this study is shown in Figure 1.

2.2 Nutritional and Texture Profile Analysis

Product samples were obtained using a random sampling method, consisting of two packages of pork meatballs with a total weight of 2,000 g, twenty packages of pressed Vietnamese sausage totaling 2,000 g, and fourteen packages of Vietnamese grilled pork sausage totaling 2,100 g. Comprehensive food composition analysis and nutritional labeling assessment were carried out by the Foundation for Industrial Development, National Food Institute, Thailand. The analytical procedures and methodologies applied for the food analysis are presented in Table 2. The nutritional analysis data were utilized to calculate energy, sugar, fat, and sodium values in accordance with nutrient content specifications per unit package, as stipulated in Notification No. 446 of the Ministry of Public Health [29]. Reference unit content for these food products was categorized according to the characteristics of analogous food products, including sausages, meatballs, fermented pork, Vietnamese pork sausage (Mhoo-yor), and Bologna. Serving size determination and servings per container calculations were based on the methodological framework established by the National Bureau

of Agricultural Commodity and Food Standards, utilizing Thailand's food consumption data from 2016 and U.S. reference serving volume requirements [29].

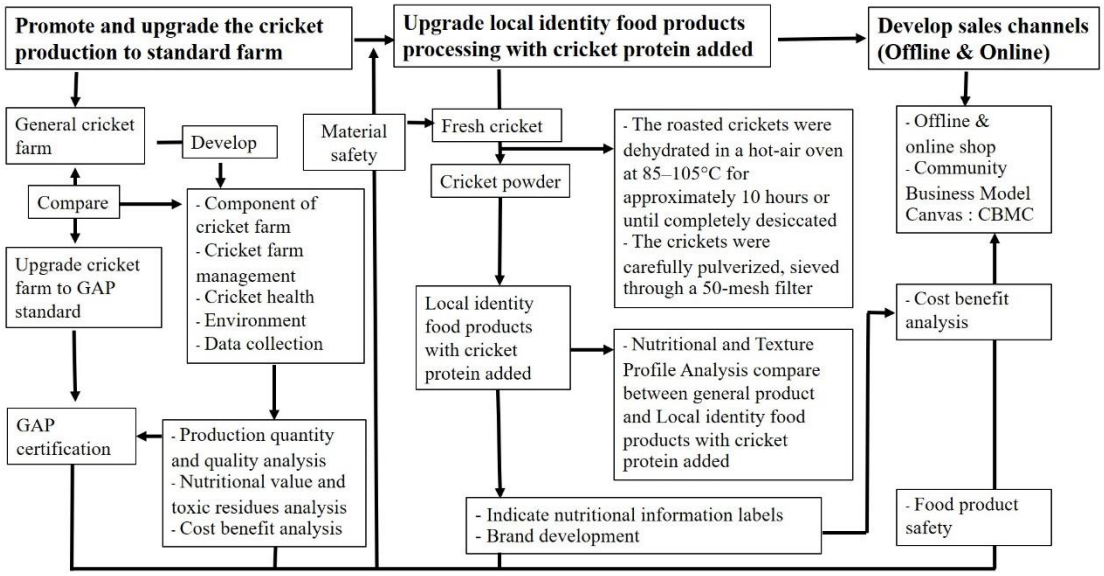

Figure 1 The steps of the research process

Table 2. Test methods for nutritional analysis of food products from cricket ingredients

Item	Test methods	References
Ash	AOAC Official Method 920.153	[30]
Calcium	In-house method T9152 based on AOAC Official Method 984.27	[30]
Calories from fat	Methods of analysis for nutrition labeling, 1993, chapter 1,5	[31]
Cholesterol	In- house method T992 based on the rapid determination of cholesterol in single and multicomponent prepared foods	[32]
Dietary fiber	In-house method T995 based on AOAC Official Method 985.29	[30]
Iron	In-house method T9152 based on AOAC Official Method 984.27	[30]
Moisture	AOAC Official Method 950.46B	[30]
Protein (N x 6.25)	In-house method T927 based on AOAC Official Method 992.	[30]
Potassium	In-house method T9152 based on AOAC Official Method 984.27	[30]
Saturated fat	In-house method T974 based on AOAC Official Method 996.06	[30]
Sodium	In-house method T9152 based on AOAC Official Method 984.27	[30]
Total carbohydrate	Methods of analysis for nutrition labeling, 1993, chapter 1,5	[32]
Total calories	Methods of analysis for nutrition labeling, 1993, chapter 1,5	[32]
Total fat	AOAC Official Method 945.38F	[30]
Total sugars	In-house method T997 based on AOAC Official Method 982.14	[30]
Vitamin A	In-house method T969 based on AOAC Official Method 992.06	[30]
Vitamin B1	In-house method T970 based on AOAC Official Method 942.23	[30]
Vitamin B2	In-house method T971 based on AOAC Official Method 970.65	[30]

Texture Profile Analysis (TPA) of the products was conducted using a texture analyzer (Brookfield, model CT3, S/N: BEL8749458_DK) equipped with a solid cylindrical probe (No. P/50). Product samples were prepared in standardized 2 cm^3 dimensions for analysis. The TPA measured multiple textural parameters, including hardness, adhesiveness, springiness (rate of deformation recovery), and cohesiveness (degree of product decomposition). Additional derived parameters were calculated as follows: gumminess, representing the energy required for food breakdown to achieve a swallowable state, was determined using the formula gumminess = hardness × cohesiveness; chewiness, indicating the total energy required for mastication, was calculated as chewiness = hardness × springiness × cohesiveness [33]. Color analysis was performed using a

Hunter Lab colorimeter (Konica Minolta, model CR-400) to measure lightness (L*), redness (a*), and yellowness (b*) values according to the CIE color space system. Water activity (aw) analysis was conducted to determine the available water content within the products using a Water Activity Meter (LabSwift-AW Novasina, model LabSwift-aw with battery, S/N: NOV1809006_DK). This parameter is critical for assessing product stability and microbial safety [34-36].

2.3 Acceptance Testing of Cricket Protein-Supplemented Products

Consumer acceptance testing for pork meatballs, pressed pork sausages, and grilled pork sausages supplemented with cricket protein was performed utilizing a Randomized Complete Block Design (RCBD) and assessed via the 9-point hedonic scale (where 1 = extremely dislike, 5 = neutral, and 9 = extremely like) [37]. The hedonic scale evaluated essential sensory characteristics, encompassing appearance, scent, flavor, texture, mouthfeel, and overall attractiveness. Untrained panelists were enlisted to assess 100 sensory food items, adhering to techniques outlined by Peryam and Pilgrim [38]. The gathered data were examined by Analysis of Variance (ANOVA) to identify statistically significant variations in mean sensory ratings. Duncan's New Multiple Range Test (DMRT) was utilized at a 95% confidence level ($p \leq 0.05$) to compare the means of groups. Statistical analysis was conducted utilizing Statistix software, version 8.0 (FL, USA).

2.4 Cost-benefit Analysis

The research project has secured funding allocation and generated profit from sales at the local market, OTOP fair, and university market. The study intends to assess economic impact via a benefit-cost analysis, employing the ex-ante evaluation technique for an additional five years. This comprehensive evaluation occurs during the project's execution, assessing the investment value through quantitative metrics such as the NPV, the BCR, and the IRR. Data for the assessment is collected via participant interviews, utilizing tools specifically created to analyze project cost-effectiveness [39], as illustrated in Eqs. (1-3).

$$NPV = \sum(Bt\text{-}Ct)/(1+r)t \quad (1)$$

$$BCR = \sum Bt/(1+r)t/\sum Ct/(1+r)t \quad (2)$$

$$IRR = \sum(Bt\text{-}Ct)/(1+r)t = 0 \quad (3)$$

The equations encompass the variables t (project duration in years), Bt (project benefit in year t in baht per annum), Ct (project research cost in year t in THB per annum), and r (discount rate in percentage).

The researcher protocol received approval from the Human Research Ethics Committee of Valaya Alongkorn Rajabhat University under Royal Patronage, Pathum Thani Province, with COA No. 0041/2567 and REC No. 0001/2567.

3. Results and Discussion

3.1 Texture Profile Analysis (TPA)

The development of three processed food products containing cricket protein powder—pork sausages, grilled pork sausages, and pork meatballs (Figure 2)—was followed by a texture assessment using the Texture Profile Analysis (TPA) method. The components of cricket powder ingredient were 51.65 % of protein, 22.36 % fat, 16.58 % of fiber, 12.47 % of ash, 9.97 % of moisture, and 3.55 % of carbohydrate with the 3 months of shelf life and room temperature storage conditions. The results indicated that the chewiness of pork sausages, grilled pork sausages, and pork meatballs did not significantly differ from the control groups (ns). Products containing 0.33% cricket powder by weight (pork sausages and pork meatballs) and 1.20% (grilled pork sausages) exhibited higher hardness, springiness, and gumminess compared to those with 0.45% and 1.64% cricket powder, respectively (Table 3), which is consistent with the findings of Samon and Jangchud [40]. Additionally, increasing the concentration of cricket powder was found to significantly reduce the hardness of the products.

The results showed that pork sausages containing 0.33% cricket powder by weight (Formula 1.1) and grilled pork sausages containing 1.20% (Formula 2.1) exhibited significantly greater hardness and gumminess than the other formulas ($p \leq 0.01$). Higher hardness indicates a firmer texture, while gumminess refers to the

amount of force required to chew food until it is ready to swallow. Among all formulas, Formula 1.1 and Formula 1.2—both containing lower levels of cricket powder—demonstrated a firmer and more compact texture compared to the others. However, no significant differences (ns) were observed in cohesiveness (ranging from 0.2447 to 0.3967) and springiness (11.6500–13.1000 mm) among the products, indicating similar elastic properties. These findings are consistent with the study by Dholvitayakhun et al. [41], which found no significant differences in cohesiveness (0.19–0.24) and springiness (8.91–10.15 mm) between microwave-cooked pork loin and conventionally steamed pork loin. The creation of pork sausages and grilled pork sausages (Table 1) includes pork loin and pork lard as the main ingredients, comprising 48.90–53.30% and 22.81–26.32% by weight, respectively. These are homogenously mixed with other components. Tapioca flour is added as a thickener, filler, binder, or stabilizer in meat products [42]; salt facilitates emulsification of the mixture [43]; and pepper and garlic are included to enhance flavor and aroma. Cricket powder is incorporated as an alternative protein source to support the development of nutritious food products. In addition to selecting appropriate ingredients, a critical step in the process is blending the emulsion at a temperature below 15°C [44], typically by whisking in the evening. It is not necessary to prepare a separate fat emulsion beforehand; instead, the focus should be on maintaining the chopping and mixing temperature below 10°C. The inclusion of 10% tapioca starch is considered appropriate for achieving desirable texture and overall product quality [45]. This method aligns with the present study, which controlled the blending temperature between 10°C and 15°C and incorporated ice at levels ranging from 11.01% to 14.99% by weight (Table 1). For pork meatballs, the ingredients and production method are similar to those used for pork sausages and grilled pork sausages; however, the primary component is pork loin, comprising 66.58% by weight. The formula containing 0.33% cricket powder (Formula 3.1) exhibited no significant differences in hardness, cohesiveness, or gumminess compared to the control groups (ns). This formula demonstrated a firm texture and similar chewability to conventional pork meatballs. However, when the cricket powder content was increased to 5%, significant reductions in hardness, springiness, gumminess, and chewiness were observed ($p \leq 0.05$). In other words, higher concentrations of cricket powder negatively affected the texture, firmness, elasticity, and internal binding properties of the product (Table 3). This indicates that each category of ingredient possesses specific characteristics and functions that directly influence the properties of food and the final product. According to Utaida [46], the use of pepper at concentrations of 0.2%, 0.3%, and 0.4%, and salt at 2.0%, 2.5%, and 2.9%, increased the hardness and firmness of the texture as ingredient levels rose. However, no significant differences were observed in brightness (L*) or red color values (a*), nor in consumer preferences regarding color, aroma, taste, and overall acceptability. Therefore, the results of this TPA study confirm that ingredient quantities affect the textural quality of the product. The formulas with the lowest amount of cricket powder (Formulas 1.1, 2.1, and 3.1) were selected for nutritional analysis, as their sensory acceptance scores did not significantly differ from the control groups. In contrast, formulas with higher concentrations of cricket powder had significantly lower acceptance scores compared to the other experimental groups (Table 5). The results of color measurement in food products containing cricket powder (Table 4) showed that grilled pork sausages with 1.20% cricket powder by weight (Formula 2.1) exhibited brightness (L*), red (a*), and yellow (b*) values that were not significantly different from those of the control groups (ns). However, when the concentration of cricket powder increased to 1.64%, both a* and b* values increased significantly compared to the control groups ($p \leq 0.05$), indicating that cricket powder influences the color quality of the product. This finding aligns with Gantner et al. [47], who reported that the color intensity of products increases with higher concentrations of cricket powder, reflected in elevated a* and b* values and reduced L* values. These changes are attributed to the brown color of the chitinous exoskeleton, a characteristic feature of insects [48-49]. Moreover, the inclusion of animal fats in the product can contribute to a softer texture, enhance flavor, and increase the brightness of the sausage [50]. Thus, color is a key characteristic that significantly influences consumer preferences and product acceptance. In this study, pork sausages and pork meatballs in the control groups exhibited the highest brightness values, which were significantly different from those of the experimental groups containing 0.33% and 0.45% cricket powder, respectively (Table 4). These findings are consistent with those of Wangkawa et al. [28], who reported L* values of 63.2 for pork yolks with silkworm pupae and 64.1 for the standard formula—values comparable to this study's L* value of 67.90 in Formula 1.1 (Table 4).

Therefore, the color quality of pork sausages, grilled pork sausages, and pork meatballs with the highest consumer acceptance was observed in the formulas containing the lowest amount of cricket powder (Formulas 1.1, 2.1, and 3.1). These findings are consistent with the TPA results, where acceptance scores were similar to those of the control groups, which did not contain cricket powder (Table 3). Regarding water activity (aw), the highest values were found in the control groups. While pork sausages showed no significant difference in aw, grilled pork sausages and pork meatballs containing cricket powder exhibited significantly lower aw values compared to the control groups ($p \leq 0.05$). The formulas containing cricket powder had aw values ranging from 0.901 to 0.916, which may influence microbial growth in food products (Table 4). Since aw is a critical factor in microbial control, bacteria that cause foodborne illness typically cannot grow at aw levels below 0.85 [51-52]. Moreover, low aw ensures the microbiological stability of food products, as aw values below 0.6 significantly inhibit microbial growth [53]. However, the method of storage and packaging also affects food quality. For example, storing pork meatballs in transparent vacuum packaging at 3 ± 1°C results in less microbial growth compared to LDPE packaging, with storage durations not exceeding 12 and 9 days, respectively [46].

Figure 2. Photographs of three processed food products containing cricket powder as an ingredient (pork sausages, grilled pork sausages, and pork meatballs).

3.2 Acceptance Testing

The consumer sensory acceptance test results for cricket-based products at different levels, compared to the control groups without cricket powder, showed that grilled pork sausages and pork meatballs containing the lowest amounts of cricket powder—0.33% and 1.20% by weight (Formulas 2.1 and 3.1, respectively)—received overall acceptance scores that were not significantly different from the control groups (ns). In contrast, increasing the cricket powder content to 0.45% and 1.64% (Formulas 2.2 and 3.2) resulted in significantly lower acceptance scores compared to the control groups ($p < 0.05$). Pork sausages containing 0.33% cricket powder (Formula 1.1) received the highest flavor acceptance among the experimental formulas. However, their appearance, aroma, mouthfeel, and overall acceptability did not differ significantly from the control groups. Consequently, products with the lowest levels of cricket powder—0.33% in pork sausages, 1.20% in grilled pork sausages, and 0.33% in pork meatballs—were deemed most acceptable by consumers and selected for further food analysis, including nutritional labeling and consumer information (Table 5). In addition to receiving the highest overall liking score, the selected formulas also exhibited physical and sensory characteristics comparable to the control groups. Given that crickets are a valuable source of energy and protein in the human diet, these findings support the suitability of cricket powder for the development of

nutritious local food products. The inclusion of nutritional labeling further facilitates informed consumer choices by highlighting beneficial nutrients while helping to limit the intake of undesirable or restricted nutrients [54].

Table 3. Texture profile analysis of food products in each formula (F)

Food products	Cricket ingredients in formula	Texture Profile Analysis (TPA)					
		Hardness (g)	Adhesiveness (mJ)	Cohesiveness	Springiness (mm)	Gumminess (g)	Chewiness (mJ)
Pork sausages	Control	6,584.33b	0.4333b	0.3967a	12.6100a	1,949.90b	577.43a
	1.1 (0.33%)	11,506.00a	1.0467a	0.3500a	13.1000a	2,795.93a	420.60b
	1.2 (0.45%)	6,300.33b	1.1667a	0.2667a	12.6627a	1,632.47c	230.47c
	F-test	**	**	ns	ns	**	**
	%CV	9.50	19.72	24.81	3.08	7.02	14.13
Grilled pork sausages	Control	3,026.91b	0.5800a	0.2610a	11.6500a	1,424.93b	207.06b
	2.1 (1.20%)	5,291.67a	0.1910b	0.2533a	12.5133a	2,252.53a	315.77a
	2.2 (1.64%)	2,903.29b	0.6067a	0.2447a	12.3133a	1,722.80b	193.20b
	F-test	**	*	ns	ns	*	**
	%CV	17.70	33.64	14.90	5.02	12.78	14.00
Pork meatballs	Control	9,251.33a	0.0333b	0.5053ab	12.6293b	3,996.33a	661.47a
	3.1 (0.33%)	8,566.00a	0.1667a	0.5633a	12.8867a	4,921.40a	575.49b
	3.2 (0.45%)	5,955.00b	0.0333b	0.4800b	12.0980c	2,831.67b	336.69c
	F-test	**	*	Ns	**	**	**
	%CV	6.08	74.23	7.14	0.72	13.72	6.79

Note: a, b, c = significant different at $p<0.05$ with the same row, ns = non-significant ($p>0.05$) and CV = Coefficient of Variation

Table 4. Results of color quality and water activity of food products in each formula

Products	Cricket ingredients in formula	Color quality			Water activity
		L*	a*	b*	aw
Pork sausages	Control	69.350a	3.733c	14.703c	0.914a
	1.1 (0.33%)	67.820b	4.212b	17.823a	0.908a
	1.2 (0.45%)	56.903c	4.947a	15.143b	0.910a
	F-test	**	**	**	ns
	%CV	0.92	2.19	1.05	0.35
Grilled pork sausages	Control	69.923a	3.487b	14.377b	0.912a
	2.1 (1.20%)	70.635a	3.817ab	15.073ab	0.901b
	2.2 (1.64%)	67.880a	4.173a	15.483a	0.902b
	F-test	Ns	ns	ns	**
	%CV	2.63	8.14	3.01	0.01
Pork meatballs	Control	76.463a	2.043c	11.990ab	0.916a
	3.1 (0.33%)	74.673b	2.337b	12.100a	0.909b
	3.2 (0.45%)	71.739c	3.009a	11.853b	0.908b
	F-test	**	**	*	**
	%CV	0.92	4.12	0.59	0.08

Note: a, b, c = significant different at $p<0.05$ with the same row, ns = non-significant ($p>0.05$) and CV= Coefficient of Variation

3.3 Nutritional Analysis

The formulas containing 0.33% cricket powder in pork sausages and pork meatballs (Formulas 1.1 and 3.1), and 1.20% in grilled pork sausages (Formula 2.1), were selected for nutritional analysis to provide nutritional information for consumers (Table 2). The results revealed that, per 100 g serving, pork meatballs contained the highest levels of dietary fiber, cholesterol, moisture, protein, and vitamin B1, followed by grilled

pork sausages and pork sausages, respectively. Grilled pork sausages contained the highest levels of ash, potassium, sodium, total calories, total sugars, and vitamin B1. In contrast, pork sausages were found to contain the highest levels of calcium, iron, total carbohydrates, and total fat. Vitamin A was not detected in any of the three products (Table 6). According to the nutritional information panels, a 50 g serving of grilled pork sausages provided the highest energy content at 170 kilocalories, followed by pressed pork sausages at 150 kcal and pork meatballs at 80 kilocalories. The nutrient data were evaluated based on the Thai Recommended Daily Intakes (% Thai RDI), calculated using a daily energy intake of 2,000 kilocalories, as shown in Table 7. These values align with the Nutrient Reference Values (NRVs) established by the Codex Alimentarius, which are based on the Daily Intake Reference Values (DIRVs) for a healthy population aged 19–50 years. The Thai RDIs are also set to ensure nutrient intake does not exceed the safe maximum consumption levels (Upper Levels of Intake, ULs) for individuals aged 3 years and above with normal health status [29].

Table 5. Result of acceptance testing of food products in each formula

Products	Cricket powder as an ingredient	Acceptance testing						
		Appearance	Color	Aroma	Flavor	Texture	Mouthfeel	Overall acceptability
Pork sausages	Control	5.78	5.83a	6.43a	5.80b	5.87a	5.05a	5.87a
	1.1 (0.33%)	5.61	5.43ab	5.88ab	6.37a	5.36b	5.16a	5.64a
	1.2 (0.45%)	5.55	5.23b	5.35b	5.15c	4.77c	4.69b	5.12b
	F-test	ns	*	*	**	**	**	*
	%CV	4.43	3.77	6.29	4.65	3.46	1.67	3.81
Grilled pork sausages	Control	6.21a	6.32a	6.70a	6.74a	6.08a	5.86a	6.07a
	2.1 (1.20%)	6.05ab	6.36a	6.64a	6.72a	5.68a	5.81a	6.21a
	2.2 (1.64%)	5.32b	5.43b	5.45b	3.69b	5.03b	4.99b	5.32b
	F-test	ns	**	**	**	**	**	**
	%CV	7.20	3.79	2.55	2.97	4.11	2.16	3.07
Pork meatballs	Control	5.92a	6.80a	5.94a	6.00a	5.69a	5.75a	5.87a
	3.1 (0.33%)	5.68a	5.92b	5.79a	5.93a	5.46a	5.55a	5.77a
	3.2 (0.45%)	4.93b	4.95c	4.87b	4.67b	4.49b	4.47b	4.72b
	F-test	**	**	**	**	**	**	**
	%CV	4.36	2.76	2.65	2.55	3.68	2.51	2.77

Note: a, b, c = significant different at $p<0.05$ (*), $p<0.01$ (**) with the same row, ns = non-significant ($p>0.05$) and CV = Coefficient of Variation

Table 6. Result of food composition analysis of processed pork products with cricket ingredients

Items	Units	Amount of food listed (per 100 g edible portion)		
		Pork sausages	Grilled pork sausage	Pork meatballs
Ash	g	2.01	2.60	2.02
Calcium	mg	59	17	25
Calories from fat	kcal	215	261	58
Cholesterol	mg	36	41	45
Dietary fiber	mg	0.8	0.8	2.0
Iron (Fe)	mg	0.99	0.56	0.45
Moisture	g	55.36	49.19	70.89
Potassium (K)	mg	237	292	230

Table 6. Result of food composition analysis of processed pork products with cricket ingredients (Continue)

Items	Units	Amount of food listed (per 100 g edible portion)		
		Pork sausages	Grilled pork sausage	Pork meatballs
Protein (N x 6.25)	g	13.4	16.7	19.0
Saturated fat	g	0.8	9.9	2.5
Sodium (Na)	mg	445	647	511
Total carbohydrate	g	5.3	2.5	2.5
Total calories	kcal	290	338	144
Total fat	g	23.9	29	6.5
Total sugars	g	ND	0.6	0.5
Vitamin A	μg	ND	ND	ND
Vitamin B1	mg	0.29	0.37	0.41
Vitamin B2	mg	0.02	0.03	0.01

Table 7. Nutritional information panels on food labels (per 50 g edible portion)

Items	Units	Pork sausages		Grilled pork sausage		Pork meatballs	
		This study	%Thai RDI	This study	%Thai RDI	This study	%Thai RDI
Amount per serving	g	50	-	50	-	50	-
Total Energy	kcal	150	-	170	-	80	-
Total fat	g	12	18	15	23	3.5	5
Saturated fat	g	4	20	5	25	1.5	8
Cholesterol	mg	7	-	20	7	25	8
Protein	g	7	-	8	-	10	-
Total carbohydrate	g	3	1	1	0	1	0
Dietary fiber	g	0	0	-	0	1	4
Sugars	g	0		0	-	0	-
Sodium	mg	220	11	320	16	260	13
Potassium	mg	120	3	150	4	115	3
Vitamin A	-	-	0	-	0	-	0
Vitamin B1	-	-	10	-	10	-	15
Vitamin B1	-	-	0	-	0	-	0
Calcium	-	-	4	-	0	-	< 2
Iron	-	-	4		< 2	-	< 2

Note: Percent Thai Recommended Daily Intakes (%Thai RDI) are based on a 2,000 kcal diet. Nutrition labeling is provided for net weights of 100 g of pressed sausages (2 servings per container), 150 g of grilled pork sausages (3 servings per container), and 100 g of pork meatballs (20 servings per container).

The results (Table 6) present the protein, fat, and carbohydrate content of the developed products in comparison with the Thai Community Product Standards (TCPS) for pork meatballs (TCPS 304/2012; TISI, 2012) and pork sausages (TCPS 102/2012; TISI, 2012). The analysis indicated that the products met the required protein content standard (> 13% by weight). However, the fat and carbohydrate contents exceeded the TCPS limits, which specify that pork meatballs and pork sausages should contain no more than 6% and 25% fat by weight, respectively, and that the carbohydrate content in both products should not exceed 2% by weight [47]. The developed cricket-based products, per 100 g serving, contained 13.4–19.0 g of protein, 6.5–23.9 g of total fat, 2.5–5.3 g of total carbohydrates, and 2.01–2.60 g of ash (Table 6). These values are comparable to those reported for pork sausages fortified with silkworm pupae, which contained 16.0% protein, 20.73% fat, and 3.19% ash—exceeding the nutritional value of conventional formulas that typically contain 15.2% protein, 16.0% fat, and 2.8% ash [28]. Similarly, pork sausages with Panang curry paste were found to contain 10.6 g of protein, 7.8 g of fat, and 3.0 g of carbohydrates [56]. In another example, pork meatballs with 73% of fat by weight replaced by pastry gel contained 17.16% protein, 6.23% fat, and 71.92% moisture [49]. For pork

meatballs, the protein content is 19 g per 100 g of edible portion (Table 6), which is higher than that found in blanched and fried meatball products across three levels of production—industrial, small business, and retail—commonly available in local markets and supermarkets in Bangkok. According to Chan-Urai [50], the protein content in comparable products is as follows: beef balls (13.8–16.1 g), pork balls (13.2–16.2 g), chicken balls (10.0–15.9 g), shrimp balls (12.7–13.7 g), fish balls (14.9–16.5 g), and traditional Chinese pork balls (9.9–13.2 g) per 100 g of edible portion. The ash, fat, carbohydrate, and moisture values of the developed pork meatballs are comparable to those of other meatball products.

The results showed that the nutritional values per 50 g serving of pork sausages, grilled pork sausages, and pork meatballs were 150 kcal, 170 kcal, and 80 kcal, respectively (Table 7). Grilled pork sausages had the highest energy value, with fat contributing up to 130 kcal, which corresponds to the product's total fat content of 29 g per 100 g (Table 6). This high fat content can be attributed to the inclusion of 23.35% pork lard and 1.20% cricket powder by weight (Table 1). Regarding the cricket powder, the nutritional analysis showed that the highest content was protein (50.84%), followed by fat (22.34%), fiber (16.58%), ash (12.47%), moisture (10.80%), and carbohydrate (3.55%) [24]. This aligns with the findings of Montowska et al. [6], who reported that cricket powder is rich in protein (42.0–45.8% of dry matter) and fat (23.6–29.1% of dry matter). These results suggest that the type and proportion of ingredients—such as pork loin, pork lard, cricket powder, and starch—affect the nutritional value of the final product. In the case of pork meatballs, the absence of both pork lard and cricket powder (0.33%) contributes to their lower energy value of 80 kcal. This is lower than the energy content of commercial pork meatballs, which range from 121 to 158 kcal [58]. Furthermore, the analysis indicates that all three products contribute to daily macronutrient intake based on Thai Recommended Daily Intake (Thai RDI) values, providing 220–320 mg of sodium (11–16%), 115–150 mg of potassium (3–4%), and 10% of the daily value for vitamin B1 per 50 g serving (Table 7). The nutritional values of the three products align with the Thai Recommended Daily Intakes (% Thai RDI) for individuals over 6 years of age, based on a 2,000-kcal diet [29]. The recommended daily caloric intake is 2,600–2,800 kcal for adult males and 2,000–2,200 kcal for adult females [59]. Each product has a standardized serving size of 50 g, corresponding to ½ piece of pork sausage, 1 piece of grilled pork sausage, and 5 pork meatballs (Table 7). These meat products are among the most popular foods in Thailand. They can be consumed as snacks or used as ingredients in various one-dish meals such as noodles, Thai papaya salad, spicy salads, and soups. According to consumption reports (average per person per day), the intake of pork sausage (1.22 g) and pork ball (0.7 g) products in rural provinces is approximately 8 to 10 times higher than in urban areas [58,60]. Notably, the developed pork meatballs were found to contain 1.36 to 1.44 times more protein than those available on the market, while their fat and carbohydrate contents were 4.29 and 6.56 times lower, respectively [50]. These findings suggest that pork sausage, grilled pork sausage, and pork meatballs belong to the category of traditional Thai foods that are widely consumed and have the potential to appeal to health-conscious consumers. As such, incorporating cricket protein presents a promising way to enhance the nutritional profile of these popular local food products.

3.4 Cost-benefit Analysis

An analysis of the project to add value through the use of crickets in developing three processed food products—pork sausages, grilled pork sausages, and pork meatballs—showed that fixed costs, including machinery, kitchen equipment, and personal protective gear, accounted for 93.33% of the total investment (Table 8). The remaining 6.67% consisted of variable costs, primarily raw materials. An economic evaluation of the project's value over five years showed that the returns exceeded the initial investment. The project demonstrated strong financial viability, with the NPV of 1,274,843 THB [(38,790.29 USD): 1USD=33.0880 THB at March 5, 2025], the IRR of 31.80%, and the BCR of 3.76 (BCR Year 1 = 0.94, Year2 = 1.42, Year 3 = 1.97, Year 4 = 2.55, Year 5 = 3.76). This means that for every 1 THB (0.03043 USD) invested, the return was 3.76 times the cost. A return of 3.76 THB (0.11 USD) meets standard cost-effectiveness criteria, with the NPV > 0, the Benefit-BCR > 0, and the IRR > exceeding the funding source's interest rate (5%) [31]. Therefore, the evaluation confirms the cost-effectiveness of allocating the project budget, aligning with the estimated return on investment for cricket-based processed food products, which ranges from 27.45% to 69.26% [61]. This cost-benefit analysis serves as a useful guideline for reducing production costs—particularly variable costs related to raw materials—by fostering partnerships among key stakeholders, including cricket farmers, middlemen,

and Small and Medium Enterprises (SMEs). In the long term, it is recommended that a Social Return on Investment (SROI) assessment be conducted at the project's conclusion to support the sustainable development of Thai local foods incorporating cricket protein.

4. Conclusion

The development of suitable formulas incorporating cricket powder focused on creating pork sausages, grilled pork sausages, and pork meatballs with specific proportions of the ingredient. The most effective formulas contained 0.33%, 1.20%, and 0.33% cricket powder by weight, respectively. This finding is supported by sensory evaluation results, which showed no significant differences in overall acceptance scores compared to the control groups. Therefore, the formulas containing 0.33% cricket powder in pork sausages and pork meatballs, and 1.20% in grilled pork sausages, achieved the highest levels of consumer acceptance. Specifically, the protein content in pork meatballs (19.0 g/100 g) and pork sausages (13.4 g/100 g) meets the requirements of the Thai Community Product Standard (TCPS). For the community enterprise group, 93.33% of the project costs were fixed, while 6.67% were variable costs. The project yielded a return greater than the initial investment, with the NPV of 38,790.29 USD, the IRR of 31.80%, and the BCR of 3.76. The development of pork sausage, grilled pork sausage, and pork meatball products in this project demonstrates that cricket protein is a viable alternative for enhancing the nutritional value of traditional Thai food products. Additionally, it provides a practical solution to the issue of low-value cricket yields and offers valuable insights for promoting community enterprises and supporting sustainable development.

5. Acknowledgment

This research was supported by the Fundamental Fund (fiscal year 2024) from the National Science Research and Innovation Fund (NSRF), awarded to Valaya Alongkorn Rajabhat University under the Royal Patronage, Pathum Thani Province.

Author Contributions: NT and WO contributed to the study conception and design. Material preparation, data collection, and analysis were performed by KP, NC, CJ, KR and CR. The first draft of the manuscript was written by NT and WO commented on previous versions of the manuscript. All authors read and approved the final manuscript.

Funding: This research was supported by the Fundamental Fund (fiscal year 2024) from the National Science Research and Innovation Fund (NSRF), awarded to Valaya Alongkorn Rajabhat University under the Royal Patronage, Pathum Thani Province.

Conflicts of Interest: The authors declare no conflict of interest.

References

[1] Carcea, M. Quality and Nutritional/Textural Properties of Durum Wheat Pasta Enriched with Cricket Powder. *Foods* **2020**, *9*, 1298. https://doi.org/10.3390/foods9091298

[2] Halloran, A.; Megido, R. C.; Oloo, J.; Weigel, T.; Nsevolo, P.; Francis, F. Comparative Aspects of Cricket Farming in Thailand, Cambodia, Lao People's Democratic Republic, Democratic Republic of the Congo and Kenya. *J. Insects Food Feed* **2018**, *4*, 101–114. https://doi.org/10.3920/JIFF2017.0016

[3] Kampanat, P.; Krittika, C. *Knowledge Guide for Low-Cost Cricket Food Production Using Local Food Ingredients*; Faculty of Agriculture and Technology, Nakhon Phanom University: Thailand, 2023.

[4] Bangkok Bank SME. *Crickets: Novel Food of the Future with Global Markets*; Bangkok Bank SME: Thailand, **2020**.

[5] Mayura, P. "Insect": New Food Trend. *NIF Food Innov.* **2019**, 1–3.

[6] Montowska, M.; Kowalczewski, P. L.; Rybicka, I.; Fornal, E. Nutritional Value, Protein and Peptide Composition of Edible Cricket Powders. *Food Chem.* **2019**, *289*, 130–138. https://doi.org/10.1016/j.foodchem.2019.03.062

[7] Nowakowski, A. C.; Miller, A. C.; Miller, M. E.; Xiao, H.; Wu, X. Potential Health Benefits of Edible Insects. *Crit. Rev. Food Sci. Nutr.* **2022**, *62*, 3499–3508. https://doi.org/10.1080/10408398.2020.1867053

[8] Wongthahan, P.; Chandeewanta, S.; Phromthep, K.; Hengboriboon, L. Factors Affecting Customer Attitudes towards Alternative Cricket Protein and the Concept of Novel Products in China and Thailand. *CyTA–J. Food* **2024**, *22*, Article No. (if available). https://doi.org/10.1080/19476337.2024.2326061
[9] Farkas, V. I.; Máté, M.; Takács, K.; Jánosi, A. The House Cricket (*Acheta domesticus* Linnaeus) in the Food Industry: Farming, Technological Challenges, and Sustainability Considerations. *Appl. Sci.* **2025**, *15*, 9494. https://doi.org/10.3390/app15179494
[10] Wuttichai, L.; Eurngploy, C. *Development of Cricket Alternative Protein Products*; Chiang Mai Livestock Product Research and Development Center, Department of Livestock Development: Thailand, 2024.
[11] Yaowarat, S.; Yupa, H. *Factors Influencing the Consumption of Edible Insects in the Northeast*; Khon Kaen University: Thailand, **2017**.
[12] Better Pack Co., Ltd. Introduction to Meat Processing. **2020**. https://www.betterpack.co.th/news&article/0-38-
[13] Vichasilp, C.; Poungchompu, C. Feasibility of Detecting Pork Adulteration in Halal Meatballs Using Near Infrared Spectroscopy (NIR). *CMUJ Nat. Sci.* **2014**, *13*. https://doi.org/10.12982/CMUJNS.2014.0052
[14] Visetnoi, S.; Nelles, W. Can Organic Pork Help Achieve Sustainable Development Goals in Thailand? *Agriculture* **2023**, *13*, 1822. https://doi.org/10.3390/agriculture13091822
[15] Mazumder, M. A. R.; Sangsomboon, M.; Ketnawa, S.; Rawdkuen, S. Mushroom-Based Northern Thai Style Sausages: Physicochemical Properties, Nutritional Profile, and In Vitro Digestibility. *J. Agric. Food Chem.* **2024**, *72*, 101103. https://doi.org/10.1016/j.jafr.2024.101103
[16] Trujillo-Cayado, L. A.; García-Domínguez, I.; Rodríguez-Luna, A.; Hurtado-Fernández, E.; Santos, J. Cricket Protein as an Innovative Emulsifier for Avocado Oil: Formulation and Characterization of Sustainable Emulsions. *Appl. Sci.* **2024**, *14*, 1674. https://doi.org/10.3390/app14041674
[17] Maiprasert, P.; Payackpunth, C.; Chalermchaiwat, P.; Chantaro, P.; Hirunyophat, P.; Sangteerakij, D. Product Development of Flakes with Cricket Powder and Its Application in Granola Ball. *RMUTSV Res. J.* **2024**, *16*, 772–784.
[18] Pansuntia, R.; Fanpimai, K.; Roddee, J.; Promboot, S.; Sangsawad, P.; Promyo, K.; Phahom, T. Development of Prik Ka Kleua (Original Thai Sprinkles Seasoning for Rice). *Khon Kaen Agric. J.* **2023**, *1*, 587–594.
[19] Office of the National Economic and Social Development Council. *Quarterly Report on the Economic and Social Situation*; NESDC: Thailand, **2022**.
[20] Sakaeo Provincial Office. *General Information of Sakaeo*; Thailand, **2021**.
[21] Sa Kaeo Community Development Provincial Office. *Sa Kaeo Province BMN Survey Report, FY 2025*; Community Development Department, Ministry of Interior: Thailand, **2025**.
[22] Sakaeo Provincial Administrative Organization. *Five Star Product of Sakaeo*; Thailand, **2021**.
[23] Tokhun, N.; Ounsaneha, W.; Buachoon, N.; Chotklang, N. *Project to Improve Quality of Life and Raise the Grassroots Economy, Ta Praya District, Sa Kaeo Province*; Valaya Alongkorn Rajabhat University: Thailand, **2024**.
[24] Tokhun, N.; Ounsaneha, W.; Punaaterkoon, K.; Ruengkhajhon, K.; Jansukar, C.; Chotklang, N. *Innovations for Upgrading Production, Processing, and Value Addition of Cricket Products as Community Identity Products under the Bioeconomy Concept*; Valaya Alongkorn Rajabhat University: Thailand, 2024.
[25] Wongnai Media Co., Ltd. How to Make Homemade Moo Yor. **2019**. https://www.wongnai.com /recipes/homemade-vietnamese-ham
[26] Wongnai Media Co., Ltd. How to Make Pork Meatballs. **2019**. https://www.wongnai.com/recipes/pork-balls
[27] Wongnai Media Co., Ltd. How to Make Naem Nueng. **2021**. https://www.wongnai.com/recipes/nam-neaung
[28] Wangkawa, S.; Sinlapachai, T.; Koonyotying, S.; Wisetaud, C. *Developed Recipe for Processed Silkworm Pupa*; Queen Sirikit Department of Sericulture: Thailand, **2015**.
[29] Ministry of Public Health. *Notification of the Ministry of Public Health (No. 445) B.E. 2566 (2023): Nutrition Labelling*; Thai FDA: Thailand, **2024**.
[30] AOAC. *Official Methods of Analysis of AOAC International*, 21st ed.; AOAC International: Gaithersburg, MD, **2019**.
[31] Wolf, W. R. Methods of Analysis for Nutrition Labeling. In *AOAC International*; Sullivan, D. R.; Carpenter, D. E., Eds.; AOAC International: Gaithersburg, MD, **1993**.

[32] Al-Hasani, S. M.; Hlavac, J.; Carpenter, M. W. Rapid Determination of Cholesterol in Single and Multicomponent Prepared Foods. *J. AOAC Int.* **1993**, *76*, 902–906. https://doi.org/10.1093/jaoac/76.4.902

[33] Caine, W. R.; Aalhus, J. L.; Best, D. R.; Dugan, M. E. R.; Jeremiah, L. E. Relationship of Texture Profile Analysis and Warner–Bratzler Shear Force with Sensory Characteristics of Beef Rib Steaks. *Meat Sci.* **2003**, *64*, 333–339. https://doi.org/10.1016/S0309-1740(02)00110-9

[34] Department of Medical Sciences. *Standard Methods for Food Analysis*, Vol. 2; Thailand's National Office of Buddhism Printing House: Thailand, **2014**.

[35] Saengthongpinit, W.; Luanglue, M.; Somboonphol, P.; Butrachoti, S. Pork Stick Supplemented with Pomelo Albedo Fiber. *VRU Res. Dev. J.* **2010**, *9*, 8–18.

[36] Ulu, H. Effects of Carrageenan and Guar Gum on the Cooking and Textural Properties of Low-Fat Meatballs. *Food Chem.* **2016**, *87*, 523–529. https://doi.org/10.1016/j.foodchem.2004.01.002

[37] Lawless, H. T.; Heymann, H. *Sensory Evaluation of Food: Principles and Practices*, 2nd ed.; Springer: New York, 2010. https://doi.org/10.1007/978-1-4419-6488-5

[38] Peryam, D. R.; Pilgrim, F. J. Hedonic Scale Method of Measuring Food Preferences. *Food Technol.* **1957**, *11*, 9–14.

[39] Jaijit, S.; Paoprasert, N.; Pichitlamken, J. Economic Impact Assessment of Rice Research in Thailand. *Khon Kaen Agric. J.* **2017**, *45*, 613–624.

[40] Sanom, P.; Jangchud, K. Effect of Cricket (*Acheta domesticus*) Powder, Soy Protein Isolate, and Xanthan Gum on the Qualities of Rice Flour-Based Cookies. *RMUTP Res. J.* **2020**, *14*, 72–84.

[41] Dholvitayakhun, A.; Sanguanval, A.; Khayankannawi, S. Production of Moo Yor Using Microwave. *Rajabhat Agric. J.* **2014**, *13*, 80–87.

[42] Chatterjee, D.; Brambila, G. S.; Bowker, B. C.; Zhuang, H. Effect of Tapioca Flour on Physicochemical Properties and Sensory Descriptive Profiles of Chicken Breast Meat Patties. *J. Appl. Poult. Res.* **2019**, *28*, 598–605. https://doi.org/10.3382/japr/pfy076

[43] Doungthong, S. *Study and Development of Frozen Fish Balls from Cobia (Rachycentron canadum)*; Songkhla Rajabhat University: Thailand, **2004**.

[44] Suthivanit, N. *Manual of Meat and Meat Products: Meat*; Kasetsart University: Thailand, 1976.

[45] Jomduang, S.; Meechou, J.; Kaewsuriya, S. Study on Improving Quality of Moo Yor. Rajamangala University of Technology Lanna: Thailand, **1998**; pp 27–45.

[46] Utaida, T. Pork Balls Development and Shelf-Life Study by Comparing Packaging Types. *J. Sci. Technol. Ubon Ratchathani Univ.* **2020**, *22*, 45–51.

[47] Gantner, M.; Sadowska, A.; Piotrowska, A.; Kulik, K.; Sionek, B.; Kostyra, E. Wheat Bread Enriched with House Cricket Powder (*Acheta domesticus* L.) as an Alternative Protein Source. *Molecules* **2024**, *29*, 711. https://doi.org/10.3390/molecules29030711

[48] Mafu, A.; Ketnawa, S.; Phongthai, S.; Schönlechner, R.; Rawdkuen, S. Whole Wheat Bread Enriched with Cricket Powder as an Alternative Protein. *Foods* **2022**, *11*, 2142. https://doi.org/10.3390/foods11142142

[49] Lucas-González, R.; Fernández-López, J.; Pérez-Álvarez, J. A.; Viuda-Martos, M. Effect of Drying Processes on Chemical, Physicochemical, Techno-Functional, and Antioxidant Properties of Flours from House Cricket (*Acheta domesticus*). *Eur. Food Res. Technol.* **2019**, *245*, 1451–1458. https://doi.org/10.1007/s00217-019-03301-4

[50] Leewan, V.; Ritthiruangdej, P.; Therdthai, N. Effect of Guava Powder as a Fat Substitute on Physical, Chemical, and Sensory Quality of Sausages. In *Proc. 62nd Kasetsart Univ. Annu. Conf.*; Kasetsart University: Thailand, **2024**; pp 301–309.

[51] Codex Alimentarius Commission. *Report of the 28th Session of the Codex Committee on Food Hygiene (ALINORM 97/13A)*; FAO: Rome, **1997**.

[52] Sevenich, R.; Reineke, K.; Hecht, P.; Fröhling, A.; Rauh, C.; Schlüter, O.; Knorr, D. Impact of Different Water Activities on High-Pressure High-Temperature Inactivation of *Bacillus amyloliquefaciens* Spores. *Front. Microbiol.* **2015**, *6*, 689. https://doi.org/10.3389/fmicb.2015.00689

[53] Fellows, P. J. Dehydration. In *Food Processing Technology*, 3rd ed.; Woodhead Publishing: Cambridge, 2009; pp 481–524. https://doi.org/10.1533/9781845696344.3.481

[54] U.S. Food and Drug Administration. *Nutrition Facts Label*; FDA: USA, **2024**.
[55] Thai Industrial Standards Institute. *Thai Community Product Standard for Pork Meatballs (TCPS 304/2555)*; TISI: Thailand, **2012**.
[56] Chatpanglurlurt, R.; Dholvitayakhun, A. *Development of Moo Yor with Panang Curry Paste*; Rajamangala University of Technology Lanna Tak: Thailand, **2014**.
[57] Akesowan, A. Improvement of Production of Reduced-Fat Minced and Preserved Pork and Chicken with Konjac Flour. *Food* **1999**, *29*, 37–50.
[58] Chan-Urai, P. *Nutritive Value of Meatball Products*; M.Sc. Thesis, Mahidol University: Thailand, 2004.
[59] Faizan, U.; Rouster, A. S. Nutrition and Hydration Requirements in Children and Adults. In *StatPearls*; StatPearls Publishing: Treasure Island, FL, **2003**.
[60] Department of Health. *Report of Observation on Nutritional Status of Thailand*, 4th ed.; Ministry of Public Health: Thailand, **1995**.
[61] Khwanchai, P. *Database Collection and Value Addition of Crickets for Protein Food Products*; National Research Council of Thailand: Thailand, **2021**.

ASEAN
Journal of Scientific and Technological Reports
Online ISSN:2773-8752

Research article

Development of Probiotic Soy Yogurt Containing Kale Powder: Evaluation of Functional and Plant-Based Properties

Vijitra Plongbunjong[1], Kitiya Suhem[1], and Jarupat Kanjanarong[1*]

[1] Faculty of Science and Technology, Rajamangala University of Technology Rattanakosin, Nakhon Pathom, 73170, Thailand
[*] Correspondence: jarupat.kan@rmutr.ac.th

Citation:
Plongbunjong, V.; Suhem, K.; Kanjanarong, J. Development of probiotic soy yourt containing kale powder: Evaluation of functional and plant-based properties. *ASEAN J. Sci. Tech. Report.* **2026**, *29*(2), e260295. https://doi.org/10.55164/ajstr.v29i2.260295.

Article history:
Received: July 14, 2025
Revised: October 9, 2025
Accepted: November 15, 2025
Available online: January 20, 2026

Abstract: Probiotic soy yogurt containing kale powder represents a promising plant-based functional product suitable for lactose-intolerant individuals and health-conscious consumers. This study aimed to develop and characterize soy-based probiotic yogurts containing kale powder at concentrations of 0%, 1%, 3%, and 5% (w/w). All formulations were standardized to an initial total soluble solids (TSS) content of 15 °Brix and fermented at 43 ± 1 °C for 8 hours using a commercial yogurt starter and probiotic culture. The yogurt containing 1% kale powder exhibited the most desirable physicochemical and functional properties, including favorable fermentation characteristics (pH 4.63, titratable acidity 0.75 ± 0.03%), the highest viable lactic acid bacteria (LAB) count (8.37 ± 0.05 log CFU/g), and optimal curd structure. Sensory evaluation using a 9-point hedonic scale with thirty untrained panelists confirmed its highest overall acceptability (7.93 ± 0.74). Chemical composition analysis revealed slight variations among formulations, with the 1% kale-containing yogurt showing relatively higher levels of protein (3.49 g/100 g), dietary fiber (0.95 g/100 g), carbohydrate (10.6 g/100 g), energy (65.6 Cal/100 g), and vitamin K_1 (4.94 μg/100 g), reflecting the natural contribution of kale powder rather than fortification. During 21 days of storage at 4 ± 1 °C, the 1% kale-containing yogurt maintained probiotic viability above 7.0 log CFU/g, consistent with internationally recognized efficacy criteria for probiotic products. No yeast and mold growth was detected during storage. These findings highlight, for the first time, the feasibility of formulating probiotic soy yogurt containing kale powder with desirable product quality and functional potential, aligning with current trends in plant-based fermented foods.

Keywords: Soy yogurt; probiotics; kale powder; plant-based dairy

1. Introduction

In recent years, global interest in plant-based functional foods has grown substantially, driven by heightened consumer awareness of health benefits, environmental sustainability, and ethical concerns associated with animal-derived products. This dietary shift is widely acknowledged, with recent academic literature highlighting the strong trend toward healthier and more sustainable food options enriched with bioactive compounds, thereby propelling significant market growth and innovation [1]. Among the various innovations in this sector, plant-based dairy alternatives, such as yogurts made from legumes, grains, and nuts, have become particularly prominent. These products cater to populations with lactose intolerance, milk allergies, or those adopting vegetarian or vegan lifestyles [2]. In the ASEAN region, where health-

related non-communicable diseases and aging demographics are increasingly pressing issues, functional foods have been emphasized for their potential to maintain wellness and delay disease onset [3].

Soy milk is widely acknowledged as a suitable base for developing plant-based yogurts due to its high-quality protein, beneficial lipid profile, and ability to support microbial fermentation. It also provides a lactose-free, cholesterol-free, and sustainable alternative to dairy milk, thus appealing to individuals with lactose intolerance and those seeking heart-friendly diets [4]. Fermented soy-based products, including soy yogurt, have been associated with health-promoting effects such as improved gut microbiota balance, reduced blood cholesterol, and antioxidant activity [5-6]. Furthermore, soy yogurt is recognized as an effective carrier for probiotic strains, promoting their survival through the gastrointestinal tract [7]. Despite these benefits, plant-based yogurts made from soy often require formulation improvements to enhance their sensory and textural characteristics and overall consumer acceptability.

An emerging formulation strategy is the enrichment of soy yogurt with functional vegetables such as kale (*Brassica oleracea* L. var. *acephala* DC), a leafy green vegetable increasingly regarded as a superfood. Kale is rich in essential nutrients, including fiber, vitamins, particularly K_1 and β-carotene, minerals, and biologically active phytochemicals like glucosinolates and flavonoids. These compounds offer antioxidative and anti-inflammatory benefits and are associated with reduced risks of chronic diseases such as cardiovascular disorders and cancer [8]. In Thailand, kale cultivation and consumption have been rising steadily, especially among health-focused consumers, contributing to its growing incorporation into smoothies, salads, and functional food products alongside the expansion of organic agriculture [9].

Although kale is recognized for its nutritional value and increasing popularity, it has not been extensively studied for application in fermented plant-based food products. A review of contemporary scientific literature reveals a notable absence of research exploring the integration of kale into probiotic soy yogurt, indicating an opportunity for product innovation. Prior studies have examined the use of cereals, legumes, and fruit-based powders in dairy and soy yogurts [10-11], but no peer-reviewed publications have yet evaluated kale's inclusion in soy-based fermented systems. The high content of fiber and micronutrients in kale makes it a compelling additive to enhance nutritional quality. However, its fibrous nature and pigmentation could potentially alter yogurt texture and visual appeal if used in excessive amounts. Therefore, determining the optimal fortification level is essential to maintain product quality while maximizing health benefits.

Given the growing demand for clean-label and functional plant-based fermented products, particularly in Southeast Asia, where soy-based diets are culturally entrenched, this study aims to formulate and evaluate probiotic soy yogurt containing kale powder at concentrations of 0%, 1%, 3%, and 5% (w/w). The research evaluates fermentation performance, sensory quality, physicochemical and microbiological properties, and chemical composition. Results from this work are expected to inform future development of consumer-accepted, functionally improved, and value-added plant-based yogurts that align with health and sustainability trends.

2. Materials and Methods

2.1 Preparation of Kale Powder and Soy Milk

Fresh kale leaves (1 kg) were thoroughly washed under running water to remove surface impurities and then finely chopped. The chopped leaves were dehydrated in a convection oven at 60 ± 1 °C until constant weight was achieved. The dried leaves were subsequently ground using a high-speed blender and sieved through a 425 μm mesh to obtain a uniform fine powder. The final yield of kale powder was approximately 65 g per kilogram of fresh leaves, corresponding to a drying yield of about 6.5% (w/w). The resulting kale powder was stored in airtight zip-lock bags at 4 ± 1 °C until further use. For soy milk preparation, split soybeans (*Glycine max* (L.) Merr.) (1 kg) were washed and soaked in potable water at ambient room temperature for 6 hours. To reduce off-flavors and microbial load, the soaked beans were blanched in boiling water for 2 minutes. The blanched beans were then blended with potable water at a 1:3 (w/w) ratio to form a homogenized suspension. This suspension was filtered through a double-layered muslin cloth to extract soy milk. The extracted soy milk was pasteurized at 85± 1 °C for 15 minutes, followed by a second filtration using

sterile muslin to remove any remaining solids. The prepared soy milk was cooled to room temperature and stored at 4 ± 1 °C until further use.

2.2 Fermentation of Probiotic Soy Yogurt Containing Kale Powder

For the preparation of kale containing probiotic soy yogurt, soy milk was used as the fermentation substrate, and its total soluble solids were adjusted to 15 °Brix by adding sucrose. All formulations were thoroughly mixed to ensure homogeneity, pasteurized at 85 ± 1 °C for 15 minutes, and then cooled to 45 ± 1 °C. A commercial plain soy yogurt available in Thailand was used as the inoculum source to provide lactic acid bacteria for soy milk fermentation. The yogurt starter, containing *Lactobacillus bulgaricus*, *Streptococcus thermophilus*, *Lactobacillus acidophilus*, and *Bifidobacterium animalis* subsp. *lactis*, originally optimized for plant-based fermentations, was added at 10% (w/w). Kale powder was incorporated at concentrations of 1%, 3%, and 5% (w/w), while a control sample without kale (0%) was also prepared for comparison. The mixtures were transferred into 200 mL sterile glass containers and incubated at 43 ± 1 °C for 8 hours until the pH reached 4.6–4.8, which is considered suitable for set-style yogurt. The resulting yogurts were stored at 4 ± 1 °C until further analysis.

2.3 Sensory evaluation

A sensory evaluation was conducted to assess the acceptability of probiotic soy yogurt samples containing kale. Thirty untrained panelists participated in the evaluation, rating five sensory attributes: color, odor, flavor, texture, and overall acceptability. A 9-point hedonic scale, ranging from 1 (dislike extremely) to 9 (like extremely), was used to quantify participants' preferences. The collected data were statistically analyzed to identify consumer preferences and determine the most preferred formulation based on overall liking scores. This human-subject study was conducted in accordance with the Declaration of Helsinki and the institutional ethical guidelines of Mahamakut Buddhist University. Ethical approval was obtained under protocol number COA-0056-2567(2024).

2.4 Evaluation of Shelf-Life Stability of Probiotic Soy Yogurt Containing Kale Powder

The shelf-life stability of both the control and the most acceptable kale-containing probiotic soy yogurt formulations was assessed over a 21-day refrigerated storage period at 4 ± 1 °C. All samples were stored in tightly sealed transparent glass bottles wrapped with aluminum foil to protect them from light exposure and placed in a dark refrigerated environment at 4 ± 1 °C throughout the entire storage period. Samples were collected and analyzed on days 0, 7, 14, and 21 to determine changes in physicochemical properties, microbiological quality, and product stability during storage**.** This evaluation focused on monitoring potential alterations in physicochemical parameters and microbiological quality during storage. Particular attention was given to the enumeration of lactic acid bacteria and the detection of yeast and mold at regular intervals to ensure microbial safety and product stability throughout the storage duration [12].

2.5 Textural profile analysis

After fermentation, all yogurt samples were refrigerated at 4 ± 1 °C for 48 hours before texture analysis. Before testing, each sample (approximately 50 mL) was gently transferred into a cylindrical plastic cup (50 mm diameter × 30 mm height) to obtain a uniform surface. A BRAVO Food Texture Analyzer (Model TA Prime) was used to evaluate the texture characteristics following a modified procedure adapted from Cheng et al. [13]. The analysis simulated the chewing action by performing a two-cycle compression test using a cylindrical probe (TA4/1000) with a diameter of 36 mm. The test was conducted under the following settings: pre-test speed at 1 mm/s, test speed at 1 mm/s, post-test speed at 20 mm/s, and a compression distance of 25 mm. All measurements were carried out in triplicate, and the average values were reported. Texture profile analysis included measurements of hardness, cohesiveness, springiness, and gumminess to assess the quality and consistency of each yogurt formulation.

2.6 Physicochemical analysis

The pH of the yogurt samples was measured using a digital pH meter (Mettler Toledo, USA), and total soluble solids (TSS) were determined using a digital refractometer (ATAGO MASTER-50-H, Japan). Titratable acidity was expressed as a percentage of lactic acid according to the AOAC (2023) method [14].

Color attributes (L*, a*, b*) were evaluated using a colorimeter (Konica Minolta CR-400, Japan) calibrated with a standard white plate. Syneresis was determined by centrifuging 10 g of yogurt at 4,500 rpm for 10 min at 4 °C, and the separated liquid fraction was expressed as a percentage of the total sample weight. Water-holding capacity (WHC) was measured by quantifying the retained fraction after centrifugation [15–16]. All measurements were conducted in triplicate (n = 3), and results were expressed as mean ± SD. The proximate composition, including energy, protein, carbohydrate, total fat, dietary fiber, moisture, ash, and vitamin K_1, was analyzed by an accredited laboratory following AOAC (2023) official methods. Beta-carotene was analyzed instead of vitamin A because kale primarily contains carotenoids rather than preformed vitamin A (retinol). The compound was quantified using high-performance liquid chromatography (HPLC) to represent the measurable provitamin A fraction naturally present in plant-based ingredients, following validated procedures performed by a certified private laboratory.

2.7 Microbiological determinations

The microbial analysis of kale-containing probiotic soy yogurt was performed following the methodology adapted from Mehaya et al. [17]. Total bacterial count was determined using standard plate count techniques. Lactic acid bacteria were enumerated by spread-plating on de Man, Rogosa, and Sharpe (MRS) agar, followed by incubation at 37 ± 1 °C for 48 hours under anaerobic conditions. Yeasts and molds were assessed on potato dextrose agar (PDA) and incubated at 30 ± 2 °C for 5 to 7 days. All microbial counts were expressed as log colony-forming units per gram (log CFU/g).

2.8 Statistical Analysis

A completely randomized design (CRD) was employed to evaluate the physical, chemical, and microbiological characteristics of the yogurt samples, while sensory evaluation followed a randomized complete block design (RCBD) to account for panelist variability. All data are expressed as mean ± standard deviation (SD) based on three independent replicates. One-way analysis of variance (ANOVA) was performed to determine significant differences among treatments, and mean separation was conducted using Duncan's multiple range test (DMRT) at a 95% confidence level ($p \leq 0.05$). Statistical analyses were performed using IBM SPSS Statistics software, version 28 (IBM Corp., Armonk, NY, USA).

3. Results and Discussion

3.1 Fermentation Characteristics of Probiotic Soy Yogurt Containing Kale Powder

The effect of different kale powder concentrations on the fermentation performance and structural development of probiotic soy yogurt was studied. Four treatments were prepared: a control sample (0% kale) and three samples containing 1%, 3%, and 5% kale powder. Before fermentation, each formulation was adjusted to 15 °Brix and inoculated with a commercially available probiotic culture. After incubating at 43 ± 1 °C for 8 hours, noticeable variations in fermentation dynamics and curd formation were recorded. The quality of curd structure was observed to deteriorate progressively with increasing concentrations of kale. While acceptable gel textures were retained in the control, 1%, and 3% formulations, the 5% kale yogurt presented weak coagulation and a watery appearance. This decline in curd firmness at higher levels of kale fortification may be linked to interactions between bioactive compounds in kale and the soy protein matrix during acidification, potentially disrupting the aggregation and gelation of protein structures [18].

As presented in Figure 1, the pH values of all yogurt formulations consistently decreased during the 8-hour fermentation period, ultimately falling within the range of 4.63 to 4.80. Notably, the 1% kale-containing sample exhibited the most substantial acidification, achieving the lowest final pH (4.63 ± 0.03), which may reflect enhanced lactic acid bacterial activity stimulated by moderate levels of kale addition. The acidification process plays a vital role in curd formation, as casein begins to coagulate when the pH nears its isoelectric point (approximately 4.6), promoting gel network development [10, 17]. In parallel with the reduction in pH, titratable acidity steadily increased across all samples. During the 8-hour incubation period, lactic acid contents ranged between 0.62% to 0.75%. The highest acidity was found in the 1% kale formulation (0.75 ± 0.03%), while the 5% kale sample recorded the lowest value (0.62 ± 0.02%). All measured values

exceeded the minimum lactic acid content of 0.6%, as required by Thailand's Ministry of Public Health under Notification No. 353 [19] for fermented milk products.

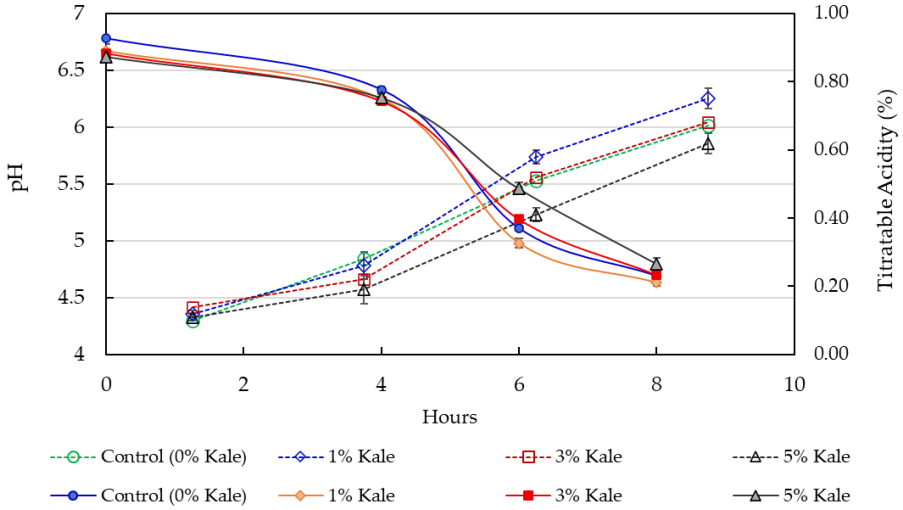

Figure 1. pH (—) and titratable acidity (---) profiles of probiotic soy yogurt containing kale powder (0%, 1%, 3%, and 5%) during 8 hours of fermentation at 43 ± 1 °C.

The TSS of the fermented soy yogurt samples ranged from 10.67 ± 0.58 to 12.33 ± 0.58 °Brix (Table 1). A statistically significant increase in TSS was observed as the kale powder concentration increased from 0% to 5%. This trend is likely due to the addition of kale powder, which contains naturally occurring sugars, soluble fibers, and other water-soluble phytochemicals. These components may have dissolved during heat treatment and contributed to the higher TSS values observed following pasteurization and after fermentation [10, 20]. Although sugar consumption by fermenting microbes typically reduces TSS during yogurt production, the enrichment with kale appears to have mitigated this reduction, particularly in the 5% formulation, which retained the highest TSS after the 8-hour fermentation. Syneresis, an indicator of gel network stability, was found to increase proportionally with higher kale inclusion. The yogurt containing 5% kale showed the greatest syneresis value (39.17 ± 1.04%) (Table 1), suggesting that elevated kale levels may weaken gel integrity. It is generally acknowledged that soy-based yogurts exhibit more pronounced syneresis compared to their dairy counterparts due to inherent differences in protein and lipid composition [21-22]. Conversely, WHC demonstrated a declining pattern, ranging from 71.33 ± 1.25% in the control to 60.17 ± 0.76% in the 5% kale sample. This decline suggests that increased kale content might interfere with the protein network formation, thereby leading to greater whey separation. These findings align with results from Arab et al. [23], which indicated that WHC in soy-based yogurts is influenced by fermentation dynamics, stabilizer use, and the protein content of the formulation. Kale addition also significantly altered the color properties of the yogurt. The visual appearance and color of the kale containing yogurt samples at four concentration levels are shown in Figure 2. As the kale concentration increased, the lightness value (L*) decreased, indicating a darker appearance. Simultaneously, the a* values shifted negatively, reflecting increased greenness, while b* values progressively decreased, indicating reduced yellowness. These changes are largely attributed to pigments such as chlorophylls and carotenoids inherent in kale, which not only affect product appearance but also offer health-related benefits [10, 24]. The addition of kale powder may enhance the functional quality of soy yogurt due to the presence of bioactive compounds such as vitamin K_1, β-carotene, lutein, and dietary fiber, which are known to support antioxidant activity and digestive health [10, 24, 25]. Although the 1% addition used in this study is relatively small, these components can still contribute to improving the nutritional and functional properties of the product rather than providing direct health claims.

In terms of microbiological quality, all yogurt formulations maintained LAB counts above 7 log CFU/g (approximately 10^7 CFU/g), which exceeds the minimum level generally recommended for probiotic foods to ensure functional efficacy [25]. The 1% kale formulation recorded the highest LAB population (8.37 ± 0.05 log

CFU/g), possibly due to prebiotic support from moderate kale enrichment. This finding aligns with Kim et al. [8], who demonstrated enhanced LAB survival in kale-based fermentations due to antioxidant-rich fibers, and with Rashwan et al. [10], who reported stabilized probiotic viability in yogurts containing plant-based bioactives. Additionally, no yeast and mold growth was detected in any sample, underscoring the microbiological safety of all formulations. Collectively, the soy yogurt containing 1% kale demonstrated the most desirable combination of quality traits, including strong gel structure, minimal syneresis, enhanced LAB viability, and improved color, making it the most favorable option among the variants tested.

Figure 2. Visual appearance and color of probiotic soy yogurt containing kale powder (0%, 1%, 3%, and 5%) at 8 hours of fermentation at 43 ± 1 °C.

Table 1. Physicochemical properties of probiotic soy yogurt containing different levels of kale powder after fermentation

Properties	Control (0% Kale)	1% Kale	3% Kale	5% Kale
Physical:				
TSS (°Brix)	10.67 ± 0.58^{b}	10.83 ± 0.29^{b}	11.50 ± 0.50^{ab}	12.33 ± 0.58^{a}
Syneresis (%)	28.83 ± 2.02^{c}	31.16 ± 1.04^{c}	35.17 ± 0.76^{b}	39.17 ± 1.04^{a}
Water-Holding Capacity (WHC, %)	71.33 ± 1.25^{a}	68.17 ± 1.04^{b}	65.10 ± 1.00^{c}	60.17± 0.76^{d}
Color L*	78.83 ± 0.51^{a}	70.48 ± 0.71^{b}	59.22 ± 1.00^{c}	52.41 ± 0.74^{d}
a*	-1.71 ± 0.04^{a}	-3.64 ± 0.06^{b}	-4.57 ± 0.12^{c}	-4.72 ± 0.07^{d}
b*	17.32 ± 0.85^{a}	15.83 ± 0.87^{ab}	14.37 ± 0.65^{b}	12.33 ± 0.89^{c}
Microbiology:				
Total Bacteria (log CFU/g)	8.30 ± 0.02^{b}	8.42 ± 0.06^{a}	8.23 ± 0.05^{b}	7.11 ± 0.08^{c}
Lactic Acid Bacteria (log CFU/g)	8.28 ± 0.03^{ab}	8.37 ± 0.05^{a}	8.19 ± 0.08^{b}	7.05 ± 0.07^{c}
Yeast and Mold (log CFU/g)^{ns}	ND	ND	ND	ND

Note: Values are presented as mean ± SD (n = 3). Different superscript letters in the same row indicate significant differences ($p \leq 0.05$), ND indicates not detected, while ns indicates non-significant differences ($p > 0.05$), as determined by one-way ANOVA.

3.2 Textural Attributes of Probiotic Soy Yogurt Containing Kale Powder

Texture Profile Analysis (TPA) demonstrated that the inclusion of kale powder had a dose-dependent impact on the structural attributes of probiotic soy yogurt (Table 2). The control sample (0% kale) exhibited the highest hardness (2.39 ± 0.05 N), cohesiveness (0.51 ± 0.07), and gumminess (2.72 ± 0.08 N), with moderate springiness (0.18 ± 0.04 s). When 1% kale was added, hardness decreased slightly to 2.25 ± 0.02 N, and cohesiveness remained statistically unchanged (0.49 ± 0.05). Interestingly, springiness significantly increased to 0.27 ± 0.07 s ($p \leq 0.05$), while gumminess was maintained (2.66 ± 0.06 N), indicating that moderate kale supplementation preserved gel integrity and even improved the elastic recovery of the matrix. However, higher concentrations of kale (3% and 5%) severely compromised the yogurt's textural parameters. Hardness dropped sharply to 0.40 ± 0.03 N and 0.32 ± 0.02 N, respectively, and gumminess was reduced to 0.00 N in both cases. Cohesiveness and springiness were also dramatically reduced, with values approaching zero, signifying an almost complete breakdown of the gel structure. The total loss of springiness (0.00 ± 0.00 s) particularly

reflects the absence of elasticity, a key factor in yogurt mouthfeel. This complete loss of springiness and gumminess clearly indicates a gel failure or non-gelling structure rather than merely a compromised texture. These formulations were therefore considered unsuccessful products in terms of textural integrity, as the excessive kale content disrupted the protein–polysaccharide network formation and reduced water-binding capacity, leading to weak or non-existent gel matrices. This phenomenon is consistent with the inherently weaker gelation ability of plant proteins compared with casein micelles in dairy systems [28]. These results align with previous findings that low levels of dietary fiber may enhance yogurt structure, whereas excessive fiber can disrupt the formation of a stable protein network [26–27]. The degradation observed at higher levels of kale is likely due to the interference of insoluble fibers with protein–protein interactions and competition for water within the matrix, impairing both casein and soy protein gelation. In plant-based yogurt systems, where the gel structure is inherently weaker than in dairy-based counterparts due to the absence of casein micelles, such interference becomes more pronounced and often leads to gel collapse [28].

Therefore, the findings suggest that a 1% kale addition level provides an optimal balance by enhancing the functional and quality attributes of the yogurt without compromising its texture. In contrast, higher concentrations (≥3%) negatively affect the physical structure of the yogurt, highlighting the importance of precise formulation when incorporating plant-based ingredients into functional food systems.

Table 2. Texture profile analysis (TPA) results of probiotic soy yogurt containing kale powder

Texture profile analysis (TPA)	Hardness (N)	Cohesiveness (-)	Springiness (s)	Gumminess (N)
Control (0% Kale)	2.39 ± 0.05^{a}	0.51 ± 0.07^{a}	0.18 ± 0.04^{b}	2.72 ± 0.08^{a}
1% Kale	2.25 ± 0.02^{b}	0.49 ± 0.05^{a}	0.27 ± 0.07^{a}	2.66 ± 0.06^{a}
3% Kale	0.40 ± 0.03^{c}	0.03 ± 0.02^{b}	0.00 ± 0.00^{c}	0.00 ± 0.00^{b}
5% Kale	0.32 ± 0.02^{c}	0.01 ± 0.00^{b}	0.00 ± 0.00^{c}	0.00 ± 0.00^{b}

Note: Values are presented as mean ± SD. Different superscript letters within the same column indicate significant differences ($p \leq 0.05$), as determined by one-way ANOVA.

3.3 Sensory Acceptability of Probiotic Soy Yogurt Containing Kale Powder

The impact of kale powder supplementation on the sensory attributes of probiotic soy yogurt was assessed using a 9-point hedonic scale with 30 untrained panelists evaluating color, odor, flavor, texture, and overall liking (Table 3). The yogurt sample containing 1% kale powder received the highest overall acceptability score (7.93 ± 0.74), which was significantly higher than the control (7.43 ± 1.04; $p \leq 0.05$), indicating enhanced consumer preference at this fortification level. The 1% kale sample also achieved favorable scores across all other sensory attributes, including flavor (7.57 ± 0.94) and texture (7.33 ± 1.06), suggesting that low-dose kale incorporation may contribute to a well-balanced mouthfeel and a pleasant vegetal note without compromising product quality. These findings align with prior studies reporting that moderate inclusion of green vegetable powders can improve consumer perception in plant-based and dairy matrices by subtly enhancing flavor complexity and functional appeal [29]. The mild enrichment may also have influenced perceived creaminess and color uniformity due to kale's chlorophyll and fiber content, which has been associated with a smoother texture and more vibrant appearance in fermented products [30–31]. In contrast, higher fortification levels (3% and 5%) resulted in significantly lower scores across all sensory parameters, with the 5% kale yogurt receiving the lowest overall liking score (5.63 ± 0.72). Panelist feedback indicated that these samples exhibited unpleasant bitterness, off-flavors, and an overly dark green coloration, which negatively affected consumer acceptance. These undesirable attributes are likely due to elevated concentrations of chlorophylls, phenolic compounds, and insoluble fibers, which are known to contribute to sensory imbalances when used excessively in food formulations [32–33]. Overall, the results indicate that incorporating 1% kale powder provides the most favorable formulation, improving sensory characteristics and overall product acceptability. This finding supports its potential application in developing plant-based yogurt alternatives that are both palatable and suitable for consumers seeking dairy-free options.

Table 3. Sensory evaluation scores of kale-containing probiotic soy yogurt samples

Treatments	Color	Odor	Flavor	Texture	Overall liking score
Control (0% Kale)	7.27 ± 0.78[a]	7.23 ± 0.82[a]	7.50 ± 1.01 [a]	7.27 ± 1.08 [a]	7.43 ± 1.04 [b]
1% Kale	7.43 ± 1.55[a]	7.26 ± 0.98[a]	7.57 ± 0.94 [a]	7.33 ± 1.06 [a]	7.93 ± 0.74 [a]
3% Kale	6.60 ± 1.22[b]	6.07 ± 1.25[b]	6.50 ± 1.07 [b]	6.73 ± 1.11 [b]	6.87 ± 0.63 [c]
5% Kale	5.93 ± 1.36[c]	4.40 ± 1.00[c]	5.10 ± 0.92 [c]	5.47 ± 0.82 [c]	5.63 ± 0.72 [d]

Note: Values are presented as mean ± SD (n = 30). Different superscript letters within the same column indicate significant differences ($p \leq 0.05$), as determined by one-way ANOVA.

3.4 Chemical Composition of Probiotic Soy Yogurt Containing Kale Powder

The chemical components of the two most consumer-preferred formulations of control (0% kale) and 1% kale-containing soy yogurt were compared to evaluate the functional impact of kale supplementation (Table 4). The yogurt containing kale powder exhibited modest yet meaningful improvements in several key nutritional metrics. Energy content increased by approximately 6.3% (65.6 vs. 61.7 Cal/100 g), coinciding with slight rises in protein (3.49 vs. 3.24 g/100 g), total fat (1.03 vs. 0.88 g/100 g), and total carbohydrate (10.6 vs. 10.2 g/100 g). These enhancements are consistent with the compositional attributes of kale, which is rich in macronutrients and phytochemicals. Dietary fiber content also improved in the 1% kale yogurt (0.95 vs. 0.81 g/100 g), which aligns with kale's established role as a dietary fiber source. Notably, vitamin K_1 (phylloquinone) levels increased significantly, from 0.68 to 4.94 μg/100 g (approximately sevenfold), highlighting kale's potential as a concentrated source of phylloquinone, a nutrient important for blood coagulation and bone health [34]. However, this amount is still below 10% of the Thai Recommended Daily Intake (RDI) for vitamin K (60 μg/day) as specified in the Thailand Ministry of Public Health Notification No. 445 (B.E. 2566) and reflects a functional improvement in formulation. Although beta-carotene (provitamin A) was not detected under the analytical conditions used, previous research has identified kale as a valuable source of carotenoids, including β-carotene and lutein [35]. The relatively low vitamin K_1 level compared with the theoretical content in kale powder may be due to its susceptibility to degradation by heat, light, and oxygen during drying, pasteurization, and fermentation processes. Oxidative reactions and dilution within the yogurt matrix could also contribute to further losses during storage. To improve vitamin K_1 retention in future studies, researchers may consider using higher kale concentrations, applying gentle drying methods such as freeze-drying, protecting the product from light and oxidation, incorporating microencapsulation techniques, or adding natural antioxidants before incorporation. While the addition of 1% kale powder improved the nutritional profile, particularly in dietary fiber and vitamin K_1, the quantity used in this study does not meet the minimum thresholds for nutrient fortification or enrichment claims according to the Thailand Ministry of Public Health Notification No. 445 (B.E. 2566). A slight increase in ash content (0.43 vs. 0.40 g/100 g) and a minor reduction in moisture (84.5% vs. 85.3%) were also observed, suggesting a more nutrient-dense matrix in the kale-added sample. These trends are in line with previous findings that reported compositional improvements in soy-based fermented products following the addition of green vegetable powders [36]. The results confirm that incorporating 1% kale powder into soy yogurt can enhance its chemical composition and functional properties, particularly in protein, dietary fiber, and vitamin K_1 content, without compromising sensory attributes. This formulation presents a promising plant-based functional product for consumers seeking improved product quality and functional potential in non-dairy alternatives.

Table 4. Chemical composition of probiotic soy yogurt with and without kale powder

Parameters	Control (0% Kale)	Soy Yogurt with 1% Kale
Energy (Cal/100g)	61.7	65.6
Protein (g/100g)	3.24	3.49
Total Carbohydrate (g/100g)	10.2	10.6
Total Fat (g/100g)	0.88	1.03
Moisture (g/100g)	85.3	84.5
Ash (g/100g)	0.40	0.43
Total Dietary Fiber (g/100g)	0.81	0.95
Vitamin K_1 (ug/100g)	0.68	4.94
Vitamin A (Beta-carotene) (ug/100g)	ND	ND

Note: ND = Not detected.

3.5 Storage Stability of Probiotic Soy Yogurt Containing Kale Powder

The shelf-life characteristics of probiotic soy yogurt containing 1% kale powder were evaluated over 21 days, focusing on key physicochemical and microbiological parameters. The storage stability of both control (0% kale) and 1% kale-containing probiotic soy yogurts was monitored on days 0, 7, 14, and 21 under refrigerated conditions (4 ± 1 °C) to assess changes in their physicochemical and microbiological properties. In both formulations, the pH gradually decreased throughout storage, indicating post-acidification caused by the residual metabolic activity of LAB. The control sample decreased from 4.68 ± 0.01 (Day 0) to 4.47 ± 0.05 (Day 21), whereas the 1% kale-containing yogurt showed a slightly greater reduction, from 4.64 ± 0.02 to 4.39 ± 0.02 (Table 5). Titratable acidity increased significantly ($p \leq 0.05$) in both formulations, from 0.67% to 0.93% for the control and from 0.72% to 1.05% for the kale yogurt, which is consistent with continued LAB fermentation during refrigerated storage [7, 37]. Syneresis (%) decreased steadily in both yogurts, from 28.85 ± 1.29% to 25.02 ± 2.24% in the control and 31.53 ± 0.62% to 25.30 ± 0.33% in the kale yogurt, suggesting improved serum retention and gel stability over time. The improvement observed in the kale formulation may be attributed to the WHC of kale fiber and its contribution to the stabilization of the protein–polysaccharide network [23, 38]. WHC and color parameters remained stable ($p > 0.05$) in both samples, with only a slight reduction in lightness (L) observed in the 1% kale yogurt, likely due to partial oxidation of chlorophyll pigments. Microbiologically, both formulations maintained high probiotic viability throughout the 21-day storage period. Total bacterial counts in the control yogurt decreased slightly from 8.25 log CFU/g (Day 0) to 7.21 log CFU/g (Day 21) (data not shown), while the 1% kale containing yogurt retained 8.32 log CFU/g to 7.41 log CFU/g. Likewise, LAB counts showed minimal reductions, decreasing from 8.21 to 7.14 log CFU/g in the control and from 8.31 to 7.37 log CFU/g in the 1% kale yogurt, indicating that kale addition contributed to better microbial protection, possibly due to its prebiotic fibers and antioxidant compounds [8, 38]. Microbiologically, both formulations maintained viable counts of lactic acid bacteria (LAB) exceeding 7 log CFU/g, which meets the requirement for probiotic foods as specified by the Thailand Ministry of Public Health Notification No. 346 (B.E. 2555). According to the accompanying Thai FDA guidelines, probiotic-containing foods are recommended to contain at least 10^6 CFU/g (6 log CFU/g) of viable microorganisms throughout the shelf life to ensure functional efficacy. No yeast and mold growth was detected in any samples, confirming the microbiological safety of the products during storage. Overall, both yogurt formulations exhibited stable physicochemical and microbiological properties during refrigerated storage. The addition of 1% kale slightly improved LAB survivability and gel consistency, indicating that kale fortification can serve as a functional strategy to enhance probiotic stability and product quality in soy-based yogurts during cold storage [7, 8, 38].

Table 5. Physicochemical properties of probiotic soy yogurt during refrigerated storage for 21 days

Properties /Days	pH	Titratable acidity(%)	Syneresis (%)	WHC (%)	Color		
					L*	a*	b*
Control (0% Kale):							
0	4.68 ± 0.01^{a}	0.67 ± 0.01^{d}	28.85 ± 1.29^{ns}	71.55 ± 1.29^{ns}	78.31 ± 0.60^{a}	-1.73 ± 0.02^{ns}	17.30 ± 0.15^{ns}
7	4.61 ± 0.02^{b}	0.73 ± 0.02^{c}	27.83 ± 1.60^{ns}	72.17 ± 1.60^{ns}	78.13 ± 0.57^{a}	-1.70 ± 0.01^{ns}	17.28 ± 0.24^{ns}
14	4..58 ± 0.02^{c}	0.84 ± 002^{b}	27.27 ± 1.96^{ns}	72.73 ± 1.96^{ns}	77.53 ± 0.10^{b}	-1.71 ± 0.03^{ns}	17.10 ± 0.27^{ns}
21	4.47 ± 0.05^{d}	0.93 ± 0.02^{a}	25.02 ± 2.24^{ns}	74.98 ± 2.24^{ns}	76.53 ± 0.38^{c}	-1.70 ± 0.03^{ns}	17.08 ± 0.11^{ns}
Soy Yogurt (1% Kale):							
0	4.64 ± 0.02^{a}	0.72 ± 0.02^{c}	31.53 ± 0.62^{a}	68.62 ± 0.45^{d}	70.73 ± 0.10^{a}	-3.64 ± 0.15^{c}	16.57 ± 0.26^{a}
7	4.60 ± 0.01^{b}	0.76 ± 0.01^{c}	28.08 ± 0.45^{b}	71.92 ± 0.45^{c}	69.63 ± 0.19^{b}	-3.52 ± 0.12^{bc}	16.33 ± 0.18^{a}
14	4.57 ± 0.01^{c}	0.89 ± 002^{b}	26.62 ± 0.20^{c}	73.38 ± 0.20^{b}	69.40 ± 0.39^{b}	-3.43 ± 0.14^{b}	16.12 ± 0.22^{a}
21	4.39 ± 0.02^{d}	1.05 ± 0.03^{a}	25.30 ± 0.33^{d}	74.70 ± 0.33^{a}	69.27 ± 0.51^{b}	-3.27 ± 0.13^{a}	15.52 ± 0.25^{b}

Note: Values are presented as mean ± SD (n = 3). Different superscript letters within the same column indicate significant differences ($p \leq 0.05$) among storage periods for each sample, while *ns* indicates non-significant differences ($p > 0.05$), as determined by one-way ANOVA.

4. Conclusions

This study demonstrated the successful development of probiotic soy yogurt containing kale powder, confirming its potential as a functional, plant-based fermented product. Among the tested formulations, the yogurt containing 1% kale powder exhibited the most desirable characteristics, including optimal fermentation performance, improved texture, high sensory acceptability, and favorable chemical composition, particularly in protein, dietary fiber, and vitamin K_1. This formulation also maintained probiotic viability above 7 log CFU/g throughout 21 days of refrigerated storage, with no detectable yeast and mold, indicating good microbiological safety and shelf-life stability. In contrast, higher kale concentrations (3% and 5%) negatively affected gel structure, taste, and overall product quality, likely due to interference of excessive fiber with the protein network. These findings highlight the feasibility of incorporating low levels of kale powder to enhance the functional quality of soy yogurt without compromising its sensory and structural integrity. Further research is recommended to explore the use of stabilizers or fiber modification techniques to improve product quality and consumer acceptance of plant-based yogurt products.

5. Acknowledgements

The authors would like to thank the Department of Food Processing and Culinary Science and the Department of Environmental Science, Faculty of Science and Technology, Rajamangala University of Technology Rattanakosin, for providing the essential research facilities.

Author Contributions: Conceptualization, V.P. and J.K.; Methodology, J.K., V.P., and K.S.; Formal analysis and investigation, V.P., J.K., and K.S.; Writing – original draft preparation, J.K. and V.P.; Writing – review and editing, J.K. and V.P.; Supervision, V.P. and J.K.; Project administration, J.K.; Funding acquisition, J.K.

Funding: This research was supported by the Thailand Science Research and Innovation (TSRI) and Fundamental Fund of Rajamangala University of Technology Rattanakosin (RMUTR) with funding under contract No. FRB6741/2567/ Project code 192967 / Research project: Probiotic Yogurt from Soy Milk with Kale Powder for Health to a Prototype Community Product in Nakhon Pathom Province (2024).

Conflicts of Interest: The authors declare no conflict of interest.

References

[1] Fekete, M.; Lehoczki, A.; Kryczyk-Poprawa, A.; Zábó, V.; Varga, J. T.; Bálint, M.; Fazekas-Pongor, V.; Csípő, T.; Rząsa-Duran, E.; Varga, P. Functional Foods in Modern Nutrition Science: Mechanisms, Evidence, and Public Health Implications. *Nutrients* **2025**, *17*(13), 2153. https://doi.org/10.3390/nu17132153

[2] Silva, A. R. A.; Silva, M. M. N.; Ribeiro, B. D. Health Issues and Technological Aspects of Plant-Based Alternative Milk. *Food Res. Int.* **2022**, *152*, 110936. https://doi.org/10.1016/j.foodres.2019.108972

[3] Garza-Juárez, A.; Pérez-Carrillo, E.; Arredondo-Espinoza, E. U.; Islas, J. F.; Benítez-Chao, D. F.; Escamilla-García, E. Nutraceuticals and Their Contribution to Preventing Noncommunicable Diseases. *Foods* **2023**, *12*(17), 3262. https://doi.org/10.3390/foods12173262

[4] Granato, D.; Nunes, D. S.; Barba, F. J. An Integrated Strategy between Food Chemistry, Biology, Nutrition, Pharmacology, and Statistics in the Development of Functional Foods: A Proposal. *Trends Food Sci. Technol.* **2017**, *62*, 13–22. https://doi.org/10.1016/j.tifs.2016.12.010

[5] Arumugam, S.; Dioletis, E.; Paiva, R.; Fields, M. R.; Weiss, T. R.; Secor, E. R.; Ali, A. Fermented Soy Beverage Q CAN Plus Consumption Improves Serum Cholesterol and Cytokines. J. Med. *Food* **2020**, 23(5), 560–563. https://doi.org/10.1089/jmf.2019.0116

[6] Jung, S. M.; Haddad, E. H.; Kaur, A.; Sirirat, R.; Kim, A. Y.; Oda, K.; Fraser, G. E.; Sabaté, J. A Non-Probiotic Fermented Soy Product Reduces Total and LDL Cholesterol: A Randomized Controlled Crossover Trial. *Nutrients* **2021,** *13*(2), 535. https://doi.org/10.3390/nu13020535

[7] Ranadheera, C. S.; Vidanarachchi, J. K.; Rocha, R. S.; Cruz, A. G.; Ajlouni, S. Probiotic Delivery through Fermentation: Dairy vs. Non-Dairy Beverages. *Fermentation* **2017**, *3*(4), 67. https://doi.org/10.3390/fermentation3040067

[8] Kim, G. Y.; Kim, S. A.; Kong, S. Y.; Seong, H.; Bae, J. H.; Han, N. S. Synergistic Antioxidant and Anti-Inflammatory Activities of Kale Juice Fermented with Limosilactobacillus reuteri EFEL6901 or Limosilactobacillus fermentum EFEL6800. *Antioxidants* **2023,** *12*(10), 1850. https://doi.org/10.3390/antiox12101850

[9] Mobility Foresights. Thailand Superfood Market Size and Forecasts 2030. Available online: https://mobilityforesights.com/product/thailand-superfood-market (accessed on 12 July 2025).

[10] Rashwan, A. K.; Osman, A. I.; Chen, W. Natural Nutraceuticals for Enhancing Yogurt Properties: *A Review. Environ. Chem. Lett.* **2023,** *21*(3), 1907–1931. https://doi.org/10.1007/s10311-023-01588-0

[11] Rasika, D. M. D.; Vidanarachchi, J. K.; Luiz, S. F.; Azeredo, D. R. P.; Cruz, A. G.; Ranadheera, C. S. Probiotic Delivery through Non-Dairy Plant-Based Food Matrices. *Agriculture* **2021**, *11*(7), 599. https://doi.org/10.3390/agriculture11070599

[12] Ziarno, M.; Zaręba, D.; Ścibisz, I.; Kozłowska, M. Comprehensive Studies on the Stability of Yogurt Type Fermented Soy Beverages during Refrigerated Storage Using Dairy Starter Cultures. Front. *Microbiol.* **2023,** *14*, 1230025. https://doi.org/10.3389/fmicb.2023.1230025

[13] Cheng, J.; Xie, S.; Yin, Y.; Feng, X.; Wang, S.; Guo, C.; Ni, C. Physiochemical, Texture Properties, and the Microstructure of Set Yogurt Using Whey Protein–Sodium Tripolyphosphate Aggregates as Thickening Agents. *J. Sci. Food Agric*. **2017**, *97*, 2819–2825. https://doi.org/10.1002/jsfa.8110

[14] AOAC International. Official Methods of Analysis; 21st ed.; AOAC International: Gaithersburg, MD, **2023.**

[15] Keum, D. H.; Lee, H. J.; Ryoo, J. H.; Han, S. G. Enhancing the Texture of Fat-Free Yogurt with Panax ginseng Leaf-Stem Extract and Casein: Focusing on Their Softening Effect. *Food Chem.* **2025,** *26*, 102242. https://doi.org/10.1016/j.fochx.2025.102242

[16] Abdelmoneim, A. H.; Sherif, A. M.; Sameh, K. A. Rheological Properties of Yoghurt Manufactured by Using Different Types of Hydrocolloids. *Austin J. Nutr. Food Sci.* **2016,** *4*(2), 1–6.

[17] Mehaya, F. M.; El-Shazly, A. I.; El-Dein, A. N.; Farid, M. A. Evaluation of Nutritional and Physicochemical Characteristics of Soy Yogurt by *Lactobacillus plantarum* KU985432 and *Saccharomyces boulardii* CNCM I-745. *Sci. Rep.* **2023**, *13*(1), 13026. https://doi.org/10.1038/s41598-023-40207-4

[18] Lee, W. J.; Lucey, J. A. Structure and Physical Properties of Yogurt Gels: Effect of Inoculation Rate and Incubation Temperature. *J. Dairy Sci.* **2004,** *87*(10), 3153–3164. https://doi.org/10.3168/jds.S0022-0302(04)73450-5

[19] Thai Ministry of Public Health. Notification No. 353; Fermented Milk Products Standards; Ministry of Public Health: Nonthaburi, Thailand, **2023.**

[20] Deshpande, H. W.; Katke, S. D.; Kulkarni, A. S. Process Standardization and Quality Evaluation of Yogurt Fortified with Noni Juice. *Int. J. Curr. Microbiol. Appl. Sci.* **2019,** *8*(10), 179–186. https://doi.org/10.20546/ijcmas.2019.810.018

[21] Mistry, V. V.; Hassan, H. N. Manufacture of Nonfat Yogurt from a High Milk Protein Powder. *J. Dairy Sci.* **1992,** *75*(4), 947–957. https://doi.org/10.3168/jds.S0022-0302(92)77835-7

[22] Granato, D.; Branco, G. F.; Nazzaro, F.; Cruz, A. G.; Faria, J. A. F. Functional Foods and Nondairy Probiotic Food Development: Trends, Concepts, and Products. *Compr. Rev. Food Sci. Food Saf.* **2010,** *9*(3), 292–302. https://doi.org/10.1111/j.1541-4337.2010.00110.x

[23] Arab, M.; Yousefi, M.; Khanniri, E.; Azari, M.; Ghasemzadeh-Mohammadi, V.; Mollakhalili-Meybodi, N. A Comprehensive Review on Yogurt Syneresis: Effect of Processing Conditions and Added Additives. *J. Food Sci. Technol.* **2023,** *60*(6), 1656–1665. https://doi.org/10.1007/s13197-022-05403-6

[24] Fan, X.; Li, X.; Du, L.; Li, J.; Xu, J.; Shi, Z.; Pan, D. The Effect of Natural Plant-Based Homogenates as Additives on the Quality of Yogurt: A Review. *Food Biosci.* **2022,** *49*, 101953. https://doi.org/10.1016/j.fbio.2022.101953

[25] Tripathi, M. K. ; Giri, S. K. Probiotic functional foods: Survival of probiotics during processing and storage. *J. Funct. Foods*. **2014,** *9*, 225–241**.** https://doi.org/10.1016/j.jff.2014.04.030

[26] Mousavi, M.; Taheri, M.; Daraei Garmakhany, A.; Heshmati, A. The Effects of Flaxseed Powder on Physicochemical, Rheological, Microbiological and Sensory Properties of Yogurt. *Brazilian Arch. Biol. Technol.* **2022**, *65*, e22120705. https://doi.org/10.1590/1678-4324-2022210012

[27] Güler-Akın, M.; Goncu, B.; Akın, M. Some Properties of Bio-Yogurt Enriched with Cellulose Fiber. *Adv. Microbiol.* **2018,** *8*, 54–64. https://doi.org/10.4236/aim.2018.81005

[28] Khalesi, M.; Glenn-Davi, K.; Mohammadi, N.; FitzGerald, R. J. Key Factors Influencing Gelation in Plant vs. Animal Proteins: A Comparative Mini-Review. *Gels* **2024,** *10*(9), 575. https://doi.org/10.3390/gels10090575

[29] Postolache, A. N.; Veleșcu, I. D.; Stoica, F.; Crivei, I. C.; Arsenoaia, V. N.; Usturoi, M. G.; Rațu, R. N. A Clean-Label Formulation of Fortified Yogurt Based on Rhododendron Flower Powder as a Functional Ingredient. *Foods* **2023,** *12*(23), 4365. https://doi.org/10.3390/foods12234365

[30] Canazza, E.; Tessari, P.; Mayr Marangon, C.; Lante, A. Nutritional Profile and Chlorophyll Intake of Collard Green as a Convenience Food. *Nutrients* **2024,** *16*(23), 4015. https://doi.org/10.3390/nu16234015

[31] Bankole, A. O.; Irondi, E. A.; Awoyale, W.; Ajani, E. O. Application of Natural and Modified Additives in Yogurt Formulation: Types, Production, and Rheological and Nutraceutical Benefits. *Front. Nutr.* **2023,** *10*, 1257439. https://doi.org/10.3389/fnut.2023.1257439

[32] Plaskova, A.; Mlcek, J. New Insights of the Application of Water or Ethanol-Water Plant Extract Rich in Active Compounds in Food. *Front. Nutr.* **2023**, *10*, 1118761. https://doi.org/10.3389/fnut.2023.1118761

[33] Sharafi, M.; Hayes, J. E.; Duffy, V. B. Masking Vegetable Bitterness to Improve Palatability Depends on Vegetable Type and Taste Phenotype. *Chem. Percept.* **2013**, *6*(1), 8–19. https://doi.org/10.1007/s12078-012-9137-5

[34] Satheesh, N.; Fanta, S. W. Kale: Review on Nutritional Composition, Bio-Active Compounds, Anti-Nutritional Factors, Health Beneficial Properties and Value-Added Products. *Cogent Food Agric.* **2020**, *6*(1), 1811048. https://doi.org/10.1080/23311932.2020.1811048

[35] Ortega-Hernández, E.; Antunes-Ricardo, M.; Jacobo-Velázquez, D. A. Improving the Health-Benefits of Kales (Brassica oleracea L. var. acephala DC) through the Application of Controlled Abiotic Stresses: A Review. *Plants* **2021**, *10*(12), 2629. https://doi.org/10.3390/plants10122629

[36] Dabija, A.; Codină, G. G.; Gâtlan, A. M.; Sănduleac, E. T.; Rusu, L. Effects of Some Vegetable Proteins Addition on Yogurt Quality. *Sci. Study Res. Chem. Chem. Eng. Biotechnol. Food Ind.* **2018**, *19*(2), 181–192.

[37] Mani-López, E.; Palou, E.; López-Malo, A. Probiotic Viability and Storage Stability of Yogurts and Fermented Milks Prepared with Several Mixtures of Lactic Acid Bacteria. *J. Dairy Sci.* **2014**, *97*(5), 2578–2590. https://doi.org/10.3168/jds.2013-7551

[38] Zhang, W.; Al-Wraikata, M.; Shu, Q.; Hu, J.; Li, L.; Liu, Y. Enhancement Effect of Kale Fiber on Physicochemical, Rheological and Digestive Properties of Goat Yogurt. *LWT* **2024**, *207*, 116649. https://doi.org/10.1016/j.lwt.2024.116649

ASEAN
Journal of Scientific and Technological Reports
Online ISSN:2773-8752

Research article

Organic White Corn (*Zea mays* L. IPB var. 6) Production through the Integration of Bio-fertilizer on Chicken Manure

Daniel B. Tangpos[1], Mary Joy L. Pineda[1], Julius D. Caritan[1], Noriel Jay A. Magsayo[1], and Pet Roey L. Pascual[2]

[1] Graduate School, Cebu Technological University-Barili Campus, Barili, 6306 Cebu, Philippines
[2] Food Science, Agribusiness and Development Communication, Cebu Technological University-Barili Campus, 6306 Cebu, Philippines
* Correspondence: danieltangpos143@gmail.com

Citation:
Tangpos, B.D.; Pineda, L.J.M.; Caritan, D.J.; Magsayo, A.J.N.; Pascual, L.R. Organic white corn (*Zea mays* L. IPB var. 6) production through the integration of bio-fertilizer on chicken manure. *ASEAN J. Sci. Tech. Report.* **2026**, *29*(2), e260397. https://doi.org/10.55164/ajstr.v29i2.260397.

Article history:
Received: July 18, 2025
Revised: October 10, 2025
Accepted: November 15, 2025
Available online: January 20, 2026

Abstract: White corn is the most important substitute staple in periods of rice shortage. Currently, there is an increasing global trend toward reducing dependence on synthetic fertilizers. The increasing demand for organic produce among health-conscious consumers is driving the adoption of sustainable agricultural practices, including the use of organic fertilizers and bio-fertilizers to meet plant nutrient needs. A field experiment was conducted to evaluate the effectiveness of bio-fertilizer added to chicken manure in terms of growth, yield, and physicochemical characteristics of corn. The study used a Randomized Complete Block Design (RCBD) consisting of five treatments with three replications each, and data were collected on the growth, yield, and physicochemical parameters of corn. Data were analyzed using Analysis of Variance (ANOVA) in RCBD, and Comparisons among means were performed using Duncan Multiple Range Test (DMRT) to determine the specific significant differences among treatments. One-half the recommended rate of *Azospirillum* combined with half the recommended rate of Mykovam® at half the amount of chicken manure was comparable to using the full-recommended inorganic fertilizer in terms of plant height, days to silking, ear height, and average length of ears. Moreover, the same treatment combination significantly affected all growth and yield parameters, except for plant stand and average number of ears, which were comparable to using the full-recommended rate of chicken manure. The overall results of this study suggest that combining bio-fertilizer with organic amendments, like chicken manure, using only half the recommended rate, can effectively enhance corn production.

Keywords: Bio-fertilizer; organic fertilizer; chemical fertilizer; sustainable agricultural practices, bio-enhancer

1. Introduction

Corn (*Zea mays* L.) ranks as the second most important crop in the Philippines after rice, with around 1.8 million Filipino farmers or one third of the farming population relying on it as their primary source of income. White corn serves as the main alternative staple during times of rice shortage, particularly for those living in rural communities [1]. It is known to be a rich source of vitamins A, B, and E, as well as various essential minerals. Corn production in the Philippines, harvest area, and yield per hectare increased by 11%, 7.2%, and 3.5%, respectively, in 2019 compared with 2018. In Central Visayas, Cebu had the widest area dedicated to corn cultivation, making up 55.2% of the region's total, and emerged as the top corn producer in 2018,

contributing 54.63% to the region's overall corn production [2]. Chemical fertilizers have been used for decades to increase crop yield. However, the extensive use of chemical fertilizers has also led to environmental challenges, including water pollution and soil degradation [3]. Farmers employ alternative and economical techniques to make food production more sustainable, including crop rotation, biological pest management, composts, and organic fertilizers, which contribute to reducing negative environmental impacts. Currently, there is an increasing global trend toward reducing dependence on synthetic fertilizers, driven by environmental concerns, rising costs, and the pursuit of sustainable agriculture. Additionally, the growing demand from health-conscious consumers for organically produced crops has sparked greater interest in foliar feeding, the use of organic fertilizers, and the use of bio-fertilizers as effective alternatives to meet plants' nutritional needs during the growing season [4].

Bio-fertilizers (microbial inoculants) and organic materials such as chicken manure are cost-effective nutrient sources that can act as alternatives to chemical fertilizers and enhance crop production in low-input farming systems. Application of organic amendments like chicken manure increases soil organic carbon and stimulates microbial activity, which provides N and P to the soil [3]. Microbial inoculants, on the other hand, are agricultural enhancements that utilize beneficial microbes to improve both plant and soil health. These are used to enhance plant nutrition and can also support plant growth by stimulating the production of plant hormones. *Azospirillum* is a microbial-based fertilizer that makes use of nitrogen-fixing microbial inoculants, which have been shown to effectively improve root development and lead to higher crop yields [5]. *Azospirillum* forms an associative symbiotic relationship with many plants, especially those that utilize the C4 dicarboxylic acid pathway of photosynthesis (Hatch and Slack pathway), as it thrives and fixes nitrogen using organic acid salts like malic and aspartic acids [21]. On the other hand, Mykovam® is a soil-based bio-fertilizer containing spores. According to Dr. Jocelyn T. Zarate of UPLB BIOTECH, these fungi, when inoculated to seedlings, will infect the roots, help absorb water and nutrients, particularly phosphorus, and prevent root infection by pathogens. Moreover, they boost the plant's ability to handle stress, such as drought or soil diseases [16]. Furthermore, they are involved in interactions with plant roots, either symbiotically or as free-living, improving plant nutrient uptake, bolstering crop production, and improving soil quality [6].

However, under field conditions, studies are still very limited. A study on determining the comparative performance of *Azospirillum*, Mykovam® on Chicken manure in terms of plant growth, yield, and physicochemical characteristics is deemed necessary, especially towards full organic white corn production.

2. Methodology

2.1 Location

The study was conducted at Barangay Cagay, experimental area of Cebu Technological University-Barili Campus, from the months of November 2024 to February 2025, situated at approximately 10° 8' North, 123° 32' East in the island of Cebu and located approximately 8.5 kilometers away from the market proper. Elevation at these coordinates is estimated at 145.2 meters or 475.4 feet above mean sea level. The soils vary in color from dark brown to yellowish brown, becoming hard when dry but plastic and sticky when wet. They have a high clay content (46-70%) and a water-holding capacity greater than 40%. Chemically, these soils have an alkaline pH of 7.83.

2.2 Experimental Design and Treatment

A single-factor experiment having five treatments replicated three times, arranged in a Randomized Complete Block Design (RCBD) was used in the study. Since both *Azospirillum* and Mykovam® do not provide nutrients to plants but instead allow more efficient utilization of available nutrients, the sole application of both bio-inoculants was not considered, but instead used with chicken manure. The following were the treatments of the study.

T1- Full Recommended Rate Inorganic Fertilizer (120 N- 60 P_2O_5 – 60 K_2O)
T2- *Azospirillum* + Half-Recommended Rate (RR) Chicken Manure
T3- Mykovam® + Half- Recommended Rate Chicken Manure

T4- Half-Recommended Rate *Azospirillum* + Half-Recommended Rate Mykovam® +Half-Recommended Rate Chicken Manure
T5- Full Recommended Rate Chicken Manure (20 tons/ha)

Figure 1. Location of the study within Cebu Technological University-Barili Campus

2.3 Land Preparation

The experiment was set up in a 100 m^2 land, which was divided into three major blocks. The area was plowed twice and harrowed once before furrowing. Rocks and residues were removed. Furrows were established 75 cm apart across the plots. Each treatment plot measured 5 meters in length and 3 meters in width, with a one-meter space allocated between blocks and replications to facilitate data collection and regular inspection.

2.4 Inputs, Treatments, and Application

Farm supplies such as urea (46-0-0) and complete fertilizer (14-14-14) were acquired from an Agrivet supplier in Barili, Cebu City. White Corn IPB var. 6 used in the study was purchased from a reliable seed farmer in Barili, Cebu City. Chicken manure was sourced from the Department of Animal Science of the Cebu Technological University- Barili Campus, while *Azospirillum* and Mykovam® were purchased online. Basal application of chicken manure was done 1 week before sowing at 20 tons per hectare. The application of synthetic fertilizer was based on the recommended rate of 120kg N, 60kg P, and 60kg K per hectare. Mykovam® was applied at the rate of 10 g per hill, and *Azospirillum* was applied by coating 3 kilograms of corn seeds with a 200-gram pack of BIO-N. The amounts of fertilizers and bio-fertilizers were reduced by half the recommended rate, depending on the treatments of the study.

2.5 Seed Planting and Hilling-up

White Corn IPB var. 6 seeds were soaked in coconut water for twenty-four (24) hours to improve germination rate and were directly planted with a row spacing of 75cm and plant spacing of 25 cm. Hilling up, on the other hand, was performed at 30 DAP.

2.6 Care and Maintenance of Experimental Plants

Watering was done at three days interval, one week after germination. Weeding was done just before thinning and fertilizer application. Constant check-ups and regular monitoring were done to monitor pest and disease infestation.

2.7 Data Gathered

2.7.1 Agronomic Characteristics of Corn

- Plant height (cm) was determined by measuring from the base of the plant to the base of the tassel using a measuring tape.
- Days to silking were obtained by counting the number of days of silk emergence after planting.

- Ear height (cm) was measured at the maturity stage; it was measured from the ground to the base of the ear.
- The Plant Stand was done by counting the number of live plants in a row per treatment.
- The number of Ears was determined by counting the total number of ears of the plants within the row per treatment.
- Fresh Weight of Ears with Husk (kg) was measured by weighing the total ears taken from the plants within the row per treatment.
- Average Length of Ears (cm) was measured by getting the total length of ears without husks divided by ten.
- The average weight of unshelled ears (g) was measured by weighing all the total sample ears without husks, divided by ten per treatment.
- The average weight of shelled ears (g) was measured by weighing all the total sample grains divided by ten per treatment.
- Total yield (kg). The total yield with 18% moisture content was computed using this formula:

$$\text{Total } Yield\ (t/ha) = \frac{SW(g)\ x\ 55{,}000\ x\ (100-MC)}{(100-18)x\ (1{,}000{,}000)}$$

Where:

SW = shelled weight (g)
55,000 = assumed plant population per hectare (constant)
MC = actual harvest moisture
18 = standard moisture basis used
1,000,000 = conversion factor from grams to metric tons

2.7.2 Physicochemical characteristics of Corn

- Total Soluble Solid (TSS). Twenty (20) grams of kernels were blended and homogenized with 100 mL of distilled water. TSS in Brix% was measured using a hand-held refractometer (model HI-96801 manufactured by Hanna Instruments Ltd.) calibrated with distilled water by placing 1-3 drops of juice on the instrument's prism and taking the reading.
- Titratable Acidity (TA). Five mL of corn juice was taken, and homogenized samples prepared from TSS were diluted with 45 mL of distilled water. The 50 mL extract (aliquot) was measured and put into an Erlenmeyer flask and a beaker, and 2 drops of 1% phenolphthalein indicator were added. This was titrated with 0.1% NaOH until a pale pink color was achieved using a Cordial 1642TF Glass burette.

2.8 Statistical Analysis

Analysis of variance (ANOVA) for a randomized complete block design (RCBD) was used to analyze any significant difference in all the parameters gathered. Comparisons among means were done using Duncan Multiple Range Test (DMRT) to determine the specific significant differences among treatments.

3. Results and Discussion

3.1 Agronomic Characteristics

The agronomic characteristics of corn, such as plant height, days to silking, and ear height, as affected by *Azospirillum* and Mykovam® Biofertilizers and chicken manure, are shown in Table 1. Treatment applied with half the amount of *Azospirillum* combined with half the rate of Mykovam® at half the amount of chicken manure has a plant height mean of 218.93, which is statistically comparable with treatment applied with inorganic fertilizer (225.10 cm) and *Azospirillum* combined with half the amount of chicken manure (213.47 cm). These treatments showed to be significantly different compared to treatments with Mykovam® combined with half the amount of chicken manure and chicken manure alone. These results are similar to those obtained in [3] that the application of biofertilizer on poultry manure significantly produced taller plants compared to the control poultry manure alone. Furthermore, the inoculation of maize with biofertilizers had a beneficial

effect on the plant growth due to the stimulation of root development and the supply of combined nitrogen. The symbiotic association of microorganisms with plant roots is one of the most enhanced biological activities in the soil. Soil microorganisms that colonize the rhizosphere assist plants in the uptake of phosphorus, potassium, and nitrogen from the soil [7]. Similar to the study of Rotor [14] that inoculation of maize with *Azospirillum* bacteria (Bio-N) contributed to an increase in plant vigour. Plants were taller with the inoculation of *Azospirillum*. Similarly, [15] found that biofertilizers have a positive effect on the plant height and other agronomic characteristics.

In mean differences of the days to silking, treatment applied with chicken manure alone has a significant difference among all the treatments. In mean differences of the ear height, treatment applied with inorganic fertilizer has the highest mean of 130.03 cm, which is statistically comparable with using half the recommended rate *of Azospirillum* combined with half the recommended rate of Mykovam® at half the amount of chicken manure (124.30 cm), but showed to be significantly different compared to other treatments. On the other hand, treatment applied with chicken manure alone has the significantly shortest mean ear height of 108.50 cm. The positive effects of bio-fertilizer and poultry manure on plant growth, as observed in this study, have also been reported by some workers (Abdullahi et al. 2013) using various organic amendments. They observed that inoculated plants grown with organic amendments produced plants with higher growth characteristics than uninoculated ones. Positive growth response of inoculated plants could be due to the provision of nutrients, especially nitrogen and growth-promoting hormones by *Azospirillum*, and enhanced uptake of phosphorus and other nutrients due to mycorrhizal colonization. Enhanced nutrient availability could also be attributed to the decomposition of organic manure or the transformation of inorganic substances to an available form by microorganisms [3]. Moreover, the study conducted by Chen et al. (2024) also supported this, highlighting that microorganisms such as bacteria, fungi, and actinomycetes help decompose complex organic substances into simpler forms that plants can readily absorb. For instance, studies have shown that greater microbial diversity is closely associated with increased rates of organic matter decomposition, resulting in quicker nutrient release and enhanced soil quality [8].

Table 1. Agronomic characteristics of corn as affected by the integration of biofertilizer on chicken manure application to corn.

Treatment	Plant Height (cm)	Days to Silking	Ear Height (cm)
Full RR Inorganic Fertilizer	225.10 ^{a}	51.63 ^{b}	130.03 ^{a}
Azospirillum + ½ RR Chicken Manure	213.47 ^{b}	51.63 ^{b}	118.73 ^{bc}
Mykovam® + ½ RR Chicken Manure	200.30 ^{c}	51.87 ^{b}	114.33 ^{cd}
½ RR *Azospirillum* + ½ RR Mykovam® + ½ RR Chicken Manure	218.93 ^{ab}	51.77 ^{b}	124.30 ^{ab}
Full RR Chicken Manure	187.97 ^{d}	52.40 a	108.50 ^{d}
CV (%)	2.32	0.33	2.74

3.1 Plant Stand, number of ears, and fresh weight of ears with husk

Table 2a presents the yield and yield components of corn as affected by the application of biofertilizers and chicken manure. Table 2a shows that there is a significant difference in the fresh weight of ears with husk among all the treatments. Treatment applied with inorganic fertilizer had the highest mean fresh weight of ears with husk of 4.96 kg, followed by half the recommended rate *of Azospirillum* and Mykovam® at half the amount of chicken manure, with the mean of 4.14 kg. On the other hand, treatment applied with chicken manure alone has the significantly lowest mean of fresh weight of ears with husk of 2.90 kg. The results are consistent with those of Cleyet-Marel [9], who found that inoculation of plants with plant growth-promoting rhizobacteria at the early stage of development made a positive impact on biomass through direct effect on root growth, production, and production of phytohormones by bacteria, mineral enhancement uptake, and

transfer of nitrogen to the plant. Similar findings were reported in [10], stating that nitrogen-fixing microorganisms such as *Azospirillum* and beneficial fungi like Mykovam®, commonly found in biofertilizers, can enhance plant growth and yield. They achieve this by capturing atmospheric nitrogen and solubilizing soil phosphate, making it more accessible to plants. Additionally, they produce growth-promoting hormones like IAA (Indole-3-acetic acid), cytokinins, gibberellins, and auxins, which significantly contribute to improved plant development and productivity. Moreover, numerous studies, including Fadlalla [11], have demonstrated that combining biofertilizers with organic amendments can enhance the availability and uptake of plant nutrients, leading to improved crop yields.

Table 2a. Yield and yield components of corn as affected by the integration of biofertilizer on chicken manure application to corn.

Treatment	Plant Stand	Number of Ears	Fresh Weight of Ears with Husk (kg)
Full RR Inorganic Fertilizer	24.67	23.67	4.96 [a]
Azospirillum + ½ RR Chicken Manure	24.00	23.33	3.63 [c]
Mykovam®+ ½ RR Chicken Manure	24.00	23.33	3.44 [d]
½ RR *Azospirillum* + ½ RR Mykovam® + ½ RR Chicken Manure	24.33	24.00	4.14 [b]
Full RR Chicken Manure	24.67	23.00	2.90 [e]
CV (%)	1.50	2.19	2.26

3.2 Average weight of unshelled ears, average weight of shelled ears, average length of ears, and total yield

Table 2b shows that there is a significant difference in the average weight of unshelled ears and the average weight of shelled ears, among all the treatments. Treatment applied with half the amount of *Azospirillum* combined with half of the recommended rate of Mykovam® at half the amount of chicken manure has the average weight of unshelled ears mean of 179.30 g, and inorganic fertilizer has the highest mean of 203.06 g. On the other hand, treatment applied with chicken manure alone has the lowest mean of average weight of unshelled ears with 118.98 g. In the mean differences of the average of shelled ears, the highest average of shelled ears was recorded on corn in inorganic fertilizer with 170.64 g, followed by *Azospirillum* combined with Mykovam® at half the amount of chicken manure with 148.42 g. On the other hand, according to Pascual [5], the combined application of BIO-N and VAMRI with only half of the recommended fertilizer rate consistently produced optimal outcomes in ear dry weight without husk, average ear diameter, and kernel dry weight—showing results comparable to the full-recommended rate of inorganic fertilizer. Moreover, the study by Haserirad [12] and Rokhzadi [13] showed that inoculation of biofertilizers containing Azotobacter and *Azospirillum* increased plant height, number of leaves per plant, and corn weight compared to those without biofertilizer. Furthermore, Amba [6] stated that the mixed application of Mykovam® and inorganic fertilizer gave the heaviest corncobs. The increase in the average weight of both unshelled and shelled ears was attributed to enhanced traits like the number of leaves, ear length, and plant height, which ultimately led to greater assimilate production.

Figure 2. Comparing the corn yield using full chicken manure with the yield from a combination of *Azospirillum* and Mykovam® applied alongside half the usual amount of chicken manure.

Table 2b. Yield and yield components of corn as affected by biofertilizer on chicken manure application to corn.

Treatment	Ave. weight of unshelled ears (g)	Ave. weight of shelled ears (g)	Ave. Length of Ears (cm)	Total yield (kg)
Full RR Inorganic Fertilizer	203.06 ^{a}	170.64 ^{a}	14.05 ^{a}	8.04 ^{a}
Azospirillum + ½ RR Chicken Manure	145.82 ^{c}	118.93 ^{c}	12.25 ^{bc}	5.83 ^{c}
Mykovam® + ½ RR Chicken Manure	138.68 ^{c}	116.47 ^{c}	11.62 ^{cd}	5.52 ^{c}
½ RR *Azospirillum* + ½ RR Mykovam® + ½ RR Chicken Manure	179.30 ^{b}	148.42 ^{b}	13.10 ^{ab}	7.10 ^{b}
Full RR Chicken Manure	118.98 ^{d}	94.98 ^{d}	10.80 ^{d}	4.71 ^{d}
CV (%)	3.94	4.19	4.78	3.94

In terms of average ear length, the treatment using half the recommended rate of *Azospirillum* combined with 50% of the recommended rate of Mykovam® and half the amount of chicken manure recorded a mean ear length of 13.10 cm. This result was statistically comparable to the treatment with inorganic fertilizer (14.05 cm) and the treatment combining *Azospirillum* with half the amount of chicken manure (12.25 cm). On the other hand, treatment applied with chicken manure alone has the significantly lowest ear height mean of 10.80 cm. Pascual [5] observed similar results, which showed that using BIO-N and VAMRI together with just half of the recommended fertilizer rate was comparable with treatment applied with the full-recommended rate of inorganic fertilizer in terms of average length of ears. Bakry [17] stated that triple treatment of combinations of Micronutrients, Chicken Manure, and Rhizobium Inoculation achieved a considerably greater increase, which reached 53.80, 29.10, 29.93, 31.14, and 42.27 % for length, ear diameter, ear weight, raw number/ear, and grain number/raw over the control treatment, respectively. The improvements in the examined ear characteristics resulting from the applied treatments may be attributed to their ability to release plant growth-promoting substances, which likely enhanced plant growth and increased the uptake of water and nutrients from the soil. Differences in treatment means of total yield showed significant differences at α0.05. The highest total yield was recorded on corn in inorganic fertilizer with 8.04 kg, followed by *Azospirillum* combined with Mykovam® at half the amount of chicken manure with 7.10 kg. However, treatment applied with chicken manure alone has the significantly lowest total yield of 4.71 kg. These findings are consistent with those reported by Purwani [18] that the treatment using 50% of the recommended NPK rate combined with bio-fertilizer resulted in a higher maize yield compared to the treatment with 100% of the recommended NPK rate. Mahato and Neupane [19] reported similar results, demonstrating that the combined use of chemical

fertilizers and biofertilizers produced higher corn yields compared to using chemical fertilizers alone, thereby lowering the required amount of chemical fertilizers during cultivation. Zarabi [20] stated that the application of organic fertilizer enhances water use efficiency, improves photosynthesis, and promotes plant growth and development. Furthermore, Rattin [22] reported that the improvement in growth parameters was linked to the activity of arbuscular mycorrhizal fungi and other microorganisms, which enhanced plant biomass and phosphorus content. Additionally, Javier [23] noted that the microorganisms in biofertilizers help develop a strong root system, enhancing the plant's ability to absorb nutrients, which in turn promotes better plant growth and higher biomass production.

3.3 Total Soluble Solid and Titratable Acidity

Table 3 indicates that the total soluble solids of corn in *Azospirillum* combined with Mykovam® at half the amount of chicken manure showed significantly different results compared to other treatments, especially in the treatment applied with chicken manure alone. Treatment applied with inorganic fertilizer had the highest total soluble solids (2.13), followed by *Azospirillum* combined with Mykovam® at half the amount of chicken manure (1.93). In contrast, the chicken manure treatment has the significantly lowest total soluble solids (1.67). Mahdi [24] also reported similar findings, indicating that the application of mixed bio-fertilizer significantly enhanced the levels of starch, protein, and dry matter. Whereas, Azotobacter spp. T2 fertilizer was most effective in enhancing potassium availability (339 mg/kg) and total sugar content (0.507%), showing clear differences from other biofertilizers. Meanwhile, *Azospirillum* spp. T1 treatment led to the highest increase in total soluble solids (6.763%), significantly outperforming the other treatments. This is consistent with other studies showing that mineral nutrients—particularly sulfur and nitrogen from ammonium sulfate—enhance the photosynthetic activity of chloroplasts, facilitate the transport of photosynthates through the phloem to sink tissues, and ultimately improve fruit quality and yield, which is linked to higher sugar content [25].

Table 3. Physicochemical characteristics of corn as affected by the integration of biofertilizer on chicken manure application to corn.

Treatment	Total Soluble Solid (TSS)	Titratable Acidity (TA).
Full RR Inorganic Fertilizer	2.13 [a]	1.01 a
Azospirillum + ½ RR Chicken Manure	1.83 [c]	0.73 c
Mykovam® + ½ RR Chicken Manure	1.80 [c]	0.75 c
½ RR *Azospirillum* + ½ RR Mykovam® + ½ RR Chicken Manure	1.93 [b]	0.86 b
Full RR Chicken Manure	1.67 [d]	0.69 c
CV (%)	1.82	4.99

In titratable acidity, differences in treatment means showed significant differences at α0.05. Treatment applied with inorganic fertilizer has the highest titratable acidity with 1.01, followed by *Azospirillum* combined with Mykovam® at half the amount of chicken manure with 0.86. On the other hand, treatment applied with chicken manure alone has the lowest titratable acidity with 0.69. According to Bhattacharjee [26], bio-fertilizers such as plant growth-promoting rhizobacteria (PGPR) promote plant growth through various mechanisms, typically by solubilizing phosphorus, enhancing nutrient uptake, or producing plant growth hormones. Moreover, Di-ammonium Phosphate (DAP) often leads to higher acid accumulation, which can influence the flavor and shelf life of corn varieties. The phosphorus supplied by DAP fertilizers can stimulate the synthesis of organic acids in plants, potentially increasing acidity in specific tissues, including fruits or kernels like corn [27].

4. Conclusions

Based on the results, the use of integration of biofertilizers on chicken manure significantly improved the growth, yield, and physicochemical characteristics of corn. Under the CTU-Barili Cebu Condition, the application of *Azospirillum* and Mykovam® singly or in combination with chicken manure at half the recommended rate is generally more effective than using chicken manure alone at the full recommended rate

for the production of corn. This also indicates that using a combination of biofertilizer on chicken manure has greater potential to reduce reliance on inorganic fertilizers in corn production.

5. Acknowledgements

The authors would like to acknowledge Cebu Technological University, Barili Campus, and the DOST-Strand N for their support in making this study a success.

Author Contributions: Conceptualization, P.R.P.; methodology, D.B.T., and M.L.P.; software, D.B.T., validation, J.D.C., E.D.J.; formal analysis, D.B.T.; investigation, D.B.T., N.J.M., and M.L.P.; resources, D.B.T., N.J.M., and J.D.C.; data curation, D.B.T., and M.I.C.; writing-original draft preparation, D.B.T.; writing-review and editing, D.B.T., and P.R.P.; visualization, , D.B.T.; supervision, P.R.P.; project administration, D.B.T., M.L.P., J.D.C., and N.J.M.; funding acquisition D.B.T.; All authors have read and agreed to be published version of the manuscript.

Funding: This research was made possible through the support provided by the Department of Science and Technology (DOST) STRAND N program and the Cebu Technological University - Barili Campus.

Conflicts of Interest: The author declares no conflict of interest, as the funding agency did not influence the study's design, methodology, data analysis, or conclusions.

References

[1] Gerpacio, R. V.; Labios, J. D.; Labios, R. V.; Diangkinay, E. I. *Maize in the Philippines: Production Systems, Constraints, and Research Priorities*; Maize Production Systems Paper No. 7650; CIMMYT (International Maize and Wheat Improvement Center): Mexico, 2004. https://doi.org/10.22004/ag.econ.7650

[2] Abello, N. F.; Remedios, E.; Carabio, D. E.; Pascual, P. Fermented Japanese Snail Fertilizer Reduced Vapor Pressure Deficit Which Improved Indigenous Corn Growth (*Zea mays* var. Tiniguib). *Asian J. Agric. Biol.* **2021**, *4*, 202102087. https://doi.org/10.35495/ajab.2021.02.087

[3] Abdullahi, R.; Sheriff, H.; Lihan, S. Combined Effect of Biofertilizer and Poultry Manure on Growth, Nutrient Uptake, and Microbial Population Associated with Sesame (*Sesamum indicum*) in Northeastern Nigeria. *IOSR J. Environ. Sci. Toxicol. Food Technol.* **2013**, *5*(5), 60–65.

[4] Ibanez, R. Y.; Balansag, G. C.; Puod, N. Effects of Different Manures on the Growth Performance of Petchay (*Brassica rapa* L.) under Visayas State University Conditions. *J. Sci. Technol. Rep.* **2025**, *28*(1), e255634.

[5] Pascual, P. L.; Monsulod, C. F.; Monsulod, R. G.; Brown, M. B. Reduction of White Corn (*Zea mays* IPB Var. 6) Dependency on Inorganic Fertilizer through VAMRI and BIO-N Inoculation. *Trop. Technol. J.* **2015**, *18*, ISSN 1656-0264.

[6] Amba, O.; Masnar, A. L.; Bangi, J. C.; Jambaro, G. Growth and Yield of Open-Pollinated Young Corn (*Zea mays* Linn.) as Influenced by Different Levels of Mykovam® Biofertilizer. *Int. J. Sci. Basic Appl. Res.* **2022**, *62*(2), 448–459.

[7] Iwuagwu, M.; Chukwuka, K.; Uka, U.; Amandianeze, M. Effect of Biofertilizers on the Growth of *Zea mays* L. *Asian J. Microbiol. Biotechnol. Environ. Sci.* **2013**, *15*(2), 235–240.

[8] Chen, Q.; Song, Y.; An, Y.; Lu, Y.; Zhong, G. Soil Microorganisms: Their Role in Enhancing Crop Nutrition and Health. *Diversity* **2024**, *16*(12), 734. https://doi.org/10.3390/d16120734

[9] Cleyet-Marel, J.-C.; Larcher, M.; Bertrand, H.; Rapior, S.; Pinochet, X. Plant Growth Enhancement by Rhizobacteria in Nitrogen Assimilation by Plants: Physiological, Biochemical, and Molecular Aspects; Science Publishers: Enfield, NH, 2001; pp 185–199.

[10] Kantikowati, E.; Yusdian, K.; Suryani, C. Chicken Manure and Biofertilizer for Increasing the Growth and Yield of Potato (*Solanum tuberosum* L.) of Granola Varieties. *IOP Conf. Ser.: Earth Environ. Sci.* **2019**, *393*, 012017. https://doi.org/10.1088/1755-1315/393/1/012017

[11] Fadlalla, H.; Abukhlaif, H.; Mohamed, S. Effects of Chemical and Biofertilizers on Yield, Yield Components, and Grain Quality of Maize (*Zea mays* L.). *Afr. J. Agric. Res.* **2016**, *11*(45), 4654–4660. https://doi.org/10.5897/AJAR2016.11619

[12] Naserirad, H.; Soleymanifard, A.; Naseri, R. Effect of Integrated Application of Biofertilizer on Grain Yield, Yield Components, and Associated Traits of Maize Cultivars. *Am.-Eurasian J. Agric. Environ. Sci.* **2011**, *10*(2), 271–277.

[13] Rokhzadi, A.; Asharzadeh, A.; Darvish, F.; Ghorban, N.; Eslam, M. Influence of Plant Growth-Promoting Rhizobacteria on Dry Matter Accumulation and Yield of Chickpea (*Cicer arietinum* L.) under Field Conditions. *Am.-Eurasian J. Agric. Environ. Sci.* **2008**, *3*, 253–257.

[14] Rotor, A.; Delima, P. Mycorrhizal Association, Nitrogen Fertilization, and Biocide Application on the Efficacy of Bio-N Corn (*Zea mays* L.) Growth and Productivity. *E-Int. Sci. Res. J.* **2010**, *2*.

[15] Migahed, H.; Ahmed, A.; Abd, B.; Ghany, E. Effect of Different Bacterial Strains as Biofertilizer Agents on Growth, Production, and Oil Content of *Apium graveolens* under Calcareous Soil. *Arab Univ. J. Agric. Sci.* **2004**, *12*(2), 511–525.

[16] Laraño, G. J. V.; Amper, C. D. Analysis of Soil Planted to Sweet Corn Applied with Mycorrhizal Inoculants and Varied Fertilizer Rates. *Nativa* **2023**, *11*(4), 500–504. https://doi.org/10.31413/nativa.v11i4.16654

[17] Barky, M.; Soliman, Y.; Moussa, S. Importance of Micronutrients, Organic Manure, and Biofertilizer for Improving Maize Yield and Its Components Grown in Desert Sandy Soil. *Res. J. Agric. Biol. Sci.* **2009**, *5* (1), 16–23.

[18] Purwani, J.; Nurjaya. Effectiveness of Inorganic Fertilizer and Biofertilizer Application on Maize Yield and Fertilizer Use Efficiency on Inceptisol from West Java. *J. Trop. Soils* **2020**, *25*(1), 11–20. https://doi.org /10.5400/jts.2020.v25i1.11

[19] Mahato, S.; Neupane, S. Comparative Study of Impact of *Azotobacter* and *Trichoderma* with Other Fertilizers on Maize Growth. *J. Maize Res. Dev.* **2017**, *3*(1), 1–16. https://doi.org/10.3126/jmrd.v3i1.18915.

[20] Zarabi, M.; Alahdadi, I.; Akbari, G. A. Effects of Different Biofertilizer Combinations on Yield, Its Components, and Growth Indices of Corn (*Zea mays* L.) under Drought Stress Conditions. *Afr. J. Agric. Res.* **2011**, *6* (3), 681–685. https://doi.org/10.5897/AJAR10.870

[21] Wani, F.; Ahmad, L.; Mushtaq, A. Role of Microorganisms in Nutrient Mobilization and Soil Health: A Review. *J. Pure Appl. Microbiol.* **2015**, *9*(2), 1401–1410.

[22] Ratti, N.; Kumar, S.; Verma, H. N.; Gautam, S. P. Improvement in Bioavailability of Tricalcium Phosphate to *Cymbopogon martinii* var. *motia* by Rhizobacteria, AMF, and *Azospirillum* Inoculation. *Microbiol. Res.* **2001**, *156*(2), 145–149. https://doi.org/10.1078/0944-5013-00095

[23] Javier, A.; Brown, M. *Biofertilizer and Biopesticides Research and Development at UPLB*; Food and Fertilizer Technology Center for the Asian and Pacific Region, 2009.

[24] Mahdi, R.; Manea, A.; Aubied, I. Effect of Biofertilizer and Potassium Spraying on the Growth and Yield of Potatoes for Autumn Season. *IOP Conf. Ser.: Earth Environ. Sci.* **2023**, *1158*(4), 042050. https://doi.org/10.1088/1755-1315/1158/4/042050

[25] Aryakia, E.; Roosta, H. R.; Rahmizade, N. Effects of Cow Manure, Ammonium Sulfate, and Potassium Sulfate on Physicochemical Indices of Fruit and Leaf of Mazafati Date (*Phoenix dactylifera* L.). *J. Hortic. Sci.* **2017**, *31*(3), 457–468. https://doi.org/10.22067/jhorts4.v31i3.36474

[26] Bhattacharjee, R.; Dey, U. Biofertilizer, a Way Towards Organic Agriculture: A Review. *Afr. J. Microbiol. Res.* **2014**, *8* (24), 2332–2342. https://doi.org/10.5897/AJMR2013.6374

[27] Fageria, N. K.; Baligar, V. C.; Li, Y. C. The Role of Nutrient-Efficient Plants in Improving Crop Yields in the Twenty-First Century. *J. Plant Nutr.* **2008**, *31*(6), 1121–1157. https://doi.org/10.1080/01904160802116068

ASEAN
Journal of Scientific and Technological Reports
Online ISSN:2773-8752

Research article

Early Root Development and Yield Performance of Different Corn (*Zea mays* L.) Varieties Under Alkaline Soil

Elvira D. Jamio[1*], Bernie C. Bacalso[1], Noriel Jay A. Magsayo[1], Melissa I. Canunayon[1], Daniel B. Tangpos[1], Julius D. Caritan[1], and Pet Roey L. Pascual[2]

[1] Graduate School, Cebu Technological University – Barili Campus, Barili, Cebu, 6036, Philippines
[2] Agribusiness and Development Communication, Cebu Technological University– Barili Campus, Barili, Cebu, 6036, Philippines
* Correspondence: jamioelvira28@gmail.com

Citation:
Jamio, D.E.; Bacalso, C.B.; Pascual, L.P.R. Early root development and yield performance of different corn (*Zea mays* L.) varieties under alkaline soil. *ASEAN J. Sci. Tech. Report.* **2026**, *29*(2), e259735. https://doi.org/10.55164/ajstr.v29i2.259735.

Article history:
Received: June 10, 2025
Revised: October 11, 2025
Accepted: November 15, 2025
Available online: January 20, 2026

Abstract: Early root vegetative stages of corn are critical in transitioning to the independent phase, wherein roots support development and improved nutrient uptake that may influence yield. Thus, the study assessed the root development of different corn varieties at the vegetative 4 (V4) stage and its relationship to yield, and to evaluate its performance under alkaline soil using a Randomized Complete Block Design. Data on root morphological traits were measured at the V4 stage, while yield parameters were assessed after harvest. Data were analyzed using ANOVA in RCBD, and the relationship between early root growth and yield was assessed using Pearson's correlation. The results showed that varieties TCT 476A and TCT 1868 significantly outperformed, producing higher yields across parameters, with computed yields of 9.23 t/ha and 9.27 t/ha, respectively, while CGUARD VII-002 exhibited reduced performance, having significantly lower yield. Results demonstrated that differences in yield performance among varieties can be attributed to genotype-environment interactions. Moreover, root morphological traits at the V4 stage showed no significant differences, indicating that all varieties exhibit comparable root morphological characteristics at this stage. However, root morphological traits at the V4 stage revealed no significant linear relationship with yield and yield components, suggesting that the early vegetative stage is not a reliable predictor of yield. The findings highlight that the V4 stage primarily supports establishment rather than yield formation, and fertilizer application strategies must align with efficient nutrient demand to optimize yield. Further research on later stages of root development is suggested to corroborate the preliminary findings.

Keywords: V4 stage; corn; alkaline soil, root morphological traits, yield performance

1. Introduction

Corn (*Zea mays* L.), a member of the Poaceae family, is the most widely produced and consumed cereal globally, with multiple uses primarily for feed and food crops [1]. According to the USDA (United States Department of Agriculture), worldwide corn production in 2024 was 1.23 billion metric tons, with the United States, China, and Brazil being the top-producing countries [2]. In the Philippines, corn is considered the second most important crop after rice [3], with a production decrease of 0.3% from 2.533 to 2.526 metric tons in the third quarter of 2024. In Cebu, corn is a vital component of the rural

community, with the white corn variety predominantly grown for human consumption, underscoring its significance to the local diet and economy [4]. The diverse uses of corn, including its significant role in human consumption, industrial purposes, and livestock feed, solidify it as a fundamental commodity that plays a vital role in global food security [5]. Environmental condition plays a significant role in crop production. Abiotic stresses are one of the constraints that substantially limit corn production growth and development [6]. According to the study of [7], maize grown in saline-alkaline soil can experience a yield reduction of 20-46% and inhibit root penetration. In alkaline soil conditions, the utilization of essential nutrients by plants is limited due to decreased solubility. The edaphic condition in Barili, Cebu, Philippines, exhibits an alkaline pH above 7.5 and a CaCO3 content greater than 70%, resulting from a limestone parent material, as reported by [8].

The root system sustains plant life by anchoring in the ground and serving as a storage organ, absorbing and translocating water and nutrients from the soil, which are the primary fuel for plant productivity. Reports from [9] highlighted that root growth is little influenced by external pH in the range of 5.0–7.5. Abiotic stress factors may influence the growth and development of crops at any stage. In corn, the critical growth phase occurs during the vegetative stages of V4, V6, and V8, during which plants can take up nutrients and water that directly influence the crop yield, according to [10]. Notably, the V4 stage marks the onset of rapid dry matter accumulation, during which available resources directly influence biomass and reproductive potential. At this phase, the plant shifts from relying on seed reserves to actively absorbing nutrients through the newly developed nodal roots. This process initiates stalk elongation, which establishes the structural and physiological foundation necessary for succeeding growth and optimal yield formation [11, 12]. This is supported by [13], which states that the root-to-shoot ratio of cereal crops is significantly affected by plant age, being higher during the vegetative growth stage (21-40 days of growth period), indicating that more photosynthetic products are translocated to the roots and decrease during the reproductive or grain-filling stage. At this stage, the mesocotyl root plays a crucial role below the soil, which is accompanied later by nodal roots [14]. The mesocotyl is described as a structure similar to the stem in young maize seedlings that links the first true leaves and the seed. Its primary role is to facilitate the development of the shoot from the soil surface by securing the seedling as it emerges, allowing it to begin photosynthesis, which permits the plant to access light and establish itself more efficiently. Additionally, mesocotyl roots exhibit a distinct response to abiotic stress [15]. Meanwhile, nodal roots serve as the foundation of the whole root system, making the uptake of water and nutrients efficient.

These root systems are essential for the better transition in order to achieve optimal development and productivity of crops, ensuring they can prosper in diverse soil conditions. However, the majority of previous studies have focused on shoot development, while only a few have assessed the yield by examining root systems. Therefore, this study aims to evaluate the development of roots at the vegetative 4 (V4) stage of different corn varieties and their relationship with yield, and to evaluate varieties that potentially performed well under alkaline soil conditions. It is hypothesized that enhanced root development at the V4 stage will lead to increased dry matter accumulation and yield.

2. Materials and Methods

2.1 Experimental Site

The study was conducted at Cebu Technological University – Barili Campus, Barili, Cebu, Philippines, located at coordinates 10°07′53″ N, 123°32′45″ E from September 2024 to January 2025. The soil in the area is classified as alkaline with a pH above 7.5.

2.2 Land Preparation and Planting of Corn

The land area was plowed twice to eliminate weeds and harrowed to provide enough soil aeration and drainage. A basal application was made before planting to provide the optimum nutrients required by the seeds during germination. During planting, seeds were soaked with water to hasten germination by providing enough moisture to break their dormancy. The planting distance used in the study was 75 cm x 25 cm, with two seeds per hill.

2.3 Fertilization

The split fertilizer application was used in the study. The first fertilizer application was made ten days after planting, using a complete fertilizer. After one month, a mixture of complete and urea fertilizers was applied, and the final application was made during the flag leaf stage using urea and potash.

2.4 Collection of roots

Root samples were obtained through destructive sampling using a shovel by carefully extracting the roots from the soil during the V4 stage (four leaves with a visible collar were present) at a depth of 20 cm and a diameter of 40 cm around the stem, providing an overall root biomass per unit volume of soil following the methods of [16]. The gathered roots were rinsed under running water to eliminate any excess soil. After cleansing, root length, root diameter, and fresh weight were measured. Subsequently, the root samples were dried in an oven at 70°C until a constant weight was reached, and the root dry weight was obtained.

2.5 Experimental design and Treatments

The experiment was laid out in a Randomized Complete Block Design (RCBD) with a land area of approximately 100 m², divided into three blocks to separate each replication. Each block contained three rows with twenty plants per row. Three different corn varieties were used: CGUARD VII-002 (Variety 1), TCT 476A (Variety 2), and TCT 1868 (Variety 3). Each variety was replicated three times, and a total of ten (10) samples were collected for each variety per replication.

2.6 Data Collection

2.6.1. Root Parameters

Length of mesocotyl (cm). The length of the mesocotyl was carefully measured from the root base to the tip using a digital caliper at the V4 stage.

Diameter of mesocotyl (cm). It was taken at the midpoint of the mesocotyl, as this point provides a representative measure of the overall thickness of the structure.

Length of nodal root (cm). The measurement was taken from the base of the node to its tip using a digital caliper.

Diameter of nodal root (cm). The measurement was taken at the midpoint along the root axis using a digital caliper to ensure consistency.

Fresh weight (g). The fresh weight was carefully measured immediately after cleaning, using a digital weighing scale to ensure accuracy.

Dry weight (g). It was obtained after drying the samples in an oven.

2.6.2. Yield Parameters

Weight of ears (g). All harvested ears in each plot were weighed using a digital weighing scale.

Ear length (cm). The measurement was taken from the base of the ear to the tip using a ruler.

Ear diameter (cm). The measurement was taken at the midpoint of the ears using a ruler.

Weight of kernels (g). All the threshed kernels in every ear in a plot were weighed using a digital weighing scale.

Grain moisture content (%). Grain samples were placed in a calibrated grain moisture meter to record moisture content.

Computed yield (t/ha). It was calculated using the formula below:

$$Computed\ Yield = \frac{shelled\ weight(g)\ x\ 55{,}000\ x\ (100 - MC)}{(100 - 18)\ x\ \ (1{,}000{,}000)}$$

Where:

55,000 = plant population per hectare
MC = actual harvest moisture
18 = standard moisture basis used
1,000,000 = grams to metric tons conversion

2.7 Statistical Analysis

The data was analyzed using the analysis of variance (ANOVA) in RCBD, and further tests were done using Tukey's Honestly Significant Difference (Tukey's HSD) for significant differences between treatment means using Statistical Tool for Agricultural Research (STAR) software.

To evaluate the linear association between root development and corn yield across all treatments, Pearson's correlation coefficient was measured using SPSS (*Ver. 25*).

r	Interpretation
>0.70	Very strong positive correlation
0.40 to 0.69	Strong positive correlation
0.30 to 0.39	Moderate to strong correlation
0.20 to 0.29	Weak positive correlation
0.01 to 0.19	No relationship
-0.01 to -0.19	No relationship
-0.20 to -0.29	Weak negative correlation
-0.30 to -0.39	Moderate negative correlation
-0.40 to -0.69	Strong negative correlation
<-0.70	Very strong negative correlation

3. Results and Discussion

3.1 Yield and yield components of different corn varieties

The performance of three different corn varieties—CGUARD VII-002 (Var1), TCT 476A (Var2), and TCT 1868 (Var3)—was evaluated based on yield and yield component traits. Statistical analysis (Table 1) revealed that TCT 476A and TCT 1868 produced significantly higher yields across all measured parameters, with computed yields of 9.23 t/ha and 9.27 t/ha, respectively. In contrast, CGUARD VII-002 exhibited reduced performance in alkaline soil, showing a significantly lower yield compared to TCT 476A and TCT 1868.

Table 1. Analysis of variance for yield traits of different corn varieties.

Variety	Ear weight (g)	Ear length (cm)	Ear diameter (cm)	Weight of Kernels (g)	Moisture Content (%)	Computed yield (t/ha)
1. CGUARD VII-002	132.91^{b}	14.10^{b}	4.35^{b}	111.01^{b}	15.00^{b}	5.88^{b}
2. TCT 476A	223.95^{a}	17.50^{a}	4.85^{a}	186.16^{a}	20.76^{a}	9.23^{a}
3. TCT 1868	225.80^{a}	17.85^{a}	4.89^{a}	186.77^{a}	21.09^{a}	9.27^{a}
Mean	194.22	16.49	4.70	161.31	18.95	8.12
Cv (%)	5.56	2.74	0.73	8.69	7.22	4.45

This means that the columns with the different letters are significantly different from each other at a 5% level of significance in Tukey's Honest Significant Difference (HSD) Test.

The differences in yield performance among the three different corn varieties can be attributed to genotype-environment interactions, wherein not all varieties exhibit similar performance under abiotic conditions. This is further supported by the findings of [17], which showed that certain corn varieties consistently outperformed others under varied irrigation and moisture conditions, demonstrating their adaptability. Additionally, the yield performance of three different corn varieties under alkaline soil conditions aligns with the findings of [18], which indicated significant differences in morpho-physiological traits of corn hybrids under Claveria conditions. Moreover, TCT 476A and TCT 1868 showed remarkable yield performance under alkaline soil. This may be due to their improved nutrient uptake and root adaptability. These findings align with [19], who found that corn varieties applied with ammonium fertilizers in alkaline soils show significant differences in yield traits. In particular, high-performing genotypes demonstrate better nitrogen absorption and greater physiological resilience. These findings highlight the genetic variability

among different corn varieties and emphasize the importance of selecting suitable varieties to optimize productivity under alkaline soil conditions.

3.2 Root morphological traits of different corn varieties at the V4 stage

Table 2 shows the statistical analysis of root traits in maize at the V4 stage. The findings revealed no significant differences among varieties across all the measured parameters. The results suggest that all varieties exhibited comparable root morphological characteristics at the V4 stage, indicating similar responses under the given growing conditions. Similar results were reported by [20], who state that early vegetative stages showed conserved root morphology across different genotypes.

Table 2. Analysis of variance for root morphological traits of different maize varieties during the V4 stage

Variety	Mesocotyl length (cm)	Mesocotyl diameter (cm)	Nodal root length (cm)	Nodal root diameter (cm)	Root fresh weight (g)	Root dry weight (g)
1. CGUARD VII-002	46.19	0.44	177.42	0.24	0.62	0.18
2. TCT 476A	40.90	0.51	196.12	0.24	0.60	0.18
3. TCT 1868	42.80	0.31	175.84	0.08	0.50	0.17
Mean	43.29	0.42	183.13	0.19	0.57	0.18
Cv (%)	33.22	31.36	6.73	68.85	13.87	14.19

Early-stage assessments are incapable of detecting genotypic differences under stress conditions, indicating that varietal divergence becomes more evident in later stages. According to the findings of [21], abiotic stress tolerance influences significant morphological differences in root traits as plants mature. This is further supported by the results of [22], suggesting that root morphology changes over time, highlighting its relevant differences at a later growth stage. It implies that the genetic differences of corn varieties do not influence root morphological traits during the early vegetative stage under alkaline soil, reinforcing the importance of evaluating root morphological traits beyond the early vegetative stages to fully understand the tolerance of different corn varieties.

3.3 Relationship between mesocotyl root traits and yield parameters of corn

The influence of mesocotyl root traits, specifically diameter and length, during the early vegetative (V4) stage on corn yield parameters was assessed. Results found that mesocotyl root diameter showed no significant relationship with any measured yield traits, including ear weight, ear length, ear diameter, kernel weight, computed yield, or grain moisture content. The correlation coefficients (r) values range from –0.103 to 0.077, indicating that mesocotyl thickness does not affect yield parameters. This conforms with the findings of Zhan [23], who reported that mesocotyl and root thickness primarily contribute to early seedling establishment rather than final yield outcomes. Likewise, mesocotyl root length showed no significant correlations with yield components, with r-values ranging from –0.122 to –0.068. This indicates that variations in mesocotyl elongation do not directly influence ear development, kernel weight, or grain moisture during the V4 stage. Furthermore, previous studies corroborate these findings, indicating that mesocotyl elongation is more critical for seedling emergence, particularly under deep sowing or compacted soil conditions, than for yield formation [24, 25]. Overall, mesocotyl development at the V4 stage is not a reliable predictor of yield. Instead, root characteristics, including length density, branching, and nutrient uptake efficiency, may be more reliable indicators of productivity, particularly under stress such as drought or nutrient limitations.

3.4 Relationship between nodal root traits and yield parameters of corn

Correlation analysis between nodal root diameter and yield-related parameters showed no significant relationships, with correlation coefficients ranging from -0.031 to -0.183. Similarly, nodal root length at the V4 stage showed correlation coefficient values between -0.050 and -0.134, which indicates that variations in nodal root length and diameter do not directly affect yield performance under the studied conditions in corn. The

findings confirm that nodal root diameter during the early vegetative (V4) stage does not have a significant linear relationship with yield or morphological traits. While roots are essential for water and nutrient uptake, the minimal correlations observed suggest that variation in nodal root diameter does not directly impact yield performance. This observation aligns with previous findings indicating that root structural traits are more important under stress adaptation, such as during drought or low nitrogen conditions, than under optimal growth environments [26].

3.5 Relationship between root biomass and yield parameters of corn

The relationship between root fresh and dry weight and various yield-related traits in corn was evaluated to determine the influence of root biomass at the early vegetative stage (V4) on yield-related performance. Root fresh weight did not exhibit a significant relationship with six yield parameters: ear weight, ear length, ear diameter, kernel weight, and computed yield. The correlation coefficients (r) ranged from -0.164 to -0.062, indicating no associations. Similarly, root dry weight showed no significant relationships with yield parameters, with r values ranging from -0.019 to -0.102. Generally, root fresh and dry weight showed no linear associations with corn yield parameters. While root biomass indicates early plant vigor, it does not directly predict final yield at the V4 stage. Instead, root functional traits, including root length density, nutrient uptake efficiency, and stress-responsive architecture, are likely more critical for determining yield outcomes under environmental stress, as supported by previous research [24, 25].

4. Conclusions

Corn varieties, TCT 476A and TCT 1868, significantly outperformed, having higher yields across all the measured parameters, implying that these varieties are suitable for cultivation in alkaline conditions. Furthermore, all root morphological traits of different corn varieties at the V4 stage show no significant differences, reinforcing the importance of assessing root morphological traits beyond early vegetative stages. On the other hand, root morphological traits at the V4 stage show no significant linear relationship with yield and yield components, suggesting that yield outcomes cannot be reliably predicted at this stage. In relation to this, fertilizer application during the V4 stage has minimal benefits, as it does not significantly influence the final yield. Thus, it is strongly advised to evaluate root development in later stages, and fertilizer application strategies should be well-timed as nutrient demand increases during the early reproductive stage. To optimize nutrient efficiency and improve yield outcomes, nutrient assimilation analysis will provide valuable insights into nutrient utilization and uptake dynamics.

5. Acknowledgements

The authors extend their sincere gratitude to Cebu Technological University – Barili Campus, for letting them use the land in conducting the research, to DOST-Strand N and CTU – Barili Campus, Graduate School, for the remarkable opportunity offered in making this study possible.

Author Contributions: Conceptualization, P.R.P., and E.J.; methodology, E.J., and B.B.; software, E.J.; validation, E.J.; formal analysis, E.J.; investigation, E.J., and B.B.; resources, E.J., and B.B.; data curation, E.J.; writing—original draft preparation, E.J.; writing—review and editing, E.J., and P.R.P; visualization, E.J.; supervision, P.R.P.; project administration, E.J., and B.B. All authors have read and agreed to the published version of the manuscript**.**

Funding: The research was made possible through the support of the Department of Science and Technology – Science Education Institute (DOST-SEI) under the STRAND-N Scholarship Program.

Conflicts of Interest: The authors declare no conflict of interest.

References

[1] Erenstein, O.; Jaleta, M.; Sonder, K.; Mottaleb, K.; Prasanna, B. M. Global maize production, consumption and trade: Trends and R&D implications. *Food Secur.* **2022,** *14*(5), 1295–1319. https://doi.org/10.1007/s12571-022-01288-7

[2] U.S. Department of Agriculture, Foreign Agricultural Service. *Corn: Production Data*; USDA: Washington, DC, 2024. https://www.fas.usda.gov/data/production/commodity/0440000

[3] Biñas, E. E., Jr. The use of organic and inorganic fertilizers and its effect on the quality of corn products in the Philippines: A review. *Galaxy Int. Interdiscip. Res. J.* **2021,** *9*(5), 83–100. https://doi.org/10.17605/osf.io/puc7a

[4] Amper, B. M., Jr.; Amper, Z. H. S. Precarity among corn farmers in the uplands of Cebu, the Philippines. *Aghamtao* **2021,** *29*, 42–57.

[5] Amanullah; Fahad, S. Corn – Production and Human Health in Changing Climate; *IntechOpen*, **2018**. https://doi.org/10.5772/intechopen.74074.

[6] Gaikwad, D. J.; Ubale, N. B.; Pal, A.; Singh, S.; Ali, M. A.; Maitra, S. Abiotic stresses impact on major cereals and adaptation options—A review. *Res. Crops* **2022,** *23*(4), 913–920. https://doi.org/10.31830/2348-7542.2022.roc-913

[7] Fu, J.; Xiao, Y.; Wang, Y.-F.; Liu, Z.-H.; Yang, K. Saline–alkaline stress in growing maize seedlings is alleviated by *Trichoderma asperellum* through regulation of the soil environment. *Sci. Rep.* **2021,** *11*(1), 11546. https://doi.org/10.1038/s41598-021-90675-9

[8] Enojada, G. R.; Asio, V. B. Morphological, physical, and chemical characteristics of soils derived from limestone rocks in Barili, Cebu. *ResearchGate* **2015.** https://www.researchgate.net/publication/327366666

[9] Lynch, J.; Marschner, P.; Rengel, Z. Effect of internal and external factors on root growth and development. In *Marschner's Mineral Nutrition of Higher Plants*; Marschner, P., Ed.; Elsevier Ltd.: London, 2012; pp 331–346. https://doi.org/10.1016/B978-0-12-384905-2.00013-3

[10] De Araujo Rufino, C.; Fernandes-Vieira, J.; Martín-Gil, J.; De Souza Abreu Júnior, J.; Tavares, L. C.; Fernandes-Correa, M.; Martín-Ramos, P. Water stress influence on the vegetative period yield components of different maize genotypes. *Agronomy* **2018,** *8*(8), 151. https://doi.org/10.3390/agronomy8080151

[11] Nleya, T.; Chungu, C.; Kleinjan, J. Chapter 5: Corn growth and development. In *iGrow Corn: Best Management Practices*; *South Dakota State University*, **2016**. Chapter 5.

[12] Penn State Extension. Corn Growth Stages; *Penn State College of Agricultural Sciences*, **n.d**. https://extension.psu.edu/corn-growth-stages (accessed October 8, 2025).

[13] Fageria, N. K. The Role of Plant Roots in Crop Production; *CRC Press: Boca Raton, FL*, **2012**. https://doi.org/10.1201/b12365

[14] Rodríguez, M. N. S.; Cassab, G. I. Primary root and mesocotyl elongation in maize seedlings: Two organs with antagonistic growth below the soil surface. *Plants* **2021,** *10*(7), 1274. https://doi.org/10.3390/plants10071274

[15] Niu, L.; Hao, R.; Wu, X.; Wang, W. Maize mesocotyl: Role in response to stress and deep-sowing tolerance. *Plant Breeding* **2020,** *139* (3), 466–473. https://doi.org/10.1111/pbr.12804

[16] Poffenbarger, H. J.; Barker, D. W.; Helmers, M. J.; Miguez, F. E.; Olk, D. C.; Sawyer, J. E.; Six, J.; Castellano, M. J. Genotypic variation on root growth and nutrient uptake in corn and soybean. *Agric. Environ. Lett.* **2019,** *4*(1), 180018.

[17] Gu, S.; dos Santos Diniz, M. H.; Mukhametov, A.; Kondrashev, S. Comparative study on the response of corn hybrids to different irrigation techniques and moisture levels. *Arch. Agron. Soil Sci.* **2025**, *71*(1), 1–15.

[18] Elmundo, E. M.; Alcantara, C. G.; Bautista, E. R. Yield performance of ten white corn hybrids under Claveria condition. *Mindanao J. Sci. Technol.* **2011,** *9*(1), 45–58.

[19] Puyod, S.E.G.; Pascual, P.R. Varietal performance of hybrid corn fertilized with ammonium fertilizers in an alkaline soil under drought conditions. *ASEAN J. Sci. Tech. Report.* **2025**, *28*(4), e257403. https://doi.org/10.55164/ajstr.v28i4.257403

[20] Vilas-Boas, J. K.; Steiner, F.; Zuffo, A. M.; González Aguilera, J.; Zaratin Alves, C. Tolerance of high-yielding corn hybrids to drought stress during the early growth stage. *Rev. Ciênc. Agron.* **2025**, *56*, e20250040. https://doi.org/10.5935/1806-6690.20250040

[21] Tripathi, S.; Tiwari, K.; Mahra, S.; Victoria, J.; Rana, S.; Tripathi, D. K.; Sharma, S. Nanoparticles and root traits: Mineral nutrition, stress tolerance, and interaction with rhizosphere microbiota. *Planta* **2024,** *260*(2), 409.

[22] Rasheed, A.; Li, H.; Tahir, M. M.; Mahmood, A.; Nawaz, M.; Shah, A. N.; Aslam, M. T.; Negm, S.; Moustafa, M.; Hassan, M. U.; Wu, Z. The role of nanoparticles in plant biochemical, physiological, and molecular responses under drought stress: A review. *Front. Plant Sci.* **2022,** *13,* 976179.

[23] Zhan, A.; Lynch, J. P. Reduced frequency of lateral root branching improves water and nitrate capture in maize (*Zea mays* L.) under low nitrogen stress. *Plant Physiol.* **2015,** *168*(1), 117–129.

[24] Gao, Y.; Lynch, J. P. Reduced crown root number improves water acquisition under water deficit stress in maize (*Zea mays* L.). *J. Exp. Bot.* **2016,** *67*(15), 4545–4557. https://doi.org/10.1093/jxb/erw243

[25] Hund, A.; Trachsel, S.; Stamp, P. Rooting depth and water use efficiency of tropical maize inbred lines differing in drought tolerance. *Plant Soil* **2009,** *318,* 311–325. https://doi.org/10.1007/s11104-008-9843-6

[26] Magsayo, N. J.; Jamio, E.; Canunayon, M.; Tangpos, D.; Caritan, J.; Pascual, P. R. Root length and diameter at flag leaf stage correlate with important yield parameters in corn (*Zea mays* L.) grown in alkaline soil under drought conditions. *ASEAN J. Sci. Technol. Rep.* **2025,** *28*(5), e259419. https://doi.org/10.55164/ajstr.v28i5.259643

ASEAN
Journal of Scientific and Technological Reports
Online ISSN:2773-8752

Research article

Fiber Yield and Characterization of Locally Grown Abaca (*Musa textilis* Née) Cultivars in Aklan, Philippines

Gene T. Señeris[1, 2], Franz Marielle N. Garcia[2, 5*], Rosemarie T. Tapic[2], Ariel G. Mactal[2], Fernan T. Fiegalan[3], and Anna Maria Lourdes S. Latonio[4]

[1] College of Agriculture, Forestry and Environmental Sciences, Aklan State University, Banga, Aklan 5601, Philippines
[2] College of Agriculture, Central Luzon State University, Science City of Muñoz, Nueva Ecija, 3120, Philippines
[3] College of Agriculture, Central Luzon State University, Science City of Muñoz, Nueva Ecija, 3120, Philippines
[4] College of Science, Central Luzon State University, Science City of Muñoz, Nueva Ecija, 3120, Philippines
[5] Crops and Resources Research and Development Center, Central Luzon State University, Science City of Muñoz, Nueva Ecija, 3120, Philippines
* Correspondence: fmcnogoy@clsu.edu.ph

Citation:
Señeris, G.; Garcia, F.M.; Tapic, R.; Mactal A.G.; Fiegalan F.T.; Latonio A.M. L., Fiber yield and characterization of locally grown abaca (*Musa textilis* Née) cultivars in Aklan, Philippines. *ASEAN J. Sci. Tech. Report.* **2026**, *29*(2), e259173. https://doi.org/10.55164/ajstr.v29i2.259173.

Article history:
Received: May 6, 2025
Revised: November 3, 2025
Accepted: November 15, 2025
Available online: January 20, 2026

Abstract: Abaca (*Musa textilis* Née) is a natural fiber-producing plant that is endemic to the Philippines. It is primarily grown for its fibers in textile and industrial applications. Currently, five locally described Abaca cultivars are grown in Aklan: *Tabukanon*, *Bisaya*, *Agbayanon*, *Negro*, and *Totoo*. Limited information exists, and no in-depth research has been conducted on the yield of these Abaca cultivars. The study investigated the fiber yield performance of Abaca cultivars in Aklan using a linear mixed-effects model (LMM) and Tukey's HSD method at a 5% level to determine differences between cultivars. Findings highlighted highly significant differences among cultivars in terms of tuxy weight, extracted fiber weight, dry weight, moisture content, fiber length, and fiber count. Findings revealed that significant differences were observed in the inner layers of tuxy, extracted fibers, moisture content, and fiber length, while in the outer layers, significant differences were observed only in dry weight and fiber count. Moreover, no significant differences were observed in the tuxy weight, extracted fiber, moisture content, and fiber length for the outer layers, whereas extracted fiber and dry weight were significantly different for the inner layers. The study highlighted that *Bisaya* and *Tabukanon* exhibited high inner fiber yield and tuxy weight but have shorter fiber lengths and potential for commercial production. In contrast, the *Totoo* cultivar produced a high fiber count; however, it had lower tensile strength, shorter length, and lower dry weight. Among all cultivars, *Negro* exhibited significantly longer fibers (both layers), and *Agbayanon* had moderate fiber characteristics, which are desirable for industrial applications.

Keywords: Abaca; fiber; manila hemp; textile

1. Introduction

Abaca (*Musa textilis* Née) is a native plant thriving in the Philippines. It is mainly cultivated for its fibers for textile and industrial applications. Due to its export value, the Philippines is the top exporter of Abaca fibers, supplying 85% of global demand and ranking as a top crop dollar earner. Its fiber is considered the strongest among natural fibers due to its high durability and tensile strength, and is primarily used for ropes, cords, marine cordage, and reinforcing materials [1, 2]. Additionally, Abaca is widely used in specialty

papers, non-woven products, pulp production, and other specialized products, both locally and internationally [3]. Despite its economic significance, this fiber crop faces several challenges, including poor fiber yield, limited varietal information, limited research on fiber yield, and limited adoption of other technologies, resulting in an overall decline in production. The demand for Abaca fiber is expected to grow due to global demand in the pulp, paper, and fiber industries [4, 5].

Fiber characterization of locally described Abaca fiber yield is vital for optimizing and increasing production to meet the global demand for Abaca fiber. According to Research and Markets [6], the global Abaca fiber market is expected to grow at a CAGR of 15.2% from 2025 to 2030, driven by the government's push for the adoption of natural fibers as substitutes for hazardous synthetic fibers. The Abaca plant has emerged as an important material to address environmental concerns, such as forest conservation, and to attract other industries because of its potential properties and increasing demand locally and internationally. There is a need for Abaca cultivars with desirable agronomic traits and quality attributes to meet the increasing demand for high-quality fiber in the international market [5]. However, there is limited information on the fiber yield of Abaca cultivars, which is rarely discussed in research and literature, especially for unregistered cultivars.

Several varieties and hybrids exist in the Philippines, and as many as 200 Abaca cultivars thrive in the Philippines, which has not yet been fully explored. Studies have shown that these varieties exhibit different morphological and fiber yield performance [7], and there are only three registered varieties under the National Seed Industry Council (NSIC), including Inosa, Abuab, and Tangongon. Aklan is the top abaca-producing province in the Western Visayas Region and one of the leading Abaca-producing provinces in the Philippines. There are five locally described Abaca cultivars identified in Aklan: *Bisaya*, *Agbayanon*, *Tabukanon*, *Negro*, and *Totoo*. However, no in-depth research has been conducted on fiber yield performance. Exploring the fiber yield of these unregistered cultivars can provide valuable insights and reveal superior fiber traits that can be introduced to the market, contributing to fiber productivity, boosting the Abaca industry, and advancing scientific research.

Evaluating the fiber yield of these Abaca cultivars and comparing them with other varieties will provide new insights into the fiber yield in the Abaca industry. Hence, this study aimed to provide comprehensive information to assess the fiber yield characteristics of Abaca cultivars, which are crucial for improving production, enhancing economic viability, and optimizing their use. This study aimed to evaluate and identify specific fiber yield traits, including tuxy weight, extracted fibers, fiber yield, dry weight, moisture content, fiber length, and fiber number, for the five cultivars used in the Province of Aklan. The generated information will be valuable to all farmers, breeders, stakeholders, and industries to optimize the yield performance of this Abaca to meet the high demand for high-quality fiber in the global market.

2. Materials and Methods

The study employed an observational comparative study with inferential analysis to determine, assess, and evaluate the fiber yield traits of Abaca fibers extracted from different cultivars in the province of Aklan. It was carried out in the municipality of Libacao, where fibers from the *Bisaya*, *Agbayanon*, *Tabukanon*, and *Negro* (Figure 1a – d) cultivars were collected and extracted, as these cultivars were grown in the Eastern Aklan (1st District) of the Province of Aklan. Meanwhile, the *Totoo* (Figure 1e) cultivar was exclusively grown in the municipality of Makato in Western Aklan (2nd District). Figure 2 shows the site of the study.

2.1 Harvesting and Sample Collection

Fibers were gathered from ten (10) samples of each cultivar at every sampling location to obtain a representative yield per cultivar–location combination. The fiber yields of the Abaca cultivars from the ten samples were averaged to represent each cultivar in that location. Tuxying was conducted in separating several layers of the leaf sheaths (outer layer and inner layer) by inserting a tuxy-knife between the layers. This was followed by manual hand stripping to extract all the fibers from the tuxies [8-10]. Moreover, PhilFIDA provided all the modified Abaca stripping knives (MASK) used in the study to the farmers. All extracted fibers were separately sun-dried per plant/cultivar to remove moisture and prevent fungal growth.

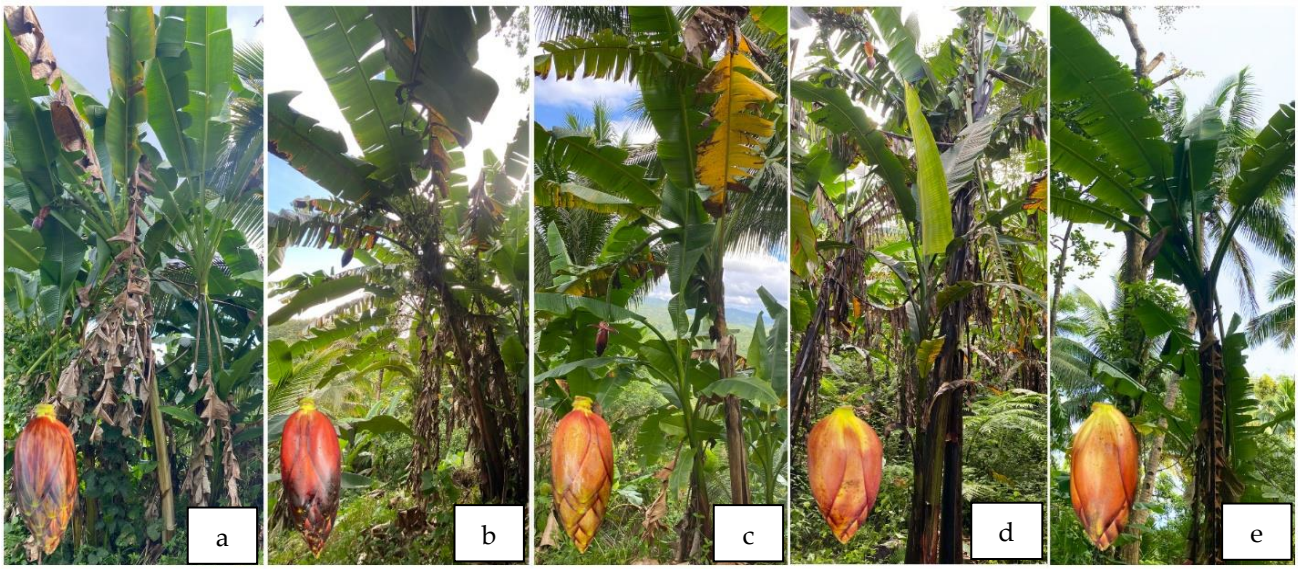

Figure 1. Aklan Abaca cultivars: (a) *Bisaya*, (b) *Agbayanon*, (c) *Tabukanon*, (d) *Negro*, and (e) *Totoo*.

2.2 Agroclimatic Conditions

Data on agroclimatic conditions in Makato and Libacao, Aklan, including soil, climate, and topography, were gathered from various government agencies and legitimate sources. Climate data, including rainfall, humidity, and temperature, were sourced from the Philippine Atmospheric, Geophysical, and Astronomical Services Administration (PAGASA), Global Historical Weather and Climate Data to determine annual rainfall, humidity, and average temperature during data collection. Soil data, including soil type, were obtained from the Bureau of Soil and Water Management. Furthermore, the National Mapping and Resource Information Authority (NAMRIA) obtained the land cover and topography.

2.3 Tuxy and Fresh Weight

The outer and inner layers of the leaf sheath were immediately separated to gather the weight using a digital weighing scale (kg). The tuxy (inner and outer) was weighed three times, and the average was used to ensure data accuracy. In terms of fiber weight, after stripping the fibers and removing non-fibrous material, the freshly extracted fibers were immediately weighed using a digital weighing scale, recorded three times, and the average was calculated to ensure uniformity and minimize human error and variation.

2.4 Dry Weight

This was measured and weighed using a digital weighing scale in grams (g). It was calibrated before the measurement session with a precision of at least 0.01 g. The fibers were measured and labeled separately, and the procedure was repeated three times by the same observer to ensure data accuracy and minimize inter-observer variability. The average dry weight of the repeated readings was used in the analysis.

2.5 Moisture content

This was measured after the fresh weight and dry weight of the sample plants were recorded using the digital weighing scale in grams (g). To compute the moisture content percentage, the formula below was used:

$$\text{Moisture Content (\%)} = \frac{(Fresh\ Weight - Dry\ Weight)}{Fresh\ Weight} \times 100\% \quad (1)$$

2.6 Fiber Length

Ten (10) representatives with the longest air-dried fibers in each cultivar were measured using a meter roll in centimeters. Visual inspections were carefully conducted to ensure that the fibers were not stretched or tangled. Upon measuring, the fibers were carefully straightened to avoid curling. At least two people conducted the process to ensure data accuracy by holding and carefully aligning the fiber. Data on fiber length were carefully tabulated for each cultivar.

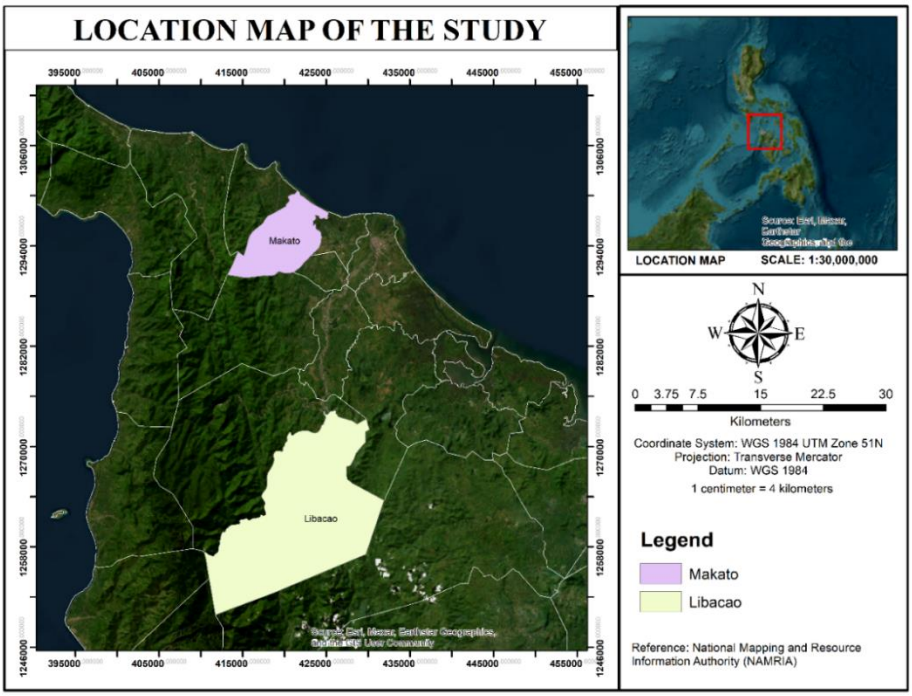

Figure 2. Study site.

2.7 Number of Fibers

The fibers extracted were manually counted to determine the fiber count or total number of fibers produced per cultivar. The fibers were carefully separated to ensure their accuracy. This process was repeated three times for each batch, and the average fiber count was recorded to reduce human error.

2.8 Statistical Tool Analysis

The data were analyzed using R statistical software (version 4.4.3, R Core Team, 2023), and the study employed a linear mixed-effects model (LMM) to handle the variability in data and unbalanced designs, where some cultivars are absent in specific locations. In the model, location was included as a random effect to account for variability across sampling sites, while cultivars were treated as fixed effects to assess differences in fiber characteristics. This modeling choice reflects the study's focus on the fixed effects of Abaca cultivars rather than on comparing specific locations. Although some cultivars were limited to fewer locations, recent literature supports the inclusion of random effects with fewer than five levels when the grouping variables serve as a nuisance factor rather than a primary target of inference [11]. Tests of fixed effects were performed using Satterthwaite's approximation for denominator degrees of freedom. For models with very small degrees of freedom (DenDF ≤ 3), a parametric bootstrap test with 1000 simulations was conducted to validate the significance of the fixed effect. In cases where the bootstrap test disagreed with the F-test result, inference was based on the bootstrap p-value.

3. Results and Discussion

3.1 Agroclimatic Conditions

According to the Global Historical Weather and Climate Data and the Philippine Atmospheric, Geophysical and Astronomical Services Administration (PAGASA), the municipality of Libacao has an average monthly rainfall of 243.85 mm, a temperature of 28.35°C, and a humidity of 79.54%. Meanwhile, the Municipality of Makato has an average monthly rainfall of 166.77 mm, a temperature of 29.98°C, and a humidity of 84.09% [12]. Studies show that Abaca ideally thrives in areas with temperatures of 22 °C to 28 °C [13], high relative humidity (78-85%) and evenly distributed rainfall [9]. In terms of soil, Makato and Libacao have clay loam soils according to the BSWM, with Libacao having alimodian clay and san manuel clay loam. On the other hand, Makato has alimodian clay loam, makato clay, and buang clay. Abaca thrives in loamy

soils, as they provide proper drainage and ideal moisture retention, which are vital for the roots and growth and development of the Abaca plant [14]. Meanwhile, the vegetative cover data provided by NAMRIA shows that the majority of the land area of Makato is classified as perennial crops (62.18%), whereas the majority of the vegetative cover of Libacao has 41.88% brush/shrub land. Abaca is a shade-loving plant that thrives well under shady conditions. Several studies have shown that it is widely intercropped with other perennial crops, such as fruit trees and timber, but still produces a high fiber yield [15-17]. Additionally, topography shows that both municipalities have gentle to moderate terrain (8-8%). According to PhilFIDA, Abaca is grown in areas with sloping, rolling, hilly, or mountainous terrain, as it provides proper drainage and reduces the risk of waterlogging. Overall, the municipality of Makato has a suitable climate and vegetative cover favorable to Abaca fiber production. Meanwhile, Libacao's climate and vegetative cover are slightly lower than Makato's, but they still have good potential for Abaca cultivation.

3.2 Fiber Characteristics of Abaca Cultivars in Aklan

The study presents the fiber yield characteristics of the five Abaca cultivars. Findings revealed significant variation in fiber characteristics across all cultivars. There were significant differences in tuxy weight, extracted fiber weight, moisture content, fiber length, and fiber count on the inner layer of all cultivars. In the outer layer, only fiber dry weight and fiber number differed significantly, but not tuxy weight, extracted fiber weight, moisture content, or fiber length. No significant differences across the outer layer of cultivars were observed for any fiber morphology measured (fiber weight, moisture content, and fiber length). The results of the linear mixed-effects model (LMM) ANOVA for the fiber characteristics of Abaca cultivars are presented in Table 1. The estimated marginal means (EMMs), which account for random effects, are shown in Table 2. Pairwise comparisons of fiber characteristics among Abaca cultivars are summarized in Table 3.

3.3 Tuxy Weight

The results indicate significant differences in tuxy weight for the inner layer, $F(4, 6) = 104.97$, $p < 0.001$, whereas the outer layer showed no significant differences, $F(4, 6) = 1.70$, $p = 0.267$ (Table 1). Tuxy weight varied across cultivars, ranging from 1.44 to 3.54 in the outer layer and 1.53 to 6.28 in the inner layer (Figure 3a). Among the cultivars, *Totoo* exhibited the heaviest tuxy weight in the outer layer (M = 3.54, 95% CI [2.55, 4.71]) but had the lightest tuxy weight in the inner layer (M = 1.53, 95% CI [1.24, 1.88]) as presented in Table 2. For the inner layer tuxy weight, *Agbayanon* exhibited significantly lighter values than *Tabukanon* (MD = −2.86, SE = 0.28) and *Negro* (MD = −2.22, SE = 0.44), but was heavier than *Totoo* (MD = 1.88, SE = 0.27). *Tabukanon* demonstrated significantly heavier weights than *Totoo* (MD = 4.74, SE = 0.27), *Agbayanon* (MD = 2.86, SE = 0.28), and *Bisaya* (MD = 2.06, SE = 0.27). Additionally, *Negro* was significantly heavier than *Totoo* (MD = 4.11, SE = 0.27), as shown in Table 3.

Totoo exhibited lighter tuxy weight in the inner layer, which may be due to genetic differences and could indicate lower fiber yield. The inner layer of all cultivars weighs more than the outer layer, except for the *Totoo* cultivar, contributing to the significant variation in tuxy weight across all cultivars. The inner layer consists of secondary fibers and pulpy material, resulting in a heavier weight, while the outer layers contain primary fibers, resulting in a lower, finer density[18, 8]. Moreover, cultivars (*Tabukanon*, *Negro*, and *Bisaya*) have higher inner tuxy weight, which can be optimized for pulp production and used for paper, bank notes, tea bags, and other applications [19-21]. There is an increasing demand for pulp production, underscoring the urgent need to increase fiber yield. There is an urgent need to increase fiber production [22]. The demand for Abaca pulp across several industries is rapidly increasing and expanding, and it contributes 70 to 80% of the total income in these industries, highlighting its importance to economic growth [23]. Furthermore, Abaca pulp has a substantial addressable market, as the global Abaca pulp market is anticipated to expand at a compound annual growth rate of 13.9% between 2024 and 2030, amounting to USD 1.0 billion by 2030, according to Grandview Research [24]. In comparison, other NSIC varieties also produce more pulp, such as Inosa, and were recommended for pulp and paper production [22].

Table 1. ANOVA Results for Fiber Characteristics of Abaca Cultivars Using Linear Mixed-Effects Model (LMM).

Characteristics	Fixed Effects	Sum Square	Mean Square	NumDF	DenDF	F-value	p-value	p-value (PB)
Tuxy Weight								
Outer Layer	Cultivars	6.00	1.50	4	6	1.70	0.267	
Inner Layer	Cultivars	31.86	7.96	4	6	104.97	p<0.001 **	
Extracted Fiber Weight								
Outer Layer	Cultivars	1.71	0.43	4	4.94	3.81	0.088	
Inner Layer	Cultivars	8.99	2.25	4	5.33	15.56	0.004 **	
Fiber Yield Recovery								
Outer Layer	Cultivars	0.25	0.06	4	6	9.06	0.010 *	
Inner Layer	Cultivars	0.17	0.04	4	4.84	5.16	0.053	
Fiber Dry Weight								
Outer Layer	Cultivars	0.11	0.03	4	2	53.83	0.018 *	0.051
Inner Layer	Cultivars	0.07	0.02	4	6	0.66	0.640	
Moisture Content								
Outer Layer	Cultivars	0.06	0.01	4	2	1.58	0.423	0.572
Inner Layer	Cultivars	0.10	0.03	4	6	6.40	0.023 *	
Length of Fiber								
Outer Layer	Cultivars	6270	1567.50	4	6	3.05	0.108	0.027*
Inner Layer	Cultivars	11145	2786.20	4	2	27.05	0.036 *	
Number of Fiber								
Outer Layer	Cultivars	5939908	1484977	4	6	36.12	p<0.001 **	
Inner Layer	Cultivars	14112901	3528225	4	6	65.75	p<0.001 **	

*Significant at 5% level. **Significant at 1% level. NumDf= Numerator Degrees of freedom; DenDf = Denominator Degrees of freedom. F-tests were performed using Satterthwaite's method to approximate Dendf. For models with DenDF≤3, parametric bootstrap (PB) tests with 1000 simulations were additionally performed to validate fixed-effect significance. Random effect (Location) was included as a random intercept in all models; variance estimates were small but retained for model validity.

3.4 Extracted Fiber

Findings revealed that the extracted fiber weight in the outer layer was similar across Abaca cultivars ($F(4, 4.94) = 3.81$, $p = 0.088$). However, significant differences were observed in the inner layer $F(4, 5.33) = 15.56$, $p = 0.004$, as shown in Table 1. Moreover, Table 2 presents that extracted fiber weight ranged from 0.21 to 1.35 in the outer layer and the inner layer, with *Tabukanon* garnering the highest extracted fiber (2.63 kg), followed by *Bisaya* (2.11 kg), *Negro* (2.01 kg), *Agbayanon* (0.75 kg), and *Totoo* (0.26 kg) having least weight (Figure 3b). The pairwise comparisons in Table 3 confirm that *Totoo* weighed significantly less than *Tabukanon* (MD = 2.37, SE = 0.39) and *Bisaya* (MD = 1.84, SE = 0.32). The study highlighted that the outer layer is relatively uniform across all cultivars, whereas the inner layer shows significant differences. Generally, cultivars such as *Tabukanon* and *Bisaya* contain heavier fibers, which attract farmers and industries to commercial fiber production due to a per-kilo payment structure, in addition to grading and classification, which influence the profitability of Abaca farmers [25]. In a previous study, most of the cultivars used in the Province of Aklan were *Tabukanon* and *Bisaya,* as these cultivars produce more suckers and fiber [26]. It has an economic and industrial impact that is key to profitability in fiber-processing industries. Meanwhile, *Totoo* exhibited relatively low extracted fiber yields, which may contain a high density of non-fibrous materials and result in biomass loss [15].

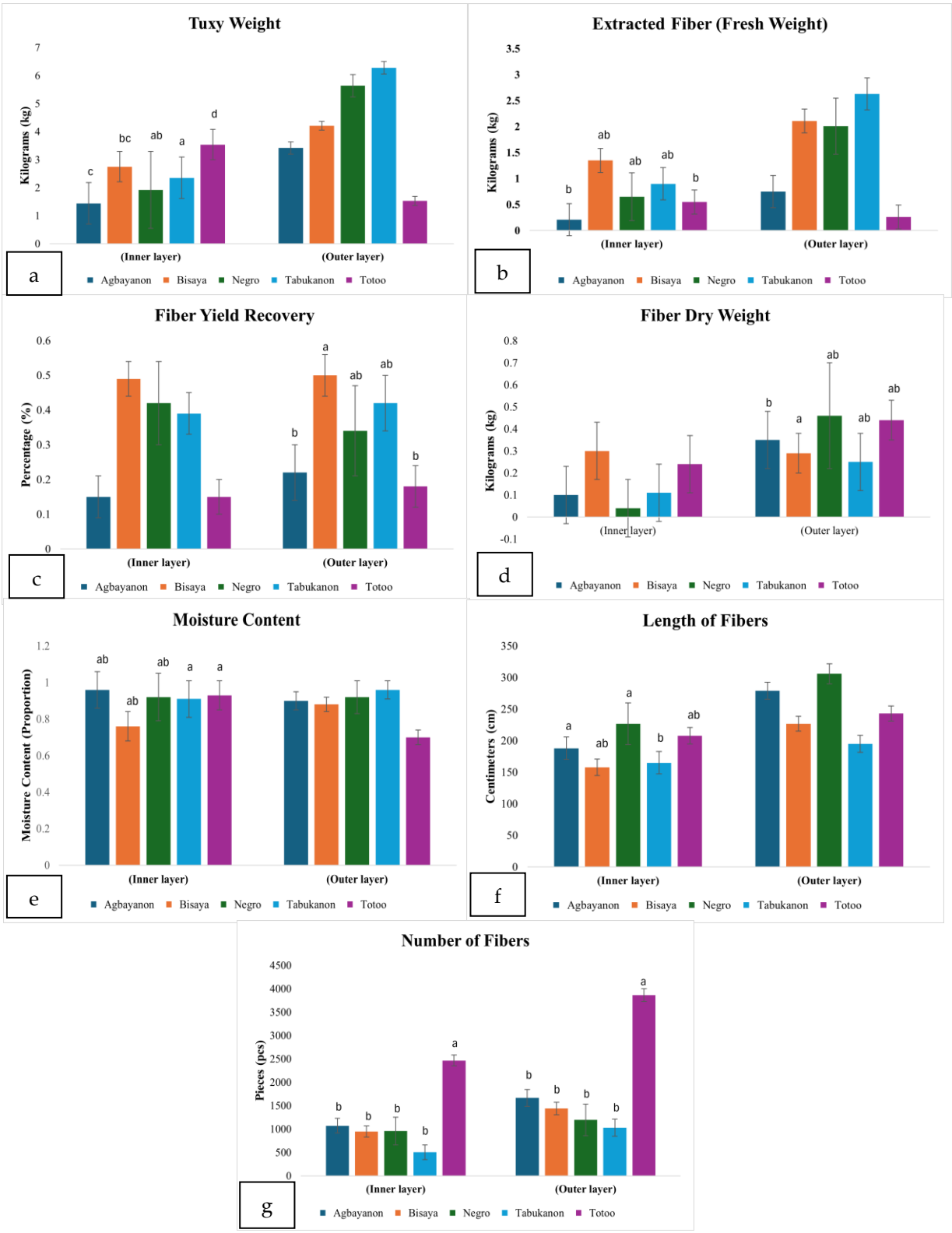

Figure 3. Fiber yield characteristics of the five Abaca cultivars: (a) tuxy weight, (b) extracted fiber, (c) fiber yield recovery, (d) fiber dry weight, (e) moisture content, (f) length of fibers, and (g) number of fibers. Statistical analysis was conducted with a Linear Mixed-Effects Model (LMM) with F-tests being performed using method of Satterthwaite for approximating the denominator degrees of freedom. Different superscript letters indicate significant difference among cultivars

3.5 Fiber Yield Recovery

Significant differences were observed among cultivars for the outer layer ($p = 0.010^*$, F -value = 9.06) as shown in Table 1. This study result implies that different Abaca cultivars can produce different percentages of fiber from the outer layer, which is relevant in identifying Abaca cultivars that produce a high yield. In contrast, the inner layer did not yield significant differences in fiber at the 5% level ($F(4, 4.84) = 5.16$, $p = 0.053$). The estimated marginal means (Table 2) reveal that fiber yield varied from 0.15 to 0.49 in the outer layer and 0.18 to 0.50 in the inner layer, with *Totoo* consistently showing the lowest yield (M = 0.15, 95% CI [0.08, 0.29]) in the outer layer and (M = 0.18, 95% CI [0.07, 0.26]) in the inner layer. In contrast, *Bisaya* had the highest fiber yield (M = 0.49, 95% CI [0.40, 0.58] in the outer layer and (M = 0.50, 95% CI [0.39, 0.60]) in the inner layer (Figure 3c). Table 3's pairwise comparison further confirms that *Bisaya* exhibited significantly higher fiber than *Agbayanon* (MD = -0.34, SE = 0.08), and *Totoo* exhibited significantly lower outer fiber yield than *Bisaya* (MD = 0.34, SE = 0.07) and other cultivars. Hence, the study indicates that cultivars *Bisaya* and *Tabukanon* are the best choices for fiber production due to their higher fiber yield potential, which encourages farmers to cultivate them and optimize yields, thereby increasing their profitability. Several factors affect fiber yield, including environmental factors (wind, drought, location, temperature, and rainfall), nutrient availability, and water availability [16]. Studies have shown that the Abaca thrives in high humidity, less sunlight, and wind [9], thus producing more fiber yield. Some studies reported that the location of the Abaca greatly impacts the fiber yield. For instance, Abaca planted in hilly areas produced lower fiber yields and lower fiber quality [27]. Moreover, intercropping (coconut, coffee, mango, cacao, and bamboo) greatly benefits Abaca plants and farmers by providing shading and protection from the sun and strong winds, thereby enhancing fiber yield and farmers' income [8; 14]. Most Abaca plantations were also intercropped with leguminous trees (nitrogen-fixing plants), which enhanced fiber yield. Studies have shown that planting legumes significantly affects the overall vigor of the Abaca plant by producing longer, wider pseudostems with wider leaves, thus increasing fiber yield [1].

3.6 Fiber Dry Weight

LMM ANOVA (Table 1) revealed that, in terms of dry weight, fiber significantly differs in the outer layer across Abaca cultivars ($F(4, 2) = 53.83$, $p = 0.018$), while the inner layer displayed similar dry weight ($F(4, 6) = 0.66$, $p = 0.640$). The outer layer demonstrated a significant difference ($p = 0.018^*$), and the corresponding F-value (53.83) indicated significant differences between the cultivars in outer layer fiber dry weight. This could be important for fiber processing as dry weight affects handling and quality. In contrast, the inner layer of all cultivars did not have significance at all ($p = 0.640$); likewise, the F-value (0.66) is very low. *Agbayanon* was the lightest cultivar in the outer layer (M = -0.01, 95% CI [0.3, 0.27]), while *Bisaya* was the heaviest (M = 0.30, 95% CI [0.40, 0.58]). In the inner layer, *Tabukanon* was the lightest (M = 0.25, 95% CI [-0.27, 0.51]), and *Negro* was the heaviest (M = 0.46, 95% CI [0.26, 0.59]) as presented in Table 2. A pairwise comparison of outer-layer fiber dry weight revealed that *Agbayanon* had significantly lower values than *Bisaya* (MD = −0.31, SE = 0.02). According to the data, *Totoo* obtained the maximum value of inner layer fiber dry weight (0.44g), while *Agbayanon* obtained the minimum value (0.35g). In the outer layer, the highest fiber dry weight was found in *Bisaya* (0.30g), and the lowest in *Agbayanon* (0.10g) (Figure 3d). Abaca fibers contain polymers such as hemicelluloses, cellulose, and lignin, which contribute to a high crystalline index (≥65%) [28] and also affect the total weight of the Abaca fiber. Moreover, Abaca cultivars can yield highly extracted fiber but also experience significant biomass loss during sun drying, which greatly affects dry weight. A study found that 15% to 30% shrinkage was observed after drying [15]. Other studies showed that 48 tons of biomass waste were produced for every ton of dry fiber [15;29]. Proper drying is vital for removing moisture from fibers and greatly affects fiber quality [30]. Moreover, dried fibers have an economic impact on farmers, as traders prefer properly dried Abaca fibers for several reasons. The high moisture content of the fibers can easily deteriorate and grow mold and mildew, thereby degrading fiber quality [4]. Likewise, the payment scheme for Abaca fibers is per kilo; thus, traders avoid paying the water weight rather than the actual fiber weight [25].

3.7 Moisture Content

Moisture content across Abaca cultivars was similar in the outer layer, F (4, 2) = 1.58, p = 0.423, but significantly differed in the inner layer, F (4, 6) = 6.40, p = 0.023 (Table 1). Regarding the outer layer, the study found no significant effect of cultivar (p = 0.423), indicating that moisture content in the outer fiber layer is relatively similar across cultivars. However, in the inner layer, the difference is significant (p = 0.023), demonstrating that the moisture content is different between cultivars. The F-value (6.40) indicates that genetic determinants might be involved in moisture retention of the inner fibers and may have implications on drying and storage properties. Table 2 shows the estimated marginal means (EMMs) for moisture content, which ranged from 0.76 to 0.96 in the outer layer and from 0.70 to 0.96 in the inner layer (Figure 3e). These cultivars have almost identical moisture content in the outer and inner layers, except for *Totoo,* which has the lowest inner-layer moisture content (0.70%). Moreover, further testing (Table 3) indicates that *Tabukanon* had significantly higher inner-layer moisture content than *Totoo* (MD = 0.26, SE = 0.06). High moisture content in Abaca fibers significantly affects the mechanical performance of composite materials due to their hydrophilic nature, which allows them to absorb more moisture from the environment and thereby affects the overall performance of Abaca fiber composites [31]. Abaca is highly saturated with water and has high initial moisture uptake [9]. According to other studies [32,33], Abaca's pseudostems comprise 93% - 96% water and 1.3-5% fiber. Hence, the present findings aligned with other studies showing that extracted fibers from different cultivars exhibited varying levels of moisture. Additionally, a study shows that the moisture content of newly harvested Abaca fibers can be reduced to 8% after 2-3 hours of sun exposure under summer heat conditions [34]. The present study indicates that the inner layer of *Totoo* (70%) may dry faster than *Tabukanon* (96%) and is less prone to microbial damage and fiber deterioration, such as mold. In contrast, *Tabukanon* may take longer to dry to the recommended 8% moisture content for safe storage and processing.

3.8 Fiber Length

Fiber length was significantly different in the inner layer, F (4, 2) = 27.05, p = 0.036, but not in the outer layer, F (4, 6) = 3.05, p = 0.108, as shown in Table 1. The only other variable for which a significant difference was detected (p = 0.036*) was the inner layer, indicating differences in inner fiber lengths between cultivars. A high F-value (27.05) indicates that cultivar selection may be essential for obtaining longer inner-layer fibers , which might be preferred in some industrial applications (Milosevic *et al*., 2022). Fiber length also varied significantly, ranging from 158 cm to 227 cm in the outer layer and 195 cm to 306 cm in the inner layer (Figure 3f). *Negro* had the longest fibers among cultivars, both in the outer layer (M = 227 cm, 95% CI [182, 274]) and the inner layer (M = 306 cm, 95% CI [285, 327]), followed by *Agbayanon* (M = 279 cm, 95% CI [263, 293]), *Totoo* (M = 243 cm, 95% CI [233, 256]), *Bisaya* (M = 227 cm, 95% CI [216, 238]) and *Tabukanon* (M = 195 cm, 95% CI [179, 256]) has the shortest as shown in Table 2. The fibers in the inner layer are generally longer, and the longest fibers are produced by *Negro* in both layers, while *Bisaya* (outer) and *Tabukanon* (inner) have the shortest. Moreover, the pairwise comparison further confirmed that *Tabukanon* consistently produced shorter fibers in the inner layer compared to *Negro* (MD = −111.0, SE = 13.3) and *Agbayanon* (MD = −83.8, SE = 10.1), as presented in Table 3. As a result, *Negro* fibers are considerably longer than those of *Bisaya* and *Tabukanon*. On the other hand, *Agbayanon* fibers are much longer than *Tabukanon* fibers. Abaca can reach up to 7.5 meters in height, with an average monthly increment of 14 cm [9; 16]. Hence, plant height may also directly influence fiber length and can be attributed to some factors (physiological and genetic). Generally, as the height of the Abaca plant increases, the leaf sheath elongates, thereby increasing fiber length. Several studies concluded that plant height significantly influences fiber elongation [35]. A previous study reported that among cultivars, *Negro* is the tallest plant (5 – 6 m), while *Tabukanon* (3 -3.5 m) and *Bisaya* are the shortest (4 m)[26]. Typical fiber length ranges from 1.5 to 3.5 meters, depending on the cultivar. In comparison, the fiber length of Abaca cultivars in Aklan was shorter than in other studies [2; 36]. The length of Abaca fibers is pivotal in grading and classifying fiber grades. As mentioned, Abaca fibers are not homogeneous and vary according to cultivars, growth , and development. The minimum requirements for normal grades are no less than 60 cm, while the residual grade is less than 60 cm according to the Philippine National Standards for grading and classifying Abaca fibers. However, some studies reported that fiber strength and abrasion resistance decline at the initial feet of the fiber top portion, although longer fiber length can be beneficial for other industrial applications [37].

Table 2. Estimated Marginal Means (EMMs) for Fiber Characteristics of Abaca Cultivars.

Characteristics	Outer Layer				Inner Layer			
			95% CI				95% CI	
	EMM	SE	Lower Bound	Upper Bound	EMM	SE	Lower Bound	Upper Bound
Tuxy Weight								
Agbayanon	1.44	0.74	0.11	2.81	3.42	0.22	3.03	3.82
Bisaya	2.75	0.54	1.68	3.74	4.21	0.16	3.90	4.51
Negro	1.92	1.37	0.09	3.89	5.64	0.40	5.10	6.22
Tabukanon	2.35	0.74	1.03	3.73	6.28	0.22	5.89	6.68
Totoo	3.54	0.54	2.55	4.71	1.53	0.16	1.24	1.88
Extracted Fiber weight								
Agbayanon	0.21	0.31	-0.27	0.71	0.75	0.31	0.21	1.30
Bisaya	1.35	0.23	0.97	1.71	2.11	0.23	1.67	2.51
Negro	0.65	0.46	-0.02	1.39	2.01	0.54	1.27	2.81
Tabukanon	0.90	0.31	0.42	1.39	2.63	0.31	2.09	3.18
Totoo	0.55	0.23	0.196	0.96	0.26	0.23	-0.14	0.74
Fiber Yield								
Agbayanon	0.15	0.06	0.03	0.27	0.22	0.08	0.09	0.35
Bisaya	0.49	0.05	0.40	0.58	0.50	0.06	0.39	0.60
Negro	0.42	0.12	0.26	0.59	0.34	0.13	0.16	0.54
Tabukanon	0.39	0.06	0.27	0.51	0.42	0.08	0.29	0.55
Totoo	0.15	0.05	0.07	0.26	0.18	0.06	0.08	0.29
Fiber Dry Weight								
Agbayanon	0.01	0.13	-0.04	0.03	0.35	0.13	0.11	0.58
Bisaya	0.30	0.13	0.28	0.33	0.29	0.09	0.10	0.46
Negro	0.04	0.13	-0.01	0.08	0.46	0.24	0.14	0.80
Tabukanon	0.11	0.13	0.08	0.15	0.25	0.13	0.02	0.48
Totoo	0.24	0.13	0.22	0.27	0.44	0.09	0.27	0.65
Moisture Content								
Agbayanon	0.96	0.10	0.80	1.08	0.90	0.05	0.81	0.99
Bisaya	0.76	0.08	0.65	0.86	0.88	0.04	0.80	0.94
Negro	0.92	0.13	0.71	1.10	0.92	0.09	0.80	1.05
Tabukanon	0.91	0.10	0.73	1.03	0.96	0.05	0.87	1.05
Totoo	0.93	0.08	0.83	1.05	0.70	0.04	0.64	0.78
Length of Fiber								
Agbayanon	188	17.7	156	221	279	13.5	263	293
Bisaya	158	13.1	133	182	227	11.8	216	238
Negro	227	32.9	182	274	306	16.0	285	327
Tabukanon	165	17.7	133	198	195	13.5	179	210
Totoo	208	13.1	184	236	243	11.8	233	256
Number of Fiber								
Agbayanon	1072	158	786	1369	1667	181	1340	2007
Bisaya	948	117	719	1163	1440	134	1177	1685
Negro	958	295	561	1382	1195	337	742	1679
Tabukanon	504	158	219	800	1029	181	704	1367
Totoo	2466	117	2254	2719	3865	134	3622	4154

SE= standard error; CI= confidence interval. EMM confidence intervals were computed using parametric bootstraps with 1000 simulations to improve the reliability of the estimates.

Table 3. Pairwise Comparisons of Fiber Characteristics of Abaca Cultivars.

Cultivars		Inner Layer Tuxy Weight (kg)		Inner Layer Extracted Fiber Weight (kg)		Outer Layer Fiber Yield (%)	
i	**j.**	**Estimate (MD)**	**SE**	**Estimate (MD)**	**SE**	**Estimate (MD)**	**SE**
Agbayanon	***Bisaya***	-0.80	0.27	-1.35	0.38	-0.34	0.08
	Negro	-2.22 *	0.44	-1.26	0.58	-0.27	0.13
	Tabukanon	-2.86 **	0.28	-1.88	0.38	-0.24	0.08
	Totoo	1.88 **	0.27	0.49	0.39	-0.01	0.08
Bisaya	***Negro***	-1.43	0.43	0.09	0.58	0.07	0.13
	Tabukanon	-2.06 **	0.27	-0.53	0.38	0.10	0.08
	Totoo	2.68 **	0.23	1.84 **	0.32	0.34 **	0.07
Negro	***Tabukanon***	-0.63	0.44	-0.62	0.58	0.03	0.13
	Totoo	4.11 **	0.43	1.75	0.59	0.27	0.13
Tabukanon	***Totoo***	4.74 **	0.27	2.37 **	0.39	0.24	0.08

Cultivars		Inner Layer Moisture Content (%)		Inner Layer Length of Fiber (cm)		Outer Layer Number of Fiber		Inner Layer Number of Fiber	
i	**j.**	**Estimate (MD)**	**SE**	**Estimate (MD)**	**SE**	**Estimate (MD)**	**SE**	**Estimate (MD)**	**SE**
Agbayanon	***Bisaya***	0.02	0.06	51.3	10.5	123.67	197	227	225
	Negro	-0.02	0.10	-27.2	13.3	114.00	321	472	366
	Tabukanon	-0.06	0.06	83.8 *	10.1	568.00	203	638	232
	Totoo	0.20	0.06	35.3	17.9	-1394.33*	197	-2198 **	225
Bisaya	***Negro***	-0.04	0.10	-78.5	13.5	-9.67	317	245	362
	Tabukanon	-0.09	0.06	32.5	10.5	444.33	197	411	225
	Totoo	0.17	0.05	-16.0	16.7	-1518.00*	166	-2426 **	189
Negro	***Tabukanon***	-0.04	0.10	111.0 *	13.3	454.00	321	166	366
	Totoo	0.21	0.10	62.5	19.9	-1508.33 *	317	-2670 **	362
Tabukanon	***Totoo***	0.26 *	0.06	-48.5	17.9	-1962.33*	197	-2836 **	225

Cultivars i and j denote the two Abaca cultivars being compared. MD=Mean difference; SE=standard error. *Significant at 5% level. **Significant at 1%. The Tukey's HSD method was used for post-hoc pairwise comparisons to control for family-wise error rates.

3.9 Number of Fibers

Fiber count differed significantly among Abaca cultivars both in the outer layer, $F(4, 6) = 36.12$, $p < 0.001$, and inner layer, $F(4, 6) = 65.75$, $p < 0.001$ (Table 1). There was a highly significant difference ($p < 0.001$) among cultivars in the outer layer. The F-value was very high (36.12). The high sum of squares (5,939,908) indicates that cultivar choice significantly influenced fiber production potential. The inner layer was also observed to have a highly significant difference ($p < 0.001$), with a higher F-value (65.75). That means genetic variation influences the inner layer's fiber count even more heavily than the outer layers. The exceptionally large sum square (14,112,901) supports the idea that choosing a cultivar makes a huge contribution to fiber content.

Findings revealed that the number of fibers varied widely across cultivars. *Tabukanon* produced the fewest fibers, with an average of 504 fibers (95% CI [219, 800]) in the outer layer and 1029 fibers (95% CI [704, 1367]) in the inner layer. In contrast, *Totoo* had the largest fiber count, averaging 2466 fibers (95% CI [3622, 4154]) in the outer layer and 3865 fibers (95% CI [2254, 2719]) in the inner layer (Table 2 and Figure 3g). Thus,

Totoo has the highest number of fibers in both layers, while *Tabakanon* has the lowest. This result contrasts with the findings on fiber yield, where *Tabukanon* shows the highest extracted fiber yield while *Totoo* shows the lowest, this is primarily due to the diameter of the *Totoo* fiber extracted, which ranged from 0.10 – 0.20 (EF fiber grade), whereas *Tabukanon* fibers ranged from 0.20-0.50 (S2), resulting in a greater number of fibers extracted from *Totoo*.

Fiber grades, quality, and fiber counts sometimes vary depending on the extraction process, leaf sheaths, and stripping knives used. Other studies confirmed that knife serrations greatly influenced the Abaca fiber [38]. The Philippine National Standard for fiber grading and classification indicates that thinner fibers (smaller strand sizes) produce excellent fiber grades (excellent soft) compared to other fibers with larger strands [18]. Cultivars producing smaller fiber sizes yield higher fiber counts and excellent fiber grade, which will generate more income for the farmer [9]. Hence, the study indicates that *Tabukanon* may produce a higher fiber yield; however, *Totoo* produces excellent-quality fiber, generating higher prices and income for the farmers. Further tests confirmed that *Totoo* displayed a significantly lower number of fibers in the outer layer compared to *Tabukanon* (MD = −1962.33, SE = 197), *Bisaya* (MD = −1518.00, SE = 166), *Totoo* (MD = −1508.33, SE = 317), and *Agbayanon* (MD = −1394.33, SE = 197). Similarly, the inner layer fiber count of *Totoo* significantly differed from the other Abaca cultivars, with mean differences as follows: *Tabukanon* (MD = −2836, SE = 197), *Negro* (MD = −2670, SE = 362), *Bisaya* (MD = −2426, SE = 189), and *Agbayanon* (MD = −2198, SE = 225) as presented in Table 3. In addition, *Totoo* has many more fibers than other cultivars. *Tabukanon*, on the other hand, has much less fiber than most cultivars.

Statistical Considerations and Limitations

The study acknowledged that certain tests had low degrees of freedom due to the limited number of replicates, which could affect the validity of the F-statistics. Linear Mixed-Effects Models (LMM) with Satterthwaite's approximation were used to address this issue and supplemented with parametric bootstrap validation for models with low DenDF. Moreover, results demonstrate consistent trends in fiber yield traits among cultivars and are cautiously interpreted. Future studies with larger sample sizes are recommended to replicate the findings in multiple locations, thereby enhancing statistical power and strengthening and confirming the results and trends.

4. Conclusions

The study investigated the fiber characteristics of Abaca cultivars in Aklan. Findings highlighted highly significant differences among cultivars in terms of tuxy weight, extracted fiber weight, dry weight, moisture content, fiber length, and fiber count. In terms of the fiber yield traits, findings revealed that significant differences were observed in the inner layers of tuxy, extracted fibers, moisture content, and fiber length, while, for the outer layers, significant differences were observed only in dry weight and fiber count. Moreover, no significant differences were observed in the tuxy weight, extracted fiber, moisture content, and fiber length for the outer layers, whereas extracted fiber and dry weight were significantly different for the inner layers. The study highlighted that *Bisaya* and *Tabukanon* exhibited high inner fiber yield and tuxy weight but have shorter fiber lengths and potential for commercial production. While *Totoo* produced a high fiber count, it showed the lowest performance among all fiber characteristics. Among all cultivars, *Negro* exhibited significantly longer fibers (both layers), and *Agbayanon* had moderate fiber characteristics, which are desirable for industrial applications. The results of the study provide valuable information for stakeholders, farmers, breeders, and researchers, and are used in industrial applications, breeding programs, further research, policy development, and to optimize fiber production.

5. Acknowledgments

The researchers would like to acknowledge the Department of Agriculture – Bureau of Agricultural Research (DA-BAR) for their Thesis/Dissertation Support Program and Aklan State University for the financial support to the researchers. Likewise, the Philippine Fiber Industry Development Authority and the Provincial Environment and Natural Resources Office of Aklan provided technical assistance and support. The

researchers also extend their gratitude to all the faculty and staff of Central Luzon State University for their guidance and support.

Author Contributions: Conceptualization, data gathering and writing , G.T.S..; monitoring, supervision, review and editing, F.M.N.G.; methodology, formal analysis, review and editing, R.T.T., A.G.M and F.T.F.; statistical analysis, A.M.L.S.L. All authors have read and agreed to the published version of the manuscript.
Funding: Department of Agriculture – Bureau of Agricultural Research (DA-BAR)

Conflicts of Interest: The authors declare no conflict of interest.

References

[1] Armecin, R.B.; Seco, M.H.P.; Caintic, P.S.; Milleza, E.J.M. Effect of leguminous cover crops on the growth and yield of abaca (Musa textilis Née). *Ind. Crops Prod.* **2005**, *21*(3), 317–323. https://doi.org/10.1016/j.indcrop.2004.04.028

[2] Barba, B.J.D.; Madrid, J.F.; Penaloza, J.R.D.P. A review of abaca fiber-reinforced polymer composites: Different modes of preparation and their applications. *J. Chil. Chem. Soc.* **2020**, *65*(3), 4919–4924. http://dx.doi.org/10.4067/s0717-97072020000204919

[3] Galvez, L.C.; Meinhardt, L.W.; Goenaga, R.; Zhang, D. Accurate identification of abaca (Musa textilis Née) cultivars using single nucleotide polymorphisms (SNP) markers developed for banana (Musa acuminata Colla). *Int. J. Plant Biol. Res.* **2021**, *9*(1), 1125. https://doi.org/10.47739/2333-6668/1125

[4] Armecin, R.B.; Sinon, F.G.; Moreno, L.O. Abaca fiber: A renewable bioresource for industrial uses and other applications. In *Biomass and Bioenergy*; Hakeem, K.R., Jawaid, M., Rashid, U., Eds.; Springer Nature: **2014**; pp. 108–116. https://doi.org/10.1007/978-3-319-07641-6_3

[5] Lalusin, A.G.; Villavicencio, M.L.H. Abaca (Musa textilis Nee) breeding in the Philippines. In *Industrial Crops: Breeding for Bioenergy and Bioproducts*; **2015**; pp. 265–289. https://doi.org/10.1007/978-1-4939-1447-0_12

[6] Research and Markets. Trends and strategies in the $2.32 billion abaca fiber industry, 2025–2030, segmented by product and region. *GlobeNewswire*, March 3, 2025. Available online: https://www.globenewswire.com/news-release/2025/03/03/3035348/0/en/Trends-and-Strategies-in-the-2-32-Bn-Abaca-Fiber-Industry-2025-2030-Segmented-by-Product-and-Region.html (accessed on 28 April 2025).

[7] Galvez, L.C.; Catalla, J.L.; Borromeo, T.H.; Alvoteros, N.C. *Abaca Germplasm Conservation*; Philippine Fiber Industry Development Authority: Quezon City, Philippines, **2018**.

[8] Göltenboth, F.; Mühlbauer, W. Abacá – cultivation, extraction and processing. In *Industrial Applications of Natural Fibres*; Müssig, J., Ed.; John Wiley & Sons, Ltd.: Chichester, UK, **2010**; pp. 163–179.

[9] Waller, V.; Wilsby, A. Abaca in the Philippines, an overview of a potential important resource for the country: Relating the tensile strength of the single fiber to the microfibrillar angle.

[10] Philippine Fiber Industry Development Authority. *Abaca: Improvement of Fiber Extraction and Identification of Higher-Yielding Cultivars*; PhilFIDA Progress Report, **2002**.

[11] Gomes, D. G. E. Should I use fixed effects or random effects when I have fewer than five levels of a grouping factor in a mixed-effects model? *PeerJ.* **2022**, 10, e12794. https://doi.org/10.7717/peerj.12794

[12] Global Historical Weather and Climate. Aklan Climate Summary. Available online: https://weatherandclimate.com/philippines/aklan (accessed on 15 January 2025).

[13] Araya-Gutiérrez, D.; Monge, G. G.; Jiménez-Quesada, K.; Arias-Aguilar, D.; Cordero, R. Q. Abaca: A general review on its characteristics, productivity, and market in the world. Rev. Fac. Nac. Agron. Medellín **2023**, *76*(1), 10263–10273.

[14] Armecin, R.B.; Cosico, W.C.; Badayos, R.B. Characterization of the different abaca-based agro-ecosystems in Leyte, Philippines. *J. Nat. Fibers* **2011**, *8*(2), 111–125. https://doi.org/10.1080/15440478.2011.576114.

[15] Cortez, J.R.C.; Alcantara, A.; Pacardo, E.; Rebancos, C. Life cycle assessment of Manila hemp in Catanduanes, Philippines. *J. Environ. Sci. Manag.* **2015**, *18*(2). https://doi.org/10.47125/jesam/2015_2/06.

[16] Bande, M.M.; Asio, V.B.; Sauerborn, J.; Romheld, V. Growth performance of abaca (Musa textilis Née) integrated in multi-strata agroecosystems. *Ann. Trop. Res.* **2016**, *38*(1), 19–35. https://doi.org/10.32945/atr3813.2016

[17] Bande, M.M.; Grenz, J.; Asio, V.B.; Sauerborn, J. Fiber yield and quality of abaca (Musa textilis var. Laylay) grown under different shade conditions, water, and nutrient management. *Ind. Crops Prod.* **2013**, *42*, 70–77. https://doi.org/10.1016/j.indcrop.2012.05.009

[18] Bureau of Agriculture and Fisheries Standards. Abaca fiber – grading and classification – hand-stripped and spindle/machine stripped (Philippine National Standard). Available online: https://philfida.da.gov.ph/images/Publications/PNS/PNSBAFS1802016AbacaFiberHandstrippedandMachineStripped.pdf (accessed on 28 April 2025).

[19] Aiyedun, P.O.; Abdulkadir, B.; Owoeye, F.T.; Borokinni, F.; Azodo, A.P. Development of pulp and paper using stem and fruit stem of Musa species. *J. Amasya Univ. Inst. Sci. Technol.* **2023**, *4*(1), 20–32. https://doi.org/10.54559/jauist.1140132

[20] Shahri, W.; Tahir, I.; Ahad, B. Abaca fiber: A renewable bio-resource for industrial uses and other applications. In *Biomass and Bioenergy: Process and Properties*; **2014**; pp. 47–61.

[21] Mari, E.L.; Austria, C.O.; Torres, A.S.; Domingo, E.P. Residual grade and waste abaca fibers as reinforcement for packaging and printing/writing papers from recycled fiber. *Philipp. J. Sci.* **2019**, *148*(2).

[22] Moreno, L.O.; Protacio, C.M. Chemical composition and pulp properties of abaca (Musa textilis Née) cv. Inosa harvested at different stages of stalk maturity. *Ann. Trop. Res.* **2012**, *34*(2), 45–62. https://doi.org/10.32945/atr3423.2012

[23] Abamo, A.P.; Mascariñas, A.M.; Villarin, B.S.; Alan, E.G.; Galve, J.R. Abaca fiber industry in the Philippines. In *Exploring the Opportunities Towards Competitiveness: Supply Chain Improvement of Selected Commodities in AFNR (Phase I)*; PCARRD, DOST: Los Baños, Laguna, Philippines, **2011**, p. 61.

[24] Grandview Research. Abaca pulp market size, share & trends analysis report by product (medical filter papers, food preparation papers), by region (North America, Europe, Asia Pacific, Central & South America), and segment forecasts, 2024–2030. Available online: https://www.grandviewresearch.com/industry-analysis/abaca-pulp-market-report (accessed on 28 April 2025).

[25] Sagocsoc, R.A. Farmers' practices in marketing abaca fiber in Caraga Region. *J. Biodivers. Environ. Sci.* **2023**, *22*(6), 72–79.

[26] Señeris, G.T.; Vedasto, E.P.; Teodosio, M.M.; Ragaas, M.L.; Teodosio, L.J. Morphological characteristics of abaca (Musa textilis Nee') cultivars grown in two municipalities of Aklan, Philippines. *Univ. J. Agric. Res.* **2022**, *10*(2), 175–183. https://doi.org/10.13189/ujar.2022.100209

[27] Armecin, R.B.; Gabon, F.M. Biomass, organic carbon and mineral matter contents of abaca (Musa textilis Née) at different stages of growth. *Ind. Crops Prod.* **2008**, *28*(3), 340–345. https://doi.org/10.1016/j.indcrop.2008.03.014.

[28] De Souza, N.C.R.; D'Almeida, J.R.M. Tensile, thermal, morphological and structural characteristics of abaca (Musa textilis) fibers. *Polym. Renew. Resour.* **2014**, *5*(2), 47–60. https://doi.org/10.1177/2041247914005002.

[29] Van Dam, J.E.G.; Bos, H.L. The environmental impact of fibre crops in industrial applications. In: Van Dam, J.E.G., Ed.; *Hintergrundpapier zu: Van Dam JEG*; 2004.

[30] Ramadevi, P.; Sampathkumar, D.; Srinivasa, C.V.; Bennehalli, B. Effect of alkali treatment on water absorption of single cellulosic abaca fiber. *BioResources* **2012**, *7*(3).

[31] Punyamurthy, R.; Sampathkumar, D.; Srinivasa, C.V.; Bennehalli, B. Effect of alkali treatment on water absorption of single cellulosic abaca fiber. *BioResources* **2012**, *7*(3), 3515–3524.

[32] Hillman, J. Plant resources of South-East Asia No. 17. Fibre plants. In *Plant Resources of South-East Asia*; Brink, M., Escobin, R.P., Eds.; Backhuys Publishers: Leiden, The Netherlands, **2004**; p. 456.

[33] Castañeda-Niño, J.P.; Mina Hernandez, J.H.; Solanilla Duque, J.F. Potential of plantain pseudostems (Musa AAB Simmonds) for developing biobased composite materials. *Polymers* **2024**, *16*(10), 1357. https://doi.org/10.3390/polym16101357

[34] Sinon, F.G. *Manual on Abaca Harvesting and Processing into Fiber*; National Abaca Research Center, Visayas State University: Baybay, Philippines, 1997.

[35] Alcober, E.R. Morphological characteristics and yield of abaca and related Musa clones in Baybay, Leyte, Philippines. *Ann. Trop. Res.* **1986**, *8*(4), 193–197.

[36] Bledzki, A.K.; Franciszczak, P.; Osman, Z.; Elbadawi, M. Polypropylene biocomposites reinforced with softwood, abaca, jute, and kenaf fibers. *Ind. Crops Prod.* **2015**, *70*, 91–99. https://doi.org/10.1016/j.indcrop.2015.03.013

[37] Milosevic, M.; Dzunic, D.; Valasek, P.; Mitrovic, S.; Ruggiero, A. Effect of fiber orientation on the tribological performance of abaca-reinforced epoxy composite under dry contact conditions. *J. Compos. Sci.* **2022**, *6*(7), 204. https://doi.org/10.3390/jcs6070204

[38] Richter, S.; Stromann, K.; Müssig, J. Abacá (*Musa textilis*) grades and their properties—A study of reproducible fibre characterization and a critical evaluation of existing grading systems. *Industrial Crops and Products.* **2013**, 42, 601–612. https://doi.org/10.1016/j.indcrop.2012.06.025

ASEAN
Journal of Scientific and Technological Reports
Online ISSN:2773-8752

Research article

A Bibliometric Analysis of Sustainable Livestock Systems: Soil and Plant Health Perspectives

Annie Rose C. Permano[1*]

[1] Office of Provincial Agriculturist-Antique, College of Agriculture and Forestry-West Visayas State University, Iloilo City, 5000, Philippines
* Correspondence: permanoannierose@g.mail.com

Citation:
Permano, A. A bibliometric analysis of sustainable livestock systems: soil and plant health perspectives. *ASEAN J. Sci. Tech. Report.* **2026**, *29*(2), e259393. https://doi.org/10.55164/ajstr.v29i2.259393.

Article history:
Received: May 17, 2025
Revised: November 4, 2025
Accepted: November 18, 2025
Available online: January 20, 2026

Abstract: This Bibliometric analysis evaluates research on sustainable livestock systems, emphasizing plant and soil health, and examining the major trends in publications and partnerships. Analyzing 104 published articles from 2013 to 2024, the study reveals a significant increase in publication trends since 2016, peaking in 2021. An average of 5.8 authors per article reflects a strong inclination toward collaborative research—significantly higher than the 1.4–1.6 average in social sciences and humanities, and more aligned with biomedical and environmental sciences, where five or more authors are common. Despite this, co-authorship networks remain fragmented, lacking interdisciplinary collaborations essential for holistic solutions. The United States leads as a central research hub, maintaining collaborations with China and Brazil, though geographic and language clustering affect partnerships. Most studies were published by prestigious journals such as Science of the Total Environment (7 articles), Journal of Environmental Management (5), and Agriculture Ecosystems and Environment (9), with the majority available as open access. The study underscores the crucial role of open access in disseminating knowledge and fostering sustainable agricultural practices worldwide. It highlights the importance of incentivizing interdisciplinary research and fostering international collaboration. Establishing platforms for knowledge sharing, funding applied research, implementing supportive policy frameworks, investing in stakeholder training, and creating monitoring systems are essential actions. These will ensure effective and adaptive initiatives to bridge collaboration gaps and address challenges in sustainable livestock systems. These efforts contribute to resilient livestock systems, climate mitigation, biodiversity enhancement, and foster global collaboration —core elements of SDGs 2, 13, 15, and 17.

Keywords: Sustainable livestock systems; soil health; plant biodiversity; grazing management; environmental sustainability.

1. Introduction

Sustainable livestock systems have garnered significant attention in recent years due to their important part in promoting environmental sustainability, improving soil health, and enhancing plant biodiversity. These systems aim to balance agricultural productivity with ecological integrity by mitigating the negative impacts of conventional livestock farming, such as biodiversity loss, soil degradation, pollution, and greenhouse gas emissions. Numerous studies have demonstrated that sustainable practices like rotational grazing reduce stocking rates and improve pasture management, thereby

enhancing soil health, nutrient cycling, and encouraging diverse vegetations, making them a vital component of resilient agricultural landscapes [1,2].

The link between livestock management and soil health is particularly significant to support the growing need for sustainable food systems. Livestock contribute to these systems by providing manure, a critical source of natural fertilizer, and serving as draft animals to boost productivity in regions with low mechanization. However, overgrazing, improper land use, and poor soil management have been the reason the concerning soil erosion and nutrient depletion in many agricultural regions. Researchers have explored innovative grazing strategies that can increase productivity without compromising soil health [3,4]. For instance, rotational grazing has improved soil aeration and prevented soil compaction, resulting in healthier soil that supports diverse vegetation [5]. Recent bibliometric reviews also highlight the role of technology and ecological restoration in improving soil processes under sustainable grazing regimes [8,10]. Plant Biodiversity supports sustainable livestock systems through ecosystem functions such as nutrient cycling, water retention, and pest control. Studies highlight that integrating diverse forage species within grazing systems increases resilience against drought, diseases, and other environmental stressors [6,7]. The interconnectedness of livestock management and plant health is thus a key area of study in order to advance sustainable agricultural practices. Moreover, sector-wide collaboration among livestock stakeholders has been shown to drive innovation and improve biodiversity outcomes in grazing landscapes [13].

Despite the growing number of studies focusing on sustainable livestock systems, a persistent gap in interdisciplinary and international collaboration remains. Co-authorship networks are fragmented, which usually focus only on specific subject areas. The lack of international and interdisciplinary collaborations limits the development of comprehensive solutions to complex issues faced by sustainable livestock systems. Bibliometric analyses of agrifood transitions and SDG-related research emphasize the importance of cross-disciplinary partnerships to address these gaps [9,12]. Strengthening these networks is essential for fostering innovation and achieving sustainability targets. Recent bibliometric reviews of plant-based feeds and forage research from 2013 to 2024 further reinforce this gap, revealing fragmented co-authorship networks and limited collaboration between major contributors such as the United States and China. Thematic trends emphasize forage quality, crop resilience, and interdisciplinary integration across agriculture, environmental science, and animal production. Institutions like Lanzhou University and the USDA Agricultural Research Service emerged as key drivers of innovation, highlighting the importance of robust infrastructure and international partnerships to accelerate progress in sustainable livestock systems [21]. To address these limitations, this study introduces a novel analytical framework that integrates bibliometric mapping with thematic evolution analysis, offering deeper insights into interdisciplinary linkages and emerging research frontiers.

This study will provide an in-depth analysis of sustainable livestock systems research from 2013 to 2024. It identifies key contributors, research clusters, and emerging topics related to soil and plant health within sustainable livestock systems. By mapping the evolution of research in this area, this study provides a more integrated approach to sustainable livestock research. This study's findings can guide future research efforts and policy decisions to enhance environmental, economic, and social outcomes in sustainable agriculture. Recent bibliometric studies suggest that fostering interdisciplinary collaboration is essential for holistic sustainability planning in livestock systems [11,14]. Aligned with the United Nations Sustainable Development Goals (SDGs), this study contributes to several key global targets. It supports SDG 2: Zero Hunger by promoting sustainable food production systems and resilient agricultural practices that enhance soil and plant health. It advances SDG 15: Life on Land through the conservation of biodiversity and the sustainable use of terrestrial ecosystems, particularly in grazing landscapes. By addressing climate-resilient livestock practices and reducing environmental degradation, the study aligns with SDG 13: Climate Action. Finally, by emphasizing the importance of interdisciplinary and international research collaborations, it contributes to SDG 17: Partnerships for the Goals, fostering innovation and integrated approaches to sustainability planning.

The study aims to systematically analyze bibliometric patterns in sustainable livestock systems. Specifically, the study seeks to identify citation trends, highlighting influential works and emerging research trajectories. Additionally, it aims to map co-authorship networks, identifying key contributors and

collaborative relationships that shape the field. Another critical focus is the exploration of significant keywords, particularly those related to soil health, plant biodiversity, and grazing management, to uncover thematic concentrations within existing literature. Furthermore, the research examines the distribution of articles based on dimensions such as study type, authorship patterns, and source journals, providing insight into the structural characteristics of scholarly output. By addressing these objectives, the study contributes to a deeper understanding of research impact, collaboration dynamics, and thematic evolution within the domain of sustainable livestock systems.

2. Materials and Methods

The bibliometric analysis was conducted using peer-reviewed academic publications focused on sustainable livestock systems. The study aimed to identify patterns in authorship, keyword co-occurrence, institutional contributions, and thematic clusters. Articles were sourced exclusively from the Scopus database, selected for its comprehensive indexing of high-impact journals across agricultural and environmental sciences. While Scopus offers extensive coverage, its indexing bias toward English-language and high-impact journals may underrepresent regional or non-English contributions. This could influence geographic collaboration patterns and thematic diversity observed in the results. It is acknowledged that reliance on a single database may have excluded relevant literature indexed in other platforms such as Web of Science and Dimensions. Future studies should consider multi-database triangulation to enhance comprehensiveness and reduce selection bias.

Search strings were developed through a structured process combining preliminary scoping reviews of existing literature, expert consultation to refine thematic focus, and application of Boolean logic using ChatGPT to assist in generating and refining initial keyword combinations based on thematic relevance and co-occurrence patterns observed in prior studies. The final Boolean search strings were manually reviewed and adjusted to ensure precision and reproducibility. The search was conducted on July 12, 2024, using the Boolean combinations applied to titles, abstracts, and keywords: “sustainable livestock systems” AND “soil health” AND “plant biodiversity”, “grazing management” OR “rotational grazing” AND “sustainable agriculture”, “soil conservation” AND “pasture management” AND “biodiversity” OR “ecosystem services”, “sustainable livestock systems” AND “carbon sequestration” AND “environmental sustainability” and “regenerative agriculture” OR “organic farming” AND “rangeland management” AND “soil erosion”.

A total of 104 articles were filtered after applying criteria to focus on articles ranging from 2013 to 2024, in the English language, and within the subject areas of Agricultural and Biological Sciences and Environmental Sciences. This final count reflects the saturation point at which thematic patterns and co-authorship networks stabilized, ensuring both relevance and analytical depth. To validate the search strategy, a manual screening of titles and abstracts was performed to ensure relevance and consistency with the study’s objectives. The filtered articles were exported in CSV format and analyzed using VOSviewer version 1.6.20 (October, 2023). This software was selected for its effectiveness in visualizing complex data, robust capability in mapping co-authorship networks, keyword occurrences, and identifying research clusters, thereby providing a comprehensive overview of the research landscape and thematic evolution within the field of sustainable livestock systems.

3. Results and Discussion

The result section consists of two subchapters; the first one describes the VOSviewer computations, and the second part is about the ratio of documents per year, per year by source, by author, by affiliation, by country/territory, by type, by funding sponsors, and by subject area.

3.1 Result of VOSviewer computations

3.1.1 Co-Authorship Analysis

The co-authorship analysis (Figures 1- 3) highlights researchers such as Dong Shikui, Richard Teague, and Sarah E. MacDonald, whose contributions were thematically distinct - focusing on soil health, plant biodiversity, and grazing management- but largely isolated. This fragmentation suggests that comprehensive

solutions to sustainable livestock challenges may be constrained by limited interdisciplinary collaboration. Temporal analysis from 2019 to 2023 shows that Richard Teague maintained a consistent focus on adaptive grazing and ecosystem services, while Dong Shikui expanded into broader ecological and land-use dynamics. These shifts highlight the importance of continuous engagement and the need for the emergence of new collaborators in the field. However, the lack of interconnected networks raises concerns about knowledge and the synthesis of ideas. Fragmented co-authorship networks limit innovation and the development of scalable solutions for soil degradation, biodiversity loss, and sustainable grazing. Strengthening interdisciplinary ties is essential for advancing holistic livestock sustainability. As emphasized by Mittal and Bansal, cross-disciplinary collaboration is essential for holistic sustainability approaches, enabling the integration of ecological, technological, and social dimensions [14].

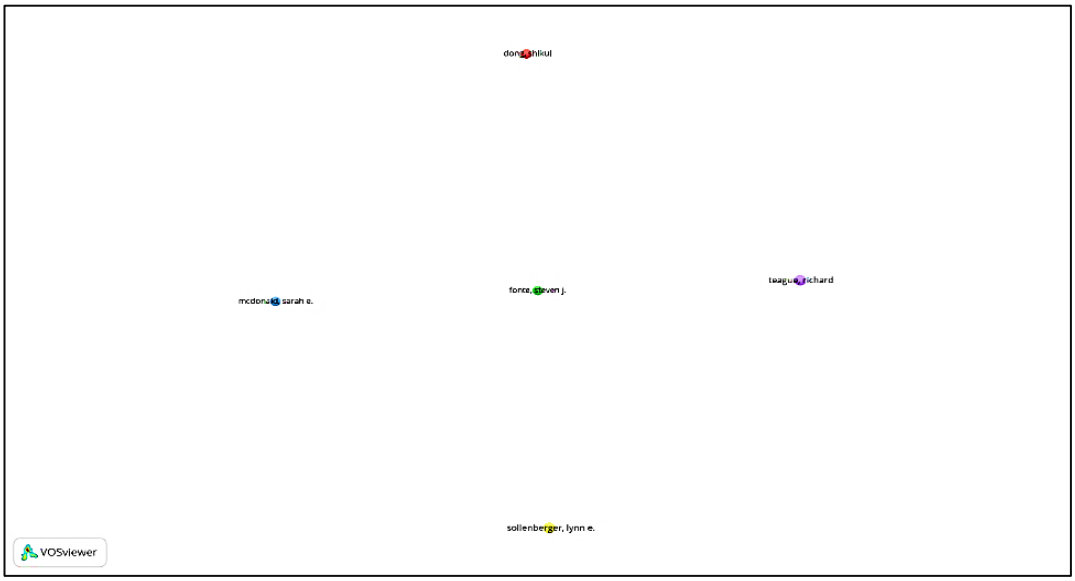

Figure 1. VOSviewer Network Visualization of Co-Authorship

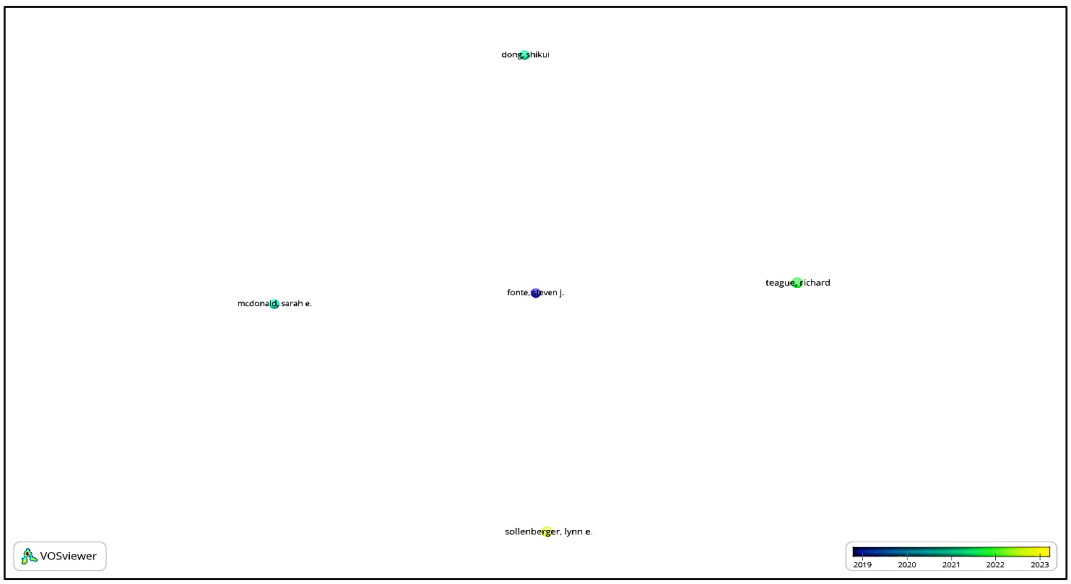

Figure 2. VOSviewer Overlay Visualization of Co-Authorship

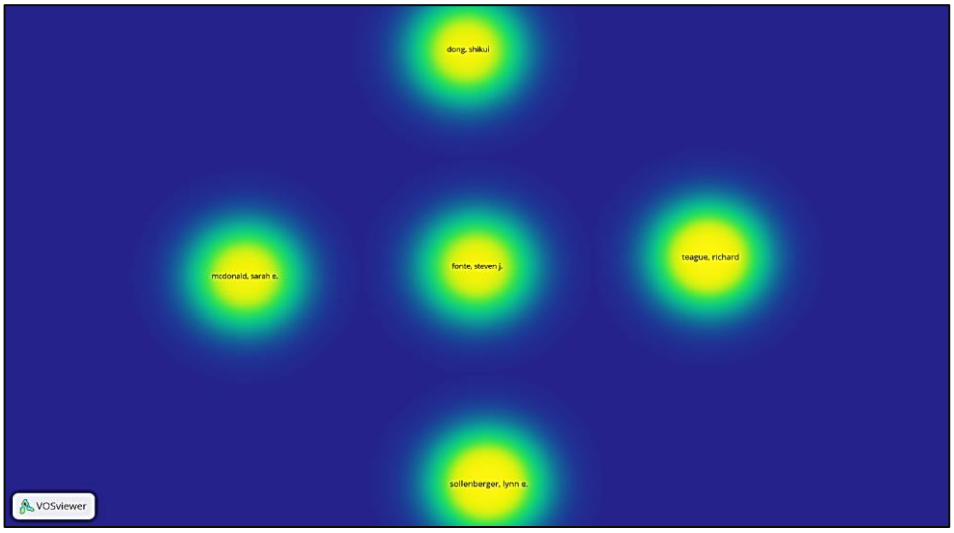

Figure 3. VOSviewer Density Visualization of Co-Authorship

3.1.2 Co-Authorship between countries

The network of research collaborations through co-authorship between countries in Figures 4, 5 & 6 has shown that the United States dominates plant-based feed and forage research, with strong connections to countries like China and Brazil forming central nodes in the global research landscape. While other countries like Australia and the United Kingdom are influenced by geography and language, forming clusters. Many other nations exhibit sparse connections, indicating limited international collaboration and underrepresentation in global research efforts. The changing temporal overlay from 2019 to 2024 shows that the nature of collaboration was still evolving. Recent articles show activity from countries Brazil and Spain, while earlier collaborations involved China, Germany, and the United Kingdom. This significantly suggests that clusters with the same geographical distributions, language, and historical identity have recognized contributions to the field, but also highlights the limited cross-cluster engagement. Limited international collaboration may result in regionally siloed policies and missed opportunities for knowledge transfer. For example, adaptive grazing techniques developed in the US may not be easily adopted in Southeast Asia without collaborative validation and localized adaptation. Encouraging more inclusive and diverse co-authorship networks could enhance the sharing of knowledge and innovation, leading to comprehensive solutions for soil degradation, biodiversity loss, and sustainable grazing practices. Strengthening global research connectivity is essential for designing adaptable livestock systems across diverse agroecological zones.

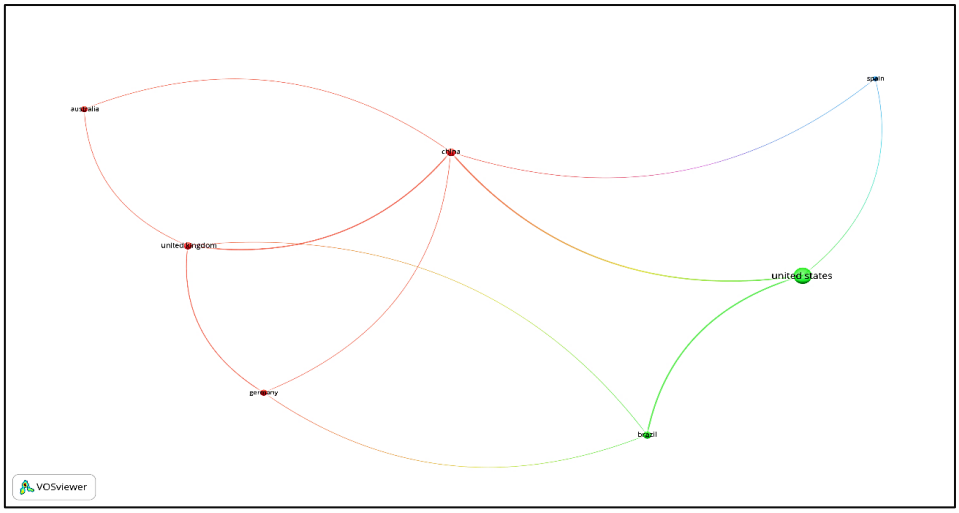

Figure 4. VOSviewer Network Visualizations of countries

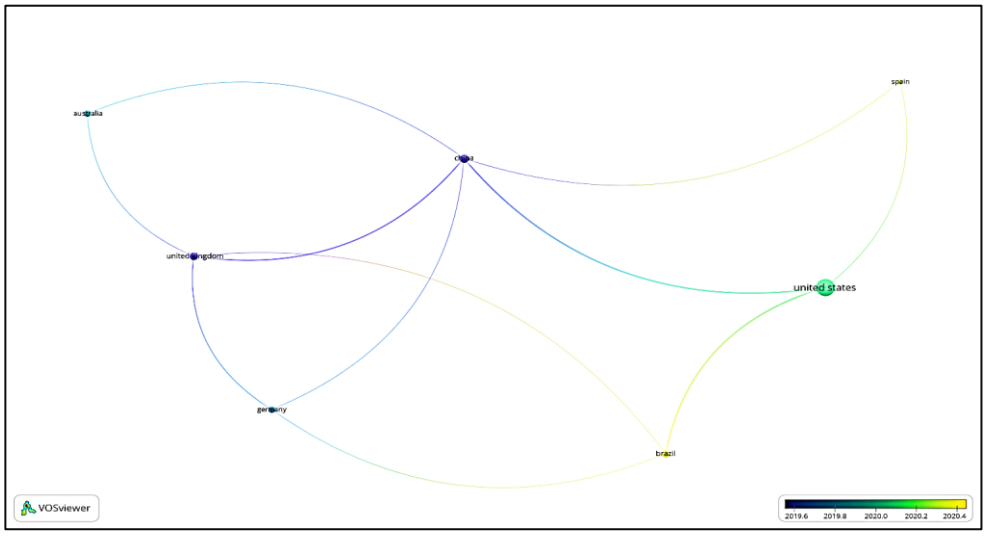

Figure 5. VOSviewer Overlay Visualization of countries

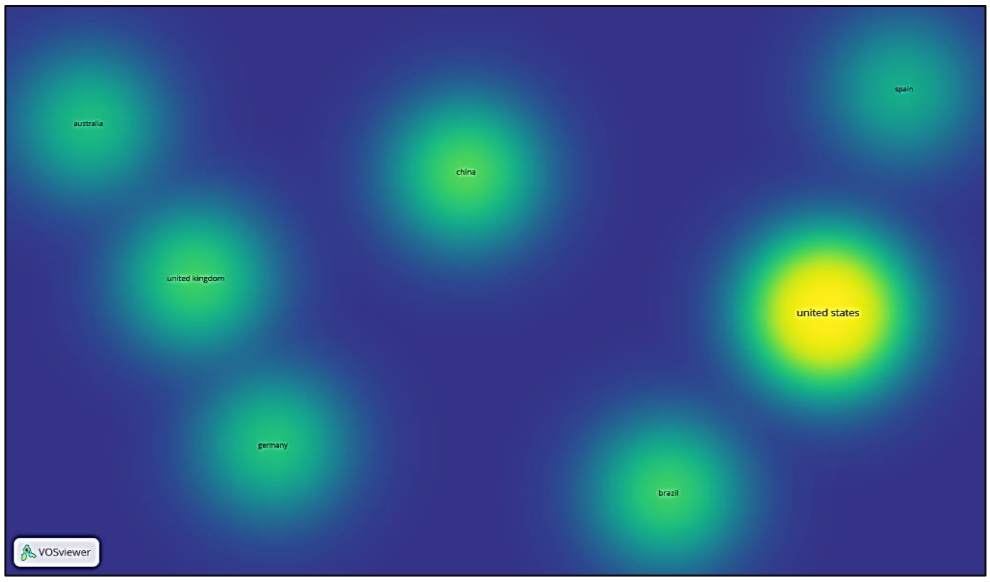

Figure 6. VOSviewer Density Visualization of countries

3.1.3 Keywords Co-occurrence

The density visualization of keywords co-occurrence in Figure 9 reveals that "grazing management" is the most prominent word, frequently co-occurring with "ecosystem services" and "biodiversity." This pattern reflects the dominant research focus on land use practices, pasture systems, and livestock–environment interactions. While "grazing management" anchors productivity-focused studies—such as pasture rotation, stocking rates, and land use optimization— "ecosystem services" bridges ecological and agricultural domains, and "biodiversity" reflects conservation-oriented themes. Overlay visualizations (Figures 8 and 11) show a temporal shift: earlier studies emphasized grazing practices, while recent ones focus on biodiversity. "Ecosystem services" consistently links these themes, reinforcing its role as a conceptual bridge. Their positioning in the visualization suggests more peripheral thematic roles, often linked to ecological outcomes or broader sustainability frameworks rather than direct agricultural interventions. This fragmentation underscores the need for interdisciplinary research to bridge conceptual and methodological gaps. Integrated policy frameworks that align grazing practices with biodiversity and ecosystem service goals are essential. Embedding ecological indicators—such as nutrient cycling, water regulation, and carbon sequestration—into livestock planning can help balance productivity with long-term sustainability.

The VOSviewer Network Visualization (Figure 7) further illustrates this convergence. Studies by Dey et al. [15], Kumar et al. [16], and Rao et al. [17] demonstrate the dual economic and ecological benefits of forage alternatives, multifunctional legumes, and the LivestockPlus framework—each integrating grazing management with ecosystem service enhancement. Recent bibliometric clusters also reflect emerging interdisciplinary themes. Kibria et al. [18] link cereal-based agriculture in South Asia to greenhouse gas emissions and biodiversity concerns, while Bo et al. [19] show how mixed cropping systems improve forage quality and plant–soil health. Attia et al. [20] explore phytogenic feed additives as sustainable inputs that support livestock health and indirectly enhance ecosystem services. To translate these insights into practice, policymakers and funding agencies should support interdisciplinary research clusters that explicitly link agronomic practices with ecological outcomes. This could include joint calls for proposals across agriculture and environment ministries, or the development of livestock sustainability frameworks that embed ecosystem service metrics. Such approaches would enable climate-resilient, biodiversity-enhancing livestock systems aligned with global sustainability goals.

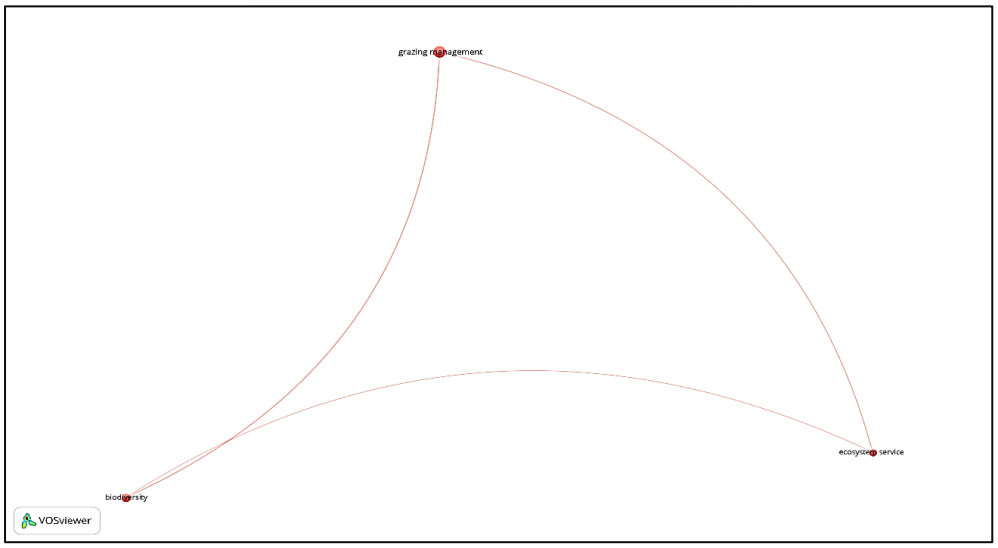

Figure 7. VOSviewer Network Visualization of keywords

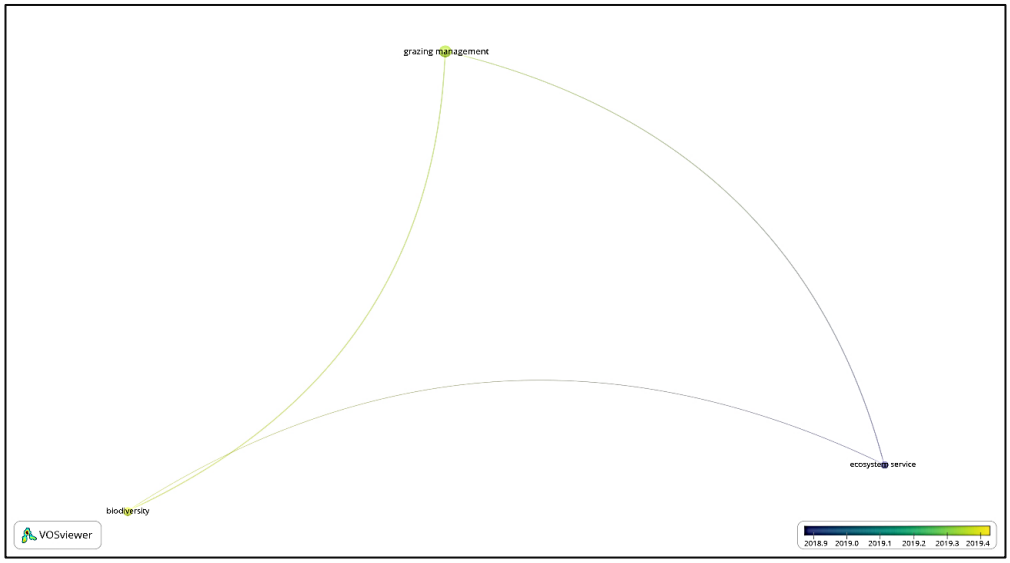

Figure 8. VOSviewer Overlay Visualization of keywords

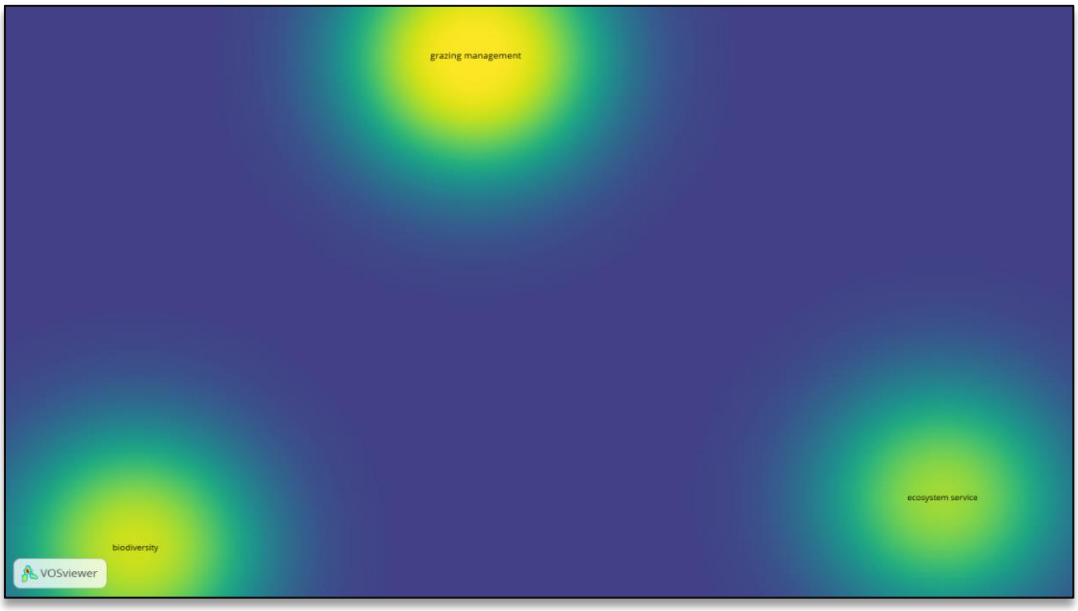

Figure 9. VOSviewer Density Visualization of keywords

3.1.4 Author Keywords

The three highlighted clusters of keywords are "grazing management", "biodiversity", and "ecosystem service". The string of colors connecting these keywords in the VOSviewer Network Visualization (Figure 10) illustrates their co-occurrence and thematic prominence, with yellow areas indicating the high relevance and frequency of the two keywords (Figure 12). The central positioning of the keyword "ecosystem service" indicates that it conceptually bridges the connection between the two keywords, forming a relationship. This suggests that most of the studies evaluate how grazing management practices influence "ecosystem services" that eventually affect "biodiversity". The strength of these connections emphasizes the degree of association in research contexts, which indicates the strong interdisciplinary nature of these themes. The Overlay Visualization (Figure 11) reveals that "grazing management" was associated with earlier studies, while "biodiversity" is linked to recent ones. "Ecosystem services" consistently bridge this temporal and thematic gap, highlighting the evolving focus on grazing practices and their impacts on "biodiversity" and ecosystem processes. This also highlights the evolving integration of ecological and agricultural research, where ecosystem services serve as a mediating framework to connect land use practices with conservation outcomes. These insights have direct implications for sustainable livestock policy and management. Integrating ecosystem service metrics into grazing policies enables decision-makers to assess trade-offs between productivity and ecological resilience. For example, pasture strategies that enhance soil health and water retention can simultaneously support biodiversity goals. Embedding such indicators into land use zoning, livestock incentive schemes, and biodiversity monitoring frameworks can ensure agricultural interventions align with broader sustainability targets. This integration is critical for advancing sustainability science, enabling researchers and policymakers to co-design interventions that balance agronomic performance with long-term ecosystem integrity.

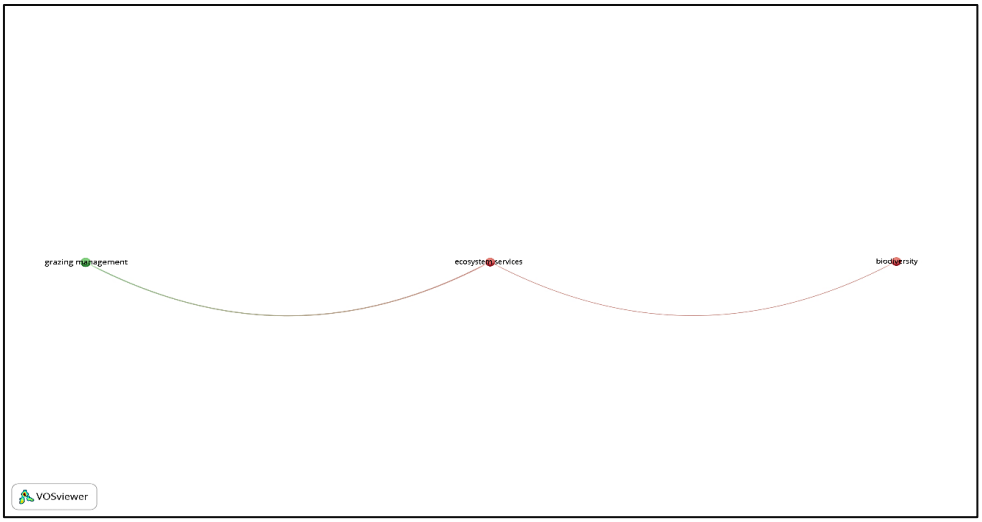

Figure 10. VOSviewer Network Visualization of author keywords

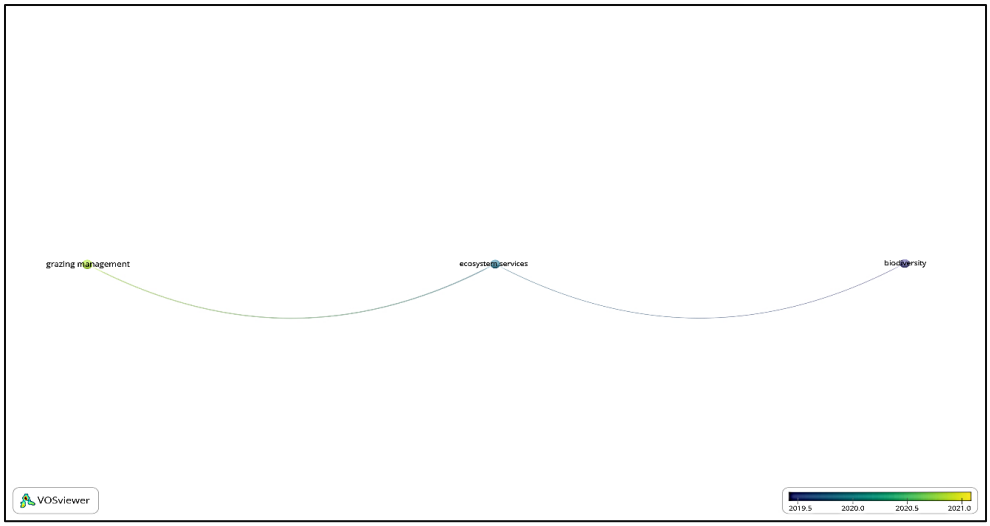

Figure 11. VOSviewer Overlay Visualization of author keywords

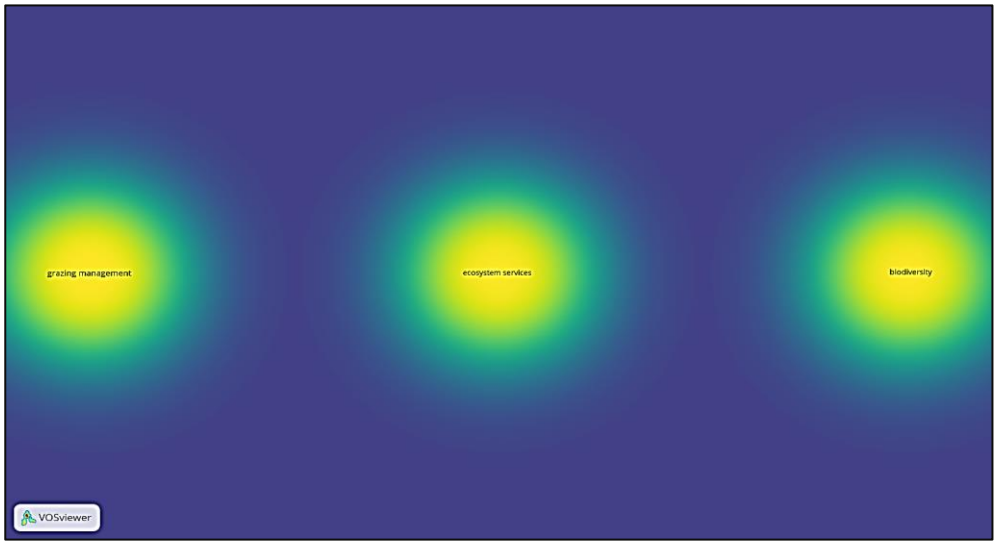

Figure 12. VOSviewer Density Visualization of author keywords

3.2 Ratio of documents per year, per year by source, by author, by affiliation, by country/territory, by type, by funding sponsors, and by subject area

3.2.1 Documents per year

The publication trends for articles focusing on sustainable livestock systems have shown significant fluctuations over the years, as shown in Figure 13. Initial output was low, with only two (2) articles in 2013 and 2015, which doubled to four (4) by 2014. There was a substantial increase in 2016, with the number of articles reaching 11. For the year 2017-2018, the number of publications remained at 8 per year, indicating a sustained scholarly interest. In 2019, the number of articles slightly declined to 7 and gradually rebounded to 11 by 2020. CY 2021 marked the peak of publication with 14 publications, the highest recorded in the dataset. From 2023 to the present, the number of articles has stabilized at 13 per year.

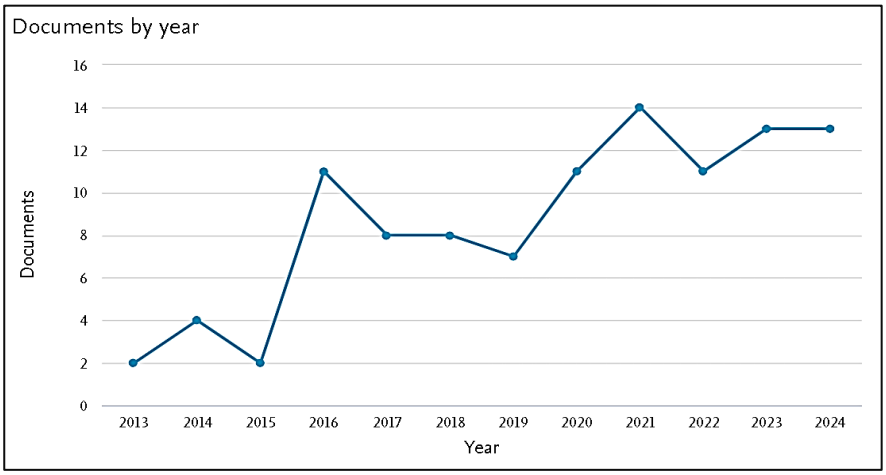

Figure 13. Ratio of documents per year

3.2.2 Documents per year by source

Figure 14 shows that from 2013 to 2024, the Top 5 Publishers of articles related to sustainable livestock management have been consistent in their contributions to the field. Top of the list was "Agriculture Ecosystems and Environment, having a total of 9 contributions. Followed by "Science of the Total Environment" with 7 publications. The "Journal of Environmental Management" and "Rangeland Ecology and Management" have 5 articles each, and lastly, "Geoderma" has 4 published articles throughout the years. This distribution highlights the sustained engagement of key environmental science journals in advancing research on sustainable livestock systems. The steady output across these sources suggests a stable and interdisciplinary interest in the topic, with each journal contributing to different facets of ecological, soil, and rangeland management.

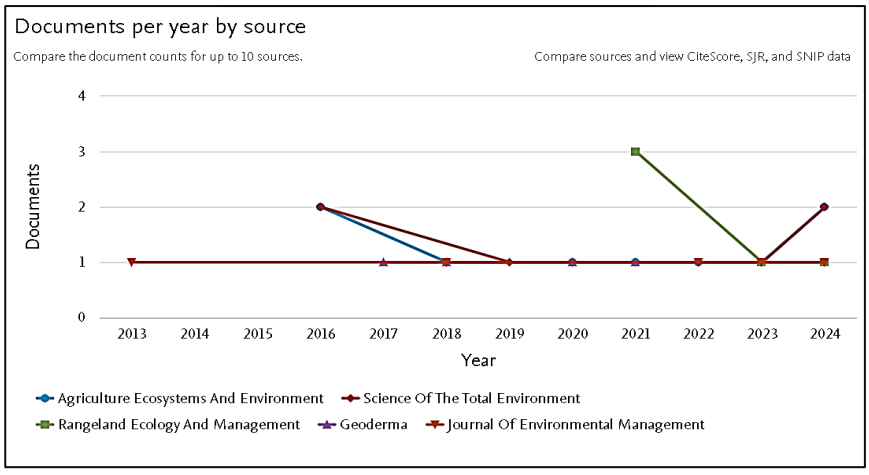

Figure 14. Ratio of documents per year by source

3.2.3 Documents by author

Here are the top 15 authors who published related articles on sustainable livestock systems, as shown in Figure 15. Note that while the dataset includes 15 authors, Figure 15 only displays the top 10 based on document count. The Top leading author was Sollenberger, L.E., with 4 publications focusing on sustainable grazing systems and forage management. Following Sollenberger, L.E., was Teague, R., also with 4 publications, renowned for the studies of holistic management practices and their impact on soil health and livestock sustainability. With 3 publications, the line was followed by Dong, S., whose articles contribute to the livestock production and environmental interactions in pastoral systems, Fonte, S.J., with a focus on soil fertility, sustainable agriculture practices, and integration of livestock systems, and McDonald, S.E., who focuses on biodiversity and sustainable livestock systems. The remaining authors such as Ashworth, A.J. (nutrient management and environmental impact of livestock farming), Byck, P. (sustainable livestock practices and socio-economic aspects of livestock systems), Engle, D.M. (grassland management and its role in sustainable livestock production), Farias, G.D. (innovative farming techniques and their applications in livestock systems), Franzluebbers, A.J. (soil health, carbon sequestration and sustainable grazing system), Fu, B. (landscape ecology and sustainable land use practices involving livestock's), Fuhlendorf, S.D. (rangeland ecology and sustainable management of grazing lands), Gao, J. (land management and environmental impacts of livestock farming), Haney, R.L. (soil health assessment and the role of livestock in sustainable agriculture), Hovick, T.J. (wildlife-livestock interactions and ecosystem management) composes the top 15 with 2 publications each. The average of 5.8 authors per article in this dataset reflects a moderate level of collaboration in sustainable livestock systems research. This figure is notably higher than typical averages in social sciences and humanities (1.4–1.6 authors per publication), and more aligned with collaborative norms in environmental and biomedical sciences, where multi-authorship is common. These disciplinary patterns are consistent with science-wide author metrics reported by Ioannidis et al. [22].

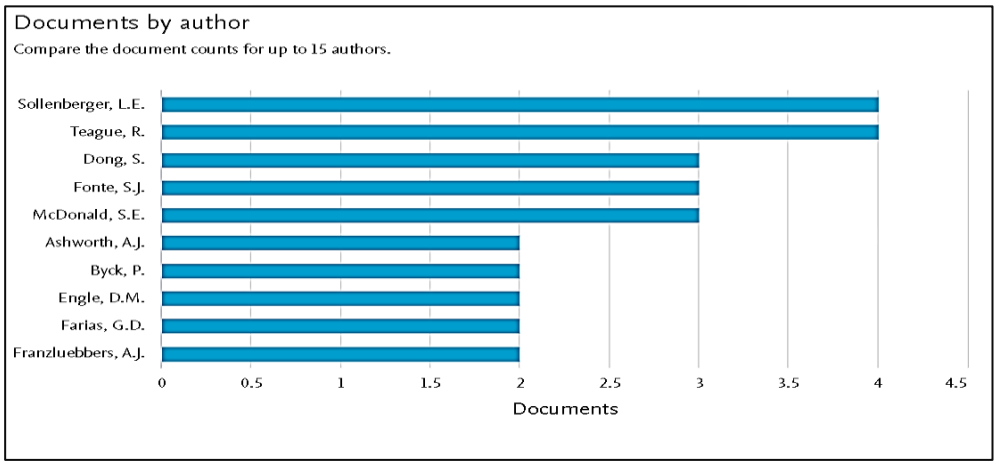

Figure 15. Ratio of documents by author

3.2.4 Documents by affiliation

From 2013 to 2024, numerous institutions have made notable contributions in the researches in sustainable livestock systems. The Top 10 known contributors are shown in Figure 16 with their document counts. It shows that the USDA Agricultural Research Service has published a total of 9 research documents showing their strong commitment to advancing agricultural practices and sustainability. It was followed closely by Texas A&M AgriLife Research with 8 publications and the United States Department of Agriculture, which contributed 6 documents, highlighting their active participation and support in sustainable agriculture. Other notable institutions were NSW Department of Primary Industries (5 articles), Colorado State University (5), Wageningen University and Research (4), Oklahoma State University (4), University of Florida (4), Texas A&M University (4), and Lanzhou University (4). Note that while the dataset includes more affiliations, Figure 16 highlights only the top 10 based on document count. This distribution reflects a diverse and international

research landscape, with institutions from North America, Europe, Asia, and Oceania actively shaping the discourse on sustainable livestock systems.

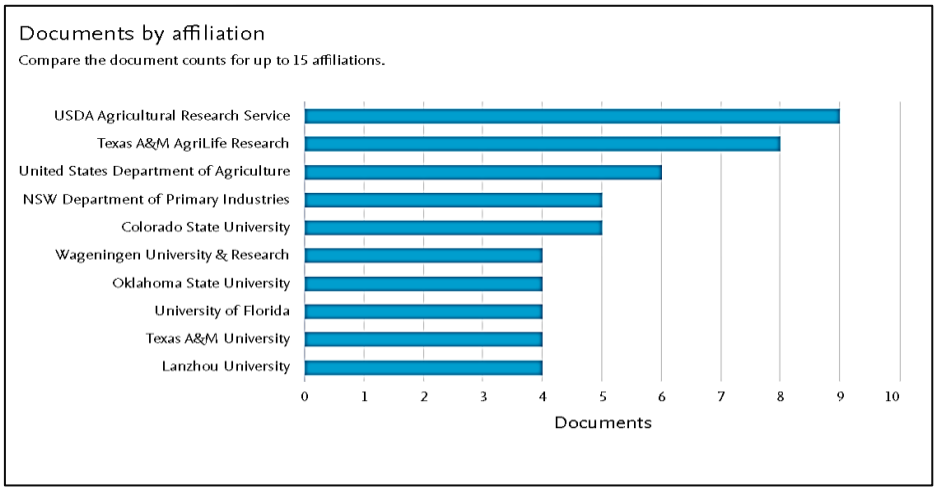

Figure 16. Ratio of documents by affiliation

3.2.5 Documents by country

Various countries have contributed significantly in researches on sustainable livestock systems. As shown in Figure 17, the United States, as the highest contributors had published 51 documents, followed by China with 14 published documents. These underscore their commitments to advancing sustainable agriculture practices amidst the rapid agricultural development. Brazil (11) and the United Kingdom (10) also share their dedication to sustainable agricultural research and integration of such in the vast livestock industries. Both Australia and Germany had contributed 8 documents each, showcasing their innovative practices and policy-driven approaches. Other countries also take part in contributing, such as Spain (6 documents), Argentina (4), the Netherlands (4), and lastly Colombia (3), which is still emerging. Note that Figure 17 highlights only the top countries based on document count. This illustrates the global commitment to sustainable livestock practices and is significant in addressing global agricultural sustainability concerns across diverse ecological and socio-economic contexts.

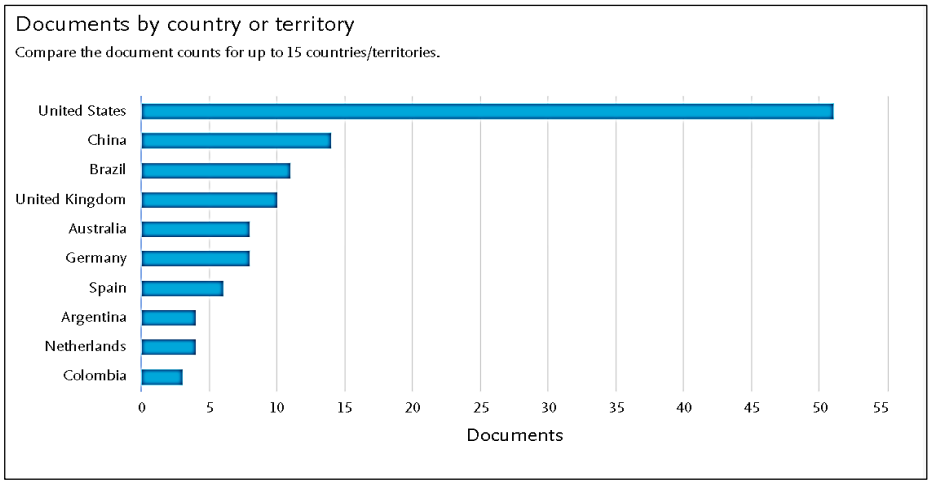

Figure 17. Ratio of documents by country

3.2.6 Documents by type

All documents used in this bibliometric analysis was 100% research articles with a varying range of formats, reflecting diverse methodological approaches and findings as shown in Figure 18. This uniformity in document type reflects a strong emphasis on the empirical and theoretical contributions within the field of sustainable livestock systems. The majority of these research papers were original research papers written to

present new data, insights from experiments, field studies, and modeling approaches that explore the ecological, agronomic, and socio-economic dimensions of livestock sustainability. These studies often investigate topics such as grazing management, soil health, biodiversity impacts, carbon sequestration, and integrated farming systems. While the dataset is composed entirely of articles, it is important to note that some of these also include review-type content, which forms a significant part of the literature.

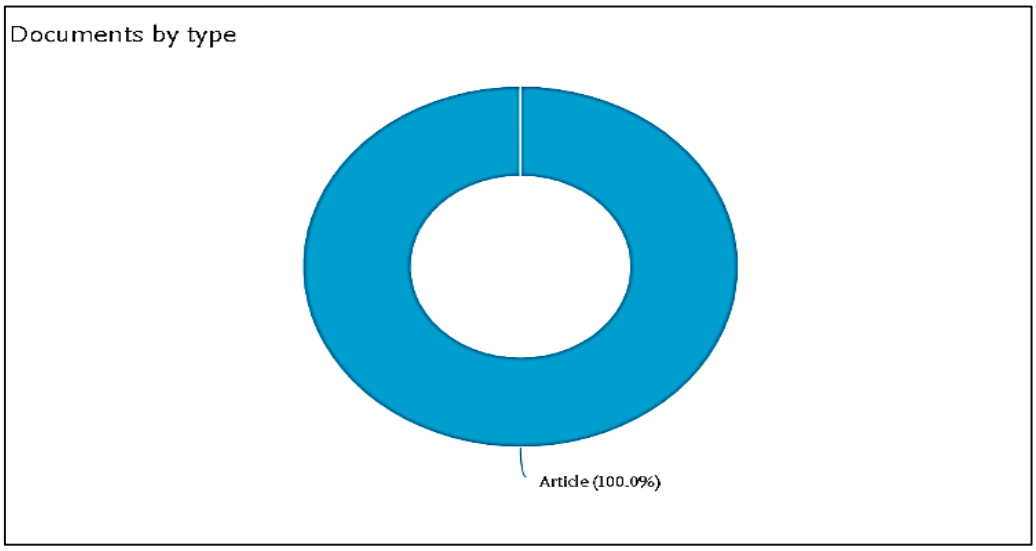

Figure 18. Ratio of documents by type

3.2.7 Documents by subject area

The articles published from 2013 to 2024 relative to sustainable livestock systems span an array of subject areas, reflecting the interdisciplinary nature of the field. The most prominent subject area, as shown in Figure 19, is Agricultural and Biological Sciences with 71 published documents, followed by Environmental Science with 70 contributions. Together, these two areas dominate the research landscape, highlighting the critical role of sustainable practices in agriculture and their impact on environmental aspects. Most studies in these areas focus on soil health, biodiversity, ecosystem services, and innovative farming systems. The Social Sciences, with 9 documents, emphasize the socio-economic aspects of sustainable livestock systems. These studies explore community engagement, farmers' behavior and acceptability, community engagement and policy implications. It illustrates the importance of social dynamics in the adoption and long-term success of sustainability interventions. The field of Biochemistry, Genetics, and Molecular Biology has also published 8 documents that explore the genetic and molecular mechanisms that influence livestock health and productivity, including the development of new disease-resistant varieties. Various areas such as Neuroscience (4 documents), Decision Science (3 documents), Energy (3 documents), Veterinary Science (2 documents), Computer Science (1 document) Earth and Planetary Sciences (1 document), Economics, and Finance (1 document) and Multidisciplinary (1 document) shows that researches in sustainable livestock systems does not only confine to a single discipline rather it also intersects with fields like data analysis, earth sciences, economic sustainability, and integrated multidisciplinary approaches.

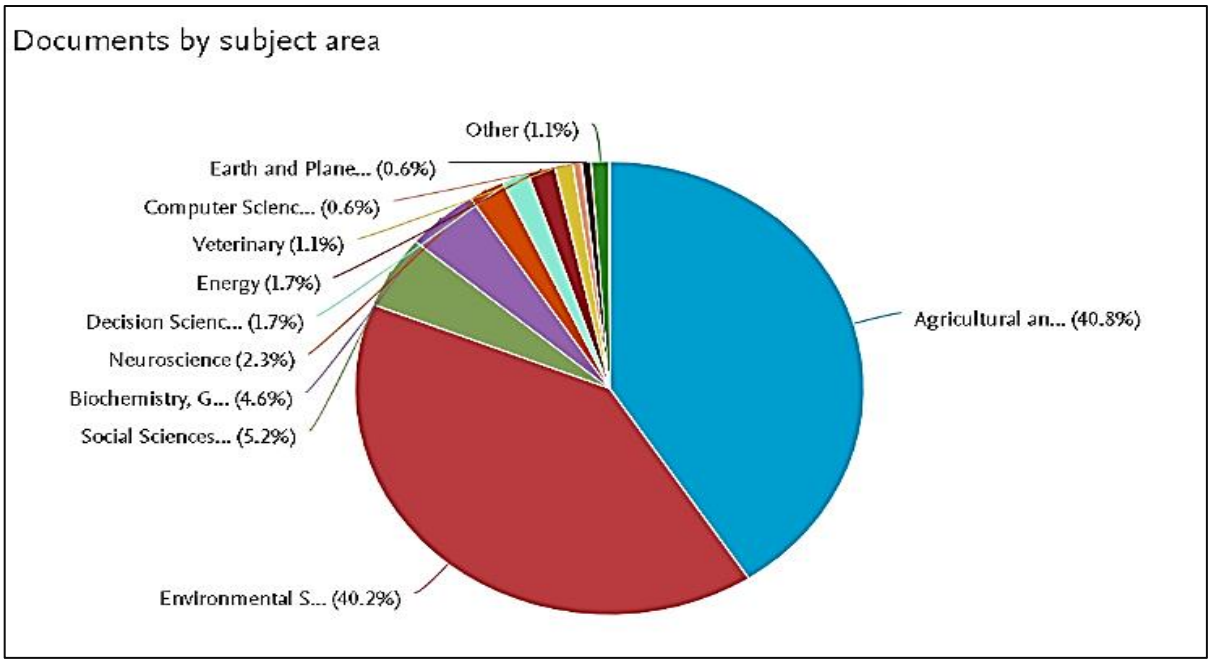

Figure 19. Ratio of documents by subject area

3.2.8 Documents by funding sources

Various funding sponsors have played a very important role in the advancement of research on sustainable livestock systems. As shown in Figure 20, the U.S. Department of Agriculture (USDA) leads the list with 14 funded documents, reflecting its strong commitment to promoting sustainable agricultural practices, ecological stewardship, and innovation in livestock management. This leadership is consistent with the USDA's long-standing support for integrated farming systems and climate-resilient agriculture. It was followed by the National Natural Science Foundation of China with 8 documents, highlighting China's growing investment in sustainable land use and livestock-environment interactions. The National Institute of Food and Agriculture has funded 7 documents emphasizing the improvement of food production systems while maintaining ecological balance. The Coordenação de Aperfeiçoamento de Pessoal de Nível Superior (CAPES) in Brazil contributed 5 documents in advancements of academic research and the sustainability of the livestock system. Other significant contributors include the Agricultural Research Service with 4 documents, Bundesministerium für Bildung und Forschung (Federal Ministry of Education and Research) with 4 documents. China's Ministry of Science and Technology and the National Key Research and Development Program have also contributed 4 documents each, showcasing their comprehensive research efforts. This funding landscape reveals a strong international commitment to sustainable livestock systems, with support spanning North America, Asia, South America, and Europe. It also underscores the importance of multi-level collaboration—from national agencies to academic institutions.

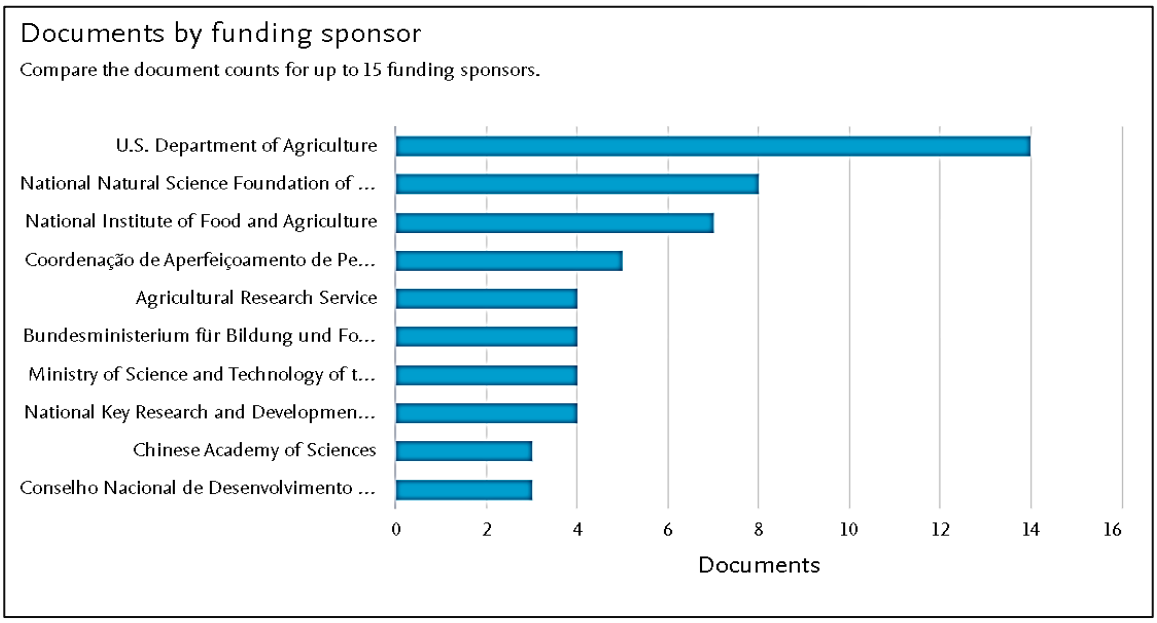

Figure 20. Ratio of documents by funding sources

4. Conclusions

This Bibliometric analysis focuses on several critical aspects of sustainable livestock research. The analysis shows that the co-authorship network is fragmented, where authors prefer to work alone within specific subject areas such as soil health, plant biodiversity, and grazing management. This lack of interdisciplinary collaborations has become a challenge in the development of a holistic solution to complex issues faced by sustainable livestock systems. As shown in Figure 15, the average of 5.8 authors per article is indicative of moderate collaboration, is significantly higher than the 1.4–1.6 average in social sciences and humanities, and is more aligned with biomedical and environmental sciences, where five or more authors are common. Notably, the involvement of other authors continues to decline while their focus shifted. However, between 2019 and 2023, there was a notable increase in active participation, indicating renewed interest in collaborative and thematic expansion. Geographically, the United States remains a central hub of research, maintaining strong collaborations with countries like China and Brazil. However, geography and language clustering also affect these collaborations, with countries such as the United Kingdom and Australia forming confined clusters. This pattern is visualized in Figure 16, which shows author affiliations and geographic clustering, highlighting the need for cross-regional integration. The keyword analysis highlights the top 3 used keywords, which are “grazing management”, biodiversity”, and “ecosystem service”. These three keywords, although interconnected, also suggest three different foci. Grazing management is tied to agricultural and land-use practices, biodiversity to ecological diversity and conservation, while ecosystem services are linked to the sustainable benefits of the ecosystem to humans. Figures 9 and 11 show that “ecosystem services” bridge the temporal and thematic gap between earlier grazing-focused studies and more recent biodiversity research. This convergence underscores the importance of interdisciplinary approaches that integrate ecological indicators into livestock planning. The dominance of "grazing management" underscores its crucial role in maintaining soil health, ensuring pasture productivity, and supporting livestock welfare. Effective grazing management helps mitigate overgrazing, soil erosion, and biodiversity loss, which are essential for sustainable agriculture. This focus also reflects the need to adapt livestock systems to climate change, emphasizing innovative techniques like rotational grazing and holistic management. These findings align with the subject area distribution in Figure 19, where Agricultural and Biological Sciences and Environmental Science dominate the literature. The top contributor in the field was the “Agriculture Ecosystems and Environment” with 9 contributions, followed by publishers such as “Science of Total Environment”, “Journal of Environmental Management”, Rangeland Ecology and Management”, and “Geoderma”. These publishers showed consistency in their contributions over the years. Prominent authors include Sollenberger, L.E.,

Teague, R., Dong, S., Fonte, S.J. McDonald, S.E., Ashwort, A.J., Byck, P., Engle, D.M., Farias, G.D., Franzluebbers, A.J., Fu, B., Fuhlendorf, S.D., Gao, J., Haney, R.L., and Hovick, T.J., affiliated with institutions such as United States Department of Agriculture (USDA) Agricultural Research Service, Texas A&M AgriLife, United States Department of Agriculture (USDA), showing a strong commitment to advancing agricultural practices and sustainability. Overall, this analysis underscores the critical need for a collaborative and integrated approach to sustainable livestock systems research. Policymakers and funding agencies can take several specific actions to address the gaps in collaboration and research focus in sustainable livestock systems. Firstly, policymakers and funding agencies should incentivize interdisciplinary research by establishing grant programs that reward collaboration among researchers from diverse fields such as agriculture, ecology, economics, and social sciences, fostering comprehensive approaches to sustainability challenges. Promoting international partnerships by developing funding schemes that encourage cross-border research, particularly between countries with different geographical and cultural backgrounds, can enhance global knowledge exchange and innovation. Moreover, allocating funding to studies exploring the interconnectedness of emerging keywords like "grazing management," "biodiversity," and "ecosystem services, as identified in Figures 9 and 11. Support for knowledge-sharing platforms—such as international conferences, workshops, and online forums - can foster dialogue and co-creation of solutions. Practical research on farming techniques, tools, and technologies should be prioritized to ensure real-world impact. In addition, investment in education and training programs for farmers, researchers, and policymakers is essential to raise awareness about the importance of sustainable agriculture and provide the necessary skills and knowledge to implement effective practices. Establishing systems to monitor and evaluate the impact of funded projects and policies will ensure the effectiveness of initiatives and allow for adjustments based on feedback and results. By taking these actions, the funding agencies and policymakers can bridge the gaps in collaboration and research focus, leading to more integrated and effective solutions for sustainable livestock systems.

5. Acknowledgements

The author sincerely thanks Professor Greta G. Gabinete for her invaluable guidance and support throughout the study.

Author Contributions: -

Funding: This research received no external funding.

Conflicts of Interest: The author declares no conflict of interest.

References

[1] Kjaer, E. L.; Limb, R.; Geaumont, B.; Harmon, J.; Hovick, T.; Sedivec, K. Fire and Grazing Reduce Invasive Grass Thatch in Rangelands. *Rangeland Ecol. Manag.* **2024**, *98*, 414–418. https://doi.org/10.1016/j.rama.2024.06.009

[2] Navasardyan, M.; Sargsyan, T.; Daveyan, H.; Mezhlumyan, T. Effect of Grazing on Plant and Soil Parameters in Drylands. *Land* **2024**.

[3] Dahal, S.; Franklin, D.; Subedi, A.; Cabrera, M.; Hancock, D.; Mahmud, K.; Ney, L.; Park, C.; Mishra, D. Strategic Grazing in Beef-Pastures for Improved Soil Health and Reduced Runoff-Nitrate—A Step Towards Sustainability. *Sustainability* **2020**, *12*, 20558. https://doi.org/10.3390/su12020558

[4] Read, Z. J.; King, H. P.; Tongway, D. J.; Ogilvy, S. Landscape Function Analysis to Assess Soil Properties under Different Grazing Regimes. *Eur. J. Soil Sci.* **2016**.

[5] Nobilly, F.; Atikah, S. N.; Yahya, M. S.; Jusoh, S.; Cun, G. S.; Norhisham, A. R.; Tohiran, K. A.; Zulkifli, R.; Azhar, B. Rotational Cattle Grazing Improves Understory Vegetation Biodiversity and Structural Complexity in Oil Palm Plantations. *Weed Biol. Manag.* **2022**. https://doi.org/10.1111/wbm.12246

[6] Read, Z. J.; King, H. P.; Tongway, D. J.; Ogilvy, S.; Greene, R. S. B.; Hand, G. Landscape Function Analysis to Assess Soil Processes on Farms Following Ecological Restoration and Changes in Grazing Management. *Eur. J. Soil Sci.* **2016**. https://doi.org/10.1111/ejss.12352

[7] Atikah, S. N.; Jusoh, S.; Yahya, M. S. Cattle Grazing Effects on Plant Growth in Tropical Ecosystems. *Weed Biol. Manag.* **2021**.

[8] Ramírez-Durán, J. A.; Niebles, W. A.; Gallego, G.; Guerra-Cogollo, J. A. Use of Technology for Sustainable Livestock Processes: A Bibliometric Review. *Afr. J. Food Agric. Nutr. Dev.* **2024**, *24*(7), 23934–23956. https://doi.org/10.18697/ajfand.132.23515

[9] Jamala, A.; Elangob, B.; Joseph, M. K. A Bibliometric Analysis of Sustainability Transitions in Agrifood Systems. *Cogent Soc. Sci.* **2025**, *11* (1), 2556226. https://doi.org/10.1080/23311886.2025.2556226

[10] Manyike, J. Z.; Taruvinga, A.; Akinyemi, B. E. Mapping the Research Landscape of Livestock Adaptation to Climate Change: A Bibliometric Review Using Scopus Database (1994–2023). *Front. Clim.* **2025**, *7*, 1567674. https://doi.org/10.3389/fclim.2025.1567674

[11] Romero Riaño, E. Agronomy Research Co-Authorship Networks in Agricultural Innovation Systems. *Rev. UIS Ing.* **2020**, *20* (1). https://doi.org/10.18273/REVUIN.V20N1-2021015

[12] Payumo, J.; He, G.; Manjunatha, A. C.; Higgins, D.; Calvert, S. Mapping Collaborations and Partnerships in SDG Research. *Front. Res. Metr. Anal.* **2020**, *5*, 612442. https://doi.org/10.3389/frma.2020.612442

[13] Maree, E.; Blignaut, J.; Gilliland, J.; Lee, M. R. F.; Manzano, P.; McCosker, T.; du Toit, L.; Truter, W.; Weinheimer, B.; Polkinghorne, R. Ruminant Livestock Farmers and Industry Are Leading Innovation Through Sector Lifecycle Collaboration: A Review of Case Studies. *Anim. Front.* **2025**, *15*(1), 55–71. https://doi.org/10.1093/af/vfae050

[14] Mittal, P.; Bansal, R. Role of Cross-Disciplinary Collaborations for Holistic Approach to Sustainability. In *Community Engagement for Sustainable Practices in Higher Education*; Springer: Cham, **2024**; pp 143–160. https://doi.org/10.1007/978-3-031-63981-4_9

[15] Dey, B.; Notenbaert, A.; Makkar, H.; Mwendia, S.; Rao, I. Realizing Economic and Environmental Gains from Forage Alternatives. *CAB Rev.* **2022**.

[16] Kumar, R.; Yadav, M. R.; Arif, M.; Mahala, D. M.; Kumar, D.; Ghasal, P. C.; Yadav, K. C.; Verma, R. K. Multiple Agroecosystem Services of Forage Legumes towards Agriculture Sustainability: An Overview. *Indian J. Agric. Sci.* **2020**, *90*(8), 1367–1377. https://doi.org/10.56093/ijas.v90i8.105882

[17] Rao, I.; Peters, M.; Castro, A.; et al. LivestockPlus – The Sustainable Intensification of Forage-Based Agricultural Systems to Improve Livelihoods and Ecosystem Services in the Tropics. *Trop. Grassl.–Forrajes Trop.* **2015**, *3*(2), 59–82. https://doi.org/10.17138/TGFT(3)59-82

[18] Kibria, M. G.; Aspy, N. N.; Ullah, E.; Dewan, M. F.; Hasan, M. A.; Hossain, M. A.; Haseeb, M.; Hossain, M. E. Quantifying the Effect of Agricultural Greenhouse Gas Emissions, Food Production Index, and Land Use on Cereal Production in South Asia. *J. Clean. Prod.* **2023**, *432*, 139764. https://doi.org/10.1016/j.jclepro.2023.139764

[19] Bo, P. T.; Bai, Y.; Dong, Y.; Shi, H.; Soe Htet, M. N.; Samoon, H. A.; Zhang, R.; Tanveer, S. K.; Hai, J. Influence of Different Harvesting Stages and Cereals–Legume Mixture on Forage Biomass Yield, Nutritional Compositions, and Quality under Loess Plateau Region. *Plants* **2022**, *11*(20), 2801. https://doi.org/10.3390/plants11202801

[20] Attia, Y. A.; El-Hack, M. E. A.; Alagawany, M. M.; Elnaggar, A. S. *Phytogenic and Phytochemical as Alternative Feed Additives for Animal Production*; Bentham Science Publishers: Sharjah, UAE, 2025; pp 1–198. https://doi.org/10.2174/9789815227671250101

[21] Napalinga, C. Plant-Based Feed and Forage Research for Livestock: A Bibliometric Review. *ASEAN J. Sci. Technol. Rep.* **2025**, *28*(5), e259394. https://doi.org/10.55164/ajstr.v28i5.259394

[22] Ioannidis, J. P. A.; Boyack, K. W.; Baas, J. Updated Science-Wide Author Databases of Standardized Citation Indicators. *PLoS Biol.* **2020**, *18*, e3000918. https://doi.org/10.1371/journal.pbio.3000918

ASEAN
Journal of Scientific and Technological Reports
Online ISSN:2773-8752

Academic article

Agri-Fishery Practices through Product Resource Management, Value Addition and Commercialization Enhancement Project of Villages in Daram, Samar

Jose Marlon Refuncion Jr.[1], Dennis Durango[1], Ma. Winna Mae Agbon[1], and Jonafe Matugas[2]

[1] College of Arts and Sciences, Samar State University, Samar, 6700, Philippines
[2] Basey Campus, Samar State University, Samar, 6720, Philippines
* Correspondence: josemarlon.refuncion@ssu.edu.ph

Citation:
Refuncion, J.M.; Durango, D.; Agbon, W.M.; Matugas, J. Agri-Fishery practices through product resource management, value addition and commercialization enhancement project of villages in Daram, Samar. *ASEAN J. Sci. Tech. Report.* **2026**, *29*(2), e259686. https://doi.org/10.55164/ajstr.v29i2.259686.

Article history:
Received: July 3, 2025
Revised: October 9, 2025
Accepted: October 18, 2025
Available online: January 20, 2026

Abstract: The study revealed the prevailing conditions of agri-fishery practices and value-added production in Barangays Marupangdan and Astorga in Daram, Samar. Findings indicated that Barangay Marupangdan remained dependent on traditional crop and fish harvests with minimal post-harvest technology, no value-added processing, and limited market access, resulting in low profit margins. Overproduction of hawol-hawol (Bali Sardinella) and vegetables led to waste due to the absence of storage, processing, and market linkages. In contrast, Barangay Astorga demonstrated active value addition through products galunggong-based fish balls, significantly increasing income per unit sold. Porter's Value Chain analysis showed that Astorga's community benefited from interventions by DTI and LGU Daram in providing equipment, packaging materials, and access to trade fairs. However, both barangays still lacked essential post-harvest facilities, ICT integration, and formal marketing strategies. Women in both communities actively participated in agri-fishery production, but their associations in Marupangdan remained unregistered, limiting support opportunities. Farmers and fisherfolk expressed willingness to adopt technology and undergo training, showing potential for scaling up productivity. The study highlighted the importance of institutional aid and local government support in capacitating communities to develop sustainable agri-fishery value chains. With targeted interventions, Marupangdan could replicate Astorga's best practices to enhance food security, income, and community resilience.

Keywords: Agri-fishery production and management; value addition; porter's value chain; market access; sustainable agriculture

1. Introduction

Asia bears a major share of global hunger. In 2018, 513.9 million Asians were undernourished—over 60% of the world's hungry. Although this number declined to 384.5 million by 2023, the region still accounts for more than half of the global undernourished population [1]. A contributing factor to this persistent hunger is the high proportion of income that low-income households in Asia allocate to food. For instance, households in the Philippines spend approximately 41.9% of their income on food [2]. This substantial expenditure leaves limited resources for other essential needs, making these households particularly vulnerable to fluctuations in food prices. As a result, they are

significantly impacted by higher and more volatile food prices, which have hindered progress in reducing poverty across the region. With Asia becoming increasingly urbanized and prosperous, upward pressure on food prices is expected to persist. If food supply fails to keep pace with rising demand and agricultural productivity challenges are not addressed, food security will likely remain a persistent concern both globally and regionally. This could potentially threaten Asia's long-term economic growth [3]. Addressing hunger in Asia necessitates not only increasing food production but also implementing policies that enhance food affordability and accessibility for the poor. Without such measures, the region's progress in reducing poverty and hunger may remain stagnant. The community must harness innovation, marketing, and the commercialization of agri-aqua raw materials to create value-added products.

The Cooperative Development Authority [4] reported that among 9,432 cooperatives, only four are engaged in agriculture and three in fisheries. This suggests either a lack of interest in these sectors or a failure to report cooperative activities, which highlights gaps in engagement with agriculture and fisheries at the cooperative level. Policymakers must address several critical challenges to support community development. First, revitalizing growth in agricultural productivity is essential, especially in the face of climate change. Second, Asia's 350 million small farmers—typically working on less than two hectares—must be integrated into modern food value chains. Third, persistent malnutrition among preschool children has long-term consequences on human capital. Livelihood is essential for survival, as it fuels the daily lives of people. Agriculture remains a major source of livelihood globally, but fewer people—particularly in rural areas—are engaging in farming activities. This trend threatens the sustainability of food security. Sustainable strategies such as the intensification of agri-aqua production and livelihood have shown promise. Utilizing local resources for livelihood purposes can stimulate the national economy. However, despite the availability of rich natural resources, many communities lack the knowledge or infrastructure to process and utilize them effectively [5]. Many areas still rely on traditional farming methods, despite the availability of advanced agricultural technologies that could boost productivity and streamline marketing. A study [6] emphasized that natural resources are underutilized. Revisiting their potential through development projects could enhance agri-aqua entrepreneurial activities. Government extension programs, especially when partnered with private companies, play a significant role in supporting vulnerable groups such as barangay associations, women, and the unemployed [7]. Common challenges include a lack of knowledge, capital, and agricultural inputs, as highlighted by World Vision.

Projects focused on farming and fishing education, scientific practices, and entrepreneurial training can empower communities. Teaching value addition—through product creation, branding, packaging, and marketing—enhances income and sustainability. Successful value addition requires access to training, resources, market linkages, and an environment that supports innovation and entrepreneurship. Cultural authenticity and sustainable practices are also crucial. An author [8] noted that marketing is a major challenge for value-added products. Poor farmers often lack the knowledge to market their products effectively, leading them to sell raw materials at low prices. Training in branding, quality assessment, retailing, and sustainable production is essential to improve profitability and market competitiveness. Barangay Marupangdan and Barangay Astorga are two coastal communities situated in the municipality of Daram, Samar, Philippines. As of the 2020 Census, Marupangdan had a population of 573 individuals, comprising approximately 1.38% of Daram's total population, while Astorga had a population of 1,849, representing about 4.44% of the municipality's populace [9]. Both barangays are located at low elevations—Marupangdan at 16.1 meters and Astorga at 12 meters above sea level—making them naturally suited for agri-fishery activities. The main sources of livelihood in these communities include farming and small-scale fishing, which are typical economic activities across the municipality of Daram. However, these sectors face numerous challenges, particularly the degradation of marine resources due to overfishing and illegal practices, which threaten the long-term viability of fishing as a livelihood [4].

Poverty remains a persistent issue in the area. In 2003, Daram registered a poverty incidence of 77.96%, which gradually declined to 38.80% by 2021. Despite this improvement, poverty levels in the municipality continue to exceed the national average, indicating that a significant proportion of residents in Marupangdan and Astorga still experience economic hardship (10]. In response, various development

interventions have been implemented to improve the quality of life in these barangays. Programs like the "SAVE-FAITH" initiative have promoted transformative governance, sustainable agriculture and fishery practices, and better access to health, nutrition, and livelihood opportunities [4]. These efforts aim to empower local communities by building their capacity for value addition, entrepreneurship, and sustainable resource management. This research contributes to agricultural development by promoting the use of technologies like the "three sisters" intercropping system. The goal is to help communities transition from poverty to productivity by establishing viable agribusinesses.

Agri-fishery practices play a vital role in achieving community sustainability. They help maintain environmental balance, ensure food security, create jobs, and generate income. This can improve living standards and contribute significantly to poverty reduction. To conduct a value chain analysis of the agri-science sector to assess and optimize the journey of products from production to market through stakeholder collaboration and value chain mapping. To identify bottlenecks and opportunities for value addition and commercialization within the agri-fishery value chain, thereby providing comprehensive insights into the agri-fishery ecosystem.

2. Materials and Methods

2.1 Research Design

This study employed a qualitative-descriptive research design, specifically utilizing Value Chain Analysis (VCA) and Focus Group Discussions (FGDs) to explore the agri-fishery production, processing, and marketing practices of local communities. This design enabled a comprehensive understanding of the value chain and the identification of gaps and opportunities for value addition and commercialization. It was particularly suited for contextualizing local knowledge, practices, and perspectives in agricultural development [11]. This is a qualitative study with descriptive elements; no statistical tests were performed. Quantitative estimates provided are illustrative and not inferential. This study utilized Porter's Value Chain Analysis (1985) to examine the sequence of value-adding activities in the local agri-fishery enterprises of Barangay Astorga (galunggong fish balls). The framework guided the identification of both primary activities (inbound logistics, operations, outbound logistics, marketing and sales, and service) and support activities (infrastructure, human resources, technology, and procurement). Data gathered from interviews, focus group discussions, and field observations were categorized according to these value chain components. The analysis focused on: Identifying gaps and inefficiencies in each stage of the chain, Mapping cost and profit contributions, and Assessing the institutional and technical support available to producers.

2.2 Participants and Sampling Technique

The participants consisted of members from the Farmers Association and Women's Association in Barangay Marupangdan and Barangay Astorga in Daram. A purposive sampling technique was employed to select individuals actively involved in agricultural and fishery activities. 30 participants, including farmers, fisherfolk, and women, were selected based on their involvement in farming and small-scale fishing. Selection was also guided by their availability and willingness to participate in the FGDs. A total of 30 participants were selected to ensure diversity across livelihood sectors (farming, fishing, and processing) and gender representation. This size allowed for in-depth discussions while maintaining manageability during FGDs.

Table 1. Demographic Profile

Variable	Frequency	Percentage
Gender (Male/Female)	14 / 16	47% / 53%
Age Range	25–60 years	—
Occupation	Farmers (18), Fisherfolk (7), Women Entrepreneurs (5)	—
Barangay	Marupangdan (15), Astorga (15)	—

2.3 Research Instrument

The primary research instruments were semi-structured FGD guides and value chain mapping tools. The FGD guide included open-ended questions focused on current agricultural practices, challenges in production and marketing, and opportunities for value addition. The value chain mapping tool helped identify key stages in the agri-fishery value chain and determine bottlenecks and inefficiencies across the system.

2.4 Data Gathering Procedure

The research team first sought permission and support from the Local Government Unit (LGU) of Daram, followed by coordination with community associations. An initial orientation was conducted to explain the purpose and scope of the study. Two FGDs were conducted: the first focused on identifying current practices and challenges, and the second on exploring strategies for value addition and marketing. All sessions were facilitated by trained moderators and documented through note-taking and audio recordings (with consent).

2.5 Data Analysis Procedure

Data collected from FGDs were transcribed and subjected to thematic analysis, identifying recurring themes, issues, and insights. Concurrently, Value Chain Analysis was conducted by mapping the stages from production to market, highlighting areas for improvement, and recommending potential interventions. Findings were cross-referenced with existing literature and used to inform the next phase of project implementation.

2.6 Data Validation

To ensure credibility, triangulation was achieved through multiple FGDs and cross-validation with LGU records. Member checking was conducted by sharing summaries of findings with participants for verification.

2.7 Ethical Considerations

The study adhered to ethical research standards from Samar State University, namely the Institutional Human Research Ethics Committee (IHREC). Informed consent was obtained from all participants, who were assured of the confidentiality and anonymity of their responses. Participation was voluntary, and participants were informed of their right to withdraw at any point without consequence. The research team also ensured that no physical or psychological harm was posed to participants throughout the process. Ethical clearance was sought from the appropriate institutional review board before data collection.

3. Results and Discussion

3.1 Value Chain Framework of Barangay Marupangdan, Daram, Samar

3.1.1 Community Production and Marketing Practices

Figure 1 presents the current value chain analysis of the existing agri-fishery resources in Barangay Marupangdan, Daram, Samar. Based on data gathered from community participants, several key characteristics and gaps were identified throughout the value chain. There is an absence of value-adding activities that could enhance the productivity and marketability of raw products. The community currently does not use any agri-fishery technology during production and lacks fabricated tools for post-harvest processing or value addition. Although a potential Post-Harvest and Processing Facility (PHPF) exists, it remains non-functional and requires substantial repair. Marketing of agricultural and fishery produce is limited to nearby localities such as Catbalogan and selected municipalities, restricting profitability. Transportation costs are high, limiting return on investment. Furthermore, participants reported no Information, Education, and Communication (IEC) activities from government agencies to enhance local capacity. Surplus harvests often go to waste due to a lack of market access, though some overripe produce is recycled into organic fertilizer.

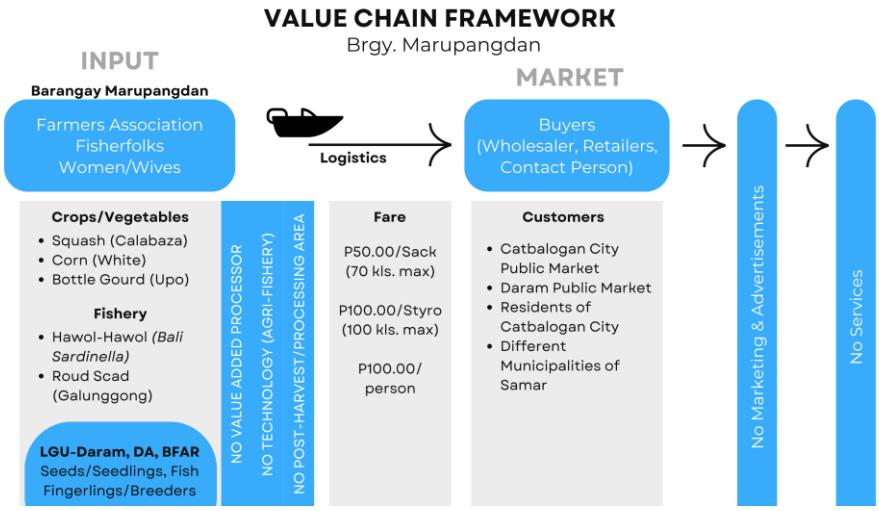

Figure 1. Value Chain Framework of Barangay Marupangdan

3.1.2 Implications for Value Chain Efficiency

The lack of value-adding activities and market linkages reflects inefficiency across the value chain. As supported by prior studies [12], value addition and the integration of technology can significantly improve income stability and market competitiveness. The limited use of ICT and logistics support constrains producers' access to broader markets, while the absence of pre-harvest contractors weakens production continuity. A comparison with Barangay Astorga reveals the potential benefits of community-led processing and digital marketing. Their success illustrates that integrating value-added strategies within Marupangdan can improve profitability and reduce post-harvest losses.

3.2 Value Chain Analysis for Galunggong in Barangay Astorga

3.2.1 Results: Application of Porter's Value Chain Analysis

Figure 2 illustrates the value chain analysis for Galunggong (Round Scad) Fish Balls using Porter's framework. The analysis evaluates both primary activities (inbound logistics, operations, marketing, sales, and service) and support activities (infrastructure, technology, and human resource management). In Barangay Astorga, galunggong is converted into fish balls, increasing total product value from ₱100.00 to ₱250.00 per kilo. Table 2 presents the cost-benefit analysis, excluding labor costs, which are governed by member participation stipulations. These figures highlight the profitability potential of value-added processing. However, without technological support, product standardization, and reliable logistics, sustainability remains uncertain. Support activities, such as infrastructure and technology, are critical gaps in both barangays. Porter's framework underscores that improving these areas would enhance efficiency, quality, and market access. Astorga's adoption of community-led processing demonstrates how local value chains can evolve toward self-sustaining enterprises. Replicating these practices in Marupangdan, alongside institutional support (DTI, LGU, and DA), can bridge the gap between production and profitability.

Table 2. Simplified Cost–Benefit Analysis

Product	Raw Material Cost	Processing Cost	Packaging Cost	Transport Cost	Total Cost	Selling Price/kg	Value Added
Galunggong (GG) Fish Balls	₱100.00	₱50.00	₱20.00	₱30.00	₱200.00	₱250.00	₱150.00

Note: Value added refers to the difference between the selling price and the raw material cost, reflecting the economic value created through processing rather than net profit. Labor costs are excluded in accordance with association-based participation stipulations.

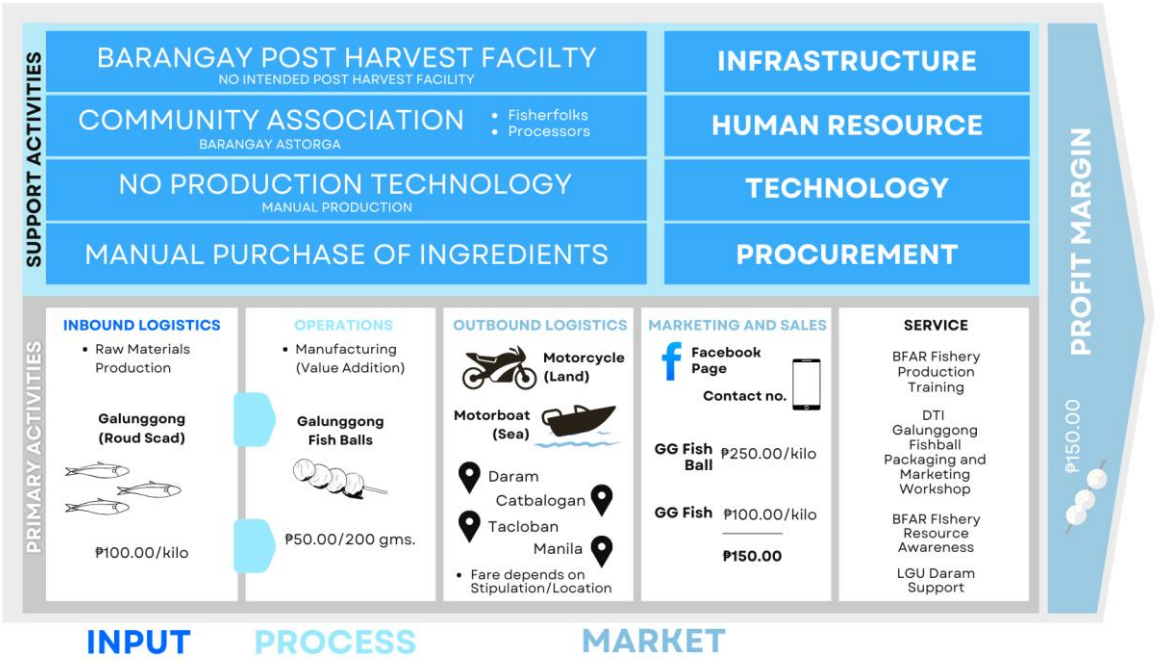

Figure 2. Value Chain Framework of Barangay Astorga

3.3 Community Human Resource Management

In Barangay Marupangdan, the Barangay Farmers Association is the only formally registered organization. The Women's Association is pending DOLE registration. Farming and fishing are primarily male-led, though women contribute significantly when available. The Farmers Association president oversees logistics and marketing. Meanwhile, Astorga's registered association engages in value-added processing supported by DTI and the LGU. The organizational gap between the two barangays indicates differing stages of institutional readiness. Astorga's formalization and external support networks have enabled sustained production. Marupangdan's informal structures, while participatory, require technical and administrative strengthening to access similar benefits. Strengthening women's involvement in processing could enhance social inclusion and community capacity.

3.4 Agri-Fishery Production Management

Barangay Marupangdan produces squash, corn, and bottle gourd, with squash sold at ₱20/kg and bottle gourd at ₱15/kg. Transport cost per sack (₱50) and lack of proper packaging limit profits. Marine resources include hawol-hawol (Bali sardine) and galunggong, with seasonal surpluses leading to waste. Farmers have requested training on organic hybrid seeds and post-harvest processing. These findings highlight inefficiencies caused by logistical constraints and a lack of value-adding practices. As noted in related literature [15], rural communities benefit economically when post-harvest losses are minimized and value-addition is introduced. Improved infrastructure and access to hybrid seeds can enhance productivity and resilience.

3.5 Agri-Fishery Technology

Farmers and fishers lack access to mechanized tools, ICT applications, or post-harvest equipment. Production remains manual, relying on traditional techniques. Neighboring Astorga has acquired equipment and packaging tools from DTI and LGU Daram. Technology adoption is essential for production efficiency and quality assurance. Consistent with [16], limited awareness and cost barriers hinder technology use. Investment in training and machinery is a prerequisite for modernizing the agri-fishery systems in Marupangdan.

3.6 Value-Added Agri-Fishery Food Production and Processing

Marupangdan has not yet implemented structured value-adding activities. Astorga, however, has established production of Galunggong Fish Balls, sold at ₱50 per 200-gram pack, respectively. The contrast between the two barangays shows the transformative effect of training and capital support. Processed products typically yield greater profit margins compared to raw materials, supporting the strategic transition toward value-added forms of entrepreneurship.

Similar findings were reported by Mustacisa, who demonstrated that participatory, science-based interventions in root crop production significantly improved yields and enhanced value creation at the community level, reinforcing the role of localized innovation in strengthening agri-fishery value chains [19].

3.7 Product Advertisement and Marketing

Barangay Marupangdan lacks formal marketing initiatives. No advertisement or government support currently exists. Astorga, by contrast, benefits from DTI and LGU-led promotion during trade fairs and social media campaigns. Effective marketing and communication are essential for sustaining agri-fishery enterprises [17,18]. Establishing digital presence, market linkages, and promotional materials can empower local producers to access wider markets and stabilize income. This study was limited to two barangays in Daram, Samar; thus, findings may not represent all coastal communities in the region. The cost analysis excluded labor and indirect expenses. Future research should include longitudinal data and broader geographic coverage.

4. Conclusions

This study revealed the critical gaps and opportunities in the agri-fishery value chain of Barangay Marupangdan and Barangay Astorga, highlighting the communities' strong reliance on farming and fishing as primary livelihoods. Despite the abundance of natural resources and initial steps toward value-added production—such galunggong fish balls—there remains limited access to agri-fishery technologies, post-harvest facilities, and effective marketing strategies. Value chain analysis showed that most agricultural and fishery products are sold as raw goods, significantly limiting income potential for local producers. The lack of processing centers, packaging technology, and entrepreneurial skills further constrains these communities from fully capitalizing on value addition. However, the research also uncovered a high level of community interest and willingness to adopt innovative practices, particularly among women and local associations. The findings underscore the need for targeted interventions such as technology provision, skills training, product development support, and improved market linkages. Strengthening institutional support from LGUs, DTI, DA, Bureau of Fisheries and Aquatic Resources (BFAR), and other stakeholders is crucial to building sustainable agrifishery enterprises. The development of inclusive and localized value chain strategies can help transform subsistence farming and fishing into viable economic activities. This shift has the potential to improve food security, generate income, and contribute to poverty reduction in rural coastal communities

5. Acknowledgements

The authors would like to express their heartfelt gratitude to Samar State University and the Center for Lifelong Learning (CeLL) for their unwavering support and for granting us the opportunity to be among the recipients of institutional funding. We also extend our sincere thanks to the entire project team for their invaluable contributions and commitment throughout the course of this endeavor.

Author Contributions: Conceptualization, Jose Marlon J. Refuncion Jr. and Jonafe O. Matugas; methodology, Jose Marlon J. Refuncion Jr.; data gathering, Jose Marlon J. Refuncion, Mar June Gabon, Rinaliza Gabon, Bryan G. Cabadora; validation, Jose Marlon J. Refuncion Jr.; formal analysis, Jose Marlon J. Refuncion Jr.; Jonafe O. Matugas, Dennis B. Durango, Ma. Winna Mae A. Agbon; writing—original draft preparation, Jose Marlon J. Refuncion Jr.; writing—review and editing, Jose Marlon J. Refuncion Jr.; visualization, Jose Marlon J. Refuncion Jr.; supervision and administration, Jose Marlon J. Refuncion Jr. All authors have read and agreed to the published version of the manuscript.

Funding: This research was funded by the Department of Science and Technology – Philippine Council for Agriculture, Aquatic and Natural Resources Research and Development (DOST-PCAARRD) and supported by institutional research funding from Samar State University (SSU).

Conflicts of Interest: The authors declare no conflict of interest.

References

[1] News Bharati. Asia Has 60% of World's Hungry Population. *News Bharati*, July 16, 2019. https://www.newsbharati.com/Encyc/2019/7/16/Asia-has-60-of-hungry-people-.html.

[2] World Economic Forum. This Map Shows How Much Each Country Spends on Food. *World Econ. Forum*, December 21, 2016. https://www.weforum.org/stories/2016/12/this-map-shows-how-much-each-country-spends-on-food.

[3] Asian Development Bank. *Food Security in Asia and the Pacific*; Asian Development Bank: Manila, Philippines, 2013. https://www.adb.org/publications/food-security-asia-and-pacific.

[4] Cooperative Development Authority. *Performance of Cooperatives by Type as of December 2015–2016*; Cooperative Development Authority: Quezon City, Philippines, 2016; based on reporting data of 9,432 cooperatives. https://cda.gov.ph/resources/updates/statistics.

[5] Khan, N.; Fahad, S.; Naushad, M.; Faisal, S. Analysis of Livelihood in the World and Its Impact on World Economy. *SSRN* **2020**. https://doi.org/10.2139/ssrn.3717265

[6] Israr, M.; Khan, H. An Analysis of Livelihood Sources in Hilly Areas of Northern Pakistan. *Sarhad J. Agric.* **2010**, *26*(4), 665–672.

[7] Babu, S. C.; Davis, K. Private Technical Assistance Approaches in Brazil. In *Knowledge Driven Development*; **2015**. https://doi.org/10.1016/B978-0-12-802231-3.00006-1

[8] Kuldeep; et al. Livelihood Enhancement through Value Addition and Marketing of Turmeric in Dang District of Gujarat. *Int. J. Commer. Bus. Manag.* **2013**, *6*(2).

[9] PhilAtlas. Barangay Marupangdan and Astorga, Daram, Samar. *PhilAtlas* **2020**. https://www.philatlas.com.

[10] Philippine Statistics Authority. *Poverty Statistics*; Philippine Statistics Authority: Manila, Philippines, **2021**.

[11] Kaplinsky, R.; Morris, M. *A Handbook for Value Chain Research*; Institute of Development Studies: Brighton, UK, **2001**.

[12] Hasan, K.; Sambo, M.; Muchlis, R. A.; Yahya, M. Optimization of Marketing Communications of Fisheries, Marine and Food Agriculture of Lhokseumawe City. *Proc. Int. Conf. Soc. Sci. Polit. Humanit. (ICoSPOLHUM 2020)* **2021**. https://doi.org/10.2991/ASSEHR.K.210125.008

[13] Dieffenbacher, S.; Dieffenbacher, S. Michael Porter Value Chain Analysis Model: Examples & Applying Steps. *Digital Leadership*, April 30, **2024**. https://digitalleadership.com/unite-articles/porters-value-chain/.

[14] Tejaswini, C.; Rao, T. S.; Reddy, M. K. Value Addition in Horticulture: A Sustainable Approach for Farmer Income Enhancement. *Int. J. Agric. Sci.* **2021**, *13*(3), 8991–8994.

[15] Ayoo, C.; Bonti-Ankomah, S.; Aryee, A. N. Constraints to Value Addition to Agricultural Byproducts. In *Byproducts from Agriculture and Fisheries*; Wiley: Hoboken, NJ, **2019**. https://doi.org/10.1002/9781119383956.ch32

[16] Secretaria, M. B. Resistance to Technological Adoption in Philippine Agri-Fisheries: Barriers and Solutions. *Philipp. J. Rural Dev.* **2019**, *41*(1), 85–98.

[17] Gartanti, W. T.; Triwardhani, I. J.; Putra, R. P. The Development of Village Entrepreneurship through Digital Marketing Communication. *Adv. Soc. Sci. Humanit. Res.* **2020**. https://doi.org/10.2991/assehr.k.200225.029

[18] Luthfiana, N.; Widodo, H.; Susanti, R. Digital Marketing Strategies for Empowering Farmers in Southeast Asia. *J. Agric. Econ. Dev.* **2024**, *15*(1), 23–35.

[19] Mustacisa-Lacaba, M.; Villanueva, R.; Tadios, L.K.; Tan, N. Increasing Sweet Potato (Ipomoea batatas) Root Crop Yield Based Scientific Participatory Research. *ASEAN J. Sci. Technol. Rep*. **2023**, 26(3), 24–35. https://doi.org/10.55164/ajstr.v26i3.249375

ASEAN
Journal of Scientific and Technological Reports
Online ISSN:2773-8752

Research article

Experimental Investigation of Ozone Generation in Multi-Cell Dielectric Barrier Discharge Reactors

Phurin Chonpan[1], Kampanart Theinnoi[1, 2], and Sak Sittichompoo[1, 2*]

[1] College of Industrial Technology, King Mongkut's University of Technology North Bangkok, Bangkok, 10800, Thailand
[2] Research Centre for Combustion Technology and Alternative Energy (CTAE), Science and Technology Research Institute, King Mongkut's University of Technology North Bangkok, Bangkok, 10800, Thailand
* Correspondence: sak.s@cit.kmutnb.ac.th

Citation:
Chonpan, P.; Theinnoi, K.; Sittichompoo, S. Experimental investigation of ozone generation in multi-cell dielectric barrier discharge reactors. *ASEAN J. Sci. Tech. Report.* **2026**, *29*(2), e261804. https://doi.org/10.55164/ajstr.v29i2.261804.

Article history:
Received: October 9, 2025
Revised: November 18, 2025
Accepted: December 3, 2025
Available online: January 20, 2026

Publisher's Note:
This article is published and distributed under the terms of the Thaksin University.

Abstract: Ozone is a sustainable oxidant with applications in water treatment, air purification, and food sterilisation. Dielectric barrier discharge (DBD) reactors are attractive for ozone generation because of their simplicity and scalability. Performance depends on both plasma processes and power supply characteristics. This research examined single-, two-, and three-cell dielectric tubes DBD reactor operated under varying voltages and frequencies to assess ozone yield and energy efficiency. FTIR spectroscopy confirmed ozone as the main product and enabled extended quantification beyond portable ozone detector saturation through calibration with detector readings (R^2 = 0.9997). Reactor scaling-up enhanced ozone generation, with the three-cell reactor achieving 11946 ppm and 17.25 g/h at 40 kV_{pp} and 100 Hz, for discharge voltage and frequency, respectively. However, ozone concentrations from the two- and three-cell reactors were nearly identical across the SEI (Specific Energy Input) range due to high-voltage power supply (HVPS) limitations rather than reactor design. Efficiency analysis revealed two perspectives, based on discharge power, the ozone production efficiency (OPE) peaked at 396 g/kWh in a two-cell configuration at low SEI but declined at higher SEI owing to non-productive energy losses. Conversely, the overall ozone production efficiency (OOPE), referenced to system input power, increased with SOEI (specific overall energy input), with the two-cell reactor outperforming (16.0–22.3 g/kWh). These findings highlight the combined influence of plasma on ozone generation, offering guidance for scaling DBD reactors in industrial applications.

Keywords: Ozone generation; nonthermal plasma; dielectric barrier discharge; FTIR spectroscopy; ozone production efficiency

1. Introduction

Ozone (O_3) is a colourless gas consisting of three oxygen atoms and characterised by a sharp, irritating odour [1]. Its physical and chemical properties are summarised in Table 1. Ozone is regarded as a strong oxidising agent [2], possessing an oxidation potential of 2.07 V [3] and exhibiting significantly lower stability than ambient oxygen, decomposing rapidly to oxygen in both air and water [4]. This rapid decomposition, which leaves no harmful residues, combined with high oxidising potential, makes ozone particularly advantageous for applications. In the food industry, it is used to inactivate microorganisms [5] and extend product shelf life [6], including vegetables, fruits [7], meat, and grain products [6]. As well as in drinking water treatment, ozone removes taste and

odour compounds (for example, geosmin and 2-methylisoborneol (MIB) by combining direct oxidation with ozone and indirect oxidation by hydroxyl (OH) radicals [8]. Ozone is also employed to enhance air quality through the removal of volatile organic compounds (VOCs), which pose direct risks to the eyes and the respiratory system [9].

Table 1. Physical and chemical properties of ozone.

Property	Value	Ref
Molecular weight (g/mol)	48	[1, 10]
Gaseous density (kg/m^3) @ 0 °C and 1 atm	2.1415	[11]
Solid density @ -195.75 °C (kg/m^3)	1728	[1]
Melting point (°C)	-192.5 ± 0.4	[1, 11, 12]
Boiling point (°C)	-111.9 ± 0.3	[1, 11, 12]
Half-life in air (min)	20 - 1524	[1]
Half-life in water (min)	10 -80	[1]
Dielectric constant at -183 °C	4.74	[1, 11]

A range of techniques has been developed for the generation of ozone, including vacuum ultraviolet (VUV) [13], electron-beam processes [14], water electrolysis [15], and electrical discharge plasmas such as Corona Discharge [16] and Dielectric Barrier Discharge (DBD) [17]. Among these, electrical discharge plasma remains the only practical approach capable of producing the quantities of ozone required for large-scale applications [18].

DBD is widely recognised as a non-thermal plasma (NTP) technique for ozone generation, an important oxidising agent with diverse industrial applications [19]. In this method, a high voltage AC (Alternating current) or pulsed DC (Direct current) is applied across a gas restricted between two electrodes separated by a dielectric barrier [20]. The resulting discharge produces reactive oxygen species (e.g., O), which subsequently interact with molecular oxygen to form ozone. DBD offers diverse advantages compared to other reactor types, including high efficiency, relatively low operating cost, and straightforward scalability, making it a desirable reactor design for ozone generation. Consequently, many researchers have investigated methods and operating strategies to produce high concentrations of ozone with low energy consumption to achieve greater efficiency. Xie Linjie et al. [21] studied the use of a coaxial DBD reactor with water as both the high-voltage and ground electrodes. The water electrodes effectively controlled the gas temperature, keeping the rotational temperature near ambient (305–308 K), which favoured ozone synthesis. As a result, the reactor achieved high ozone generation efficiency and stable long-term performance (6000 ppm ozone, which was maintained for 400 min). Sun Shukai et al. [22] developed a needle–plate DBD ozone generator with a magnetic field and showed that the field increased discharge power up to 23.9% and ozone concentration up to 35.4%. The findings suggested that magnetic fields enhanced ozone generation but did not improve the efficiency in this reactor design. Most studies emphasized the ozone production mechanisms at the laboratory scale, while fewer works focus on the effect of increased parallel DBD cell of a scale-up system.

The objective of this research is to investigate ozone generation in non-thermal plasma dielectric barrier discharge (NTP-DBD) reactors with different levels of DBD cell scaling, represented by single, two, and three-cell configurations. In this design, each "cell" corresponds to one dielectric tube discharge unit, and increasing the number of cells increases the effective discharge volume and surface area available for plasma reactions. To extend the high ozone concentration measure range, the study focused on quantifying ozone formation and byproducts using FTIR spectroscopy calibrated with an electrochemical-based ozone analyser. Moreover, evaluating the effects of applied voltage, frequency, and reactor scaling on ozone concentration and production rate, and assessing energy efficiency through both discharge-based ozone production efficiency (OPE) and system-based overall ozone production efficiency (OOPE). In addition, the work aimed to provide insights that support the optimisation and scale-up of multi-cell DBD reactors for practical environmental and industrial applications.

2. Materials and Methods

This research investigated how the number of reactor cells affects the electrical characteristics, ozone concentration, and ozone production efficiency in a DBD-NTP system. To evaluate the effect of system scaling, the reactor was operated in three configurations comprising one, two, and three cells, respectively, while the experimental arrangement for ozone generation is illustrated in Figure 1. The reactor was constructed from stainless steel and incorporates three borosilicate glass tubes as a dielectric barrier, each with an outer diameter of 63 mm, a glass tube thickness of 2 mm, and a length of 50 cm, which resulted in a discharge gap of 1.15 mm. The capacitance of the DBD reactors was measured by a Hioki LCR impedance analyser (model IM 3570). The measured values were 392.6 pF, 839.1 pF, and 1140.2 pF for the one, two, and three cells, respectively. The square-wave signal was generated using a digital storage oscilloscope (DSO) (KEYSIGHT, model DSOX1204G) and subsequently amplified using a high-voltage power supply (HVPS) (Trek 20/20C-HS) to generate plasma discharge. The discharge voltage was adjusted to 24, 30, and 40 kV_{pp} at frequencies of 50 Hz and 100 Hz. The electrical signals' instantaneous voltage and current were continuously monitored with the DSO to characterise the discharge behaviour. Additionally, the power consumption of the HVPS was also captured via a power meter. The feed gas consisted of air and oxygen, where the oxygen was supplied by an oxygen concentrator (purity is 93 %Vol.±3). Before entering the reactor, the gases were cooled and dehumidified to improve the stability of the discharge and enhance ozone generation efficiency [23, 24]. This step was particularly important, as water vapour can promote the formation of undesirable nitrogen oxides (NOx) through the generation of OH radicals originating from water molecules [25].

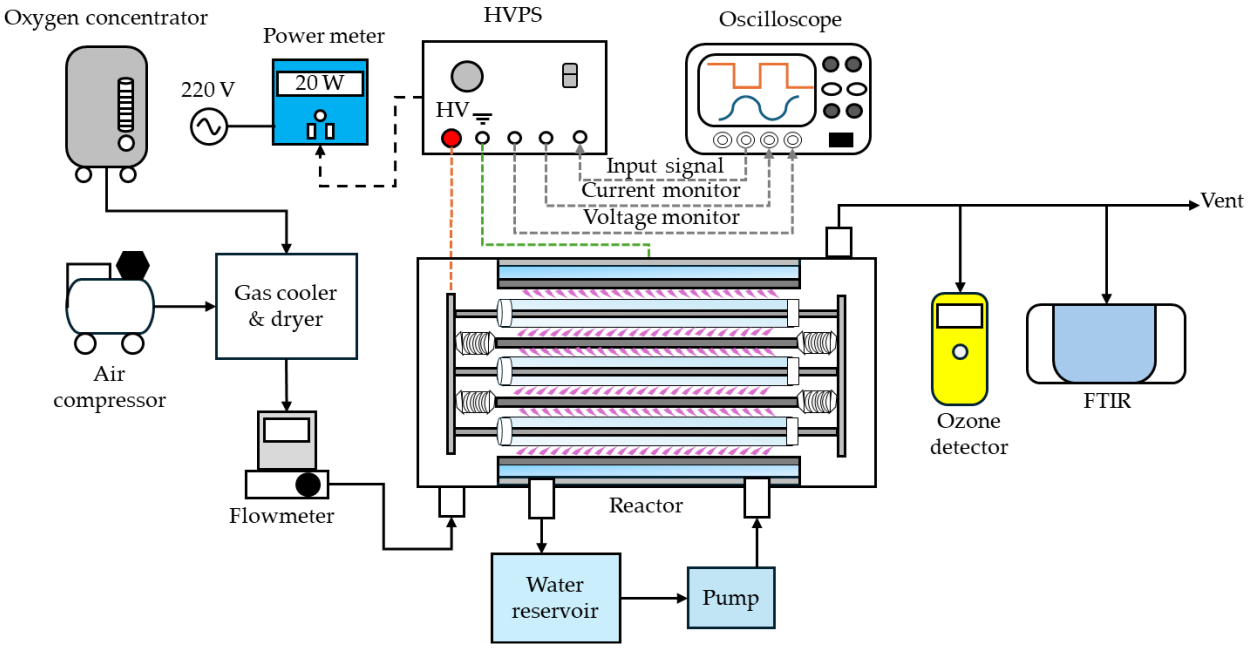

Figure 1. The schematic diagram of multi-cell DBD-NTP ozone generation.

The gas flow was controlled at 12 LPM with a flow meter (SMC, model: PF2A750 – F02 - 27) before entering the reactor. Moreover, the operating temperature of the reactor was regulated by a water-cooling system to prevent overheating of the reactor. This cooling system comprised a water reservoir and a pump, which circulated cooling water around the outer electrodes of the reactor.

UV absorption spectroscopy at 254 nm, based on the Beer–Lambert law, is a common approach [26] for ozone concentration measurement, though it can be affected by cross-interference, saturation at high concentrations, and sensitivity to temperature, pressure, and optical losses. Electrochemical sensing provides a simpler alternative by generating an electrical signal from ozone's reaction with an electrolyte [27], but this method is limited by electrolyte degradation and a restricted detection range. In this research, ozone concentration was initially monitored using an ozone analyser (SKZ, model: 1050-O_3). Due to the analyser's

measurement limit of 5000 ppm, a Fourier Transform Infrared Spectroscopy (FTIR) instrument (Bruker INVENIO R) was employed for higher concentrations. A calibration curve was established by plotting analyser readings against the integrated absorbance of ozone obtained from FTIR spectra, followed by linear regression to derive the calibration equation. This calibration enabled reliable quantification of ozone beyond the analyser's detection limit, allowing accurate measurement under varying operating conditions and reactor configurations. The ozone production efficiency (OPE, g/kWh), defined in Eq. (1), represents the efficiency of ozone generation based on the discharge power. The overall ozone production efficiency (OOPE, g/kWh), given in Eq. (2), accounts for the proportion of ozone generated relative to the total input energy, including the contribution from the HVPS.

$$OPE = \frac{OPR}{P_D} \times 1000 \tag{1}$$

$$OOPE = \frac{OPR}{P_m} \times 1000 \tag{2}$$

Where OPR is the ozone production rate (g/h), which describes how much ozone is produced per unit time and can be calculated using Eq. (3). P_D is the discharge power (W) calculated from Eq. (4) [28]. P_m (W) represents the total power consumed by the HVPS as measured directly with a power meter.

$$OPR = C_{O_3} \times Q \times 60 \tag{3}$$

Where C_{O_3} is ozone concentration (g/L), and Q is the gas flow rate (LPM)

$$P_D = f \times \int_0^T I(t) \times V(t) dt \tag{4}$$

Which I(t) and V(t) are the current and voltage signals, respectively. f is the frequency (Hz) and T is the period of discharge.

The Lissajous diagram of the DBD ozone generator requires both the reactor voltage and the corresponding charge. In the conventional approach, a measurement capacitor is connected in series with the reactor, and the charge (Q) is determined from the voltage across this capacitor multiplied by its capacitance. However, the addition of a measurement capacitor can increase the overall capacitance of the reactor, thereby altering its electrical characteristics. To avoid this effect, a virtual measurement capacitor was introduced, and the charge was reconstructed by integrating the measured discharge current. As the oscilloscope provides discrete data points, numerical integration was applied, and the accumulated charge is expressed as eq. (5) [29].

$$Q(t) = \sum_{i=1}^{N} I(t_i)\, \Delta t \tag{5}$$

Where I (t_i) is the discharge current at time (t_i), Δt is the data sampling interval, and N is the number of samples.

The energy consumption and the formation of reactive species in the discharge process were directly related to the specific energy input (SEI, J/L), which was calculated as shown in Eq. 6 [30]. Furthermore, the total energy supplied by the HVPS, expressed as the specific overall energy input (SOEI, J/L), is defined in Eq. (7).

$$SEI = \frac{P_D}{Q} \times 60 \tag{6}$$

$$SOEI = \frac{P_m}{Q} \times 60 \tag{7}$$

3. Results and Discussion

3.1 Electrical behaviours

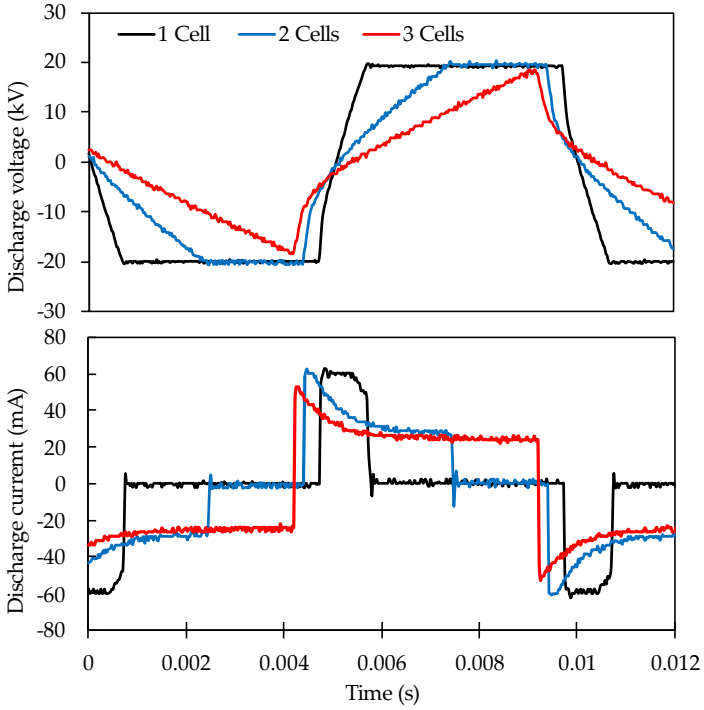

Figure 2. Discharge voltage and discharge current waveform.

Figure 2 demonstrates the discharge voltage and discharge current waveform of one, two, and three DBD cells when applying a discharge voltage at 40kVpp 100 Hz. The discharge voltage waveform indicated a difference when increasing the number of DBD cells. For the single-cell configuration, the discharge voltage shows a slightly skewed square wave as the result of the limited slew rate of the HVPS (800 V/μs) and the substantial capacitance of the DBD reactor. On the other hand, the 2 and 3-cell configuration indicated a significantly lower gradient of voltage waveform during both positive and negative phases. This phenomenon is due mainly to the capacitive load characteristic of the DBD reactor, whose capacitance of the reactor increased with the number of DBD (borosilicate glass) and affected the charge and discharge characteristics. In the case of the configuration with three DBD cells, the maximum voltage attained was lower than that observed with one or two DBD cells. This discrepancy is attributed to insufficient time for complete reactor charging, which consequently led to a reduction in discharge power. A detailed analysis of this effect will be presented in a subsequent section. The current waveform was steep and narrow in the single-cell case, whereas the two- and three-cell configurations exhibit broader waveforms with peak amplitudes half as high. The peak current reaches approximately 60 mA, which was the peak current limited (clipped) by the HVPS. Moreover, the current waveforms show a more leading phase characteristic as the number of cells increases. The ability of the HVPS to deliver high voltage is constrained by its slew rate, which for the Trek 20/20C-HS is limited to 800 V/μs, which means it requires at least 50 μs to drive the output stage to 40kV. The high capacitance of our proposed DBD reactor imposed a significant capacitive load, preventing the HVPS from supplying current rapidly enough to effectively charge it in a finite period.

The dielectric properties of the DBD reactors were further evaluated using Lissajous diagrams, which provided insight into the capacitive behaviour of the multi-cell DBD. As shown in Figure 3, the slope of the charge–voltage (Q–V) curve, corresponding to dQ/dV [31], indicated the dielectric capacitance of the reactor. Linear fitting of each curve revealed capacitance values of 471.1 pF, 998.39 pF, and 1219.2 pF for the one, two, and three cell configurations, respectively. These values increased proportionally with the number of cells and indicated good agreement with the measurement values obtained from the LCR meter. In addition, the

enclosed area of each Lissajous parallelogram represents the energy dissipated per cycle of discharge. It is evident that the area becomes larger with the addition of more cells, reflecting higher discharge power and increased energy deposition into the plasma

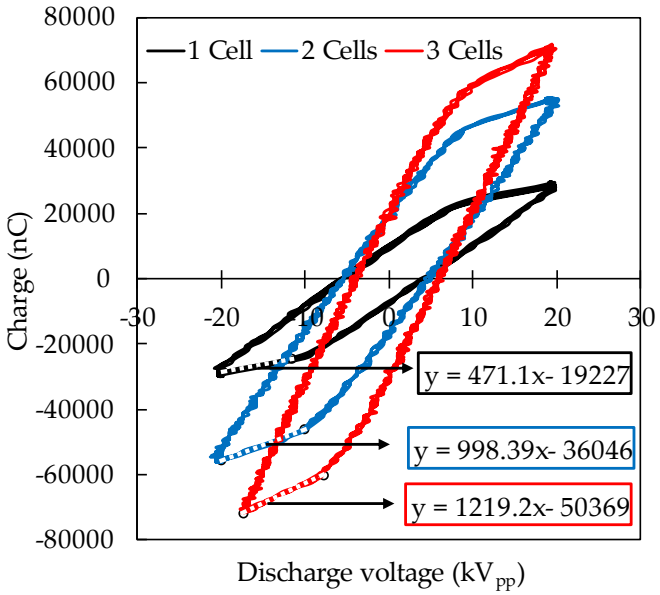

Figure 3. Lissajous diagram of multi-cell DBD at 40kV$_{pp}$ and 100 Hz.

3.2 Ozone formation and quantification

Ozone is produced from oxygen dissociation mechanisms (R1) and (R2), followed by three-body recombination to ozone (R3) [32].

$$e + O_2 \rightarrow e + O\ ^3P + O\ ^3P \quad \text{(R1)}$$

$$e + O_2 \rightarrow e + O\ ^3P + O\ ^1D \quad \text{(R2)}$$

$$O + O_2 + M \rightarrow O_3 + M \quad \text{(R3)}$$

Which M is the third body that removes excess energy, e.g., O, O_2, or N_2.

Figure 4 presents the FTIR spectra obtained during ozone generation with a three-cell DBD configuration operated at different applied voltages (24, 30, and 40 kV$_{pp}$) at a fixed frequency of 100 Hz and utilising air+O_2 at 12 LPM. The spectra revealed the main gaseous products formed in the discharge corresponding to the ozone band. Besides, minimising other absorption is byproduct NOx species from nitrogen in air, such as nitrous oxide (N_2O), dinitrogen pentoxide (N_2O_5), and carbon dioxide (CO_2). The absorption bands for these gases are summarised in Table 2. At 24 kV$_{pp}$, the ozone absorbance was relatively weak, indicating limited generation efficiency at lower discharge power. Increasing the voltage to 30 kV$_{pp}$ resulted in a significant rise in the absorbance, and at 40 kV$_{pp}$, the ozone peak became dominant. This confirmed the strong dependence of ozone formation on the discharge intensity. This trend was consistent with higher applied voltages enhancing the electron energy distribution, thereby promoting more effective oxygen dissociation and subsequent ozone formation.

Table 2. Reference infrared absorption bands of ozone and related species.

Species	Band/cm^{-1}	Ref
O_3	1050, 2100	[33]
N_2O	1300, 2211, 2237	
N_2O_5	1247, 1720	[34]
CO_2	2360, 2340	

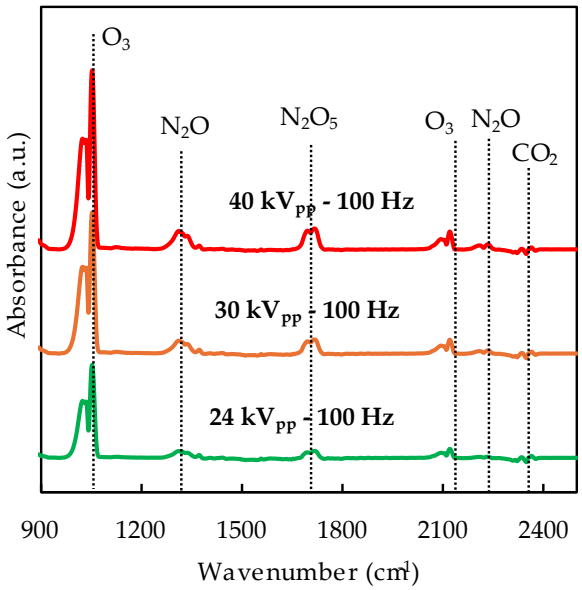

Figure 4. FTIR spectra of ozone generation at 3 cells configuration.

The NOx species originated from N_2 in the air feed, with pathways such as N_2O formed via (R4) – (R5) and N_2O_5 formed via (R6) – (R9) [34].

$$N_2^* + O_2 \rightarrow N_2O + O \quad \text{(R4)}$$

$$NO_2 + N_2 \rightarrow N_2O + O \quad \text{(R5)}$$

$$N + O_2 \rightarrow NO + O \quad \text{(R6)}$$

$$NO + O_3 \rightarrow NO_2 + O_2 \quad \text{(R7)}$$

$$NO_2 + O_3 \rightarrow NO_3 + O_2 \quad \text{(R8)}$$

$$NO_2 + NO_3 + M \rightarrow N_2O_5 \quad \text{(R9)}$$

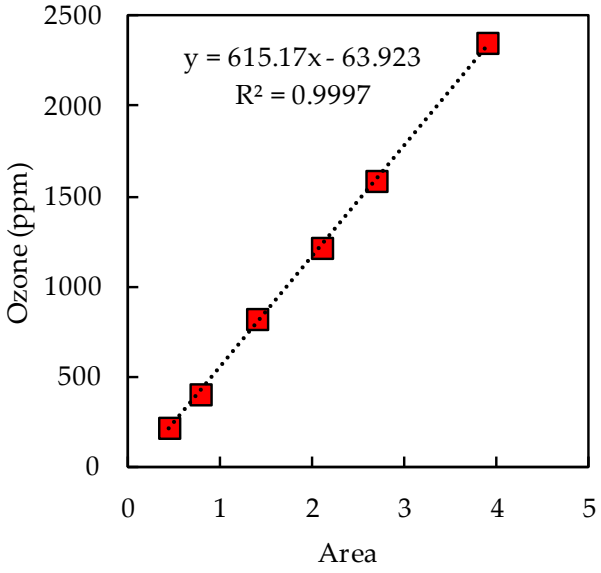

Figure 5. Calibration curve for ozone concentration.

The ozone analyser (SKZ1050) alone was unable to measure concentrations exceeding 5000 ppm-vol. FTIR spectroscopy was calibrated with the ozone analyser to extend quantification beyond this range. The calibration curve was established by correlating the ozone analyser readings with the integrated area under the ozone absorption curve obtained from FTIR spectra. As illustrated in Figure 5, this calibration produced a strong linear relationship, expressed as $y = 615.17x - 63.923$ with a coefficient of determination (R^2) of 0.9997. During the experiments, the discharge power of the reactor was incrementally adjusted, and data from both the ozone analyser and FTIR were collected simultaneously. The data's linearity confirms this approach's reliability, demonstrating that FTIR can be utilised to accurately quantify ozone concentrations once the ozone analyser's detection range exceeds the measurement range of SKZ1050.

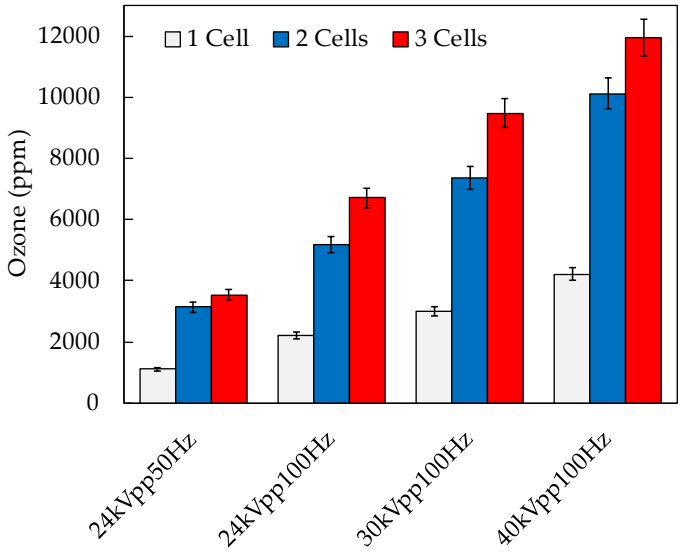

Figure 6. Compares the ozone concentrations produced for one, two, and three cells.

Figure 6 demonstrates the comparison of the ozone concentrations produced under four different operating conditions (24–40 kV_{pp} at 50–100 Hz) for one, two, and three cell configurations. The results demonstrated that ozone concentrations increased with the number of cells. Increasing the number of cells from one to three significantly enhanced ozone generation across all condition voltages and frequencies. This can be explained by the fact that the larger effective discharge volume and surface area are provided by increasing the dielectric tubes, which promoted a greater number of micro discharges per cycle. As a result, a larger fraction of the input energy was converted into plasma reactions, leading to higher ozone concentrations. In addition, at 24 kV_{pp} and 50 Hz, the ozone concentrations were approximately 1100 ppm, 3100 ppm, and 3500 ppm for one, two, and three cell configurations, respectively. When the frequency was increased to 100 Hz while maintaining the same voltage (24 kV_{pp}), ozone production increased, reaching approximately 2200 ppm, 5150 ppm, and 6700 ppm for one, two, and three cells, respectively. A similar increasing trend was observed at higher discharge voltages. At both 30 kV_{pp} (50 Hz) and 40 kV_{pp} (100 Hz), ozone production rose further across all cell configurations, demonstrating that both applied voltage and operating frequency have a significant effect on ozone generation [7]. The highest ozone concentration was obtained at 40 kV_{pp}, 100 Hz in the three-cell configuration, highlighting the combined benefit of higher voltage, higher frequency, and reactor scaling.

Figure 7(a). reveals the variation in the concentration of ozone with SEI. The ozone concentration rose linearly with SEI in all reactor configurations. The three-cell setup produced the highest concentration, reaching 11946 ppm-vol at 627 J/L, while the single cell configuration only generated ozone below 6000 ppm compared to the same conditions. However, the concentrations obtained with the two- and three-cell reactors were nearly identical within the same SEI range. This similarity was attributed to the HVPS's inability to provide enough power to fully charge the three-cell setup, caused by the high reactor's capacitance. Figure 7(b). showed a similar trend, with the ozone production rate increasing gradually with SEI. The three-cell

setup achieved a maximum production rate of 17.25 g/h. This demonstrated how increasing the number of discharge cells increased not only the effective discharge volume but also enhanced the ozone generation. Contrasting with the linear increase in ozone concentration, the ozone production efficiency decreased with increasing SEI, as shown in Figure 7(c). At low SEI below 100 J/L, the three-cell reactor achieved approximately 305 g/kWh. At higher SEI (340 - 630 J/L), OPE dropped significantly and remained around 140 g/kWh for all configurations. This was caused by an increasing amount of input energy to the reactor, dissipated as heat and other non-productive processes at higher discharge powers. Although the multi-cell systems maintain improving on the single-cell configuration, the relative advantage is reduced at high SEI. A different trend showed when the overall ozone production efficiency (g/kWh) was calculated based on the system input power shown in Figure 7(d). During the SOEI range, the two-cell reactor consistently produced the highest OOPE (16.0→22.3 g/kWh), followed by the three-cell reactor (14.6→22.6 g/kWh) and the single-cell reactor (6.6→13.9 g/kWh). This behaviour indicated the correlation between wall-plug efficiency and HVPS operating conditions. At low input power, the supply exhibited lower conversion efficiency and power factor. As SOEI increased, relative electrical losses decreased, and apparent efficiency improved. The three-cell's slightly lower OOPE when compared to two cells was due to the significantly greater capacitive load, which utilised the HVPS over its current/slew-rate limits (as indicated by broadened current pulses and softened voltage slopes), introducing additional supply losses and preventing full utilisation of the extra discharge capacity. OOPE provides a realistic measure of the energy cost of ozone generation from the end-user's perspective, while OPE (discharge-based) only reflects the intrinsic plasma efficiency of the reactor.

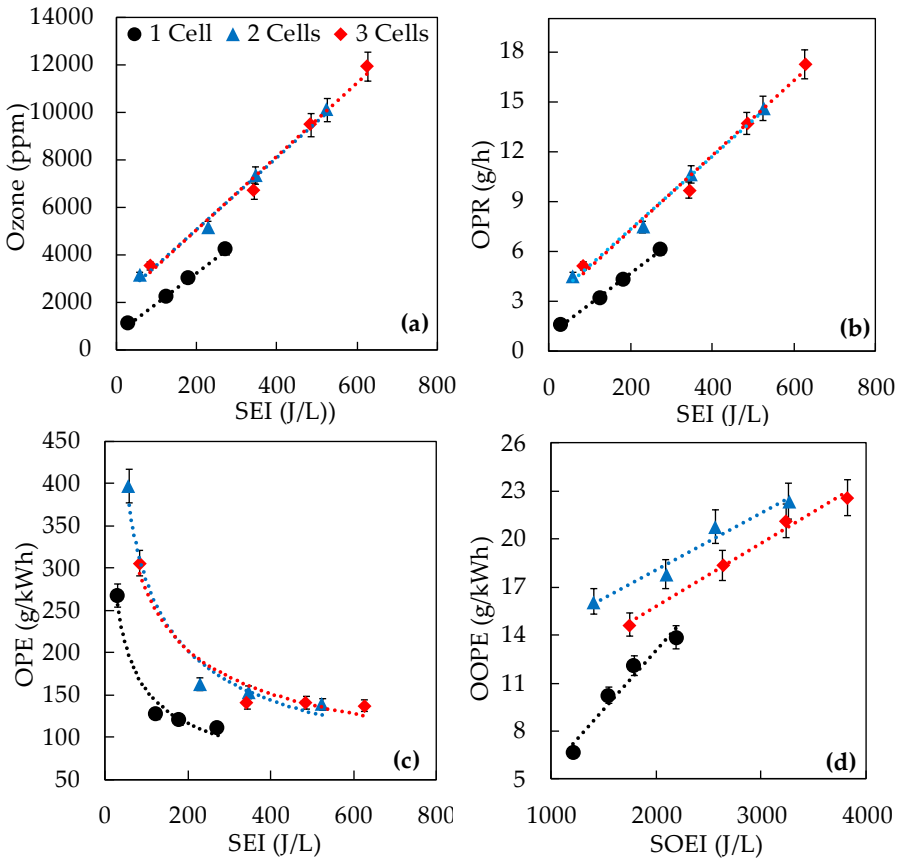

Figure 7. The Ozone production as a function of specific energy input, expressed in terms of (a) concentration (ppm), (b) ozone production rate (g/h), (c) ozone production efficiency based on discharge power (g/kwh), and (d) overall ozone production efficiency based on HVPS power (g/kwh).

The limits of the HVPS under various capacitive loads are presented in Figure 8, where each curve corresponds to a different load's capacitance. The shaded area indicated the discharge voltage and frequency

window utilised in this research, thereby additionally ensuring that all experimental operating points were located within stable supply conditions. The one-cell (471 pF), two-cell (998 pF), and three-cell (1219 pF) reactors' capacitances were all found in this region, demonstrating that the HVPS could drive each configuration at the given frequencies. Increasing the number of cells expanded the discharge volume and raised the energy input. However, this did not transfer into an improvement in ozone concentration, OPR, or OPE. In contrast, when efficiency is assessed from the perspective of the actual power drawn from the wall socket, the OOPE improved consistently with each additional cell.

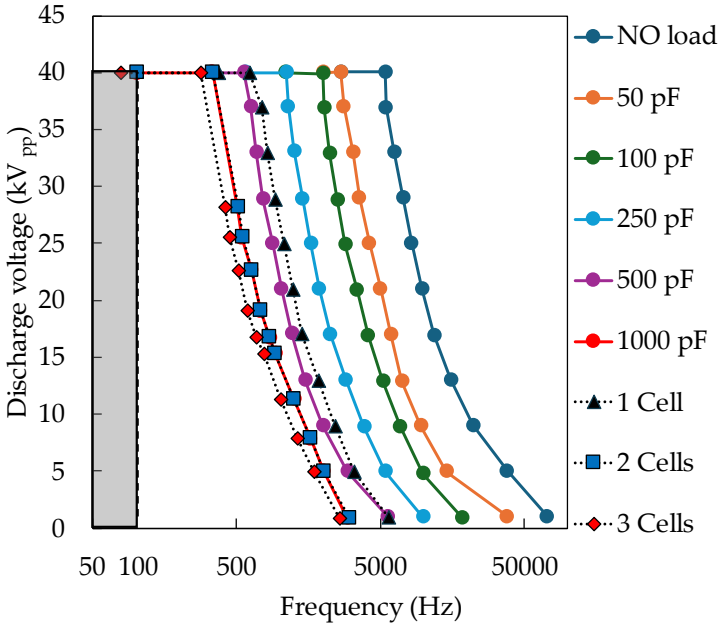

Figure 8. Operational frequency range of HVPS under different capacitive loads and DBD Cell Configurations (Adapted from Advanced Energy).

4. Conclusions

This research has demonstrated that scaling DBD reactors from one to three cells significantly enhances ozone generation by increasing the effective discharge volume and effective surface area. However, the merits of increasing reactor capacity were limited by the output capacity of the HVPS. The observed reduction of discharge voltage slope was restricted by the slew rate of the HVPS, while the broadened current pulses resulted from the current clipping function of the HVPS. Energy efficiency analysis revealed two complementary perspectives. OPE, referenced to discharge power, was highest at low SEI. On the other hand, OOPE, which accounts for HVPS performance, provided a more realistic measure of system efficiency and real ozone production cost. In this respect, the two-cell reactor achieved the most favourable balance between ozone yield and power utilisation, while the three-cell configuration was restricted by the limitations of the HVPS. In summary, ozone generation efficiency in DBD reactors was governed by both plasma processes and HVPS performance. While reactor scaling enhances ozone yield, system-level efficiency was maximised when the power supply could operate efficiently under the corresponding electrical load. These findings provided valuable guidance for developing energy-efficient ozone generators for practical applications in water treatment, air purification, and food sterilisation. Future work should focus on applying multi-cell DBD reactors in practical fields such as water and wastewater treatment, air purification, and food sterilisation, where high ozone yields are required. The results also provide valuable guidance for engineers who wish to scale up ozone generators for industrial applications, enabling more sustainable and energy-efficient processes.

5. Acknowledgements

The authors would like to thank the Research Centre for Combustion Technology and Alternative Energy (CTAE), King Mongkut's University of Technology North Bangkok, for providing access to research facilities and measurement equipment.

Author Contributions: Conceptualisation, P.C., K.T. and S.S.; methodology, P.C.; validation, P.C., K.T. and S.S.; formal analysis, P.C.; investigation, P.C.; resources, K.T. and S.S.; data curation, P.C.; writing—original draft preparation, P.C.; writing—review and editing, K.T. and S.S.; supervision, K.T. and S.S. All authors have read and agreed to the published version of the manuscript.

Funding: The authors gratefully acknowledge the financial support provided by the College of Industrial Technology, King Mongkut's University of Technology North Bangkok, under Contract No. CIT-2023-GRAD-29, which supported the author's scholarship.

Conflicts of Interest: The authors declare no conflict of interest

References

[1] Epelle, E. I.; Macfarlane, A.; Cusack, M.; Burns, A.; Okolie, J. A.; Mackay, W.; Rateb, M.; Yaseen, M. Ozone Application in Different Industries: A Review of Recent Developments. *Chem. Eng. J.* **2023**, *454*, 140188. https://doi.org/10.1016/j.cej.2022.140188

[2] Ghaitaoui, E. A.; Nassour, K.; Nemmich, S.; Oulad Naoui, B. E. K.; Ghaitaoui, T.; Tilmatine, A.; Ramdani, N. Experimental Comparative Study between Simple and Multi-Tube DBD Ozone Generator with Same Volume Discharge for Wastewater Treatment. *J. Korean Phys. Soc.* **2024**, *85*(10), 798–809. https://doi.org/10.1007/s40042-024-01179-4

[3] Chen, T.; Delgado, A. G.; Yavuz, B. M.; Proctor, A. J.; Maldonado, J.; Zuo, Y.; Westerhoff, P.; Krajmalnik-Brown, R.; Rittmann, B. E. Ozone Enhances Biodegradability of Heavy Hydrocarbons in Soil. *J. Environ. Eng. Sci.* **2016**, *11*(1), 7–17. https://doi.org/10.1680/jenes.16.00002

[4] Powell, A.; Scolding, J. W. S. Direct Application of Ozone in Aquaculture Systems. *Rev. Aquacult.* **2018**, *10*(2), 424–438. https://doi.org/10.1111/raq.12169

[5] Niveditha, A.; Pandiselvam, R.; Prasath, V. A.; Singh, S. K.; Gul, K.; Kothakota, A. Application of Cold Plasma and Ozone Technology for Decontamination of *Escherichia coli* in Foods: A Review. *Food Control* **2021**, *130*, 108338. https://doi.org/10.1016/j.foodcont.2021.108338

[6] Xue, W.; Macleod, J.; Blaxland, J. The Use of Ozone Technology to Control Microorganism Growth, Enhance Food Safety and Extend Shelf Life: A Promising Food Decontamination Technology. *Foods* **2023**, *12*(4), 814. https://doi.org/10.3390/foods12040814

[7] Sumaiyah, S.; Nugraha, R.; Suhartono, S.; Yulianto, E.; Fuskhah, E.; Al-Baarri, A. N.; Usman, A.; Nur, M. Analysis of Low Frequency on Dielectric Barrier Discharge Plasma Reactor for Ozone Production. *Trends Sci.* **2025**, *22*(4). https://doi.org/10.48048/tis.2025.9335

[8] Soyluoglu, M.; Williams, C. F.; Karanfil, T. Advancing Water Treatment: Ozone Nanobubbles for Geosmin and 2-Methylisoborneol Control. *Chem. Eng. J.* **2025**, *513*, 162892. https://doi.org/10.1016/j.cej.2025.162892

[9] Asilevi, P. J.; Boakye, P.; Oduro-Kwarteng, S.; Fei-Baffoe, B.; Sokama-Neuyam, Y. A. Indoor Air Quality Improvement and Purification by Atmospheric Pressure Non-Thermal Plasma (NTP). *Sci. Rep.* **2021**, *11*(1), 22830. https://doi.org/10.1038/s41598-021-02276-1

[10] Varga, L.; Szigeti, J. Use of Ozone in the Dairy Industry: A Review. *Int. J. Dairy Technol.* **2016**, *69*(2), 157–168. https://doi.org/10.1111/1471-0307.12302

[11] Joseph, C. G.; Farm, Y. Y.; Taufiq-Yap, Y. H.; Pang, C. K.; Nga, J. L. H.; Li Puma, G. Ozonation Treatment Processes for the Remediation of Detergent Wastewater: A Comprehensive Review. *J. Environ. Chem. Eng.* **2021**, *9*(5), 106099. https://doi.org/10.1016/j.jece.2021.106099

[12] Guzel-Seydim, Z. B.; Greene, A. K.; Seydim, A. C. Use of Ozone in the Food Industry. *LWT–Food Sci. Technol.* **2004**, *37* (4), 453–460. https://doi.org/10.1016/j.lwt.2003.10.014

[13] Fu, P.; Feng, J.; Yang, H.; Yang, T. Degradation of Sodium *n*-Butyl Xanthate by Vacuum UV–Ozone (VUV/O_3) in Comparison with Ozone and VUV Photolysis. *Process Saf. Environ. Prot.* **2016**, *102*, 64–70. https://doi.org/10.1016/j.psep.2016.02.010

[14] Cleland, M. R.; Galloway, R. A. Ozone Generation in Air during Electron Beam Processing. *Phys. Procedia* **2015**, *66*, 586–594. https://doi.org/10.1016/j.phpro.2015.05.078

[15] Zhu, Z.; Song, Q.; Jiang, L.; Yan, M.; Chen, S.; Duan, J. Perspective of Water Electrolysis to Ozone Production: Electrocatalyst Design and Development. *Mater. Horiz.* **2025**. https://doi.org/10.1039/D5MH01341K

[16] Feng, C.; Zheng, Y.; Zhang, R.; Tian, E.; Zou, X.; Liu, K. Characterizing the Pin-to-Ring Direct-Current Air Corona Discharge by Its Ultrasonic Signal and Ozone Production. *Appl. Acoust.* **2025**, *237*, 110738. https://doi.org/10.1016/j.apacoust.2025.110738

[17] Liu, P.; Song, Y.; Zhang, Z. A Novel Dielectric Barrier Discharge (DBD) Reactor with Streamer and Glow Corona Discharge for Improved Ozone Generation at Atmospheric Pressure. *Micromachines* **2021**, *12*(11), 1287. https://doi.org/10.3390/mi12111287

[18] Hyun-Ha, K.; Abdelaziz, A. A.; Yoshiyuki, T.; Tomohiro, N.; Dae-Young, K.; Brandenburg, R.; Schiorlin, M.; Hensel, K.; Young-Hoon, S.; Dae-Hoon, L.; Woo-Seok, K.; Akira, M. Revisiting Why DBDs Can Generate O_3 against the Thermodynamic Limit. *Int. J. Plasma Environ. Sci. Technol.* **2023**, *17*(2), 1–20.

[19] Li, S.; Dang, X.; Yu, X.; Abbas, G.; Zhang, Q.; Cao, L. The Application of Dielectric Barrier Discharge Non-Thermal Plasma in VOCs Abatement: A Review. *Chem. Eng. J.* **2020**, *388*, 124275. https://doi.org/10.1016/j.cej.2020.124275

[20] Sharma, M.; Alhashmialameer, D.; Ali, S. K.; Alzahrani, A.; Khan, M. S.; Sowjanya, M.; Rashid, M. S.; BaQais, A.; Khleefa, F. A.; Shariq, M. Enhancement of Ozone Production by Increasing Number Density of Plasma Channels in Volume DBD Using Ceramic Foam for Water Treatment and Industrial Applications. *J. Electrostat.* **2025**, *135*, 104088. https://doi.org/10.1016/j.elstat.2025.104088

[21] Xie, L.; Yuan, D.; Jin, C.; Xu, H.; Li, Y.; Wei, L.; Wu, W.; Ling, Z. Characteristics of Dielectric Barrier Discharge and Ozone Production in Synthetic Air. *Vacuum* **2024**, *226*, 113359. https://doi.org/10.1016/j.vacuum.2024.113359

[22] Sun, S.; Chen, Y.; Yuan, P.; Xu, L.; Zhang, Y.; Wei, L. Effect of Magnetic Field on Multi-Parameters of Needle–Plate DBD Ozone Generator. *Ozone: Sci. Eng.* **2022**, *44*(4), 384–397. https://doi.org/10.1080/01919512.2021.1960146

[23] Bang, S.; Snoeckx, R.; Cha, M. S. Temperature-Dependent Kinetics of Ozone Production in Oxygen Discharges. *Plasma Chem. Plasma Process.* **2023**, *43*(6), 1453–1472. https://doi.org/10.1007/s11090-023-10370-7

[24] Siriprom, W.; Teanchai, K.; Jitchot, N.; Chamchoi, N. The Comparison of Ozone Production with Oxygen Concentration and Feed Gas Flow Rate at Atmospheric Pressure. *Mater. Today Proc.* **2022**, *65*, 2336–2339. https://doi.org/10.1016/j.matpr.2022.05.225

[25] Huang, C.-L.; Liao, T.-Y.; He, Y.-T.; Lin, G.-J.; Lai, W.-H.; Chen, Y.-C.; Lin, K.-M. Characterization of OH Species in kHz Air/H_2O Atmospheric Pressure Dielectric Barrier Discharges. *Plasma Sources Sci. Technol.* **2024**, *33*(6). https://doi.org/10.1088/1361-6595/ad4ddd

[26] Petruci, J. F. d. S.; Barreto, D. N.; Dias, M. A.; Felix, E. P.; Cardoso, A. A. Analytical Methods Applied for Ozone Gas Detection: A Review. *TrAC Trends Anal. Chem.* **2022**, *149*, 116552. https://doi.org/10.1016/j.trac.2022.116552

[27] Han, P.; Mei, H.; Liu, D.; Zeng, N.; Tang, X.; Wang, Y.; Pan, Y. Calibrations of Low-Cost Air Pollution Monitoring Sensors for CO, NO_2, O_3, and SO_2. *Sensors* **2021**, *21*(1), 256. https://doi.org/10.3390/s21010256

[28] Guragain, R. P.; Baniya, H. B.; Pradhan, S. P.; Pandey, B. P.; Subedi, D. P. Influence of Plasma-Activated Water (PAW) on the Germination of Radish, Fenugreek, and Pea Seeds. *AIP Adv.* **2021**, *11*(12), 125214. https://doi.org/10.1063/5.0070800

[29] Tang, X.; Liang, T.; Zhou, Y.; Li, J.; Li, X.; Zhang, M. A Parameter Measurement Method for DBD-Type Ozone Generators Based on Data Fitting. *Measurement* **2025**, *256*, 118127. https://doi.org/10.1016/j.measurement.2025.118127

[30] Hegemann, D. Plasma Activation Mechanisms Governed by Specific Energy Input: Potential and Perspectives. *Plasma Process. Polym.* **2023**, *20*(5), e2300010. https://doi.org/10.1002/ppap.202300010

[31] Chen, Y.; Wang, Q.; Wang, Y. Analysis and Comparison of DBD Power Supplies with Different Control Methods. *IEEE Trans. Plasma Sci.* **2024**, *52*(5), 1747–1757. https://doi.org/10.1109/TPS.2024.3381748

[32] Kogelschatz, U. Dielectric-Barrier Discharges: Their History, Discharge Physics, and Industrial Applications. *Plasma Chem. Plasma Process.* **2003**, *23*(1), 1–46. https://doi.org/10.1023/A:1022470901385

[33] Shaban, M.; Merkert, N.; van Duin, A. C. T.; van Duin, D.; Weber, A. P. Advancing DBD Plasma Chemistry: Insights into Reactive Nitrogen Species Such as NO_2, N_2O_5, and N_2O Optimization and Species Reactivity through Experiments and MD Simulations. *Environ. Sci. Technol.* **2024**. https://doi.org/10.1021/acs.est.4c04894

[34] Yuan, D.; Wang, Z.; Ding, C.; He, Y.; Whiddon, R.; Cen, K. Ozone Production in Parallel Multichannel Dielectric Barrier Discharge from Oxygen and Air: The Influence of Gas Pressure. *J. Phys. D: Appl. Phys.* **2016**, *49*(45), 455203. https://doi.org/10.1088/0022-3727/49/45/455203

ASEAN
Journal of Scientific and Technological Reports
Online ISSN:2773-8752

Research article

Valorization of White Shrimp Shell Waste: Development of Chitosan-Based Pellet Feed for Enhanced Nile Tilapia (*Oreochromis niloticus*) Nutrition

Kanokkan Worawut[1*], Baramee Phungpis[1], and Pakin Noppawan[2, 3]

[1] Faculty of Natural Resources, Rajamangala University of Technology Isan Sakon Nakhon Campus, Sakon Nakhon, 47160, Thailand
[2] Faculty of Science, Mahasarakham University, Maha Sarakham, 44150, Thailand
[3] Sustainable Approaches for Materials, Agriculture, and Health Technology (SAMAHT) Research Unit, Mahasarakham University, Maha Sarakham, 44150, Thailand
* Correspondence: kanokkan_pom@hotmail.co.th; (Kanokkan Worawut)

Citation:
Worawut, K.; Phungpis, B.; Noppawan, P. Valorization of White Shrimp Shell Waste: Development of Chitosan-Based Pellet Feed for Enhanced Nile Tilapia (*Oreochromis niloticus*) Nutrition. *ASEAN J. Sci. Tech. Report.* **2026**, *29*(2), e260098. https://doi.org/10.55164/ajstr.v29i2.260098.

Article history:
Received: July 1, 2025
Revised: October 6, 2025
Accepted: October 18, 2025
Available online: January 20, 2026

Abstract: This study demonstrates the development and application of an eco-friendly Nile tilapia (*Oreochromis niloticus*) feed formulation incorporating chitosan extracted from white shrimp shells. The extraction process yielded purified chitosan through ultrasonic deproteinization, acid demineralization, and alkaline deacetylation, confirmed by FTIR spectrophotometry. Three experimental feed formulations containing varying chitosan levels (10%, 15%, and 20%) were prepared and evaluated through proximate analysis. Formula 2 (15% chitosan) was identified as optimal, meeting standard nutritional requirements for aquafeeds while maximizing protein content and minimizing ash levels. A 14-week growth trial using the optimal feed showed that tilapia exhibited healthy growth performance, with an average weight of 14.90 g, length of 10.05 cm, and a survival rate of 77.50%. Water quality parameters remained within acceptable ranges, confirming the environmental compatibility of the feed. These results align with previous findings that chitosan supplementation enhances feed conversion and growth in aquaculture species. This work underscores the value of converting shrimp shell waste into a functional feed additive, offering a sustainable solution for improving aquafeed quality and promoting circular economy practices in aquaculture. By integrating waste valorization and local feed production, this research contributes to safer, more sustainable fish farming while reducing reliance on chemical additives. The approach supports both environmental stewardship and community livelihood development in regions where aquaculture is an essential economic sector.

Keywords: Tilapia; chitosan; white shrimp; pellet feed

1. Introduction

Animal feed plays a vital role in supporting livestock health, growth, reproduction, and milk production. Typically sourced from plant and animal materials, these feeds provide varying nutritional profiles. In recent years, chemical additives have been widely incorporated into feed formulations to boost productivity. However, prolonged use of such additives can lead to harmful residues in animal products, posing significant risks to consumers. This has led to increased interest in natural, environmentally friendly alternatives that promote both animal health and consumer safety. One promising approach

involves utilizing naturally derived compounds to enhance feed efficiency and overall productivity. For example, the outer shells and heads of crustaceans, particularly shrimp, are commonly ground and added to animal feed. Beyond their nutritional value, shrimp shells offer greater potential due to their rich content of chitin and chitosan, two biopolymers with diverse functional applications. Chitin is a fibrous, structural carbohydrate structurally similar to cellulose, but distinguished by the presence of a nitrogen-containing acetylamino group (–$NHCOCH_3$) at the C-2 position of the glucose monomer, which gives it distinctive reactivity. The chemical formula of its monomer is $C_8H_{13}NO_5$. Chitosan, derived from chitin via alkaline deacetylation, is a copolymer consisting of anhydro-*N*-acetyl-D-glucosamine and anhydro-D-glucosamine (commonly known as glucosamine, $C_6H_{11}NO_4$). This process modifies the structure of chitin, especially the nitrogen-based functional groups. While chitosan is insoluble in water, it dissolves readily in organic acids. Its solutions are viscous, transparent, and exhibit non-Newtonian behavior. Chitosan can naturally form flexible, plastic-like films and be processed into various forms, including membranes, gels, beads, fibers, colloids, and coatings.

Thanks to its unique physicochemical and biological properties, biocompatibility, non-toxicity, and biodegradability, chitin and chitosan are regarded as safe and versatile materials. They are widely used in agriculture, food technology, water treatment, separation processes, medicine, pharmaceuticals, and cosmetics. Chitin is naturally found in shrimp shells, crab carapaces, squid pens, mollusk shells, and the cell walls of certain fungi [1]. Chitosan is a white, odorless biopolymer that is biodegradable and exhibits low toxicity, with an LD_{50} in rats of approximately 16 g/kg body weight, comparable to common table salt or sugar [2-4]. In aquaculture, chitosan has been applied in various roles, including water purification, flocculation of suspended solids, waste adsorption, and bacterial control [5, 6]. It has also been used to manage phytoplankton in aquaculture ponds [7], stimulate immune responses in aquatic species [8, 9], control drug and vaccine release [10], and enhance stress resistance and survival in post-larval white shrimp [11]. Given these beneficial properties, the present study aims to develop an eco-friendly aquafeed by chemically extracting chitosan from shrimp shells and incorporating it into a high-quality, sustainable feed formulation. This initiative also seeks to transfer knowledge to local aquaculture communities, supporting the development of environmentally responsible practices and sustainable livelihoods.

2. Materials and Methods

2.1 Extraction of chitin and chitosan from Pacific white shrimp shells

First, selected white shrimp shells are thoroughly washed with clean water and sun-dried for two days. Once completely dry, the shells, approximately 12 kilograms, are weighed and subjected to deproteinization to remove residual proteins. This is carried out by soaking the shells in water using an ultrasonic cleaner operating at 30 kHz and 80 °C for 12 hours. This step is repeated twice more to ensure complete deproteinization. After ultrasonic treatment, the shrimp shells are washed again, then sun-dried for an additional two days. The resulting shells should appear cleaner and lighter in color. The dried shells are then coarsely ground to increase their surface area for the subsequent chemical treatments that remove impurities and minerals. Next, the ground shrimp shells are soaked in a 4% hydrochloric acid (HCl) solution for four days to eliminate residual minerals and contaminants. After soaking, the shells are thoroughly washed with clean water and filtered through a fine cloth until the rinse water is neutral. The cleaned shells are then sun-dried for another two days, yielding approximately 7 kilograms of dried material. The dried shells (7 kg) are then finely ground using an electric blender to produce a light brownish powder known as purified chitin. The purified chitin is weighed to calculate the yield percentage using the following formula:

$$\text{Yield (\%)} = (\text{Final weight of ground shrimp shells} \times 100) / \text{Initial weight of shrimp shells}$$

To convert the purified chitin into chitosan, the chitin powder is stirred in a 40% sodium hydroxide (NaOH) solution using a heated magnetic stirrer at 100 °C for four hours. This step removes the *N*-acetyl groups through deacetylation. After heating, the mixture is allowed to cool to room temperature (approximately 30-40 °C) for 30-40 minutes, and the deacetylation step is repeated once more to ensure completeness. The resulting mixture is filtered to separate the solid product from the NaOH solution. The

solid chitosan is then soaked and rinsed repeatedly with clean water until a neutral pH is reached, followed by filtration through a sintered crucible to remove residual solution. Finally, the chitosan powder is air-dried in a well-ventilated area for two days, producing a light brown purified chitosan powder ready for use in Nile tilapia feed formulations.

2.2 Formulation of Nile tilapia feed using chitosan extracted from Pacific white shrimp shells

The study focused on developing and testing feed formulations for Nile tilapia using chitosan extracted from white shrimp shells. The prepared ingredients were thoroughly mixed in a designated container, and clean water was added to achieve the desired consistency, maintaining a water-to-feed ratio of 14 liters per 10 kilograms of feed mixture. The moistened mixture was then processed through an animal feed pelletizer. The resulting pellets were sun-dried outdoors for one day and subsequently packed in suitable storage bags for later use. Three experimental feed formulations were initially developed to identify the optimal chitosan-based feed for Nile tilapia. All three formulations contained the same base ingredients: fish meal, duck eggs, ground broken rice, soybean meal, brewer's grains, distillery by-products, rice bran, ground corn, lead tree leaves (*Leucaena leucocephala*), water hyacinth, vegetable oil, and chitosan derived from shrimp shells. The only difference among the three formulations was the proportion of chitosan relative to the total feed:

Formula 1: 10% chitosan, 90% other ingredients

Formula 2: 15% chitosan, 85% other ingredients
Formula 3: 20% chitosan, 80% other ingredients

All three formulations will undergo proximate analysis to determine their protein, fat, fiber, ash, and moisture contents. These results will then be compared to select the single most suitable formulation, which will be used in further studies to assess its impact on the growth performance of Nile tilapia.

2.3 Growth performance testing of Nile tilapia fed with experimental diets

Before the feeding trial began, Nile tilapia fingerlings were obtained from a private farm. The fish had an average total length of approximately 6 centimeters (measured from head to tail). To allow the fingerlings to acclimate to the experimental conditions, they were kept in a holding pond and fed a commercial pellet feed for seven days. After the acclimation period, the fish were randomly sampled to measure their initial length and weight. They were then stocked into experimental cement tanks measuring 100 × 100 centimeters, each filled with water to a depth of 30 centimeters, at a stocking density of 50 fish per tank. The fish were fed the experimental diets twice daily (morning and evening) at a feeding rate of 3% of their body weight per feeding. Tank maintenance involved weekly partial water changes by draining half of the old water and refilling with clean water to maintain the original water level. Aeration was provided throughout the trial to ensure adequate dissolved oxygen levels. Growth performance data, including fish length, body weight, and survival rate (%), were recorded regularly to evaluate the effects of the feed formulations on the growth of Nile tilapia.

2.4 Water quality monitoring during the growth performance study of Nile tilapia

Water quality parameters were monitored weekly using standard methods. The parameters measured included temperature (electrometric method) [12], pH (electrometric method) [12], dissolved oxygen (membrane-electrode method) [12], nitrate as nitrogen (colorimetric brucine method) [13], and phosphate as phosphorus (ascorbic acid method) [14].

2.5 Statistical analysis

Data were statistically analyzed using analysis of variance (ANOVA), and mean differences were compared using Duncan's Multiple Range Test (DMRT) with the aid of statistical software.

3. Results and Discussion

3.1 Extraction of chitosan from white shrimp shells using a chemical method

The extraction of chitosan from white shrimp shells begins with 12 kilograms of raw, unpurified shrimp shells as the starting material. In the initial step, chitin is extracted from the shells and obtained as a light brown powder (Figure 1). This chitin is then converted into chitosan through a deacetylation reaction,

which removes the *N*-acetyl groups from the chitin molecules, resulting in purified chitosan in the form of a light brown powder in 58.33 % yield (Figure 1). The chemical equation for the deacetylation of chitin is presented in Figure 2.

Figure 1. Chitin (left) and chitosan (right) purified from white shrimp shells after chemical extraction

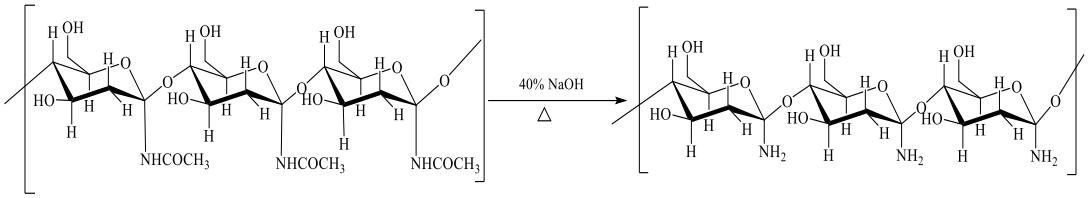

Figure 2. Deacetylation of chitin to chitosan using NaOH

3.2 Characterization of chitin and chitosan from white shrimp shells

The conversion of functional groups during the deacetylation of chitin was verified by confirming the transformation of *N*-acetyl groups into amino groups in chitosan. Functional group analysis was conducted using FTIR spectroscopy to characterize the chitin and chitosan extracted from white shrimp shells. The resulting spectra were compared with a standard chitosan reference. The FTIR spectra of chitin and chitosan from the shrimp shell samples are presented in Figures 3–5. As shown in Figure 3, the FTIR spectrum of chitin extracted from white shrimp shells exhibits a carbonyl (C=O) functional group characteristic of the amide molecule at a wavenumber of 1664 cm^{-1}. Additionally, an N–H bending vibration of the amide group appears around 1554 cm^{-1}. The FTIR spectrum for chitosan from the same shrimp shell sample is presented in Figure 4. Figure 4 shows that the FTIR spectrum of chitosan derived from white shrimp shells displays a similar pattern to that of chitin, with an N–H bending vibration of the amine group observed at approximately 1589 cm^{-1}. However, the C=O stretching vibration decreases significantly, confirming the success of the deacetylation process. This peak closely matches the spectrum of the standard chitosan shown in Figure 5.

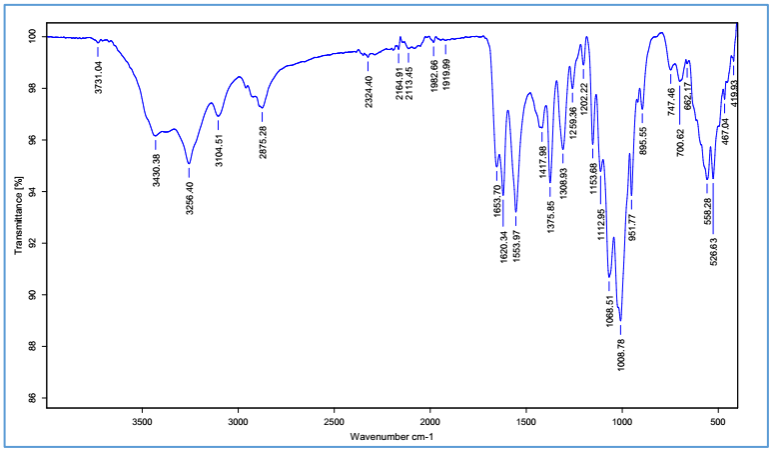

Figure 3. FTIR spectrum of chitin extracted from white shrimp shells

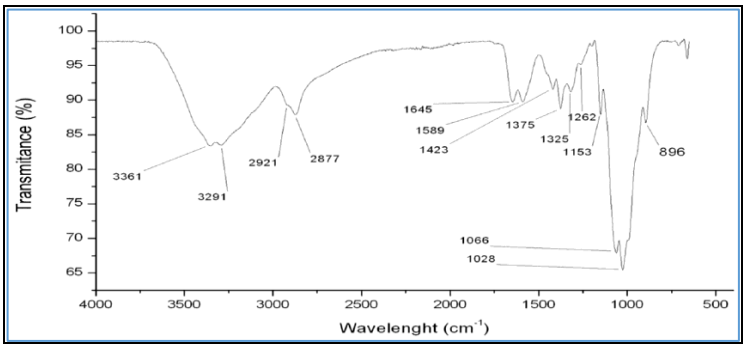

Figure 4. FTIR spectrum of chitosan extracted from white shrimp shells

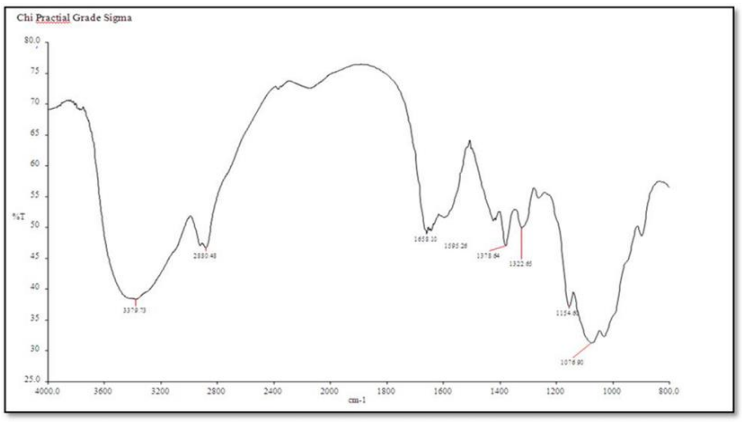

Figure 5. FTIR spectrum of standard chitosan

3.3 Identification of the optimal chitosan-based feed formulation from white shrimp shells

The optimal chitosan-based feed formulation for Nile tilapia includes the following ingredients: fish meal, duck eggs, ground broken rice, soybean meal, brewer's grains, distillery by-products, rice bran, ground corn, *Leucaena* leaves, water hyacinth, vegetable oil, and chitosan extracted from white shrimp shells. The experiment tested three variations of this base formula by adjusting the proportion of chitosan relative to the other feed components. The feed mixtures were as follows:

Formula 1: 10% chitosan and 90% other ingredients (fish meal, duck eggs, ground broken rice, soybean meal, brewer's grains, distillery by-products, rice bran, ground corn, *Leucaena* leaves, water hyacinth, and vegetable oil)

Formula 2: 15% chitosan and 85% other ingredients (same as above)

Formula 3: 20% chitosan and 80% other ingredients (same as above)

These three formulations were analyzed using a proximate analysis instrument to determine their protein, fat, fiber, moisture, and ash contents. The results are presented in Table 1.

Table 1. Standard requirements and proximate composition of the three chitosan-based feed formulations

Composition (%)	Standard Maximum	Standard Minimum	Formula 1	Formula 2	Formula 3
Protein	42	30	30.05	31.67	31.85
Fat	6	3	3.06	3.04	3.04
Fiber	6	5	4.60	5.07	5.04
Moisture	12	-	11.54	11.49	11.48
Ash	-	-	15.25	10.81	11.90

Note: The standard feed quality criteria are based on the Animal Feed Quality Control Act B.E. 2558 [15].

The results show that the protein content in Formulas 2 and 3 did not differ significantly and both fell within the standard range for aquafeeds [15]. Formula 1 had the lowest protein content at 30.05%. The fat content was similar across all three formulations. The fiber content was highest in Formula 2, followed by Formula 3 and then Formula 1. In contrast, the ash content was highest in Formula 1, followed by Formula 3, with Formula 2 having the lowest ash content. The moisture content was comparable across all three formulations. Based on the proximate analysis and in reference to the standard feed quality requirements, which specify minimum protein and fat levels and maximum fiber and moisture levels, Formula 2 was identified as the most suitable formulation. This feed will be used in further trials to evaluate its effects on the growth performance of Nile tilapia. The composition of the optimal chitosan-based feed formulation is as follows:

Fish meal — 10% by weight

Duck eggs — 10% by weight

Ground broken rice — 10% by weight

Soybean meal — 10% by weight

Brewer's grains — 5% by weight

Distillery by-products — 5% by weight

Rice bran — 10% by weight

Ground corn — 10% by weight

Leucaena leaves — 5% by weight

Water hyacinth — 5% by weight

Vegetable oil — 5% by weight

Chitosan from white shrimp shells — 15% by weight

3.4 Application of the optimal chitosan-based feed formulation from white shrimp shells to growth performance testing

3.4.1 Fish growth in terms of weight, length, and survival rate (%)

In this trial, Nile tilapia were fed the optimal chitosan-based feed formulation derived from white shrimp shells for a rearing period of 14 weeks. Throughout the experiment, all fish remained healthy, exhibited normal behavior, and showed no visible external deformities. Figure 6 presents the feed used and the general appearance of the fish at the end of the trial. By the conclusion of the experiment, the tilapia showed an average survival rate of 77.50% and demonstrated steady increases in both weight and length over time. The average final weight and length were 14.90 grams and 10.05 centimeters, respectively. Detailed results for fish weight and length are summarized in Table 2.

Figure 6. The experimental feed and the general appearance of the fish at the end of the trial

These findings are consistent with the reports by Wu (2020) and Rangkuti et al. (2025), who observed that tilapia fed chitosan-supplemented diets exhibited improved feed conversion ratios (FCR) and greater body weight compared to fish fed conventional diets. [16,17]. Similarly, Harikrishnana et al. (2012) reported that grouper (*Epinephelus bruneus*) fed chitosan-supplemented diets showed significantly better growth performance than those fed standard diets [18].

3.4.2 Water quality during the experiment

Water quality was monitored throughout the experiment, and the average values were as follows: pH 7.66, dissolved oxygen (DO) 4.11 mg/L, total phosphorus 1.18 mg/L, and nitrate-nitrogen 0.67 mg/L, as presented in Table 2.

Table 2. Growth performance and water quality parameters of Nile tilapia fed the optimal chitosan-based feed formulation

Week	Fish Weight (g)	Fish Length (cm)	pH	DO (mg/L)	Nitrate-Nitrogen (mg/L)	Total Phosphorus (mg/L)
1	6.66^{k}	6.05^{h}	8.62^{a}	3.63^{e}	0.00^{g}	0.00^{d}
2	7.62^{k}	6.69^{gh}	8.36^{b}	4.89^{a}	0.05^{fg}	0.51^{c}
3	9.08^{j}	7.69^{fgh}	7.81^{c}	3.66^{e}	0.44^{d}	0.80^{b}
4	10.17^{ij}	8.07^{fgh}	7.63^{cde}	3.70^{e}	0.45^{cd}	0.96^{b}
5	11.11^{i}	8.51^{fg}	7.50^{defg}	3.98^{cde}	0.26^{e}	1.33^{a}
6	12.62^{h}	9.11^{ef}	7.66^{cd}	4.88^{a}	0.15^{ef}	1.43^{a}
7	15.66^{g}	$9.96d^{ef}$	7.53^{defg}	3.70^{e}	0.44^{d}	1.51^{a}
8	16.94^{f}	11.02^{cde}	7.60^{def}	4.36^{b}	0.59^{c}	1.38^{a}
9	17.86^{ef}	11.87^{bcd}	7.41^{fg}	4.41^{b}	1.00^{b}	1.40^{a}
10	18.68^{de}	12.44^{abc}	7.46^{efg}	3.87^{de}	1.19^{a}	1.49^{a}
11	19.14^{cd}	13.30^{abc}	7.41^{fg}	4.29^{bc}	1.19^{a}	1.43^{a}
12	20.05^{bc}	13.70^{ab}	7.46^{efg}	3.89^{de}	1.21^{a}	1.46^{a}
13	20.86^{b}	14.07^{ab}	7.37^{g}	4.15^{bcd}	1.22^{a}	1.41^{a}
14	22.10^{a}	14.52^{a}	7.39^{g}	4.32^{bc}	1.24^{a}	1.48^{a}
Average	14.90	10.50	7.66	4.11	0.67	1.18
CV (%)	5.83	15.77	1.82	6.43	15.69	11.18

Note: Means in the same column with different superscript letters are significantly different at $P<0.01$.

The average pH values in the experimental tanks ranged from 7.37 to 8.62, which is within the optimal range for Nile tilapia growth. Generally, a pH range of 6.5-9.0 is considered suitable for aquaculture, allowing fish to maintain homeostasis without expending additional energy on osmoregulation [19]. If pH levels are too high or too low, they can stress or harm aquatic organisms. Specifically, pH values below 4.0 can be lethal; values between 4.0-6.0 may slow growth and disrupt reproduction; 6.5-9.0 is optimal; 9.0-11.0 is suboptimal for long-term survival; and levels above 11.0 are toxic [20,21]. The dissolved oxygen levels during the trial ranged from 3.63 to 4.89 mg/L, which is considered safe for tilapia. According to Abdel-Tawwab et al. (2014), the optimal DO range for Nile tilapia culture is 6.0-6.5 mg/L, but levels should not fall below 3.0 mg/L [22].

Insufficient DO can reduce respiration efficiency, growth, and metabolic function [23]. Nitrate-nitrogen levels ranged from 0.00 to 1.24 mg/L, and total phosphorus ranged from 0.00 to 1.48 mg/L, both of which are within safe limits for tilapia culture. Nitrate, as the final product of nitrification, should not accumulate beyond 50 mg/L; although not directly toxic at that threshold, high levels can stress fish and increase susceptibility to disease. Both nitrate and phosphorus are important nutrients for primary productivity in ponds and are not harmful at the levels observed.

4. Conclusions

This study successfully demonstrates the extraction, formulation, and application of an environmentally friendly tilapia feed enriched with chitosan derived from white shrimp shells. The optimized extraction process produced purified chitosan, confirmed by FTIR analysis, ensuring the functional integrity of the biopolymer for feed use. Among the three experimental formulations tested, the feed containing 15% chitosan (Formula 2) was identified as the most effective, meeting the required nutritional standards for protein, fat, fiber, and moisture content under the Animal Feed Quality Control Act B.E. 2558. When applied in a 14-week growth trial, the optimal chitosan-based feed supported healthy and consistent growth of Nile tilapia, with fish showing normal behavior, no visible deformities, and an acceptable survival rate of 77.50%. Importantly, the water quality parameters throughout the trial remained within safe and optimal ranges for aquaculture, indicating that the feed formulation does not adversely affect the culture environment. These findings are consistent with previous studies highlighting the benefits of chitosan in improving feed conversion efficiency and growth performance in various aquaculture species. Beyond demonstrating technical feasibility, this research emphasizes the significance of transforming crustacean shell waste, often discarded as an environmental pollutant, into a high-value, functional feed additive. This not only contributes to waste valorization and the circular bioeconomy but also offers practical benefits for small-scale farmers seeking cost-effective and safe alternatives to chemical feed additives. By integrating local waste resources into feed production, the approach strengthens the sustainability and self-reliance of rural aquaculture communities.

5. Acknowledgements

This research was completed thanks to the support and facilities provided by the Department of Fisheries, Faculty of Natural Resources, Rajamangala University of Technology Isan, Sakon Nakhon Campus. The research team would like to express their sincere gratitude for the use of laboratory facilities, experimental areas, and all the assistance extended throughout the course of this study.

Author Contributions: Conceptualization, K.W.; methodology, K.W.; writing—original draft preparation, K.W.; writing—review and editing, K.W., P.N. and B.P. All authors have read and agreed to the published version of the manuscript.

Funding: This research received no external funding.

Conflicts of Interest: The authors declare no conflict of interest.

References

[1] Hoffmann, K.; Gabriele, D.; Marina, K.; Werner-Michael, K.; Heike, M.; Bernward, B.; Friedhelm, M. Genetic Improvement of *Bacillus licheniformis* Strains for Efficient Deproteinization of Shrimp Shells and Production of High-Molecular-Mass Chitin and Chitosan. *Appl. Environ. Microbiol.* **2010**, *76*, 8211–8221. https://doi.org/10.1128/AEM.01404-10

[2] van der Lubben, I. M.; Verhoef, J. C.; Borchard, G.; Junginger, H. E. Chitosan and Its Derivatives in Mucosal Drug and Vaccine Delivery. *J. Pharm. Sci.* **2001**, *90*, 207–214. https://doi.org/10.1016/S0928-0987(01)00172-5

[3] Qurashi, M. T.; Blair, H. S.; Allen, S. J. Studies on Modified Chitosan Membrane. II. Dialysis of Low Molecular Weight Metabolites. *J. Appl. Polym. Sci.* **1992**, *46*, 263–269. https://doi.org/10.1002/app.1992.070460207

[4] Singh, D. K.; Ray, A. R. Graft Copolymerization of 2-Hydroxyethyl Methacrylate onto Chitosan Films and Their Blood Compatibility. *J. Appl. Polym. Sci.* **1994**, *53*, 1115–1121. https://doi.org/10.1002/app.1994.070530814

[5] Chung, Y.-C.; Li, Y.-H.; Chen, C.-C. Pollutant Removal from Aquaculture Wastewater Using the Biopolymer Chitosan at Different Molecular Weights. *J. Environ. Sci. Health A* **2005**, *40*, 1775–1790. https://doi.org/10.1081/ESE-200068058

[6] Huang, C.; Chen, S.; Pan, J. R. Optimal Condition for Modification of Chitosan: A Biopolymer for Coagulation of Colloidal Particles. *Water Res.* **2000**, *34*, 1057–1062. https://doi.org/10.1016/S0043-1354(99)00211-0

[7] Lertsutthiwong, P.; Sutti, S.; Powtongsook, S. Optimization of Chitosan Flocculation for Phytoplankton Removal in Shrimp Culture Ponds. *Aquacult. Eng.* **2009**, *41*, 188–193. https://doi.org/10.1016/j.aquaeng.2009.07.006

[8] Dautremepuits, C.; Betoulle, S.; Paris-Palacios, S.; Vernet, G. Immunology-Related Perturbations Induced by Copper and Chitosan in Carp (*Cyprinus carpio* L.). *Arch. Environ. Contam. Toxicol.* **2004**, *47*, 370–378. https://doi.org/10.1007/s00244-004-3115-0

[9] Kumar, S. R.; Ahmed, V. P. I.; Parameswaran, V.; Sudhakaran, R.; Babu, V. S.; Hameed, A. S. S. Potential Use of Chitosan Nanoparticles for Oral Delivery of DNA Vaccine in Asian Sea Bass (*Lates calcarifer*) to Protect from *Vibrio (Listonella anguillarum)*. *Fish Shellfish Immunol.* **2008**, *25*, 47–56. https://doi.org/10.1016/j.fsi.2007.12.004

[10] Polk, A.; Amsden, B.; Scarlett, D.; Gonzalez, A.; Okonmafe, O.; Goosen, M. Oral Delivery in Aquaculture: Controlled Release of Proteins from Chitosan–Alginate Microcapsules. *Aquacult. Eng.* **1994**, *13*, 311–323. https://doi.org/10.1016/0144-8609(94)90018-3

[11] Niu, J.; Liu, Y. J.; Lin, H. Z.; Mai, K. S.; Yang, H. J.; Liang, G. Y.; Tian, L. X. Effects of Dietary Chitosan on Growth, Survival, and Stress Tolerance of Postlarval Shrimp, *Litopenaeus vannamei*. *Aquac. Nutr.* **2011**, *17*, 406–412. https://doi.org/10.1111/j.1365-2095.2010.00775.x

[12] APHA. *Standard Methods for the Examination of Water and Wastewater*, 20th ed.; American Public Health Association: Washington, DC, 1998; pp 1–1325.

[13] USEPA. *Method 352.1: Nitrogen, Nitrate (Colorimetric, Brucine) by Spectrophotometer*; United States Environmental Protection Agency: Washington, DC, **1971**; pp 11–15.

[14] APHA. *Standard Methods for the Examination of Water and Wastewater*, 18th ed.; American Public Health Association: Washington, DC, **1992**; pp 1–1100.

[15] Somsueb, P. Aquafeed Analysis for Monitoring and Feed Quality Control. *E-Thai Fish. Gaz.* **2021**, *4*, 102–128.

[16] Wu, S. Growth Performance, Body Composition, and Nonspecific Immunity of Tilapia (*Oreochromis niloticus*) Affected by Chitosan. *Int. J. Biol. Macromol.* **2020**, *145*, 682–685. https://doi.org/10.1016/j.ijbiomac.2019.12.235

[17] Rangkuti, P.; Suharman, I.; Siagian, D. R. Effect of Chitosan Extracted from Vannamei Shrimp (*Litopenaeus vannamei*) Shells in Feed on the Growth Performance and Digestibility of Nile Tilapia (*Oreochromis niloticus*). *J. Nat. Indones.* **2025**, *23*, 1–9. https://doi.org/10.31258/jnat.23.1.1-9

[18] Harikrishnan, R.; Kim, J. S.; Balasundaram, C.; Heo, M.-S. Immunomodulatory Effects of Chitin and Chitosan-Enriched Diets in *Epinephelus bruneus* against *Vibrio alginolyticus* Infection. *Aquaculture* **2012**, *326–329*, 46–52. https://doi.org/10.1016/j.aquaculture.2011.11.034

[19] El-Sherif, M. S.; El-Feky, A. M. I. Performance of Nile Tilapia (*Oreochromis niloticus*) Fingerlings. I. Effect of pH. *Int. J. Agric. Biol.* **2009**, *11*, 297–300.

[20] Boyd, C. E. *Water Quality in Warmwater Fish Ponds*; Auburn University, Agricultural Experiment Station: Auburn, AL, **1979**; p 359.

[21] Boyd, C. E. *Water Quality in Ponds for Aquaculture*; Auburn University, Agricultural Experiment Station: Auburn, AL, **1990;** p 482.

[22] Abdel-Tawwab, M.; Hagras, A. E.; Elbaghdady, H. A. M.; Monier, M. N. Dissolved Oxygen Level and Stocking Density Effects on Growth, Feed Utilization, Physiology, and Innate Immunity of Nile Tilapia, *Oreochromis niloticus*. *J. Appl. Aquac.* **2014**, *26*, 340–355. https://doi.org/10.1080/10454438.2014.959830

[23] Tsadik, G.; Kutty, M. Influence of Ambient Oxygen on Feeding and Growth of the Tilapia *Oreochromis niloticus* (Linnaeus). Port Harcourt, Nigeria, **1987**.

ASEAN
Journal of Scientific and Technological Reports
Online ISSN:2773-8752

Research article

Rapid Identification of Orange Juice Adulteration Using Voltammetric Profiling and Machine Learning

Nguyen Duc Thanh[1, 4], Nguyen Manh Son[1], Nguyen Duc Phong[1], Pham Huu Vang[1], Ninh Duc Ha[2] , Nguyen Thi Van Anh[3], Le Thi Hong Hao[1, 5], Nguyen Manh Ha[1], Nguyen Thi Kim Thuong[1], and Ta Thi Thao[1*]

[1] University of Science, Vietnam National University - Hanoi, Hanoi, Vietnam
[2] Institue of Chemistry and Materials, Academy of Military Science and Technology, Vietnam
[3] Vietnam University of Traditional Medicine and Pharmacy, Hanoi, Vietnam
[4] Vietnam Military Medical University, Hanoi, Vietnam
[5] National Institute for Food Control, Hanoi, Vietnam
[*] Corresponding author: tathithao@hus.edu.vn

Citation:
Thanh, D.N.; Son, M.N.; Phong, D.N.; Vang, H.P.; Ha, D.N.; Anh, V.T.N.; Hao, H.T.; Ha, M.N.; Thuong, K.T.N.; Thao, T.T. Rapid identification of orange juice adulteration using voltammetric profiling and machine learning *ASEAN J. Sci. Tech. Report.* **2026**, *29*(2), e260129. https://doi.org/10.55164/ajstr.v29i2.260129.

Article history:
Received: July 3, 2025
Revised: October 12, 2025
Accepted: October 18, 2025
Available online: January 21, 2026

Abstract: In this study, the differential pulse voltammetry with a gold electrode and machine learning was employed to detect adulteration in orange juices. The method assessed both natural and commercial juices, along with their mixtures containing known proportions of natural juice. Initially, an unsupervised machine learning algorithm, Cluster Analysis (CA), was used to highlight differences, demonstrating the ability to distinguish between natural and flavored orange juices. Subsequently, supervised machine learning methods, including Interval Partial Least Squares – Linear Discriminant Analysis (iPLS-LDA) and Interval Partial Least Squares – Random Forest (iPLS-RF), were applied for classification purposes. The RF model achieved up to 95% classification accuracy, greatly exceeding 67.5% of iPLS- LDA. This enables reliable detection of orange juice adulteration. The RF model struggled to accurately distinguish between the "Natural" and "Mixed" categories, particularly for samples containing a medium proportion of natural orange juice (around 45–50%). The integration of voltammetric fingerprints with machine learning enabled a fast, cost-effective classification method for on-site analysis with portable sensors. This approach proved more efficient than other complex analytical techniques.

Keywords: Voltammetry; machine learning; orange juice adulteration; Interval Partial Least Squares (iPLS); Linear Discriminant Analysis (LDA);

1. Introduction

In the food industry, classifying and controlling the quality of agricultural products, especially fruits, is essential for maintaining standards and protecting consumer health. Among these fruits, oranges are highly valued for their rich content of vitamins, fiber, and antioxidants. However, due to their popularity, fresh orange juice products are frequently targeted for adulteration with chemical flavorings [1], leading to counterfeit products [2, 3] and commercial fraud involving natural orange juice. Recent advancements in machine learning have greatly improved the processing of large datasets, enabling rapid chemical analysis of various products. This has enhanced adulteration detection and geographical indication verification with high sensitivity and accuracy. As a result, machine learning has become a valuable tool in safeguarding food integrity and ensuring the authenticity of agricultural and food products [4, 5]. To

identify and classify analytical samples, two basic approaches are commonly employed: i) Targeted analysis: This method utilizes datasets containing the concentrations of specific compounds in multiple samples. Certain compounds serve as markers to assess authenticity and classify products. For example, polyphenol content can help detect adulteration in different types of orange juice [6, 7], while flavonoid content can distinguish grapefruit juice from other citrus juices [8] or differentiate concentrated and non-concentrated orange juices with high accuracy [9]. However, targeted analysis requires high analytical costs, as managing multiple parameters across samples demands significant resources. ii) Non-targeted analysis: This approach considers the entire dataset, including all measured signals, without identifying specific compounds. Spectroscopic techniques such as UV-VIS, NIR [11], Raman [10], and NMR [12] have been effective in providing data for statistical analysis, enabling the detection and quantification of adulteration in orange and grapefruit juices [10].

Machine learning algorithms enhance classification accuracy in non-targeted analysis. Unsupervised methods like Principal Component Analysis (PCA), Support Vector Machines (SVM), Data-Driven SIMCA, and soft-PLS-DA outperform traditional PLS-DA. Additionally, algorithms such as logistic regression, PCA, SVM, and Artificial Neural Networks (ANN) have proven effective in handling high-dimensional and complex analytical data. These techniques not only aid in identifying characteristic chemical markers but also optimize classification through highly accurate predictive models [14, 15]. Recently, the integration of multivariate analysis (chemometrics) with electrochemical analysis has offered outstanding advantages, including high sensitivity and selectivity, rapid analysis time, effective data processing, and the ability to eliminate background noise [16]. This approach enables not only the simultaneous quantification of organic acids [17] or polyphenols [18] in fruit juices (e.g., orange, lemon, and others) but also the classification of fruits with an accuracy exceeding 90% [18].

This study aims to assess the feasibility of the voltammetric method with a gold electrode for analyzing natural and commercial orange juice. It focuses on different orange varieties and mixtures of natural and commercial juices. Data from voltammograms (current intensity vs. potential matrices) are combined with machine learning to develop models for classifying natural and commercial orange juice and predicting adulteration ratios. This approach not only enhances the accuracy of food fraud detection but also opens up broader application potential in the food industry.

2.1 Reagents, Reference, and Standard Solutions

Hydrochloric acid (HCl, 37%) was procured from Sigma Aldrich (Singapore). Methanol (Merck, Germany) was utilized for preparing standard solutions, while Milli-Q water used for dilutions was obtained from a Milli-Q water system (Merck, Germany).

2.2 Sampling and sample preparation

All orange samples belonged to the *Citrus sinensis* variety and were collected from various regions of Vietnam. A total of 80 samples were sourced from 8 provinces: Hoa Binh, Ha Giang, Ben Tre, Vinh Long, Nghe An, Bac Giang, Hung Yen, and Quang Ninh. Each fruit was cut and juiced. Additionally, 50 commercial orange juice samples were collected from supermarkets in Hanoi, Vietnam. These samples included bottled or canned juices from brands such as Mirinda, Fanta, TH, Splash. For the adulteration study, two samples of pure natural orange juice were mixed with commercial orange juice at nine different adulteration levels: 10%, 20%, 30%, 40%, 50%, 60%, 70%, 80%, and 90% natural orange juice. Each adulteration level was prepared in triplicate. A total of 54 blended samples was synthesis. Additionally, there is one sample of difference that was mixed (the other orange juice sample was mixed with a commercial sample at 10, 40, 60, and 90%) and added to the data. The sample preparation was simple, starting with centrifugation of the juices for 10 minutes at 13,500 rpm. After that, a 1:4 dilution with 0.1 M HCl was performed to reach a pH of about 1.2. Each sample was prepared in triplicate. The samples were freshly prepared and measured immediately without storage.

2.3 Data Acquisition

Electrochemical measurements were conducted using the 797 VA Computrace instrument (Metrohm, Switzerland). This instrument, controlled by VA Computrace software, consisted of a complete measurement system, including a gold working electrode, an Ag/AgCl reference electrode, and a platinum auxiliary

electrode. For each sample, a 100 μL droplet was used as the sample volume. Differential pulse voltammetry (DPV) was employed to record voltammograms under the following experimental conditions: Scan range: -0.2 V to +1.2 V (vs. Ag/AgCl); Pulse amplitude: 50 mV; Step potential: 5 mV; Scan rate: 10 mV/s. The raw data matrices (I-E) extracted from Voltammograms of samples under the conditions

2.4 Data Analysis

To perform an exploratory analysis of the data, Cluster Analysis (CA) was employed. Raw data from all samples were utilized, and the mean value of the three replicates for each sample was calculated and used in the analysis. To assess the effectiveness of the methodology, confusion matrices were generated, and performance metrics such as accuracy were determined. Accuracy was calculated as the ratio of correctly classified samples to the total number of samples, providing a clear measure of the model's classification performance.

2.5 Methods

2.5.1 Cosine similarity

$$\cos(\theta) = \frac{x \cdot y}{\|x\| \, \|y\|}$$

Where x and y are vectors for which the similarity is to be computed.

2.5.2 SNV

To standardize the spectral data, each spectrum x = (x1, x2,…,xk) is first centered by removing its mean, and then scaled using the standard deviation. This process results in a normalized vector z = (z1, z2,…, z k) where the data have zero mean and unit variance, facilitating comparison across different spectra.

$$z_i = \frac{x_i - \bar{x}}{\sqrt{\sum_j^k (x_i - \bar{x})^2 / k}}$$

The data is standardized using the SNV (Standard Normal Variate) method to remove variations caused by scattering effects and correct baseline shifts. After standardization, the data is further processed using the Savitzky-Golay filter with a window length of 15, a polynomial order of 3, and a second derivative calculation. This step smooths the data, reduces noise, and enhances important spectral features for subsequent analysis.

2.5.3 iPLS.

The data X (p features) is divided into n intervals, and a local PLS model is built for each interval to select the best interval. In PLS regression, similar to PCR, we aim to find components z that are linear combinations of the inputs; however, unlike PCR, PLS seeks components that not only represent the predictors x well but also serve as strong predictors of the response y y, under the assumption that both X and y can be explained by a smaller set of components Z with k < p.

$$X = ZV^T + E$$

2.5.4 Random Forest

Random Forest is an ensemble learning method that builds multiple decision trees using bootstrap samples and random feature subsets at each split, which increases diversity and reduces correlation among trees. For regression, the final output is the average of predictions from all trees, while for classification, majority voting is used.

$$y = \frac{1}{T} \sum_{t=1}^{T} h_t(x)$$

where ht is the predicted value of the t-th tree for the input x, and T is the total number of trees

3. Results and discussion

3.1 Electrochemical Fingerprint of Orange Juices

The voltammetric results of 198 orange juice samples are shown in Fig. 1 (A, B, C). The signal intensity (I) is clearly observed in the range of potential (V) from 0.8 to 1.2 V (versus Ag/AgCl electrode), with intensity of peak currents reaching a maximum between 0.04 mA and 0.6 mA. Some blended samples of natural and artificial orange juice exhibited lower peak maxima, ranging from 0.02 mA to 0.04 mA. However, most signals showed slight differences depending on the geographical origin of the samples and were quite similar to those of natural and commercial samples. This resemblance in peak shapes and minimal variations in peak heights made visual classification impractical. Even within the same category, whether natural or artificial, there were significant variations in peak maxima, which could introduce considerable noise into classification models. Therefore, signal preprocessing is essential before performing discrimination and classification.

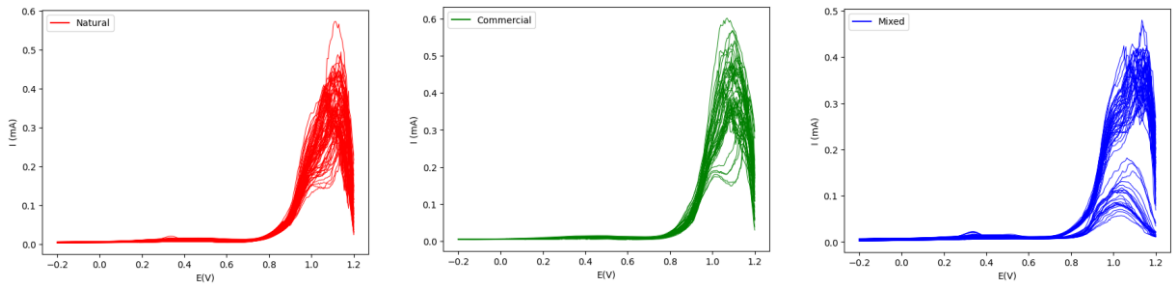

A B C

Figure 1. Voltammograms of orange juice (A- natural samples; B- commercial samples, and C- blended samples) (sửa lại trục tung)

The Standard Normal Variate (SNV) algorithm was used to normalize the data, followed by second-order derivation and smoothing using the Savitsky-Golay algorithm. The preprocessed voltammograms are shown in Figure 2. These preprocessing algorithms significantly reduced background noise, including sample background noise and noise caused by the equipment and experimental environment. Additionally, the second-order derivation enhanced the signal differences between samples. These results contributed to the stability and objectivity of classification models, thereby improving the classification performance of the models. After preprocessing, the entire voltammetric dataset was randomly split into 158 samples (80%) for the training and 40 samples (20% remaining) for testing to perform machine learning methods. The dataset was first preprocessed using Standard Normal Variate (SNV) to correct for scattering effects and variations in sample thickness. Subsequently, the SNV-corrected spectra were smoothed and differentiated using the Savitzky–Golay filter with a 15-point window, a third-order polynomial, and calculation of the second derivative, to enhance subtle spectral features while reducing noise.

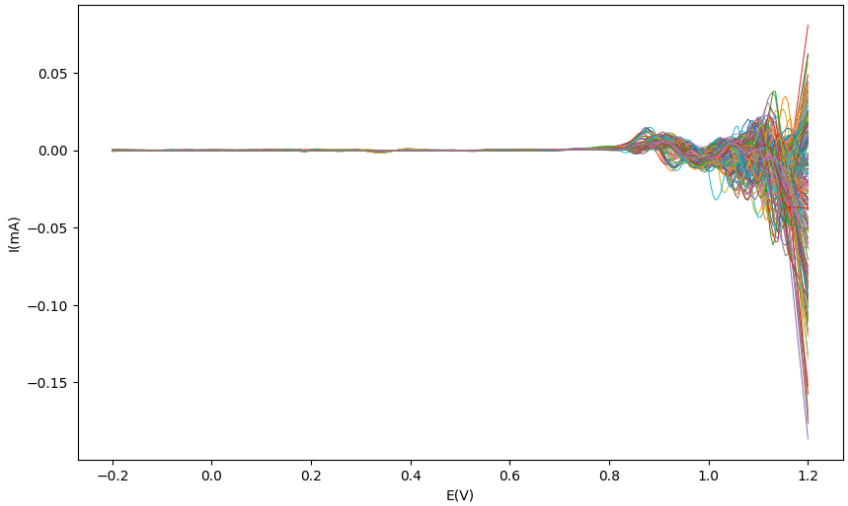

Figure 2. Voltammograms of orange juice after normalization using the SNV algorithm, second-order derivation, and smoothing with the Savitzky-Golay algorithm.

3.2. Identification and authentication of orange juice

Figure 3 illustrates the results of hierarchical clustering analysis (HCA) performed on the entire dataset of preprocessing with SNV using cosine similarity. Cosine similarity was selected as the distance metric for hierarchical clustering because it emphasizes the similarity of signal patterns rather than absolute intensity. In voltammetric data, current intensity may vary due to sample preparation, dilution, or instrumental noise, while the overall shape of the voltammogram remains characteristic of the sample type. The dendrogram shows that, even with unsupervised methods, it is possible to distinguish three data clusters: natural orange juice, commercial orange juice, and mixed orange juice (Table 1).

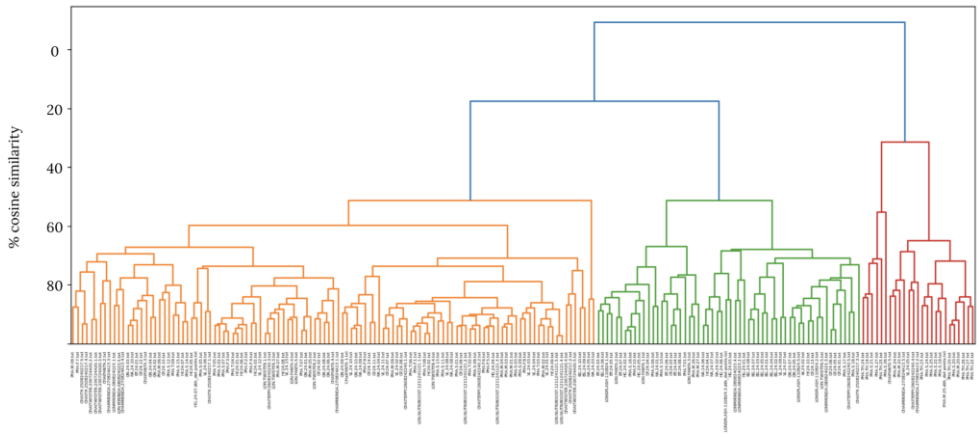

Figure 3. Hierarchical clustering using cosine similarity

The results indicate that 80% of the mixed juice samples belong to the first group, while 62% of the natural orange juice samples appear in the second group. However, in the third cluster, the distribution of samples across the three categories does not show a clear distinction. Thus, unsupervised algorithms reveal a clear difference between the blended orange juice and natural orange juice groups, providing a foundation for using supervised machine learning models for classification.

Table 1. Percentage of each sample type in each group classified.

Sample Cluster	Mixed	Commercial	Natural
1	80%	16%	4%
2	16%	22%	62%
3	33%	27%	40%

3.3 Supervised learning for the detection of orange juice adulteration

After second-order derivation, the dataset showed a relatively large number of features (284 features obtained), requiring dimensionality reduction. Therefore, the iPLS algorithm was applied to the training dataset to reduce the number of features for building machine learning models. The iPLS algorithm selects the most relevant spectral regions with strong discriminatory power, eliminating noisy or low-information regions, which helps prevent overfitting and enhances model accuracy. The results of the features retained by the iPLS algorithm are displayed in Fig. 4. Among these, 205 features, which do not have good classification potential (highlighted in pink in the figure), were removed, leaving 79 features with the best potential for classification. The test dataset will also use these 79 features for accuracy evaluation.

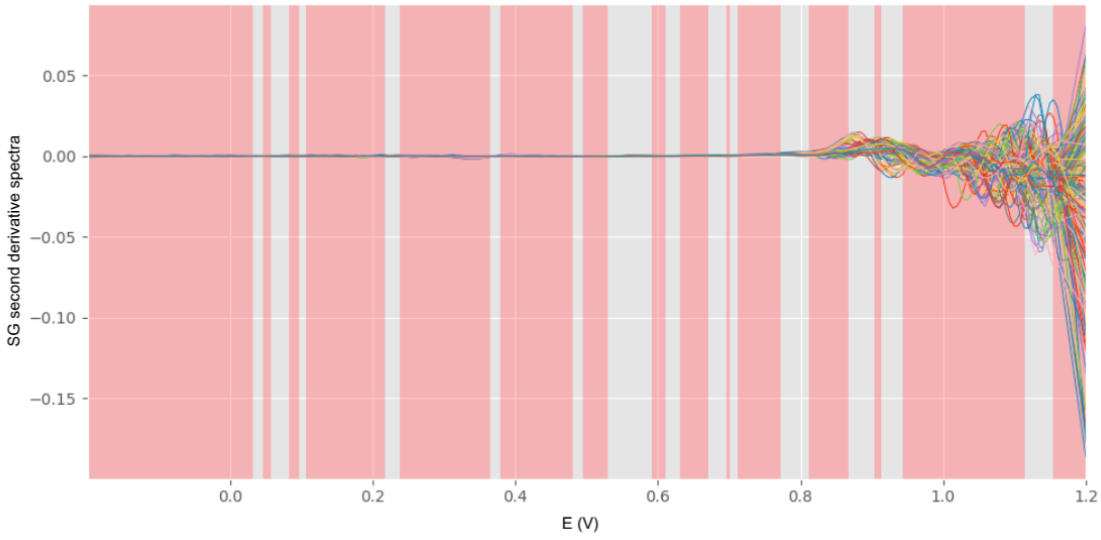

Figure 4. Features selected by the iPLS algorithm

In model selection, factors such as linearity, accuracy, label differentiation (especially between natural and commercial juices), and performance on small datasets were considered. Typically, PLS-DA, Random Forest, Support Vector Machine (SVM), and Artificial Neural Network (ANN) with hyperparameter optimization using GridSearchCV are preferred for classification. However, both ANN and SVM initially achieved only 75% prediction accuracy, making them unsuitable for this study. Additionally, the small dataset restricted the ANN's ability to capture information, while SVM strongly misclassified between natural and commercial orange juices, further reducing its applicability. Therefore, this study only focuses on two models: iPLS-LDA and Random Forest.

3.3.1 iPLS-LDA

The iPLS algorithm was applied for dimensionality reduction using a 158×79 training dataset, consisting of 158 samples classified into three groups (natural, commercial, and blended orange juice) with 79 features extracted from the raw data. An LDA model was then built to classify these groups, but some blended orange juice samples were misclassified as either natural or commercial juice. Linear separation was not achieved due to overlap between the natural and blended orange juice groups. A deeper evaluation of the percentage of natural orange juice in the samples is shown in Fig.5, with the sample colors gradually transitioning from white to dark, representing an increasing proportion of natural orange juice. The triangle markers represent samples from the training dataset, while the circular markers represent samples from the

test dataset. The results indicate that the LDA model struggles to differentiate between natural and blended samples. This suggests that the compounds in natural orange juice may be masking the signals, making classification more challenging.

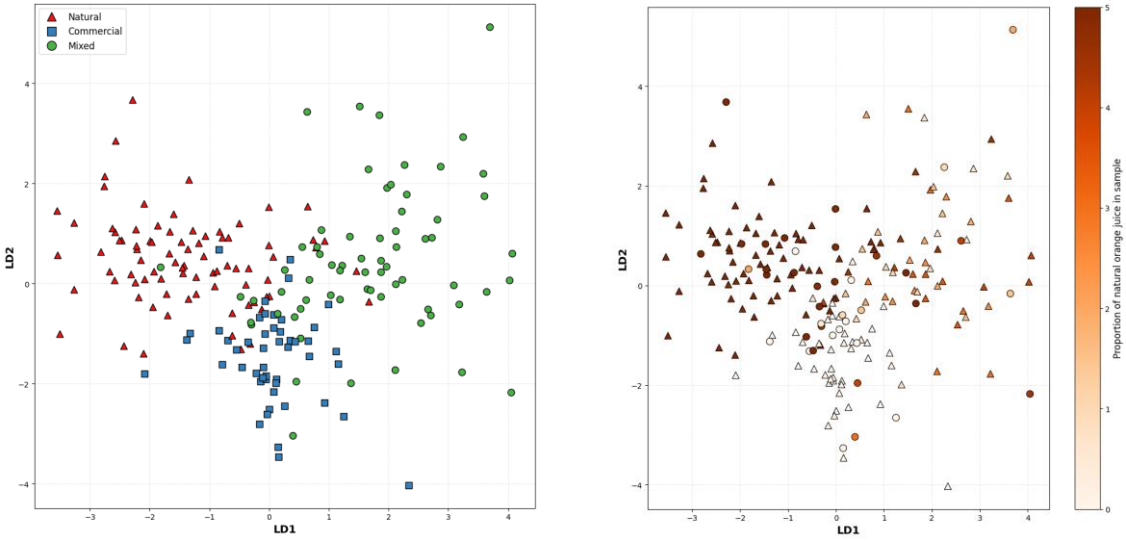

A B

Figure 5. LDA plot of training dataset and test dataset projected onto LDA model space according to: A- corresponding labels and B- the proportion of natural orange juice in each sample.

Based on Fig. 5A, it can be observed that when the training and testing datasets are projected onto the LDA space according to their corresponding labels, there is a significant overlap between the clusters of the "Mixed" and "Commercial" labels. This explains why certain samples are misclassified into the "Mixed" group. This phenomenon reflects the characteristic similarity between commercial and mixed juice samples, especially when the proportion of natural orange juice in these products fluctuates, making it challenging for the model to distinguish between them. Additionally, Fig. 5B provides further insights as the samples are projected onto the LDA space based on the proportion of natural orange juice. It reveals that samples with natural orange juice proportions near the threshold between "Mixed" and "Natural" or "Commercial" are prone to misclassification. Moreover, this issue may stem from the insufficiently strong boundaries between clusters in the LDA space, which fail to fully capture the differences in natural orange juice proportions among the groups.

3.3.2 iPLS- RF

Using the test dataset, the iPLS-RF model achieved 95% classification accuracy, demonstrating a significant improvement over the LDA algorithm (67.5%) (Fig. 6). Based on the iPLS-RF model, only one natural sample was misclassified as a blended one, and one blended sample was predicted as a natural one. No confusion occurred between the blended and commercial groups, highlighting the superior potential of the RF algorithm and, more broadly, ensemble learning methods in classifying objects based on selected spectral features.

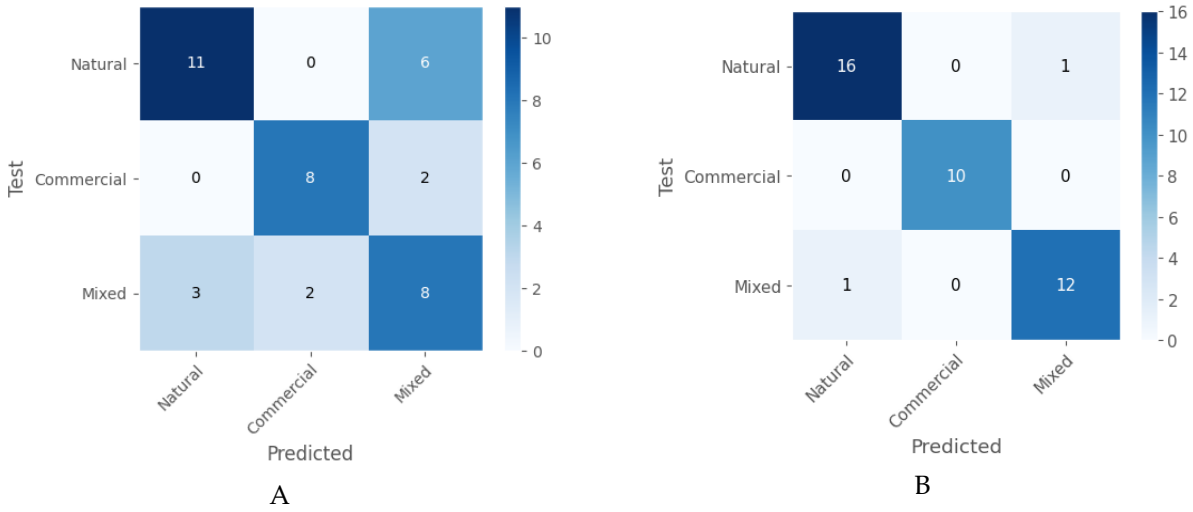

Figure 6. Confusion matrix of: A- LDA model on the test dataset, and B- Random Forest model on the test dataset

The Random Forest model also struggled to accurately distinguish between the "Natural" and "Mixed" categories, especially for samples with a medium proportion of natural orange juice (around 45-50%). This issue may stem from the inadequacy of the data features to effectively separate these two categories within the feature space.

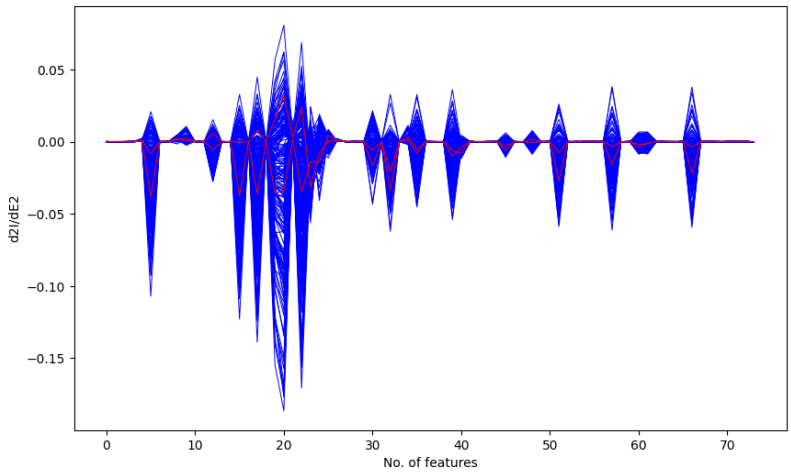

Figure 7. The second-order derivative signals vs. features of the samples classified by iPLS-LDA (red lines: misclassification samples; blue line: correct classification samples)

To check the reasons why iPLS-DA gave the low accuracy prediction, the second-order derivative signals of the misclassified samples (red lines) compared to the correctly classified samples (blue lines) were shown in Fig. 7. It can be observed that the shape of the second derivative data across features differs between correctly classified and misclassified samples. Misclassified samples exhibit abnormalities such as missing peak points and flattened or unchanged signals. These irregularities are also associated with outliers at peak or shoulder points in the voltammogram. This suggests that samples with abnormal shapes compared to the overall dataset within the same group should be identified and excluded before processing. Compared with previously reported classification results, our machine learning model achieved higher accuracy. The limitation of working on a single device is that accurate results can only be obtained for experiments conducted on that same device. However, when switching to another device, it is necessary to calibrate the measurement signals and ensure similar operating conditions to the original device to maintain accuracy.

4. Conclusion

The feasibility of using voltammetric data combined with machine learning as a screening method for determining the authenticity of juice was confirmed. Cluster analysis revealed the differences between natural orange juice, chemical-based juices, and blends of natural and chemical juices. Based on this, supervised machine learning models such as iPLS-LDA and random forest were developed for classification purposes, with the random forest model showing promising results in classification and prediction. The obtained results also highlight the usefulness of the voltammetric method using a gold electrode to assess the authenticity of orange juice. The limitations of the sample recognition method were addressed by increasing the sample size and creating stronger models. Moreover, the electrochemical approach has shown that it is capable of fast classification, low cost, and suitability for on-site analysis. This approach would enable the monitoring of raw material procurement concerning the orange variety and growing regions.

5. Acknowledgement

This research received funding support from the QG.23.68 project.

Author Contributions: Thanh, D.N. :Writing – original draft preparation; Data curation ; Son, M.N. : Writing – original draft preparation, Software; Formal analysis; Phong, D.N.: Software, Visualization; Vang, H.P. Data curation, Visualization; Ha, D.N.: Resources ; Anh, V.T.N.: Investigation; Hao, H.T.: Validation, Resources; Ha: , M.N.: Conceptualization, Writing – review, proofreading and editing; Thuong, K.T.N.: Methodology; Writing – review, proofreading and editing; Thao, T.T: Writing – review, proofreading and editing, Methodology; Supervision.

Funding: This research received funding support from the QG.23.68 project.

Conflicts of Interest: The authors have no conflics of interest.

References

[1] Pei, X.; Tandon, A.; Alldrick, A.; Giorgi, L.; Huang, W.; Yang, R. The China Melamine Milk Scandal and Its Implications for Food Safety Regulation. *Food Policy* **2011**, *36*, 412–420. https://doi.org/10.1016/j.foodpol.2011.03.008

[2] Šejvl, J.; Šíma, J.; Rubešová, K.; et al. Public Health Response to Methanol Mass Poisoning in the Czech Republic in 2012: A Case Study. *Cent. Eur. J. Public Health* **2019**, *27*(Suppl.), 29–39. https://doi.org/10.21101/cejph.a5764

[3] Feng, S.; Yi, L.; Wu, X.; et al. Differentiation between Flavors of Sweet Orange (*Citrus sinensis*) and Mandarin (*Citrus reticulata*). *J. Agric. Food Chem.* **2018**, *66*, 203–211. https://doi.org/10.1021/acs.jafc.7b04968

[4] Mac, H. X.; Chen, Y.; Shao, Y.; et al. Current Techniques for Fruit Juice and Wine Adulterant Detection and Authentication. *Beverages* **2023**, *9*, 84. https://doi.org/10.3390/beverages9040084

[5] Manikandan, V. S.; Adhikari, B.; Chen, A. Nanomaterial-Based Electrochemical Sensors for the Safety and Quality Control of Food and Beverages. *Analyst* **2018**, *143*, 4537–4554. https://doi.org/10.1039/C8AN00497H

[6] Abad-García, B.; Berrueta, L. A.; López-Márquez, D. M.; et al. Polyphenolic Contents in Citrus Fruit Juices: Authenticity Assessment. *Eur. Food Res. Technol.* **2014**, *238*, 803–818. https://doi.org/10.1007/s00217-014-2160-9

[7] Lozano-Sánchez, J.; Segura-Carretero, A.; Fernández-Gutiérrez, A. Chromatographic Technique: High-Performance Liquid Chromatography (HPLC). In *Modern Techniques for Food Authentication*; Elsevier: Amsterdam, 2018; pp 459–526. https://doi.org/10.1016/B978-0-12-814264-6.00013-X

[8] Guccione, C.; Russo, M.; Cacciola, F.; et al. A Simple and Rapid HPLC–PDA–MS Method for the Profiling of Citrus Peels and Traditional Italian Liquors. *Planta Med.* **2016**, *82*, 1039–1045. https://doi.org/10.1055/s-0042-108735

[9] Sun, R.; Yang, J.; Xia, Y.; et al. UPLC-QTOF-MS Coupled with Machine Learning to Discriminate between NFC and FC Orange Juice. *Food Control* **2023**, *145*, 109487. https://doi.org/10.1016/j.foodcont.2022.109487

[10] Varnasseri, M.; Xu, Y.; Goodacre, R. Rapid Detection and Quantification of the Adulteration of Orange Juice with Grapefruit Juice Using Handheld Raman Spectroscopy and Multivariate Analysis. *Anal. Methods* **2022**, *14*, 1663–1670. https://doi.org/10.1039/D2AY00219A

[11] Ehsani, S.; Yazdanpanah, H.; Parastar, H. An Innovative Screening Approach for Orange Juice Authentication Using Dual Portable/Handheld NIR Spectrometers and Chemometrics. *Microchem. J.* **2023**, *194*, 109304. https://doi.org/10.1016/j.microc.2023.109304

[12] Marchetti, L.; Berrué, F.; Caro, Y.; et al. Use of ^{1}H NMR to Detect the Percentage of Pure Fruit Juices in Blends. *Molecules* **2019**, *24*, 2592. https://doi.org/10.3390/molecules24142592

[13] Cuny, M.; Vigneau, E.; Le Gall, G.; et al. Fruit Juice Authentication by ^{1}H NMR Spectroscopy in Combination with Different Chemometrics Tools. *Anal. Bioanal. Chem.* **2008**, *390*, 419–427. https://doi.org/10.1007/s00216-007-1708-y

[14] Ranbir; Kumar, R.; Singh, S.; et al. Machine Learning-Based Analytical Systems: Food Forensics. *ACS Omega* **2022**, *7*, 47518–47535. https://doi.org/10.1021/acsomega.2c05632

[15] Islam, M.; Wahid, K.; Dinh, A. Assessment of Ripening Degree of Avocado by Electrical Impedance Spectroscopy and Support Vector Machine. *J. Food Qual.* **2018**, *2018*, 4706147. https://doi.org/10.1155/2018/4706147

[16] Hassan, M. M.; El-Naggar, A. E.; Rodríguez-González, I.; et al. Recent Progress in Chemometrics-Driven Biosensors for Food Application. *TrAC, Trends Anal. Chem.* **2022**, *156*, 116707. https://doi.org/10.1016/j.trac.2022.116707

[17] Silva, A. C.; Lourenço, A. S.; de Araujo, M. C. U. Simultaneous Voltammetric Determination of Four Organic Acids in Fruit Juices Using Multiway Calibration. *Food Chem.* **2018**, *266*, 232–239. https://doi.org/10.1016/j.foodchem.2018.06.005

[18] Monago-Maraña, O.; Palenzuela, A. Z.; Crevillén, A. G. Untargeted Authentication of Fruit Juices Based on Electrochemical Fingerprints Combined with Chemometrics: Adulteration of Orange Juice as a Case Study. *LWT* **2024**, *209*, 116797. https://doi.org/10.1016/j.lwt.2024.116797

ASEAN
Journal of Scientific and Technological Reports
Online ISSN:2773-8752

Research article

Ellipsoidal Coverage Function (ECF) – a Modified Mahalanobis Radial Basis Function with Geometrical Coverage Learning (GCL) Algorithm

Tanat Piumsuwan[1*], and Prompong Sugunnasil[2]

[1] Faculty of Engineering, Chiang Mai University, 50200, Thailand
[2] DAKSH Research Group, Chiang Mai University, 50200, Thailand
* Correspondence: tanat_pi@cmu.ac.th

Citation:
Piumsuwan, T.; Sugunnasil, P. Ellipsoidal coverage function (ECF) – a modified mahalanobis radial basis function with geometrical coverage learning (GCL) algorithm. *ASEAN J. Sci. Tech. Report.* **2026**, *29*(2), e259894. https://doi.org/10.55164/ajstr.v29i2.259894.

Article history:
Received: July 14, 2025
Revised: October 9, 2025
Accepted: November 15, 2025
Available online: January 21, 2026

Abstract: This research presents an Ellipsoidal Coverage Function (ECF) with the addition of the Geometrical Coverage Learning (GCL) algorithm concept for classification. The motivation for this research stems from inefficiencies in nonlinear Deep Neural Networks (DNNs). The implementation of a higher-order function for neurons, while less popular than a deeper linear design, has been claimed to improve the robustness of the model in dealing with noisy environments and to negate the need for a deeper network. The ECF is a higher-order neuron design based on the Mahalanobis distance Radial Basis Function (MRBF) design, but with the number of parameters linearly scaled instead of quadratically with respect to the input dimension. This means that the ECF neuron can approximate the volume coverage of an MRBF in the feature space under a non-rotating constraint and is more suitable for integration into a neural network for further backpropagation (BP) optimization. The integration of the GCL into the ECF for classification architectures boosts learning efficiency, underscoring the versatility and potential impact of this research. The results from experiments with computer vision tasks in a transfer learning environment suggest that the integrated GCL ensures that the ECF can map all the data and correct the training parameters of the network faster. Furthermore, the ECF with the GCL algorithm demonstrates competitive performance relative to other nonlinear neuron designs in a transfer learning setup across different datasets, including itself without GCL. These findings point to a better nonlinear machine learning model in terms of performance and efficiency combined.

Keywords: Machine learning; deep learning; nonlinear neuron; artificial neural networks; smart initialization

1. Introduction

Deep Neural Networks (DNNs) have become the focus of machine learning research in the past few years. This is mainly due to their scalability, performance in various tasks (including natural language processing (NLP) and computer vision), and the availability of more capable hardware. DNNs can map complex structures and have been applied to both classification and clustering tasks [1, 2]. However, the field lacks major developments in terms of the fundamental structure, mainly the neuronal models and their training paradigms. The most well-known neuron is the McCulloch and Pitts (M-P) neuron, introduced in 1943 [3]. Since then, artificial neural networks have been

developed based on this model, along with various gradient-descent-based learning algorithms [4–11]. However, the model suffers from linear separability, as the M-P model is fundamentally a linear discriminator. The most popular remedy to this problem is increasing the number of hidden layers while implementing different structural designs [12–21]. However, some studies also claim that multiple-layer linear designs are vulnerable to adversarial examples [22–28].

There have been several attempts at developing new neuron structures to enhance each neuron's capability with nonlinear designs, including the radial basis function (RBF) neurons introduced by Broomhead and Lowe [29]. However, the RBF network is easily outperformed by multilayer linear designs in terms of accuracy, rendering it unpopular. Nevertheless, despite the lower performance, studies illustrate that the RBF network can be more robust toward adversarial samples that normal deep linear designs fail to handle and is less prone to overfitting due to the nonlinear locality of the classifier [23, 25, 28]. Moreover, works suggest that the RBF is not yet irrelevant, including in industry domains [30–34], finance [35–39], and more [40–42]. We further speculate that the unpopularity of RBF-based neural networks is due to two reasons: 1) the increased number of training parameters, since multiple RBF neurons are needed to cover a large data structure, and 2) training a deeper network with integrated RBF neurons is more computationally expensive without guaranteeing better performance. One could implement the RBF network with clustering initialization in a transfer learning environment to circumvent the second problem [43–45], but the first problem persists. While the implementation of different distance metrics, particularly the Mahalanobis distance, which is known to perform well in pattern recognition [46–52], to the RBF neuron addresses coverage flexibility. However, it does not solve problem 1, and problem 2 becomes even more severe even when proper initialization is applied. The Mahalanobis distance RBF, for example, has $d^2 + d$ trainable parameters for a d-dimensional input space. If utilized in a DNN, gradient descent becomes extremely inefficient compared to a more capable, deeper linear network. More recent works focusing on nonlinear neuron designs include the High-order Coverage Function Neural Network (HCFNN) [53] and the Hyper-Sausage Coverage Function (HSCF) [54]. Both claim to outperform traditional neuron designs on some datasets. However, these models even require extra optimization algorithms during training, including Genetic Algorithms (GA). Other works, such as QuadraNet [55], integrate the nonlinear neuron design only partially to keep computational costs low.

In this work, we aim to investigate whether we can formulate an approach to assist a network of nonlinear neurons before performing backpropagation (BP). We are motivated by a study in 1999 by Zhang et al., in which they proposed an interpretation of the M-P neuron for classification tasks [56]. Each neuron could be viewed as a linear discriminator in the d-dimensional space for a dataset with d features. They proposed a training algorithm by introducing a new bounding parameter, which transforms the space into a $(d + 1)$-dimensional space in which the training data is contained within a d-dimensional sphere. The neuron is then built upon each data point until all points from the same class are covered by the corresponding class neurons. Another work that inspires our approach is the HSCF [54]. They perform clustering using a Gaussian Mixture Model (GMM) within a class of data points and then build HSCF neurons upon the obtained intra-class clusters. The two furthest data points in each cluster are used to calculate the orientation of the HSCF, while the variance of distances between data points in the intra-class cluster determines its "fatness." The Gaussian kernel activation is used similarly to the RBF design. They also introduce a novel loss, called the volume coverage loss. L_{VC}, for the BP process, which takes the HSCF volume into account and keeps the HSCF compact. We consider the HSCF work novel because the authors propose a design similar to the Mahalanobis distance RBF, but with far fewer parameters. In a d-dimensional input space, an HSCF neuron has only $2d + 1$ parameters compared to $d^2 + d$ parameters for the Mahalanobis distance RBF. However, HSCF has its own drawbacks. Training requires an iterative approach: starting BP on a small number of neurons created from initial clustering, and then gradually increasing the number of neurons from subsequent clustering of predicted negative samples to achieve the design's maximum capability. Furthermore, under our replication attempts, we found that HSCF exhibits long computation time per step during optimization, suffers from floating-point precision issues, and fails to perform at all without the prior clustering construction. We suspect that its complicated functional form is the underlying cause of these issues.

Instead, we found that we could reduce the number of parameters to $2d$ by removing the rotatability of the Mahalanobis distance RBF. This is an acceptable compromise when combined with the supervised clustering approach from [43], in which samples from each class are clustered separately. We also start with a specific number of neurons to avoid excessive BP each time a new set of clusters is introduced. We then modified this non-rotating Mahalanobis distance RBF by adding a boundary bias and replacing the Gaussian kernel activation function with the hyperbolic tangent. This results in a total of $2d + 1$ trainable parameters, like the HSCF, but with a much simpler functional form. These modifications allow the ECF to perform effectively even when randomly initialized. The bias and choice of activation function create a hard boundary for the neuron, enabling us to initialize its parameters such that it covers all samples belonging to each sub-cluster; hence, starting hypothetically closer to an optimal state, giving rise to the name Geometrical Coverage Learning (GCL). Moreover, we refer to this neuron design as the Ellipsoidal Coverage Function (ECF) from now on. In short, our goals are to study how well our nonlinear ECF design performs when integrated into DNNs, explore whether this GCL initialization paradigm truly improves training efficiency and nonlinear model performance, and aim to inspire further research on smart initialization.

2. Materials and Methods

2.1 Ellipsoidal Coverage Function (ECF)

First, we describe how we modify the Mahalanobis distance RBF to get our ECF. For an arbitrary i^{th} RBF neuron with Gaussian kernel activation function in an d-dimensional input space, its output from an input $\mathbf{x}$ is given by:

$$y_i = \exp[-\beta_i \|\mathbf{x} - \mathbf{c}_i\|^2]. \tag{1}$$

The training parameters are $\mathbf{c}_i$ and β_i, which represent the RBF center and its size, respectively. $\|\mathbf{x} - \mathbf{c}_i\|$ is the distance between the input $\mathbf{x}$ and the center $\mathbf{c}_i$. Any distance metric can be used here, but we focus on the Mahalanobis distance. The metric is defined as:

$$\|\mathbf{x} - \mathbf{c}_i\| = \sqrt{(\mathbf{x} - \mathbf{c}_i)^T \mathbf{\Sigma}^{-1} (\mathbf{x} - \mathbf{c}_i)}, \tag{2}$$

where $\mathbf{\Sigma}^{-1}$ is a $d \times d$ positive semi-definite covariance matrix. In the context of a machine learning model, this matrix is determined during the training process. Compared to the basic Euclidean distance, $\mathbf{\Sigma}^{-1}$ transforms an RBF unit into an ellipsoid in Euclidean space. Since we are integrating the RBF neuron into DNNs, it can be randomly initialized with a constraint ensuring that it remains a positive semi-definite matrix. However, a problem arises if we want to include it as an additional training parameter. The total number of trainable parameters from $\mathbf{\Sigma}^{-1}$ alone is d^2. We can use Cholesky decomposition, $\mathbf{\Sigma}^{-1} = \mathbf{L}\mathbf{L}^T$, where $\mathbf{L}$ is a lower triangular matrix. This guarantees symmetry during BP training, but the number of trainable parameters remains $\mathcal{O}(d^2)$. Nevertheless, there is a special case that allows us to reduce the number of parameters from $\mathbf{\Sigma}^{-1}$ to only d: when $\mathbf{\Sigma}^{-1}$ is fixed as a diagonal matrix, which prevents the ellipsoid from rotating relative to the basis vectors. Assuming $\mathbf{\Sigma}^{-1}$ is strictly a diagonal, Equation (2) can be rewritten as:

$$\|\mathbf{x} - \mathbf{c}_i\| = \sqrt{\mathbf{v}^T [(\mathbf{x} - \mathbf{c}_i) \circ (\mathbf{x} - \mathbf{c}_i)]}, \tag{3}$$

where $\mathbf{v}$ is a vector of length d containing the diagonal elements of $\mathbf{\Sigma}^{-1}$, and $\circ$ denotes element-wise multiplication. The square root applies to the scalar sum of all weighted squared components, i.e., $\sqrt{\sum_j v_j (x_j - c_{ij})^2}$, as in the Euclidean norm rather than element-wise. By substituting this back into Equation (1) and replacing the exponential function with an arbitrary activation function σ, we obtain:

$$y_i = \sigma\{\mathbf{w}^T [(\mathbf{x} - \mathbf{c}_i) \circ (\mathbf{x} - \mathbf{c}_i)]\}. \tag{4}$$

Now, $\mathbf{w} = -\beta_i \mathbf{v}$ is our new vector weight, which determines how the ellipsoid stretches and has only d parameters. However, this also means that we can no longer rotate the ellipsoid relative to the basis vectors (in this case, the feature vectors). We found that the resulting reduction in classification accuracy is acceptable when considering the time required for a full BP epoch to train the Mahalanobis distance RBF. We attempted to initialize ellipsoids at arbitrary angles, decompose $\mathbf{\Sigma}^{-1}$, and train only the vector of length d that performs the same function as $\mathbf{w}$. However, this yielded only negligible to no improvement, since Σ^{-1} must be reconstructed via matrix multiplication. We suspect that this matrix multiplication is required to reacquire the $d \times d\ \Sigma^{-1}$, interferes with the gradient flow during BP. Lastly, we added a new scalar bias parameter ϕ. This transforms Equation (4) into our ECF:

$$y_i = \sigma\{\mathbf{w}^T[(\mathbf{x} - \mathbf{c}_i) \circ (\mathbf{x} - \mathbf{c}_i)] - \phi\}. \tag{5}$$

This will play a major role in our subsequent GCL algorithm. As a result, each ECF unit in a d-dimensional input space has a total of $2d + 1$ trainable parameters. We chose the hyperbolic tangent as our activation function σ because the introduction of ϕ can produce negative outputs in the original Mahalanobis distance RBF. To reduce the number of parameters from $\mathcal{O}(d^2)$ to $\mathcal{O}(d)$, we constrain Σ^{-1} to be diagonal, resulting in a non-rotating Mahalanobis RBF. Conceptually, the ECF can be viewed as a soft indicator of an ellipsoid obtained by applying a tanh kernel to a diagonal Mahalanobis quadratic, similar to how a traditional RBF applies an exponential (Gaussian) bump to the same quadratic. With diagonal covariance, both share the same ellipsoidal level sets, but tanh allows negative outputs, which are essential for GCL to detect where the neuron output crosses zero and define coverage regions in feature space. Therefore, the choice of tanh is motivated by its similarity to the Gaussian kernel, its compatibility with the bias ϕ, and its natural interaction with the non-rotating structure of the ECF within the GCL framework. Since we are comparing our ECF to the HSCF design from [54], we provide a brief description of its main function. In [54], the authors express their HSCF as:

$$y_i = \sigma\left\{-\frac{\|\mathbf{x} - [\lambda \mathbf{q}_{i1} + (1 - \lambda)\mathbf{q}_{i2}]\|}{dr^2}\right\}. \tag{6}$$

$\mathbf{q}_{i1}$ and $\mathbf{q}_{i2}$ are vectors of length d pointing from the origin to the two endpoints of the function, where d is the input dimension. r is the radius of the HSCF, also referred to as the "fatness" of the function by the authors. λ represents the projection length of the vectors $(\mathbf{x} - \mathbf{q}_{i1})$ and $(\mathbf{q}_{i2} - \mathbf{q}_{i1})$. The authors provide an explicit form for λ as:

$$\lambda = \begin{cases} 1, & \mathbf{k} \cdot (\mathbf{q}_{i2} - \mathbf{q}_{i1}) < 0 \\ \|\mathbf{k}\|, & \dfrac{\|\mathbf{k}\|}{\|\mathbf{q}_{i2} - \mathbf{q}_{i1}\|} < 1, \mathbf{k} \cdot (\mathbf{q}_{i2} - \mathbf{q}_{i1}) \geq 0 \\ 0, & \dfrac{\|\mathbf{k}\|}{\|\mathbf{q}_{i2} - \mathbf{q}_{i1}\|} \geq 1, \mathbf{k} \cdot (\mathbf{q}_{i2} - \mathbf{q}_{i1}) > 0 \end{cases}, \tag{7}$$

where $\mathbf{k}$ is the projection vector of $(\mathbf{x} - \mathbf{q}_{i1})$ onto $(\mathbf{q}_{i2} - \mathbf{q}_{i1})$:

$$\mathbf{k} = \frac{(\mathbf{x} - \mathbf{q}_{i1}) \cdot (\mathbf{q}_{i2} - \mathbf{q}_{i1})}{\|\mathbf{q}_{i2} - \mathbf{q}_{i1}\|^2} (\mathbf{q}_{i2} - \mathbf{q}_{i1}). \tag{8}$$

The trainable parameters are the endpoints, $\mathbf{q}_{i1}$, $\mathbf{q}_{i2}$, and the radius r, resulting in a total of $2d + 1$ parameters per neuron unit. The authors also introduce an additional loss function, L_{VC}, which concerns the volume of the shape. Since the HSCF is essentially a hypercylinder with two hyperspheres as end caps, the L_{VC} given in [54] roughly corresponds to the combined volume of a hypersphere and a hypercylinder:

$$L_{VC} = \frac{\pi^{\frac{d-1}{2}}}{\Gamma\left(\frac{d-1}{2}+1\right)} r^{d-1} \times h + \frac{\pi^{\frac{d}{2}}}{\Gamma\left(\frac{d}{2}+1\right)} r^{d}, \tag{9}$$

or explicitly as:

$$L_{VC} = \begin{cases} \frac{2^{\frac{d}{2}} \pi^{\frac{d-2}{2}}}{(d-1)!!} r^{d-1} \times h + \frac{\pi^{\frac{d}{2}}}{\left(\frac{d}{2}\right)!} r^{d}, & d = 2l \\ \frac{\pi^{\frac{d-1}{2}}}{\left(\frac{d-1}{2}\right)!} r^{d-1} \times h + \frac{2^{\frac{d+1}{2}} \pi^{\frac{d-1}{2}}}{d!!} r^{d}, & d = 2l+1 \end{cases}. \tag{10}$$

$h = \|\mathbf{q}_{i2} - \mathbf{q}_{i1}\|$ is the height of the cylinder, and $\Gamma(x)$ is Euler's gamma function. In [54], the authors provide an explicit expression for this gamma function, and L_{VC} is given as Equation (10).

Compared to our ECF, given by Equation (5), the HSCF is considerably more complicated. We also suspect that this functional form is why, in our replication, it requires higher floating-point precision, from 32 to 64 bits, to allow proper gradient flow. In our replication attempts, we found that BP on HSCF cannot be performed at all without this increased precision, whereas BP on other designs, including the Mahalanobis distance RBF, works fine with float32 precision. Furthermore, this issue is compounded by multiple vector multiplications. Overall, under our setup, HSCF requires 87 ms and 185 ms per optimization step when working with CIFAR10 and CIFAR100. The time per step is significantly longer than reported in [54], making reliable implementation for comparison impractical. As a result, HSCF has been omitted from our comparisons; this limitation is acknowledged, and a fair comparison could not be obtained.

2.2 Computational and Parameter Complexity Analysis

To clarify the reduction from $\mathcal{O}(d^2)$ to $\mathcal{O}(d)$ parameters and to support claims about computational efficiency, we summarize the parameter and complexity characteristics of all neuron designs considered in this work. Table 1 reports per-unit trainable parameters and asymptotic time and space complexities with respect to feature dimension d. The analysis assumes forward and backward computations for a single batch, where matrix multiplications dominate cost. While HSCF has $\mathcal{O}(d)$ asymptotic complexity, its practical runtime is slower than ECF due to multiple sequential vector operations, conditional branching, and the need for 64-bit precision. This analytical comparison highlights that the proposed ECF achieves the same representational capacity order as full Mahalanobis RBFs while remaining linear in d and suitable for large-scale feature embeddings.

Table 1. Analytical parameter and complexity comparison across neuron designs in d-dimension.

Neuron Design	Parameters per Neuron	Forward Complexity (per neuron)	Backward Complexity (per neuron)	Memory (Space) Complexity	Notes
M-P	$d+1$	$\mathcal{O}(d)$	$\mathcal{O}(d)$	$\mathcal{O}(d)$	Standard fully connected neuron
Euclidean RBF	$d+1$	$\mathcal{O}(d)$	$\mathcal{O}(d)$	$\mathcal{O}(d)$	Spherical RBF
Mahalanobis RBF	d^2+d	$\mathcal{O}(d^2)$	$\mathcal{O}(d^2)$	$\mathcal{O}(d^2)$	Requires matrix multiplication for $\mathbf{\Sigma}^{-1}$
ECF (proposed)	$\boldsymbol{2d+1}$	$\boldsymbol{\mathcal{O}(d)}$	$\boldsymbol{\mathcal{O}(d)}$	$\boldsymbol{\mathcal{O}(d)}$	**Diagonal covariance approximation**

HSCF [54]	$2d+1$	$\mathcal{O}(d)$	$\mathcal{O}(d)$	$\mathcal{O}(d)$	Slower in practice due to sequential ops, branching, and 64-bit precision

2.3 Geometrical Coverage Learning (GCL)

This process helps the ECF initialize closer to its optimal state by ensuring it covers a subset of the training data; hence, the name Geometrical Coverage. Assuming we have a set of classification labels K with k elements, we perform supervised clustering on the training data **x.** We then obtain a set of m different intra-class clusters X_a^t with $a = 1, 2, \cdots, m$ for each label $t \in K$:

$$G^t = \{X_1^t, X_2^t, \cdots, X_m^t\}. \tag{11}$$

We then build ECFs based on these subsets of training data. For each subcluster X_a^t, we first obtain its center, denoted as $\mathbf{c}^{a,t}$. We translate each input $\mathbf{x} \in X_a^t$ with $\mathbf{x} - \mathbf{c}$ to obtain $\mathbf{x}' = (x_1', x_2', \cdots, x_d')$. Next, we determine each i^{th} component of the stretching weights, $\mathbf{w}^{a,t} = \left(w_1^{a,t}, w_2^{a,t}, \cdots, w_d^{a,t}\right)$ for subset a of class t by:

$$w_i^{a,t} = \begin{cases} \left(\frac{1}{\Delta_i}\right)^2, & 0 < \Delta_i < \frac{\Delta_{\max}}{\delta} \\ \left(\frac{\delta}{\Delta_{\max}}\right)^2, & \text{otherwise} \end{cases}. \tag{12}$$

Δ_i is the maximum separation of the i^{th} component among $\mathbf{x} \in X_a^t$, while $\Delta_{\max}$ is $\max\{\Delta_i\}$ and δ is a hyperparameter set by the user. The latter is used to prevent $w_i^{a,t}$ from blowing up when Δ_i is very small or zero. After $\mathbf{w}^{a,t}$ are determined, we scale them to prevent gradient explosion or vanishing during BP by mimicking the mean and variance of the positive half of the Xavier Glorot uniform initialization [57]. This is a widely used method for initializing neurons while taking the sizes of the previous and current layers into account [58, 59]. Normally, the Xavier Glorot uniform initialization takes the form:

$$U\left[-\frac{\sqrt{6}}{\sqrt{\text{fan}_{\text{in}} + \text{fan}_{\text{out}}}}, \frac{\sqrt{6}}{\sqrt{\text{fan}_{\text{in}} + \text{fan}_{\text{out}}}}\right], \tag{13}$$

where U indicates a uniform distribution, fan_{in} is the number of input units in the weight tensor $\mathbf{w}$, and fan_{out} is the number of the output units of the layer. However, since the weights $\mathbf{w}$ of our ECF are defined on the positive half of the real space $\mathbb{R}^+$, we modify the distribution to the positive half so that $\mathbf{w}$ is scaled as follows:

$$w_i^{a,t} \sim U\left[0, \frac{\sqrt{6}}{\sqrt{\text{fan}_{\text{in}} + \text{fan}_{\text{out}}}}\right]. \tag{14}$$

The mean of our weight tensor is scaled to:

$$\bar{\mathbf{w}} = \frac{\sqrt{6}}{2\sqrt{\text{fan}_{\text{in}} + \text{fan}_{\text{out}}}}, \tag{15}$$

and its variance is scaled to:

$$\sigma_{\mathbf{w}}^2 = \frac{1}{2(\text{fan}_{\text{in}} + \text{fan}_{\text{out}})}. \tag{16}$$

After this scaling, we determine the bias parameter for subcluster a of label t as follows:

$$\phi^{a,t} = \max_{\mathbf{x} \in X_a^t}\{(\mathbf{w}^{a,t})^T[(\mathbf{x} - \mathbf{c}^{a,t}) \circ (\mathbf{x} - \mathbf{c}^{a,t})]\}. \tag{17}$$

From this, we can see that ϕ determines how far the ellipsoid boundary extends before the output changes from negative to positive, instead of starting at zero at the center like a normal RBF. This ϕ sets a specific

boundary for our ECF, allowing us to define our GCL such that each ECF unit fully covers its corresponding subcluster before BP. This, in turn, helps the ECF start closer to its optimal state before further gradient descent training. The overall algorithm for the GCL is shown in Algorithm 1:

Algorithm 1 Geometrical Coverage Learning (GCL)

1: **Input:** Training set X, labels y, nodes per class num, hyperparameter δ
2: **Output:** Cluster centers $\mathbf{c}^{a,t}$, stretching weights $\mathbf{w}^{a,t}$, biases $\phi^{a,t}$
3: $\text{fan}_{\text{in}} = \text{num\_features}(X)$
4: $\text{fan}_{\text{out}} = num \times |unique(y)|$
5: $PXGU = U\left[0, \frac{\sqrt{6}}{\sqrt{\text{fan}_{\text{in}}+\text{fan}_{\text{out}}}}\right]$ ◁ positive-half Xavier initialization
6: **for** each class $t \in unique(y)$ **do**
7: $X^t = \{\mathbf{x} \in X : y = t\}$
8: $X_{\text{clu}} = KMeans(X^t, n\_clusters = num)$
9: **for** each subcluster $X_a^t \in X_{\text{clu}}$ **do**
10: $\mathbf{c}^{a,t} = \text{mean}(X_a^t)$
11: $X'_a = X_a^t - \mathbf{c}^{a,t}$ ◁ translate samples to subcluster center
12: $\Delta = \max(X'_a, \text{axis} = 0) - \min(X'_a, \text{axis} = 0)$ ◁ vector of max-min per dimension
13: $\Delta_{\max} = \max(\Delta)$
14: $\mathbf{w}^{a,t} = \begin{cases} (1/\Delta_i)^2 & \text{if } 0 < \Delta_i < \Delta_{\max}/\delta \\ (\delta/\Delta_{\max})^2 & \text{otherwise} \end{cases}, \ \forall i = 1, \ldots, d$ ◁ element-wise weights computation
15: Scale $\mathbf{w}^{a,t}$ to match mean and variance of $PXGU$
16: $\phi^{a,t} = \max_{x' \in X'_a}\{(\mathbf{w}^{a,t})^T (x' \circ x')\}$ ◁ compute bias
17: **end for**
18: **end for**

The main computational overhead of GCL comes from the supervised clustering step (Line 6 in Algorithm 1, for which we use K-Means with a time complexity in practice of $\mathcal{O}(nmdki)$ (n elements, m classes, d dimension, k clusters per class, and i number of iterations). While this may appear expensive at first, GCL is performed only once before backpropagation, and its runtime is roughly equivalent to a single BP epoch. The vectorized computations of the stretching weights $\mathbf{w}^{a,t}$ and biases $\phi^{a,t}$ (Lines 9–17) further improve efficiency, ensuring that GCL does not add significant overhead to the overall training process.

2.4 Experiments

We perform experiments on image classification tasks. We used an AMD Ryzen 9 5900HX, 3301 MHz, 8 cores, 16 logical processors. All custom modules used in the experiments are vectorized and parallelized to utilize all CPU cores. Our experimental setup employs transfer learning on the following backbone models: ResNet18 (512 embedded features), ResNet50 (1024 embedded features), and VGG16 (4096 embedded features). All backbones are trained on the ImageNet1K dataset and provided via the timm open-source library [60, 61]. The backbone models are frozen, and BP is performed only on a classifier consisting of one input layer, one hidden layer, and one output layer. Hidden layer units are varied to test different neuron designs. The classification layers are optimized using ADAM (learning rate of 0.0002 and a batch size of 64) via TensorFlow. ADAM is considered one of the best optimizers for DNNs in terms of convergence speed [7, 10, 62]. We test our models on three benchmarks: CIFAR10, CIFAR100 [63], and MNIST [64], and three industrial image datasets: Magnetic Tile Defect Dataset (MTD) [65], Kylberg Texture dataset v1.0 (KTv1.0) [66], and SDNET2018 [67]. All datasets are separated into training, validation, and test sets. The model selected for evaluation is based on the checkpoint achieving the best validation accuracy during backpropagation, ensuring that overfitting is mitigated. Our experiments use identical train and validation splits and paired random seeds across methods. Although confidence intervals or formal statistical significance tests are rarely reported in standard deep learning experiments, due to the high computational cost and the non-independence of training runs, we report ± deviations across multiple seeds for each dataset, backbone, and metric. These deviations capture the variability of the results and enable meaningful comparisons across

neuron designs under identical splits and paired seeds. Each experiment was repeated more than 10 times, providing an effective "n" for these comparisons and ensuring that the reported values are statistically meaningful. To ensure reproducibility and fair per-neuron comparisons, training uses a fixed validation set. Hyperparameters for each neuron design were selected via grid search on a high-performance computing cluster before CPU-based experiments. Head-level work is measured on frozen features, with forward and backward computation costs reported per step and per batch; multi-epoch training scales linearly with the number of samples. Reported per-method times and parameter counts reflect CPU execution. This setup isolates each model's intrinsic neuron capability without bias from differing hidden-unit counts.

We compare the following designs:

- **M-P with hyperbolic tangent activation**: Note that the original embedders are trained with this linear design and frozen; thus, it is unlikely that any nonlinear design will outperform it. However, we consider it useful to monitor the accuracy loss when different nonlinear designs are implemented.
- **Euclidean distance RBF with Gaussian kernel activation**: Supervised K-Means clustering is used to initialize the center of each RBF neuron. This highlights the limitations of the spherical shape of the RBF.
- **ECF with GCL**: The main design proposed in this work.
- **ECF without GCL**: Used to study whether GCL significantly affects the performance of the ECF.

We avoid using the full Mahalanobis distance RBF in the following experiments because the number of trainable parameters becomes prohibitively large. Even with a single unit in the smallest backbone, ResNet18, BP would require approximately 10^5 parameters, compared to roughly 10^3 for other designs. We aim to keep the number of parameters across designs roughly comparable for the same dataset, though not exactly. This is because the M-P and Euclidean distance RBF neurons have $d + 1$ parameters per unit, whereas the other designs have $2d + 1$ parameters per unit. For instance, with the ResNet18 backbone (512 features), at least 1025 M-P neurons are needed to match the number of parameters of 513 ECF neurons. This is a clearly excessive number of hidden units. We count per-neuron trainable parameters inside each coverage unit. **Fairness controls:** To ensure valid comparisons on frozen embeddings, all neuron designs are trained under identical optimization and evaluation protocols, including the same optimizer (ADAM), learning rate, batch size, and checkpointing policy. Experiments use identical train/validation/test splits and paired random seeds. Hyperparameters are selected under parameter-parity considerations (see Table 4 and Table 5 for per-head trainable counts), and reported throughput and timings are measured per batch on the same CPU hardware. These measures isolate architectural effects from differences in optimization or resource allocation. We note that the backbone was originally trained with an M-P head, which may introduce alignment bias favoring that baseline; comparisons are therefore interpreted as competitive under fixed-budget frozen-backbone transfer rather than definitive superiority claims.

With this setup, we divide our experiments into two parts.

2.4.1. 20 epochs of training

We test our BP-trained models to assess how close each design is to its optimal state after a limited number of epochs.

2.4.2. 200 epochs of training

We carry out the same experiment on CIFAR10 and CIFAR100 using the ResNet18 backbone, but with many more BP epochs. This allows all models to reach their validated states at some point, enabling us to evaluate their final performance.

3. Results and Discussion

First, an observation is made for 100 units of ECF with and without GCL. Figure 1 indicates that the GCL does boost the optimization efficiency of our ECF. The ECF initialized with GCL can reach the best

validated state faster than the ECF without GCL. For the CIFAR10 used in the observation with 10 classes, the total time used during the GCL process is approximately 10 seconds. The time taken is roughly equivalent to one epoch optimization under the mentioned setup, while the performance gain with GCL requires the ECF without GCL more than one epoch to catch up.

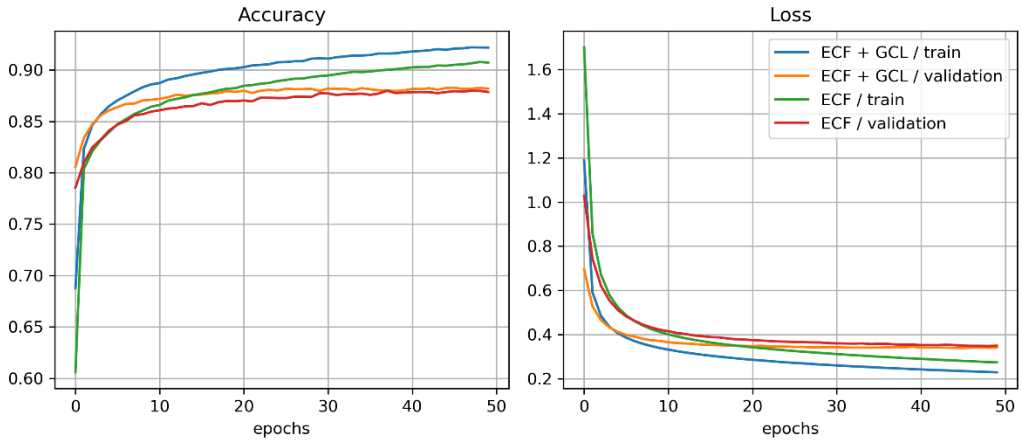

Figure 1. Observation on the training performance of ECF with and without GCL initialization on the CIFAR10 dataset, the backbone network used is pre-trained ResNet18 trained on ImageNet1k by [60, 61].

3.1 Comparison with other neuron designs

3.1.1. 20 epochs of training

The test accuracy results for this short training are shown in Table 2. At this limited number of training epochs, most of the nonlinear models fail to reach a more optimal state. However, ECF with GCL can reach a better state in most situations. Another key takeaway is that the ECF with GCL beats itself without GCL across all situations, which aligns with the previous observation made in Figure 1. Meanwhile, the accuracy loss from the M-P model is minor compared to the other models. The RBF design struggles the most when it comes to the VGG16 backbone; the limitation is likely due to the spherical shape resulting from the Euclidean distance, which does not perform well under high dimensional environment (4096 features returned from VGG16).

Table 2. Top-1 test accuracy score across different models and datasets after 20 epochs of training.

Neuron Design	Backbone Model	Top-1 Test Accuracy (%)					
		CIFAR10	**CIFAR100**	**MNIST**	**MTD**	**KTv1.0**	**SDNET2018**
M-P	ResNet18	88.48 ± 0.06	68.46 ± 0.04	97.48 ± 0.03	74.4 ± 0.4	96.64 ± 0.07	88.01 ± 0.05
	ResNet50	92.1 ± 0.1	74.93 ± 0.05	97.83 ± 0.03	76.0 ± 0.2	98.75 ± 0.04	90.92 ± 0.03
	VGG16	84.38 ± 0.09	62.66 ± 0.09	97.24 ± 0.03	82 ± 1	98.6 ± 0.1	87.10 ± 0.08
RBF	ResNet18	83.23 ± 0.07	31.1 ± 0.2	94.35 ± 0.03	72.4 ± 0.3	46.9 ± 0.4	83.61 ± 0.04
	ResNet50	87.8 ± 0.1	30.7 ± 0.4	94.34 ± 0.04	72.8 ± 0.5	27.9 ± 0.8	85.5 ± 0.1
	VGG16	10.00 ± 0.01	1.00 ± 0.01	11.35 ± 0.01	71.88 ± 0.07	5.89 ± 0.09	47 ± 4
ECF + GCL	ResNet18	87.69 ± 0.05	64.18 ± 0.01	96.39 ± 0.02	72.7 ± 0.3	90.5 ± 0.1	87.61 ± 0.05
	ResNet50	**91.06 ± 0.06**	**70.87 ± 0.03**	**96.58 ± 0.02**	72.4 ± 0.3	95.5 ± 0.1	**89.97 ± 0.03**
	VGG16	82.03 ± 0.09	56.4 ± 0.2	96.37 ± 0.03	**74.9 ± 0.6**	**96.1 ± 0.1**	86.35 ± 0.08
ECF	ResNet18	86.83 ± 0.03	61.67 ± 0.05	95.66 ± 0.02	72.1 ± 0.2	86.8 ± 0.1	86.40 ± 0.04
	ResNet50	90.85 ± 0.04	69.9 ± 0.1	96.20 ± 0.02	72.3 ± 0.3	94.69 ± 0.08	89.31 ± 0.06
	VGG16	82.0 ± 0.1	57.7 ± 0.1	93.97 ± 0.09	72.1 ± 0.2	92.78 ± 0.09	85.78 ± 0.07

3.1.2. 200 epochs of training

After letting all designs train further and save the best validated checkpoint for the final model, again, the ECF with GCL overcame itself without GCL, even after optimizing the network further, as shown in Tables 4 and 5.

Table 4. Top-1 test accuracy score on CIFAR10 across different models after 200 epoch training with a trained ResNet18 backbone. The number of steps per epoch is 625.

Neuron Design	Number of Parameters	Time per step (ms)	Top-1 Test Accuracy (%)
M-P	104,610	2	88.6 ± 0.1
RBF	104,610	20	**88.01 ± 0.04**
ECF + GCL	103,410	15	87.91 ± 0.07
ECF	103,410	15	87.82 ± 0.04

Table *5*. Top-1 and Top-5 test accuracy scores on CIFAR100 across different models after 200 epoch training with a trained ResNet18 backbone. The number of steps per epoch is 625.

Neuron Design	Number of Parameters	Time per step (ms)	Top-1 Test Accuracy (%)	Top-5 Test Accuracy (%)
M-P	245,300	3	68.44 ± 0.07	92.36 ± 0.03
RBF	245,300	38	57.9 ± 0.2	87.69 ± 0.05
ECF + GCL	224,900	30	**66.37 ± 0.07**	**91.45 ± 0.04**
ECF	224,900	30	65.92 ± 0.09	91.04 ± 0.07

Note again that the number of parameters could not be exactly matched since some designs have $d + 1$ parameters per unit and others have $2d + 1$ parameters per unit. This is an unexpected effect since GCL is meant to only jump the training process of ECF by some epochs, but it turns out it also seems to help prevent the model from falling into a worse local optimum. From Table 4, the Euclidean distance RBF does reach a better optimal state. However, it struggles when the number of labels increases to 100 with fewer training instances per class, as seen in Table 5, where ECF with GCL dominates other nonlinear designs. Note that this time per step is recorded from the first few epochs, where more corrections are made, requiring more computational power. The loss of performance of the ECF with GCL compared to the popular M-P model is also minimal compared to other nonlinear approaches.

4. Conclusions

The ECF models proposed can be optimized to perform image classification tasks more efficiently than other nonlinear neuron designs, while keeping the number of parameters low compared to the original Mahalanobis distance RBF. Although the increase in time per step compared to the Euclidean distance RBF is higher, ECF reaches its optimal state faster with GCL, mitigating this cost. Observations also suggest that GCL helps prevent ECF from experiencing confusion during training, which could otherwise lead to worse local optima. Taken together, these results indicate that ECF provides competitive performance under fixed-budget, frozen-backbone transfer settings, with favorable efficiency and parameter usage compared to alternative nonlinear designs. It also highlights that smart initialization in neural networks is possible and may lead to gains in optimization efficiency. A formal theoretical analysis of the convergence properties of the ECF with GCL is left as future work, which will further validate these empirical findings. It is undeniable that GCL is formulated for cases where the data is well-structured. However, GCL still performs significantly well in boosting efficiency despite the arbitrary, non-semantic features from black-box extractors. The ECF with GCL could also be integrated with ease into tasks where it has been proven that RBF networks remain relevant. The next interesting questions could be as follows: How would ECF perform when the backbone models are unfrozen? Does it perform well under attacks from adversarial samples or noisy data? Does a similar smart initialization exist for the M-P networks? While the results demonstrate the potential of ECF with GCL, several constraints should be noted. Experiments focus on plug-in classification heads under fixed compute budgets with frozen encoders. Benchmarks are moderate-scale image classification datasets (CIFAR10, CIFAR100, MNIST, and selected industrial datasets), which are not web-scale and have limited diversity. All main experiments were conducted on CPU due to resource constraints, with custom operations vectorized across

cores; reported per-method times and parameter counts reflect this environment. Hyperparameters were selected via grid search on a high-performance computing cluster prior to CPU experiments, but searches were modest and oriented toward parameter parity, not exhaustive optimization. The full Mahalanobis RBF baseline was evaluated only under parameter- and PCA-width-parity conditions; full evaluation is prohibitive at high-dimensional frozen-backbone features (e.g., $d = 512$ for ResNet18, $d = 4096$ for VGG16). Other tasks: end-to-end fine-tuning, detection/segmentation, sequence or graph tasks, adversarial robustness, calibration/uncertainty, and distribution-shift evaluations, were not explored. The inverse covariance matrix in ECF is diagonal, reducing rotational capacity, and GCL relies on supervised K-Means (choice of k, sensitivity). Although the ECF head is theoretically domain-agnostic, evidence is limited to transfer-learning heads on frozen CV embeddings; extension to other modalities or unfrozen backbones is anticipated but unverified. Reported results reflect asymptotic complexity and throughput/time-to-best; absolute performance may vary with hardware or computational budget.

5. Acknowledgements

This work was supported by Erawan HPC Project, Information Technology Service Center (ITSC), Chiang Mai University, Chiang Mai, Thailand. Financial and institutional support was provided by Chiang Mai University.

Author Contributions: Conceptualization, T.P.; methodology, T.P.; validation, T.P.; writing—review and editing, T.P.; supervision, P.S.

Funding: The APC was funded by Chiang Mai University.

Conflicts of Interest: The authors declare no conflict of interest.

References

[1] LeCun, Y.; Bengio, Y.; Hinton, G. Deep Learning. *Nature* **2015**, *521*(7553), 436–444. https://doi.org/10.1038/nature14539

[2] Strazzeri, F.; Sánchez-García, R. J. Possibility Results for Graph Clustering: A Novel Consistency Axiom. *Pattern Recognition* **2022**, *128*, 108687. https://doi.org/10.1016/j.patcog.2022.108687

[3] McCulloch, W. S.; Pitts, W. A Logical Calculus of the Ideas Immanent in Nervous Activity. *The bulletin of mathematical biophysics* **1943**, *5*(4), 115–133. https://doi.org/10.1007/BF02478259

[4] Nesterov, Y. A Method for Unconstrained Convex Minimization Problem with the Rate of Convergence O (1/K2). In *Dokl. Akad. Nauk. SSSR*; **1983**; Vol. 269, p 543.

[5] Mammone, R. J.; Zeevi, Y. Y. *Neural Networks: Theory and Applications*; Academic Press Professional, Inc., **1992**.

[6] Qian, N. On the Momentum Term in Gradient Descent Learning Algorithms. *Neural Networks* **1999**, *12*(1), 145–151. https://doi.org/10.1016/S0893-6080(98)00116-6.

[7] Ruder, S. An Overview of Gradient Descent Optimization Algorithms, 2017. https://arxiv.org/abs/1609.04747.

[8] Duchi, J.; Hazan, E.; Singer, Y. Adaptive Subgradient Methods for Online Learning and Stochastic Optimization. *Journal of Machine Learning Research* **2011**, *12*(61), 2121–2159.

[9] Zeiler, M. D. ADADELTA: An Adaptive Learning Rate Method, **2012**. https://arxiv.org/abs/1212.5701.

[10] Kingma, D. P.; Ba, J. Adam: A Method for Stochastic Optimization, **2014**.

[11] Dozat, T. Incorporating Nesterov Momentum into Adam. **2016**.

[12] Krizhevsky, A.; Sutskever, I.; Hinton, G. E. ImageNet Classification with Deep Convolutional Neural Networks. In *Advances in Neural Information Processing Systems*; Pereira, F., Burges, C. J., Bottou, L., Weinberger, K. Q., Eds.; Curran Associates, Inc., **2012**; Vol. 25.

[13] Simonyan, K.; Zisserman, A. Very Deep Convolutional Networks for Large-Scale Image Recognition, **2015**. https://arxiv.org/abs/1409.1556.

[14] Szegedy, C.; Liu, W.; Jia, Y.; Sermanet, P.; Reed, S.; Anguelov, D.; Erhan, D.; Vanhoucke, V.; Rabinovich, A. Going Deeper With Convolutions. In *Proceedings of the IEEE Conference on Computer Vision and Pattern Recognition (CVPR)*; **2015**; pp 1–9.

[15] He, K.; Zhang, X.; Ren, S.; Sun, J. Deep Residual Learning for Image Recognition. In *Proceedings of the IEEE Conference on Computer Vision and Pattern Recognition (CVPR)*; **2016**; pp 770–778.
[16] Howard, A. G.; Zhu, M.; Chen, B.; Kalenichenko, D.; Wang, W.; Weyand, T.; Andreetto, M.; Adam, H. MobileNets: Efficient Convolutional Neural Networks for Mobile Vision Applications, **2017**. https://arxiv.org/abs/1704.04861.
[17] Huang, G.; Liu, Z.; van der Maaten, L.; Weinberger, K. Q. Densely Connected Convolutional Networks. In *Proceedings of the IEEE Conference on Computer Vision and Pattern Recognition (CVPR)*; **2017**; pp 4700–4708.
[18] Zhang, X.; Zhou, X.; Lin, M.; Sun, J. ShuffleNet: An Extremely Efficient Convolutional Neural Network for Mobile Devices. In *Proceedings of the IEEE Conference on Computer Vision and Pattern Recognition (CVPR)*; 2018; pp 6848–6856.
[19] Chen, Y.; Li, J.; Xiao, H.; Jin, X.; Yan, S.; Feng, J. Dual Path Networks. In *Advances in Neural Information Processing Systems*; Guyon, I., Luxburg, U. V., Bengio, S., Wallach, H., Fergus, R., Vishwanathan, S., Garnett, R., Eds.; Curran Associates, Inc., **2017**; Vol. 30.
[20] Tan, M.; Le, Q. EfficientNet: Rethinking Model Scaling for Convolutional Neural Networks. In *Proceedings of the 36th International Conference on Machine Learning*; Chaudhuri, K., Salakhutdinov, R., Eds.; Proceedings of Machine Learning Research; PMLR, **2019**; Vol. 97, pp 6105–6114.
[21] Xie, Q.; Luong, M.-T.; Hovy, E.; Le, Q. V. Self-Training With Noisy Student Improves ImageNet Classification. In *Proceedings of the IEEE/CVF Conference on Computer Vision and Pattern Recognition (CVPR)*; **2020**; pp 10687–10698.
[22] Szegedy, C.; Zaremba, W.; Sutskever, I.; Bruna, J.; Erhan, D.; Goodfellow, I.; Fergus, R. Intriguing Properties of Neural Networks, **2014**. https://arxiv.org/abs/1312.6199.
[23] Goodfellow, I. J.; Shlens, J.; Szegedy, C. Explaining and Harnessing Adversarial Examples, 2015. https://arxiv.org/abs/1412.6572.
[24] Nguyen, A.; Yosinski, J.; Clune, J. Deep Neural Networks Are Easily Fooled: High Confidence Predictions for Unrecognizable Images. In *Proceedings of the IEEE Conference on Computer Vision and Pattern Recognition (CVPR)*; **2015**; pp 427–436.
[25] Fawzi, A.; Moosavi-Dezfooli, S.-M.; Frossard, P. Robustness of Classifiers: From Adversarial to Random Noise. In *Advances in Neural Information Processing Systems*; Lee, D., Sugiyama, M., Luxburg, U., Guyon, I., Garnett, R., Eds.; Curran Associates, Inc., **2016**; Vol. 29.
[26] Moosavi-Dezfooli, S.-M.; Fawzi, A.; Frossard, P. DeepFool: A Simple and Accurate Method to Fool Deep Neural Networks. In *Proceedings of the IEEE Conference on Computer Vision and Pattern Recognition (CVPR)*; **2016**; pp 2574–2582.
[27] Carlini, N.; Wagner, D. Adversarial Examples Are Not Easily Detected: Bypassing Ten Detection Methods. In *Proceedings of the 10th ACM Workshop on Artificial Intelligence and Security*; AISec '17; Association for Computing Machinery: New York, NY, USA, **2017**; pp 3–14. https://doi.org/10.1145/3128572.3140444
[28] Zadeh, P. H.; Hosseini, R.; Sra, S. Deep-RBF Networks Revisited: Robust Classification with Rejection, 2018. https://arxiv.org/abs/1812.03190
[29] Broomhead, D. S.; Lowe, D. *Radial Basis Functions, Multi-Variable Functional Interpolation and Adaptive Networks*; RSRE memorandum; Royal Signals and Radar Establishment, **1988**.
[30] Moradi, M. J.; Roshani, M. M.; Shabani, A.; Kioumarsi, M. Prediction of the Load-Bearing Behavior of SPSW with Rectangular Opening by RBF Network. *Applied Sciences* **2020**, *10*(3). https://doi.org/10.3390/app10031185
[31] Zhang, D.; Zhang, N.; Ye, N.; Fang, J.; Han, X. Hybrid Learning Algorithm of Radial Basis Function Networks for Reliability Analysis. *IEEE Transactions on Reliability* **2021**, *70*(3), 887–900. https://doi.org/10.1109/TR.2020.3001232
[32] Meng, X.; Zhang, Y.; Qiao, J. An Adaptive Task-Oriented RBF Network for Key Water Quality Parameters Prediction in Wastewater Treatment Process. *Neural Computing and Applications* **2021**, *33*(17), 11401–11414. https://doi.org/10.1007/s00521-020-05659-z

[33] Lin, M.; Zeng, X.; Wu, J. State of Health Estimation of Lithium-Ion Battery Based on an Adaptive Tunable Hybrid Radial Basis Function Network. *Journal of Power Sources* **2021**, *504*, 230063. https://doi.org/10.1016/j.jpowsour.2021.230063

[34] Karamichailidou, D.; Alexandridis, A.; Anagnostopoulos, G.; Syriopoulos, G.; Sekkas, O. Modeling Biogas Production from Anaerobic Wastewater Treatment Plants Using Radial Basis Function Networks and Differential Evolution. *Computers & Chemical Engineering* **2022**, *157*, 107629. https://doi.org/10.1016/j.compchemeng.2021.107629

[35] Liu, Z.; Dang, Z.; Yu, J. Stock Price Prediction Model Based on RBF-SVM Algorithm. In *2020 International Conference on Computer Engineering and Intelligent Control (ICCEIC)*; IEEE, **2020**; pp 124–127. https://doi.org/10.1109/ICCEIC51584.2020.00032

[36] Sermpinis, G.; Karathanasopoulos, A.; Rosillo, R.; de la Fuente, D. Neural Networks in Financial Trading. *Annals of Operations Research* **2021**, *297*(1), 293–308. https://doi.org/10.1007/s10479-019-03144-y

[37] Li, X.; Sun, Y. Application of RBF Neural Network Optimal Segmentation Algorithm in Credit Rating. *Neural Computing and Applications* **2021**, *33*(14), 8227–8235. https://doi.org/10.1007/s00521-020-04958-9

[38] Kumar, R.; Srivastava, S.; Dass, A.; Srivastava, S. A Novel Approach to Predict Stock Market Price Using Radial Basis Function Network. *International Journal of Information Technology* **2021**, *13*(6), 2277–2285. https://doi.org/10.1007/s41870-019-00382-y

[39] Sohrabi, P.; Jodeiri Shokri, B.; Dehghani, H. Predicting Coal Price Using Time Series Methods and Combination of Radial Basis Function (RBF) Neural Network with Time Series. *Mineral Economics* **2023**, *36*(2), 207–216. https://doi.org/10.1007/s13563-021-00286-z

[40] Amirian, M.; Schwenker, F. Radial Basis Function Networks for Convolutional Neural Networks to Learn Similarity Distance Metric and Improve Interpretability. *IEEE Access* **2020**, *8*, 123087–123097. https://doi.org/10.1109/ACCESS.2020.3007337

[41] Jiang, Q.; Zhu, L.; Shu, C.; Sekar, V. An Efficient Multilayer RBF Neural Network and Its Application to Regression Problems. *Neural Computing and Applications* **2022**, *34*(6), 4133–4150. https://doi.org/10.1007/s00521-021-06373-0

[42] Papadimitrakis, M.; Alexandridis, A. Active Vehicle Suspension Control Using Road Preview Model Predictive Control and Radial Basis Function Networks. *Applied Soft Computing* **2022**, *120*, 108646. https://doi.org/10.1016/j.asoc.2022.108646

[43] Cevikalp, H.; Larlus, D.; Jurie, F. A Supervised Clustering Algorithm for the Initialization of RBF Neural Network Classifiers. In *2007 IEEE 15th Signal Processing and Communications Applications*; IEEE, **2007**; pp 1–4. https://doi.org/10.1109/SIU.2007.4298803

[44] Wang, D.; Zeng, X.-J.; Keane, J. A. A Clustering Algorithm for Radial Basis Function Neural Network Initialization. *Neurocomputing* **2012**, *77*(1), 144–155. https://doi.org/10.1016/j.neucom.2011.08.023

[45] Czarnowski, I.; Jędrzejowicz, P. Kernel-Based Fuzzy C-Means Clustering Algorithm for RBF Network Initialization. In *Intelligent Decision Technologies 2016*; Czarnowski, I., Caballero, A. M., Howlett, R. J., Jain, L. C., Eds.; Springer International Publishing: Cham, **2016**; pp 337–347.

[46] Beheim, L.; Zitouni, A.; Belloir, F. New RBF Neural Network Classifier with Optimized Hidden Neurons Number. **2004**.

[47] Ibrikci, T.; Brandt, M. E.; Wang, G.; Acikkar, M. Mahalanobis Distance with Radial Basis Function Network on Protein Secondary Structures. In *Proceedings of the Second Joint 24th Annual Conference and the Annual Fall Meeting of the Biomedical Engineering Society] [Engineering in Medicine and Biology*; **2002**; Vol. 3, pp 2184–2185. https://doi.org/10.1109/IEMBS.2002.1053230

[48] Mahalanobis, P. C. ON THE GENERALIZED DISTANCE IN STATISTICS. *Sankhyā: The Indian Journal of Statistics, Series A (2008-)* **2018**, *80*, S1–S7.

[49] Lee, S.; Kil, R. M. A Gaussian Potential Function Network with Hierarchically Self-Organizing Learning. *Neural Networks* **1991**, *4*(2), 207–224. https://doi.org/10.1016/0893-6080(91)90005-P

[50] Park, J.; Sandberg, I. W. Universal Approximation Using Radial-Basis-Function Networks. *Neural Computation* **1991**, *3*(2), 246–257. https://doi.org/10.1162/neco.1991.3.2.246

[51] Valls, J. M.; Aler, R.; Fernández, O. Using a Mahalanobis-Like Distance to Train Radial Basis Neural Networks. In *Computational Intelligence and Bioinspired Systems*; Cabestany, J., Prieto, A., Sandoval, F., Eds.; Springer Berlin Heidelberg: Berlin, Heidelberg, **2005**; pp 257–263.

[52] Li, Z.; and Fox, J. M. Integrating Mahalanobis Typicalities with a Neural Network for Rubber Distribution Mapping. *Remote Sensing Letters* **2011**, *2*(2), 157–166. https://doi.org/10.1080/01431161.2010.505589

[53] Ning, X.; Tian, W.; Yu, Z.; Li, W.; Bai, X.; Wang, Y. HCFNN: High-Order Coverage Function Neural Network for Image Classification. *Pattern Recognition* **2022**, *131*, 108873. https://doi.org/10.1016/j.patcog.2022.108873

[54] Ning, X.; Tian, W.; He, F.; Bai, X.; Sun, L.; Li, W. Hyper-Sausage Coverage Function Neuron Model and Learning Algorithm for Image Classification. *Pattern Recognition* **2023**, *136*, 109216. https://doi.org/10.1016/j.patcog.2022.109216

[55] Xu, C.; Yu, F.; Xu, Z.; Liu, C.; Xiong, J.; Chen, X. QuadraNet: Improving High-Order Neural Interaction Efficiency with Hardware-Aware Quadratic Neural Networks. In *2024 29th Asia and South Pacific Design Automation Conference (ASP-DAC)*; IEEE, **2024**; pp 19–25. https://doi.org/10.1109/ASP-DAC58780.2024.10473936

[56] Zhang, L.; Zhang, B. A Geometrical Representation of McCulloch-Pitts Neural Model and Its Applications. *IEEE Transactions on Neural Networks* **1999**, *10*(4), 925–929. https://doi.org/10.1109/72.774263.

[57] Glorot, X.; Bengio, Y. Understanding the Difficulty of Training Deep Feedforward Neural Networks. In *Proceedings of the Thirteenth International Conference on Artificial Intelligence and Statistics*; Teh, Y. W., Titterington, M., Eds.; Proceedings of Machine Learning Research; PMLR: Chia Laguna Resort, Sardinia, Italy, 2010; Vol. 9, pp 249–256.

[58] Kumar, S. K. On Weight Initialization in Deep Neural Networks, 2017. https://arxiv.org/abs/1704.08863.

[59] Narkhede, M. V.; Bartakke, P. P.; Sutaone, M. S. A Review on Weight Initialization Strategies for Neural Networks. *Artificial Intelligence Review* **2022**, *55*(1), 291–322. https://doi.org/10.1007/s10462-021-10033-z.

[60] Wightman, R. PyTorch Image Models. *GitHub repository*, 2019. https://doi.org/10.5281/zenodo.4414861

[61] Wightman, R.; Touvron, H.; Jégou, H. ResNet Strikes Back: An Improved Training Procedure in Timm, **2021**. https://arxiv.org/abs/2110.00476

[62] Luo, L.; Xiong, Y.; Liu, Y.; Sun, X. Adaptive Gradient Methods with Dynamic Bound of Learning Rate, **2019**. https://arxiv.org/abs/1902.09843

[63] Krizhevsky, A.; Hinton, G.; others. Learning Multiple Layers of Features from Tiny Images. **2009**.

[64] Lecun, Y.; Bottou, L.; Bengio, Y.; Haffner, P. Gradient-Based Learning Applied to Document Recognition. *Proceedings of the IEEE* **1998**, *86*(11), 2278–2324. https://doi.org/10.1109/5.726791

[65] Huang, Y.; Qiu, C.; Yuan, K. Surface Defect Saliency of Magnetic Tile. *The Visual Computer* **2020**, *36*(1), 85–96. https://doi.org/10.1007/s00371-018-1588-5

[66] Kylberg, G. *Kylberg Texture Dataset v. 1.0*; External report (Blue series); 35; Centre for Image Analysis, Swedish University of Agricultural Sciences and Uppsala University, **2014**; p 4. www.cb.uu.se/~gustaf/texture.

[67] Maguire, M.; Dorafshan, S.; Thomas, R. J. SDNET2018: A Concrete Crack Image Dataset for Machine Learning Applications. **2018**. https://doi.org/10.15142/T3TD19

ASEAN
Journal of Scientific and Technological Reports
Online ISSN:2773-8752

Research article

Process Capability Assessment Using SPC and Cpk in the Analysis of Clay Soil Atterberg Limits: A Case Study in Pathum Thani Province

Pattaraporn Nueasri[1], and Rattanachot Thongpong[1*]

[1] Faculty of Industrial Technology, Valaya Alongkorn Rajabhat University under The Royal Patronage, Pathum Thani Province, 13180, Thailand
* Correspondence: rattanachot.thong@vru.ac.th

Citation:
Nueasri, P.; Thongpong, R. Process capability assessment using SPC and Cpk in the analysis of clay soil atterberg limits: a case study I Pathum Thani Province *ASEAN J. Sci. Tech. Report.* **2026**, *29*(2), e260404. https://doi.org/10.55164/ajstr.v29i2.260404.

Article history:
Received: July 14, 2025
Revised: October 9, 2025
Accepted: November 15, 2025
Available online: January 21 2026

Publisher's Note:
This article is published and distributed under the terms of the Thaksin University.

Abstract: This study evaluated the consistency and capability of the testing process for the Plasticity Index (PI) of fine-grained soils, a parameter critical for soil classification and geotechnical design, particularly in compaction and foundation analyses. Statistical Process Control (SPC) was applied using X–MR control charts to monitor process stability, while process capability was assessed through Cp and Cpk indices under specification limits of LSL = 2.00 and USL = 10.00. Trend analysis and uncertainty evaluation were also conducted to strengthen the assessment framework. Results showed that the PI testing process was statistically stable, with all data points within control limits. However, process capability indices (Cp = 0.702, Cpk = 0.616) were below the benchmark value of 1.33, indicating insufficient performance due to inherent variability. Linear regression revealed no significant time-related trend (R^2 = 0.1%, p = 0.864), confirming temporal consistency. Uncertainty analysis yielded an expanded uncertainty of ±0.537 at 95% confidence, equivalent to 9.7% of the mean PI. Such uncertainty suggests possible misclassification of results near specification thresholds. In conclusion, although the PI testing process was under statistical control and free of time-related drift, it exhibited substantial variability and high uncertainty. These findings emphasize the need to reduce variation and incorporate uncertainty into quality management practices, providing a more reliable basis for decision-making in geotechnical engineering applications.

Keywords: Plasticity index; statistical process control; capability; soil compaction

1. Introduction

Soil is a natural material that plays a fundamental role in civil engineering, serving as the foundation for essential infrastructure such as buildings, roads, dams, and other load-bearing structures. The geotechnical suitability of local soil properties is a decisive factor influencing structural stability and safety, particularly in rapidly urbanizing regions such as Pathum Thani Province, located within the Bangkok Metropolitan Region. The predominant clay soils in this area are highly sensitive to fluctuations in moisture content; variations in water can induce swelling or shrinkage, thereby affecting load-bearing capacity and potentially compromising structural integrity. Therefore, accurate and reliable soil characterization is imperative for effective infrastructure planning and design. A widely accepted approach for evaluating the behavior of fine-grained soils involves determining the Atterberg Limits, which include the Liquid Limit (LL), Plastic Limit (PL), and Plasticity

Index (PI). These parameters are essential for classifying clay types and predicting soil performance under varying moisture conditions and applied loads [1]. However, the results of Atterberg Limit tests often exhibit variability due to differences in operator expertise, equipment calibration, sample preparation, and environmental factors, which may undermine data reliability and reproducibility.

To address such inconsistencies, researchers have recently introduced Statistical Process Control (SPC) and the Process Capability Index (Cpk) from industrial engineering as systematic tools for assessing the stability and performance of laboratory testing processes. For example, Hasan and Abuel-Naga [2] applied electrochemical techniques to improve the precision of PI measurements, enabling more reliable process capability assessments. Marušić and Jagodnik [3] demonstrated that the fall cone method produces more consistent LL results compared to the conventional Casagrande apparatus. Likewise, Rosas et al. [4] and Knadel et al. [5] emphasized the potential of integrating machine learning and spectroscopy techniques to reduce measurement bias and enhance test accuracy. Despite these advancements, most previous studies have focused primarily on improving individual testing methods rather than evaluating the overall process capability and measurement uncertainty of soil characterization procedures. Furthermore, the application of SPC and Cpk analysis to geotechnical testing, particularly for Atterberg Limits of clay soils, remains limited, especially within the ASEAN region, where heterogeneous soil conditions and diverse laboratory practices can lead to inconsistent results. Accordingly, the present study aims to analyze the PI of clay soils in Pathum Thani Province and to evaluate the consistency and capability of the testing process through the application of SPC and Cpk methodologies. The ultimate objective is to systematically quantify data reliability and process stability, thereby ensuring that the test results are robust and suitable for incorporation into geotechnical design frameworks in rapidly developing urban environments.

2. Theoretical Framework and Related Research

The evaluation of soil properties, particularly the Atterberg Limits of clayey soils, is fundamental in civil engineering as it influences the design and long-term stability of infrastructure [1–3]. The Liquid Limit (LL), Plastic Limit (PL), and Plasticity Index (PI) are essential parameters for soil classification and for predicting deformation behavior under variable moisture and load conditions. However, traditional testing methods often face variability stemming from operator technique and equipment inconsistencies, which may compromise data reliability [6]. To improve precision and consistency, industrial engineering approaches such as Statistical Process Control (SPC) and the Process Capability Index (Cpk) have been integrated into soil testing [4,7]. Recent studies have explored alternative measurement techniques, including electrical resistivity modeling [8], diffuse reflectance spectroscopy [9], and machine learning-based estimations [10], aiming to reduce human-induced errors and enhance rapid analysis. Moreover, the inherent variability of geotechnical properties significantly affects design safety, highlighting the importance of robust statistical evaluations [6]. The strong correlation between Atterberg Limits and compaction characteristics further emphasizes PI as a key predictor for field performance [11]. Additionally, chemical and electrochemical stabilization techniques have proven effective in modifying soil plasticity in tropical soils [12]. These integrated approaches underscore the necessity of combining advanced measurement techniques and process control strategies to enhance data reliability and structural safety in geotechnical engineering.

Therefore, the theoretical foundation of this study is built upon the integration of geotechnical testing principles with industrial quality management methodologies. By combining the deterministic nature of soil mechanics (through Atterberg Limits and classification) with statistical control concepts (SPC, Cp, Cpk) and uncertainty quantification, the framework provides a holistic approach to assess both the accuracy and consistency of soil property testing. This integration is particularly novel in the ASEAN context, where laboratory variability often challenges the reliability of soil classification for design and construction.

2.1 Atterberg Limits and Soil Classification

Atterberg Limits are quantitative indices used to describe the consistency and moisture-related behavior of clay soils. These limits provide systematic insight into strength, shrinkage potential, and plasticity under varying water contents [13]. Standardized testing procedures follow ASTM D4318–17 [1] and comprise:

- Liquid Limit (LL): The moisture content at which soil transitions from a plastic to a liquid state.
- Plastic Limit (PL): The moisture level at which soil shifts from semi-solid to plastic behavior.
- Shrinkage Limit (SL): The lowest moisture content at which further drying does not result in volume reduction. Soil classification based on the PI is derived using the equation 1.

$$PI = LL - PL \quad (1)$$

This index allows the classification of soils according to the Unified Soil Classification System (USCS), where the Plasticity Index (PI) and Liquid Limit (LL) thresholds define the soil type and its expected engineering behavior. The USCS categorizes fine-grained soils based on LL and PI values using the Casagrande Plasticity Chart, which delineates soil boundaries through the empirical A-line relationship, as shown in equation 2.

$$PI = 0.73(LL - 20) \quad (2)$$

This relationship helps differentiate clay and silt behavior and is widely applied in geotechnical engineering practice for soil classification purposes.

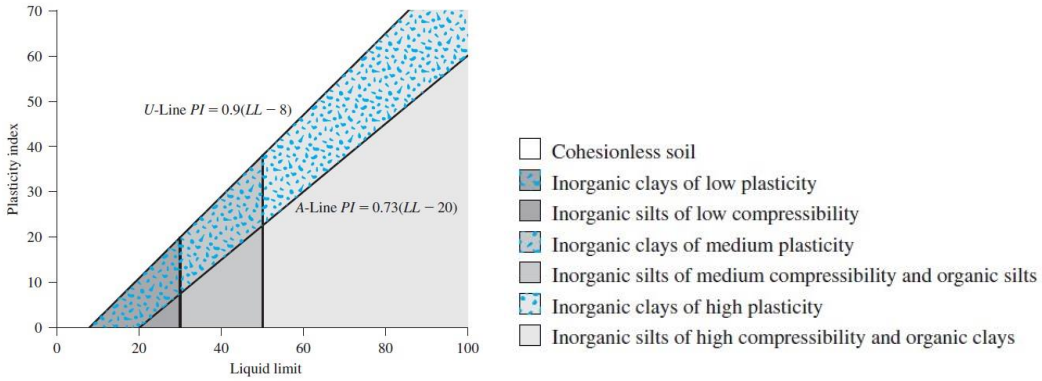

Figure 1. Casagrande plasticity chart showing classification of fine-grained soils based on LL and PI [14].

The A-line separates silts (ML/MH) from clays (CL/CH), with plasticity and liquidity thresholds guiding the classification [14]. Soil groups are interpreted not only by index values but also by their geotechnical behavior in construction and load-bearing scenarios.

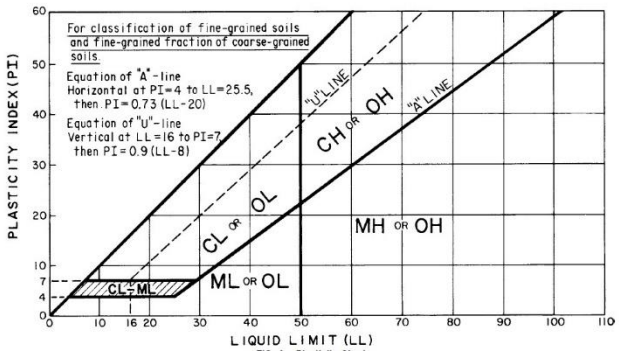

Figure 2. Plasticity chart for the USCS classification according to ASTM D4318-17 [1]

Table 1. Soil classification criteria according to USCS

Soil Group (USCS)	LL (%)	PI (%)	Key Characteristics
CL – Clay, Low Plasticity	LL ≤ 50	PI below A-line and PI < 7 (or ~7–17: medium)	Acceptable settlement; easily compacted
CH – Clay, High Plasticity	LL > 50	PI above A-line and PI > 17	High shrink–swell potential; requires stabilization (e.g., lime/cement)
ML / MH – Silt (Low/High Plasticity)	varies with LL	PI below A-line	Low shear strength; easily saturated and flow-prone

Recent advancements in soil characterization have introduced alternative methods to assess Atterberg Limits with improved precision and reproducibility. These approaches range from spectroscopic techniques to machine learning models and geotechnical interrelationships.

This study introduces a process-oriented framework for Atterberg Limits evaluation by integrating Statistical Process Control (SPC), process capability indices, and uncertainty assessment. Unlike previous works that emphasized prediction, correlation, or material characterization, this approach bridges geotechnical testing with quality management tools, providing a new perspective on the reliability, stability, and interpretive confidence of soil property testing, as summarized in Table 2.

Table 2. Summary of Recent Studies on Atterberg Limits and Identified Research Gaps

Reference	Atterberg Limits Focus	Spectroscopy / Indirect Estimation	Machine Learning (ML)	Correlation / Empirical Analysis	Soil Structure	SPC / Process Capability	Uncertainty & Guard Band
Knadel, Rehman et al. [5]	LL, PL, PI	x					
Rosas et al. [4]	LL, PL, PI		x				
Bhavya & Nagaraj [10]	LL, PL, PI				x		
Karakan et al. [15]	LL, PI			x			
Dehghanian & İpek [16]	PI				x		
This Study	LL, PL, PI					x	x

As summarized in Table 2, most previous studies focused on improving test precision or correlation analysis but rarely quantified process capability and uncertainty. This identified gap forms the foundation of the present study.

2.2 Statistical Process Control (SPC)

Statistical Process Control (SPC) refers to a set of statistical tools used to monitor, analyze, and control variability within testing or production processes. In this study, the primary SPC tool applied is the Individual Control Chart, also known as the X-MR Chart, which consists of two components [17].

2.2.1. X-Chart (Individual Value Chart) is used to monitor the central tendency of measured data.

- Mean of the data series:

$$\bar{X} = \frac{1}{n}\sum_{i=1}^{n} X_i \tag{3}$$

- Control limits for the X-Chart:

$$\mathrm{UCL_X} = \bar{X} + 2.66 \cdot \overline{MR}, \quad \mathrm{LCL_X} = \bar{X} - 2.66 \cdot \overline{MR} \tag{4}$$

Where :

$\bar{X}$ = Mean of the data series

n = Number of samples

X_i = Individual measurement

$\overline{MR}$= Average moving range

$\mathrm{UCL_X}$ = Upper control limit

$\mathrm{LCL_X}$ = Lower control limit

2.2.2 ***The MR-Chart (Moving Range Chart)*** is used to assess short-term variability between successive measurements.

- Moving range for each data pair:

$$MR_i = |X_i - X_{i-1}| \tag{5}$$

- Mean of the moving ranges:

$$\overline{MR} = \frac{1}{n-1}\sum_{i=2}^{n} MR_i \tag{6}$$

2.2.3 Process Capability Index (Cpk)

The Process Capability Index (Cpk) is a quantitative metric used to evaluate how well a process can produce outputs within predefined specification limits. It considers both process variability and the location of the process mean relative to the specification range.

The standard formula is:

$$\mathrm{Cpk} = \min\left(\frac{USL - \mu}{3\sigma}, \frac{\mu - LSL}{3\sigma}\right) \tag{7}$$

Where:

USL = Upper Specification Limit

LSL = Lower Specification Limit

μ = Process mean

σ = Standard deviation of the data

Common interpretation criteria include:

Cpk < 1.00, meaning the process is incapable or poorly controlled

Cpk = 1.00, meaning marginally acceptable

Cpk > 1.33, meaning the process exhibits high capability and statistical control

Integrating Cpk into the evaluation of soil properties, such as PI, enables a quantitative link between geotechnical characteristics and the ability to maintain testing consistency and quality. This approach supports data-driven decision-making in soil classification and construction design.

3. Research Framework

This study is grounded in an integrative framework combining concepts from civil engineering and industrial engineering. Its primary focus is the assessment of clay soil properties using Atterberg Limits, specifically the LL, PL, and PI. These parameters are essential for classifying clay soils according to the USCS and for predicting soil behavior under real-world conditions, such as mechanical loading and moisture variation. The data obtained from laboratory tests are subsequently analyzed statistically to evaluate process consistency and quality through the application of SPC and the computation of the Cpk [18]. The independent variables in this study include the Atterberg Limit values (LL, PL, PI) and fundamental soil sample characteristics such as sampling location and initial moisture content, which directly influence soil behavior. The dependent variables are the Cp and Cpk indices, which reflect the capability of the testing process. A Cpk

≥ 1.33 is typically required for high capability relative to specification limits; values between 1.00–1.33 indicate marginal capability as shown in Figure 3.

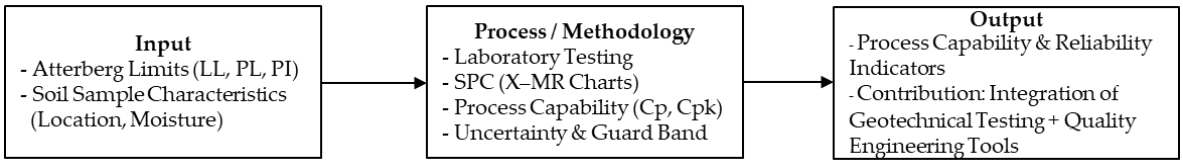

Figure 3. Research framework for Atterberg Limits testing with SPC, Cp/Cpk, and uncertainty analysis.

4. Methodology

4.1 Study Area and Soil Sampling

This study was conducted in Pathum Thani Province, located in the lower Chao Phraya River basin. The region's predominant soil type is moisture-saturated clay, which is particularly sensitive to environmental fluctuations. A total of 50 soil samples were collected across diverse subzones with varying environmental conditions to ensure a broad representation of local variability. Samples were gathered in their natural moisture state, stored in sealed containers, and subsequently transferred to the laboratory for formal testing.

4.2 Soil Property Testing

The collected soil samples were subjected to standard laboratory tests to determine their Atterberg Limits, including Liquid Limit (LL), Plastic Limit (PL), and Shrinkage Limit (SL), in accordance with ASTM D4318-17 [1]. Following the completion of these tests, the Plasticity Index (PI) was calculated using the equation. The complete test results are summarized in Table 3, providing a statistical foundation for subsequent analysis of process stability and capability.

Table 3. Atterberg Limits of Clay Soil Samples from Laboratory Testing

Sample No.	Liquid Limit (LL, %)	Plastic Limit (PL, %)	Shrinkage Limit (SL, %)	Plasticity Index (PI, %)	VLL	VPL	VSL
1	60.65	57.52	33.57	3.13	0.9	0.46	0.07
2	52.06	46.47	32.24	5.6	0.88	0.75	0.4
3	61.52	57.99	28.22	3.52	0.98	0.59	0.47
4	40.29	35.26	23.95	5.03	0.8	0.65	0.06
5	48.46	40.76	27.08	7.7	0.89	0.74	0.48
6	47.84	43.1	26.39	4.74	0.75	0.59	0.41
7	51.87	45.64	26.12	6.23	0.8	0.68	0.51
8	48.45	39.34	29.27	9.11	0.93	0.44	0.32
9	59.83	53.79	33.99	6.04	0.82	0.4	0.28
10	50.14	44.68	34.02	5.46	0.99	0.86	0.46
…	…	…	…	…	…	…	…
48	56.51	51.64	41.32	4.87	0.83	0.57	0.15
49	53.56	49.37	31.4	4.19	0.75	0.52	0.25
50	42.03	36.33	26.91	5.7	0.74	0.42	0.31

*Note: Table 3 shows selected samples for illustration. Full results are included in the Supplementary Appendix.

The relationship between moisture content and the volume ratio of soil samples (n = 50) exhibits a consistently convex upward trend. This pattern reflects the expansion behavior of clayey soil mass as moisture increases, a characteristic attributable to its high-water adsorption and retention capacity. In the low moisture range (below 20%), the volume ratio remains relatively stable within 0.2–0.4, indicating that the soil remains in a semi-solid state with preserved internal structure and limited deformability. When moisture rises to

approximately 25–40%, the volume ratio increases noticeably, suggesting a transition into the plastic state where the soil demonstrates enhanced deformability without fracturing. This behavior aligns with the defined thresholds of PL and LL, as described by Atterberg [19]. Beyond 45% moisture content, the graph shows a rapid increase in volume ratio, indicating entry into the liquid state. In this condition, the soil loses its shape-retention capacity, and interparticle bonding weakens significantly. Such moisture levels exceed the LL and can adversely affect the structural integrity of geotechnical applications, including foundations and compacted fills.

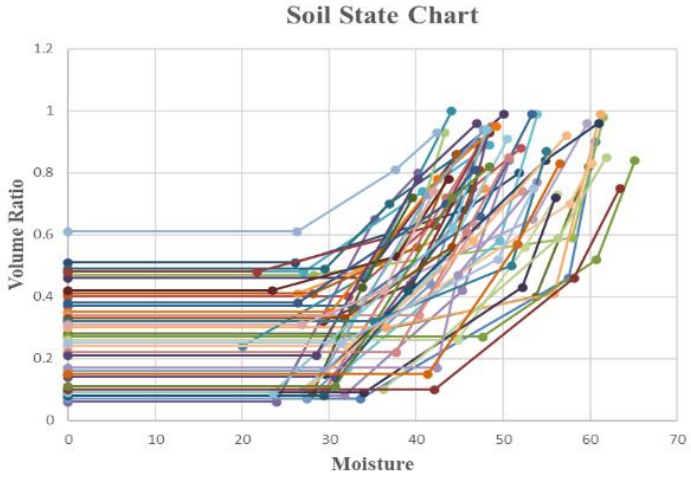

Figure 4. The relationship between moisture content and the volume ratio of soil samples

Figure 4 illustrates this volumetric transition clearly. The slope of the curve across different intervals also suggests sample-specific responses to moisture variation. Notably, soils with higher PI values tend to exhibit greater expansion, potentially due to differences in clay mineral composition. These PI values are consequently used as key indicators for evaluating soil behavior and serve as the basis for statistical process analysis in subsequent research stages.

Table 4. Statistical Analysis of Atterberg Limit Variables

Variable	N	Mean	SE Mean	StDev	Minimum	Q1	Median	Q3
LL	50	51.454	0.917	6.484	39.600	47.080	50.325	56.330
PL	50	45.944	0.988	6.987	33.770	40.627	44.750	51.785
SL	50	31.184	0.821	5.806	20.030	27.365	29.835	33.995
PI	50	5.510	0.269	1.902	2.170	4.250	5.335	6.230

The statistical analysis of 50 clay soil samples revealed Atterberg Limit values that reflect distinctive geotechnical characteristics of the study area in Pathum Thani Province. Specifically, the average LL was 51.45%, with a standard deviation of 6.48, indicating that local soils exhibit a broad moisture transition range from liquid to plastic states. Liquid Limit values exceeding 50% suggest that most samples belong to high water-retention clays with pronounced plasticity behavior. The PL had an average of 45.94% and a median of 45.77%, reflecting a symmetrically distributed dataset and indicating that most soils transition from semi-solid to plastic form at relatively high moisture levels. This range aligns with favorable workability for foundation and compaction applications. Shrinkage Limit (SL) values averaged 31.18%, suggesting that the minimum moisture level at which volume reduction ceases remains relatively high. This behavior is typical of deep-layer clays with fine-grained structures capable of preserving volumetric stability upon drying. The Plasticity Index (PI), defined as the difference between LL and PL, averaged 5.51% with a range of 2.17–10.75%, classifying the soil samples within the low to medium plasticity range based on USCS criteria. The concentration of PI values within a narrow bandwidth indicates a high degree of consistency in soil characteristics across the sampled region. This observation aligns with initial control chart results (X-MR), which confirmed process stability. The statistical data suggest that clay soils in Pathum Thani exhibit low to moderate plasticity, making them

suitable for compaction work with manageable moisture sensitivity. These findings provide a sound foundation for subsequent process capability evaluation using the Cpk index and SPC methodology.

5. Results

5.1 Process Consistency Evaluation of Plasticity Index Testing

The consistency of the Plasticity Index (PI) testing process was assessed using an Individual Control Chart (X-MR Chart), which includes two components: the Individual Value Chart (X-Chart) and the Moving Range Chart (MR-Chart). These charts evaluate both central tendency and short-term variability across successive measurements of PI values. The statistical control parameters derived from the test data are summarized in Table 5.

Table 5. Control Chart Parameters from X-MR Analysis of PI Data

Process Mean	Mean Moving Range	Upper Control Limit X Chart	Lower Control Limit X Chart	Upper Control Limit MR Chart	Lower Control Limit MR Chart
5.51	2.426	11.96	-0.94	7.925	0

The analysis revealed that the average Plasticity Index (PI) from 50 test samples was 5.51%, with a standard deviation of 1.90. Based on the Individual Value Chart, all data points were found within the statistical control boundaries. Upper Control Limit (UCL) = 11.96 and Lower Control Limit (LCL) = –0.94 with no observations falling outside the acceptable range. This indicates the absence of special cause variation or systematic irregularities. Similarly, the Moving Range Chart showed an average moving range ($\overline{MR}$) of 2.43, and no individual MR values exceeded the UCL of 7.93. These results confirm that the PI testing process was statistically stable and consistent across the entire dataset, as shown in Figure 5.

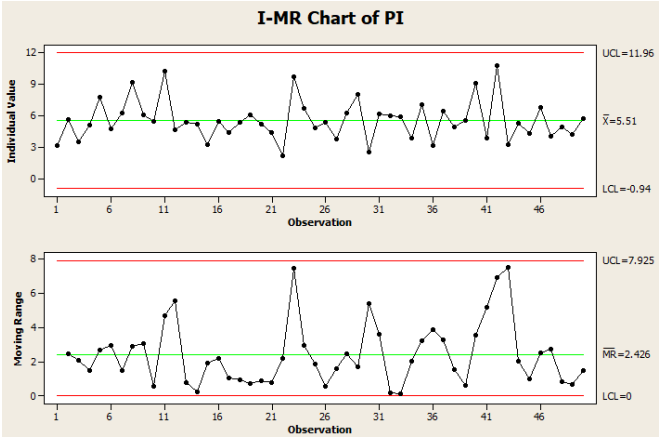

Figure 5. X-MR Control Chart of Plasticity Index

Upon examining the data distribution, no systematic bias or directional drift was observed, and the variation appeared random throughout the dataset. This confirms that the PI testing process was statistically "in control," in accordance with the principles of Statistical Process Control (SPC) [17]. There were no signs of abnormal behavior caused by process shifts or external disturbances. As such, the test results from all 50 samples can be considered sufficiently reliable, serving as a strong foundation for evaluating the process capability index (Cpk) in the subsequent section.

5.2 Process Capability Assessment of Plasticity Index Testing.

The capability of the Plasticity Index (PI) testing process was evaluated using the Cp and Cpk indices under predefined specification limits: a Lower Specification Limit (LSL) of 2.00 and an Upper Specification Limit (USL) of 10.00. This specification range is grounded in geotechnical engineering considerations. A PI value below 2.00 generally indicates non-plastic material, which is unsuitable for compaction applications due to poor deformation capacity. Conversely, PI values exceeding 10.00 suggest highly plastic clays that may

cause structural instability, such as shrinkage upon drying or excessive swelling when exposed to moisture. This rationale aligns with the classification criteria defined by the Unified Soil Classification System (USCS), which categorizes clays into three ranges: Low plasticity: PI < 7**,** Medium plasticity: 7 ≤ PI ≤ 17, and High plasticity: PI > 17**.** Therefore, selecting a specification range of 2–10 effectively encompasses materials within the "low to medium plasticity" category, consistent with the characteristics of Pathum Thani clay soils observed in this study. These threshold values support the engineering suitability of the materials for foundational and fill applications while setting boundaries that protect against undesirable behaviors under field conditions, as presented in Figure 6.

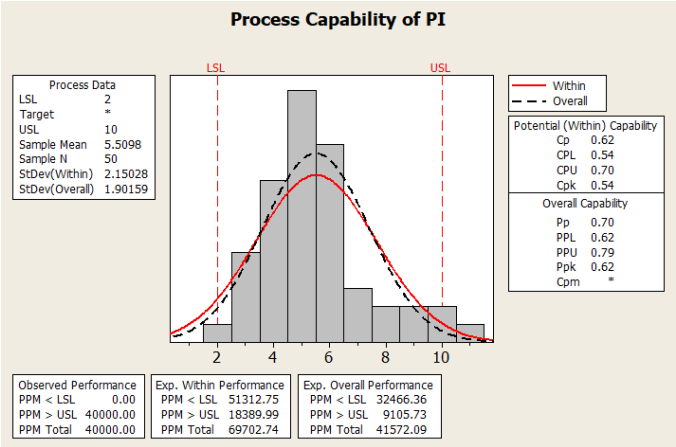

Figure 6. Process Capability Analysis of Plasticity Index

The analysis revealed that the process capability index values were Cp = 0.702 and Cpk = 0.616, both below the commonly accepted benchmark of 1.00 or higher for quality control. A Cp value less than 1.00 indicates that the process variation exceeds the tolerance defined by the specification limits. In addition, the Cpk value of 0.616 confirms that the process mean is not centered within the specification range. This conclusion is supported by the observation that the upper capability (CPU) exceeds the lower capability (CPL), which indicates that the process distribution is skewed toward the Lower Specification Limit (LSL). Cp reflects the theoretical capability of the process, assuming perfect centering. The low value suggests substantial internal variation. On the other hand, Cpk considers the position of the process mean, and the resulting value reveals that the process average deviates from the midpoint of the specification range. Such misalignment may introduce performance risks under field conditions. The Parts Per Million (PPM) analysis showed that approximately 4 percent of the results exceeded the Upper Specification Limit (USL), which is equivalent to 40,000 PPM. Although no values fell below the LSL, the presence of high-side outliers negatively affects overall process conformity. According to structural engineering standards, a Cpk value of at least 1.33 is typically required to ensure reliable performance. The observed Cpk falls short of this requirement, even when material-specific variability is taken into account. In conclusion, while the PI testing process demonstrates statistical stability, the overall capability remains low. To address this issue, it is recommended to improve moisture control, enhance sample preparation procedures, and refine measurement techniques. These adjustments can help reduce process variation and increase the Cpk value to meet engineering reliability standards more effectively.

5.3 Trend Analysis

Trend analysis of the Plasticity Index (PI) values across 50 test samples revealed a randomly distributed pattern, with no observable upward or downward trend throughout the testing sequence. The corresponding sample sequence chart confirms that the data remained statistically stable over time. This indicates that the testing process did not experience time-based drift or variation induced by external factors, such as environmental fluctuations or procedural inconsistency during sample handling, as shown in Figure 7.

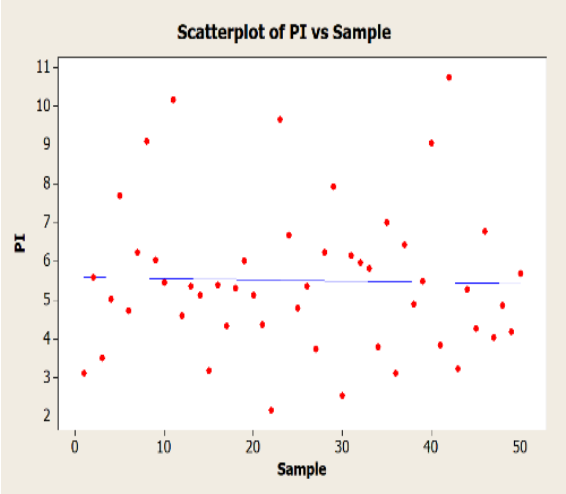

Regression Analysis: PI versus Sample

The regression equation is
PI = 5.59 - 0.0032 Sample

Predictor	Coef	SE Coef	T	P
Constant	5.5923	0.5515	10.14	0.000
Sample	-0.00323	0.01882	-0.17	0.864

S = 1.92070 R-Sq = 0.1% R-Sq(adj) = 0.0%

Analysis of Variance

Source	DF	SS	MS	F	P
Regression	1	0.109	0.109	0.03	0.864
Residual Error	48	177.077	3.689		
Total	49	177.186			

Figure 7. Trend Analysis of the Plasticity Index (PI)

To investigate the temporal behavior of the PI and determine whether a systematic trend exists across the sequence of measurements, a Linear Trend Analysis was performed using Minitab 16. The dataset consisted of PI values from 50 consecutively measured soil samples. The results were visualized through a scatterplot with an overlaid linear trend line to assess directional movement. The analysis indicated that PI values were distributed across the range of approximately 2 to 11, without exhibiting any clear upward or downward trajectory. The linear trend line displayed an extremely shallow slope, suggesting no significant temporal change in PI values throughout the testing sequence. If evaluated using a regression model, the coefficient of determination (R^2) was found to be lower than 0.10, implying that linear trends explain only a minimal portion of the observed variability. This finding supports the interpretation that the PI testing process is temporally stable and free from progressive drift or systematic deviation. The absence of trend-related anomalies aligns with the results from the X-MR control chart, which demonstrated that the process operates within statistically stable conditions. Therefore, there is no indication of abnormal variation at any specific point in the sample sequence. The trend-free nature of the data reinforces earlier SPC results and confirms that the testing process was conducted under controlled and repeatable conditions, without interference from special causes. The estimated linear regression equation, using Sample Order as the independent variable and PI as the dependent variable, is expressed as:

$$\widehat{PI} = 5.5923 - 0.0032 \cdot \text{Sample}$$

This equation further illustrates that the slope is nearly zero, and the process mean remains consistent throughout the sample order.

Table 6. The regression analysis results

Slope	R-Squared (R^2)	P-Value	Residual Standard Deviation
−0.0032	0.1%	0.864	1.9207

Based on the regression analysis results, the slope of –0.0032 indicates a slight negative trend in PI values as sample order increases. However, the associated p-value of 0.864 demonstrates that this trend is not statistically significant. The coefficient of determination (R^2) equals just 0.1%, meaning that the linear trend line explains only 0.1% of the variation in PI values. This suggests that the trend has virtually no influence on the overall behavior of the dataset. Accordingly, it can be concluded that the PI testing process does not exhibit a clear temporal pattern across the sample sequence. This finding supports the earlier X-MR chart analysis, which confirmed the statistical stability of the testing process and the absence of systematic time-dependent changes.

5.4 Uncertainty Analysis

The uncertainty of the mean PI was evaluated using a 95 % confidence interval to assess the reliability and precision of the testing results. The computed mean PI was 5.51, with a 95 % confidence interval ranging from 5.08 to 5.94, indicating a relatively narrow dispersion and confirming the stability of the dataset. This narrow range reflects good measurement precision and supports confidence in the reliability of soil quality assessments. According to the statistical summary presented in Table 3, the descriptive values are as follows: Mean = 5.51, Standard Deviation = 1.90, and 95 % Confidence Interval of the Mean = [5.08, 5.94]. Subsequently, the expanded uncertainty was determined using the following equation 8.

$$U = k \cdot \frac{\sigma}{\sqrt{n}} \tag{8}$$

Where:

U = Expanded Uncertainty
k = Coverage factor (for 95% confidence, typically k = 2)
σ = Standard deviation
n = Sample size

This expanded uncertainty offers a quantitative expression of the range within which the true mean value is expected to fall with high confidence. A relatively low uncertainty indicates high reproducibility and test consistency.

$$U = 2 \cdot \frac{1.90}{\sqrt{50}}$$
$$\text{by } k = 2 \text{ (95\% confidence interval)}$$
$$= \pm 0.537$$

The expanded uncertainty of ±0.537 represents the confidence interval of the true process mean, not the deviation of individual test results. This indicates that the estimated mean PI lies within this range at a 95% confidence level. This becomes especially critical when considered alongside specification limits. For instance, if a measured PI value approaches the Upper Specification Limit (USL) of 10.00 such as 9.5 units the inclusion of uncertainty may result in values exceeding the allowable threshold. Therefore, caution is advised when interpreting PI results, and it is recommended to evaluate uncertainty in conjunction with specification criteria to minimize engineering risk. On the other hand, a narrow confidence interval reflects the consistency of the testing process and reduces the likelihood that the results will deviate substantially from standard thresholds. This reinforces the reliability of the PI measurements and supports their use in process capability evaluation.

Table 7. Summary of Expanded Uncertainty (±U) and Percent Error

Summary	Value	Description
PI (μ)	5.51	Based on the Plasticity Index results from 50 soil samples
(σ)	1.90	Calculated using Minitab statistical analysis
Factor (k)	2	Corresponds to a 95% confidence level
Uncertainty (±U)	±0.537	$U = 2 \cdot \frac{1.90}{\sqrt{50}}$
% Uncertainty of Mean	9.74	$\frac{U}{\mu} \times 100 = 0.537 \div 5.51 \times 100$

To enhance decision reliability near specification boundaries, a Guard Band was established based on the expanded uncertainty (±0.537). This approach is especially critical when assessing Plasticity Index (PI) values that approach the Lower Specification Limit (LSL = 2.00) or Upper Specification Limit (USL = 10.00).

Table 8. Guard Band Assessment for Specification-Based Decision-Making

Specification Limit	Value	Guard Band (±U)	Cautionary Interpretation
Lower Spec Limit	2.00	2.00 + 0.537 = 2.537	PI ≤ 2.537 should be considered near the LSL boundary.
Upper Spec Limit	10.00	10.00 – 0.537 = 9.463	PI ≥ 9.463 should be considered near the USL boundary.

Values falling within the range of 2.537 to 9.463 are considered to lie within the compliance zone, representing acceptable conformity to the specification limits. However, PI values approaching either limit should be interpreted with engineering caution, as measurement uncertainty may influence the classification outcome. For instance, a sample yielding a PI of 9.2 lies within the upper cautionary zone. Considering the expanded uncertainty of ±0.537, the true value could potentially exceed the Upper Specification Limit (USL = 10.00) in practice. Therefore, such borderline cases should be treated conservatively and not be conclusively classified as within specification, particularly in quality control applications such as soil compaction or fill material evaluation. Incorporating guard bands into process capability evaluation enhances the robustness and reliability of engineering decisions near specification boundaries. This approach helps reduce false acceptance or rejection risks, ensuring more dependable quality assurance under conditions of measurement uncertainty.

6. Discussion

In the process capability analysis using Statistical Process Control (SPC), the X–MR charts for Liquid Limit (LL), Plastic Limit (PL), and Plasticity Index (PI) demonstrated that all test results were within control limits, confirming statistical stability and the absence of abnormal variation. This outcome indicates that the testing procedure is consistent and reliable for laboratory practice. Process capability indices were recalculated for PI with respect to the specification limits (LSL = 2.00, USL = 10.00). The results showed Cp = 0.702 and Cpk = 0.616, both lower than the Automotive Industry Action Group benchmark of 1.33. These findings reveal that although the process is statistically stable, its capability remains limited, reflecting moderate internal variability. Compared with the initially reported values, the corrected indices suggest that the process is closer to acceptable levels, but further improvements are still necessary. Enhancements in operational parameters, particularly moisture regulation, sample preparation, and instrument calibration, could help reduce variability and improve performance toward capability benchmarks. The corrected uncertainty analysis provided additional insights. The expanded uncertainty was calculated as ±0.537, equivalent to approximately 9.7% of the mean PI value (5.51). This is substantially lower than previously reported and demonstrates that the measurement system has reasonable precision. Considering guard band adjustments, this uncertainty improves the reliability of decisions regarding specification compliance. These results align with prior studies by Hasan and Abuel-Naga [2] and Abdallah et al. [7], which emphasized the value of statistical indices in geotechnical testing. Overall, the findings indicate that while the current process is not fully capable, it remains stable, reasonably precise, and suitable for preliminary geotechnical assessments.

7. Conclusion

This study aimed to evaluate the consistency and capability of the soil property testing process, with emphasis on the Plasticity Index (PI), a key parameter for classifying clay soil based on the Unified Soil Classification System (USCS). Plasticity Index serves as a critical indicator in geotechnical engineering applications, such as compaction assessment and subgrade stability analysis. The research methodology integrated Statistical Process Control (SPC), Process Capability Index (Cpk) evaluation, trend analysis, and uncertainty analysis to provide a comprehensive view of temporal stability, process reliability, and data limitations. The analysis demonstrated that the X-MR Control Chart, comprising the X Chart and Moving Range Chart, effectively captured process stability. All 50 PI data points were located within control limits, with no sign of abnormal patterns or systemic interference, confirming statistical stability of the measurement process. Process capability was assessed using Cp and Cpk indices under specified limits: Lower Specification Limit (LSL) = 2.00 and Upper Specification Limit (USL) = 10.00. Results showed Cp = 0.702 and Cpk = 0.616,

both falling below the industry-accepted benchmark of 1.33 for quality assurance. These values indicate that although the process is statistically stable, it remains incapable of fully meeting specification requirements due to internal variability, particularly in relation to results near the upper limit of the specification range. Trend analysis using linear regression revealed no statistically significant time-based drift in PI values ($R^2 = 0.1\%$, p-value = 0.864), reinforcing the stability of the process over sequential measurements. No embedded anomalies or directional bias were detected, corroborating findings from SPC. Uncertainty was quantified using a Type A evaluation based on actual test data. The corrected expanded uncertainty (±U) was ±0.537, representing approximately 9.7% of the mean PI value (5.51). This relatively moderate level of uncertainty indicates that the measurement system is more precise than previously reported, providing higher confidence in results even when values approach specification boundaries. When integrated with Guard Band considerations, this level of uncertainty improves interpretive safety and reduces decision-making error in material quality control for engineered fill. In summary, the PI testing process demonstrated temporal stability and statistical control. However, limited process capability ($Cpk = 0.616 < 1.33$) underscores the need for stricter control of influencing factors such as moisture regulation, sample preparation, and measurement precision. Furthermore, the corrected uncertainty analysis highlights the importance of including measurement uncertainty as an integral component of engineering judgment when interpreting PI results near specification limits.

Author Contributions: Conceptualization, P.N. and R.T.; methodology, P.N. (industrial engineering) and R.T. (civil engineering); software, P.N.; validation, P.N. and R.T.; formal analysis, P.N. (industrial engineering) and R.T. (civil engineering); investigation, P.N.; resources, R.T.; data curation, P.N.; writing—original draft preparation, P.N.; writing—review and editing, R.T.; visualization, P.N. All authors have read and agreed to the published version of the manuscript.

Funding: This research received no external funding.

Conflicts of Interest: The authors declare no conflict of interest.

References

[1] ASTM D4318-17. *Standard Test Methods for Liquid Limit, Plastic Limit, and Plasticity Index of Soils*; ASTM International: West Conshohocken, PA, USA, **2017**.

[2] Hasan, M. F.; Abuel-Naga, H. Determining Liquid Limit and Plastic Limit of Clay Soils by Electrical Surface Conduction and Diffuse Double Layer Thickness. *Minerals* **2024**, *143*), 210. https://doi.org/10.3390/min14030210

[3] Marušić, D.; Jagodnik, V. Determination of the Atterberg Limits Using a Fall Cone Device on Low Plasticity Silty Sands. *Min. Geol. Pet. Eng. Bull.* **2023**, *38*(3), 133–145. https://doi.org/10.17794/rgn.2023.3.11

[4] Rosas, D. A.; Burgos, D.; Branch, J. W.; Corbi, A. Automatic Determination of the Atterberg Limits with Machine Learning. *DYNA* **2022**, *89*(224), 102619. https://doi.org/10.15446/dyna.v89n224.102619

[5] Knadel, M.; Rehman, H. U.; Pouladi, N.; de Jonge, L. W.; Moldrup, P.; Arthur, E. Estimating Atterberg Limits of Soils from Reflectance Spectroscopy and Pedotransfer Functions. *Geoderma* **2021**, *402*, 115300. https://doi.org/10.1016/j.geoderma.2021.115300

[6] Phoon, K. K.; Kulhawy, F. H. Characterization of Geotechnical Variability. *Can. Geotech. J.* **1999**, *36*(4), 612–624.

[7] Abdallah, A.; Russo, G.; Cuisinier, O. Statistical and Predictive Analyses of the Strength Development of a Cement-Treated Clayey Soil. *Geotechnics* **2023**, *3*(2), 465–479. https://doi.org/10.3390/geotechnics3020026

[8] Alsharari, N.; Olenko, A.; Abuel-Naga, H. Modeling of Electrical Resistivity of Soil Based on Geotechnical Properties. *arXiv* **2019**, arXiv:1911.06501. https://arxiv.org/abs/1911.06501

[9] Weber, P.; Knadel, M.; Arthur, E. Diffuse Reflectance Spectroscopy for Rapid Estimation of Soil Atterberg Limits. *Geoderma* **2018**, *361*, 114083. https://doi.org/10.1016/j.geoderma.2018.07.018

[10] Bhavya, K.; Nagaraj, T. Influence of Soil Structure and Clay Mineralogy on Atterberg Limits. *Sci. Rep.* **2025**, *15*, 11292. https://doi.org/10.1038/s41598-025-98729-y

[11] Prasanna, H. S.; Harshitha, D. Correlation of Compaction Characteristics of Fine-Grained Soils Using Atterberg Limits. *Int. J. Eng. Res. Technol.* **2017**, *6*(6). https://doi.org/10.17577/IJERTV6IS060051

[12] Ayodele, A. L.; Pamukcu, S.; Agbede, O. A. Plasticity Modification of a Tropical Laterite by Electrochemical Stabilization. *Electrochim. Acta* **2020**, *341*, 136047. https://doi.org/10.1016/j.electacta.2020.136047

[13] Holtz, R. D.; Kovacs, W. D.; Sheahan, T. C. *An Introduction to Geotechnical Engineering*, 2nd ed.; Prentice Hall: Upper Saddle River, NJ, **2011**.

[14] Das, B. M.; Sobhan, K. *Principles of Geotechnical Engineering*, 8th ed., SI Version; Cengage Learning: Stamford, CT, **2014**.

[15] Karakan. Comparative Analysis of Atterberg Limits, Liquidity Index, Flow Index, and Undrained Shear Strength in Binary Clay Mixtures. *Appl. Sci.* **2022**, *12*, 8616. https://doi.org/10.3390/app12178616

[16] Dehghanian, K.; İpek, S. Ö. A Survey on the Relationships between Compression Index, Coefficient of Consolidation, and Atterberg Limits. *J. Sustain. Constr. Mater. Technol.* **2022**, *7*(4). https://doi.org/10.47481/jscmt.1161504

[17] Abdallah, A.; Russo, G.; Cuisinier, O. Statistical and Predictive Analyses of the Strength Development of a Cement-Treated Clayey Soil. *Geotechnics* **2023**, *3*(2), 465–479. https://doi.org/10.3390/geotechnics3020026

[18] Montgomery, D. C. *Introduction to Statistical Quality Control*, 7th ed.; John Wiley & Sons: Hoboken, NJ, USA, **2019**.

[19] Terzaghi, K.; Peck, R. B.; Mesri, G. *Soil Mechanics in Engineering Practice*, 3rd ed.; John Wiley & Sons: Hoboken, NJ, **1996**.

[20] Saied, E.; Besees, A. Y.; Wazeer, A.; Abd-Eltwab, A. A. Process Performance Analysis in Cement Industry. *Int. J. Sci. Technol. Res.* **2020**, *9*(6), 844–860.

ASEAN
Journal of Scientific and Technological Reports
Online ISSN:2773-8752

Research article

Colonization of Potassium-Solubilizing Purple Nonsulfur Bacteria and Their Role in Promoting the Growth of Hybrid Maize

Vo Yen Ngoc[1], Le Thi My Thu[1], Nguyen Duc Trong[1], Tran Trong Khoi Nguyen[1], Tran Chi Nhan[2], Le Thanh Quang[1], Nguyen Thanh Toan[3], Ly Ngoc Thanh Xuan[2], Phung Thi Hang[3], La Cao Thang[1], and Nguyen Quoc Khuong[1*]

[1] Faculty of Crop Science, College of Agriculture, Can Tho University, Can Tho, Vietnam
[2] An Giang University, Vietnam National University Ho Chi Minh City, An Giang, Vietnam
[3] School of Education, Can Tho University, Can Tho, Vietnam
[*] Correspondence: nqkhuong@ctu.edu.vn

Citation:
Ngoc, Y.V.; Thu, M.T.L.; Trong, D.N.; Nguyen, K.T.T.; Nhan, C.T.; Quang, T.L.; Toan, T.N.; Xuan, T.N.L.; Hang, T.P.; Thang, C.L.; Khuong, Q.N. Colonization of potassium-solubilizing purple nonsulfurbacteria and their role in promoting the growth of hybrid maize. *ASEAN J. Sci. Tech. Report.* **2026**, *29*(2), e260654. https://doi.org/10.55164/ajstr.v29i2.260654.

Article history:
Received: August 2, 2025
Revised: October 19, 2025
Accepted: November 15, 2025
Available online: January 21, 2026

Abstract: The use of biofertilisers to replace conventional chemical fertilisers has been widely investigated. However, the colonization of microbes in plants and their effects on plant growth are still unclear. The experiment aimed to (i) determine the ability of potassium-solubilizing purple nonsulfur bacteria (Ksol-PNSB) to colonize in hybrid maize and (ii) measure their capacity to promote plant growth. A randomised complete block design experiment was conducted in undeposited alluvial soil collected from An Phu, An Giang, under nethouse conditions with five treatments and six replications. The treatments were: (i) the control, (ii) *Cereibacter sphaeroides* M-Sl-09, (iii) *Rhodopseudomonas thermotolerans* M-So-11, (iv) *Rhodospeudomonas palustris* M-So-14, and (v) a combination of the three strains. Results revealed the presence of bacteria in soft tissues of the cortex and medulla in the root hair region of hybrid maize plants. Supplying one or three strains of Ksol-PNSB increased crop height (20.7–34.4%), root length (17.0–40.5%), root biomass (20.9–154.0%), and stem-leaf biomass (73.8–173.8%) compared to the control. The current study has successfully revealed the inhabitation locations of the beneficial bacteria within plant tissues, along with the improved growth characteristics of the hybrid maize. The current study is a good reference for studies investigating the works of beneficial microbes in plants. However, further molecular investigations should explore the potassium-solubilizing traits of the bacteria.

Keywords: Biofertilizer; *Cereibacter sphaeroides*; *Rhodospeudomonas palustris*; *Rhodopseudomonas thermotolerans*; root anatomy.

1. Introduction

Maize (*Zea mays* L.) globally provides food for human beings and livestock [1]. In Vietnam, maize is highly important in agricultural production and livelihoods [2]. Sandhu *et al.* [3] estimated that approximately 80% of maize is consumed in animal husbandry. Recently, the rice-rice-maize cropping system has been developed in the Mekong Delta. However, maize cultivation faces different difficulties due to the excessive use of chemical fertilizers, leading to nutrient imbalances, reduced efficiency, soil degradation, and biodiversity loss [4].

Potassium (K) is vital in photosynthesis, water storage, and stomatal control [5]. Deficiency in K reduces photosynthesis efficiency and leaf size [6]

and affects osmotic regulation [7]. Thus, K fertilization in maize can improve crop nutrient uptake and crop yield [8]. Potassium exists in soil under soluble, exchangeable, non-exchangeable, and structural forms [9]. Nevertheless, a large portion of K is immobilised in clay minerals, making it unavailable to plants. Sun *et al.* [10] suggested exploring biological nutrient sources to replace chemical fertilisers, solubilise soil K, and enhance plant growth. For hybrid maize cultivation, using biofertiliser is a sustainable approach to improve productivity and to remediate the environment [11]. The microorganisms within biofertilisers can improve soil nutrient availability and facilitate plant nutrient uptake [12].

Biofertilisers, containing beneficial microorganisms, can improve plant nutrition through multiple mechanisms, such as nitrogen fixation, phosphate and potassium solubilization, organic acid production, siderophore release, and phytohormone synthesis [12–14]. Among them, purple nonsulfur bacteria (PNSB) are a metabolically versatile group capable of photosynthesis, nitrogen fixation, and nutrient solubilization [15,16]. PNSB has been successfully applied as biofertilisers to enhance potassium availability for various crops [17,18]. Several PNSB species, such as *Rhodopseudomonas* and *Cereibacter* spp., have been reported to enhance soil fertility and plant growth through their potassium-solubilizing capacity and plant growth–promoting (PGP) traits [17–19]. PNSB may promote crop development not only by increasing nutrient bioavailability but also by synthesizing auxins and gibberellins, regulating reactive oxygen species, and improving chlorophyll formation and root development [20–22]. In Vietnam, different potassium-solubilizing PNSB (Ksol-PNSB) strains have been isolated from hybrid maize rhizosphere soils, including *Cereibacter sphaeroides* M-Sl-09, *Rhodopseudomonas thermotolerans* M-So-11, and *Rhodopseudomonas palustris* M-So-14 [23]. However, limited information exists regarding their colonization patterns within maize tissues and their effects on plant growth under early vegetative stages.

Therefore, this study aimed to: (i) assess the colonization potential of Ksol-PNSB during hybrid maize growth stages and (ii) determine their plant growth-promoting capabilities. The findings are expected to provide insight into the interaction between beneficial PNSB and maize roots and support the development of microbial biofertilizers for sustainable maize cultivation in alluvial soils.

2. Materials and Methods

2.1 Materials

Location and duration: The experiment was conducted from September 21 to October 6, 2024, in a greenhouse at the Faculty of Crop Science, College of Agriculture, Can Tho University.

Pots: Plastic containers with a dimension of top diameter x bottom diameter x height at 14 x 11 x 12 (cm). At the bottom, there were 5 five drainage holes.

Soil: Undeposited alluvial soil collected from An Phu - An Giang (0-20 cm depth), air-dried and cleaned from plant debris. Each pot contained 2 kg of prepared soil. Before the experiment, the soil was analyzed for key physicochemical properties: pH = 5.33, electrical conductivity = 0.27 mS cm^{-1}, total N = 0.07%, total P = 0.06 % P_2O_5, and exchangeable K = 0.21 meq 100 kg^{-1}. These values represent moderately fertile, slightly acidic conditions typical of in-dyked alluvial soils in the Mekong Delta.

Plant material: Hybrid maize seeds, NK7328 (Bayer company, Germany).

Bacterial strains: Three Ksol-PNSB strains, including *Cereibacter sphaeroides* M-Sl-09, *Rhodopseudomonas thermotolerans* M-So-11, and *Rhodospeudomonas palustris* M-So-14 [19], were obtained from the Faculty of Crop Science, College of Agriculture, Can Tho University.

2.2 Methods

The experiment followed a randomised complete block design with five treatments: (i) the control, (ii) M-Sl-09, (iii) M-So-11, (iv) M-So-14, and (v) a combination of the three strains. The control group was treated identically to the inoculated groups except that seeds were soaked and watered with sterilized distilled water instead of bacterial suspension. This ensured that any observed differences were due solely to bacterial effects. No fertilizer was used in this experiment. Every day, 100 mL of water was applied to each pot at 5:00 p.m.

Bacterial inoculation: Maize seeds were surface-sterilised using 70% ethanol and 1% sodium hypochlorite before being rinsed with sterilised deionised water. Sanitised seeds were germinated in darkness

for 24 hours, then immersed in the corresponding Ksol-PNSB solution suspension (1 x 10^8 CFU mL^{-1}) for 1 hour before sowing, achieving a final bacterial load of 2 x 10^8 CFU per seed as 2 seeds × 1 × 10^8 from 50 seeds/50 mL = 2 × 10^8 [20].

Biofertiliser application: Biofertilisers of *C. sphaeroides* M-Sl-09, *R. thermotolerans* M-So-11, and *R. palustris* M-So-14 were applied into the soil at a rate of 10 mL pot^{-1} on days 5, 10, and 15 after planting (DAP). For the three-strain treatment (v), 3.33 mL of each strain was used.

Tissue microtomy was conducted following the slicing method and cell wall staining by Carmin aluné –vert d' iode for vegetative organs (stem-leaf) at 15 DAP. Samples were soaked with Javen solution (3%) and acetic acid (5%) before being dyed [21]. In particular, carmine made cellulose-made cell walls pink, and vert d' iode turned lignin-made cell walls green.

Anatomic positions: Root samples with zones of division, elongation, and maturation were randomly selected. Stem samples were collected from the middle of the second internode from the ground. Leaf samples were mature leaves at the vegetative positions, including leaf sheath (the third leaf from the tip), leaf blade (0.5 cm from the leaf margin), and midrib (a large bump in the middle of the leaf). All samples were cut in cross-section. The anatomical characteristics of the vegetative organs of maize had the general structure of a monocotyledonous plant (a big herbaceous form).

The presence of bacteria within plant organs: An anatomic method without bleaching and fuchsine staining was applied. In brief, samples were surface-sterilised with alcohol 70°. Then, the samples were quickly dissected, cut in cross-section, and stained with fuchsine to detect tissue and cell structures. This was the scientific evidence to determine the habitat and movement of bacteria among treatments. The samples were observed and sized by the light microscope (Olympus CX23) and Toupview software.

Vegetative parameters were determined on two plants per pot at 15 DAP. Plants were harvested at 15 DAP to focus on the early vegetative stage, when initial colonization and root–microbe interactions occur. Although longer trials could reveal yield responses, this short-term evaluation aimed to visualize colonization patterns and detect early physiological responses before external nutrient limitations or senescence occur in pots.

- Plant height (cm): Measure the height of the plant in each pot, from the ground to the tip of the tallest leaf on top.
- Stem diameter (cm): Measure at the top, middle, and base to calculate the average.
- Leaf length (cm): Measure from the leaf collar to the leaf tip of the top leaf.
- Leaf width (cm): Measure the widest part of the top leaf.
- Root length (cm): Measure from base to root tip.
- Root biomass (g): Cut and weigh the roots.
- Stem-leaf biomass (g): Weigh the whole plant.
- SPAD: The chlorophyll content was measured by SPAD 520 at the $^2/_3$ position of the leaf from the petiole to the leaf tip [22].
- The chlorophyll a and b: Leaf samples were cut into 1.0 cm-wide circles. The leaf samples were let react with 3 mL of NN-Dimethyl Formamidecho in a 50 mL test tube. The tube was kept from light for 24 hours. The solution was measured by spectrophotometry at 663 and 647 nm. The chlorophyll a and b contents were calculated according to Porra *et al.* [23] as follows:

Chlorophyll a = $12.00*A_{663.2} – 3.11*A_{646.8}$ µg Chl/mL

Chlorophyll b = $20.78*A_{663.2} – 4.88*A_{646.8}$ µg Chl/mL

Chlorophyll a+b = $17.67*A_{663.2} + 7.12*A_{646.8}$ µg Chl/mL

- Proline content: Samples (0.5 g) were ground in 10 mL of sulfosalicylic acid 3%. The ground sample was added into a centrifugal tube, shaken by a reciprocal shaker for 30 min, centrifuged at 3,500 rpm for 10 min, and collected for the clear extract. The extracted solution was reacted with 2 mL of Ninhydrin and 2mL of glacial acetic acid, boiled in a double boiler at 90 ℃ for 1 h, cooled by ice, and then 4 mL of toluene, shaken for 15 - 20 seconds, and measured by spectrophotometry at 520 nm [24].

2.3 Statistical analysis

The SPSS 13.0 software was applied to compare differences between means by the Duncan test at 5% significance.

3. Results and Discussion

3.1 Colonization patterns of the Ksol-PNSB in hybrid maize

Microscopic observation of maize tissues revealed clear anatomical differentiation across root, stem, and leaf sections (Figure 1–3).

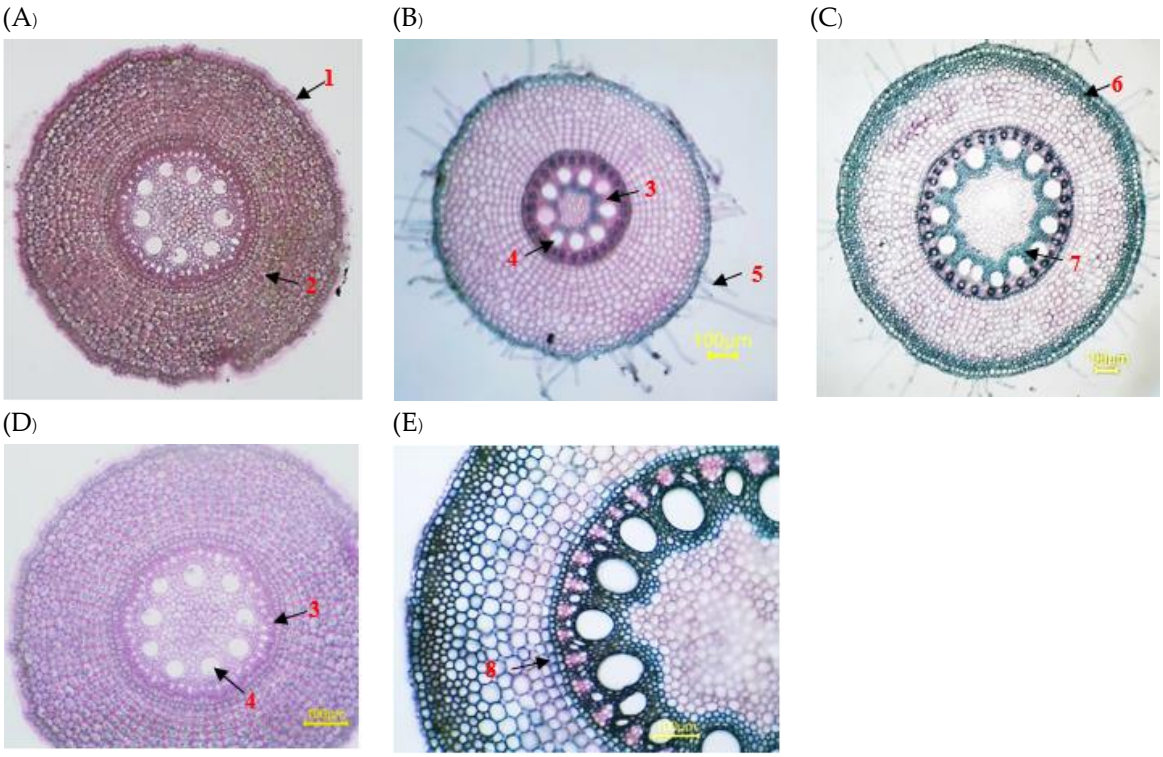

Figure 1. Cross-section anatomy of maize root. A, D: division zone, B: elongation zone, C, E: maturation zone; 1: epidermis; 2: cortex parenchyma; 3: phloem; 4: xylem; 5: root hairs; 6: suberin-impregnated zone; 7: sclerenchyma surrounding xylem; 8: endodermis with U-shaped suberine frame.

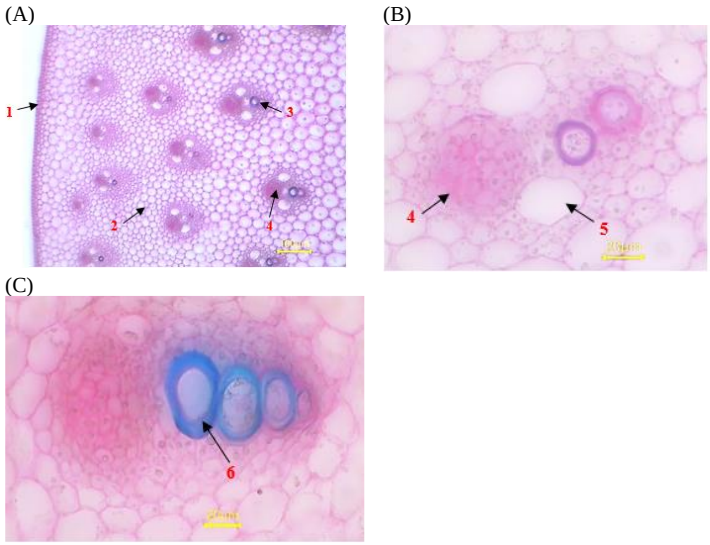

Figure 2. Cross-section anatomy of maize culm. A: stem structure, B, C: vascular bundle development from young to older stages. 1: epidermis; 2: parenchyma; 3: xylem; 4: phloem; 5: newly formed xylem; 6: lignified xylem

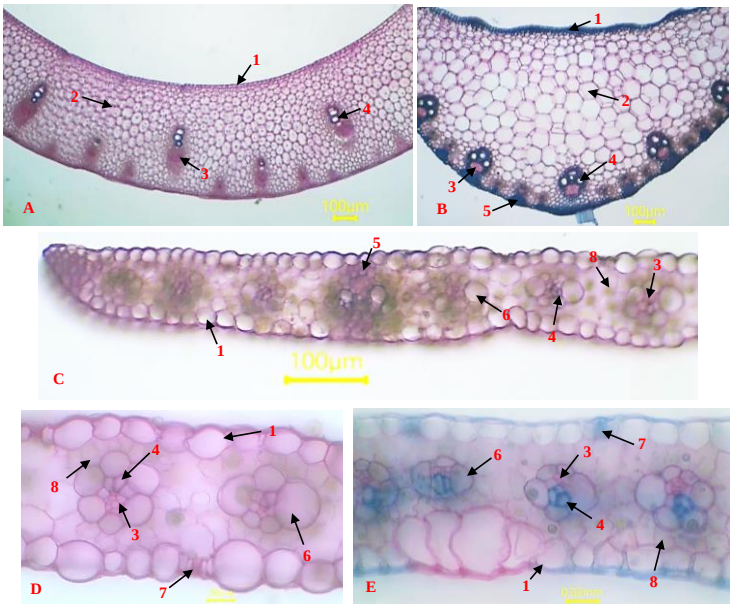

Figure 3. Cross-section anatomy of maize leaf. Leaf sheath structure (A). Anatomical structure of leaf blade: midrib region (B), leaf margin region (C), leaf blade in young leaf stage (D), leaf blade in older leaf stage (E); 1: epidermis; 2: parenchyma; 3: phloem; 4: wood; 5: sclerenchyma; 6: bundle sheath cells; 7: stomata; 8: anabolic tissue

Root anatomy: The root exhibited distinct zones in cross-section, including division (uppermost zone from root tip with active cell generation) (Figure 1A, 1D), elongation (Figure 1B), and maturation zones (Figure 1C, 1E). Cells and tissues were arranged in concentric layers from exterior to interior. The root epidermis consisted of thin-cell-wall cells closely packed together to form a layer that covers the inner parts, along with elongated unicellular root hairs (Figure 1). The thickness of the suberised cork layer varied with tissue maturity. The following layer was the soft cortical tissue that occupied a large area with mostly soft tissues. The endodermis was a layer of rectangular cells arranged in a characteristic U-shaped pattern with suberised cell walls. Numerous vascular bundles formed a ring, with centripetal xylem arrangement alternating with phloem tissues.

Stem anatomy: The cross-section of the maize stem was circular. The tissue arrangement from outside to inside. The outermost epidermis was a layer of small cells packed closely together. In the maize stem, the cross-section of the maize did not distinguish between the cortex and the medulla. The vascular bundles were scattered, and the parenchyma occupied all the remaining space. A few layers of thick tissue (hypodermis) laid just below the epidermis. For the bundle area, the more peripheral positions were, the smaller the bundles (closer to the epidermis) became in size but more numerous, while the bundles in the central region were larger and farther apart. The vascular bundles were arranged in a superimposed pattern, phloem above and xylem below. The xylem resembled a 'Y' shape, but the two xylem (sides) usually had delayed lignification (Figure 2).

Leaf anatomy: Different positions had different structures, with a distinct patterns in the leaf sheath, midrib, and blade regions.

Leaf sheath: The vascular bundles were arranged in parallel rows of different sizes. Each vascular bundle contained both xylem and phloem tissues. The remaining space was filled with parenchyma tissue. (Fig. 3A).

Leaf blade: The leaf blade had an isosurface structure (the upper and lower surfaces of the leaf cannot be distinguished). The microscopic observations revealed that the leaf blade cross-sections displayed specialised cellular organization characteristics of C4 photosynthesis. The mesophyll tissue contained prominent bundle sheaths with regularly spaced vascular bundles. Each vascular bundle showed well-defined

xylem and phloem tissues. The bundles maintained consistent spacing and size throughout the leaf blade sections examined (Figure 3B, 3C).

Lead midrib: Cross-sections of the midrib region demonstrated distinct anatomical features dominated by a large central vascular bundle. Ground tissue surrounded the vascular elements, which maintained typical organization with adaxial xylem and abaxial phloem arrangement (Figure 3D, 3E).

Bacterial colonization: Presumed bacterial cells, stained red with fuchsine, were visible in the cortex and medulla of maize roots supplied with *C. sphaeroides* M-Sl-09, *R. thermotolerans* M-So-11, and *R. palustris* M-So-14 (Figure 4–7), but not in the control (Figure 8). This could be assumed that according to the treatment description, there was the presence of M-Sl-09 (Figure 4), M-So-11 (Figure 5), M-So-14 (Figure 6), and a mixture of three strains M-Sl-09, M-So-11, and M-So-14 (Figure 7) compared to the control case (Figure 8). The microorganisms were localized primarily in thin-walled parenchyma cells and near the xylem and phloem vessels. These regions are known to facilitate endophytic movement through apoplastic flow. The bacteria likely entered through root hairs and epidermal micro-cracks, then migrated via intercellular spaces and xylem sap.

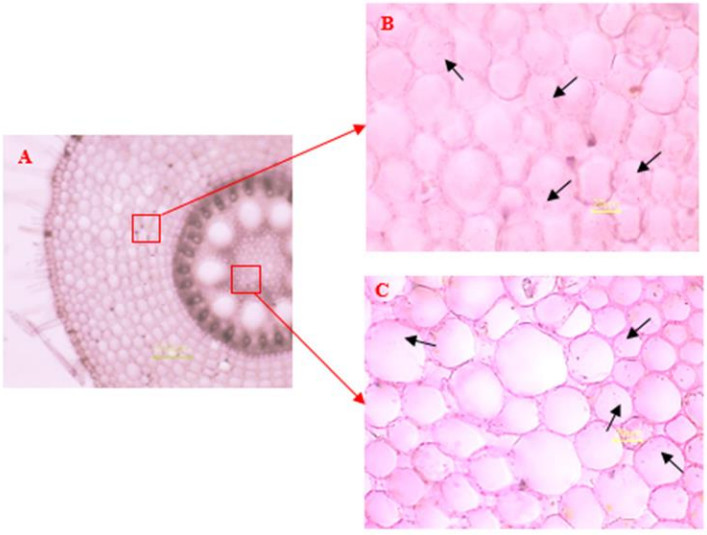

Figure 4. Presence of bacteria in maize supplied with potassium-solubilizing purple nonsulfur bacteria M-Sl-09. A: structure of elongation zone; B: cortex region; C: stele region.

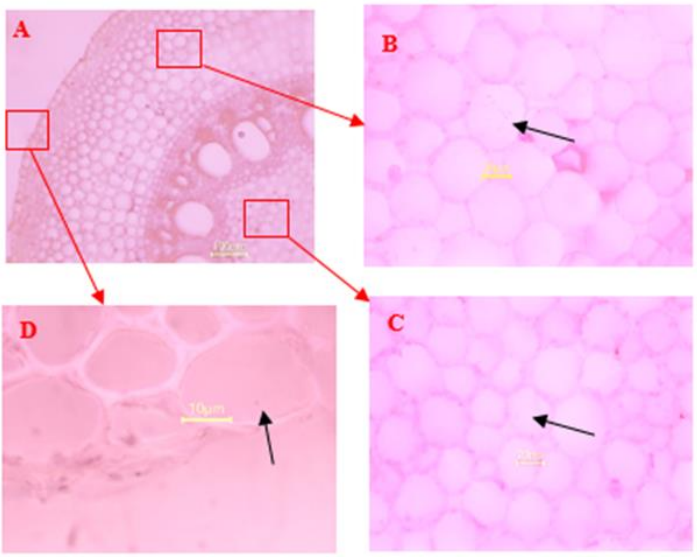

Figure 5. Presence of bacilli in maize supplied with potassium-solubilizing purple nonsulfur bacteria M-So-11. A: structure of maturation zone; B: cortex region; C: stele region; D: Epidermis

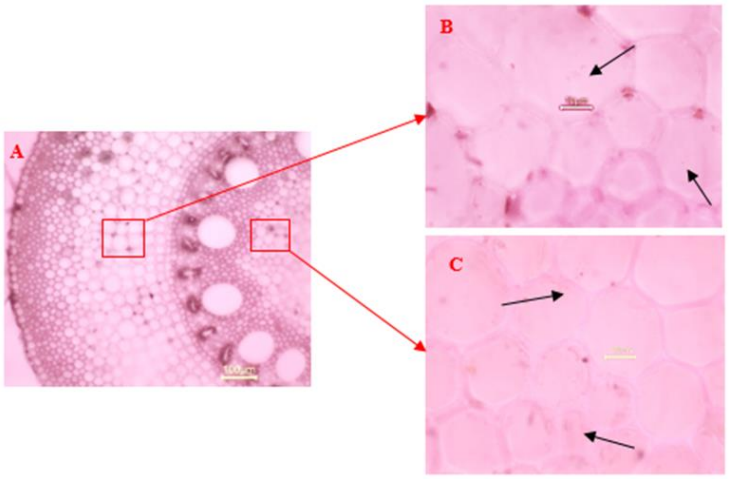

Figure 6. Presence of bacilli in maize supplied with potassium-solubilizing purple nonsulfur bacteria M-So-14. A: structure of maturation zone; B: cortex region; C: stele region

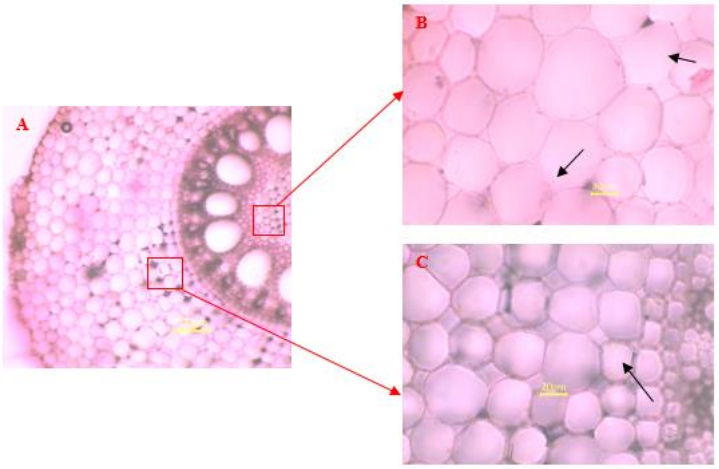

Figure 7. Presence of bacteria in maize supplied with potassium-solubilizing purple nonsulfur bacteria M-Sl-09, M-So-11, and M-So-14. A: structure of maturation zone; B: cortex region; C: stele region

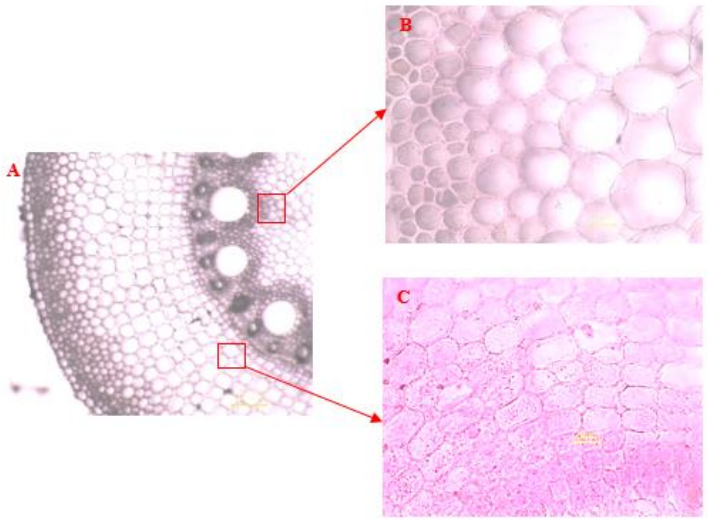

Figure 8. Presence of bacilli in maize without potassium-solubilizing purple nonsulfur bacteria. A: structure of maturation zone; B: cortex region; C: stele region

In conclusion, the soft tissue surrounding the xylem and the medullary parenchyma gradually became impregnated with the xylem, causing the cell walls to thicken and turn green when stained. The medullary parenchyma cells were loosely arranged and contained numerous starch granules. Microsamples at different locations also revealed a development trend that increased the rigidity of the root, the thin-walled tissues made of cellulose (living cells) were gradually replaced by thicker-walled cells impregnated with xylem/lignin (becoming dead cells) (Figure 1-3). Bacteria were observed in the cortex and medulla, areas with thin-walled cellulose structures (Figure 4-7). Normally, the soft tissues contain many storage substances, which are the environment for bacteria to grow. Some bacteria appeared in the epidermal area (in small numbers); however, they did not penetrate deeply due to the presence of suberin-impregnated cells that form a protective barrier. Bacteria inside the plant likely followed the water transport route, entering through the root hairs and moving through the internal structures. However, because only anatomical staining was used, the bacterial cells observed cannot be definitively confirmed as the inoculated PNSB strains. Other naturally occurring microorganisms could exhibit similar morphology. Therefore, molecular or fluorescence-based confirmation, such as PCR amplification of species-specific genes, is recommended for future studies.

3.2 Influencing capacity of Ksol-PNSB on growth and biochemical traits of hybrid maize

3.2.1 Growth traits

The treatments with Ksol-PNSB showed significant increases by 10.1 - 16.8 cm in plant height, by 1.01 - 1.58 cm in stem diameter, by 9.70 - 15.3 cm in leaf length, by 1.02 - 1.69 cm in leaf width, by 8.00 - 19.0 cm in root length, by 0.41 - 3.02 g in root biomass, and by 4.80 - 11.3 g in stem-leaf biomass (Table 1).

Table 1. Effectiveness of potassium-solubilizing purple nonsulfur bacteria in improving hybrid maize growth in undeposited alluvial soil in An Phu, An Giang, under nethouse conditions

Treatment	Crop height	Stem diameter	Leaf length	Leaf width	Root length	Root biomass	Culm-leaf weight
			(cm)				(g)
Control	48.7^{c}	1.92^{c}	33.7^{c}	1.98^{d}	46.8^{c}	1.96^{c}	6.50^{d}
M-Sl-09	64.4^{a}	3.50^{a}	45.3^{b}	3.40^{ab}	62.7^{a}	4.27^{b}	17.8^{a}
M-So-11	64.5^{a}	3.30^{a}	45.3^{b}	3.25^{bc}	57.2^{b}	4.31^{b}	13.9^{b}
M-So-14	58.8^{b}	2.93^{b}	43.4^{b}	3.00^{c}	54.8^{b}	2.37^{c}	11.3^{c}
Mix	65.5^{a}	3.30^{a}	49.0^{a}	3.67^{a}	65.8^{a}	4.98^{a}	17.7^{a}
Significance	*	*	*	*	*	*	*
CV (%)	3.07	7.33	3.12	6.12	4.18	7.65	8.56

Note: In the same column, numbers followed by different letters are significantly different at 5% (*); ns: no significance. M-Sl-09: *Cereibacter sphaeroides* M-Sl-09, M-So-11: *Rhodopseudomonas thermotolerans* M-So-11, M-So-14: *Rhodospeudomonas palustris* M-So-14. Mix: the mixture of three strains *Cereibacter sphaeroides* M-Sl-09, *Rhodopseudomonas thermotolerans* M-So-11, *Rhodospeudomonas palustris* M-So-14.

Table 1 shows that strains of Ksol-PNSB significantly improved hybrid maize growth compared to the control. Previous studies have demonstrated the ability of PNSB strains, such as *R. palustris*, to enhance the growth of different crops, *e.g.*, Chinese cabbage Pak choi (*Brassica chinensis* L.) [25], stevia (*Stevia rebaudiana* Bert.) [26], urad bean (*Vigna mungo* L.) [27], and rice (*Oryza sativa* L.) [28–30]. In this study, *C. sphaeroides* M-Sl-09, *R. thermotolerans* M-So-11, and *R. palustris* M-So-14 significantly increased crop height, stem diameter, leaf length, leaf width, root length, root biomass, and stem-leaf weight, resulting in significantly higher fresh biomass of hybrid maize (Table 1). Ksol-PNSB releases organic acids (e.g., citric, malic, and gluconic acids) that chelate K from insoluble minerals such as mica and feldspar, increasing soluble K concentration in the rhizosphere [31,32]. Moreover, PNSB synthesise indole-3-acetic acid (IAA) and gibberellins that promote cell elongation and root development, leading to enhanced nutrient uptake [33]. Unlike other microorganisms, PNSB can function under both aerobic and microaerobic light conditions, contributing to improved root oxygenation and carbon metabolism [34]. These combined effects indicate that Ksol-PNSB stimulates maize growth primarily through physiological activation rather than simple nutrient supplementation.

3.2.2 Biochemical traits

By improving nutrient balance and metabolic efficiency, PNSB increases chlorophyll content and photosynthetic capacity, as supported by higher SPAD values observed in this study. Chlorophyll content (SPAD index) significantly increased under Ksol-PNSB treatments (37.5 - 45.5) compared to the control (35.9) (Table 2). The SPAD index, a reliable indicator of the N nutritional status in leaves, is positively correlated with leaf N content [35]. A SPAD index below 35 indicates that the plant is in an N-insufficient status [36]. Table 2 revealed that Ksol-PNSB M-Sl-09, M-So-11, and M-So-14 improved the SPAD index. The a and a+b chlorophyll contents peaked in the M-So-14 treatment (8.26 μg g^{-1} and 13.1 μg g^{-1}, respectively). The a and a+b chlorophyll in the Ksol-PNSB treatments were significantly greater than those of the control at 15 DAP. The b chlorophyll ranged from 4.71 to 4.87 μg g^{-1} (Table 2). The enhancement of chlorophyll accumulation reflects improved N assimilation and photosynthetic performance. Similar findings were reported by Xu et al. [26,27] and Sundar et al. [37], who demonstrated that PNSB inoculation improved photosynthetic pigments and plant vigor in *Stevia rebaudiana* and rice, respectively.

Table 2. Effectiveness of potassium-solubilizing purple nonsulfur bacteria in improving hybrid maize biochemistry in undeposited alluvial soil in An Phu-An Giang, under nethouse conditions

Treatment	SPAD	Proline (μmol g^{-1} DW)	Chlorophyll a	Chlorophyll b	Chlorophyll a+b
			(μg g^{-1})		
Control	35.9^{d}	19.7^{c}	6.80^{c}	4.85	11.7^{c}
M-Sl-09	42.5^{a}	21.2^{bc}	8.06^{ab}	4.87	12.9^{ab}
M-So-11	37.5^{c}	23.2^{ab}	7.57^{b}	4.71	12.3^{bc}
M-So-14	39.9^{b}	26.5^{a}	8.26^{a}	4.87	13.1^{a}
Mix	40.4^{b}	17.5^{bc}	7.64^{ab}	4.83	12.5^{ab}
Significance	*	*	*	ns	*
CV (%)	2.22	14.7	5.44	4.09	3.90

Note: In the same column, numbers followed by different letters are significantly at 5% (*); ns: no significance. M-Sl-09: *Cereibacter sphaeroides* M-Sl-09, M-So-11: *Rhodopseudomonas thermotolerans* M-So-11, M-So-14: *Rhodospeudomonas palustris* M-So-14. Mix: the mixture of three strains *Cereibacter sphaeroides* M-Sl-09, *Rhodopseudomonas thermotolerans* M-So-11, *Rhodospeudomonas palustris* M-So-14.

Proline content, an indicator of stress tolerance, was highest in the M-So-14 treatment (26.5 μmol g^{-1} DW) and decreased progressively in the treatments with M-Sl-09 (24.2 μmol g^{-1} DW), M-So-11 (21.2 μmol g^{-1} DW), and the combination of M-Sl-09, M-So-11, and M-So-14 (17.5 μmol g^{-1} DW). In comparison, the proline content in the control was 19.7 μmol g^{-1} DW (Table 2). Furthermore, the significantly increased proline content in maize treated with Ksol-PNSB compared to the control suggested that supplying Ksol-PNSB enhanced maize tolerance against stresses. Proline is synthesised to maintain cell osmosis and protect enzymes, proteins, membranes, and cell structures under water scarcity [38]. Proline is commonly used as a biomarker for stress response and osmotic regulation in plants [39]. However, since no abiotic stress was imposed in this experiment, the elevated proline level is more likely linked to enhanced metabolic activity and amino acid turnover during rapid vegetative growth rather than to stress tolerance [40]. The lower proline level in the mixed treatment may reflect a more balanced physiological state, where the combined bacterial consortium improved osmotic stability and nitrogen assimilation efficiency, reducing the need for proline accumulation [41]. The proline accumulation increases crop tolerance and yield [42]. Thus, the increased proline production by the Ksol-PNSB application improved crop growth and yield and minimised the adverse effects on plants.

Overall, these findings suggest that the PNSB strains may contribute to maize vigor through coordinated effects on nutrient mobilization, photosynthesis, and amino acid metabolism rather than by inducing stress-related pathways. The presence of presumed PNSB in maize tissues corresponds with enhanced morphological and biochemical performance. However, colonization alone does not directly prove causality for growth promotion. It is plausible that the bacterial metabolites and solubilised nutrients exerted systemic effects on plant physiology independent of internal colonization. Future studies should integrate

molecular detection with metabolomic profiling to verify bacterial persistence and identify the specific bioactive compounds responsible for growth enhancement.

4. Conclusions

This study demonstrated that potassium-solubilizing purple nonsulfur bacteria (*Cereibacter sphaeroides* M-Sl-09, *Rhodopseudomonas thermotolerans* M-So-11, and *Rhodopseudomonas palustris* M-So-14) are presumed to colonize the soft tissues of hybrid maize roots, particularly in the cortex and medulla regions near the vascular system. Their application significantly enhanced early vegetative growth, including plant height, leaf expansion, root elongation, and biomass accumulation, compared with the uninoculated control. The positive effects of Ksol-PNSB on maize growth are likely associated with multiple plant growth–promoting mechanisms such as potassium solubilization, phytohormone synthesis, and improved chlorophyll formation, rather than from direct bacterial colonization alone. Increased proline content observed in certain treatments reflected enhanced metabolic activity during active growth rather than a stress-related response, while the lower proline level in the mixed inoculation suggested a balanced physiological state under optimal nutrient conditions. These results support the potential use of Ksol-PNSB as promising biofertilizer candidates to improve nutrient efficiency and promote sustainable maize cultivation in alluvial soils of the Mekong Delta. However, because this experiment focused on short-term colonization, further studies are required to confirm bacterial identity within plant tissues using molecular or fluorescence-based methods; evaluate their persistence and physiological influence throughout the full growth cycle; and examine the interaction between Ksol-PNSB and potassium fertilizers under field conditions.

5. Acknowledgements

Author Contributions: Conceptualization, V.Y.N. and N.Q.K.; methodology, V.Y.N., L.T.M.T., and N.Q.K.; validation, L.T.M.T., N.D.T., and T.T.K.N.; formal analysis, N.D.T., T.T.K.N., T.C.N., L.T.Q., and N.T.T.; investigation, T.C.N., N.T.T., L.N.T.X., and P.T.H.; resources, L.N.T.X., P.T.H., L.C.T.; data curation, P.T.H., L.C.T., and N.Q.K.; writing—original draft preparation, V.Y.N.; writing—review and editing, N.Q.K. and L.T.Q.; supervision, N.Q.K.; project administration, N.Q.K.; funding acquisition, N.Q.K. All authors have read and agreed to the published version of the manuscript.

Funding: This research was funded by CAN THO UNIVERSITY, grant number CTCS2024-14-02.

Conflicts of Interest: The authors declare no conflict of interest.

References

[1] Reddy, V.R.; Seshu, G.; Jabeen, F.; Rao, A.S. Specialty maize types with reference to quality protein maize (*Zea mays* L.)—A review. *Int. J. Agric. Environ. Biotechnol.* **2012**, *5*, 393–400.

[2] Tran, A.T.M.; Eitzinger, J.; Manschadi, A.M. Response of maize yield under changing climate and production conditions in Vietnam. *Ital. J. Agrometeorol.* **2020**, *1*, 73–84. https://doi.org/10.13128/ijam-764

[3] Sandhu, H.; Scialabba, N.E.H.; Warner, C.; Behzadnejad, F.; Keohane, K.; Houston, R.; Fujiwara, D. Evaluating the holistic costs and benefits of maize production systems in Minnesota US. *Sci. Rep.* **2020**, *10*, 3922. https://doi.org/10.1038/s41598-020-60826-5

[4] Peñuelas, J.; Coello, F.; Sardans, J. A better use of fertilizers is needed for global food security and environmental sustainability. *Agric. Food Secur.* **2023**, *12*, 9. https://doi.org/10.1186/s40066-023-00409-5

[5] Rawat, J.; Pandey, N.; Saxena, J. Role of potassium in plant photosynthesis transport growth and yield. In *Role of Potassium in Abiotic Stress*; Iqbal, N., Umar, S., Eds.; Springer: Singapore, 2022; pp. 1–14. https://doi.org/10.1007/978-981-16-4461-0_1

[6] Nguyen, H.K.; Le, V.Q.; Tran, H.T.; Van Tra, T.; Nguyen, T.V.; Tran, K.T.; Ho, T.T.T. Reuse shrimp pond sedimentation to produce organic fertilizer in industrial scale. *Sci. Technol. Dev. J. Sci. Earth Environ.* **2021**, *5*, 273–283. https://doi.org/10.32508/stdjsee.v5i1.536

[7] Sardans, J.; Peñuelas, J. Potassium control of plant functions: Ecological and agricultural implications. *Plants* **2021**, *10*, 419. https://doi.org/10.3390/plants10020419

[8] Adnan, M. Role of potassium in maize production: A review. *Open Access J. Biol. Sci. Res.* **2020**, *3*, 1–4. https://dx.doi.org/10.46718/JBGSR.2020.03.000083

[9] Azadi, A.; Shakeri, S. Effect of different land use on potassium forms and some soil properties in Kohgiluyeh and Boyer-Ahmad Province, Southwest Iran. *Iran Agric. Res.* **2020**, *39*, 121–133. https://doi.org/10.22099/iar.2020.36758.1387

[10] Sun, F.; Ou, Q.; Wang, N.; Guo, Z.X.; Ou, Y.; Li, N.; Peng, C. Isolation and identification of potassium-solubilizing bacteria from *Mikania micrantha* rhizospheric soil and their effect on *M. micrantha* plants. *Glob. Ecol. Conserv.* **2020**, *23*, e01141. https://doi.org/10.1016/j.gecco.2020.e01141

[11] Gao, C.; El-Sawah, A.M.; Ali, D.F.I.; Alhaj Hamoud, Y.; Shaghaleh, H.; Sheteiwy, M.S. The integration of bio and organic fertilizers improve plant growth, grain yield, quality and metabolism of hybrid maize (*Zea mays* L.). *Agronomy* **2020**, *10*, 319. https://doi.org/10.3390/agronomy10030319

[12] Nosheen, S.; Ajmal, I.; Song, Y. Microbes as biofertilizers: A potential approach for sustainable crop production. *Sustainability* **2021**, *13*, 1868. https://doi.org/10.3390/su13041868

[13] Verma, P.; Yadav, A.N.; Khannam, K.S.; Saxena, A.K.; Suman, A. Potassium-solubilizing microbes: Diversity, distribution and role in plant growth promotion. In *Microorganisms for Green Revolution: Volume 1: Microbes for Sustainable Crop Production*; Panpatte, D., Jhala, Y., Vyas, R., Shelat, H., Eds.; Springer: Singapore, 2017; pp. 125–149. https://doi.org/10.1007/978-981-10-6241-4_7

[14] Jiao, H.; Wang, R.; Qin, W.; Yang, J. Screening of rhizosphere nitrogen-fixing, phosphorus- and potassium-solubilizing bacteria of *Malus sieversii* (Ldb.) Roem. and the effect on apple growth. *J. Plant Physiol.* **2024**, *292*, 154142. https://doi.org/10.1016/j.jplph.2023.154142

[15] Hamid, B.; Zaman, M.; Farooq, S.; Fatima, S.; Sayyed, R.Z.; Baba, Z.A.; Suriani, N.L. Bacterial plant biostimulants: A sustainable way towards improving growth, productivity and health of crops. *Sustainability* **2021**, *13*, 2856. https://doi.org/10.3390/su13052856

[16] Khatoon, Z.; Huang, S.; Rafique, M.; Fakhar, A.; Kamran, M.A.; Santoyo, G. Unlocking the potential of plant growth-promoting rhizobacteria on soil health and the sustainability of agricultural systems. *J. Environ. Manag.* **2020**, *273*, 111118. https://doi.org/10.1016/j.jenvman.2020.111118

[17] Khuong, N.Q.; Sakpirom, J.; Oanh, T.O.; Thuc, L.V.; Thu, L.T.M.; Xuan, D.T.; Quang, L.T.; Xuan, L.N.T. Isolation and characterization of novel potassium-solubilizing purple nonsulfur bacteria from acidic paddy soils using culture-dependent and culture-independent techniques. *Braz. J. Microbiol.* **2023**, *54*, 2333–2348. https://doi.org/10.1007/s42770-023-01069-0

[18] Koh, R.H.; Song, H.G. Effects of application of *Rhodopseudomonas* sp. on seed germination and growth of tomato under axenic conditions. *J. Microbiol. Biotechnol.* **2007**, *17*, 1805–1810.

[19] Thu, L.T.M.; Xuan, L.N.T.; Nhan, T.C.; Quang, L.T.; Trong, N.D.; Thuan, V.M.; Nguyen, T.T.K.; Nguyen, P.C.; Thuc, L.V.; Khuong, N.Q. Characterization of novel species of potassium-dissolving purple nonsulfur bacteria isolated from in-dyked alluvial upland soil for maize cultivation. *Life* **2024**, *14*, 1461. https://doi.org/10.3390/life14111461

[20] Khuong, N.Q.; Huu, T.N.; Nhan, T.C.; Tran, H.N.; Tien, P.D.; Xuan, L.N.T.; Kantachote, D. Two strains of *Luteovulum sphaeroides* (purple nonsulfur bacteria) promote rice cultivation in saline soils by increasing available phosphorus. *Rhizosphere* **2021**, *20*, 100456. https://doi.org/10.1016/j.rhisph.2021.100456

[21] Mondolot, L.; Roussel, J.L.; Andary, C. New applications for an old lignified element staining reagent. *Histochem. J.* **2001**, *33*, 379–385. https://doi.org/10.1023/A:1013798426161

[22] Yuan, D.Q.; Wang, Y. Effects of solution conditions on the physicochemical properties of stratification components of extracellular polymeric substances in anaerobic digested sludge. *J. Environ. Sci.* **2013**, *25*, 155–162. https://doi.org/10.1016/S1001-0742(12)60038-2

[23] Porra, R.J.; Thompson, W.A.; Kriedemann, P.E. Determination of accurate extinction coefficients and simultaneous equations for assaying chlorophylls a and b extracted with four different solvents: Verification of the concentration of chlorophyll standards by atomic absorption spectroscopy. *Biochim. Biophys. Acta - Bioenerg.* **1989**, *975*, 384–394. https://doi.org/10.1016/S0005-2728(89)80347-0

[24] Bates, L.S.; Waldren, R.P.A.; Teare, I.D. Rapid determination of free proline for water-stress studies. *Plant Soil* **1973**, *39*, 205–207. https://doi.org/10.1007/BF00018060

[25] Xu, J.; Feng, Y.; Wang, Y.; Luo, X.; Tang, J.; Lin, X. The foliar spray of *Rhodopseudomonas palustris* grown under *Stevia* residue extract promotes plant growth via changing soil microbial community. *J. Soils Sediments* **2016**, *16*, 916–923. https://doi.org/10.1007/s11368-015-1269-1

[26] Xu, J.; Feng, Y.; Wang, Y.; Lin, X. Effect of rhizobacterium *Rhodopseudomonas palustris* inoculation on *Stevia rebaudiana* plant growth and soil microbial community. *Pedosphere* **2018**, *28*, 793–803. https://doi.org/10.1016/S1002-0160(18)60043-8

[27] Batool, K.; Tuz Zahra, F.; Rehman, Y. Arsenic-redox transformation and plant growth promotion by purple nonsulfur bacteria *Rhodopseudomonas palustris* CS2 and *Rhodopseudomonas faecalis* SS5. *BioMed Res. Int.* **2017**, *2017*, 6250327. https://doi.org/10.1155/2017/6250327

[28] Iwai, R.; Uchida, S.; Yamaguchi, S.; Sonoda, F.; Tsunoda, K.; Nagata, H.; Miyasaka, H. Effects of seed bio-priming by purple non-sulfur bacteria (PNSB) on the root development of rice. *Microorganisms* **2022**, *10*, 2197. https://doi.org/10.3390/microorganisms10112197

[29] Dat, L.T.; Tran, N.V.N.B.; Xuan, D.T.; Xuan, L.N.T.; Quang, L.T.; Khuong, N.Q. Effects of P-solubilizing bacteria *Cereibacter sphaeroides* ST16 and ST26 on soil fertility, P uptake and rice yield grown on salt-affected soils under greenhouse conditions. *J. Crop Sci. Biotechnol.* **2024**, *27*, 509–523. https://doi.org/10.1007/s12892-024-00247-2

[30] Anh, N.H.; Hai, T.T.; Duc, N.V.; Xuan, D.T.; Quang, L.T.; Khuong, N.Q. Use of nitrogen-fixing purple nonsulfur bacteria to produce available nitrogen for rice (*Oryza sativa* L.) cultivated in saline acidic soil. *Geomicrobiol. J.* **2024**, *42*, 64–72. https://doi.org/10.1080/01490451.2024.2433202

[31] Sarikhani, M.R.; Ebrahimi, M. Potassium Releasing Bacteria (KRB): Role of KRB in Horticultural Crops. In *Bio-Inoculants in Horticultural Crops*; Woodhead Publishing: Cambridge, UK, 2024; pp. 175–195. https://doi.org/10.1016/B978-0-323-96005-2.00004-0

[32] Sharma, R.; Sindhu, S.S.; Glick, B.R. Potassium Solubilizing Microorganisms as Potential Biofertilizer: A Sustainable Climate-Resilient Approach to Improve Soil Fertility and Crop Production in Agriculture. *J. Plant Growth Regul.* **2024**, *43*, 2503–2535. https://doi.org/10.1007/s00344-024-11297-9

[33] Wu, J.Y.; Chen, H.W.; Sundar, L.S.; Tu, Y.K.; Chao, Y.Y. Exploring the Potential of Purple Non-Sulfur Bacteria Strains A3-5 and F3-3 in Sustainable Agriculture: A Study on Nutrient Solubilization, Plant Growth Promotion, and Acidic Stress Tolerance. *J. Soil Sci. Plant Nutr.* **2025**, *25*, 2294–2313. https://doi.org/10.1007/s42729-025-02268-4

[34] Maeda, I. Potential of Phototrophic Purple Nonsulfur Bacteria to Fix Nitrogen in Rice Fields. *Microorganisms* **2021**, *10*, 28. https://doi.org/10.3390/microorganisms10010028

[35] IRRI (2000) 'Adaptation of the chlorophyll meter technology for N management in rice.' (IRRI: Manila, Philippines).

[36] Ghosh, M.; Swain, D.K.; Jha, M.K.; Tewari, V.K. Precision Nitrogen Management Using Chlorophyll Meter for Improving Growth Productivity and N Use Efficiency of Rice in Subtropical Climate. *J. Agric. Sci.* **2013**, *5*(2), 253. https://doi.org/10.5539/jas.v5n2p253

[37] Sundar, L.S.; Chao, Y.Y. Potential of Purple Non-Sulfur Bacteria in Sustainably Enhancing the Agronomic and Physiological Performances of Rice. *Agronomy* **2022**, *12*, 2347. https://doi.org/10.3390/agronomy12102347

[38] Khanna-Chopra, R.; Semwal, V.K.; Lakra, N.; Pareek, A. Proline—A Key Regulator Conferring Plant Tolerance to Salinity and Drought. In *Plant Tolerance to Environmental Stress*; Hasanuzzaman, M., Fujita, M., Oku, H., Islam, M.T., Eds.; CRC Press: Boca Raton, FL, USA, 2019; pp. 59–80. https://doi.org/10.1201/9780203705315

[39] Ghosh, U.K.; Islam, M.N.; Siddiqui, M.N.; Cao, X.; Khan, M.A. Proline, a Multifaceted Signalling Molecule in Plant Responses to Abiotic Stress: Understanding the Physiological Mechanisms. *Plant Biol.* **2022**, *24*(2), 227–239.

[40] Kishor, P.K.; Sangam, S.; Amrutha, R.N.; Laxmi, P.S.; Naidu, K.R.; Rao, K.S.; Rao, S.; Reddy, K.J.; Theriappan, P.; Sreenivasulu, N. Regulation of Proline Biosynthesis, Degradation, Uptake and Transport in Higher Plants: Its Implications in Plant Growth and Abiotic Stress Tolerance. *Curr. Sci.* **2005**, *88*, 424–438.

[41] Khan, M.Y.; Nadeem, S.M.; Sohaib, M.; Waqas, M.R.; Alotaibi, F.; Ali, L.; Zahir, Z.A.; Al-Barakah, F.N. Potential of Plant Growth Promoting Bacterial Consortium for Improving the Growth and Yield of Wheat under Saline Conditions. *Front. Microbiol.* **2022**, *13*, 958522. https://doi.org/10.3389/fmicb.2022.958522

[42] Khan, P.; Abdelbacki, A.M.; Albaqami, M.; Jan, R.; Kim, K.M. Proline Promotes Drought Tolerance in Maize. *Biology* **2025**, *14*, 41. https://doi.org/10.3390/biology14010041

ASEAN
Journal of Scientific and Technological Reports
Online ISSN:2773-8752

Research article

Public Health Implications of Antimicrobial-Resistant Bacteria in the U-Tapao Canal, South of Thailand: A Study of *Escherichia coli* and Associated Gram-Negative Bacteria

Pharanai Sukhumungoon[1*], Chanitnan Putchu[1], Thodsaphon Palee[1], Phattharanit Bunkraiwong[1], Passaraporn Yong-un[1], and Pattamarat Rattanachuay[2]

[1] Faculty of Science, Prince of Songkla University, Songkhla, 90110, Thailand
[2] Faculty of Science and Technology, Prince of Songkla University, Pattani campus, 94000, Thailand
* Correspondence: pharanai82@gmail.com

Citation:
Sukhumungoon, P.; Putchu, C.; Palee, T.; Bunkraiwong, P.; Yong-un, P.; Rattanachuay, P. Public health implications of antimicrobial-resistant bacteria in the u-tapao canal, south of Thailank: a study of *Escherichia coli* and associated gram-negative bacteria. *ASEAN J. Sci. Tech. Report.* **2026**, *29*(2), e260502. https://doi.org/10.55164/ajstr.v29i2.260502.

Article history:
Received: July 24, 2025
Revised: November 24, 2025
Accepted: December 3, 2025
Available online: January 21, 2026

Abstract: Water-borne diseases are a major global public health concern, leading to significant morbidity and mortality worldwide. In this study, *E. coli* and the associated culturable bacteria were investigated from 7 water sampling locations along the 26 kilometers of U-Tapao Canal, an important aquatic source in southern Thailand. Five *E. coli* strains were obtained from 3 water samples (3/21, prevalence of 14%). Two of five were multidrug-resistant (MDR) *E. coli*. One *E. coli* strain was resistant to imipenem, suggesting that it was a carbapenem-resistant *E. coli*. All five *E. coli* strains exhibited γ-hemolysis on blood agar and produced catalase, suggesting their virulence to some extent. Fifteen diverse bacterial strains other than *E. coli* were also found and classified into 12 distinct bacterial species using MALDI-TOF MS. The finding of *E. coli* and other bacterial species in the U-Tapao Canal in this study highlights the microbial contamination inhabiting this canal and emphasizes the potential risk of water-borne diseases among inhabitants residing in the vicinity. This study strengthens the need for systematic microbiological monitoring of water quality, promoting public health and environmental safety.

Keywords: Bacterial diversity; *Escherichia coli*; fecal; multidrug resistance; water-borne

1. Introduction

Fecal contamination of water has been a major public health concern since it is a source of numerous pathogens [1]. Fecal indicator bacteria are a group of bacteria used to assess water fecal contaminations and their abundance should correspond to the presence of fecal pathogens [2]. One of the major pathogens that serves as an indicator of fecal water contamination supplies is *Escherichia coli* [3]. *E. coli* contamination at a level of zero per 100 mL is considered the threshold for safe potable water [4]. Numerous *E. coli* strains carry distinct virulent genes that are capable of causing a wide variety of diseases, including diarrhea, septicemia, and urinary tract infection [5, 6]. Water-borne outbreaks have been reported to implicate Shiga toxin-producing *E. coli* (STEC) and enteropathogenic *E. coli* (EPEC) [7]. STEC producing Shiga toxin 2 can result in hemorrhagic colitis (HC) and hemolytic uremic syndrome (HUS), leading to high mortality rates [8]. In addition, EPEC, comprising *bfp* (coding for bundle-forming pili) and *eae* (coding for intimin), including locus of enterocyte

effacement (LEE), can lead to non-bloody diarrhea [5]. More importantly, they can acquire antimicrobial-resistant genes through horizontal gene transfer, contributing to their intractability.

The U-Tapao Canal originates from the Thai-Malaysian border and terminates at the lower area of Songkhla Lake, covering a distance of approximately 130 kilometers [9]. It serves as a catchment area and effectively aggregates microbial contaminants from diverse upstream sources traversing Hat-Yai city, which is an urban center with a population exceeding hundreds of thousands of people. This hydrological pathway is serving as a potential stream for the spread of water-borne pathogens to the urban populations. In Thailand, there is a report of a high level of multidrug-resistant (MDR) and extended-spectrum beta-lactamases (ESBL)-producing *E. coli* from river water. However, the data on *E. coli*, including other bacterial species, are scarce in southern Thailand. Therefore, this study discovers the information in terms of prevalence, virulence, antimicrobial resistance (AMR), and bacterial diversity in fresh water in the southern Thai area. This is beneficial to Thailand's public health intervention.

2. Materials and Methods

2.1 Sample collection and bacterial isolation

Water samples were collected from 7 locations, including 5 locations along 26 kilometers of U-Tapao Canal (UTP-1 to UTP-5), and the 2 water reservoirs near cattle farms (Rattana farm, RTN, and Ruengkitt farm, RKF) (Figure 1). Briefly, 100 mL of water was acquired at a depth of 30 cm below the water surface. Ten mL of water was mixed with 90 mL of tryptic soy broth (TSB) (Becton Dickinson, Sparks, USA) and incubated at 37℃ for 1 h. One loop-full of the bacterial culture was streaked on eosin methylene blue agar (EMB agar) (Becton Dickinson, Sparks, USA) and incubated at 37℃ for 18 h for *E. coli* isolation. Green metallic sheen colonies were selected and kept in stock at -80℃ using 10% glycerol (final concentration) as the cryoprotectant.

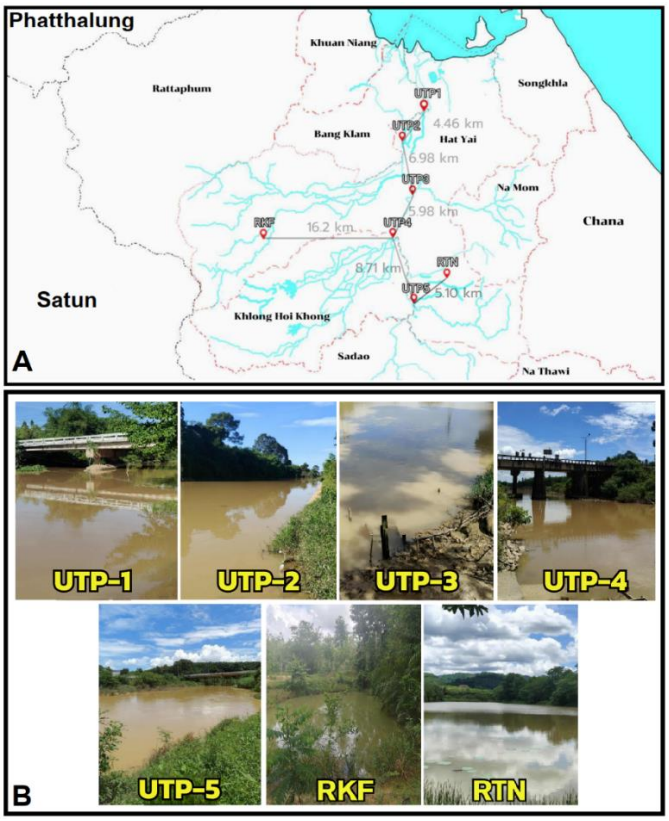

Figure 1. Water sampling locations. A. Water samples were collected from 7 locations, including 5 locations (UTP-1 to UTP-5) along the 26 kilometer-U-Tapao Canal, and 2 water reservoirs from nearby farms (Ruengkitt farm, RKF, and Rattana farm, RTN farm) to assess the bacterial contamination. B, actual field sites where water samples were collected.

2.2 Bacterial identification by matrix-assisted laser desorption ionization-time of flight mass spectrometry (MALDI-TOF MS)

A total of 27 suspected *E. coli* isolates were subjected to bacterial identification by MALDI-TOF MS [10]. In brief, a tiny amount of bacterial colony was spotted onto a steel target plate. The sample was overlaid with 1 µl of 100% formic acid. After drying, 1 µl of Bruker HCCA matrix (α-Cyano-4-hydroxycinnamic acid) was prepared followed the manufacturer's instructions, and was added. The sample was processed and analyzed in a Microflex Biotyper (Bruker Daltonik GmbH, Germany). All isolates were done in duplicates. The highest score value and the identification provided by MALDI-TOF MS were recorded. Score values ≤ 2.0 and ≥1.7 were established as the cut-off for species-level and genus-level identification, respectively [11]. Species-level sample identities were determined by the MTB software searching against the Bruker BDAL MSP library database.

2.3 Hemolysis and catalase production

Hemolysis on blood agar and catalase production were also examined to seek their additional virulence characteristics. For the hemolysis assay, an overnight bacterial colony was spotted on human blood agar and incubated at 37ºC for 18 hours. Alpha (α), beta (β), or gamma (γ) hemolysis was observed macroscopically. Catalase production assay was examined using 3% H_2O_2 solution as described by Sukhumungoon et al. [12].

2.4 Antimicrobial susceptibility assay

All *E. coli* strains were examined for antimicrobial susceptibility using the disk diffusion method [13]. Twelve antimicrobial agents used in this assay were amikacin, AK (30 µg), ampicillin, AMP (10 µg), ceftazidime, CAZ (10 µg), ceftriaxone, CRO (30 µg), cephalothin, KF (30 µg), chloramphenicol, C (30 µg), ciprofloxacin, CIP (5 µg), gentamicin, CN (10 µg), kanamycin, K (30 µg), imipenem, IPM (10 µg), streptomycin, S (10 µg), and tetracycline, TE (30 µg) (Oxoid Hampshire, UK). The clear zone was measured by a vernier caliper. *E. coli* ATCC 25922 was used as a control. MDR was determined by the resistance to 2 or more antibiotic classes.

2.5 Statistical analyses

Fisher's Exact Test was employed to determine the significant difference in the relationship between the detection of *E. coli* and the sampling locations along the U-Tapao Canal. *P*-value was set at 0.05.

3. Results and Discussion

3.1. Bacterial isolation and bacterial identification by matrix-assisted laser desorption ionization-time of flight mass spectrometry (MALDI-TOF MS)

The existence of *E. coli* in natural aquatic sources constitutes a critical public health concern, as these sources supply water to municipal systems for domestic consumption. In this study, a total of five *E. coli* strains were isolated. These 5 strains were recovered from 3 positive water samples (out of 21 total samples, prevalence of 14%). The 3 positive samples were obtained from three distinct locations: one from UTP-1 (yielding 1 isolate), one from UTP-2 (yielding 1 isolate), and the last one from the RKF cattle farm (yielding 3 isolates). (Figure 1 and Table 1). Despite the fact that the presence of *E. coli* was not significantly associated with the water sampling sites (*P*-value > 0.05), its detection is still a public health problem (Table 1). In the course of *E. coli* investigation from the northeastern region of Thailand, a total of 34 surface water samples were collected and yielded 89 *E. coli* isolates, suggesting a high level of *E. coli* contamination [14]. Likewise, the detection of *E. coli* in water has also been documented in several countries worldwide. Bong et al [15] investigated the prevalence and diversity of antimicrobial-resistant *E. coli* under anthropogenic pressure in the Larut River, Malaysia. *E. coli* was detected at all sampling sites, and its estimated abundance was up to 4.1 × 10^5 CFU/100 mL.

Table 1. Prevalence of *E. coli* from U-Tapao Canal, May, 2025

Sample	GPS location	No. of positive sample / No. of total sample (%)	No. of positive isolate / No. of total isolate (%)
*UTP-1	7°04'30.3"N 100°28'32.6"E	1/3 (33)	1/6 (17)
UTP-2	7°02'31.3"N 100°27'06.8"E	1/3 (33)	1/4 (25)
UTP-3	6°58'48.5"N 100°27'48.1"E	0/3 (0)	0/2 (0)
UTP-4	6°55'53.0"N 100°26'24.2"E	0/3 (0)	0/5 (0)
UTP-5	6°51'22.7"N 100°27'52.3"E	0/3 (0)	0/4 (0)
RKF	6°55'48.5"N 100°17'30.6"E	1/3 (33)	3/3 (100)
RTN	6°53'06.4"N 100°30'09.0"E	0/3 (0)	0/3 (0)
Total		3/21 (14%)	5/27 (19)

*UTP, U-Tapao, RKF, Ruengkitt farm, RTN, Rattana farm.

In addition to the detection of *E. coli*, we demonstrated a high degree of bacterial diversity within the fluvial environment. A total of 15 associated culturable Gram-negative isolates recovered from 6 of 7 sampling locations were classified into 12 distinct bacterial species using MALDI-TOF MS, including *Aeromonas caviae*, *Aeromonas hydrophila*, *Enterobacter kobei*, *Klebsiella pneumoniae*, *Kluyvera geogiana*, *Kosakonia radicincitans*, *Enterobacter cloacae*, *Phytobacter ursingii*, *Pantoea dispersa*, *Aeromonas veronii*, *Raoultella ornithinolytica*, and *Leclercia adecarboxylata,* all of which were capable of growing on the selective EMB agar. (Table 3). These bacteria are classified in the families *Enterobacteriaceae* and *Aeromonadaceae*. In addition, some of them are opportunistic pathogens such as *Aeromonas caviae*, *Aeromonas hydrophila*, *and Klebsiella pneumoniae* [16, 17]. Hence, our result underscores the complexity of bacterial communities inhabiting the U-Tapao Canal and highlights the possibility of infection caused by bacteria other than *E. coli* in the future. Based on the results of our investigation, the presence of multiple bacterial species detected in the U-Tapao Canal strongly suggests that these microorganisms are likely introduced through fecal discharges from both humans and animals. Nopprapun et al. [18] examined the origins of fecal bacterial contamination in the Mae Klong River by employing the H8 biomarker, a human-associated genetic marker specific to *Escherichia coli*. Using real-time PCR, 500 *E. coli* isolates were analyzed from ten sampling sites distributed longitudinally from the upstream to the downstream reaches of the river. Their findings revealed that between 10% and 46% of the isolates carried the human-associated H8 marker, indicating a substantial contribution of untreated or inadequately treated domestic wastewater to the river. This serves as compelling evidence that household effluents constitute a major source of microbial pollution in the aquatic environment. Moreover, Díaz-Gavidia et al. [19] reported that humans and cattle constitute the primary sources of fecal microorganism contamination in the Maipo and Maule Rivers of central Chile.

3.2. Hemolysis and catalase production

Hemolysis of blood indicates the bacterial virulence potential to humans. In this study, five *E. coli* strains from U-Tapao Canal and the nearby cattle farm demonstrated γ-hemolysis. The absence of hemolytic activity has been previously described in certain *E. coli* strains. The study from Hai Phong, Vietnam, that investigated the *E. coli* strains isolated from chicken and duck feces reported that 47% (7 of 15) exhibited γ-hemolysis [20]. Moreover, Ibrahim et al. [21] investigated the hemolysis caused by *E. coli* isolated from water and clinical samples in Baghdad, Iraq, in 2013. They showed that 60% (12 of 20 strains) displayed γ-hemolysis. Even though *E. coli* strains in this study lacked the hemolysis capability; it cannot be conclusively inferred that these isolates possess low virulence, as numerous other virulence factors may remain uncharacterized within them. Catalase is shown to be one of the virulence factors of *E. coli*. In this study, all *E. coli* strains were found to produce it (Table 2), supporting that they were pathogenic. Macrophages are essential constituents of the human innate immune system and may be a first line of defense to combat pathogens in the intestine [22]. Macrophages can produce and release reactive oxygen species (ROS) in response to phagocytosis, leading to a bactericidal event [23]. To survive this antimicrobial process, *E. coli* needs to surmount the oxidative stress produced by macrophages. Generally, they overcome oxidative stress by producing enzymes such as

peroxidases, superoxide dismutases, and catalases [24]. The latter enzymes catalyze the decomposition of H_2O_2 into the harmless byproducts, water and oxygen, thereby protecting cells from oxidative destruction [25].

Table 3 Diversity of bacteria in U-Tapao Canal analyzed by MALDI-TOF MS, May, 2025.

Sample	Bacterial strain	Identification result	[a]MALDI-TOF MS score
UTP-1	UTP-1.3.1	*Aeromonas caviae*	2.16
	UTP-1.2.1	*Aeromonas hydrophila*	2.06
	UTP-1.2.2	*Enterobacter kobei*	2.20
	UTP-1.1.3	*Klebsiella pneumoniae*	2.21
	UTP-1.1.2	*Kluyvera geogiana*	2.24
UTP-2	UTP-2.2.2	*NOIP	0
	UTP-2.3.1	NOIP	1.42
	UTP-2.3.2	NOIP	1.50
UTP-3	UTP-3.1.1	NOIP	0
	UTP-3.1.3	*Aeromonas caviae*	2.14
UTP-4	UTP-4.1.2	*Kosakonia radicincitans*	1.75
	UTP-4.1.3	*Enterobacter cloacae*	2.31
	UTP-4.2.1	*Phytobacter ursingii*	1.78
	UTP-4.2.2	NOIP	0
	UTP-4.2.3	*Phytobacter ursingii*	2.12
UTP-5	UTP-5.1.1	*Pantoea dispersa*	2.15
	UTP-5.1.2	*Aeromonas veronii*	2.24
	UTP-5.3.1	*Raoultella ornithinolytica*	2.05
	UTP-5.3.2	*Raoultella ornithinolytica*	2.30
RTN-1	RTN-1.2	NOIP	1.46
	RTN-1.3	*Leclercia adecarboxylata*	1.95
	RTN-3.1	NOIP	1.54

*NOIP, no organism identification possible. [a]MALDI-TOF MS score, Score values 2.00-3.00 indicate high-confidence identification; 1.70-1.99 indicates low-confidence identification; 0.00-1.69 indicates no organism identification possible.

3.3. Antimicrobial susceptibility assay

Bacterial resistance to antimicrobial agents is an escalating public health concern, particularly the emergence and spread of MDR bacteria, posing a significant global health threat. In this study, among the five *E. coli* strains obtained, 2 exhibited the MDR traits. *E. coli* strain UTP-1.1.1 revealed the resistant pattern to ampicillin, ciprofloxacin, kanamycin, streptomycin, and tetracycline, while strain UTP-2.2.1 was resistant to ampicillin, cephalothin, imipenem, and streptomycin (Table 2). The detection of *E. coli* strain UTP-2.2.1 exhibiting resistance to imipenem indicates the presence of a presumptive carbapenem-resistant *Escherichia coli* (CREC). This critical finding warrants urgent confirmatory testing. The other three *E. coli* strains from the RKF cattle farm were not MDR *E. coli* but displayed similar antimicrobial resistance patterns (Table 2). The results in this study are in concordance with the work from Tabut et al. [14] that investigated the AMR of *E. coli* from surface water, wastewater, and discharged water in the Namsuay watershed, northeastern Thailand. The results exhibited that *E. coli* was resistant to fluoroquinolone, third-generation cephalosporin, polymyxin, and carbapenem. In addition, Bong et al. [15] examined the prevalence and diversity of AMR in *E. coli* from the Larut River, Malaysia, using 20 antimicrobial agents that represented 11 different antimicrobial classes. They found that the highest resistance frequency was detected for the tetracycline class, followed by quinolones, penicillins, sulfonamides, amphenicols, fluoroquinolones, and aminoglycosides. The bacterial resistance to tetracycline is not surprising. Owing to the cost-effectiveness of tetracycline, it has been widely employed for prophylaxis and treatment of infectious diseases in humans and animals. In addition, at sub-therapeutic concentrations, it is used as an animal zootechnical additive [26]. The research from Vietnam revealed that resistance to tetracycline was the major antimicrobial resistance observed in raw meat samples

[27]. More importantly, genes mediating tetracycline resistance are effectively transferred between different bacterial species. Therefore, these anthropogenic pressures might, to some extent, play a role in accelerating the AMR. The detection of imipenem-resistant *E. coli* in this study is predictable due to the consistent increase in reported cases of its incidence. The study on antimicrobial resistance of *E. coli* in natural aquatic environment in Khon Kaen Province, Thailand, using the disk diffusion approach, demonstrated an imipenem-resistant rate of 3.54%. Even though the proportion is relatively low, it reflects an escalating risk to public health.

It is estimated that antimicrobial-resistant bacteria have a great impact on around 2.8 million individuals and are responsible for at least 35,000 fatalities annually in the United States [28]. The U-Tapao River Basin covers an area of 2,840 square kilometers, spanning 7 districts of Songkhla province, including Sadao, Na-Mom, Hat-Yai, Khlong-Hoi-Khong, Bang-Klam, Rattaphum, and Khuan-Niang Districts. Therefore, the presence of diverse bacterial contaminants in U-Tapao Canal displaying high levels of antimicrobial resistance is considered a significant threat to public health. This canal serves as a water supply for domestic use, potable purposes, and recreational water activities to hundreds of thousands of people within this area. Pathogenic contaminants in significant quantities, combined with inadequate water management, are able to transmit harmful microorganisms to the residents. Consistent microbiological surveillance of river water plays a crucial role in mitigating and preventing the occurrence of water-borne disease outbreaks. In summary, Thai river systems commonly harbor substantial bacterial loads, many of which possess pathogenic potential to some extent and exhibit varying degrees of antimicrobial resistance. Consequently, practical recommendations for the public include maintaining strict personal hygiene after any contact with untreated river water, refraining from using canal or river water for bathing or other recreational activities, and avoiding the consumption of raw or undercooked aquatic organisms harvested from these waterways. Moreover, municipal authorities should rigorously inspect households and food establishments to ensure that wastewater is adequately treated before discharge into natural water bodies, and should implement routine monitoring of key water-quality indicators to safeguard public health and environmental integrity.

Table 2. Virulence and antimicrobial resistance pattern of *E. coli* strains from U-Tapao Canal, May, 2025.

Sample No.	*Strain name	Antimicrobial susceptibility												Hemolysis (human blood)	Catalase production
		**AK	AMP	C	CAZ	CRO	CIP	CN	K	KF	IPM	S	TE		
1	UTP-1.1.1	S	R	S	S	S	R	S	R	S	S	R	R	γ	+
2	UTP-2.2.1	S	R	S	S	S	S	S	S	R	R	R	S	γ	+
3	RKF-1.1	S	S	S	S	S	S	S	S	R	S	S	S	γ	+
	RKF-1.2	S	R	S	S	S	S	S	S	R	S	S	S	γ	+
	RKF-1.3	S	R	S	S	S	S	S	S	R	S	S	S	γ	+

*UTP, U-Tapao, RKF, Ruengkitt farm, RTN, Rattana farm; **AK, amikacin, AMP, ampicillin, C, chloramphenicol, CAZ, ceftazidime, CRO, ceftriaxone, CIP, ciprofloxacin, CN, gentamicin, K, kanamycin, KF, cephalothin, IPM, imipenem, S, streptomycin, TE, tetracycline; γ, gamma hemolysis; R, resistance, S, sensitive.

4. Conclusions

In the course of investigation, fecal indicator bacteria such as *E. coli* and other opportunistic pathogens (*e.g.*, *Aeromonas* spp.) were found in the U-Tapao Canal, indicating that the water is not safe for direct consumption. Even though the water undergoes water treatment in the municipal water system, water-borne illness risks remain, especially through recreational water activities. Our study raises a public health concern for the population in this area since some *E. coli* strains are MDR, with one strain identified as a presumptive carbapenem-resistant *E. coli* (CREC) and may carry crucial virulence factors. Regular water quality monitoring and stringent microbiological control measures are imperative in decreasing water-borne diseases. This study provides crucial baseline data for safeguarding public health.

5. Acknowledgement

We thank the Division of Biological Science, Faculty of Science, Prince of Songkla University, for providing the essential facilities.

Author Contributions: PS, conceptualization, original draft preparation, methodology, review, editing, validation, resource; CP, conceptualization, methodology; TP, conceptualization, methodology; PB, conceptualization, methodology; PY, methodology; PR, original draft preparation, methodology, review, resource. All authors have read and agreed to the published version of the manuscript.

Funding: The study was funded in part by Prince of Songkla University Graduate Studies Scholarship (Grant No. PSU_GSS 2567-043).

Conflicts of Interest: The authors declare no conflict of interest.

References

[1] Holcomb, D. A.; Stewart, J. R. Microbial Indicators of Fecal Pollution: Recent Progress and Challenges in Assessing Water Quality. *Curr. Environ. Health Rep.* **2020**, *7*, 311–324. https://doi.org/10.1007/s40572-020-00278-1

[2] Liu, B.; Lee, C. W.; Bong, C. W.; Wang, A. J. Investigating *Escherichia coli* Habitat Transition from Sediments to Water in Tropical Urban Lakes. *PeerJ* **2024**, *12*, 1–22. https://doi.org/10.7717/peerj.16556

[3] Jang, J.; Hur, H.-G.; Sadowsky, M. J.; Byappanahalli, M. N.; Yan, T.; Ishii, S. Environmental *Escherichia coli*: Ecology and Public Health Implications—A Review. *J. Appl. Microbiol.* **2017**, *123*, 570–581. https://doi.org/10.1111/jam.13468

[4] World Health Organization (WHO). *Guidelines for Drinking-Water Quality*. *WHO Chron.* **2011**, *38*, 104–108.

[5] Nataro, J. P.; Kaper, J. B. Diarrheagenic *Escherichia coli*. *Clin. Microbiol. Rev.* **1998**, *11*(1), 142–201. https://doi.org/10.1128/cmr.11.1.142

[6] Themphachana, M.; Kongphene, S.; Rattanachuay, P.; Khianngam, S.; Singkhamanan, K.; Sukhumungoon, P. Molecular Characterization of Virulence and Antimicrobial Susceptibility Profiles of Uropathogenic *Escherichia coli* from Patients in a Tertiary Hospital, Southern Thailand. *Southeast Asian J. Trop. Med. Public Health* **2015**, *46*(6), 1021–1030.

[7] Chandran, A.; Mazumder, A. Pathogenic Potential, Genetic Diversity, and Population Structure of *Escherichia coli* Strains Isolated from a Forest-Dominated Watershed (Comox Lake) in British Columbia, Canada. *Appl. Environ. Microbiol.* **2015**, *81*, 1788–1798. https://doi.org/10.1128/AEM.03738-14

[8] Sukhumungoon, P.; Nakaguchi, Y.; Ingviya, N.; Pradutkanchana, J.; Iwade, Y.; Seto, K.; Son, R.; Nishibuchi, M.; Vuddhakul, V. Investigation of *stx2*$^+$ *eae*$^+$ *Escherichia coli* O157:H7 in Beef Imported from Malaysia to Thailand. *Int. Food Res. J.* **2011**, *18*(1), 381–386.

[9] Royal Irrigation Department, Ministry of Agriculture and Cooperatives. *General Features of the U-Taphao River Basin*. http://irrigation.rid.go.th/rid16/sip/linkleft/knowledge_file/autapao/1-physical_autapao.pdf (accessed June 24, 2025).

[10] Marin, M.; Ruiz, A.; Iglesias, C.; Quiroga, L.; Cercennado, E.; Martin-Rabadan, P.; Bouza, E.; Rodriguez-Sanchez, B. Identification of *Nocardia* Species from Clinical Isolates Using MALDI-TOF Mass Spectrometry. *Clin. Microbiol. Infect.* **2018**, *24*(12), 1342.e5–1342.e8. https://doi.org/10.1016/j.cmi.2018.06.014

[11] Rodríguez-Sánchez, B.; Marín, M.; Sánchez-Carrillo, C.; Cercenado, E.; Ruiz, A.; Rodríguez-Créixems, M.; Bouza, E. Improvement of Matrix-Assisted Laser Desorption/Ionization Time-of-Flight Mass Spectrometry Identification of Difficult-to-Identify Bacteria and Its Impact on the Workflow of a Clinical Microbiology Laboratory. *Diagn. Microbiol. Infect. Dis.* **2014**, *79*(1), 1–6. https://doi.org/10.1016/j.diagmicrobio.2014.01.021

[12] Sukhumungoon, P.; Nuwilai, L.; Boontaworn, M.; Rattanachuay, P. Prevalence, Antimicrobial Resistance, and Genetic Relationship of Methicillin-Resistant *Staphylococcus aureus* from Meats, Hat-Yai, Thailand. *ASEAN J. Sci. Technol. Rep.* **2025**, *28*(3), 1–7. https://doi.org/10.55164/ajstr.v28i3.256114

[13] Clinical and Laboratory Standards Institute (CLSI). *Performance Standards for Antimicrobial Susceptibility Testing*, 30th ed.; CLSI Supplement M100; Clinical and Laboratory Standards Institute: Wayne, PA, **2020**; pp 1–294.

[14] Tabut, P.; Yongyod, R.; Ungcharoen, R.; Kerdsin, A. The Distribution of Mobile Colistin-Resistant Genes, Carbapenemase-Encoding Genes, and Fluoroquinolone-Resistant Genes in *Escherichia coli* Isolated from Natural Water Sources in Upper Northeast Thailand. *Antibiotics* **2022**, *11*, 1760. https://doi.org/10.3390/antibiotics11121760

[15] Bong, C. W.; Low, K. Y.; Chai, L. C.; Lee, C. W. Prevalence and Diversity of Antibiotic-Resistant *Escherichia coli* from Anthropogenic-Impacted Larut River. *Front. Public Health* **2022**, *10*, 794513. https://doi.org/10.3389/fpubh.2022.794513

[16] Gonçalves Pessoa, R. B.; Oliveira, W. F.; Marques, D. S. C.; Correia, M. T. D. S.; de Carvalho, E. V. M. M.; Coelho, L. C. B. B. The Genus *Aeromonas*: A General Approach. *Microb. Pathog.* **2019**, *130*, 81–94. https://doi.org/10.1016/j.micpath.2019.02.036

[17] Gonzalez-Ferrer, S.; Peñaloza, H. F.; Budnick, J. A.; Bain, W. G.; Nordstrom, H. R.; Lee, J. S.; Van Tyne, D. Finding Order in the Chaos: Outstanding Questions in *Klebsiella pneumoniae* Pathogenesis. *Infect. Immun.* **2021**, *89* (4), e00693-20. https://doi.org/10.1128/iai.00693-20

[18] Nopprapun, P.; Boontanon, S. K.; Piyaviriyakul, P.; Sweattatut, R.; Fujii, S.; Harada, H. Human Source Identification by Using a Human-Associated *Escherichia coli* Genetic Marker in the Mae Klong River, Thailand. *J. Water Health* **2022**, *20*(5), 794–802. https://doi.org/10.2166/wh.2022.296

[19] Díaz-Gavidia, C.; Barría, C.; Weller, D. L.; Salgado-Caxito, M.; Estrada, E. M.; Araya, A.; Vera, L.; Smith, W.; Kim, M.; Moreno-Switt, A. I.; Olivares-Pacheco, J.; Adell, A. D. Humans and Hoofed Livestock Are the Main Sources of Fecal Contamination of Rivers Used for Crop Irrigation: A Microbial Source Tracking Approach. *Front. Microbiol.* **2022**, *13*, 768527. https://doi.org/10.3389/fmicb.2022.768527

[20] Quyen, D. V.; Lanh, P. T.; Oanh, N. K. Isolation and Characterization of *Escherichia coli* Associated with Diarrhea in Chickens and Ducks in Hai Phong Province. *Acad. J. Biol.* **2024**, *46*(3), 17–26. https://doi.org/10.15625/2615-9023/20228

[21] Ibrahim, I. A.; Al-Shwaikh, R. M.; Ismaeil, M. I. Virulence and Antimicrobial Resistance of *Escherichia coli* Isolated from Tigris River and Children Diarrhea. *Infect. Drug Resist.* **2019**, *7*, 317–322. https://doi.org/10.2147/IDR.S70684

[22] Wan, B.; Zhang, Q.; Ni, J.; Li, S.; Wen, D.; Li, J.; Xiao, H.; He, P.; Ou, H. Y.; Tao, J.; Teng, Q.; Lu, J.; Wu, W.; Yao, Y. F. Type VI Secretion System Contributes to Enterohemorrhagic *Escherichia coli* Virulence by Secreting Catalase against Host Reactive Oxygen Species (ROS). *PLoS Pathog.* **2017**, *13*(3), e1006246. https://doi.org/10.1371/journal.ppat.1006246

[23] Fang, F. C. Antimicrobial Reactive Oxygen and Nitrogen Species: Concepts and Controversies. *Nat. Rev. Microbiol.* **2004**, *2*, 820–832. https://doi.org/10.1038/nrmicro1004

[24] Imlay, J. A. The Molecular Mechanisms and Physiological Consequences of Oxidative Stress: Lessons from a Model Bacterium. *Nat. Rev. Microbiol.* **2013**, *11*, 443–454. https://doi.org/10.1038/nrmicro3032

[25] Das, D.; Bishayi, B. Staphylococcal Catalase Protects Intracellularly Survived Bacteria by Destroying H_2O_2 Produced by the Murine Peritoneal Macrophages. *Microb. Pathog.* **2009**, *47*, 57–67. https://doi.org/10.1016/j.micpath.2009.04.012

[26] Chopra, I.; Roberts, M. Tetracycline Antibiotics: Mode of Action, Applications, Molecular Biology, and Epidemiology of Bacterial Resistance. *Microbiol. Mol. Biol. Rev.* **2001**, *65*, 232–260. https://doi.org/10.1128/MMBR.65.2.232-260.2001

[27] Van, T. T. H.; Chin, J.; Chapman, T.; Tran, L. T.; Coloe, P. J. Safety of Raw Meat and Shellfish in Vietnam: An Analysis of *Escherichia coli* Isolations for Antibiotic Resistance and Virulence Genes. *Int. J. Food Microbiol.* **2008**, *124*(3), 217–223. https://doi.org/10.1016/j.ijfoodmicro.2008.03.029

[28] Centers for Disease Control and Prevention (CDC). *Antibiotic Resistance*; National Center for Emerging and Zoonotic Infectious Diseases (NCEZID), Division of Healthcare Quality Promotion (DHQP): Atlanta, GA. https://www.cdc.gov/drugresistance/about.html (accessed August 6, 2022).

ASEAN
Journal of Scientific and Technological Reports
Online ISSN:2773-8752

Research article

Influence of Dietary Fermented Mulberry (*Morus alba*) Leaf Inclusion on Growth Performance and Immune Responses in Nile Tilapia (*Oreochromis niloticus*)

Thapanakhajorn Punjam[1], Sudaporn Tongsiri[1], Jongkon Promya[1], Wassana Kongsombat[2], and Chanagun Chitmanat[1*]

[1] Faculty of Fisheries Technology and Aquatic Resources, Maejo University, Chiang Mai, 50290, Thailand
[2] Loei Freshwater Fisheries Research and Development Center, Loei, 42110, Thailand
* Correspondence: chanagun9@gmail.com

Citation:
Punjam, T.; Tongsiri, S.; Promya, J.; Kongsombat, W. Chitmanat, C. Influence of dietary fermented mulberry (*Morus alba*) leaf inclusion on growth performance and immune responses in nile tilapia (*Oreochromis niloticus*). *ASEAN J. Sci. Tech. Report.* **2026**, *29*(2), e260518. https://doi.org/10.55164/ajstr.v29i2.260518.

Article history:
Received: July 25, 2025
Revised: October 31, 2025
Accepted: December 3, 2025
Available online: January 21, 2026

Abstract: This study investigated the effects of dietary fermented mulberry leaves (FML) on growth performance, carcass traits, muscle composition, and innate immune responses of juvenile Nile tilapia (*Oreochromis niloticus*). The use of functional feed additives is increasingly emphasized in aquaculture to reduce antibiotic dependence, particularly during early life stages when fish are highly susceptible to disease. Juvenile tilapias were fed diets containing 0% (control), 1%, 2%, or 4% FML for 60 days. Dietary supplementation with FML significantly improved weight gain, length gain, average daily gain, feed conversion ratio, and survival ($P < 0.05$). The 2% FML diet produced the most favorable outcomes in muscle nutritional quality, including elevated crude protein and reduced lipid and fiber contents ($P < 0.05$). Immune parameters were also enhanced in fish receiving FML. Agglutination titers, lysozyme activity, and phagocytic efficiency increased significantly across FML-treated groups ($P < 0.05$). Moreover, the 2% inclusion level resulted in higher concentrations of the pro-inflammatory cytokines TNF-α and IL-1, indicating activation of innate immune pathways ($P < 0.05$). These findings demonstrate that FML, particularly at a 2% dietary inclusion, is an effective and environmentally sustainable feed supplement capable of improving growth performance, muscle composition, and immune competence in juvenile Nile tilapia. The incorporation of FML may therefore contribute to reduced reliance on antibiotics and support more sustainable aquaculture practices.

Keywords: Fermented mulberry leaves; nile tilapia; immunity

1. Introduction

The global aquaculture of Nile tilapia (*Oreochromis niloticus*) is continually driven by several key attributes: its rapid growth rate, significant tolerance to environmental uncertainty stressors, and relatively low production costs [1, 2]. This high-yield freshwater fish holds substantial economic importance, with its world market valuation projected to reach between USD 9.8 billion and USD 15.1 billion by 2025 [3, 4]. Despite these advantages, high fry mortality during the nursery phase remains a major constraint, largely due to the immature immune systems of juvenile fish. In recent years, the emergence and re-emergence of pathogenic threats, including *Streptococcus* spp., *Aeromonas hydrophila*, *Flavobacterium columnare*, and Tilapia

Lake Virus (TiLV) have significantly disrupted production by increasing disease incidence and mortality [5, 6]. Consequently, there is a growing trend towards seeking safe and environmentally friendly alternative products, particularly those derived from herbal plants and probiotics.

Among these, Mulberry (*Morus alba*) is recognized for its wide array of pharmacological properties, including antidiabetic, antimicrobial, antimutagenic, antioxidant, anticancer, anti-anxiety, antiparasitic, anti-stress, immunostimulating, cholesterol-lowering, kidney-protective, and liver-protective effects. Its beneficial composition includes active compounds such as carotene, vitamin B1, folic acid, isoquercetin, quercetin, tannins, flavonoids, and saponins [7-9]. These bioactive compounds are known to enhance immune function, antioxidant capacity, and disease resistance in fish species, potentially reducing mortality rates. In largemouth bass (*Micropterus salmoides*), incorporating dried mulberry leaves into the diet has been reported to enhance growth performance, improve blood lipid parameters, increase antioxidant enzyme activities, and alleviate liver inflammation [10]. Similarly, research on Indian minor carp (*Labeo bata*) demonstrated that substituting up to half of the fishmeal with fermented mulberry leaves, while keeping dietary fiber content under 5.63%, led to improved growth rates and elevated digestive enzyme activities [11]. Nevertheless, the direct use of raw mulberry leaves in animal feed has been limited by their high dietary fiber content and the presence of anti-nutritional factors (ANFs) like tannins and phytic acid, which can impede nutrient digestion and absorption in livestock [12, 13]. Biological fermentation presents a powerful solution for mitigating these adverse effects of ANFs in food and feed. This transformative process not only degrades these undesirable compounds but also significantly enhances the nutritional value of the product by releasing more digestible nutrients and fostering the growth of beneficial microorganisms [14, 15]. Fermentation by beneficial microbes such as lactic acid bacteria can reduce anti-nutritional factors while increasing the bioavailability of nutrients. The inclusion of fermented mulberry leaf meal has been demonstrated to enhance growth, boost antioxidant activity, and reduce lipid levels in largemouth bass and Indian minor carp [10, 11]. However, limited studies have investigated the effects of fermented mulberry leaf inclusion on juvenile Nile tilapia growth, immune status, and survival under controlled aquaculture conditions.

Consequently, this research aimed to explore the impact of incorporating fermented mulberry leaves into the diets of juvenile tilapia. We evaluated various inclusion ratios to assess their effects on growth performance, survival rates, and overall health of the fish. Ultimately, this study sought to minimize reliance on antibiotics and synthetic additives while promoting safer, more sustainable aquaculture practices.

2. Materials and Methods

2.1 Ethical statement

All experimental protocols, methods, and feeding regimes were approved on 30 July 2025 by the Institutional Animal Care and Use Committee of the Faculty of Fisheries Technology and Aquatic Resources, Maejo University (Chiangmai, Thailand).

2.2 Feed preparation

Experimental feeds were formulated using commercial ready-to-use pellets (Betagro 831) as the basal feed. Fermented mulberry leaves were prepared by combining 250 g of mulberry leaves, 150 g of banana shoots, and 150 g of molasses with 1 L of water and a yogurt inoculum containing 10^8 CFU/mL *Lactobacillus casei*, followed by anaerobic fermentation for 30 days. The prepared fermented mulberry leaf powder was incorporated at inclusion levels of 0% (control), 1%, 2%, and 4% per kilogram of feed. Each diet was thoroughly mixed to ensure homogeneity, coated with 3% gelatin to enhance palatability and bind the ingredients, and then redried in a hot air oven at 55 °C for 24 h to achieve a stable moisture content before storage. The finalized feed samples were packaged in airtight bags and stored at 4°C until use. Before the feeding trial, all experimental diets underwent proximate analysis to determine their nutritional composition, including moisture, ash, crude protein, crude fat, and crude fiber content, following standard methods [16]. The nitrogen-free extract (NFE), representing carbohydrate content, was determined by difference. Fish were fed twice daily, specifically between 08:30-09:30 h and 16:30-17:30 h. To ensure optimal nutrition relative to growth, the daily feed ration was adjusted every 14 days based on the incremental increase in fish biomass.

The feeding trial was conducted for a total of 60 days, with fish growth performance monitored at 30-day intervals until the experiment's conclusion. (Table 1).

Table 1. The nutrient profile in mulberry leaves, fermented mulberry leaves, and experimental feeds.

	fermented mulberry leaves (MBL)	mulberry leaves (ML)	control (MBL0)	1% (MBL1)	2% (MBL2)	4% (MBL4)
Moisture (%)	4.26 ± 0.21^{d}	6.59 ± 0.02^{c}	3.25 ± 0.02^{b}	3.22 ± 0.03^{b}	3.01 ± 0.02^{b}	2.38 ± 0.05^{a}
Ash (%)	23.91 ± 0.06^{c}	12.90 ± 0.02^{b}	10.80 ± 0.01^{a}	11.13 ± 0.02^{a}	11.27 ± 0.36^{a}	11.45 ± 0.07^{a}
Protein (%)	24.08 ± 1.32^{a}	18.98 ± 0.74^{a}	34.46 ± 0.28^{b}	34.62 ± 1.02^{b}	35.45 ± 2.58^{b}	36.13 ± 0.00^{b}
Lipid (%)	9.49 ± 0.29^{d}	6.52 ± 0.07^{c}	5.17 ± 0.04^{a}	5.51 ± 0.09^{ab}	6.09 ± 0.05^{bc}	6.34 ± 0.03^{c}
Fiber (%)	11.53 ± 0.45^{b}	16.59 ± 0.26^{c}	9.86 ± 0.06^{a}	9.93 ± 0.09^{a}	10.25 ± 0.15^{a}	10.81 ± 0.12^{ab}
NFE (%)	26.72 ± 1.54^{a}	38.42 ± 0.78^{b}	36.46 ± 0.24^{b}	35.58 ± 0.91^{b}	33.93 ± 2.50^{b}	32.89 ± 0.22^{ab}

Note:Values in the same row with different superscripts are significantly different ($P < 0.05$)

2.3. Fish and feeding trial

Nile tilapia (*Oreochromis niloticus*) fingerlings were procured from the Faculty of Fisheries Technology and Aquatic Resources, Maejo University. Before the commencement of the experiment, all fingerlings underwent a 14-day acclimatization period, during which they were housed in cages and fed a control diet to apparent satiation twice daily (morning and evening). A total of 360 fingerlings, with an initial mean body weight of 13.06±2.64 grams, were then randomly selected and their individual lengths and weights measured. Subsequently, the fingerlings were evenly distributed into experimental cages measuring 1×1×1 meter (width × length × height). The experiment consisted of five dietary treatments (control and four levels of fermented mulberry leaf meal) with three replicates per treatment, each replicate containing 30 fish per cage. Throughout the experimental duration, fish were fed a daily ration equivalent to 5% of their total body weight, administered in two equal portions per day.

2.4 Samples collection

Upon the conclusion of the feeding trial, all experimental fish underwent a 24-hour fasting period to facilitate complete gut evacuation. To minimize stress during sampling, fish from each replicate cage were first anaesthetized in a 50 ppm clove oil solution. Following anesthesia, the final total count and body weight of fish in each cage were measured to determine growth performance indices. Subsequently, six fish were randomly selected per treatment for blood collection to analyse immunological responses (bacterial agglutination, lysozyme activity, and respiratory burst assays). Blood was drawn from the caudal vein of these selected fish using a sterile 1 mL syringe and immediately transferred into Eppendorf tubes. These samples were left to coagulate for 4 hours at room temperature. The coagulated samples were then subjected to centrifugation at 3,500 × g for 5 minutes. The resulting supernatant (serum) was carefully harvested and immediately frozen at -80 °C for later biochemical and immunological analyses.

2.5 Growth Performance Evaluation

Throughout the experimental period, fish growth was periodically monitored. A random sub-sample comprising 30% of the fish from each cage was weighed (g) and measured for total length (cm). To ensure consistent nutritional intake, feed rations were meticulously adjusted biweekly based on the observed weight gain, thereby maintaining the prescribed feeding rate at 5% of the total fish biomass. At the conclusion of the 60-day feeding trial, all fish within each experimental unit were enumerated and weighed to assess final growth performance. The following parameters were subsequently calculated: average weight gain (WG, g), average length gain (LG, cm), average daily gain (ADG), feed conversion ratio (FCR), and survival rate (SR).

2.6 Carcass quality and Body composition analysis

At the end of the feeding trial, five fish were randomly sampled from each experimental replicate. To assess yield and body composition, each specimen was meticulously dissected. The key bodily components—

including the edible muscle, fins, bones, and gonads were separated and individually weighed. The weight data obtained from this detailed physical analysis were subsequently used to calculate critical morphometric and yield indicators. These parameters included the edible flesh percentage, dress-out percentage, carcass waste percentage, and the hepatosomatic index (HSI), determined according to the established methodology described by Hasan et al. [17]. To determine the nutritional profile of the fish, muscle samples were initially minced and then subjected to drying in a hot air oven until a constant weight was achieved. The dried tissue was subsequently ground into a homogeneous powder for analysis. Proximate analysis was performed to quantify moisture, ash, crude protein, crude fat, and crude fiber content. The carbohydrate fraction, reported as Nitrogen-Free Extract (NFE), was calculated using the formula: NFE (%) = 100 - (% Moisture + % Ash + % Crude Fiber + % Crude Fat + % Crude Protein). All procedures adhered to the methods outlined by AOAC [16].

2.7 Bacterial agglutination activity

Antibody levels, specifically agglutination titers, were quantified using U-bottom microtiter plates. The assay was conducted following the modification of the protocols by [18, 19]. Briefly, serum samples were subjected to two-fold serial dilutions (ranging from 1:2 to 1:128) in phosphate-buffered saline (PBS). Subsequently, 50 µL of an *Aeromonas hydrophila* bacterial suspension (optical density at 540 nm [OD_{540nm}] = 1.0; equivalent to 10^7 cells/mL) was added to each well containing the diluted serum. The plates were then incubated at room temperature for 24 hours, after which the agglutination titer of the antibody was determined. The agglutination titer was defined as the reciprocal of the highest dilution of serum that resulted in complete agglutination of the bacterial cells.

2.8 Lysozyme determination

Serum lysozyme activity was determined spectrophotometrically, based on the lysis of *Micrococcus lysodeikticus*, following the method described by [20]. Briefly, 25 µL of serum was combined with 175 µL of a *Micrococcus lysodeikticus* bacterial suspension in a microtiter plate well. The decrease in turbidity, indicating bacterial lysis, was subsequently measured at an optical density of 540 nm (OD_{540nm}) using a microplate reader. Readings were recorded every 30 seconds for a total duration of 10 minutes.

2.9 Respiratory burst activity

The respiratory burst activity of leukocytes, serving as an indicator of their oxidative killing capacity, was assessed following the method described by Secombes [21]. Briefly, isolated leukocytes were seeded into a 96-well microtiter plate and mixed with 100 µL of 0.2 % Nitro blue tetrazolium chloride (NBT) solution. The plate was then incubated at room temperature for 2 hours. Upon completion of the incubation, the supernatant was carefully discarded. The wells were then thoroughly washed with methanol, followed by an additional wash with 70% methanol, and allowed to air-dry at room temperature for 2 minutes. To solubilize the formazan product, dimethyl sulfoxide (DMSO) and 2N KOH were sequentially added to the original wells. The entire well contents were then transferred to a new 96-well microtiter plate, and the optical density at 655 nm (OD_{655nm}) was measured using a Microplate reader.

2.10 RNA extraction, cDNA synthesis, and quantitative real-time PCR (qPCR)

At the end of the feeding trial, liver samples (~0.2 g) were excised from three randomly selected fish per treatment group. Samples were immediately preserved in RNAlater® (Amnion, Cambridgeshire, UK) and stored at –80 °C until RNA extraction. Total RNA was isolated using 1 mL of QIAzol® Lysis Reagent (Qiagen, USA) and further purified using the RNeasy® Mini Kit (Qiagen, Hilden, Germany) in accordance with the manufacturer's instructions. Residual genomic DNA was eliminated by DNase I treatment (Thermo Fisher Scientific, USA). RNA purity and concentration were assessed via absorbance at 260 and 280 nm using a Synergy™ H1 Multi-Mode Microplate Reader (BioTek Instruments Inc., USA), while RNA integrity was confirmed by electrophoresis on a 2% agarose gel. First-strand cDNA synthesis was performed using 1 µg of total RNA and the RevertAid™ First-Strand cDNA Synthesis Kit (Thermo Scientific, USA) following the manufacturer's protocol. Synthesized cDNA was treated with RNase H (Invitrogen, USA) at 37 °C for 20 min and stored at –20 °C until use.

Quantitative real-time PCR was carried out on a PCRmax ECO 48 Real-Time PCR System (PCRmax, UK) using Maxima™ SYBR Green/ROX qPCR Master Mix (2×) (Thermo Fisher Scientific, Lithuania). Primer sequences used for amplification are provided in Table 2. β-actin was selected as the reference gene for normalization. Primer efficiency was validated via standard curve analysis using serially diluted cDNA, ensuring correlation coefficients (R^2) > 0.99. A melt curve analysis was performed post-amplification to confirm product specificity. Each qPCR reaction was performed in triplicate in a 20 μL volume, comprising 2 μL of 1:100 diluted cDNA, 10 μL of SYBR Green Master Mix, 1 μL of each primer (1 pmol), and 6 μL of nuclease-free water. The thermal cycling protocol included an initial denaturation at 95 °C for 3 min, followed by 40 cycles of denaturation at 95 °C for 10 s, and annealing/extension at 60 °C for 30 s. Relative gene expression was quantified using the 2^−ΔΔCt method.

Table 2. Primers used to quantify the relative gene expression

Genes	Primer sequences (5′ - 3′)	References
TNF-α	F-GCTGGAGGCCAATAAAATCA R-CCTTCGTCAGTCTCCAGCTC	Kayansamruaj et al. [22]
IL1-β	F-AAGATGAATTGTGGAGCTGTGTT R-AAAAGCATCGACAGTATGTGAAAT	Chadzinska et al. [23]
Actin	F-TGGTGGGTATGGGTCAGAAAG R- TGTTGGCTTTGGGGTTCA	XM_003443127

2.11 Statistical Analysis

All experimental data were subjected to one-way analysis of variance (ANOVA) to determine significant differences among treatment groups. When statistical significance was detected, Tukey's Honest Significant Difference (HSD) post hoc test was employed for multiple comparisons of treatment means. All statistical analyses were conducted using SPSS for Windows (Version 30.0), with a significance level established at $p < 0.05$.

3. Results and Discussion

3.1 Growth Performances

Table 3 presents the effects of dietary fermented mulberry leaf (FML) inclusion on the growth performance of juvenile Nile tilapia. Fish received FML at inclusion levels of 1%, 2%, and 4% (MBL1, MBL2, and MBL4, respectively) exhibited significantly greater ($P < 0.05$) weight gain (WG), length gain (LG), and average daily gain (ADG) compared to the control group (MBL0). Specifically, WG increased from 45.25 ± 2.79 g in the control to 78.52 ± 1.93 g (MBL1), 81.30 ± 1.81 g (MBL2), and 77.33 ± 1.90 g (MBL4). LG rose from 7.07 ± 0.17 cm to a range of 10.09 ± 0.16 to 10.66 ± 0.22 cm, while ADG improved from 0.75 ± 0.09 g/day to 1.29 ± 0.06 to 2.71 ± 0.06 g/day across FML-treated groups. No significant differences ($P > 0.05$) were observed among the FML-treated groups, indicating that increasing inclusion beyond 1% did not yield further statistical improvement.

Feed conversion ratio (FCR) was significantly reduced ($P < 0.05$) in MBL1 (1.25 ± 0.01) and MBL2 (1.24 ± 0.04) compared to MBL0 (1.43 ± 0.03), indicating improved feed efficiency. Although MBL4 (1.34 ± 0.02) showed numerically better FCR than the control, the difference was not statistically significant ($P > 0.05$). Survival rates (SR) were also significantly higher ($P < 0.05$) in all FML-supplemented groups compared to the control, with no statistical differences among the FML treatments.

These improvements in growth performances and feed efficiency align with previous findings on the use of fermented plant-based additives in aquaculture diets [24, 25]. The enhanced outcomes are likely linked to the fermentation process, which degrades anti-nutritional factors (ANFs) such as phytic acid and tannins—compounds known to inhibit nutrient digestibility and mineral bioavailability [26–28]. Fermentation not only mitigates these limitations but also promotes the release of bioactive compounds and beneficial microbial metabolites, which may further enhance digestive enzyme activity and nutrient assimilation [29-30]. Moreover, improved survival rates observed in FML-fed groups may be attributed to strengthened physiological resilience, potentially resulting from enhanced immunity and gut health, as reported in other

studies using fermented herbal additives [31-33]. However, no dose-dependent relationship was observed beyond the 2% inclusion level, suggesting a possible plateau effect in nutrient uptake or microbial stimulation. Future work may focus on investigating the optimal dosage window and long-term physiological impacts.

Table 3. Growth performances of juvenile tiapla fed with the experimental diets for 60 days.

	control (MBL0)	**1% (MBL1)**	**2% (MBL2)**	**4% (MBL4)**
WG (g)	45.25± 2.79^{a}	78.52 ± 1.93^{b}	81.30 ± 1.81^{b}	77.33 ± 1.90^{b}
LG (cm)	7.07 ± 0.17^{a}	10.11 ± 0.26^{b}	10.66 ± 0.22^{b}	10.09 ± 0.16^{b}
ADG (g/day)	0.75 ± 0.09^{a}	1.31 ± 0.06^{b}	1.35 ± 0.06^{b}	1.29 ± 0.06^{b}
FCR	1.43 ± 0.03^{b}	1.25 ± 0.01^{a}	1.24 ± 0.04^{a}	1.34 ± 0.02^{ab}
SR (%)	94.44 ±1.92^{a}	98.89 ±0.83^{b}	100 ± 0.00^{b}	98.89 ±0.63^{b}

Note: Values in the same row with different superscripts are significantly different ($P < 0.05$). WG = Weight Gain, LG = Length Gain, ADG = Average daily gain, FCR = Food Conversion Rate and SR = Survival Rate

3.2. Carcass Quality and Muscle Composition

In addition to growth performance, body composition is a critical parameter in nutritional studies, serving as a reliable indicator of feed quality, carcass yield, and the overall nutritive value of fish muscle [33-34]. The effects of dietary fermented mulberry leaf (FML) supplementation on carcass traits of juvenile *Oreochromis niloticus* are summarized in Table 4. No significant differences ($P > 0.05$) were observed among treatments in edible flesh percentage (EF: 32.96 ± 0.76% to 34.65 ± 0.62%), dress-out percentage (Do: 0.43 ± 0.01% to 0.44 ± 0.00%), or carcass waste (CW: 56.37 ± 0.26% to 57.41 ± 0.97%), indicating that FML supplementation did not adversely affect marketable yield. However, the hepatosomatic index (HSI) showed a significant increase ($P < 0.05$) in fish fed 4% FML (MBL4: 1.34 ± 0.16%) compared to the control group (MBL0: 0.61 ± 0.00%). Intermediate HSI values were recorded in the 1% and 2% FML groups (MBL1: 1.05 ± 0.09% and MBL2: 1.17 ± 0.23%), though these did not differ statistically from either the control or MBL4. Given the liver's central role in metabolism and detoxification, this elevation in HSI at higher inclusion levels may reflect hepatic metabolic stress or lipid accumulation, despite the absence of histological evidence of damage. Further studies employing liver histopathology and biochemical profiling are warranted to clarify this response.

Table 4. Effect of mulberry leaves supplemented in the Nile tilapia diet on carcass quality.

	control (MBL0)	**1% (MBL1)**	**2% (MBL2)**	**4% (MBL4)**
EF (%)	32.96 ± 0.76^{a}	34.65 ± 0.62^{a}	34.14 ± 0.29^{a}	33.86 ± 0.24^{a}
Do (%)	0.43 ± 0.01^{a}	0.43 ± 0.01^{a}	0.43 ± 0.00^{a}	0.44 ± 0.00^{a}
CW (%)	57.41 ± 0.97^{a}	56.91 ± 0.69^{a}	57.1 ± 0.21^{a}	56.37 ± 0.26^{a}
HSI (%)	0.61 ± 0.00.^{a}	1.05 ± 0.09^{ab}	1.17 ± 0.23^{ab}	1.34 ± 0.16^{b}

Note: Values in the same row with different superscripts are significantly different ($P < 0.05$)
EF = Edible flesh, Do = Dress-out percentage, CW = Carcass waste and HSI = Hepatasomatic index

Muscle proximate composition results are presented in Table 5. No significant differences ($P > 0.05$) were observed in muscle moisture or ash content across the groups. However, fish receiving 2% FML (MBL2) demonstrated a significantly higher crude protein content (53.61 ± 0.32%) compared to the control (47.05 ± 0.23%) and the 4% group (47.00 ± 0.09%) ($P < 0.05$). This enhancement in muscle protein is likely due to improved protein digestibility and assimilation, facilitated by fermentation processes that reduce anti-nutritional factors such as tannins and phytic acid, known to inhibit protein utilization. Simultaneously, the MBL2 group exhibited a marked reduction in muscle lipid content (6.61 ± 0.03%) compared to MBL0 (8.35 ± 0.09%) and MBL4 (7.85 ± 0.06%) ($P < 0.05$). These lipid-lowering effects may stem from the presence of polyphenols and flavonoids in FML, which have been shown to modulate lipid metabolism and enhance

hepatic lipid regulation in fish. A corresponding decrease in muscle crude fiber content in MBL2 (4.14 ± 0.02%) further suggests improved feed fiber utilization post-fermentation.

Additionally, the nitrogen-free extract (NFE), an indicator of carbohydrate reserves, was significantly reduced ($P < 0.05$) in MBL1 (26.45 ± 0.84%) and MBL2 (26.09 ± 0.23%) compared to MBL0 (30.89 ± 0.44%) and MBL4 (31.06 ± 0.63%). This reduction implies a shift in energy partitioning, favoring protein deposition over carbohydrate storage, supporting the observed enhancement in lean tissue accretion. These findings align with previous reports demonstrating that mulberry leaf supplementation can enhance muscle protein content in *Oreochromis niloticus* [36] and improve protein-to-fat ratios in *Megalobrama amblycephala* [29]. Overall, dietary inclusion of FML at 2% appears optimal for improving muscle nutritional quality by increasing protein and reducing lipid and carbohydrate content without compromising carcass yield. Nevertheless, the increase in HSI at higher inclusion levels suggests that caution is needed when exceeding optimal dosages. Future investigations incorporating liver enzyme assays, histological evaluation, and gut microbiome analysis could provide further insights into the metabolic and immunological responses elicited by FML supplementation.

Table 5. Muscle composition of juvenile Nile tilapia fed with the experimental diets.

	control (MBL0)	**1% (MBL1)**	**2% (MBL2)**	**4% (MBL4)**
Moisture (%)	6.84 ± 0.22^{a}	7.33 ± 0.76^{a}	6.98 ± 0.34^{a}	7.57 ± 0.77^{a}
Ash (%)	2.60 ± 0.32^{a}	2.29 ± 0.07^{a}	2.57 ± 0.04^{a}	2.35 ± 0.04^{a}
Lipid (%)	8.35 ± 0.09^{c}	7.90 ± 0.03^{b}	6.61 ± 0.03^{a}	7.85 ± 0.06^{b}
Fiber (%)	4.27 ± 0.01^{b}	4.21 ± 0.02^{ab}	4.14 ± 0.02^{a}	4.16 ± 0.02^{a}
Protein (%)	47.05 ± 0.23^{a}	51.82 ± 0.35^{b}	53.61 ± 0.32^{c}	47.00 ± 0.09^{a}
NFE (%)	30.89 ± 0.44^{b}	26.45 ± 0.84^{a}	26.09 ± 0.23^{a}	31.06 ± 0.63^{b}

Note: Values in the same row with different superscripts are significantly different ($P < 0.05$)

3.3 Immune Responses

Figures 1 and 2 illustrate the effects of dietary fermented mulberry leaf (FML) supplementation on various immune parameters in Nile tilapia, including humoral and cellular immune markers. Key immune indices analyzed included agglutination titer, lysozyme activity, bacterial phagocytic efficiency, and the expression levels of pro-inflammatory cytokines—Tumor Necrosis Factor-alpha (TNF-α) and Interleukin-1 (IL-1). Fish that received FML-supplemented diets exhibited significantly higher agglutination titers than those in the control group ($P < 0.05$), as shown in Figure 1A. Consistent titers of 6 were recorded across all treatment groups (1%, 2%, and 4% FML), compared to a value of 5 in the control, suggesting an enhancement in humoral immunity associated with FML inclusion. A dose-dependent increase in serum lysozyme activity was observed with FML supplementation ($P < 0.05$), as shown in Figure 1B. The highest activity was detected in the 2% FML group (4.73 U/ml), followed by 4% (4.59 U/ml) and 1% (4.22 U/ml), in contrast to the control group (2.84 U/ml). Given lysozyme's role in degrading bacterial cell walls, this elevation underscores the potentiation of non-specific immune defense mechanisms. Phagocytic activity of leukocytes was significantly enhanced in all FML-treated groups compared to the control ($P < 0.05$), as depicted in Figure 1C. Efficiency rose from 0.236 μg/ml in the control to 0.287 μg/ml, 0.310 μg/ml, and 0.309 μg/ml in the 1%, 2%, and 4% FML groups, respectively. This indicates that FML supports the cellular immune response by promoting more effective pathogen clearance via phagocytosis. The immunostimulatory effect of dietary mulberry leaf supplementation was confirmed by changes in TNF-α and IL-1expression (Figures 2A and 2B, respectively). Specifically, the 2% group (MBL2) exhibited the highest TNF-α mRNA level, significantly exceeding all other treatments ($P < 0.05$), suggesting a robust inflammatory response at this concentration. In contrast, IL-1 expression was significantly induced across all inclusion levels 1% (MBL1), 2% (MBL2), 4% (MBL4), with these elevated values statistically comparable to one another but significantly greater than the control group ($P < 0.05$). Collectively, these cytokine profiles indicate that the bioactive components in mulberry leaves successfully activate inflammatory signaling pathways when supplemented at appropriate dietary concentrations.

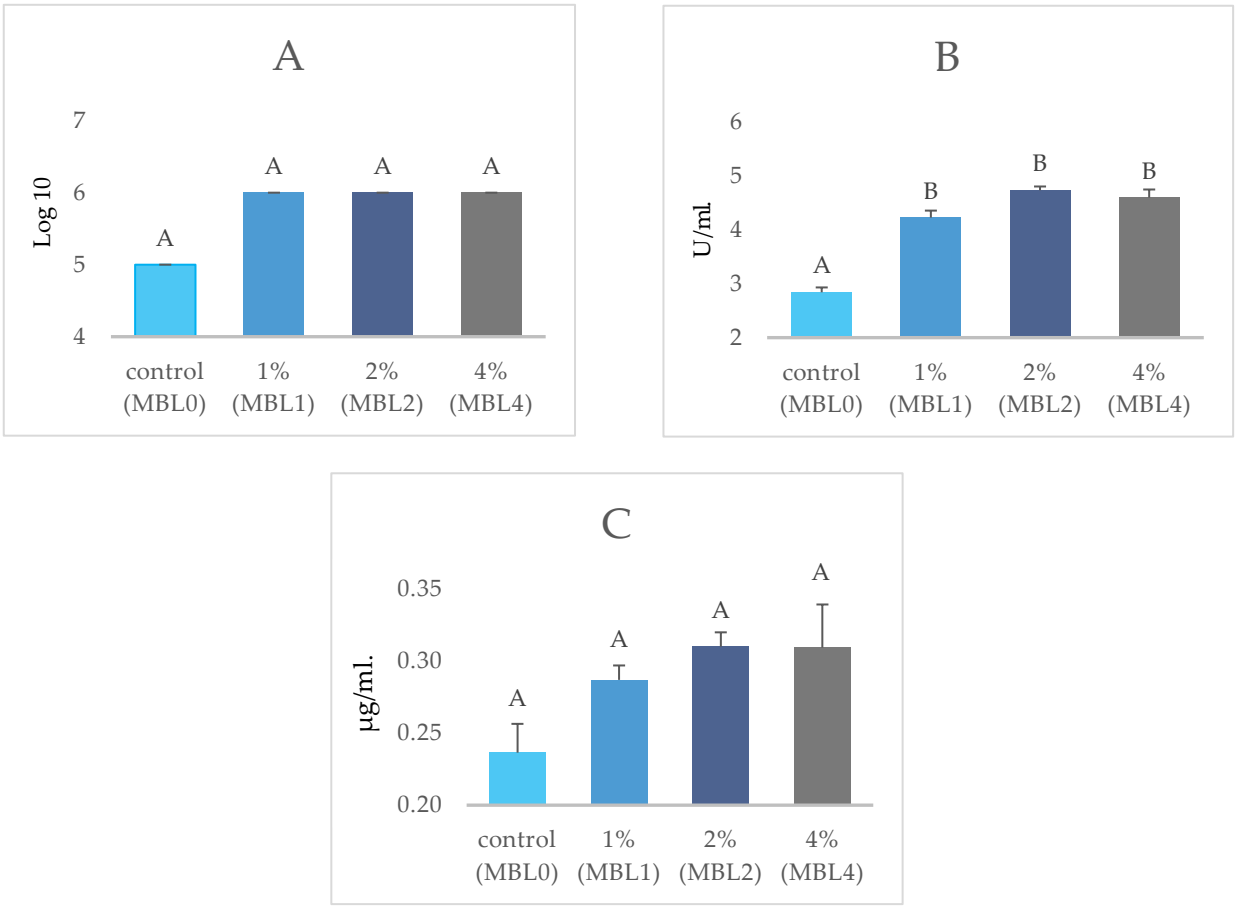

Figure 1. Agglutination titer **(**A**)**, Lysozyme determination **(**B**)**, and testing the efficiency of destroying bacteria of white blood cells (C) of fish fed experimental diets supplemented with different levels of mulberry leaves. Different power signs indicate significant differences between groups ($P < 0.05$).

These results indicate that FML supplementation significantly enhances both innate and adaptive immune responses in juvenile Nile tilapia. Improvements in humoral immunity (lysozyme activity and agglutination titers), innate cellular defense (phagocytic efficiency), and pro-inflammatory cytokine expression reflect a comprehensive upregulation of the immune system. Notably, the 2% inclusion level consistently yielded the most pronounced effects across all parameters, implying a threshold beyond which additional FML does not further enhance immunity and may even result in diminished responses. The inherent immune system is crucial for protecting fish health against microbial invaders [37 - 38]. This defense mechanism operates by inhibiting pathogen entry, mediating inflammatory reactions, and facilitating tissue repair [39]. Research suggests that immune responses in aquatic species can be significantly stimulated by dietary practices [40], gastrointestinal tract health [41], and ecological interactions, leading to increased resistance against disease and environmental stress. This enhancement occurs through the activation of immune cells and the modulation of the immune response towards anti-inflammatory cytokine production [42 - 43]. The resulting improvement in the first line of defense is frequently quantified by measuring parameters such as lysozyme activity, agglutination titers, and the rate of bacterial phagocytosis. Likely mediated by bioactive compounds in mulberry, such as flavonoids and saponins. These compounds, further potentiated through fermentation, may increase bioavailability and functional efficacy [7, 27, 44]. Furthermore, the significant upregulation of TNF-α and IL-1 aligns with previous findings in *Megalobrama amblycephala* and *Oreochromis niloticus* demonstrating that plant-derived polysaccharides can modulate immune gene expression and confer anti-inflammatory effects [29, 36]. Given that juvenile tilapia possess an underdeveloped immune system and are particularly vulnerable during early developmental stages, the

immunostimulatory effect of FML is especially valuable. The enhanced immune capacity may reduce reliance on antibiotics in aquaculture, supporting more sustainable and health-conscious farming practices.

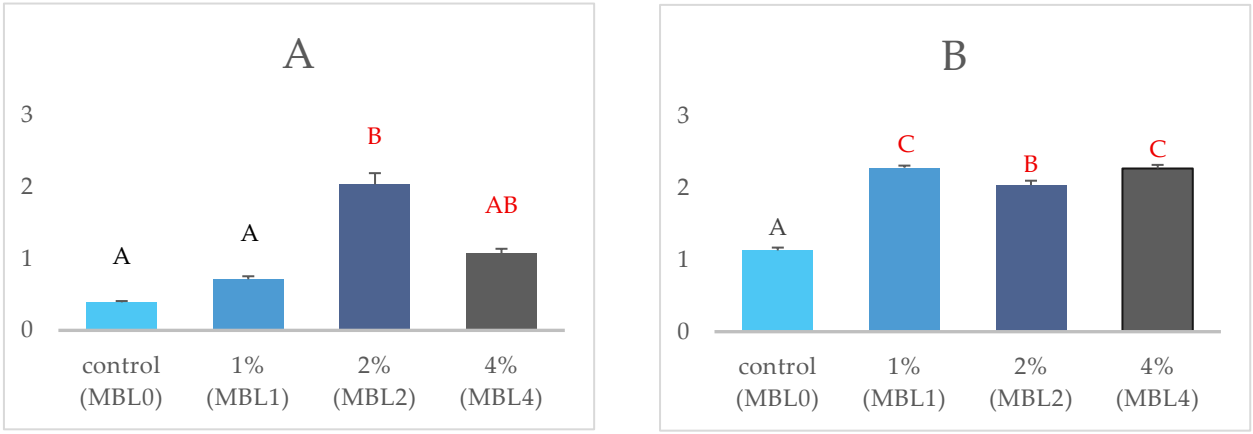

Figure 2. TNF-α (A) and IL-1 (B) of fish fed experimental diets supplemented with different levels of mulberry leaves. Different power signs indicate significant differences between groups ($P < 0.05$).

4. Conclusions

The dietary inclusion of fermented mulberry leaf meal, particularly at a 2% level, significantly enhanced innate immune responses as evidenced by increased lysozyme activity, respiratory burst activity, and upregulation of immune-related genes (TNF-α and IL-1). These results suggest that FML can improve immune competence and overall health in Nile tilapia. Moreover, FML appears to bolster the nutritional quality of the fish muscle, evidenced by an increase in protein content and a reduction in lipid content. These outcomes underscore the substantial potential of fermented mulberry leaves as a viable and sustainable feed additive in aquaculture. By fostering improved fish health and productivity through natural approaches, this study contributes significantly to the overarching objective of reducing dependence on antibiotics and promoting safer, more ecologically sound aquaculture practices. Prospective research could further explore the most effective fermentation conditions, assess the long-term impacts of FML supplementation on disease resistance under challenge conditions, and elucidate the precise molecular mechanisms through which FML modulates fish metabolism and immunity.

5. Acknowledgements

This research was supported by a research grant from the Agricultural Research and Academic Promotion Office, Maejo University, fiscal year 2025, with support from the National Research Council of Thailand (NRCT).

Author Contributions: Conceptualization, T.P. and C.C.; methodology, T.P.; S.T., W.K. and C.C.; validation, J.P.; S.T. and C.C; formal analysis, T.P. and C.C.; investigation, T.P.; S.T., W.K. and C.C.; writing—original draft preparation, T.P.; writing—review and editing, T.P.; S.T., W.K. and J.P.; supervision, C.C. All authors have read and agreed to the published version of the manuscript.

Conflicts of Interest: The authors declare no conflict of interest.

References

[1] FAO. *The State of World Fisheries and Aquaculture*; Food and Agriculture Organization of the United Nations: Rome, Italy, **2014**; 223 pp.

[2] Yue, G.; Ma, K.; Xia, J. Status of Conventional and Molecular Breeding of Salinity-Tolerant Tilapia. *Rev. Aquacult.* **2024**, *16*(1), 271–286. https://doi.org/10.1111/raq.12838

[3] Arumugam, M.; Jayaraman, S.; Sridhar, A.; Venkatasamy, V.; Brown, P. B.; Abdul Kari, Z.; Tellez-Isaias, G.; Ramasamy, T. Recent Advances in Tilapia Production for Sustainable Developments in Indian Aquaculture and Its Economic Benefits. *Fishes* **2023**, *8*(4), 176. https://doi.org/10.3390/fishes8040176

[4] Ess Team. *The Global Tilapia Market in 2025: Trends, Opportunities and Challenges*; **2025**. https://essfeed.com/the-global-tilapia-market-in-2025-trends-opportunities-and-challenges-the-global-tilapia-market-in-2025-trends-opportunities-and-challenges/ (accessed 2025).

[5] Aich, N.; Paul, A.; Choudhury, T. G.; Saha, H. Tilapia Lake Virus (TiLV) Disease: Current Status of Understanding. *Aquacult. Fish.* **2022**, *7*(1), 7–17. https://doi.org/10.1016/j.aaf.2021.04.007

[6] Wang, B.; Thompson, K. D.; Wangkahart, E.; Yamkasem, J.; Bondad-Reantaso, M. G.; Tattiyapong, P.; Jian, J.; Surachetpong, W. Strategies to Enhance Tilapia Immunity to Improve Their Health in Aquaculture. *Rev. Aquacult.* **2023**, *15*, 41–56. https://doi.org/10.1111/raq.12731

[7] Butt, M. S.; Nazir, A.; Sultan, M. T.; Schroën, K. *Morus alba* L.: Nature's Functional Tonic. *Trends Food Sci. Technol.* **2008**, *19* (10), 505–512. https://doi.org/10.1016/j.tifs.2008.06.002

[8] Devi, B.; Sharma, N.; Kumar, D.; Jeet, K. *Morus alba* Linn: A Phytopharmacological Review. *Int. J. Pharm. Pharm. Sci.* **2013**, *5*(2), 14–18.

[9] Lim, S. H.; Choi, C.-I. Pharmacological Properties of *Morus nigra* L. (Black Mulberry) as a Promising Nutraceutical Resource. *Nutrients* **2019**, *11*(2), 437. https://doi.org/10.3390/nu11020437

[10] Wei, Y.; Huang, J.; Sun, H.; Feng, Z.; He, Y.; Chen, Y.; Lin, S. Impact of Different Processing of Mulberry Leaf on Growth, Metabolism, and Liver Immune Function of Largemouth Bass (*Micropterus salmoides*). *Aquacult. Rep.* **2023**, *29*, 101508. https://doi.org/10.1016/j.aqrep.2023.101508

[11] Mondal, K.; Kaviraj, A.; Mukhopadhyay, P. K. Effects of Partial Replacement of Fishmeal by Mulberry Leaf Meal on Growth Performance and Digestive Enzyme Activities of *Labeo bata*. *Int. J. Aquat. Sci.* **2012**, *3*(1), 1–12.

[12] Mithilasri, M.; Parthiban, K.; Shankar, S. Nutritional and Antinutritional Profiling of Mulberry Genetic Resources Amenable for Animal Feed. *Range Manag. Agrofor.* **2023**, *44*(1), 210–215. https://doi.org/10.59515/rma.2023.v44.i1.26

[13] Novel Antioxidant Peptides from Mulberry (*Morus atropurpurea* Roxb.) Leaf Protein Hydrolysates with Hemolysis Inhibition Ability and Cellular Antioxidant Activity. *J. Agric. Food Chem.* **2019**, *67*(27), 7650–7659. https://doi.org/10.1021/acs.jafc.9b01115

[14] Hajimohammadi, A.; Mottaghitalab, M.; Hashemi, M. Influence of Microbial Fermentation of Sesame Meal and Enzyme Supplementation on Broiler Performance. *Ital. J. Anim. Sci.* **2020**, *19*(1), 712–722. https://doi.org/10.1080/1828051X.2020.1790045

[15] Kaviraj, A.; Mondal, K.; Mukhopadhyay, P. K.; Turchini, G. M. Impact of Fermented Mulberry Leaf and Fish Offal in Diet Formulation of *Labeo rohita*. *Proc. Zool. Soc.* **2013**, *66*(1), 64–73. https://doi.org/10.1007/s12595-012-0052-1

[16] AOAC. *Official Methods of Analysis*, 11th ed.; Association of Official Analytical Chemists: Washington, DC, **2000**; Vol. 11.

[17] Hasan, B.; Putra, I.; Suharman, I.; Iriani, D.; Muchlisin, Z. A. Growth Performance and Carcass Quality of River Catfish (*Hemibagrus nemurus*) Fed Salted Trash Fish Meal. *Egypt. J. Aquat. Res.* **2019**, *45*(3), 259–264. https://doi.org/10.1016/j.ejar.2019.07.005

[18] Yarahmadi, P.; Miandare, H. K.; Farahmand, H.; Mirvaghefi, A.; Hoseinifar, S. H. Dietary Fermentable Fiber Upregulated Immune Related Genes Expression, Increased Innate Immune Response and Resistance of Rainbow Trout (*Oncorhynchus mykiss*) against *Aeromonas hydrophila*. *Fish Shellfish Immunol.* **2014**, *41*(2), 326–331. https://doi.org/10.1016/j.fsi.2014.09.007

[19] Swain, P.; Dash, S.; Sahoo, P.; Routray, P.; Sahoo, S.; Gupta, S.; Meher, P.; Sarangi, N. Non-Specific Immune Parameters of *Labeo rohita* and Seasonal Variations. *Fish Shellfish Immunol.* **2007**, *22*(1–2), 38–43. https://doi.org/10.1016/j.fsi.2006.03.010

[20] Chandan, R.; Parry, R., Jr.; Shahani, K. Purification and Properties of Bovine Milk Lysozyme. *Biochim. Biophys. Acta* **1965**, *110* (2), 389–398. https://doi.org/10.1016/S0926-6593(65)80046-7

[21] Secombes, C. J. Isolation of Salmonid Macrophages and Analysis of Their Killing Activity. *Tech. Fish Immunol.* **1990**, *1*, 137–163.

[22] Kayansamruaj, P.; Pirarat, N.; Hirono, I.; Rodkhum, C. Increasing of Temperature Induces Pathogenicity of *Streptococcus agalactiae* and the Up-regulation of Inflammatory Related Genes in Infected Nile Tilapia (*Oreochromis niloticus*). *Vet. Microbiol.* **2014**, *172*, 265–271. https://doi.org/10.1016/j.vetmic.2014.04.013

[23] Chadzinska, M.; Savelkoul, H. F. J.; Lidy, B. M.; van Kemenade, B. M. Morphine Affects the Inflammatory Response in Carp by Impairment of Leukocyte Migration. *Dev. Comp. Immunol.* **2009**, *33*(1), 88–96. https://doi.org/10.1016/j.dci.2008.07.004

[24] Dawood, M. A.; Koshio, S. Application of Fermentation Strategy in Aquafeed for Sustainable Aquaculture. *Rev. Aquacult.* **2020**, *12*(2), 987–1002. https://doi.org/10.1111/raq.12368

[25] El-Ghafloul, M. S.; Ibrahim, M. A.; Abd El-Razek, I. M.; Abdo, S. E.; Amer, A. A.; Zaineldin, A. I.; Gewaily, M. S.; Dawood, M. A. Growth Performance and Antioxidative Status of Nile Tilapia Fed Fermented Rice Hulls. *Aquaculture* **2025**, 742586. https://doi.org/10.1016/j.aquaculture.2025.742586

[26] Siddik, M. A. B.; Julien, B. B.; Islam, S. M. M.; Francis, D. S. Fermentation in Aquafeed Processing: Achieving Sustainability in Feeds for Global Aquaculture Production. *Rev. Aquacult.* **2024**, *16*(3), 1244–1265. https://doi.org/10.1111/raq.12894

[27] Álvarez, A.; Rodríguez, A.; Chaparro, S.; Borrás, L. M.; Rache, L. Y.; Brijaldo, M. H.; Martínez, J. J. Solid-State Fermentation as a Biotechnological Tool to Reduce Antinutrients and Increase Nutritional Content in Legumes and Cereals for Animal Feed. *Fermentation* **2025**, *11*(7), 359. https://doi.org/10.3390/fermentation11070359

[28] Arbab Sakandar, H.; Chen, Y.; Peng, C.; Chen, X.; Imran, M.; Zhang, H. Impact of Fermentation on Antinutritional Factors of Legumes Seed. *Food Rev. Int.* **2023**, *39*(3), 1227–1249. https://doi.org/10.1080/87559129.2021.1931300

[29] Jiang, W.; Lin, Y.; Qian, L.; Miao, L.; Liu, B.; Ge, X.; Shen, H. Mulberry Leaf Meal as a Feed Supplement for Juvenile *Megalobrama amblycephala* "Huahai No. 1". *Fish Shellfish Immunol.* **2022**, *128*, 279–287. https://doi.org/10.1016/j.fsi.2022.07.022

[30] Ilham, I.; Sucipto, S.; Fujaya, Y. Effects of Fermented Herbal Extract as a Phytobiotic on Growth Indices, Moulting Performance, and Feed Utilization of Juvenile Tiger Shrimp (*Penaeus monodon*). *Fishes* **2024**, *9*(9), 352. https://doi.org/10.3390/fishes9090352

[31] Shi, Y.; Zhong, L.; Fan, Y.; Zhang, J.; Zhong, H.; Liu, X.; Hu, Y. Protective Effect of Mulberry Leaf Flavonoids on High-carbohydrate-induced Liver Oxidative Stress, Inflammatory Response and Intestinal Microbiota Disturbance in *Monopterus albus*. *Antioxidants* **2022**, *11*(5), 976. https://doi.org/10.3390/antiox11050976

[32] Zhang, M.; Pan, L.; Fan, D.; He, J.; Su, C.; Gao, S.; Zhang, M. Effects of Fermented Feed by Mixed Strains and Their Effects on the Survival, Growth, Digestive Enzyme Activity and Intestinal Flora of *Penaeus vannamei*. *Aquaculture* **2021**, *530*, 735703. https://doi.org/10.1016/j.aquaculture.2020.735703

[33] Neves, N. O. D. S.; De Dea Lindner, J.; Stockhausen, L.; Delziovo, F. R.; Bender, M.; Serzedello, L.; Perez Fabregat, T. E. H. Fermented Plant-Based Feeds with *Lactobacillus acidophilus* Improves the Survival and Intestinal Health of Juvenile Nile Tilapia (*Oreochromis niloticus*) Reared in a Biofloc System. *Animals* **2024**, *14*(2), 332. https://doi.org/10.3390/ani14020332

[34] Dumas, A.; France, J.; Bureau, D. P. Modelling Growth and Body Composition in Fish Nutrition: Where Have We Been and Where Are We Going?. *Aquacult. Res.* **2010**, *41*(2), 161–181. https://doi.org/10.1111/j.1365-2109.2009.02323.x

[35] Jobling, M. Fish Nutrition Research: Past, Present and Future. *Aquacult. Int.* **2016**, *24*(3), 767–786. https://doi.org/10.1007/s10499-014-9875-2

[36] Miao, L.; Charles, O.; Lin, Y.; Gong, Y.; Zhu, W.; Wang, L.; Fu, J.; Zhang, Z.; Dong, Z. Interactive Effects of Mulberry Leaf Meal and Bamboo Charcoal Additive on Growth Performance, Anti-oxidant Capacity, and Disease Resistance of Genetically Improved Farmed Tilapia (GIFT) Juvenile (*Oreochromis niloticus*). *Aquacult. Rep.* **2020**, *18*, 100483. https://doi.org/10.1016/j.aqrep.2020.100483

[37] Rombout, J.; Huttenhuis, H.; Picchietti, S.; Scapigliati, G. Phylogeny and Ontogeny of Fish Leucocytes. *Fish Shellfish Immunol.* **2005**, *19* (5), 441–455. https://doi.org/10.1016/j.fsi.2005.03.007

[38] Uribe, C.; Folch, H.; Enríquez, R.; Moran, G. Innate and Adaptive Immunity in Teleost Fish. *Vet. Med.* **2011**, *56* (10), 486–503. https://doi.org/10.17221/3294-VETMED

[39] Magnadottir, B. Immunological Control of Fish Diseases. *Mar. Biotechnol.* **2010**, *12*(4), 361–379. https://doi.org/10.1007/s10126-010-9279-x

[40] Balcázar, J. L.; De Blas, I.; Ruiz-Zarzuela, I.; Cunningham, D.; Vendrell, D.; Múzquiz, J. L. The Role of Probiotics in Aquaculture. *Vet. Microbiol.* **2006**, *114*(3–4), 173–186. https://doi.org/10.1016/j.vetmic.2006.01.009

[41] Vine, N. G.; Leukes, W. D.; Kaiser, H. Probiotics in Marine Larviculture. *FEMS Microbiol. Rev.* **2006**, *30*(3), 404–427. https://doi.org/10.1111/j.1574-6976.2006.00017.x

[42] Lim, K. C.; Yusoff, F. M.; Karim, M.; Natrah, F. M. Carotenoids Modulate Stress Tolerance and Immune Responses in Aquatic Animals. *Rev. Aquacult.* **2023**, *15* (2), 872–894. https://doi.org/10.1111/raq.12767

[43] Ahmadifar, E.; Pourmohammadi Fallah, H.; Yousefi, M.; Dawood, M. A.; Hoseinifar, S. H.; Adineh, H.; Doan, H. V. The Gene Regulatory Roles of Herbal Extracts on the Growth, Immune System, and Reproduction of Fish. *Animals* **2021**, *11*(8), 2167. https://doi.org/10.3390/ani11082167

[44] Adebo, J. A.; Njobeh, P. B.; Gbashi, S.; Oyedeji, A. B.; Ogundele, O. M.; Oyeyinka, S. A.; Adebo, O. A. Fermentation of Cereals and Legumes: Impact on Nutritional Constituents and Nutrient Bioavailability. *Fermentation* **2022**, *8*(2), 63. https://doi.org/10.3390/fermentation8020063

ASEAN
Journal of Scientific and Technological Reports
Online ISSN:2773-8752

Research article

The Batch Adsorption Process of Basic Dyes Using *Dialium Cochinchinensis* Seed Activated Carbon: Kinetics and Isotherms

Memoon Sattar[1] and Fareeda Hayeeye[2*]

[1] Faculty of Sports and Health Science, Thailand National Sports University, Yala Campus, 95000, Thailand
[2] Faculty of Science and Technology, Prince of Songkla University, Pattani Campus, 94000, Thailand
* Correspondence: fareedahayeeye@gmail.com

Citation:
Sattar, M.; Hayeeye, F. The batch adsorption process of basic dyes using *Dialium Cochinchinensis* seed activated carbon: kinetics and isotherms. *ASEAN J. Sci. Tech. Report*. **2026**, *29*(2), e260465. https://doi.org/10.55164/ajstr.v29i2.260465.

Article history:
Received: July 23, 2025
Revised: November 7, 2025
Accepted: December 3, 2025
Available online: January 21 2026

Abstract: The seeds of *Dialium cochinchinense*, an agricultural byproduct, were converted into an eco-friendly and cost-effective activated carbon (DSAC) for the adsorption of basic dyes, namely Rhodamine B (RB) and Crystal Violet (CV), from aqueous solutions. Batch adsorption experiments were performed to evaluate the effects of key parameters, including initial dye concentration, contact time, adsorbent dosage, and solution pH. The adsorption kinetics followed the pseudo-second-order model, indicating that chemisorption may play a role in the adsorption process. Equilibrium data were best fitted by the Langmuir isotherm model, with correlation coefficients (R^2) close to 1, suggesting monolayer adsorption. The maximum adsorption capacities (q_m) were 416.67 mg g^{-1} for RB and 526.32 mg g^{-1} for CV at 30 °C. These results demonstrate that DSAC is a sustainable, efficient, and economically viable adsorbent with strong potential for industrial wastewater treatment applications.

Keywords: ; *Dialium Cochinchinensis* seed; batch adsorption; basic dyes

1. Introduction

The paper, textile, and cosmetic industries extensively use synthetic dyes. Industrial effluents often contain various classes of dyes, such as anionic direct, reactive, nonionic disperse, and cationic dyes [1], many of which are toxic, resistant to degradation, and pose serious environmental concerns. Basic colors are often used on paper, wool, silk, acrylic fibers, and leather because of their high water solubility and vibrant color. Under dyeing conditions, dye molecules are also cationic dyes because the ammonium group in them carries a high positive charge [2, 3]. It has been estimated that nearly 100 tons of dyes and pigments are discharged into aquatic systems each week from industrial operations, contributing significantly to environmental contamination and posing risks to aquatic ecosystems. Additionally, the heavy metals contaminated in these dyes can be harmful, persistent, and nondegradable in the environment. These dyes pose a significant risk to aquatic life due to their potential mutagenic effects, as they greatly increase the chemical oxygen demand (COD) and biological oxygen demand (BOD) in water, indicating low oxygen levels [4]. Growing awareness of the environmental impact of organic loads has led to a steady rise in the demand for wastewater treatment over recent decades, driven by concerns about COD and BOD. The discharge of dye effluents has been identified as a cause of water pollution, requiring urgent action and remediation.

Industrial wastewater regulations mandate that BOD levels be less than 20 mg L^{-1} [5], but dye effluents can have very high BOD concentrations, sometimes reaching as high as 100,000 mg L^{-1}.

Several treatment methods have been employed to improve pollutant removal efficiency, including photocatalysis, coagulation, membrane separation, and adsorption [7, 11]. The adsorption process is widely used in wastewater treatment to eliminate pollutants. Adsorbents such as silica gel, zeolites, chitosan, natural fibers, magnetic nanocomposites, and activated carbon are commonly used in this approach [12–16]. Literature reviews have explored the synthesis of inexpensive adsorbents and the sustainability of dye adsorption using activated carbon derived from agricultural waste components [17]. *Dialium cochinchinense*, a commercially important plant grown in Thailand's Pattani province, was selected for the production of activated carbon (DSAC). DSAC is derived from agricultural waste that is abundantly available in the local area, as *Dialium cochinchinense* is commonly processed into seedless products for commercial use. Consequently, large quantities of seeds are discarded as waste. To add value to this byproduct, the seeds were utilized to produce granular activated carbon, which is easy to handle, cost-effective, and exhibits excellent adsorption performance. Rhodamine B (RB) and Crystal Violet (CV) were chosen as model adsorbates due to their toxicity. Basic dyes are visible in solution at concentrations below 1 ppm and have a high affinity for negatively charged adsorbent surfaces, facilitating the adsorption process [18]. Although the adsorption of basic dyes (RB and CV) by *Dialium cochinchinensis* seed activated carbon has been extensively studied, the adsorption capacities have often been found to be low [19–21]. Therefore, this study investigates the effectiveness of DSAC in removing RB and CV dyes.

2. Materials and Methods

2.1 Materials

Granular activated carbon derived from *Dialium cochinchinensis* seeds was prepared as follows: seeds were carbonized in a muffle furnace at 400°C for 3 h. The resulting char (DS) was then mixed with $ZnCl_2$ in a 1:1.5 ratio and activated at 450°C for an hour, representing the highest iodine number. The mixture was thoroughly washed with distilled water until the pH became neutral, followed by drying at 110 °C for 24 h. Additional details on the preparation can be found in Hayeeye et al. (2022) [22]. For pH regulation during the experiments, NaOH and HCl (Labscan, Ireland; Merck, Germany) were used. RB and CV dyes were purchased from Sigma-Aldrich. A primary stock solution (1,000 mg L^{-1}) of each dye was prepared by dissolving accurately weighed amounts in distilled water, and working solutions with concentrations ranging from 50 to 600 mg L^{-1} were obtained by appropriate dilution.

2.2 Methods

2.2.1 Characterization of DSAC

The specific surface areas of DSAC were determined using the nitrogen adsorption isotherm in the Brunauer-Emmett-Teller model, conducted with a Coulter SA 3100 analyzer at the Scientific Equipment Center, Prince of Songkla University. The pH drift method determined the point of zero charge (pH_{pzc}), where the surface of DSAC is neutral [23]. To do this, pH-adjusted 0.1 M NaCl solutions (pH 2 - 11) were prepared, and DSAC was added to 100 mL of each pH-adjusted NaCl solution. The flasks were sealed to prevent contact with air and left at ambient temperature for 24 hours. After stabilization, the final pH was recorded. The pH_{pzc} value of DSAC was determined by plotting the initial pH (pH_i) against the final pH (pH_f) and identifying the point where pH_i and pH_f were equal.

2.2.2 Batch adsorption experiments

The basic dyes (RB and CV) were selected for the adsorption process on DSAC. Batch adsorption experiments [24] were conducted to optimize various parameters, including initial dye concentration (50–600 mg L^{-1}), adsorbent dosage (0.1-0.6 g), contact time (0-20 h), and pH (2–9). Each parameter was studied individually while the other parameters were kept constant. In the experiments, 0.10 g of the adsorbent (DSAC) was added to 50 mL of the RB and CV solutions, and the mixtures were stirred in a shaking bath at 30 °C. The concentrations of RB and CV before and after the adsorption process were analyzed using the UV-Vis spectrophotometer, with absorbance measured at 554 and 591 nm for RB and CV, respectively. The RB and

CV residual concentrations were calculated based on previously determined calibration curves. The residual RB and CV concentrations were calculated based on the previously determined calibration curve. The percentage removal and the adsorption capacity, q_e (mg g^{-1}) of RB and CV on DSAC were then determined according to equations (1) and (2) [24] as follows:

$$\%RE = \frac{C_0 - C_e}{C_0} \times 100 \quad (1)$$

$$q_e = \frac{V(C_0 - C_e)}{W} \quad (2)$$

where W is the dosage of adsorbent (g), V is the volume of the basic dye solutions (L), C_0 and C_e are the initial and equilibrium liquid-phase concentrations of RB and CV (mg L^{-1}), respectively. Kinetic experiments were conducted with initial basic dye concentrations of 50 and 100 mg L^{-1} for RB and CV, maintaining a constant initial pH. The DSAC adsorbent was introduced into 50 mL of the basic dye solutions, which were then continuously shaken. At pre-determined sampling times, 1 mL solution samples were withdrawn using a syringe and analyzed for RB and CV residuals using UV-vis spectrophotometry. The experiments were repeated in triplicate to ensure the reliability of the results. The adsorption experiments were performed to investigate the different effects using 50 mL of 100 mg L^{-1} RB and CV solutions at their natural pH values: pH 4.0 for RB and pH 5.0 for CV. The equilibrium data were further evaluated using the pseudo-first-order and pseudo-second-order adsorption kinetic models as well as various adsorption isotherms, namely the Langmuir, Freundlich, Temkin, and Dubinin–Radushkevich models. [22].

2.2.3 Kinetic models for the adsorption process

The kinetic adsorption models describe the adsorption rate over time, offering insight into the underlying adsorption mechanism. The most commonly applied models are the pseudo-first-order (Lagergren's model) [25] and pseudo-second-order (Ho and McKay's model) [26]. These models are represented by equations (3) and (5), respectively, and can be expressed in their linear forms as equations (4) and (6).

$$\frac{dq_t}{dt} = k_1(q_e - q_t) \quad (3)$$

$$\ln(q_e - q_t) = \ln q_e - k_1 t \quad (4)$$

$$\frac{dq_t}{dt} = k_2(q_e - q_t)^2 \quad (5)$$

$$\frac{t}{q_t} = \frac{1}{k_2 q_e^{\,2}} + \frac{1}{q_e} t \quad (6)$$

Where q_e and q_t were the amount of dye adsorbed (mg g^{-1}) at equilibrium and at any time. k_1 and k_2 were the pseudo-first-order rate constant (min^{-1}) and the pseudo-second-order-rate constant (g mg^{-1} min^{-1}), respectively.

2.2.4 Isotherm models for the adsorption process

Several isotherm models, including the Langmuir, Freundlich, Temkin, and Dubinin–Radushkevich isotherms, were tested to fit the adsorption equilibrium data. These isotherms were represented by the following linear form in equations (7) to (10) [27 - 30]

$$\frac{C_e}{q_e} = \frac{1}{q_m b} + \frac{C_e}{q_m} \tag{7}$$

$$\log q_e = \log K_F + \frac{1}{n}\log C_e \tag{8}$$

$$q_e = B\ln A_t + B\ln C_e \;; B = \frac{RT}{b} \tag{9}$$

$$\ln q_e = \ln q_s - K_d \varepsilon^2 \;; \varepsilon = RT\ln\left(1+\frac{1}{C_e}\right) \tag{10}$$

Where C_e is the equilibrium concentration (mg L^{-1}), q_e is the amount adsorbed at equilibrium (mg g^{-1}), respectively. The parameters of q_m and b are Langmuir constants representing the maximum adsorption capacity (mg g^{-1}) and the adsorption equilibrium constant (L mg^{-1}), respectively. The values of K_F and n are Freundlich constants, indicating the adsorption capacity (L g^{-1}) and the adsorption intensity, respectively. A_t is the Temkin isotherm equilibrium binding constant (L g^{-1}), R is a universal gas constant (8.314 J $mol^{-1}K^{-1}$), T signifies temperature at 298K, and B is a constant related to the heat of sorption (J mol^{-1}). The q_s is a theoretical isotherm saturation capacity (mg g^{-1}), K_d is the Dubinin–Radushkevich isotherm constant (mol^2 kJ^{-2}), and ε is the Dubinin–Radushkevich isotherm constant.

3. Results and Discussion

3.1 Characterization of DSAC

The specific surface area of DSAC was evaluated based on the Brunauer–Emmett–Teller (BET) model [31]. As shown in Figure 1, the N_2 adsorption isotherms were interpreted according to the IUPAC classification, which distinguishes six types of adsorption isotherms [32]. Type I adsorption isotherms are typically used for tiny pores or microporous adsorbents, where the rate of adsorbate adsorption depends on available micropore volume rather than total interior surface area. Types II, III, and VI were observed in non-porous or macroporous materials. Type III and Type V isotherms indicate stronger adsorbate-adsorbate interactions compared to adsorbate-adsorbent interactions. Types IV and V were identified for mesoporous materials. The hysteresis loop type H4 suggests the presence of mesoporous particles [33-35]. DSAC predominantly exhibits mesoporous characteristics, classifying it as a Type IV adsorbent. The activated carbon prepared with $ZnCl_2$ is mainly microporous but contains a significant mesopore component, which increases with the $ZnCl_2$-to-precursor impregnation ratio [36, 37].

The BET surface area of DSAC was calculated (Table 1) and may significantly influence its adsorption efficiency. Notably, DSAC showed a substantial BET-specific surface area alongside increased mesopore volume. The physical properties of the raw materials likely influenced the porosity characteristics of the final activated carbon products. Additionally, the BET surface area values of DSAC are considerably higher than those of modified granular composite adsorbents such as chitosan-bentonite-zirconium chloride (Cs- Bn- Zr), S/modified bentonite (GOMBt), granular bentonite (GBt), ZnO-chitosan beads (CZB), chitosan beads (CB), and chitosan beads coated with ZnO (ZCB), as shown in Table 1 [38-40]. The pH_{pzc} graphs were plotted between the pH_f and the pH_i for DSAC, as shown in Figure 2. The pH_{pzc} value of DSAC was found to be 3.5, indicating that DSAC carries a positive charge. This positive charge causes electrostatic repulsion with the positive charges of basic dyes [41]. Consequently, DSAC is attracted to negatively charged species, enabling it to adsorb RB and CV solutions at pH 4 and pH 5, respectively. Moreover, the morphology of the DSAC bead shows numerous pores on the surface.

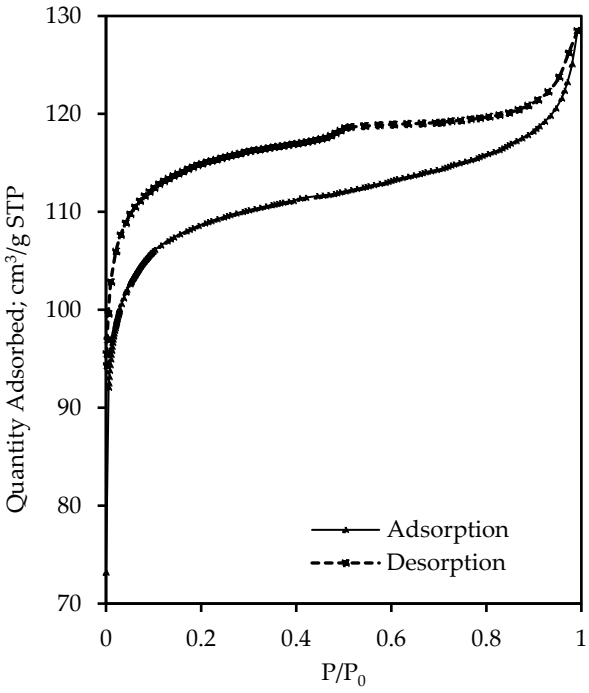

Figure 1. N_2 adsorption isotherm of DSAC: Note the hysteresis in types IV and V [32].

Table 1. BET surface area of DSAC compared with the granular adsorbents

Sample	BET Specific Surface area ($m^2\ g^{-1}$)	Micropore volume ($cm^3\ g^{-1}$)	Average pore size (nm)	Ref.
DSAC	290.19	0.109	4.96	This study
Cs-Bn-Zr	63.80	0.095	3.57	[38]
GOMBt	36.50	0.097	3.83	[39]
GBt	35.65	0.076	3.84	
CB	12.46	0.013	3.89	
CZB	13.11	0.016	3.74	[40]
ZCB	13.54	0.018	3.63	

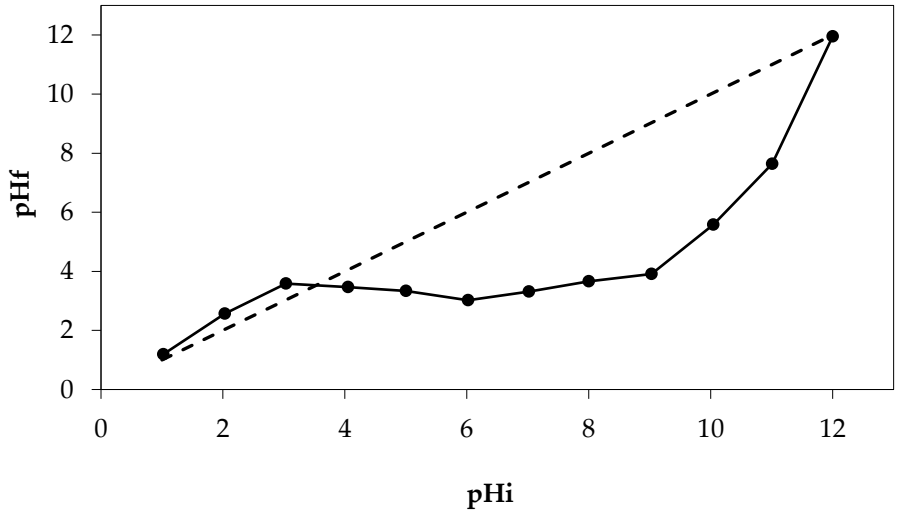

Figure 2. The pH_{pzc} of DSAC

3.2 Effects of various parameters in adsorption studies

Figure 3 illustrates the effect of contact time and initial concentrations of RB and CV on DSAC. The results reveal equilibrium times of approximately 12 hours for RB and 7 hours for CV solutions. Moreover, the amount adsorbed at equilibrium (q_e) rises with increasing initial concentrations of RB and CV solutions, suggesting potential interactions between the basic dye solutions and the adsorbents [42]. The adsorbent dosage from 0.10 - 0.60 g was used to study the effect of DCS-AC dosage for removing 100 mg L^{-1} of RB and CV solutions at 30 °C as shown in Figure 4. At equilibrium, the percentage removal of RB and CV solutions increased with increasing DSAC dosage. However, the amount of adsorbed (q_e) decreased with increasing the DSAC dosage. The result indicated that an increase in adsorbent dosage increases the surface area and availability of adsorption sites [43]. There are the highest amounts adsorbed at equilibrium, 56.97 mg g^{-1} (RB) and 71.62 mg g^{-1} (CV), on the optimal DSAC dosages, with the maximum amount of adsorbed values being 0.10 g, which is appropriate to use in this study.

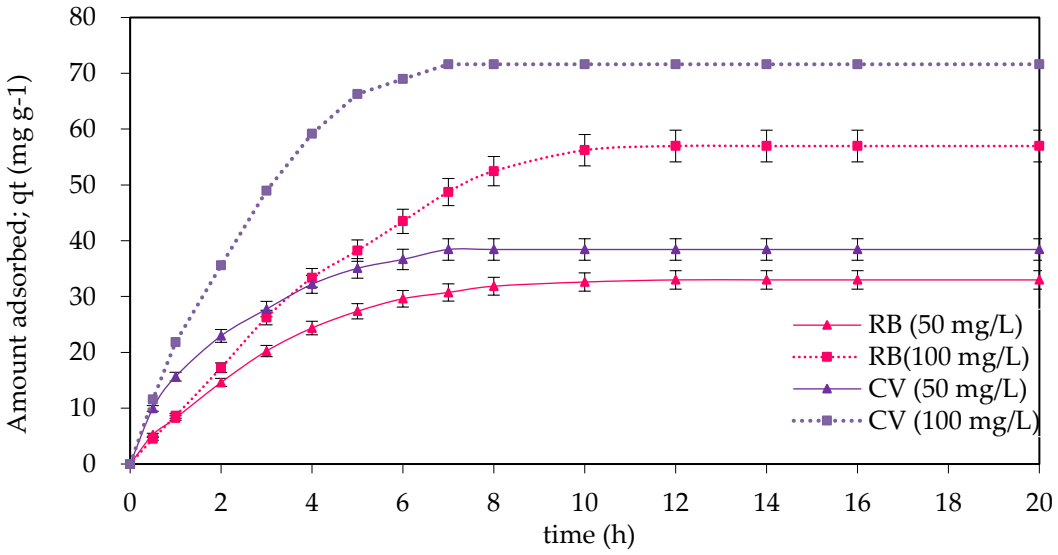

Figure 3. The effect of contact time and initial concentration of RB (pH 4.0) and CV (pH 5.0) on DSAC at 30°C (50 and 100 mg/L of basic dye solutions, 0.10 g of DSAC)

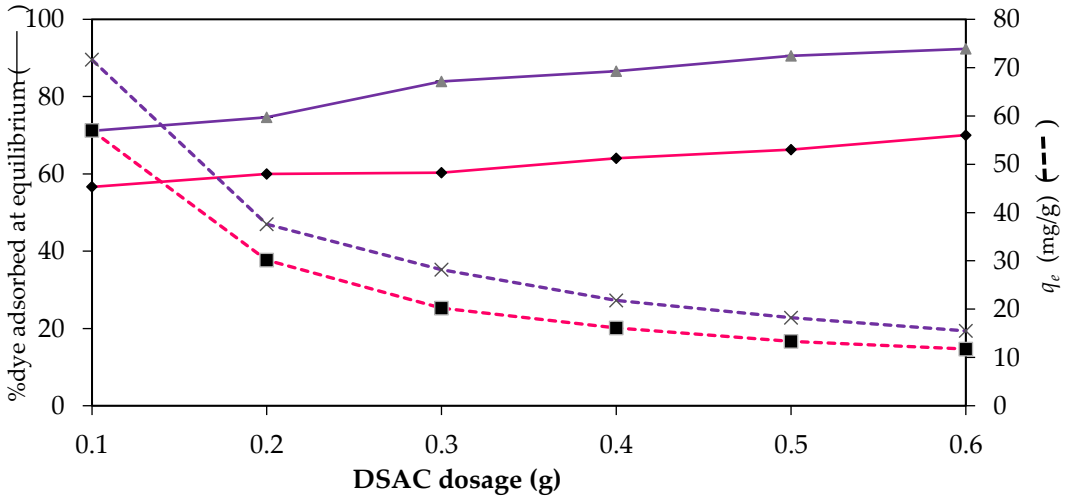

Figure 4. The effect of DSAC dosage on the adsorption of 100 mg L^{-1} of RB (pH 4) and CV (pH 5)

The pH factor is critical in adsorption, particularly for dye adsorption. As illustrated in Figure 5, the adsorption of RB and CV on DSAC increases slightly as the pH rises above 2. At lower pH levels, protonation causes H^+ ions to compete with RB and CV molecules for adsorption sites on the DSAC surface. Below the pHpzc (3.5), the DSAC surface is positively charged, whereas above pHpzc it becomes negatively charged. The pH increases, the electrical repulsion weakens, enabling more RB and CV molecules to adsorb onto the activated carbon. Conversely, at pH levels above 7, OH^- ions compete with RB and CV molecules for adsorption sites, and due to their smaller size, OH^- ions may migrate more quickly to the activated carbon surface, the generation of hydrogen bonds between the carboxylic groups of RB or CV and the beads potentially impact RB and CV of adsorption efficiency [44, 45].

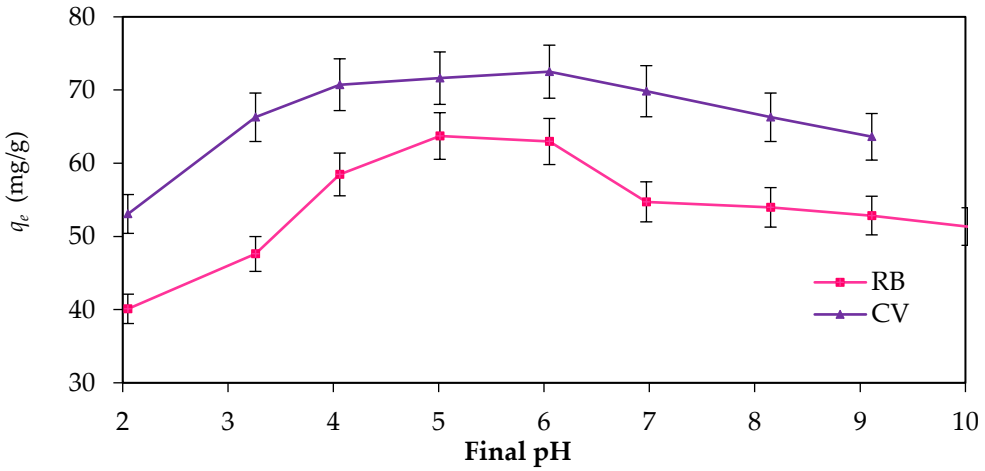

Figure 5. The effect of pH of RB and CV adsorption on DSAC at 30°C (100 mg/L of basic dye solutions, 0.10 g of DSAC)

3.3 Kinetic models for the adsorption process

The Kinetic models were employed to understand the adsorption mechanisms behind the interactions between adsorbate and adsorbent [25, 26]. The experimental results were fitted using pseudo-first-order and pseudo-second-order kinetic models. Linear plots of $ln(q_e - q_t)$ versus t for the pseudo-first-order model and t/q_t versus t for the pseudo-second-order model are shown in Figure 6. The values of k_1 and k_2 were determined from the slopes of the straight lines. Various kinetic parameters, including the correlation coefficient R^2, are listed in Table 2. The results suggest that the adsorption kinetics of RB and CV onto DSAC are most accurately represented by the pseudo-second-order model, as evidenced by the R^2 values being closest to unity. The adsorption process on porous materials proceeds through three stages: adsorption on the external surface, a gradual adsorption phase, and adsorption within the internal surface, ultimately reaching equilibrium. [46].

Table 2. Parameters of kinetic models for RB and CV solutions on DSAC

Kinetic models	Parameter	Value			
		RB (mg L^{-1})		CV (mg L^{-1})	
		50	100	50	100
Pseudo–first order	q_e (mg g^{-1})	4.91	6.41	4.96	7.31
	k_1 (× 10^{-3})	3.0	2.2	3.6	4.1
	R^2	0.97	0.96	0.98	0.95
Pseudo – second order	q_e (mg g^{-1})	52.36	136.99	49.75	131.58
	k_2 (× 10^{-5})	6.56	0.98	1.53	0.25
	R^2	0.98	0.97	0.99	0.98

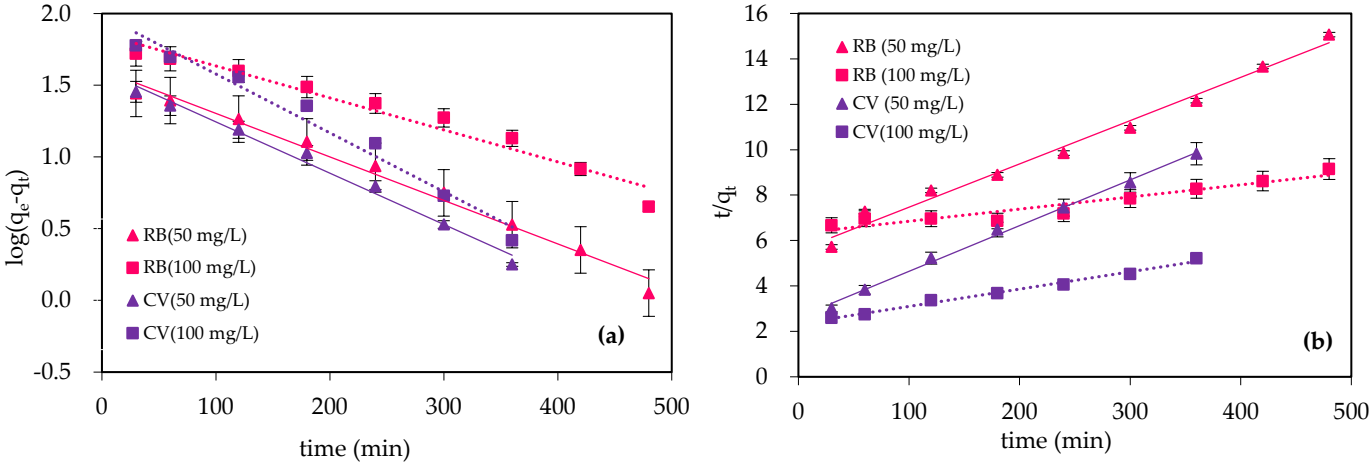

Figure 6. The kinetic adsorption models: (a) pseudo-first-order and (b) pseudo-second-order models, for RB and CV (50 and 100 mg L^{-1}) adsorption on DSAC, at 30°C and pH 5 (0.10 g of DSAC)

3.4 Isotherm models for the adsorption process

Mathematical models for representing adsorption isotherms have been developed. The Langmuir model in equations (7) suggests monolayer adsorption on a homogeneous surface of the adsorbent at the interface between the solid and liquid phases, and it also estimates the maximum adsorption capacity of the process [27]. Furthermore, the Freundlich isotherm in equations (8) is commonly used to describe the exponential adsorption of target compounds on heterogeneous surfaces. K_f indicates the strength of adsorption, with lower values indicating stronger adsorption. Another constant, *1/n*, indicates the adsorption intensity, and favorable adsorption is typically observed when the *n* value is between 1 and 10 [28, 48]. The Temkin isotherm detailed in equation (9) includes a factor that explicitly accounts for adsorbent–adsorbate interactions and assumes that the heat of adsorption of all molecules in the layer decreases linearly rather than logarithmically with coverage. This derivation features a uniform distribution of maximum binding energies. The Dubinin–Radushkevich isotherm (equation 10) is generally applied to describe the adsorption mechanism with a Gaussian energy distribution on a heterogeneous surface. This approach is often used to distinguish between physical and chemical adsorption, with the mean free energy *E* per molecule of adsorbate calculated using equation (11) [30, 47].

$$E = \frac{1}{\sqrt{2K_d}} \tag{11}$$

The mean adsorption energy (*E*) can describe adsorption properties. When the value of E was less than 8 kJ mol^{-1}, it followed physical adsorption, but when the value of E ranged from 8 to 16, it followed chemical adsorption [30, 48]. The Langmuir, Freundlich, Temkin, and Dubinin–Radushkevich isotherms were shown in Figure 7. All the parameters derived from these four isotherms, including the correlation coefficients, are summarized in Table 3. The parameters were calculated based on the slope and intercept of the respective isotherm equations. The results indicated that the adsorption process of RB and CV solutions on the DSAC corresponded more closely with the Langmuir isotherm model than with the Freundlich, Temkin, and Dubinin–Radushkevich models, as evidenced by a higher correlation coefficient (R^2). Therefore, the Langmuir equation was chosen as the best match for the adsorption isotherms. Moreover, this further means that the adsorption suggested monolayer adsorption on a homogeneous surface, according to Langmuir's theory. The DSAC surface is relatively homogenous regarding functional groups with significant interaction with RB and CV molecules [22, 49]. The Langmuir equation determined the maximum adsorption capacities (q_m) on DSAC to be 416.67 mg g^{-1} for RB and 526.32 mg g^{-1} for CV solutions. Table 4 provides the maximum uptake capacities (q_m) for RB and CV solutions compared with some reported activated carbons synthesized from different

sources. The results indicate that the qm values for RB and CV removal on DSAC were higher than those achieved with other biomass-derived activated carbons. This suggests that the DSAC adsorbent developed in the current study demonstrates superior performance. Notably, DSAC offers significant advantages over other carbon-based adsorbents; Therefore, DSAC is an effective adsorbent material for treating wastewater.

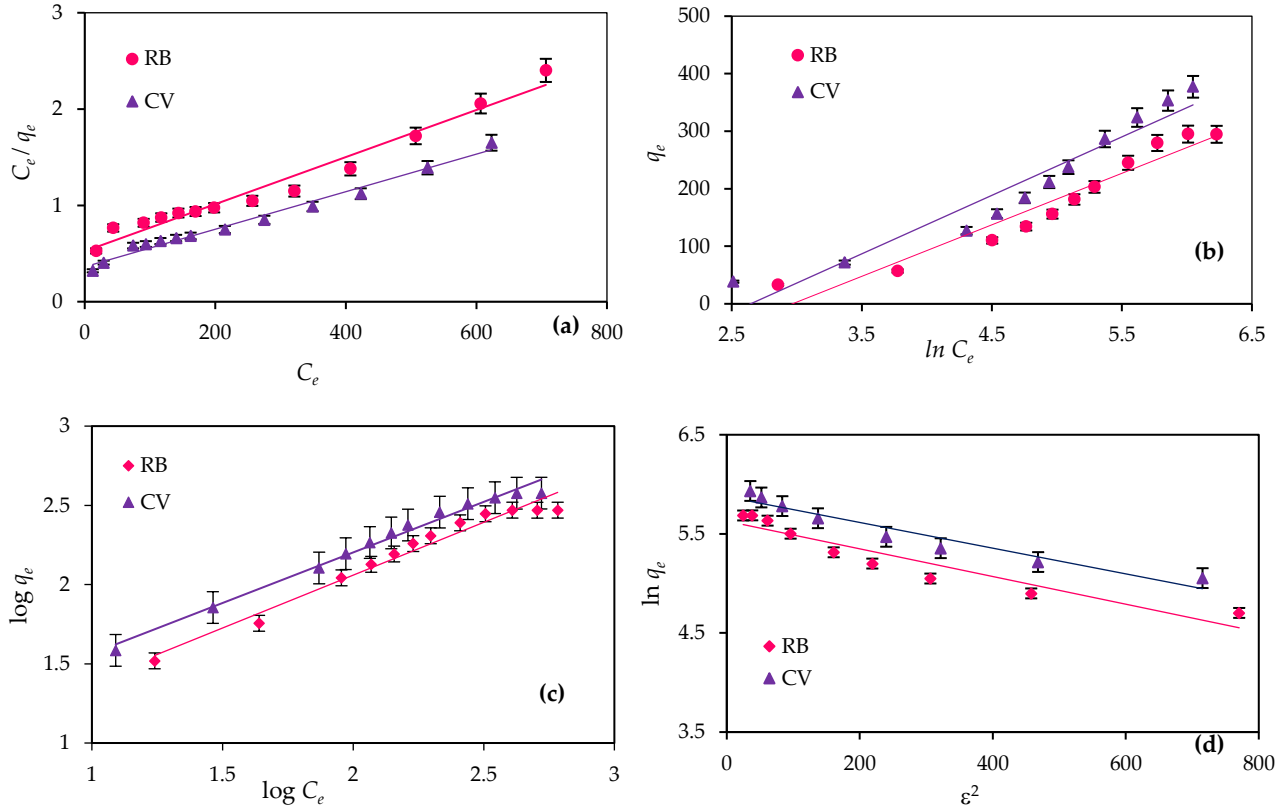

Figure 7. The (a) Langmuir, (b) Freundlich, (c) Temkin, and (d) Dubinin–Radushkevich isotherms of RB (pH 4.0) and CV (pH 5.0) solutions on DSAC (basic dye concentration 50–600 mg L^{-1}, 0.10 g of DSAC)

Table 3 Parameter of Langmuir, Freundlich, Temkin, and Dubinin–Radushkevich for RB and CV on DSAC

No.	Adsorbents	*pH*	q_m (mg g^{-1})	*Ref.*
	RB			
1.	Polysulfone - AC	4.0	25.71	[20]
2.	White sugar AC	4.0	123.46	[45]
3.	Magnetic AC	4.0	135.01	[50]
4.	Cassava peel	4.0	265.36	[51]
5.	DSAC	4.0	416.67	This study
	CV			
6.	Date palm leaves AC	5.0	37.58	[21]
7.	Korean cabbage waste	5.0	195.60	[52]
8.	NaOH-activated Aerva javanica leaf	5.0	315.20	[53]
9.	Water hyacinth plants AC	5.0	322.58	[54]
10.	DSAC	5.0	526.32	This study

Table 4. The maximum adsorption capacities of RB and CV compared with prior literature at 25 °C

Isotherms	Parameters	Value	
		RB	**CV**
Langmuir	q_m (mg g^{-1})	416.67	526.32
	b (L mg^{-1})	0.004	0.005
	R^2	0.97	0.98
Freundlich	K_F (L g^{-1})	4.65	4.35
	n	1.38	1.08
	R^2	0.96	0.97
Temkin	A_t (L g^{-1})	0.05	0.07
	B (J mol^{-1})	89.55	101.63
	R^2	0.93	0.92
Dubinin–Radushkevich	K_d (mol^2 kJ^{-2}) ×10^{-3}	1.41	1.30
	q_s (mg g^{-1})	278.66	354.25
	E (kJ mol^{-1})	0.18	0.19
	R^2	0.89	0.93

4. Conclusions

Dialium cochinchinense seed–based activated carbon (DSAC) was successfully prepared using $ZnCl_2$ activation and demonstrated high efficiency in removing Rhodamine B (RB) and Crystal Violet (CV) from aqueous solutions. The adsorption followed the pseudo-second-order kinetic model and fitted well with the Langmuir isotherm, showing maximum adsorption capacities of 416.67 mg g^{-1} for RB and 526.32 mg g^{-1} for CV at 30 °C. Removal efficiencies ranged between 80% and 90%, confirming the strong adsorption performance of DSAC. These findings highlight DSAC as a cost-effective, sustainable, and environmentally friendly adsorbent derived from agricultural waste. With its simple preparation, high adsorption capacity, and reusability potential, DSAC shows great promise for practical application in industrial wastewater treatment systems.

5. Acknowledgements

The authors wish to extend their sincere thanks to the Department of Science, Faculty of Science and Technology, Prince of Songkla University, Pattani Campus, Thailand, and the Thailand National Sport Science University, Yala Campus, for their invaluable support.

Author Contributions: Conceptualization, experimental design, Sattar, M, conducting experiments and data acquisition, Hayeeye, F., data analysis, writing and editing, Hayeeye, F., and Sattar, M. All authors have read and approved the published version of the manuscript.

Funding: None.

Conflicts of Interest: The authors declare no conflict of interest.

References

[1] Benkhaya, S.; El Harfi, S.; El Harfi, A. Classifications, Properties, and Applications of Textile Dyes: A Review. *Appl. J. Environ. Eng. Sci.* **2017**, *3*(3), 311–320.

[2] Qada, E. N.; Allen, S. J.; Walker, G. M. Adsorption of Basic Dyes from Aqueous Solution onto Activated Carbons. *Chem. Eng. J.* **2008**, *135*(3), 174–184. https://doi.org/10.1016/j.cej.2007.02.023

[3] Massoud, K.; Motaba, S.; Sahar, M. Removal of Dyes from the Environment by Adsorption Process. *Chem. Mater. Eng.* **2018**, *6*(2), 31–35. https://doi.org/10.13189/cme.2018.060201

[4] Sasan, F.; Gholian, J.; Konečný, J. J.; Baloch, A.; Kordestani, H. K. Sustainable and Optimized Values for Municipal Wastewater: Removal of BOD and COD Using Granular Activated Carbon and Genetic Algorithm-Based Simulation. *J. Clean. Prod.* **2023**, *417*, 137932. https://doi.org/10.1016/j.jclepro.2023.137932

[5] Sarakarnkosol, W. Pollution and Risk of Wastewater from Textile Dyeing Process. *Environ. J.* **2017**, *21*(1), 7–14 (in Thai).

[6] Surafel, M. B.; Venkatesa, P.; Tsegaye, S.; Abraham, G. Sugarcane Bagasse-Based Activated Carbon Preparation and Its Adsorption Efficacy for Removal of BOD and COD from Textile Effluents. *Bioresour. Technol. Rep.* **2021**, *14*, 100664. https://doi.org/10.1016/j.biteb.2021.100664

[7] Ibrahim, E. S.; Laszlo, E.; Kim, J.-H.; Kim, H. S. Adsorption and Photocatalytic Degradation of Methylene Blue over Hydrogen-Titanate Nanofibres. *Water Res.* **2013**, *47*(12), 4115–4125. https://doi.org/10.1016/j.watres.2012.12.045

[8] Vijayaraghavan, G.; Shanthakumar, S. Effective Removal of Reactive Magenta Dye in Textile Effluent by Coagulation Using Algal Alginate. *Desalin. Water Treat.* **2018**, *121*, 22–27. https://doi.org/10.5004/dwt.2018.22190

[9] Wang, Y.; Liu, C.; Ma, M.; Li, P.; Li, X.; Yu, Y. Fabrication and Evaluation of GO/TiO_2-Based Molecularly Imprinted Nanocomposite Membranes. *Sep. Purif. Technol.* **2019**, *212*, 245–254. https://doi.org/10.1016/j.seppur.2018.11.042

[10] Chakraborty, S.; Chowdhury, S.; Das Saha, P. Adsorption of Crystal Violet from Aqueous Solution onto NaOH-Modified Rice Husk. *Carbohydr. Polym.* **2011**, *86*(4), 1533–1541. https://doi.org/10.1016/j.carbpol.2011.06.058

[11] Hayeeye, F.; Sattar, M.; Tekasakul, S.; Sirichote, O. Adsorption of Rhodamine B on Activated Carbon from Rubber Fruit Pericarp. *Songklanakarin J. Sci. Technol.* **2014**, *36*(2), 177–187.

[12] Gaikwad, R. W.; Misal, S. A. Sorption Studies of Methylene Blue on Silica Gel. *Int. J. Chem. Eng. Appl.* **2010**, *1*(4), 342–345. https://doi.org/10.7763/IJCEA.2010.V1.59

[13] Imessaouden, A.; Cheikh, S.; Hadadi, A.; Hamri, N.; Bollinger, J.-C.; Amrane, A.; Tahraoui, H.; Manseri, A.; Mouni, L. Adsorption Performance of Zeolite for Congo Red Removal. *Separations* **2023**, *10* (1), 57. https://doi.org/10.3390/separations10010057

[14] Sarkar, T. K.; Chakraborty, N.; Basu, S.; Ghosh, A.; Inoue, H.; Fukumori, Y. Adsorption of Methyl Orange onto Chitosan. *J. Water Resour. Prot.* **2010**, *2*, 898–906. https://doi.org/10.4236/jwarp.2010.210107

[15] Basha, N. A.; Rathinavel, T.; Sridharan, H. Activated Carbon from Coconut Shell: Synthesis and Applications. *Appl. Sci. Eng. Prog.* **2023**, *16*(2), 6152. https://doi.org/10.14416/j.asep.2022.07.001

[16] Esvandi, Z.; Foroutan, R.; Peighambardoust, S. J.; Akbari, A.; Ramavandi, B. Uptake of Anionic and Cationic Dyes from Water Using Natural Clay and Clay/Starch/$MnFe_2O_4$ Magnetic Nanocomposite. *Surf. Interfaces* **2020**, *21*, 100754. https://doi.org/10.1016/j.surfin.2020.100754

[17] Bharathi, K. S.; Ramesh, S. T. Removal of Dyes Using Agricultural Waste as Low-Cost Adsorbents: A Review. *Appl. Water Sci.* **2013**, *3*, 773–790. https://doi.org/10.1007/s13201-013-0117-y

[18] Emad, N.; Qada, E. N.; Allen, S. J.; Walker, G. M. Adsorption of Basic Dyes from Aqueous Solution onto Activated Carbons. *Chem. Eng. J.* **2008**, *135*(3), 174–184. https://doi.org/10.1016/j.cej.2007.02.023

[19] Laktif, T.; Lakhmiri, R.; Albourine, A. *Salsola tetragona* as a New Low-Cost Adsorbent for Water Treatment: Highly Effective Adsorption of Crystal Violet. *Int. J. Phytoremediation* **2024**, *26*, 1691–1700. https://doi.org/10.1080/15226514.2024.2349703

[20] Sattar, M.; Hayeeye, F.; Chinpa, W.; Sirichote, O. Preparation and Characterization of Polysulfone/Activated Carbon Composite Beads. *Appl. Mech. Mater.* **2014**, *625*, 106–109. https://doi.org/10.4028/www.scientific.net/AMM.625.106

[21] Ghazali, A.; Shirani, M.; Semnani, A.; Zare-Shahabadi, V.; Nekoeini, M. Optimization of Crystal Violet Adsorption onto Date Palm Leaves as a Potent Biosorbent Using Response Surface Methodology and Ant Colony Optimization. *J. Environ. Chem. Eng.* **2018**, *6*, 3942–3950. https://doi.org/10.1016/j.jece.2018.05.043

[22] Hayeeye, F.; Benhawan, A.; Sattar, M. Adsorption Efficiency of Batik Dye by Modified *Dialium cochinchinense* Activated Carbon Beads: Kinetics and Thermodynamics. *Desalin. Water Treat.* **2022**, *269*, 200–211. https://doi.org/10.5004/dwt.2022.28751

[23] Jia, Y. F.; Xiao, B.; Thomas, K. M. Adsorption of Metal Ions on Nitrogen Surface Functional Groups in Activated Carbons. *Langmuir* **2002**, *18*, 470–478. https://doi.org/10.1021/la011161z

[24] Hayeeye, F.; Sattar, M.; Chinpa, W.; Sirichote, O. Kinetics and Thermodynamics of Rhodamine B Adsorption by Gelatin/Activated Carbon Composite Beads. *Colloids Surf., A* **2017**, *513*, 259–266. https://doi.org/10.1016/j.colsurfa.2016.10.052

[25] Lagergren, S. Zur Theorie der Sogenannten Adsorption Gelöster Stoffe. *Kungl. Svenska Vetenskapsakad. Handl.* **1898**, *24*, 1–39.

[26] Ho, Y. S.; McKay, G. Pseudo-Second-Order Model for Sorption Processes. *Process Biochem.* **1999**, *34*, 451–465. https://doi.org/10.1016/S0032-9592(98)00112-5

[27] Langmuir, I. Adsorption of Gases on Plane Surfaces of Glass, Mica, and Platinum. *J. Am. Chem. Soc.* **1918**, *40*, 1361–1403. https://doi.org/10.1021/ja02242a004

[28] Freundlich, H. Über die Adsorption in Lösungen. *Z. Phys. Chem.* **1907**, *57*, 385–470. https://doi.org/10.1007/BF01813604

[29] Al-Shehri, A.; Almudaifer, E. A.; Alorabi, A. Q.; Alanazi, H. S.; Alkorbi, A. S.; Alharthi, F. A. Effective Adsorption of Crystal Violet from Aqueous Solutions: Equilibrium, Mechanism Studies, and Modeling Analysis. *Environ. Pollut. Bioavailability* **2021**, *33*(1), 214–226. https://doi.org/10.1080/26395940.2021.1960199

[30] Dubinin, M. M. The Potential Theory of Adsorption of Gases and Vapors for Adsorbents with an Energetically Nonuniform Surface. *Chem. Rev.* **1960**, *60*, 235–266. https://doi.org/10.1021/cr60204a006

[31] Brunauer, S.; Skalny, J.; Bodor, E. E. Adsorption on Nonporous Solids. *J. Colloid Interface Sci.* **1969**, *30*(4), 546–552. https://doi.org/10.1016/0021-9797(69)90423-8

[32] Zeid, A.; Othman, A. Fundamental Aspects of Silicate Mesoporous Materials: A Review. *Materials* **2015**, *8*(12), 2874–2902. https://doi.org/10.3390/ma5122874

[33] Broekhoff, J. C. Mesopore Determination from Nitrogen Sorption Isotherms: Fundamentals, Scope, and Limitations. *Stud. Surf. Sci. Catal.* **1979**, *36*, 63–84.

[34] Sing, K. S. W.; Everett, D. H.; Haul, R. A. W.; Moscou, L.; Pierotti, R. A.; Rouquerol, J.; Siemieniewska, T. Reporting Physisorption Data for Gas/Solid Systems. *Pure Appl. Chem.* **1985**, *57*, 603–619. https://doi.org/10.1351/pac198557040603

[35] Abebe, B.; Murthy, H. A.; Amare, E. Summary on Adsorption and Photocatalysis for Pollutant Remediation: A Mini-Review. *J. Encapsulation Adsorpt. Sci.* **2018**, *8*, 225–255. https://doi.org/10.4236/jeas.2018.84012

[36] McEnaney, B.; Schüth, F.; Sing, K. S. W.; Weitkamp, J. *Handbook of Porous Solids*; Wiley-VCH: Weinheim, Germany, **2002**; Vol. 1.

[37] Azargohar, R. *Production of Activated Carbon and Its Catalytic Application for Oxidation of Hydrogen Sulphide*; Ph.D. Thesis, University of Saskatchewan, **2009**.

[38] Jamka, Z.; Mohammed, W. Feasibility of Modified Chitosan Beads for Nitrate Adsorption from Aqueous Solution. *J. Ecol. Eng.* **2023**, *24*(2), 265–278. https://doi.org/10.12911/22998993/156886

[39] Zhou, J.; Sun, Q. Sodium Alginate/Modified Bentonite Composite Beads for Adsorptive Removal of Norfloxacin. *Polymers* **2022**, *14*(19), 3984–4001. https://doi.org/10.3390/polym14193984

[40] Ngamsurach, P.; Namwongsa, N.; Praipipat, P. Synthesis of ZnO-Modified Chitosan Materials for Pb(II) Removal. *Sci. Rep.* **2022**, *12*, 17184. https://doi.org/10.1038/s41598-022-22182-4

[41] Hayeeye, F.; Sattar, M. Removal of Crystal Violet by Activated Carbon from Rubber Fruit Pericarp and Bagasse. *Desalin. Water Treat.* **2020**, *202*, 420–434. https://doi.org/10.5004/dwt.2020.26152

[42] Asaad, H. F.; Elhadidly, H. Production of Activated Carbons from Waste Carpets for Methylene Blue Adsorption. *J. Environ. Chem. Eng.* **2017**, *5*, 955–963. https://doi.org/10.1016/j.jece.2017.01.003

[43] Ghaedi, M.; Ansari, A.; Habibi, M. H.; Asghari, A. R. Removal of Malachite Green Using ZnO Nanoparticles Loaded on Activated Carbon. *J. Ind. Eng. Chem.* **2014**, *20*, 17–28. https://doi.org/10.1016/j.jiec.2013.04.031

[44] Porkodi, K.; Vasanth, K. K. Modeling and Simulation of Dye Sorption onto Jute Fiber Carbon. *J. Hazard. Mater.* **2007**, *143*, 311–327. https://doi.org/10.1016/j.jhazmat.2006.09.029

[45] Xiao, W.; Garba, Z. N.; Sun, S.; Lawan, I.; Wang, L.; Lin, M.; Yuan, Z. Activated Carbon from White Sugar for Rhodamine B Adsorption. *J. Clean. Prod.* **2020**, *253*, 119989. https://doi.org/10.1016/j.jclepro.2020.119989

[46] Ghaedi, M.; Ghaedi, A. M.; Negintaji, E.; Ansari, A.; Vafaei, A.; Rajabi, M. Random Forest Model for Bromophenol Blue Removal Using Activated Carbon. *J. Ind. Eng. Chem.* **2014**, *20*, 1793–1803. https://doi.org/10.1016/j.jiec.2013.08.033

[47] Dada, A. O.; Olalekan, A. P.; Olatunya, A. M. Langmuir, Freundlich, Temkin, and Dubinin–Radushkevich Isotherm Studies of Zn^{2+} Adsorption. *J. Appl. Chem.* **2012**, *3*(1), 38–45. https://doi.org/10.9790/5736-0313845

[48] Azad, M. S.; Mohd, S. H.; Shahinuzzaman, M.; Azhari, S. Removal of Copper from Aqueous Solution Using Rice Husk Activated Carbon. *Sci. Technol. Asia* **2022**, *27*(3), 69–84.

[49] Arabzadeh, S.; Ghaedi, M.; Ansari, A.; Taghizadeh, F.; Rajabi, M. Removal of Methylene Blue Using NiO and Pd Nanoparticle-Loaded Activated Carbon. *Hum. Exp. Toxicol.* **2015**, *34*, 153–169. https://doi.org/10.1177/0960327114532383

[50] Boulder, B.; Rida, K. Adsorption of Rhodamine B, Methyl Orange, and Phenol by Magnetic Activated Carbon. *Mater. Sci. Eng. B* **2024**, *307*, 117502. https://doi.org/10.1016/j.mseb.2024.117502

[51] Belcaid, A.; Beakou, B. H.; Bouhsina, S.; Anouar, A. Adsorptive Removal of Dyes by Cassava Peel Biochar. *Biofuels, Bioprod. Biorefin.* **2024**, *14*, 7783–7806. https://doi.org/10.1007/s13399-022-02928-w

[52] Sewu, D. D.; Boakye, P.; Woo, S. H. Adsorption of Cationic Dye by Biochar from Korean Cabbage Waste. *Bioresour. Technol.* **2017**, *224*, 206–213. https://doi.org/10.1016/j.biortech.2016.11.009

[53] Al-Shehri, H. S.; Almudaifer, E. A.; Alorabi, Q.; Alanazi, H. S.; Alkorbi, A. S.; Alharthi, F. A. Effective Adsorption of Crystal Violet from Aqueous Solutions. *Environ. Pollut. Bioavailability* **2021**, *33*(1), 214–226. https://doi.org/10.1080/26395940.2021.1960199

[54] Rajeswari, K. M.; Revanth, T.; Anirudh, A.; Prasad, B. Removal of Crystal Violet Using Water Hyacinth. *Resour.-Effic. Technol.* **2017**, *3*, 71–77. https://doi.org/10.1016/j.reffit.2017.01.009

ASEAN
Journal of Scientific and Technological Reports
Online ISSN:2773-8752

ASEAN
Journal of Scientific and Technological Reports
Online ISSN: 2773-8752

Article type

Type of the Paper (Article, Review, Communication, etc.) *about 8,000 words maximum*

Title (Palatino Linotype 18 pt, bold)

Firstname Lastname[1], Firstname Lastname[2] and Firstname Lastname[2*]

[1] Affiliation 1; e-mail@e-mail.com
[2] Affiliation 2; e-mail@e-mail.com
* Correspondence: e-mail@e-mail.com; (one corresponding authors, add author initials)

Citation:
Lastname, F.; Lastname, F.; Lastname, F. Title. *ASEAN J. Sci. Tech. Report.* **2023**, *26*(X), xx-xx. https://doi.org/10.55164/ajstr.vxxix.xxxxxx

Article history:
Received: date
Revised: date
Accepted: date
Available online: date

Abstract: A single paragraph of about 400 words maximum. Self-contained and concisely describe the reason for the work, methodology, results, and conclusions. Uncommon abbreviations should be spelled out at first use. We strongly encourage authors to use the following style of structured abstracts, but without headings: (1) Background: Place the question addressed in a broad context and highlight the purpose of the study; (2) Methods: briefly describe the main methods or treatments applied; (3) Results: summarize the article's main findings; (4) Conclusions: indicate the main conclusions or interpretations.

Keywords: keyword 1; keyword 2; keyword 3 (List three to ten pertinent keywords specific to the article yet reasonably common within the subject discipline.)

1. Introduction

The introduction should briefly place the study in a broad context and highlight why it is crucial. It should define the purpose of the work and its significance. The current state of the research field should be carefully reviewed and critical publications cited. Please highlight controversial and diverging hypotheses when necessary. Finally, briefly mention the main aim of the work. References should be numbered in order of appearance and indicated by a numeral or numerals in square brackets—e.g., [1] or [2, 3], or [4–6]. See the end of the document for further details on references.

2. Materials and Methods

The materials and methods should be described with sufficient details to allow others to replicate and build on the published results. Please note that your manuscript's publication implicates that you must make all materials, data, computer code, and protocols associated with the publication available to readers. Please disclose at the submission stage any restrictions on the availability of materials or information. New methods and protocols should be described in detail, while well-established methods can be briefly described and appropriately cited.

Interventional studies involving animals or humans, and other studies that require ethical approval, must list the authority that provided approval and the corresponding ethical approval code.

2.1 Subsection

2.1.1. Subsubsection

3. Results and Discussion

This section may be divided by subheadings. It should provide a concise and precise description of the experimental results, their interpretation, as well as the experimental conclusions that can be drawn.Authors should discuss the results and how they can be interpreted from previous studies and the working hypotheses. The findings and their implications should be discussed in the broadest context possible. Future research directions may also be highlighted.

3.1. Subsection

3.1.1. Subsubsection

3.2. Figures, Tables, and Schemes

All figures and tables should be cited in the main text as Figure 1, Table 1, etc.

Figure 1. This is a figure. Schemes follow the same formatting.

Table 1. This is a table. Tables should be placed in the main text near the first time they are cited.

Title 1	Title 2	Title 3
entry 1	data	data
entry 2	data	data [1]

[1] Table may have a footer.

3.3. Formatting of Mathematical Components

This is example 1 of an equation:

$$a = 1, \tag{1}$$

The text following an equation need not be a new paragraph. Please punctuate equations as regular text. This is example 2 of an equation:

$$a = b + c + d + e + f + g + h + i + j + k + l + m + n + o + p + q + r + s + t + u \tag{2}$$

The text following an equation need not be a new paragraph. Please punctuate equations as regular text. The text continues here.

4. Conclusions

Concisely restate the hypothesis and most important findings. Summarize the significant findings, contributions to existing knowledge, and limitations. What are the future directions? Conclusions MUST be well stated, linked to original research question & limited to supporting results.

5. Acknowledgements

Should not be used to acknowledge funders – funding will be entered as a separate. As a matter of courtesy, we suggest you inform anyone whom you acknowledge.

Author Contributions: For research articles with several authors, a short paragraph specifying their individual contributions must be provided. The following statements should be used "Conceptualization, X.X. and Y.Y.; methodology, X.X.; software, X.X.; validation, X.X., Y.Y. and Z.Z.; formal analysis, X.X.; investigation, X.X.; resources, X.X.; data curation, X.X.; writing—original draft preparation, X.X.; writing—review and editing, X.X.; visualization, X.X.; supervision, X.X.; project administration, X.X.; funding acquisition, Y.Y. All authors have read and agreed to the published version of the manuscript." Please turn to the CRediT taxonomy for the term explanation. Authorship must be limited to those who have contributed substantially to the work reported.

Funding: Please add: "This research received no external funding" or "This research was funded by NAME OF FUNDER, grant number XXX" and "The APC was funded by XXX". Check carefully that the details given are accurate and use the standard spelling of funding agency names at https://search.crossref.org/funding. Any errors may affect your future funding.

Conflicts of Interest: Declare conflicts of interest or state "The authors declare no conflict of interest." Authors must identify and declare any personal circumstances or interest that may be perceived as inappropriately influencing the representation or interpretation of reported research results. Any role of the funders in the design of the study; in the collection, analyses or interpretation of data; in the writing of the manuscript, or in the decision to publish the results must be declared in this section. If there is no role, please state "The funders had no role in the design of the study; in the collection, analyses, or interpretation of data; in the writing of the manuscript, or in the decision to publish the results".

References

References must be numbered in order of appearance in the text (including citations in tables and legends) and listed individually at the end of the manuscript. We recommend preparing the references with a bibliography software package, such as EndNote, ReferenceManager to avoid typing mistakes and duplicated references. Include the digital object identifier (DOI) for all references where available.

Citations and references in the Supplementary Materials are permitted provided that they also appear in the reference list here.

In the text, reference numbers should be placed in square brackets [ ] and placed before the punctuation; for example [1], [1–3] or [1, 3]. For embedded citations in the text with pagination, use both parentheses and brackets to indicate the reference number and page numbers; for example [5] (p. 100), or [6] (pp. 101–105).

Using the American Chemical Society (ACS) referencing style

[1] Author 1, A.B.; Author 2, C.D. Title of the article. *Abbreviated Journal Name* Year, *Volume*, page range.

[2] Author 1, A.; Author 2, B. Title of the chapter. In *Book Title*, 2nd ed.; Editor 1, A., Editor 2, B., Eds.; Publisher: Publisher Location, Country. **2007**, Volume 3, pp. 154–196.

[3] Author 1, A.; Author 2, B. *Book Title*, 3rd ed.; Publisher: Publisher Location, Country, **2008**, pp. 154–196.
[4] Author 1, A.B.; Author 2, C. Title of Unpublished Work. *Abbreviated Journal Name* stage of publication (under review; accepted; in press).
[5] Author 1, A.B. (University, City, State, Country); Author 2, C. (Institute, City, State, Country). Personal communication, 2012.
[6] Author 1, A.B.; Author 2, C.D.; Author 3, E.F. Title of Presentation. In Title of the Collected Work (if available), Proceedings of the Name of the Conference, Location of Conference, Country, Date of Conference; Editor 1, Editor 2, Eds. (if available); Publisher: City, Country, Year (if available); Abstract Number (optional), Pagination (optional).
[7] Author 1, A.B. Title of Thesis. Level of Thesis, Degree-Granting University, Location of University, Date of Completion.
[8] Title of Site. Available online: URL (accessed on Day Month Year).

Reviewers sugestion

1. Name, Address, e-mail
2. Name, Address, e-mail
3. Name, Address, e-mail
4. Name, Address, e-mail

URL link:

Notes for Authors >>
https://drive.google.com/file/d/1r0zegnIVeQqe4iLQyT1xDEIinNggINPD/view?usp=sharing
https://drive.google.com/file/d/1r0zegnIVeQqe4iLQyT1xDEIinNggINPD/view?usp=sharing

Online Submissions >> https://ph02.tci-thaijo.org/index.php/tsujournal/user/register

Current Issue >> https://ph02.tci-thaijo.org/index.php/tsujournal/issue/view/16516

AJSTR Publication Ethics and Malpractice >> https://ph02.tci-thaijo.org/index.php/tsujournal/ethics

Journal Title Abbreviations >> http://library.caltech.edu/reference/abbreviations

ASEAN
Journal of Scientific and Technological Reports
Online ISSN:2773-8752

ASEAN
Journal of Scientific and Technological Reports
Online ISSN:2773-8752

ASEAN Journal of Scientific and Technological Reports (AJSTR)
Institute of Research and Innovation, Thaksin University, Phatthalung Campus
222 Moo. 2, Baan Prao Sub-District, Papayom District, Phatthalung, 93210, Thailand
Tel. +668 1540 7304